

# BERICHTE

aus dem Fachbereich Geowissenschaften  
der Universität Bremen

Nr. 32

Antia, E.E.

**SEDIMENTOLOGY, MORPHODYNAMICS AND FACIES ASSOCIATION  
OF A MESOTIDAL BARRIER ISLAND SHOREFACE  
(SPIEKEROOG, SOUTHERN NORTH SEA)**

Berichte, Fachbereich Geowissenschaften, Universität Bremen, Nr. 32,  
370 S., 132 Abb., 5 Tab., Bremen 1993.



ISSN 0931-0800

Die "Berichte aus dem Fachbereich Geowissenschaften" werden in unregelmäßigen Abständen vom Fachbereich 5, Universität Bremen, herausgegeben.

Sie dienen der Veröffentlichung von Forschungsarbeiten, Doktorarbeiten und wissenschaftlichen Beiträgen, die im Fachbereich angefertigt wurden.

Die Berichte können beim:

Fachbereich 5 Geowissenschaften

Universität Bremen

Klagenfurterstr.

2800 BREMEN 33

Telefon: (0421) 218-4124

Telefax: (0421) 218-3116

angefordert werden.

Zitat:

Antia. E.E.

Sedimentology, Morphodynamics and Facies Association of a Mesotidal Barrier Island Shoreface (Spiekeroog, Southern North Sea).

Berichte, Fachbereich Geowissenschaften, Universität Bremen, Nr. 32, 370 S., 132 Abb., 5 Tab. Bremen 1993.

ISSN 0931-0800

The Deutscher Akademischer Austauschdienst, Bonn, financed the printing of this report.



SEDIMENTOLOGY, MORPHODYNAMICS AND FACIES  
ASSOCIATION OF A MESOTIDAL BARRIER ISLAND SHOREFACE  
( SPIEKEROOG, SOUTHERN NORTH SEA )

DOCTORAL DISSERTATION

Submitted to the  
Geological Sciences Institute,  
University of Bremen

By

EFFIOM EDEM ANTIA

Bremen, 1992

"They that go down to the sea in ships, that do business in great waters;  
These see the works of the Lord, and his wonders in the deep."

Psalm 107, v. 23-24.

## DEDICATION

This work is dedicated to the memory of my grandparents, and to my parents, who may neither have sailed across the great waters nor seen the wonders of their deeps, yet faithfully believed in the Supreme Being that created, controls and causes the calm and cataclysmic changes which we witness today and attempt to unravel.

## ABSTRACT

The aim of this study is to enhance our understanding of the process-response mechanisms operating on a modern, mesotidal, moderate- to high-energy barrier island shoreface (Spiekeroog, southern North Sea). Such knowledge is of particular interest because the existence and characteristics of a barrier island system or any of its constituting elements would seem to substantially depend on the nature and the dynamics of the shoreface. In this study, the shoreface is defined as extending offshore from the beach to a water depth of about 25 m.

The above objective essentially entailed:

- (1) determining the scale and structure of the flow regime;
- (2) describing the grain size distribution patterns;
- (3) deciphering sediment transport trends and pathways;
- (4) developing models of sea-floor moulding and morphodynamics;
- (5) defining the facies association; and
- (6) detailing the distinctive characteristics of transgressive and regressive shoreface stratigraphic sequences.

The above-mentioned were achieved through a very dense net-work of bottom grab samples, vibrocores, repetitive boxcoring, current metering and echosounding, as well as analyses of sounding charts spanning a 40-year period.

The acquired data support a tripartite subdivision of the shoreface, namely, an upper, a central and a lower shoreface subenvironment. The upper shoreface is a high energy, wave-dominated subenvironment. It extends to a depth of about 7 m and is composed of a diverse succession of morphological features. These include an E-W oriented sandy beach with shore-attached inner surf zone oblique bars opening eastwards; a shore-parallel barred outer surf zone; a rhythmic "sawtooth-bar" system, situated seawards of the fair-weather surf zone; and a smoothly-sloping transitional zone linking the upper and central shoreface subenvironments.

The central shoreface (8-18 m water depth) is a moderate-energy, mixed wave-current subenvironment. The main morphologic feature of the latter is a set of WNW-ESE trending shoreface-connected ridges. The lower shoreface is also a mixed but low-energy subenvironment. With the exception of a number of ridge extensions beyond 25 m isobath, the lower shoreface subenvironment is essentially smooth.

Surficial sediment distribution and facies patterns are all consistent with the above tripartite subdivision of the shoreface. The former suggests that the upper and lower shoreface sands are genetically related whereas their central shoreface counterpart are allogenetic. The central shoreface subenvironment depicts mostly medium-coarse grained, relatively poorly sorted and meso-platykurtic sands. Sedimentary structures are extremely variable but most commonly consist of graded storm sequences, tidal cross-stratified beds and, occassionally, swaley/hummocky bedding. By contrast, the upper shoreface subenvironment consists of dominantly horizontally laminated sands, whereas the lower shoreface counterpart is bioturbation-prone.

Essentially, grain sizes fine ( $< 3$  cm/s mean settling velocity), improve in sorting, and become meso-leptokurtic both seaward and shoreward of the central shoreface subenvironment. Each of the subenvironments respectively reveals a coast-parallel band of positive and negative skewness at their distal and proximal ends. Based on a conceptual model of skewness sign evolution presented, the above-noted alternating band of skewness sign can not be justified entirely by the prevailing shoreface flow regime without recourse to an influx of extraneous sediments.

In general, tidal flow and wave data show that surficial sediments on the upper and central shoreface would be mobilized in  $> 80\%$  of the time, but with a much reduced frequency on the lower shoreface. The offshore increasing bioturbation of the shoreface substrate is consistent with this finding.

Sediment size patterns on the shoreface reflect both a cross-shore and a coast-parallel current influence. These transport directions are particularly pronounced on the proximal (shoreline-surf) zone of the upper shoreface subenvironment.

Sediment budget calculations further support the above conclusion. Interestingly, in the medial and distal zones of the upper shoreface, the longshore gradient observed in sediment budget values shows a discontinuity in pattern close to the mid-island length. This observation might suggest an updrift ebb-delta-induced wave refraction and a consequent reversal in the easterly-directed longshore sediment drift.

Circumstantial field evidences coupled with theoretical models support the contention that standing infragravity edge waves are an important component of the upper shoreface storm flow regime. The sawtooth bars along the Frisian barrier island coast are interpreted as a rip channel and ridge morphology whose genesis is related to the interaction of a longshore standing edge wave with an ebb-storm surge.

A number of observations negate the previously held opinion that the above feature represents transverse bedforms migrating alongshore. Principal among these are: (i) the alongshore-varying inclination of the channels relative to the shoreline trend, and (ii) their exclusively horizontal laminated internal structure. A conceptual model is presented in which the spatially- and temporally-varying orientation and dynamic behaviour of the rip channels are related to the degree of distortion of the standing edge wave oscillation.

The fact that rip-channel locations tend to coincide in time is suggestive of the coherent nature of the edge wave generating mechanism. An attractive mechanism requires a topographic perturbation of an easterly directed transient storm flow. From the view-points of edge wave energetics and the rip channel cross-shore configuration, a Mode 1

infragravity oscillation is asserted to be dominantly excited through the above mechanism in the study area.

The development of shoreface-connected ridges seems to be very controversial. None of the currently existing models of genesis can unequivocally explain the morphometric and textural attributes of the North Sea barrier island shoreface ridges, notwithstanding the gross similarities with their counterparts along the Atlantic sea-board of North and South America.

However, more difficult to account for with the existing models in the study area are : (i) the non-occurrence of the ridges in water depths shallower as the distal margin of the ebb-deltas, (ii) the longitudinal grain-size gradient, which has an inverse trend to that anticipated for an easterly storm and net flow, (iii) the longitudinal wedging-out pattern of the ridge relief, (iv) the distally diminishing negative or positive-prone sediment budget within the ridge troughs, (v) the vertical pattern of grain sizes, and (vi) the higher tendency of ebb-flow dominance in ridge troughs.

A novel model of shoreface ridge genesis called DISEC, which is based on the divergence of an inlet storm outflow, is presented. The latter accounts for all of the characteristics of the Frisian ridge morphology in a simple and logical manner. This model can be applied at least to a section of the Mid-Atlantic ridge field of North America. However, in comparison to other shoreface-connected ridges described from other parts of the world, those investigated here are extremely mobile. Maximum cross-shore (seaward and shoreward) translation is of the order of 100-200 m annually.

Such high rates of sea-floor mobility and the associated frequency of sediment entrainment should have profound influence on engineering management of, and development practices on, the shoreface region. Similarly, the shoreface stratigraphic sequences presented should significantly aid in rock-record reconstruction of mixed tidal and storm-wave depositional settings.

## ZUSAMMENFASSUNG

Das Ziel dieser Untersuchung ist es, eine ausreichende Einsicht in den Prozess-Reaktions-Mechanismus auf dem Sockel (shoreface) einer rezenten, mesotidalen, mäßig/hochenergertischen Barriere-Insel (Spiekeroog, südliche Nordsee) zu gewinnen. Solch eine Kenntnis ist von besonderem Interesse, da die Existenz und die Merkmale einer Barriere-Insel mit ihren einzelnen Elementen von den Eigenschaften und der Dynamik des Sockels abhängig sind. In dieser Arbeit ist als Inselsockel der Bereich seewärts vom Strand bis 25 m Wassertiefe definiert.

Im Zusammenhang mit dem oben erwähnten Ziel wurden die folgenden Aufgaben durchgeführt:

- (1) Erfassung von Intensität und Art der hydrodynamischen Prozesse;
- (2) Beschreibung der Korngrößenverteilungen der Sedimente;
- (3) Rekonstruktion der Sedimenttransportwege;
- (4) Modellierung der Entstehung und Dynamik der Meeresbodenmorphologie;
- (5) Definierung der Fazies-Assoziationen;
- (6) Charakterisierung und stratigraphische Darstellung des Sockel-Ablagerungsraumes im Zuge sowohl eines Anstiegs (Transgressivphase) als auch des Sinkens (Regressivphase) des Meeresspiegels.

Die Realisierung des o.g. erfolgt anhand eines dichten Probennetzes von Oberflächensedimenten, zahlreichen ungestörten Vibrokernen und Kastengreiferproben, Strömungsmessungen, Echolotaufzeichnungen und Auswertungen aller existierenden Peilpläne, die einem Zeitraum von 40 Jahren entsprechen.

Die Ergebnisse der durchgeführten Arbeiten lassen erkennen, daß der Inselsockel in drei küstenparallele Bereiche unterteilt werden kann, nämlich in ein oberes, ein zentrales und ein unteres Subenvironment. Das obere Subenvironment ist ein hochenergertischer, wellendominierter Bereich, der sich von der Uferlinie bis ca. 7 m Wassertiefe erstreckt. Dieses

Subenvironment besteht aus unterschiedlichen Bodenmorphologien, z.B.: küstenparallelen Riffen in Strandnähe, rhythmisch angeordneten Riffen (Sägezahnriffe) seewärts der Brandungszone und einer ebenen Übergangszone, die eine stetig abnehmende Neigung aufweist und an das zentrale Subenvironment anschließt.

Das zentrale Subenvironment (8-18 m Wassertiefe) ist ein mäßig gemischter (Welle und Tide) Energiebereich. Ein System von WNW-OSO streichenden Zungenriffen (shoreface-connected ridges) stellt die einzige Morphologie in diesem Subenvironment dar. Das untere Subenvironment ist ebenfalls ein gemischter, aber niedrigenergertischer Bereich der eben ist, ausgenommen von einigen Zungenriffen in > 25 m Wassertiefe.

Die Verteilungstrends der Oberflächensedimente und Fazies spiegeln die Dreigliederung des Inselsockels wieder. Während die Sedimentmerkmale des oberen und unteren Subenvironment eine gemeinsame Herkunft vermuten lassen, sind diejenigen auf dem zentralen Subenvironment eindeutig allogetisch. Diese allogetischen Sedimente zeichnen sich deutlich durch ihre Mittel-/Grobkornigkeit, schlechte Sortierung und meso-platykurtische Tendenz aus. Außerdem sind die Sedimentgefüge aus diesem Bereich sehr variabel mit vorwiegend sturmbedingten, gradierten Laminationen (= ebengeschichteten) und Tideschrägschichtungen. Gelegentlich sind Hummocky-Schichtungen zu erkennen. Im Gegensatz dazu kommen auf dem oberen Subenvironment Horizontalschichtungen vor, während das untere Subenvironment eine Zunahme von Bioturbation aufweist.

Sowohl seewärts als auch landwärts vom zentralen Subenvironment werden die Sedimente feinkörniger, (Sinkgeschwindigkeiten < als 3 cm/s), besser sortiert und meso-leptokurtisch. Die räumliche Verteilung der Korngößen innerhalb eines Subenvironments weist einen küstenparallelen, abwechselnden Gürtel von negativer (Proximalzone) und positiver (Distalzone) Schiefe auf. Der o.g. Trend läßt sich nur mit einer Zufuhr von Sedimenten außerhalb des Inselsockels erklären.

Im Allgemeinen sind die Oberflächensedimente auf dem oberen und zentralen Subenvironment durch die Auswirkung von Wellen- und Tideströmung zu 80% zeitlich reaktiviert. Die Bioturbationszunahme auf dem unteren Subenvironment ist ein Indikator dafür, daß die Energie der hydrodynamischen Prozesse in diesem Bereich gering ist.

Die statistische Auswertung der Korngrößenverteilungen leitet einen Sedimenttransport sowohl parallel als auch senkrecht zur Küste ab, der in Strandnähe am intensivsten erscheint. Diese Schlußfolgerung wird vom Veränderungstrend des Sandhaushaltes unterstützt.

Bemerkenswert ist die Abnahme im Sandhaushalt außerhalb der Brandungszone an einer Stelle, die der Inselmitte entspricht. Diese Abnahmeregion kann als ein Divergenzbereich des küstenparallelen Sedimenttransports gesehen werden, der einer Ebb-Delta-verursachten Wellenrefraktion entspricht.

Anhand zahlreicher Feldbeobachtungen und theoretischer Überlegungen sind die vor der ostfriesischen Inselküste vorkommenden Sägezahnriffe als eine durch Ripströmung verursachte Morphologie zu sehen. Ihre Entstehung ist Folge der Interaktion zwischen entlang der Küste stehenden Randwellen und der seewärts gerichteten Strömung während der Abklingphase eines Sturmes. Faktoren wie die räumliche Variabilität des Winkels der Riffe/Rinne relativ zu Uferlinie und die vorwiegenden Horizontalschichtungen widersprechen der landläufigen Transportkörperhypothese ihrer Entstehung.

Zur Erklärung der zeitlichen und räumlichen Dynamik der Morphologie wurde ein Prozeß-Modell erstellt. Es handelt sich um die Modifikation einer Symmetrie der stehenden Randwelle durch eine nach Osten gerichtete küstenparallele Sturmströmung, die wiederum durch Interaktion am Rande des Ebb-Deltas die Randwelle erzeugt. Aus energetischem Grunde einerseits und der Rinnenkonfiguration andererseits, ist abzuleiten, daß stehende

Randwellen der 1. Ordnung im Untersuchungsgebiet am häufigsten bzw. aktivsten sein dürften.

Die Merkmale der Zungenriffe vor der südlichen Nordseeküste sind sehr ähnlich denen vor der atlantischen Küste Nord- und Südamerikas. Trotz dieser Tatsache können die z.Zt. existierenden Entstehungsmodelle der Morphologie nicht mit Zufriedenheit im Untersuchungsgebiet angewendet werden. Diese Modelle machen keine Aussage über (a) die Abwesenheit der Riffe in Wassertiefen geringer als die örtliche Position des Ebb-Delta-Randes, (b) den Korngrößentrend entlang der Morphologie, (c) die WNW abnehmende Höhe der Morphologie, (d) der WNW zunehmende Sandhaushalt (weniger negativ), (e) die vertikalen Profile der Korngrößen, und (f) die Dominanz des Ebbstromes innerhalb der Rinnen.

Die o.g. Beobachtungen und die Entstehung der Zungenriffe sind mit dem hier erstmals vorgestellten DISEC-Modell auf eine unkomplizierte Weise erklärbar. Das Modell geht davon aus, daß die bodennahe Schichtung der Staurückströmung aus den Seegatten während der Ebbphase eines Sturmes durch Interaktion mit der westlich gerichteten Inselsockelströmung divergiert wird. Auch das Vorkommen der Zungenriffe entlang einem Teil der atlantischen Küste Nordamerikas kann grundsätzlich mit diesem Modell erklärt werden.

Die Zungenriffe vor der ostfriesischen Inselküste mit see- und landwärtigen Umlagerungsraten von 100-200 m im Jahr stellen die z.Zt. weltweit größte bekannte morphologische Beweglichkeit dar. Die morphologische Dynamik der o.g. Größenordnung, zusätzlich zu der Häufigkeit der Sedimentbewegung im Untersuchungsgebiet, ist ein kritischer Faktor, der bei technischen Planungen und Bauwerken berücksichtigt werden sollte. Ebenfalls sind die dargestellten Stratigraphien des Inselsockels äußerst wichtig in der Interpretation eines fossilen von Tide, Wellen und Sturmströmung beeinflussten Ablagerungsraumes.

## ACKNOWLEDGEMENTS

This thesis is an offshoot of a very fruitful pioneering scientific cooperation between the Marine Geology Research Group (FB 5 - Geowissenschaften) of the University of Bremen and the Marine Sciences Division of the Senckenberg Institute in Wilhelmshaven.

My sincere thanks are expressed to the heads of both Geological Institutes: Prof. Dr. G. Wefer and Dr. B. W. Flemming respectively for kindly consenting to act as academic and research advisers as well as Prof. Dr. D. Fütterer (Head of Marine Geology at the Alfred Wegener Institute for Polar and Marine Research, Bremerhaven) for also reviewing the report. Their scholarly and social disposition at all times have been a great source of inspiration.

I am grateful to Senckenbergische Naturforschende Gesellschaft for facilities generously provided in the course of this study, and to all of the scientific, technical and supporting staff of the Senckenberg Institute as well as the captain and crew of FK "Senckenberg" for their dexterity and dedication. Specific mention of Drs. B. W. Flemming, F. Wunderlich, G. Hertweck, J. Dörjes (deceased), G. Irion, Prof. Dr. H. -E. Reineck, Captain K. Kommer, Messrs W. Rosenboom, and Mrs. A. Raschke does not underscore the very valuable and varied assistance rendered by the other personnel and colleagues.

The captain and crew of FK "Senckenberg" are further commended for constantly insuring safety of personnel and equipment during the frequently inclement sea-state as well as for the many sleepless current metering nights. My gratitude and apologies to all of the individuals who were unfortunate to share these sea-board experiences with me. I thank Messrs K. Lipka and K.-H. Naujokaut for their relentless efforts in this regard. Mr N. Martin was very helpful in computer operation.

Many visiting scholars have acted as informal instructors on varied "vexing problems" associated with this research for

which I express my appreciation. Notable among these are : Profs. B. Greenwood (Canada), R. W. G. Carter (Ireland), A. Chakrabarti (India), R. A. Davis jr. (USA), A. D. Short (Australia) and Xu Sheng Shao (China). Moreover, Prof. Per Bruun's (USA) invitation to a Coastal Symposium in Skagen as well as discussions with Prof. D. A. Huntley (England) during a Workshop in Bordeaux have been very illuminating. Also rewarding were the long hours of informal discussion with Mr. N. Nyandwi.

Mr. G. Frels at the Wasser- und Schiffahrtsamt, Wilhelmshaven kindly provided very useful information and data.

I am indebted to the Kissing family and Fiti Wunderlich for their untiring hospitality, welfare and thoughtfulness during those lonely and needy occasions.

The affection, encouragement and goodwill of my parents, Edem and Inyang, and family members : Mr. Allan Antia, Mrs. Victoria Adah, Dr. Richard Antia, Dr. Victor Antia, Dr. Hogan Antia and Mr. Basseyy Antia are also acknowledged.

I record my appreciation and gratitude to the Deutscher Akademischer Austauschdienst for financing my studies and generously supporting scientific activities pertinent to this research.

Finally, I thank God for making all of these happen.

# CONTENTS

page

ABSTRACT.....	i
ZUSAMMENFASSUNG (German Summary).....	v
ACKNOWLEDGEMENTS.....	ix
CONTENTS.....	xi
LIST OF TABLES.....	xvi
LIST OF FIGURES.....	xvii
LIST OF PLATES.....	xxv
LIST OF APPENDICES.....	xxvi

CHAPTER 1	INTRODUCTION.....	1
-----------	-------------------	---

1.1	Barrier Island System.....	1
1.1.1	Definition and Constitution.....	1
1.1.2	General Characteristics.....	2
1.1.2.1	Spatial distribution.....	3
1.1.2.2	Size.....	4
1.1.2.3	Shape.....	6
1.1.2.4	Stratigraphy.....	7
1.1.3	Development.....	7

CHAPTER 2	BARRIER ISLAND SHOREFACE.....	9
-----------	-------------------------------	---

2.1	Physical Boundaries.....	9
2.2	Previous Studies.....	10
2.2.1	Hydrodynamics.....	10
2.2.2	Morphodynamics.....	12
2.2.3	Sedimentology.....	16
2.3	Present Study.....	17
2.3.1	Objectives.....	17
2.3.2	Organization.....	17

CHAPTER 3	SPIEKEROOG BARRIER ISLAND.....	19
3.1	Location.....	19
3.2	Geology.....	20
3.3	Geomorphology and Vegetation.....	23
3.4	Bathymetry.....	24
3.5	Meteorology.....	26
3.6	Hydrography and Hydrodynamics.....	27
3.6.1	Salinity - Temperature - Turbidity....	27
3.6.2	Regional Water Circulation.....	29
3.6.3	Tides and Tidal Currents.....	30
3.6.4	Waves and Wave-Induced Currents.....	40
CHAPTER 4	STUDY METHODS AND DATA SET.....	47
4.1	Bathymetric Charts and Soundings.....	47
4.2	Sea-Based Operations.....	48
4.2.1	Navigation.....	48
4.2.2	Depth Sounding.....	48
4.2.3	Seabed Sampling.....	49
4.2.3.1	Grab Sampling.....	49
4.2.3.2	Boxcoring.....	49
4.2.3.3	Vibrocoring.....	52
4.2.3.4	Current Metering.....	53
4.2.3.5	Temperature-Salinity Measurements.....	59
4.3	Shore-Based Observations.....	60
4.3.1	Beach Profile Surveys.....	60
4.3.2	Beach Sedimentary Marks.....	61
4.4	Laboratory Analyses.....	62
4.4.1	Grain Size Measures and their Interrelationships.....	62
4.4.2	Relief Peels.....	68

CHAPTER 5	SHOREFACE SEDIMENT DISTRIBUTION, DYNAMICS AND BUDGET.....	70
5.1	Introduction.....	70
5.2	Sediment Distribution.....	72
5.2.1	Summary Sediment Size Statistics.....	72
5.2.1.1	Mean.....	73
5.2.1.2	Sorting.....	79
5.2.1.3	Skewness.....	81
5.2.1.4	Kurtosis.....	88
5.2.2	Sedimentation Diameter ( $\phi$ ) and Settling Velocity (cm/s) Class Fractions.....	91
5.2.2.1	Whole-Phi Size Classes: 0-1, 1-2, 2-3, 3-4 $\phi$ .....	91
5.2.2.2	Half-Phi Size Classes: 1.5-2, 2-2.5, 2.5-3, 3-3.5 $\phi$ .....	95
5.2.2.3	Quarter-Phi Classes: 2.25-2.5, 2.5-2.75, 2.75-3 $\phi$ .....	98
5.2.2.4	Settling-Velocity Fractions: >2.5, 2.5-2, 2-1.5, 1.5-1 cm/s.....	102
5.2.3	Bivariate Diagrams.....	105
5.2.3.1	Mean vs. Sorting.....	106
5.2.3.2	Mean vs. Skewness.....	107
5.2.3.3	Mean vs. Kurtosis.....	110
5.2.3.4	Sorting vs. Skewness.....	111
5.2.3.5	Sorting vs. Kurtosis.....	112
5.2.3.6	Skewness vs. Kurtosis.....	113
5.2.3.7	C-M Plot of PASSEGA.....	115
5.2.4	Log-Probability Grain-Size Curve Characteristics.....	118
5.2.4.1	Weight-% of Components A, B, and C.....	119
5.2.4.2	Phi-Median of Components A, B and C.....	121

5.2.4.3	Sorting Index of Components A, B and C.....	126
5.2.4.4	Inflection Points of Log-probability Curve Components.....	128
5.3	Summary Remarks on Shoreface Sediment Textures.....	129
5.4	Shoreface Sediment Dynamics: Comparison of Some Texture-Based Sediment Transport Models.....	130
5.4.1	Size-Sorting Model.....	131
5.4.2	VISHER'S Model.....	135
5.4.3	PASSEGA'S Model.....	138
5.4.4	MCLAREN'S Model.....	140
5.4.5	Storm-Sedimentation Model.....	141
5.4.6	Summary Remarks on Sediment Transport Models.....	144
5.5	Shoreface Sediment Budget.....	144
5.5.1	Erosional Pattern.....	146
5.5.2	Accretional Pattern.....	147
5.5.3	Summary Remarks on Sediment Budget Patterns.....	148
CHAPTER 6	HYDRODYNAMICS, MORPHODYNAMICS AND SEDIMENTARY FACIES ASSOCIATIONS OF THE SHOREFACE SUBENVIRONMENTS.....	153
6.1	Introduction.....	153
6.2	Upper Shoreface Subenvironment.....	153
6.2.1	Hydrodynamics, Morphodynamics and Facies.....	154
6.2.1.1	Shoreline-Beach Zone.....	154
6.2.1.2	Surf Zone.....	173
6.2.1.3	Saw-tooth Bar Zone: Genesis and Dynamics.....	177

6.2.1.4	Smoothly Sloping Transitional Zone...	205
6.2.2	Summary Remarks on the Upper Shoreface Subenvironments.....	209
6.3	Central Shoreface Subenvironment.....	212
6.3.1	Genesis of Shoreface-Connected Ridges: Criteria and Constraints of Existing Models.....	213
6.3.1.1	Diverged Inlet Storm Ebb-Current (DISEC) Model: A Novel Approach to Ridge Genesis.....	217
6.3.2	Hydrodynamics.....	223
6.3.3	Morphodynamics.....	225
6.3.4	Facies.....	239
6.3.4.1	Sediment Size Statistics: Cross-shore, Longitudinal and Vertical Patterns...	239
6.3.4.2	Sedimentary and Biogenic Structures..	263
6.3.4.2.1	Ridge Trough.....	266
6.3.4.2.2	Ridge Flanks.....	267
6.3.4.2.3	Ridge Crest.....	269
6.3.5	Development and Dynamic Sequence of Shoreface-Connected Ridges.....	272
6.3.6	Summary Remarks on the Central Shoreface Subenvironment.....	276
6.4	Lower Shoreface Subenvironment.....	278
6.4.1	Hydrodynamics, Morphodynamics and Facies.....	278
6.4.2	Summary Remarks on the Lower Shoreface Subenvironment.....	281
6.5	Shoreface Stratigraphic Model.....	282
6.5.1	Transgressive Sequence.....	283
6.5.2	Regressive Sequence.....	285
CHAPTER 7	GENERAL CONCLUSIONS: RESULTS, IMPLICATIONS, AND APPLICATIONS.....	287
REFERENCES.....		296

## LIST OF TABLES

	Page
1. Postulates on barrier island origin (after JONES, 1969).....	8
2. Wave regimes and their principal characteristics along the East Frisian coast.....	43
3. Factors affecting boundary-layer hydraulic parameters (after WRIGHT, 1989).....	59
4. Alongshore sediment budget data for two upper shoreface zones.....	163
5. Longitudinal variation in average settling velocities (cm/s) of shoreface sands.....	251

## LIST OF FIGURES

	Page
1. Elements of a barrier island system (after OERTEL, 1985).....	1
2. Global distribution of barrier island morphology (from HAYES, 1979).....	3
3. Morphometrics of Frisian barrier islands and inlets....	5
4. Morphodynamic beach-state classification (after WRIGHT and SHORT, 1983).....	14
5. Location of Spiekeroog Island and its Frisian counterparts (modified after POSTMA, 1982).....	19
6. Holocene sea-level variation curves of the North Sea (from FLEMMING, 1990b).....	22
7. Bathymetry of the Spiekeroog shoreface.....	25
8a. Typical sea temperature ( $^{\circ}\text{C}$ ) profile offshore of Spiekeroog Island.....	28
8b. Typical sea salinity ( $^{\circ}/\text{oo}$ ) profile offshore of Spiekeroog Island.....	28
9. Regional water circulation in the North Sea (after POSTMA, 1982).....	29
10. Pattern of tidal wave propagation in the North Sea (after POSTMA, 1982).....	30
11a. Variation in spring and neap tidal current peak velocities (cm/s) at 100 cm above sea bed.....	32
11b. Spring-neap tide velocity ( $U_{100}$ ) ratios as a function of offshore distance.....	33
11c. Variation in spring and neap tidal flow excursion....	34
11d. Variation in spring and neap flood and ebb tide-averaged velocities (cm/s) at 100 cm above sea bed.....	35
11e. Variation in spring- and neap-tide depth-averaged (1, 2, 4 and 6 m above sea bed) velocities (cm/s)....	36
11f. Average spring and neap tidal current directions for velocities $> 10$ cm/s.....	38
12a. North Sea offshore wave frequency data (modified after FORTNUM, 1978).....	41

12b.	Variation in maximum near-bed wave current velocities (cm/s) in relation to water depth for three wave regimes.....	44
12c.	Wave current sediment threshold velocities.....	44
12d.	Percentage exceedance of sediment threshold by shoaling waves on Spiekeroog shoreface as a function of both water depth and mean grain size.....	45
13.	Spiekeroog shoreface sediment sampling stations.....	50
14.	Spiekeroog shoreface subsurface coring stations.....	51
15.	Spiekeroog shoreface current metering stations.....	54
16.	Boundary-layer flow regime (after WRIGHT, 1989).....	56
17.	Typical tidal variation in logarithmic current profiles on the Spiekeroog shoreface.....	57
18.	Definition sketch of swash angle, $\theta$ , (after ANTIA, 1989d).....	61
19.	Relationship between mean settling velocity (cm/s) and sedimentation diameter ( $\phi$ ) of shoreface sediments.....	66
20.	Relationship between sorting of $\psi$ and $\phi$ distribution of shoreface sediments.....	67
21.	Relationship between skewness of $\psi$ and $\phi$ distribution of shoreface sediments.....	67
22.	Relationship between kurtosis of $\psi$ and $\phi$ distribution of shoreface sediments.....	68
23.	Shoreface distribution of sediment mean sedimentation diameter ( $\phi$ ).....	75
24.	Shoreface distribution of sediment mean settling velocity (cm/s).....	78
25.	Distribution of sorting of shoreface sediments.....	80
26.	Models of skewness sign evolution.....	83
27.	Distribution of skewness of shoreface sediments.....	85
28.	Distribution of kurtosis of shoreface sediments.....	89
29.	Shoreface distribution of wt.-% of coarse sand (0-1 $\phi$ ).....	92
30.	Shoreface distribution of wt.-% of medium sand (1-2 $\phi$ ).....	94
31.	Shoreface distribution of wt.-% of fine sand (2-3 $\phi$ ).....	96

32.	Shoreface distribution of wt.-% of very fine sand (3-4 phi).....	97
33.	Shoreface distribution of wt.-% of 2.5-3 phi fraction.....	99
34.	Shoreface distribution of wt.-% of 2.25-2.5 phi fraction.....	100
35.	Shoreface distribution of wt.-% of 2.75-3 phi fraction.....	101
36.	Shoreface distribution of wt.-% of > 2.5 cm/s fraction.....	104
37.	Bivariate plot of mean grain size versus sorting.....	107
38.	Bivariate plot of mean grain size versus skewness....	108
39.	Bivariate plot of mean grain size versus kurtosis....	110
40.	Bivariate plot of sorting versus skewness.....	112
41.	Bivariate plot of sorting versus kurtosis.....	113
42.	Bivariate plot of skewness versus kurtosis.....	114
43.	C-M plot of shoreface sediments.....	117
44.	Areal distribution of weight-% of log-probability curve components A-B-C of shoreface sediments.....	120
45.	Areal distribution of weight-% of log-probability curve component B (saltation population).....	122
46.	Areal distribution of the phi-median of component A..	123
47.	Areal distribution of the phi-median of component B..	124
48.	Areal distribution of the phi-median of component C..	125
49.	Areal distribution of sortedness of component C.....	127
50.	Patterns of grain size statistic variation between and within the shoreface subenvironments.....	130
51.	Variants of a sediment size-sorting model (after SWIFT et al., 1972b).....	132
52.	Areal distribution of shoreface grain size modes.....	134
53.	Areal distribution of C-M based shoreface sediment transport modes.....	139
54.	Sediment source-deposit predictive model (after McLAREN and BOWLES, 1985).....	141
55.	Areal distribution of the phi coarsest percentile....	143
56.	Areal pattern of shoreface erosion and accretion.....	145
57.	Negative volumetric shoreface sediment budget pattern	146

58.	Positive volumetric shoreface sediment budget pattern	148
59.	Cross-shoreface sediment budget variation.....	149
60.	Alongshore shoreface sediment budget variation.....	151
61.	Historical change in Spiekeroog's outline (after FITZGERALD et al., 1984).....	156
62a.	Spiekeroog Beach profile and brief-time change.....	160
62b.	Spiekeroog Beach Profile and intermediate to long-term change (modified from HOMEIER and LUCK, 1977).....	160
63.	Rhythmic shoreline sediment budget.....	163
64.	Mode 0, 1 edge wave effect on shoreface bed change...	167
65.	Cross-shore profiles of upper shoreface grain size statistics.....	169
66.	Alongshore profiles of upper shoreface grain size statistics.....	170
67.	Shore-normal variation in beach grain size statistics	172
68a.	Empirical relationship of bedform wavelength versus mean grain size (from FLEMMING, 1988, 1990a).....	178
68b.	Empirical relationship of bedform height versus mean grain size (from FLEMMING, 1988, 1990a).....	178
69.	Relief peels from the saw-tooth bar (rip and ridge morphology).....	179
70.	Spatial trend of rip channel axes.....	180
71.	Temporal variation in orientation of rip channel axes relative to a hinge point at a total of 12 axis clusters.....	181
72a.	Definition sketch of rip channel axis dynamic parameters.....	182
72b.	Spatial variation in mean cluster rip channel axis shore-acute angle.....	182
72c.	Mean cluster rotational asymmetry of rip channel axes	182
72d.	Mean cluster frequencies of rotational direction of rip channel axes.....	182
73.	Temporal variation in magnitude and sense of rip channel axis rotation.....	185
74.	Rip channel dynamic modes.....	186

75a.	Fair-weather tidal current measurements in a swale of the saw-tooth bar (rip and ridge) morphology.....	187
75b.	Fair-weather tidal current measurements on a crest of saw-tooth bar (rip and ridge) morphology.....	188
76.	Rip channel response to 1973 and 1982/83 storm events	190
77.	Interaction between longshore flows and a standing edge wave oscillation.....	196
78.	Surficial grain size statistics of the rip and ridge morphology.....	199
79.	Vertical variation in mean grain size across the rip and ridge morphology.....	201
80.	Vertical variation in sediment sorting across the rip and ridge morphology.....	201
81.	Vertical variation in sediment distribution skewness across the rip and ridge morphology.....	202
82.	Vertical variation in kurtosis of sediments across the rip and ridge morphology.....	202
83.	Vertical variation in wt.-% distribution of fine sand fraction across the rip and ridge morphology....	203
84.	Vertical variation in wt.-% distribution of very fine sand fraction across the rip and ridge morphology....	203
85.	Vertical sequence of sedimentary structures on the rip and ridge morphology.....	204
86.	Typical fair-weather tidal current pattern on the smoothly sloping upper shoreface transitional zone...	206
87a	Vertical variation in mean grain size on the smoothly sloping upper shoreface transitional zone.....	208
87b.	Vertical variation in sediment sorting on the smoothly sloping upper shoreface transitional zone...	208
87c.	Vertical variation in sediment distribution skewness on the smoothly sloping upper shoreface transitional zone.....	208
87d.	Vertical variation in sediment distribution kurtosis on the smoothly sloping upper shoreface transitional zone.....	208
88a.	Vertical variation in wt.-% of very fine sand on the smoothly sloping upper shoreface transitional zone...	209
88b.	Vertical variation in wt.-% of fine sand on the smoothly sloping upper shoreface transitional zone...	209

88c.	Vertical variation in wt.-% of medium-coarse sand on the smoothly sloping upper shoreface transitional zone.....	209
89.	Regression trends of cross-shore and alongshore upper shoreface grain size statistics.....	210
90.	Sediment size distribution in the German Bight (modified from DHI, 1981).....	214
91.	Principles of flow diversion (DISEC) model.....	218
92.	Heavy metal distribution pattern as a response to flow diversion (modified from HALL et al., 1987)....	220
93.	Ebb-delta retreat-path model of shoreface ridge genesis (from McBRIDE and MOSLOW, 1991).....	222
94.	Variation in peak flow velocities (at 100 cm above bottom) with distance within the ridge morphology....	225
95.	Cross-sectional profiles of the shoreface bathymetry.	227
96.	Spatial pattern of shoreface-connected ridge trough axes.....	229
97.	Headward erosion of Frisian barrier island shoreface-connected ridge troughs.....	230
98.	Temporal variations in shoreface-connected ridge trough axis trend at different locations.....	232
99.	Temporal variations in absolute magnitudes of shoreface-connected ridge trough axis translation....	233
100.	Shoreface-connected ridge trough axis translation at the eastern sector in response to 1967 and 1984 storm events.....	234
101a.	Frequency % of dynamic pattern of shoreface-connected ridge trough axes.....	235
101b.	Shoreface-connected ridge trough axis mean translation rate and % variation from the mean.....	235
102.	Relative rates of shoreface-connected ridge trough axis translation at their eastern and western sectors	236
103a.	Cross-shore variation in sediment budget of the inner shoreface ridge morphology.....	237
103b.	Longitudinal variation in sediment budget of the inner trough of the shoreface ridge morphology.....	238

104.	Temporal cross-shore variation in mean surficial grain size of the shoreface ridge morphology.....	240
105.	Temporal cross-shore variation in sorting of shoreface ridge surficial sediments.....	240
106.	Temporal cross-shore variation in skewness of grain size distribution of shoreface ridge surficial sediments.....	242
107.	Temporal cross-shore variation in kurtosis of shoreface ridge surficial sediments.....	242
108.	Bivariate plot of mean grain size versus sorting of shoreface ridge surficial sediments.....	244
109.	Bivariate plot of mean grain size versus skewness of shoreface ridge surficial sediments.....	245
110.	Bivariate plot of mean grain size versus kurtosis of shoreface ridge surficial sediments.....	245
111.	Bivariate plot of sorting versus skewness of shoreface ridge surficial sediments.....	246
112.	Bivariate plot of sorting versus kurtosis of shoreface ridge surficial sediments.....	246
113.	Bivariate plot of skewness versus kurtosis of shoreface surficial sediments.....	247
114a.	C-M pattern of shoreface ridge surficial sediments...	248
114b.	Frequency % of transportational modes reflected in the respective shoreface ridge morphozones.....	248
114c.	Frequency % of the different ridge morphozone sediments associated with a given transportational mode.....	248
115.	Progressive cross-shore size-sorting of shoreface ridge surficial sediments.....	250
116.	Longitudinal grain size statistics variation of surficial shoreface ridge crest and trough sediments.	252
117.	Vertical variation in mean grain size of the shoreface ridge sediments.....	254
118.	Vertical variation in sorting of the shoreface ridge sediments.....	256
119.	Vertical variation in skewness of the shoreface ridge sediments.....	257

120.	Vertical variation in kurtosis of the shoreface ridge sediments.....	258
121.	Bivariate plots of mean grain size versus sorting for the coarser and finer lithologic units of the inner and outer shoreface ridges.....	259
122.	Vertical variation in wt-% of very fine sand of the shoreface ridge sediments.....	260
123.	Vertical variation in wt-% of fine sand of the shoreface ridge sediments.....	260
124.	Vertical variation in wt-% of medium-coarse sand of the shoreface ridge sediments.....	261
125.	Vertical sequence of shoreface sedimentary structures.....	263
126.	Temporal variability in surficial sequence of shoreface sedimentary structures.....	264
127.	Development and dynamic sequence of the Frisian barrier island shoreface-connected ridges.....	274
128.	Cross-shore variation in grain size statistical parameters of lower shoreface sediments.....	280
129.	Alongshore variation in grain size statistical parameters of lower shoreface sediments.....	281
130.	Regression trend of cross-shore and alongshore lower shoreface grain size statistical parameters....	282
131.	Transgressive shoreface stratigraphic sequence.....	284
132.	Regressive shoreface stratigraphic sequence.....	287

## LIST OF PLATES

	Page
1a. Massive medium to pebbly sand inner trough facies.....	270
b. Swaley (hummocky?) bedded fine-medium sand outer shoreface trough facies.....	270
c. Shelly-rich medium- to coarse-grained inner landward flank facies.....	271
d. Gently dipping fine sand seaward flank facies.....	271
e. Low angle cross-stratified fine- to medium-grained crest facies.....	272
f. Completely bioturbated fine sand lower shoreface facies.....	272

## LIST OF APPENDICES

	Page
A. Sediment sample position and principal grain size statistics.....	332
B-1. Data on tidal variation in current velocities and direction as well as boundary-layer hydraulic parameters at some stations.....	346
B-2. Panels of RUBIN and McCULLOCH's (1980) bedform stability diagram.....	349
B-3. Sediment transport threshold as a function of shear velocity (after OPEN UNIVERSITY, 1989).....	351
C-1. Areal distribution in skewness of shoreface sediments.....	352
C-2. Cross-shore temporal variation in mean grain size of shoreface ridge surficial sediments.....	353
C-3. Cross-shore temporal variation in sorting of shoreface ridge surficial sediments.....	353
C-4. Cross-shore temporal variation in skewness of shoreface ridge surficial sediments.....	354
C-5. Cross-shore temporal variation in kurtosis of shoreface ridge surficial sediments.....	354
C-6. Alongshore variation in central shoreface surficial grain size statistical parameters.....	355
D-1. Shoreface distribution of wt.-% of 1.5-2 phi sand fraction.....	356
D-2. Shoreface distribution of wt.-% of 2-2.5 phi sand fraction.....	357
D-3. Shoreface distribution of wt.-% of 3-3.5 phi sand fraction.....	358
D-4. Shoreface distribution of wt.-% of 2.5-2.75 phi sand fraction.....	359
D-5. Shoreface distribution of wt.-% of 2-2.5 cm/s sand fraction.....	360

D-6.	Shoreface distribution of wt.-% of 1.5-2 cm/s sand fraction.....	361
D-7.	Shoreface distribution of wt.-% of 1-1.5 cm/s sand fraction.....	362
E-1.	Shoreface distribution of the sorting of Component A (suspension population).....	363
E-2.	Shoreface distribution of the sorting of Component B (saltation population).....	364
E-3.	Shoreface distribution of the phi fine-truncation point (suspension-saltation transition).....	365
E-4.	Shoreface distribution of the phi coarse-truncation point (saltation-traction transition).....	366
F.	Dynamic patterns of rip channels in relation to 1962 and 1965/67 storm events.....	367
G-1.	Sequence of shoreface surficial sedimentary structures: October, 1988.....	368
G-2.	Sequence of shoreface surficial sedimentary structures: May/June 1989.....	369
G-3.	Sequence of shoreface surficial sedimentary structures: October, 1989.....	370



## CHAPTER 1

### INTRODUCTION

#### 1.1 Barrier Island System

##### 1.1.1 Definition and Constitution

The term barrier island designates, in a modern sense, a constructive, subaerial, coast-parallel clastic deposit permanently or periodically detached from a mainland coast by a body of water with a linkage to an open sea. The afore-stated implies that, as a geomorphic entity, a barrier island does not exist in isolation. Indeed, OERTEL (1985) considers a barrier island to be just one of six genetically-related elements collectively defined as a barrier island system (Fig.1).

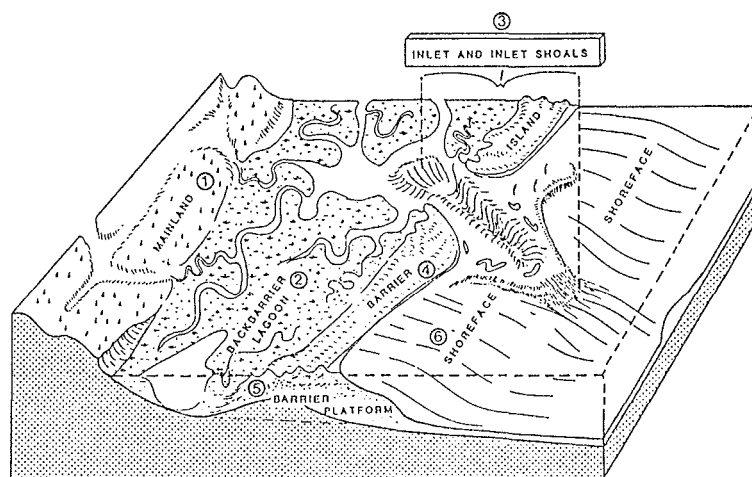


Fig. 1. Elements of a barrier island system (after OERTEL, 1985).

Although the shoreface element is the primary focus of this thesis, the complex interaction between all the elements of a barrier island system precludes a purely holistic approach. This view-point is quite evident in a number of reports

(e.g., FITZGERALD, 1988; OERTEL, 1977, 1988; LIU and ZARILLO, 1990; McBRIDE and MOSLOW, 1991) and is further corroborated by the many findings of this study.

However, in terms of direct and active fluid energy transfer and sediment transport, three interactive groups of processes and subsystems of a barrier island system are conceivable, namely, (a) barrier island - shoreface; (b) back-barrier - mainland; and (c) inlet - delta. The characteristics of the entire barrier island system and of its individual elements in any given coastal setting would depend appreciably on the relative roles of the above subsystems.

As a resource (residential, recreation etc.), the barrier element ranks topmost of all the constituting elements of the system. Given the fact that the existence of a barrier is an inevitable pre-requisite to defining a barrier island system as a whole (OERTEL, 1985), it is indeed appropriate to devote much of the subsequent discussion in this chapter to this feature.

#### 1.1.2. General Characteristics

Modern-day barrier islands are predominantly sandy. Although physically rather fragile, their widespread occurrence nevertheless renders them an immense economic and ecologic importance. The above attributes, coupled with the enigma of their evolution, underlie the century-long scientific investigations and increasing public interest on the fate and future of barrier islands world-wide.

A general overview relating to the spatial distribution, size, shape and stratigraphic characteristics of barrier islands is presented here. Some of the variations evident in the above characteristics, in addition to the diversity of thoughts on their development detailed in Section 1.1.3, clearly demonstrate the need for intensive and coordinated

geological investigations of the individual elements of a barrier island system.

The aforementioned thus defines one of the long-term objectives of the Marine Science Division of the Senckenberg Institute in Wilhelmshaven.

#### 1.1.2.1 Spatial distribution

The distribution of barrier-island coasts on a global context as shown in Fig. 2 has been discussed by LEONT'YEV and NIKIFOROV (1965), BERRYHILL et al. (1969) and CROMWELL (1971). Briefly, their data reveals:

- (a) occurrence of barrier morphology along 9-13% of the world's coastline;
- (b) > 30% of the global barrier island coast length are along the North American continent; and
- (c) > 10% of all continental coastlines, excepting Europe (5%), are constituted of barrier island morphology.

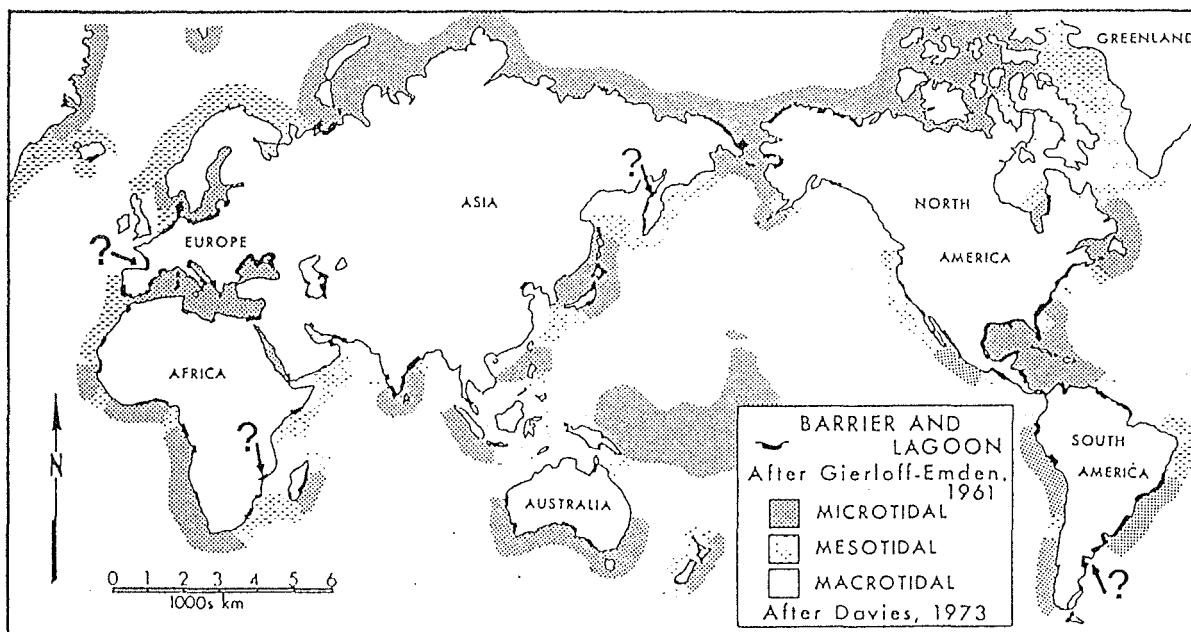


Fig. 2. Global distribution of barrier island morphology (from HAYES, 1979; modified after GIERLOFF-EMDEN, 1961).

The above distribution patterns of barriers can be related to the geographic variability in the tectonic setting and hydrodynamic characteristics of the world's coastline. GLAESER (1978), employing the tectonic continental margin classification scheme of INMAN and NORDSTROM (1971), showed that:

- (a) about 50% of global occurrences of barrier islands are associated with a trailing edge margin physiography, with subequal proportions on the collision and marginal sea counterparts; and
- (b) abundant sediment supply must complement the wide, gentle gradient characteristics of a trailing edge margin, without which barriers do not develop.

In relation to the hydrodynamic conditions, there is a consensus of opinion that barrier islands are rare along coasts of high tidal energy (GIERLOFF-EMDEN, 1961) or range (HAYES, 1975, 1979). GLAESER (1978) estimates that only about 10% of the world's barrier island systems are associated with coasts having tidal range exceeding 3 m.

#### 1.1.2.2 Size

The variability in size of barrier islands and associated inlets in modern environments is a consequence of natural factors related to their geologic setting, hydrodynamic conditions as well as human activities. Generally, island length-width ratios greater than 10 are considered typical (BERRYHILL et al., 1968). The above size ratio is an exception rather than the rule for the Frisian barrier islands (southern North Sea; see Fig. 5 for location).

The morphometrics of the Frisian barrier islands, some of which are given in (Fig. 3), can be summarized as follows :

- (a) Excepting the island length, no progressive coastwise change in width of islands and flanking inlets is apparent.

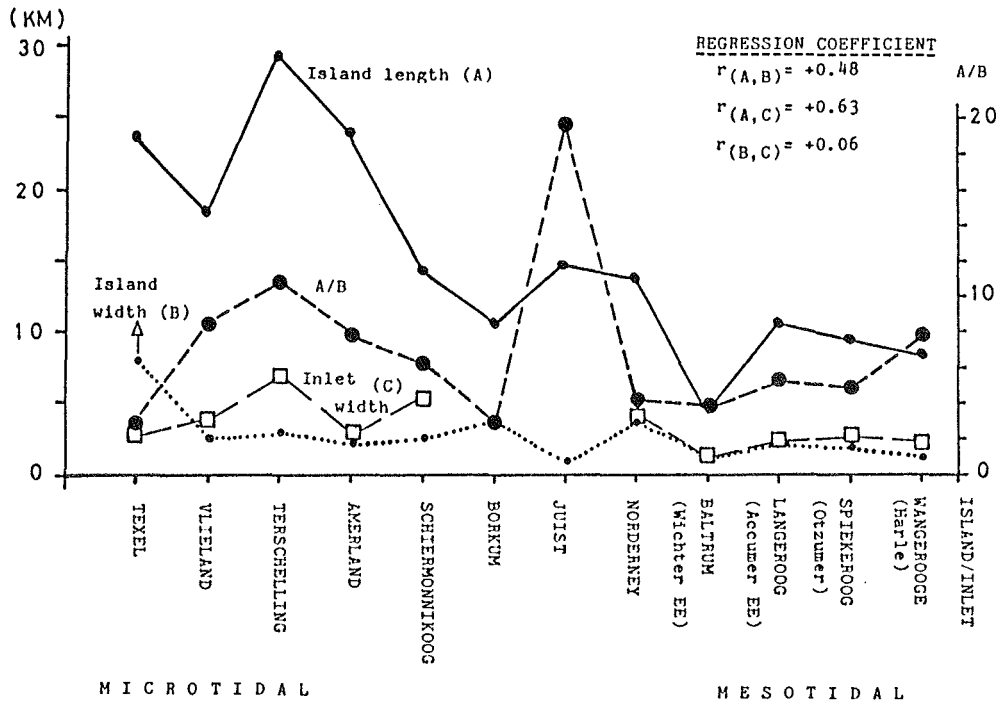


Fig. 3. Morphometrics of Frisian barrier islands and inlets.

- (b) With the exception of Terschelling and Juist, all the islands show length-width ratio considerably lower than 10.
- (c) The microtidal (mean tidal range < 2 m ; DAVIES, 1964) barrier islands show 1.5-2 order of magnitude larger island length and width, as well as inlet width than their mesotidal (2-4 m mean tidal range) counterpart.

In contrast to the above inconsistencies in the Frisian barrier island morphometrics, published data on their inlet change over a 100-470 year time-interval show that they have deepened at a comparable rate (6-10 cm/yr). Lateral inlet migration has, in many cases, been constrained by engineering structures typically at their eastern margins. The maximum easterly "lateral migration" of the East Frisian inlets of about 4 km over the time interval 1650-1960 is a consequence of 13-60% reduction in their tidal prism, which FITZGERALD et al. (1984) attribute to mainland dyking and back-barrier filling.

Considering the generally noted relationship between barrier morphology and tidal regime (HAYES, 1975, 1979), some of the variation in size characteristics of the southern North Sea barrier islands given above (e.g., mean island width and mean island length-width ratio) are inconsistent with a progressively eastward increasing mean tidal range. In some respects, the inconsistencies demonstrate the impact of human interference.

#### 1.1.2.3 Shape

Barrier islands are characterized in plan view by smoothed seaward and irregular back-barrier shorelines. This is suggestive of more intense energy and sediment transport processes acting along the seaward margin. In cross-section, lenticular and convex upward profiles are typical (DICKINSON et al., 1972).

Barrier island shapes, like the size, have commonly been attributed to the tidal range (HAYES, 1975, 1979). Barrier islands on microtidal coasts are long, linear and narrow in shape, whereas those on mesotidal coasts are short and wide with pronounced bulges at their updrift ends. However, DAVIS and HAYES (1984) have reported several exceptions to the above and concluded that the above model is most applicable to intermediate wave-energy coasts of a trailing edge continental margin.

FITZGERALD et al. (1984) relate shapes of barrier islands on mixed-energy coasts, such as those in the German Bight, to the varied position of swash bar welding on the down-drift inlet shoreline. Other existing literature suggest the dependence of barrier island shape to the often interrelated factors of tidal prism, sediment supply and the antecedent topography (DAVIS and HAYES, 1984; BELKNAP AND KRAFT, 1985; DEMAREST and LEATHERMAN, 1985; SUTER and PENLAND, 1987).

#### 1.1.2.4 Stratigraphy

Barrier island deposits are laterally flanked, landward and seaward, by a much finer-grained backbarrier/ lagoon (or bay) and offshore marine facies respectively. The vertical stratigraphic succession is primarily determined by the relative sea-level change and rate of sediment supply. Depending on the interplay between both factors, barrier island deposits may exhibit either a transgressive, regressive or a composite transgressive-regressive sequence. The precise recognition of a barrier island sequence in the stratigraphic record is critical to assessing their genesis. Some of the inherent problems in this regard indicated by HINE and SNYDER (1985) relate to the paucity and quality of subsurface data, and to uncertainties in barrier island response to changing rates of sea-level rise or fall as well as sand transport mechanisms and pathways.

#### 1.1.3 Development

Despite recent advances in marine instrumentation and observational methods, which afford greater knowledge of processes contributing to the origin of many coastal features, the precise genesis of barrier islands still remains elusive. Various hypotheses of barrier island origin, discussed and debated in the literature, are outlined in Table 1 (after JONES 1977; in FISHER, 1982). It is conceivable that barrier islands are classic examples of the principle equifinality, implying that they may have been formed by quite different processes and under different conditions. Applicable hypotheses for the southern North Sea barriers are considered in Section 3.2.

TABLE 1. Postulates on barrier island origin  
(after JONES, 1977).

HYPOTHESIS	MAJOR PROPONENT	COASTAL REGION	PRIMARY MECHANISM	SEDIMENT SOURCE
EMERGENT BAR	DeBeaumont (1845)	Northern Europe	Bar emergence/ onshore sedi- ment movement	Seaward of brea- ker zone
SHORELINE SPIT	Gilbert (1890)	Utah & Michigan Lakes	Longshore drift causing spit extension	Cliff erosion/ fluvial updrift
EMERGENT OFFSHORE BAR	Johnson (1919)	Atlantic	Shoreline emergence; onshore sedi- ment movement	Offshore
SUBMERGENT BAR	Shephard (1960)	Gulf Coast	Submerging shoreline	Offshore & fluvial
RIDGE EMBAYMENT	McIntire & Morgan (1963)	Massachu- setts	Holocene transgression/ longshore drift	Pleisto- cene/up- drift sediments
RIDGE EMBAYMENT	Hoyt (1967, 1968)	Georgia	Holocene transgression	Pleisto- cene sed- iments
COMPLEX SPIT	Fisher (1968)	Middle Atlantic	Longshore drift/wave refraction	Updrift sediments
EMERGENT SHOAL	Otvos (1970)	Gulf of Mexico	Shoal emergence/ longshore drift	Updrift sediments
RIDGE EMBAYMENT/ SPIT GENE- RATION	Pierces & Colquhoun (1970)	North Carolina	Holocene transgression or spit development	Pleisto- cene sed- iments
COMPLEX SPIT/DUNAL MIGRATION	Jones (1977)	Massachu- setts	Longshore drift/ high energy storm conditions	Updrift/ offshore sediments

## CHAPTER 2

### BARRIER ISLAND SHOREFACE

#### 2.1 Physical Boundaries

Within the context of a barrier island system comparable to that described by OERTEL (1985), SWIFT (1975a) considers the shoreface to be the most significant geomorphic element, determining both the existence and geometry as well as the behaviour of other elements.

However, the shoreface and its subdivisions are variously defined in the literature; for instance, based on one or more of the following criteria: morphology (NIEDORODA et al., 1984; NUMMEDAL and SNEDDEN, 1987); hydrodynamics (ELLIOT, 1978; NIEDORODA et al., 1984; OERTEL, 1985); and function (WRIGHT, 1987).

In view of the dynamic nature of the shoreface environment, all of the above criteria are inevitably subjective with respect to its physical boundaries and its subdivisions. For the purpose of consistency with earlier reports (reviewed in Section 2.2), the shoreface is initially viewed in two ways:

(a) as a transitional physiographic zone through which sediment is exchanged and fluid energy is transferred between the shelf and the shoreline; and

(b) following from the above, a relatively steeper, higher energy wave-dominated upper shoreface province extending shoreward of the 7 m isobath is distinguished from a gentler, less energetic lower shoreface province seaward of the above depth.

## 2.2 Previous Studies

The shoreface as designated above, and within the framework of the current study objectives (Section 2.3.1), has been investigated in the past mostly from geologic-geomorphologic, physical oceanographic and coastal engineering perspectives. It is therefore convenient to evaluate the relevant reports under three interrelated aspects: hydrodynamics, morphodynamics and sedimentology, and each presented under two categories - upper and lower shoreface.

Despite the generally recognized natural cross-shore variability in hydrodynamics, morphodynamics and sedimentology of coastal marine environments, synthesizing studies focussing on both shoreface provinces are surprisingly rare.

### 2.2.1 Hydrodynamics

Due to reasons of proximity, and the pressing and practical problems of coastal sediment transport, beach erosion and nearshore pollution as well as coastal engineering constructions, most studies deal with the hydrodynamics of the shoreline and the surf zone. Examples of principal hydrodynamic studies (theoretical, laboratory, and field) within the upper shoreface central to the understanding of the above cited coastal problems are:

- (a) behaviour and controlling factors of incident wave characteristics across the surf zone (e.g., GALVIN, 1968; BALSILLIE, 1983; THORNTON and GUZA, 1983);
- (b) wave-induced longshore current transport: theory and generating mechanisms (reviewed by GALVIN, 1967; LONGUET-HIGGINS, 1972); cross-shore variations and the role of breaker types (GUZA and THORNTON 1978; BEREK and DEAN, 1982; BODGE and DEAN, 1987);
- (c) genesis and nature of seaward flows such as undertow (DHYR-NIELSEN and SORENSEN, 1970; SVENDSON, 1984; DALLY, 1987;

SVENDSON et al., 1987) and rip currents (BOWEN, 1969; BOWEN and INMAN, 1969; DALYRYMPLE, 1975; DALYRYMPLE and LOZANO, 1978; SHORT, 1985; TALBOT and BATE, 1987; BOWMAN et al., 1988a, b); (d) excitation and structure of low frequency oscillations in shallow water (URSELL, 1952; GREENSPAN, 1956; GUZA and DAVIS, 1974; SUHAYDA, 1974; HUNTLEY, 1976; HUNTLEY and BOWEN, 1973, 1975; HUNTLEY et al., 1981; HOLMAN, 1981; SYMONDS et al., 1982; THORNTON and GUZA, 1982; YIH, 1984; and EVANS, 1988).

Although the fluid motions diminish in intensity from the upper to lower shoreface, the hydrodynamic regime of the latter is no less complex. Moreover, while normal day-to-day hydrodynamic conditions are in most cases effective in causing perceptible physical changes on the upper shoreface, processes of sedimentological and morphological significance on the lower shoreface are, on the other hand, generally less frequent. Equally limited are direct observations of these processes, being highly energetic (or stormy) in nature.

It is therefore no surprise that, due to the different indirect evidences provided by various researchers, opinions on the processes and patterns of fluid motion during storms are diversified. However, because of the variability in environmental settings and the multiplicity of physical processes on which the lower shoreface and the adjoining inner shelf hydrodynamic regimes depend, extrapolation of results of direct observations (e.g., MURRAY, 1970; GIENAPP, 1973; CSANADY, 1976; SCOTT and CSANADY, 1976; LAVELLE et al., 1978a, b; SCHWING et al., 1983; FORRISTALL et al., 1977; CACCHIONE et al., 1987; LYNE et al., 1990a, b) requires caution.

As will be shown below, and as also exemplified by WRIGHT et al., 1991, a number of flow patterns have been suggested as characteristic of storm events; however, the vertical and horizontal structure, net direction (onshore, offshore or alongshore) as well as the relative sedimentological and morphological importance of such flows on both shoreface provinces are often controversial. Until more numerous,

synoptic storm flow and in-situ sediment motion records become available, these controversies will persist.

One or more of the following fluid motion types and flow mechanisms may be significant during storm events across a shoreface-shelf environment:

- (a) wind stress-induced flow (e.g., LUDWICK, 1978; MORTON, 1979);
- (b) bottom compensatory current of surface wind drift (e.g., BAINES and KNAPP, 1965; MORTON, 1981);
- (c) coastal storm surge and associated overwash (e.g., HAYES, 1967; LEATHERMAN, 1976; ORFORD and CARTER, 1984)
- (d) pressure gradient bottom currents (upwelling and downwelling) associated with set-up and set-down of mean sea-level (e.g., NIEDORODA, et al., 1984);
- (e) edge waves (e.g., DOLAN et al., 1979; MIDDLETON et al., 1987; EVANS, 1988);
- (f) rip currents (COOK, 1970; COOK and GORSLINE, 1972);
- (g) ebb storm-surge density flows (HAYES, 1967; HAMBLIN et al., 1979);
- (h) ebb storm-surge turbulent flows (e.g., GADOW and REINECK, 1969; REINECK and SINGH, 1972; AIGNER and REINECK, 1982);
- (i) wave bottom currents (MADSEN, 1976; KOMAR et al., 1971);
- (j) wave-group-induced net seaward bottom drift (KOMAR et al., 1972; SHI and LARSEN, 1984);
- (k) geostrophic flows (SWIFT, 1976; SWIFT et al., 1986; NIEDORODA, 1985; SNEDDEN, 1985; SNEDDEN et al., 1988);
- (l) other transient complex flow patterns (e.g., helical) that may result from the interaction between the above-mentioned as well as with tidal currents, wave-generated surf zone currents, and bottom topography.

### 2.2.2 Morphodynamics

Morphological changes on the shoreface are primarily a consequence of the hydrodynamic processes. Although a tendency

towards an equilibrium state is favoured, the time scale for the latter may be either short (daily to annual), intermediate (annual to decade) or long-range (decade to century). Furthermore, modes of morphological changes may be simple or complex, periodic or aperiodic.

### Upper shoreface

The earliest efforts aimed at determining morphological changes on the upper shoreface were on beaches. A review of pioneering studies is contained in KING (1959). As demonstrated by the summer and winter beach profile nomenclature of SHEPARD (1950), early notion of beach changes was seasonal and simple. The latter nomenclature has been successively modified with increasing generability to swell and storm profiles (KOMAR, 1976), barred and non-barréd (GREENWOOD and DAVIDSON-ARNOTT, 1979) and, ultimately, to WRIGHT and SHORT's (1983) six-fold sequence of beach states (Fig. 4). SHEPARD's study is, however, foremost in a process-response approach to beach dynamic investigations in nature.

The above approach has led, within the last three decades, to numerous laboratory and field-based descriptive and semi-quantitative sequential models of beach and surf zone profile changes. These changes are usually viewed as a response to variations of a single or multiple hydrodynamic parameters and characteristics (slope and sediment size) of the beach/surf zone (e.g., SONU and VAN BEEK, 1971; DEAN, 1973; SONU, 1973; GUZA and INMAN, 1975; SUNAMURA and HORIKAWA, 1974; CHAPPELL and ELLIOT et al. 1979, SHORT, 1978, 1979, 1980; GOLDSMITH et al. 1982; WRIGHT et al., 1979; WRIGHT and SHORT, 1983; and ANTIA, 1987a).

In contrast to the above studies primarily outlining the transformation of beach and surf zone profile configuration, recent research on the upper shoreface has centered on the origin of variously scaled ( $10$ - $10^5$  m), but regularly spaced,

longshore rhythmic morphologies. These have been observed along and shoreward of the shoreline (KOMAR, 1971; GUZA and INMAN, 1975; INMAN and GUZA, 1982; ORFORD and CARTER, 1984; DOLAN et al., 1979; HAYDEN et al. 1979; DOLAN and HAYDEN, 1983; ANTIA, 1987b, 1990a,) within the surf zone (CLOS-ARCEDEC, 1962; BOWEN and INMAN, 1971, 1972; SONU, 1972; HUNTLEY, 1980), and seaward of the surf zone (REINECK, 1963; FLEMMING and ANTIA, 1989, 1990).

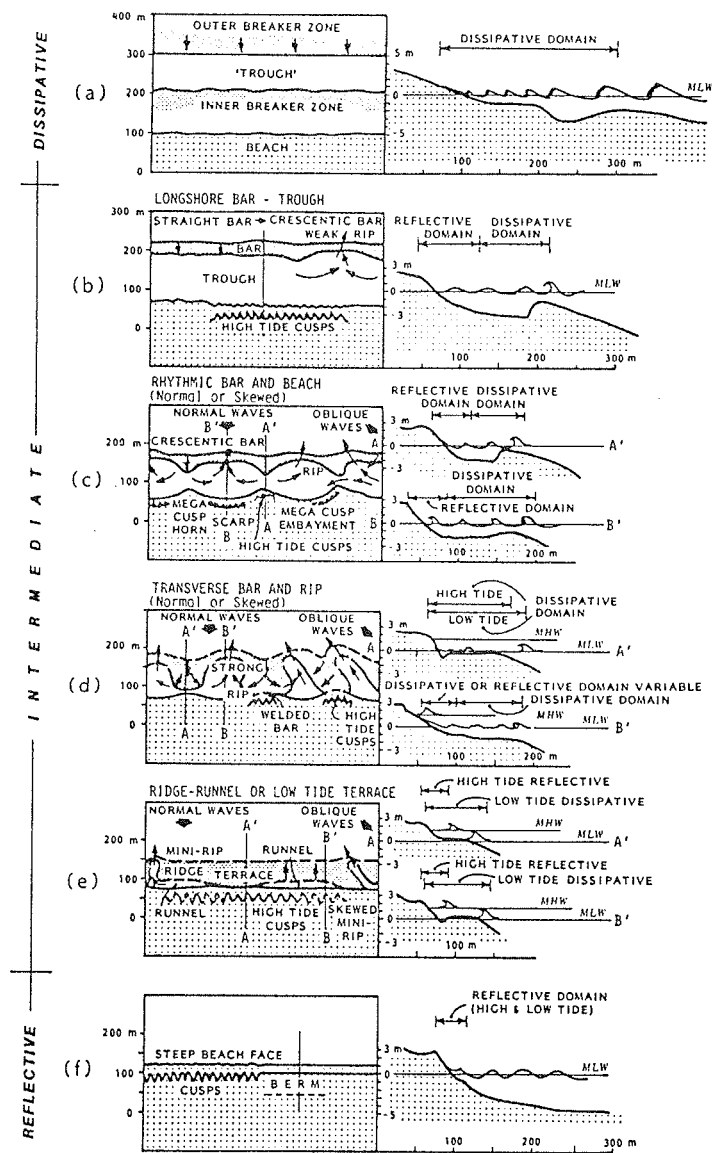


Fig. 4. Morphodynamic beach-state classification (after WRIGHT and SHORT, 1983).

## Lower shoreface

The morphologic features on the lower shoreface differ from their upper shoreface counterpart in that, under the present-day hydrodynamic conditions, their life span is considerably longer. Accordingly, their preservation potential in the stratigraphic record should be correspondingly higher.

Two large scale but genetically different ridge morphologies characterize many lower shoreface and shelf regions. For the sake of simplicity, these are referred to as tidal- and transient flow-formed ridges. The latter may be isolated or connected to the shoreface.

Whereas the development and dynamics of tidal ridges are unequivocally attributed to tidal currents (OFF, 1963; HOUBOLT, 1968; CASTON, 1972; SWIFT, 1975b; BELDERSON et al., 1982; CHIANG-SHU and JIA-SONG, 1988; DAVIS and BALSAN, 1990), most studies to-date (e.g., DUANE et al., 1972; SWIFT et al., 1972a, b, 1973, 1978, 1986; STAHL et al., 1974; STUBBLEFIELD et al., 1976; STUBBLEFIELD and SWIFT, 1981; SWIFT and FIELD, 1981; PARKER et al., 1982) associate the transient flow-formed, shore-oblique counterpart with storm events. It is, however, not clear to what extent both tides and transient storm currents may contribute to the development and dynamics of ridges along the mixed-energy Frisian coast, where both flows are, either independently or in conjunction with wave activity, sufficiently intense to frequently mobilize and transport shoreface bottom sediments.

In contrast to the latter set of studies, BOCZAR-KARAKIEWICZ and BONA (1986) and BOCZAR-KARAKIEWICZ et al. (1990) consider storm flow or prevailing sediment transport direction to be non-critical to the origin of non-tidal shoreface ridges, but may be modified by these. The authors propose progressive infragravity waves as a generating mechanism of shoreface ridges.

No existing model unequivocally explains the evolution, nature and maintenance of shoreface ridges. SWIFT (1975a) considers such knowledge to be critical to understanding the Holocene history of sea level change, barrier island evolution, and sediment transport pathways under present-day hydraulic conditions on the shoreface and shelf environments. The potential difficulties in distinguishing between tidal and non-tidal ridges in the rock record expressed by JOHNSON (1978) have been satisfactorily addressed by BELDERSON (1986).

### 2.2.3 Sedimentology

The sedimentary response to hydrodynamic processes, as in the case of morphology, is highly variable both within the upper shoreface province (e.g., KLEIN, 1970; CLIFTON et al., 1971; WUNDERLICH, 1972; DAVIDSON-ARNOTT and GREENWOOD, 1976; JAGO and HARDISTY, 1984; SHORT, 1984; GREENWOOD and MITTLER, 1985; and GREENWOOD and SHERMAN, 1986) and the lower shoreface counterpart (e.g., REINECK, 1963; REINECK and SINGH, 1972; CHOWDHURI and REINECK, 1978; HOWARD and REINECK, 1972, 1981; AIGNER and REINECK, 1982; and SHIPP, 1984).

The dissimilarities evident in these studies are attributable to the disparities in the relative roles of the hydrodynamic processes (viewed in terms of their pattern, intensity and frequency) as well as in sediment textures and bathymetric characteristics. With the exception of AIGNER and REINECK (1982), studies providing detailed information on the temporal variability in the sedimentary sequence across both the upper and lower shoreface regions are rare. Such information is basic to accurate modelling of the shoreface facies and flow dynamics most essential in rock-record reconstruction.

## 2.3 Present Study

### 2.3.1 Objectives

The overall objective of the present study is to identify and evaluate temporal and spatial variations in morphological and sedimentological responses of a modern-day barrier island shoreface to the observed and inferrable hydrodynamic regime. This is with a view to improved understanding of coastal marine sediment transport processes and facies patterns, these being central to a broad spectrum of coastal scientific and engineering tasks.

Within this framework, the data acquired from the Spiekeroog shoreface (Chapter 4) are specifically directed at:

- (a) determining the scale and structure of the flow regime;
- (b) describing grain-size distribution patterns;
- (c) deciphering sediment transport trends and pathways;
- (d) developing models of sea-floor moulding and morphodynamics;
- (e) defining the facies association; and
- (f) detailing the distinctive characteristics of transgressive and regressive shoreface stratigraphic sequences.

### 2.3.2. Organization

Whereas Chapter 1 provides some overview of the subject matter, the objectives of the current study are, in the light of literature review on shoreface hydrodynamics, morphodynamics and sedimentology, detailed in Chapter 2. Following a description of the environmental setting of the study area in Chapter 3, the data set employed in this report are presented along with brief comments and a critique of field logistics, laboratory techniques and analytical procedures in Chapter 4.

Sediment textural patterns and a sediment budget of the shoreface as a whole are discussed in Chapter 5. Characterization of the shoreface subenvironments, based on their morphology, dynamic behaviour, facies associations and hydrodynamic regime, and ultimately, constructing conceptual transgressive and regressive stratigraphic sequences of the shoreface, are dealt with in Chapter 6. Finally, a general summary of the results of the study outlining some of their geological applications and engineering implications is the subject of Chapter 7.

## CHAPTER 3

### SPIEKEROOG BARRIER ISLAND

#### 3.1 Location

Spiekerog Island is situated at the southeastern margin of the epicontinental North Sea basin. It is one of a chain of twelve Frisian barrier islands fringing the southern North Sea coast of The Netherlands and Germany (Fig. 5).

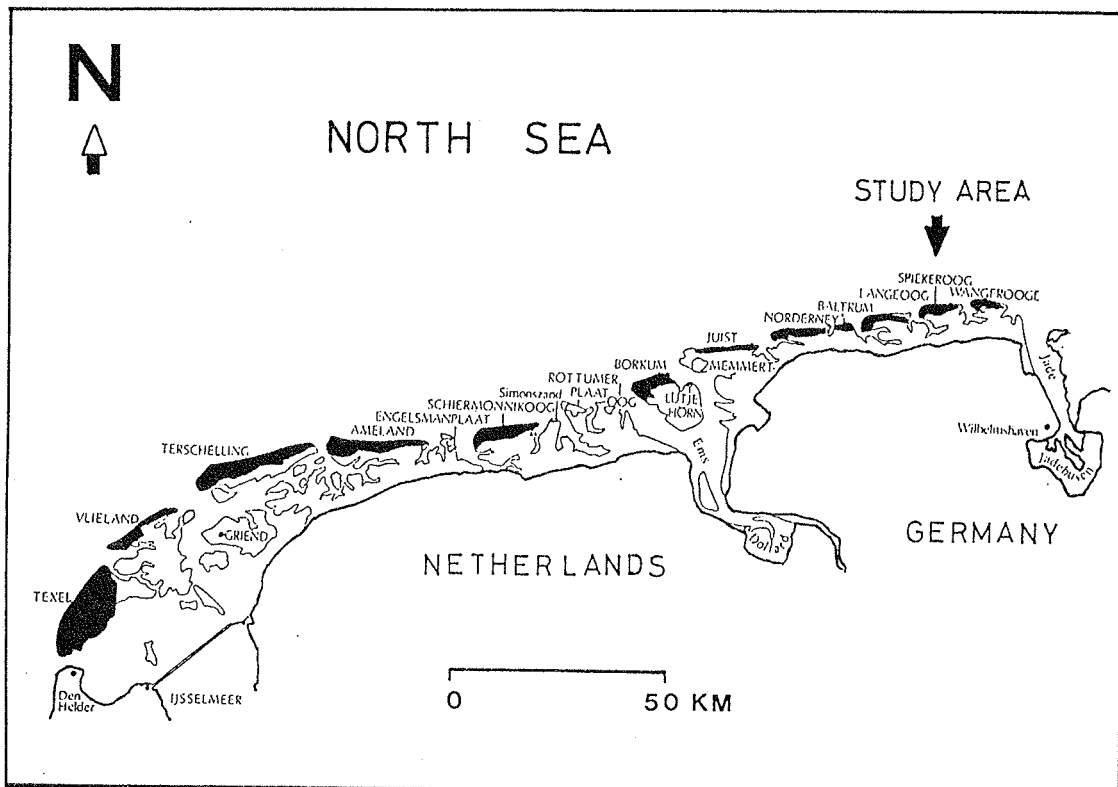


Fig. 5. Location of Spiekerog Island and its Frisian counterparts (modified after POSTMA, 1982).

The shoreface of Spiekerog covers an area of about 110 km<sup>2</sup> and is approximately delineated by latitudes 53° 47.00' and 53° 52.50' N, and longitudes 7° 40.00' and 7° 49.00' E.

### 3.2 Geology

Spiekeroog and its genetically related Frisian barrier islands are late stage products of the Quaternary evolution of the North Sea basin. The present-day physiography of the basin is a response to tectonic activities of varied spatial and temporal scales. This is vividly demonstrated by the variable geology (and age) of its flanking boundaries: Precambrian to the northeast, early Palaeozoic to the northwest, and late Palaeozoic to the south (LÜDERS, 1968).

The history of the geological evolution of the North Sea basin as a structural entity dating back to Permian is well documented by ZIEGLER and LOUWERENS (1979). CASTON (1979) provides a comprehensive summary of its Quaternary sediments. The latter study in particular shows the close correlation between Quaternary sediment deposition and the underlying Mesozoic-Tertiary tectonic features.

The sedimentary succession comprising the North Sea basin is traceable to its history of structural deformation and the alternating climatic episodes during the Quaternary. Although deposits of all geological periods occur in the basin, most of the sea-floor is blanketed by Quaternary sediments. The latter has a maximum thickness of 1 km at the centre of the southern part of the basin and linearly extends north-northwesterly along it over a 750 km distance (CASTON, 1979).

The bulk of the Quaternary sediments in the southern North Sea are Holocene and they represent, to a large extent, reworked Pleistocene deposits. CASTON's report further shows that lower and middle Pleistocene deposits outcrop on the sea-floor or exist at shallow depths predominantly south of the Dogger Bank (55° N latitude).

The Quaternary evolution and the stratigraphic succession of the German Bight are detailed in SINDOWSKI (1970, 1973), STREIF and KÖSTER (1978), BEHRE et al. (1979), LUDWIG et al.

(1981), and STREIF (1989, 1990). These reports are the source of information for the following account.

Besides the marine transgressions (Cromerian, Waalian and Tiglian) of the very early Pleistocene between about 2.5 million years and 400,000 years BP (Before Present), three glacial periods - Elster (330,000 - 400,000 years BP), Saale (125,000 - 310,000 years BP) and Weichsel (10,000 - 115,000 years BP), and two interglacials - Holstein (post-Elster) and Eem (post-Saale) constitute the central events of the Pleistocene coastal development along the German Bight.

Glaciation phases of the early Pleistocene did not extend into the coastal area (STREIF, 1990), whereas their intervening marine transgressive deposits (fine-medium quartz sands), estimated by SINDOWSKI (1973) to attain a total thickness of 20-50 m, are well documented in the East Frisian coastal region. On the contrary, the Elsterian glaciation spread across the entire North Sea basin and considerably beyond the Frisian coast (STREIF and KÖSTER, 1978; STREIF, 1990), depositing on retreat, morainic materials of Scandinavian and British-Scottish origin. During the succeeding Holsteinian interglacial high sea-level stand, the East Frisian coastal region was only marginally transgressed.

The Saalian glaciation incurred into the North Sea basin and inland, but was less extensive as the Elsterian counterpart. PRATJE (cf. LÜDERS 1968) considers the rock zones and the reef grounds of the sea basin to be the end-products of this glaciation. In contrast to the conflicting opinion on the position of the Holsteinian high sea-level stand, the Eemian transgressive deposits (sands enriched in molluscs - Venerupis senescens) are encountered in the East Frisian region at 7 m below the present mean sea level. Furthermore, this transgression advanced parallel to the present coastline trend. The last glacial phase, the Weichsel, did not advance into the East Frisian coastal area, hence its deposits are expectedly absent.

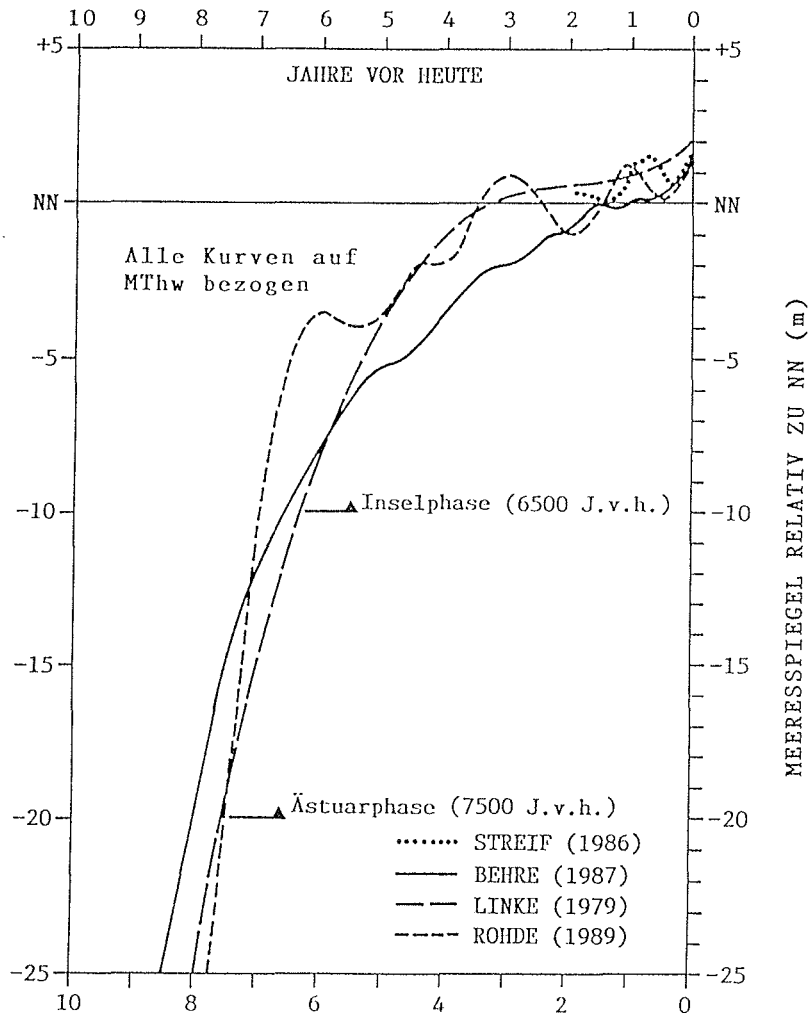


Fig. 6. Holocene sea-level variation curves of the North Sea (from FLEMMING, 1990).

As exemplified in Fig. 6 above, there are divergent views on the course of sea-level change in the North Sea basin since the beginning of the Holocene (10,000 years BP), particularly its late phase, following the Weichselian glaciation. Consensus however exists on a 110-130 m lower sea-level stand in the basin at about 18,000 years BP. Just prior to Holocene, i.e. during the late Weichselian (15,000-10,000 years BP), the North Sea coastline was situated at least 200 km away from its present position. It was in the course of the Holocene transgression that the barrier island system of the North Sea developed.

Although conclusive evidence regarding their origin is lacking, the following findings (e.g., SINDOWSKI, 1973; STREIF, 1990) are illuminating:

(a) Holocene deposits (15-20 m thick) of which barrier islands are constituted lie below chart datum and overlie a high Pleistocene platform (or relief), padded by brackish-water deposits; and

(b) Geochronologic as well as stratigraphic evidences are inconsistent with any variant of a spit-based genesis of the barrier islands (Section 1.1.3). The latter would require dated materials to young downcoast (easterly) and present barrier islands to be underlain by pre-Holocene inlet channel fills.

None of the above is evident along the East Frisian barrier island coast. An onshore-offshore based sediment transport mechanism of Frisian barrier island genesis appears more plausible, particularly in the light of evidences of erosional shoreface retreat (SWIFT et al., 1972b; SWIFT, 1975a).

### 3.3 Geomorphology and Vegetation

The barrier island system of Spiekeroog shows gross geomorphologic similarities with its other Frisian counterparts. Typically, these islands are laterally separated from each other by tidal inlets, and their shorelines show a successive seaward displacement towards the east. Thus, Spiekeroog has its shoreline displaced 2.5 km seaward of Langeoog but 1.3 km landward of Wangerooge.

Spiekeroog is presently about 10 km long and 2 km wide and is separated from the mainland coast by a 7 km wide backbarrier region or Wadden Sea. It is fringed at the sides by two 15-20 m deep and 2 km wide inlets - Otzumer Balje to the west and Harle to the east. The down-drift channel margins of the inlets have repeatedly been stabilized since 1873.

Extending seawards from the inlets by a distance of up to 3 km into water depths of about 6 m are well-developed subaqueous ebb deltas. Both deltas directly overlap half of the island's sea front. Immediately landward of the inlets are large intertidal sandy shoals.

The 20 km<sup>2</sup> surface area of the barrier element of Spiekeroog, consisting of supratidal marshes, dunes and intertidal beaches, can be evenly divided into an old dune core in the west and a younger, eastward extending sand flat. Detailed information on these are contained in EHLERS (1988) and STREIF (1990).

Some comments on dune vegetation are desirable, due to its important role in barrier island stabilization. In general, three generations of dunes can be distinguished: a primary or foredune, a secondary or white dune, and a tertiary dune. Primary dunes are aligned shore-parallel, reach 2-3 m in height and are predominantly vegetated by Agropyron junceum; secondary dunes are 10-20 m high with Ammophila arenaria and Elymus arenarius as principal plant species. The tertiary dunes constitute the western core of the island. They may be grey (principally vegetated by Koeleria albescens, Corynephorus canescentis species etc.) or black (vegetated by Empetrum nigrum and Calluna vulgaris species).

### 3.4 Bathymetry

The shoreface of Spiekeroog extends from a west-east oriented shoreline to a water depth of about 25 m, and is characterized by a succession of bottom morphologies (Fig. 7). As earlier outlined in Section 2.1, the shoreface may be subdivided into an upper and a lower province. The upper shoreface province is 2.5-3.5 km wide and has an average slope of about 1:300 to 1:400. Its morphologic features include:

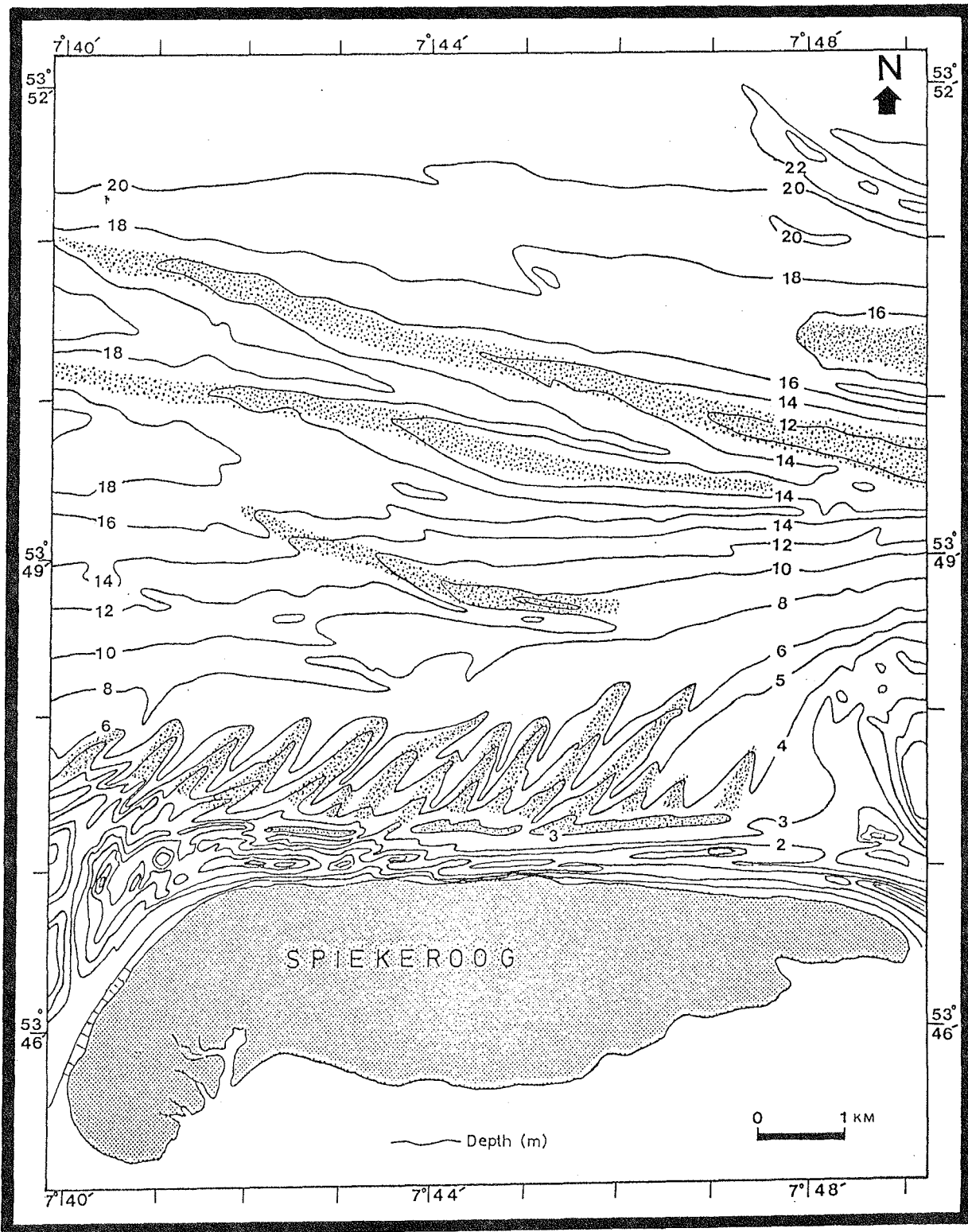


Fig. 7. Bathymetry of the Spiekeroog shoreface.

- (a) above NN-3 m : beach and obliquely attached shoreline bars and an isolated shore-parallel outer bar; these constitute the proximal upper shoreface which is about 800 m wide and has an average slope of 1:200;
- (b) NN-3 m to NN-6 m : NE-SW trending, quasi-rhythmic "saw-tooth bars" (REINECK, 1963), and represents the medial upper-shoreface zone. It is about 1.2 km wide and has an average slope of 1:600;
- (c) NN-6m to NN-8 m : a 400-800 m wide smoothly sloping (1:200 to 1:400) transitional upper shoreface zone; the latter constitutes the linkage with the lower shoreface province.

The lower shoreface province has an average slope of about 1:450 and consists of a 2.5-4 km wide WNW-ESE striking ridge and trough system (shoreface-connected ridges; DUANE et al., 1972) in NN-8 to NN-18 m water depth. It is succeeded seawards by a flat seabed surface representing the lower shoreface-inner shelf transitional zone.

The bathymetric features outlined above are discussed in greater detail with respect to their morphodynamics, sedimentary facies and processes in Chapter 6.

### 3.5 Meteorology

With an annual mean air temperature and precipitation of 9°C and 720 mm respectively at Norderney (50 km west of Spiekeroog) reported by BÄTJE (1986), the climate of the East Frisian Islands can be described as temperate marine. Two extreme weather conditions, summer and winter, characterize an annual meteorological cycle. Typical winter months (November to February) are characterized by cool, sometimes freezing temperatures and higher frequency of SW-NW originating stormy winds. The summer months (May - August), on the other hand, are normally warm (> 17-18°C) and relatively calm.

Winds of Beaufort Force 1 to 9 for the period 1947-1966 have been shown by LUCK (1976) to most frequently originate from the SW quadrant within the study region. These latter winds should significantly contribute to the inlet ebb flows. Analysis of the more stormy wind situation for the same locality as that of LUCK (island of Norderney) contained in the annual reports of the Forschungstelle für Küste for the period 1965-1986 shows as follows:

(a) 85% of wind strength > 10 Beaufort Force are confined to the winter months, 30% of which occurred in the month of November; and

(b) 47% of the above wind strength originate from NW quadrant as against 30%, 19%, and 4% from the W, SW and N quadrants respectively.

### 3.6 Hydrography and Hydrodynamics

A generalized picture of seasonal and spatial variations in the hydrographic parameters of the southern North Sea is provided in summary studies of LEE (1980), POSTMA (1982), and HOLLIGAN et al. (1989). By comparison, observations on shoreface hydrodynamic processes are still sparse; the existing information is supplemented with data acquired in the course of this study.

#### 3.6.1 Temperature - Salinity - Turbidity

The coastal waters of the study area (< 25 m depth) show:

(a) surface summer and winter temperatures of the order of 17-18°C and 3-4°C respectively; vertical temperature gradient within a season or during a tidal cycle is negligible (0.01°C per metre of water column) (Fig. 8a);

(b) surface summer and winter salinity values range between 32-34 ‰ and 30-32 ‰; vertical salinity gradient is

insignificant, being of the order of  $0.001 \text{ ‰}$  per metre of water column (Fig. 8b); and

(c) a variety of reports indicate that near surface waters may be up to 8 order of magnitude more turbid in winter than in summer.

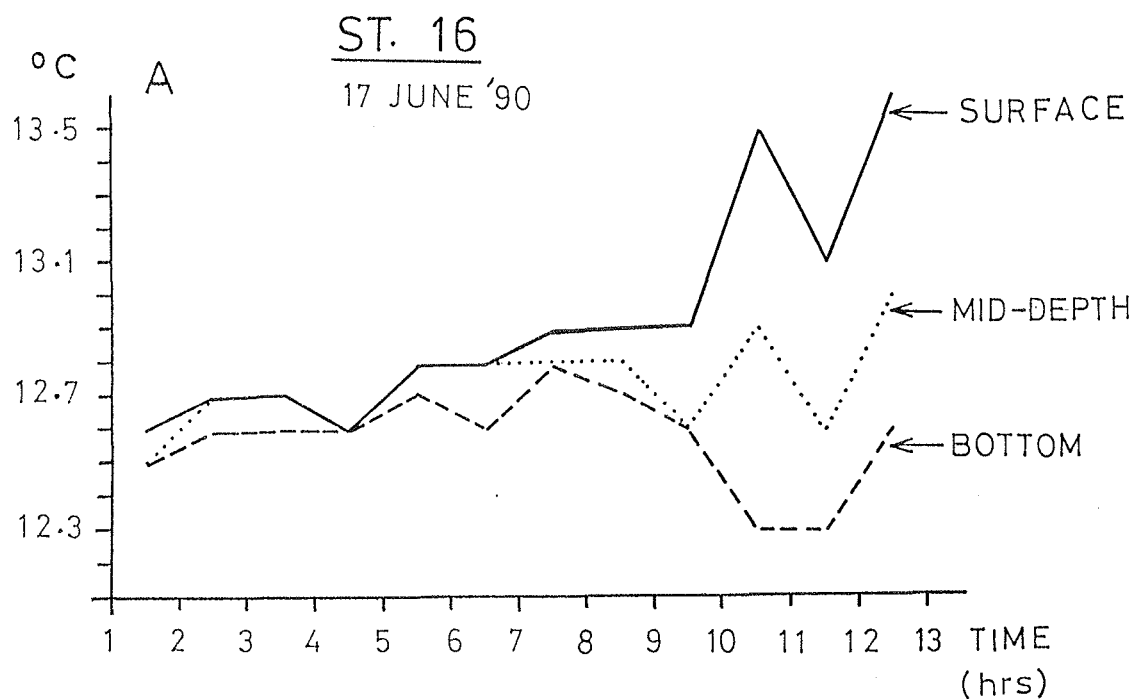


Fig. 8a. Typical sea temperature ( $^{\circ}\text{C}$ ) profile offshore of Spiekerroog.

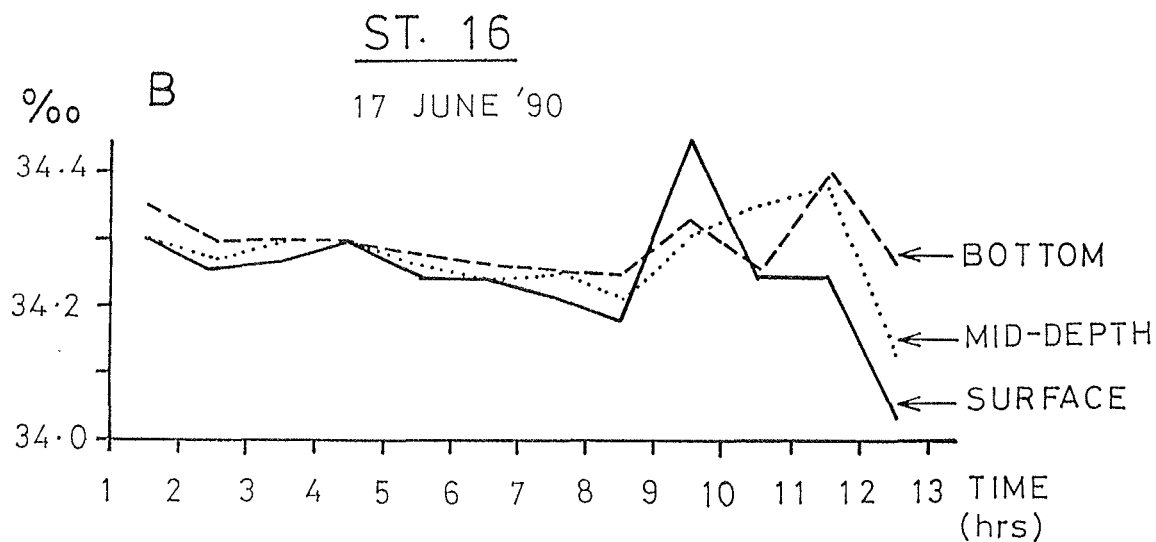


Fig. 8b. Typical sea salinity ( $\text{‰}$ ) profile offshore of Spiekerroog Island.

The above hydrographic parameters demonstrate that the coastal waters are highly homogeneous (non-stratified) and that there is much greater turbulence in the water column during winter as compared to the summer months.

### 3.6.2 Regional Water Circulation

Large-scale water mass movement in the North Sea reflects the combined effects of tidal currents, wind and pressure fields, as well as ocean circulation outside of the North Sea (POSTMA, 1982). It may thus be appropriately referred to as the residual current pattern.

Results of drift experiments within the German Bight by NEUMANN (1966) show that the residual flow in offshore waters of the East Frisian islands attains a velocity of the order of 10-15 cm/s. The latter constitutes part of the southern North Sea water circulation, which commences at the Strait of Dover, flows along the Dutch coast, to gradually veer offshore (northwesterly) along the Frisian islands toward the Danish coast (Fig. 9).

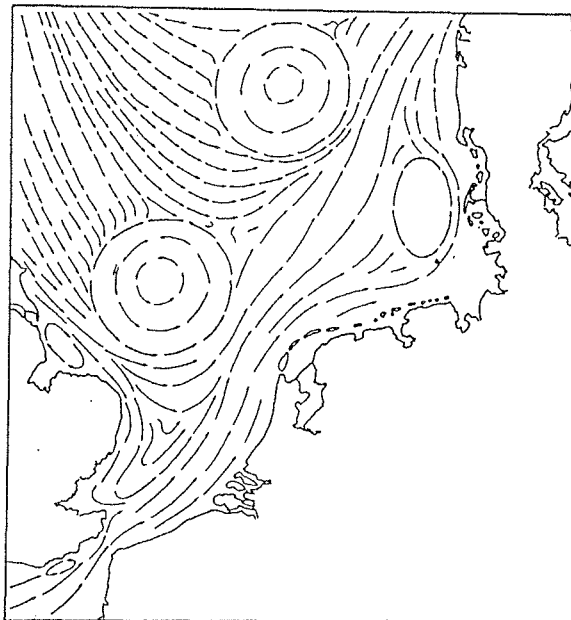


Fig. 9. Regional water circulation in the North Sea.  
(after POSTMA, 1982).

### 3.6.3 Tides and Tidal Currents

Tides in the North Sea are semi-diurnal and rotational (anti-clockwise) about three amphidromic points, two of which are shown in Fig. 10. A third one occurs in the southern North Sea Bight between England, Belgium and The Netherlands. In the southern North Sea, tidal range systematically increases eastwards along the Frisian barrier islands with increasing distance from the amphidromic point located in the east-central part of the North Sea (POSTMA, 1982).

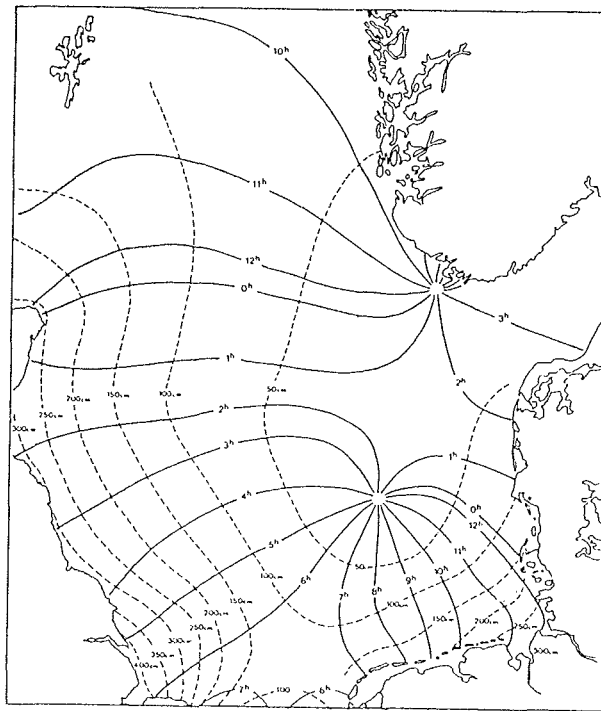


Fig. 10. Pattern of tidal wave propagation in the North Sea (after POSTMA, 1982).

Thus, with a neap, mean and spring tidal amplitude of 2.1, 2.5 and 2.9 m respectively, Spiekeroog has one of the highest tidal ranges (and energy) of all the North Sea barrier islands. The chain of the southern North Sea barrier islands terminates at the entrance of the Jade Bay, some 15-20 km eastward from the eastern tip of Spiekeroog, where the mean tidal range reaches 3.8 m.

Regional patterns of tidal currents within the German Bight are documented from repetitive measurements reported by NEUMANN and MEIER (1964). However, in relation to the present study, these data have a number of shortcomings, namely, non-documentation of flow conditions below the sea surface; non-distinction in data of different sea states (through the averaging process adopted); and finally, the measuring stations were too widely spread to adequately resolve interactions between the flow and bottom topography.

The main results of fair-weather condition (wind < 10 m/s) measurements on the shoreface of Spiekeroog are presented in Figs. 11 a-f and discussed below:

(a) Time-asymmetry of tidal currents was generally weak (typically a half-hour difference). Spring tides revealed both symmetric and evenly occurring flood and ebb time-asymmetry. Flood time-asymmetry at any location was not necessarily recurring during both neap and spring tidal conditions.

(b) In contrast to weak time-asymmetries, velocities generally show a strong flood asymmetry (Fig. 11a). Peak flood and ebb flow velocities at 100 cm above bottom ( $U_{100}$ ) at all the stations typically exceeded 25 cm/s during spring and neap tides. All-station spring flood and ebb averages were respectively  $48 \pm 6$  cm/s and  $37 \pm 9$  cm/s as against neap counterpart of  $35 \pm 7$  cm/s and  $33 \pm 6$  cm/s.

Quite instructive from Fig. 11a is the fact that even in the absence of instantaneous bottom wave currents, and assuming a threshold velocity of about 30 cm/s, all grades of sand finer than 1 phi (medium grains) would be mobilize by both flood and ebb currents during spring tide at virtually all the stations. Some sediment mobilization would also occur during neap tide, but is in this case mostly restricted to either the flood or the ebb current.

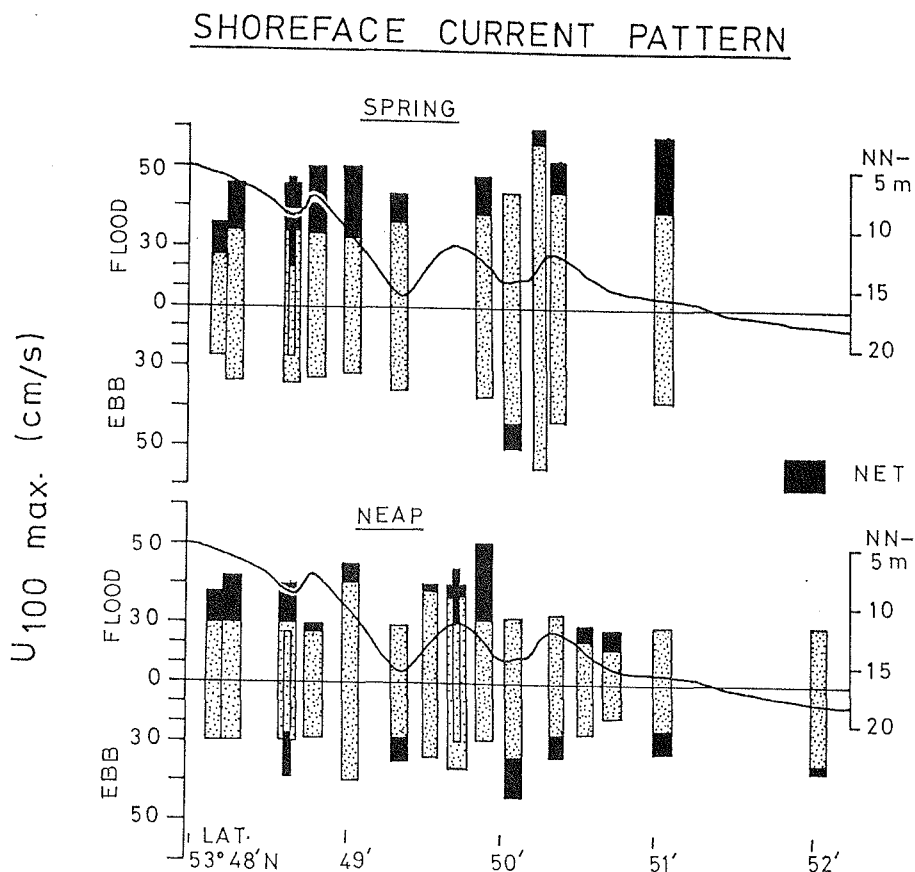


Fig. 11a. Variation in spring and neap tidal current peak velocities (cm/s) at 100 cm above sea bed.

(c) The highest peak flood and ebb  $U_{100}$  values of 58 and 56 cm/s respectively measured at spring tide was on the landward flank of a shoreface-connected ridge. It is instructive that the troughs (especially the outer one) show a strong ebb dominated tendency.

(d) Peak flood to ebb  $U_{100}$  ratios show an all-station spring and neap average of  $1.35 \pm 0.25$  and  $1.10 \pm 0.25$  respectively, thus indicating a stronger flood dominance at spring relative to neap tide. Alternatively, increasing ebb flow dominance (manifested in > 30% of the measured stations) was typical of the neap tide condition, whereas spring tide records were almost exclusively flood-asymmetric.

(e) Spring to neap peak flood and ebb  $U_{100}$  ratios respectively show an all-station average of  $1.48 \pm 0.44$  and  $1.04 \pm 0.23$ , thus indicating that maximum flood and ebb velocities respectively are on average 48% and 4% higher at spring than neap tide.

(f) As shown in Fig. 11b, these spring-neap flood and ebb peak flow ratios tend to increase with offshore distance.

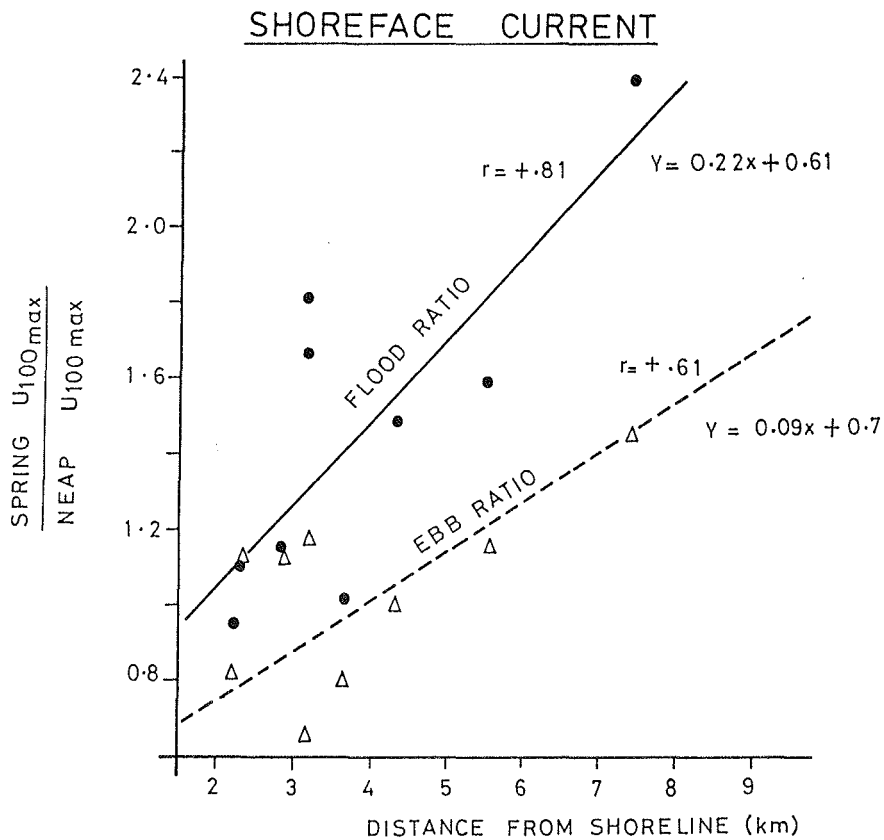


Fig. 11b. Spring-neap tide velocity ( $U_{100}$ ) ratios as a function of offshore distance.

(g) Tidal current excursion - an index of flow intensity (defined here as the area under a velocity-time curve) at 100 cm above bottom (Fig. 11c) showed a strong flood dominance at spring tide as against a weak dominance at neap tide. These are attested to by all-station average flood-ebb excursion ratios of  $1.52 \pm 0.5$  and  $1.08 \pm 0.2$ , respectively.

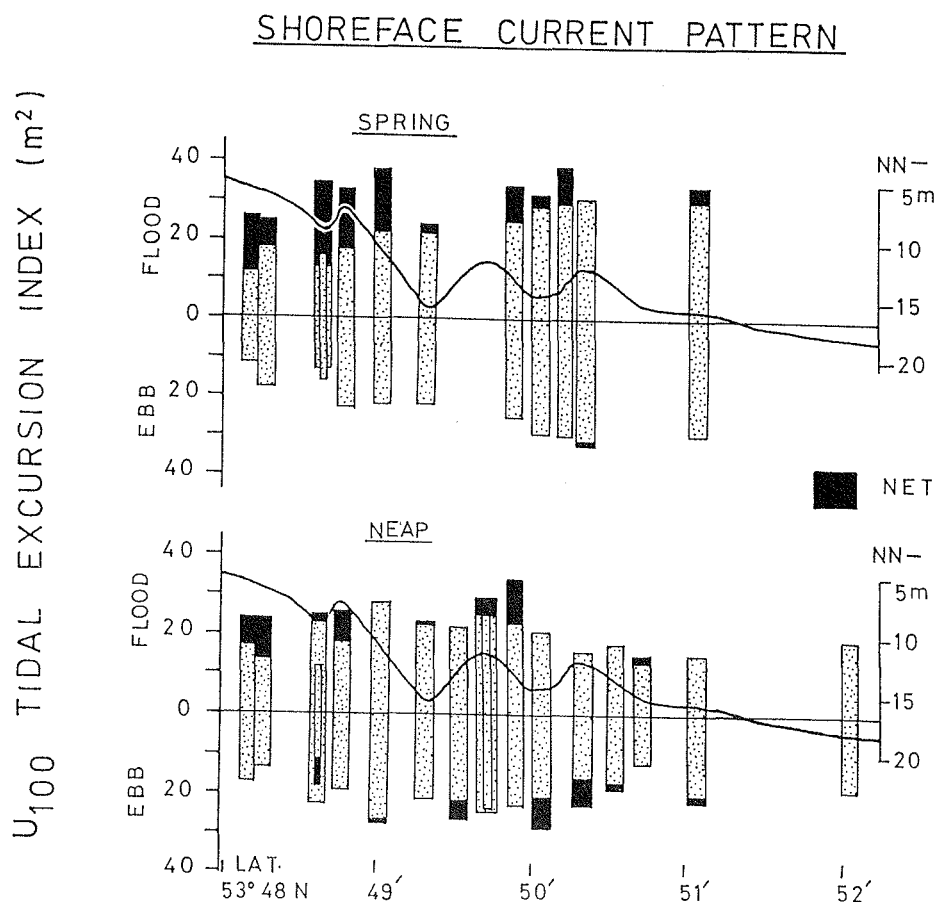


Fig. 11c. Variation in spring and neap tidal flow excursion.

(h) Maximum velocities near the surface (or at heights from the bottom greater than half of the total water column) are about 17% to over 250% of the near bottom  $U_{100}$  counterpart. The all-station average variations for the flood and ebb currents during spring are 50% and 52% respectively, with corresponding values of 77% and 59% during neap tides.

(i) Individual station tide-averaged  $U_{100}$  (mean of 9-15 time-varying readings) (Fig. 11d) and tide depth-averaged (for heights of 1, 2, 4, and 6 m) (Fig. 11e) values on the whole also showed a flood dominant tendency during spring and neap tides; instructive are the generally high values ( $> 20$  cm/s).

This indicates that, excluding the high- and low-tide slack-water stages, velocities during the remaining 80-90% of a tidal cycle are competent to sustain transport of mobilized sediments.

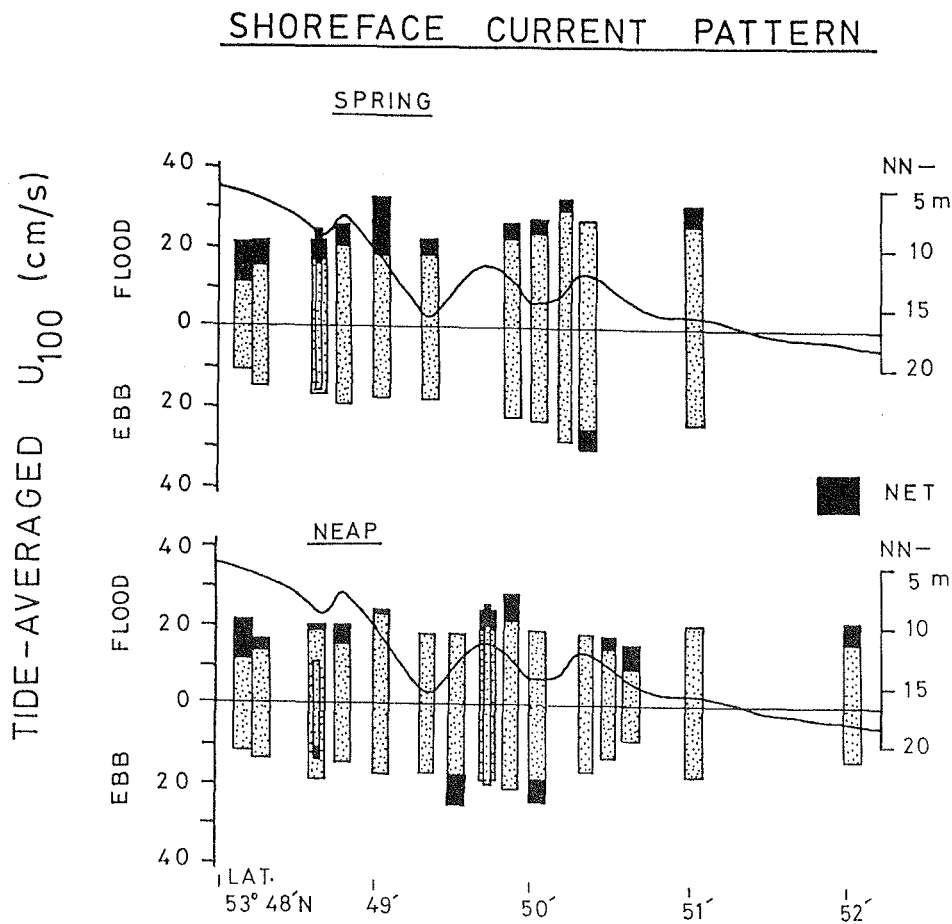


Fig. 11d. Variation in spring and neap flood and ebb tide-averaged velocities (cm/s) at 100 cm above sea bed.

(j) The acceleration and deceleration phases of  $U_{100}$  showed all-station velocity ranges and acceleration to deceleration velocity ratios (%) as follows:

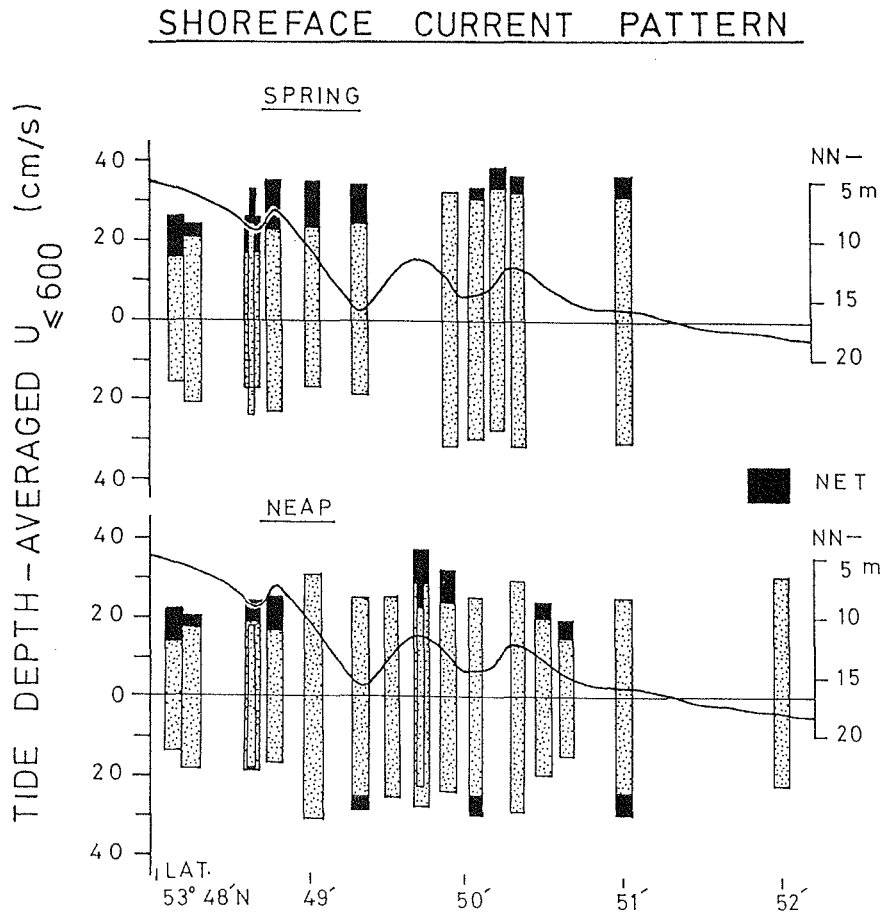


Fig. 11e. Variation in spring- and neap-tide depth-averaged (1, 2, 4, and 6 m above sea bed) velocities (cm/s).

	<u>FLOW VELOCITY (cm/s)</u>		<u>ACC/DEC ratio (%)</u>
	Acceleration	Deceleration	
spring flood	20-46	20-34	17
spring ebb	9-36	13-33	27
neap flood	10-33	9-32	3
neap ebb	13-28	12-25	25

Interestingly, at both spring and neap tides, the velocity contrast between the acceleration and deceleration phases of a

flow is more pronounced for the ebb than the flood current. This suggests that, relative to the flood current, the ebb flow at its initial or accelerating phase is "ignited" or accelerated, most probably through momentum transfer from the interacting inlet and shoreface ebb flows. A similar vertical pattern as above would, among others, result in an increase in sediment transport (WRIGHT, 1989; Section 4.2.3.4);

(k) Vertical velocity profiles had logarithmic shapes at all stages of a tidal cycle (Fig. 17, Section 4.2.3.4). However, the slopes of the profiles varied in a systematic way indicating a time-varying flow (frictional velocity,  $U_*$ ) and substrate response (bedform / suspended sediment) over a tidal cycle. Details on the theoretical background and other technicalities of the above results presented in Appendix B-1 are dealt with in Section 4.2.3.4. Important at this point are the following facts:

(i) The patterns of tidal variation of frictional velocity ( $U_*$ ) and bed-roughness ( $Z_0$ ) are comparable to that of the current velocity ( $U_{100}$ ), except for slight displacements in their peak values.

(ii) The values of bed-roughness are abnormally high and would appear to reflect not only flow retardation induced at the sea bed, but some combined effect of the latter and those well above the sea bed.

(iii) Finally, irrespective of potential errors in estimating the magnitude of  $U_*$  and  $Z_0$ , for which an appropriate scaling factor in nature is still lacking, their tidal variation pattern is considered instructive in site-specific comparisons of flow-substrate changes, especially since data acquisition methods were consistent throughout.

(l) Average directions for near-bottom flow velocities  $>10$  cm/s (revealed in over 70% of the tidal cycle) during spring and neap tides presented in Fig. 11f allows the following

generalizations about the shoreface current pattern:

(i) The flow direction-distance (cross-shore) curves are characterized by a variable segment, in which both the flood and ebb currents depict increasing veering from a shore-normal orientation with offshore distance, and a horizontal counterpart indicating attainment of equilibrium flow direction whose mean are  $105^\circ$  and  $280^\circ$  Azimuth, respectively.

(ii) The variable segment of the curve tends to be steeper for the neap flood and ebb flows than their spring counterpart; moreover equilibrium flow direction during spring tide takes place further offshore (4-5 km) from the mean shoreline as against 3-3.5 km during neap tide. This pattern attests to a stronger ebb current in the inlet at spring tide.

### SHOREFACE CURRENT PATTERN

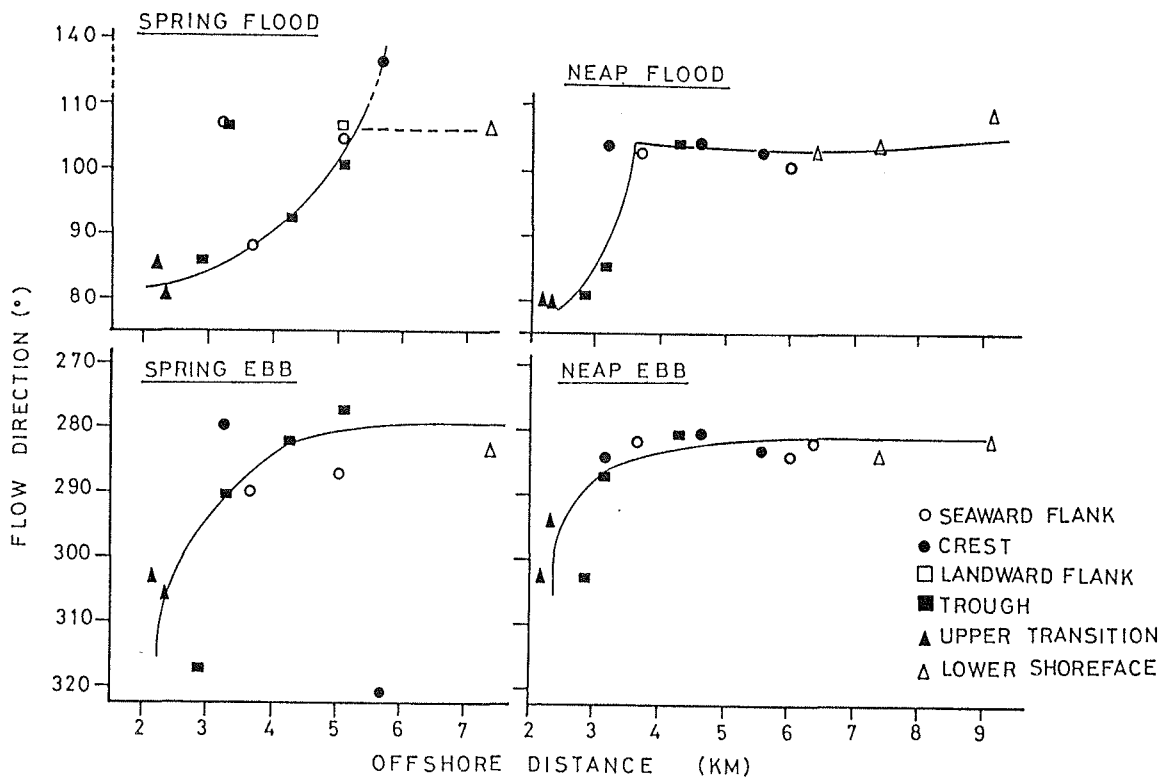


Fig. 11f. Average spring and neap tidal current directions for  $U_{100}$  velocities  $> 10$  cm/s.

(iii) Beyond about 3-4 km from the mean shoreline (in 10-12 m water depth), the flood-current direction is ENE. Coastwards from here it changes its direction through E to ESE, i.e., it become less oblique to the ridge-trough orientation. Observations of a similar ESE flow direction on the bathymetrically smooth lower shoreface suggests that the change in flow direction is not topography-induced. The almost easterly-directed flood currents in shallower water may reflect the increasing influence of a longshore component of momentum flux associated with shoaling waves.

(iv) The ebb flow directions, in contrast to their flood counterparts, show less variability, being consistently aligned WNW. However, the ebb-flow direction within about 3 km (8-10 m water depth) of the mean shoreline is somewhat more northerly (higher Azimuth values). Due to depth limitation of the offshore veering of the ebb currents, their cross-shore sediment transport effect will be insignificant on the shoreface ridges situated further offshore. This is because the ebb flow direction in deeper water is very much aligned with the different orientation of the different ridge-trough axes ( $278^{\circ}$ - $290^{\circ}$  Azimuth).

These fair-weather results are complemented by observations of KOCH and NIEMEYER (1978), which covered a spectrum of different energy conditions. Of particular interest here are the slight to severe storm situations. It must be added, however, that the location of the measuring point just landward of an inlet throat (Nordeney Seegat), the non-specification of the depth-of-measurement (the writer presumes data to be near-bottom), and the restricted applicability of their data to W and SW winds are limiting as far as a direct comparison of their results with those presented above is concerned. Nevertheless, their findings do have significant implications for the morpho-sedimentary character of the lower shoreface.

Pertinent results are :

(1) Peak inlet ebb-flow velocities (mean 136 cm/s) during

normal or "fair-weather" tide conditions are 7-32% greater than their flood counterpart. Corresponding values averaged for the waxing, peak and waning phases of a 1973 "Orkan", i.e. severe storm-tide, are 169 cm/s and 36-125%.

(2) At the peak of the above "Orkan", maximum flood and ebb velocities attained were 132 cm/s and 196 cm/s, respectively. However, the ebb-flow duration was 3 times longer.

(3) In terms of flow capacity - an integration of flow velocities and duration - the authors found an ebb to flood tide ratio of 4.25 during the "Orkan" storm condition.

(4) The above ratio increased ten-fold during the succeeding 12 hours and, thereafter, sharply reduced to a normal tide situation of 1.5.

(5) For the less stormy W-NW winds, the flow condition was identical to the severe storm situation above.

#### 3.6.4 Waves and Wave-Induced Currents

Records of nearshore wave conditions along the East Frisian barrier islands as a whole are too few and short in duration to enable an accurate definition of the local wave climate. Generally, wind-fetch considerations suggest that the most extreme wave conditions along the study area are likely to be associated with westerly to north-westerly winds.

Before a detailed evaluation of the existing nearshore wave record, an offshore record (66 m depth, 530 km NW of Spiekeroog) from FORTNUM (1978) is briefly examined (Fig. 12a). This is perhaps the only published long-term deep-water wave record from the North Sea.

Although the wave data are essentially restricted to the "high" energy periods of the year, these are, nevertheless, instructive because they are identical to the nearshore all-year wave data to be discussed. This being the case, Fig. 12a can be taken to typify the coastal wave climate of the

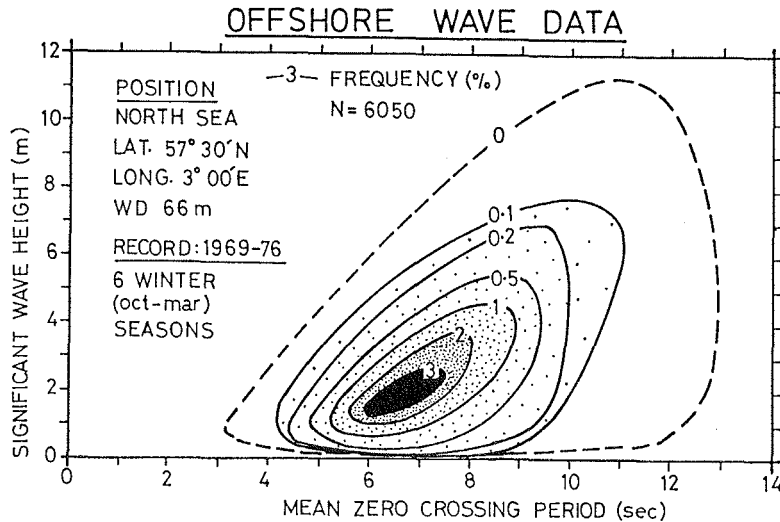


Fig. 12a. North Sea offshore wave frequency data (modified after FORTNUM, 1978).

North Sea and hence can serve as a basis for evaluating the potential role of shoaling and breaking waves in seabed dynamics.

Two nearshore (10 m depth) wave records reported by DETTE (1977) and NIEMEYER (1979) at different time intervals from two distantly situated islands (Sylt and Norderney respectively) are so strikingly similar to warrant extrapolation to the Spiekeroog shoreface. Both data-sets span a spectrum of sea-states.

A re-evaluation (based on Airy wave theory) of DETTE's summary data-set for the period 1971-1974 is presented below:

(a) In about 80% and 25% of the time, significant wave heights ( $H_{sig}$ ) are greater than 1.5 m and 3 m respectively;  $H_{sig}$  less than 1 m has lower than 1% frequency occurrence. Statistically, the wave height distribution shows a broad range (0.5-5 m), is unimodal and has a high wave asymmetric pattern. Modal (30%), mean and maximum significant wave heights were 1.5 m, 2.2 m and 5.2 m respectively. For comparison, NIEMEYER's (1979) data-set of 1976-1978 showed a significant wave height range of 1.8-4.5 m, but under extreme storm conditions reached heights

of 9 m and periods of 12 sec (NIEMEYER, 1976).

(b) Wave period range is 3.5-9.5 sec, but 4-8 sec and 5-6 sec waves respectively constitute 80% and 32% of the observed range; overall mean wave period is about 6 sec.

(c) Waves are generally short in length (L); the computed range of 19-140 m in 10 m water depth is distributed as follows:

L	< 50 m	48%
	50-100 m	38%
	> 100 m	14%

(d) Wave steepness (height to length ratio, H/L) values are considerably larger than the commonly noted value of 0.02 for the open ocean (KING, 1959); wave steepness in 10 m water depth ranges between 0.02-0.05 with a frequency distribution as follows:

H/L	> 0.03	78%
	0.03-0.02	21%
	< 0.02	1%

(e) Maximum oscillatory current velocities ( $U_m$ , computed after KOMAR, 1974) in 10 m water depth vary between 7-370 cm/s, decreasing by a factor 0.4 in 20 m water depth for similar heights and periods (or lengths). The % frequency distributions of  $U_m$  for both water depths are as follows:

		Water Depth	
		(10 m)	(20 m)
$U_m$	< 30 cm/s	17%	67%
	30-50 cm/s	25%	8%
	50-100 cm/s	25%	17%
	100-200 cm/s	23%	8%
	> 200 cm/s	10%	0%

(f) Wave orbital diameter ( $d_o$ ) in 10 m water depth ranges from 0.1-11 m, with a frequency distribution as follows:

$d_o$	< 1 m	42%
	1-3 m	33%
	3-5 m	12%
	> 5 m	13%

Employing the most commonly applied wave-breaking criterion, i.e. height-water depth ratio  $H/d = 0.78$ , to the study area, the surf zone (region of wave-generated longshore currents, rip currents, undertow etc.) in the study area can, for the day-to-day wave climate, be defined in 80% of the time to be confined shoreward of the 4 m isobath. Only in 25% of the time will waves break in 4-7 m of water depth, this corresponding to the medial (saw-tooth bar) upper shoreface zone. However, during extreme storm conditions, the surf zone may extend seaward to a water depth of 12 m.

These wave data enable a three-fold classification of the wave regime: normal or "day-to-day," sea or "windwave" and storm-swell, together accounting for 90% of the recorded wave height-period combination. The remaining "unclassified" 10% are of low sedimentologic significance, particularly on the lower shoreface. The more important wave regime characteristics (percent occurrence, height and period, breaking water depth and maximum bottom orbital velocities at different water depths) are given in Table 2 below and in Figs. 12 b, c and d.

TABLE 2. Wave regimes and their principal characteristics along the East Frisian barrier island coast.

Wave regime	%	$H_{sig}$ (m)	T sec	Breaker depth (m)	$U_m$ (10m) cm/s	$U_m$ (20m) cm/s
Normal	67	1-2	4-8	< 2.6	56 ± 25	18 ± 12
Sea	16	2.5-3.5	6-8	3.2-4.5	147 ± 25	63 ± 24
Storm-swell	8	> 3.5	8-10	> 4.5	296 ± 48	131 ± 23

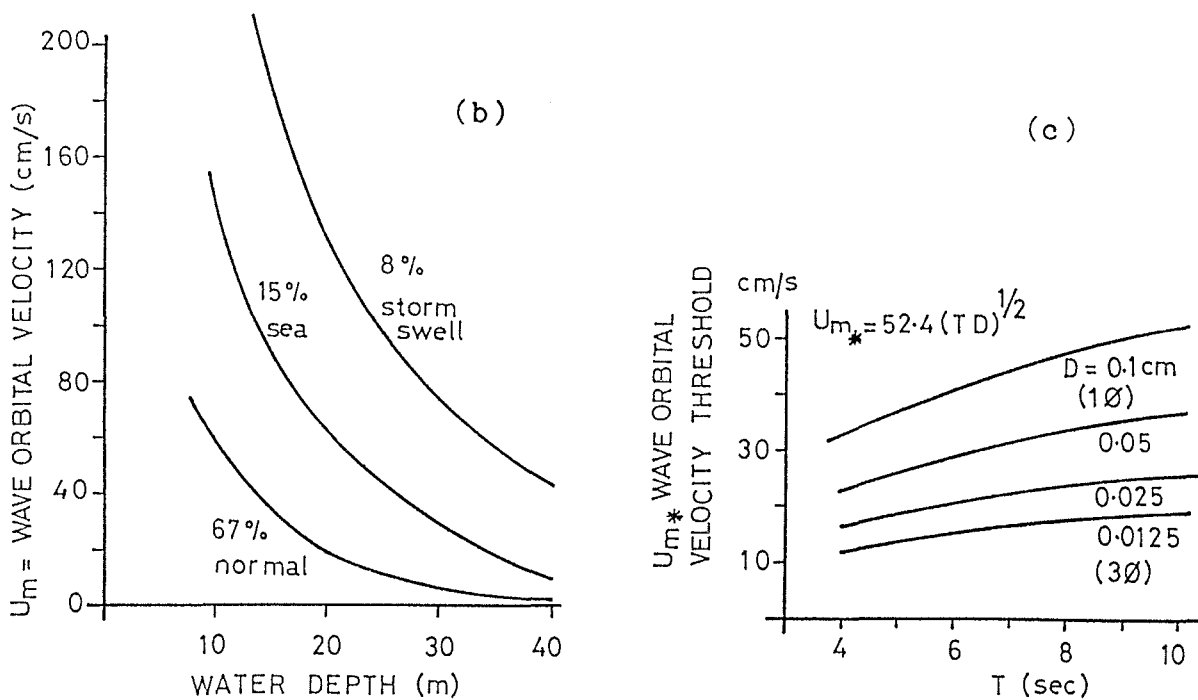


Fig. 12 (b) Variation in maximum near-bed wave-current velocities (cm/s) in relation to water depth for three wave regimes. (c) Wave current sediment threshold velocities. The employed equation is based on CLIFTON (1976).

From Figs. 12b and 12c it is evident that any sediment finer than 1 phi or 0.5 mm (medium sand) would be mobilized by bottom wave currents in virtually 100 % of the time in water depths shoaler as 10 m. Fine sand (2-3 phi; 0.125-0.25 mm) would be similarly mobilized at frequencies comparable to the latter at depths of 10-20 m.

The above results, as well as those of other grain sizes and water depths depicted in Fig. 12d below are particularly instructive, because they indicate that at depths > 30 m, medium to coarse sands would be mobilized in less than 10% of the time.

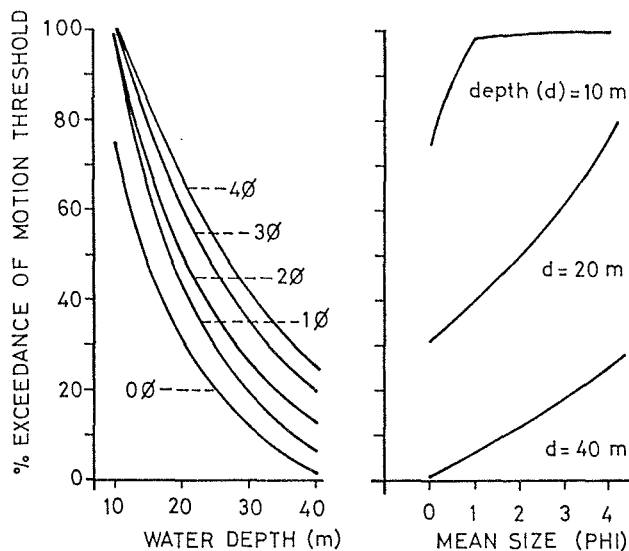


Fig. 12d. Percentage exceedance of sediment threshold by shoaling waves on Spiekeroog shoreface as a function of both water depth and grain size.

Empirical data on breaking wave-generated surf zone currents are rare for the study region. A literature survey of measurements elsewhere show, however, that rip current velocities generally exceed 0.5 m/s and may attain 1-2.5 m/s during a moderate to high wave energy events. By contrast, longshore current velocities rarely exceed 1 m/s, values of 0.2-0.6 m/s being quite commonly reported.

Longshore currents in the study region should show a net eastward flow in response to the resultant E-ESE directed deep-water wave power, whose magnitude is estimated at  $4.4 \times 10^3$  W/m (FITZGERALD, et al. 1984). However, indirect evidence from sediment budget analysis (Chapter 6) indicates that longshore currents are not likely to flow continuously eastwards along the entire length of each of the Frisian islands. Based on the reasoning adduced for the study area, it can be expected that reversals in longshore current direction would take place near the mid-point off each of the Frisian barrier islands.

The significance and implications of waves and wave-generated currents, as well as their previously discussed tidal and transient (storm) counterpart, in moulding and maintaining the morpho-sedimentary character of the shoreface are multiple and varied. These will be repeatedly addressed in several sections of this study.

## CHAPTER 4

### STUDY METHODS AND DATA SET

#### 4.1 Bathymetric Charts and Soundings

Initial information on the nature and changes on the shoreface bathymetry was based on evaluation of three types of charts: hydrographic, topographic and soundings.

Hydrographic Chart No. 89 (scale 1:50, 000) published by the Deutsches Hydrographisches Institut (DHI), now known as Bundesamt für Seeschifffahrt und Hydrographie (BSH), constituted the base map for navigational purposes and gridding of sediment sampling sites. Coastal Topographic Charts No. 7 (1960) and 2112K (1975) (scale 1:25,000), published by the Surveys Office of the State of Lower Saxony, were used to assess the nature of bottom morphology and patterns of sediment budget change for a 34 km<sup>2</sup> shoreface area (just south of Latitude 53° 47.00' N to 53° 48.00' N and just west of Longitude 7° 42.00' E to 7° 48.00' E).

Sediment budget estimates were obtained by overlaying the finely-gridded 1960 and 1975 maps and ascertaining the depth changes representative of the mid-points of the 3,375 regularly gridded cells (100 m x 100 m cell size). The resulting depth difference measures (m) were transformed into volumetric changes by multiplying them with the cell area (10<sup>4</sup> m<sup>2</sup>). The volumetric data thus obtained were subsequently hand-contoured, and the accretional and erosional areas partitioned.

Semi-sequential sounding charts of the DHI on a scale of 1:20,000, spanning the period 1950 to 1987, were processed for details relating to the temporal and spatial dynamic behaviour of shoreface morphologies. Additional data of the same kind were provided by the Wasser- und Schifffahrtsamt, Wilhelmshaven.

In general, the above soundings were contoured by hand. This enabled the delineation of the trough axis trends of two most striking shoreface morphological features, the saw-tooth bars and the shoreface-connected ridges. These axis trends were superimposed on each other to form a set of axis clusters (see Chapter 7 for further details on analytical procedure and results).

## 4.2 Sea-Based Operations

### 4.2.1 Navigation

Investigations seaward of the surf zone were conducted on board FK "Senckenberg" - a 30 x 8 m, 165 tonne research vessel of the Senckenberg Institute in Wilhelmshven. At shallower depths around and within the surf zone, a light boat (type: Dory 17) with twin out-board engines was deployed. FK "Senckenberg" is equipped, amongst others, with DECCA radio positioning facilities of the type Shipmate RS 4000, accompanied with a programmable ship tracking system (Shipmate RS 2000), and a Honeywell ELAC (electro-acoustic) echosounders, the theoretical precision of which are 18 m and 10 cm respectively. The light boat is similarly equipped with a portable and programmable DECCA navigational system as well as an analogue digital echosounder.

Besides the in-built compass and anemometer on deck FK "Senckenberg" for recording onspot wind conditions, out-deck electrical driven hydraulic winches enabled the deployment of a variety of seabed samplers and other hydrographic equipment.

### 4.2.2 Depth Sounding

Depth soundings were conducted at fixed current measurement stations, the aim being to define tidal elevation curve and

current meter position relative to the sea bed. In other cases, continuous cross-shore and coastwise seabed soundings were made to update information on the character of seabed morphologies as a basis for selecting suitable sites for repetitive coring and current measurements.

#### 4.2.3 Seabed Sampling

##### 4.2.3.1 Grab Sampling

More than 690 bottom sediment samples were obtained (Fig. 13) with two van Veen type grab samplers from a shoreface area of 110 km<sup>2</sup>. Bottom samples retrieved with both grabs (0.2 and 0.03 m<sup>2</sup> surface area) are usually somewhat disturbed. However, for consistency, only the upper 3 cm of grab sediments were subsampled. The grabs showed a very high efficiency, such that a sample can be retrieved within a few minutes of deployment.

A detailed description of the sampling grid shown in Fig. 13 is given in Appendix A. Three orders of sampling density are evident from the figure. The first and most frequent order (85%) is characterized by 4 samples per km<sup>2</sup>, whereas the second- (6%) and third- (9%) order sample patterns respectively have 17 and 25 samples per km<sup>2</sup>.

##### 4.2.3.2 Boxcoring

The screwable steel boxcores employed in this study have length, breadth and height dimensions of 20, 30, and 45 cm respectively and have been developed by REINECK (1958a, 1963) who also describes their construction and coring mechanism. Due to increased compaction of sediments in the upper shoreface region, penetration depth of cores was comparatively smaller than in the offshore region.

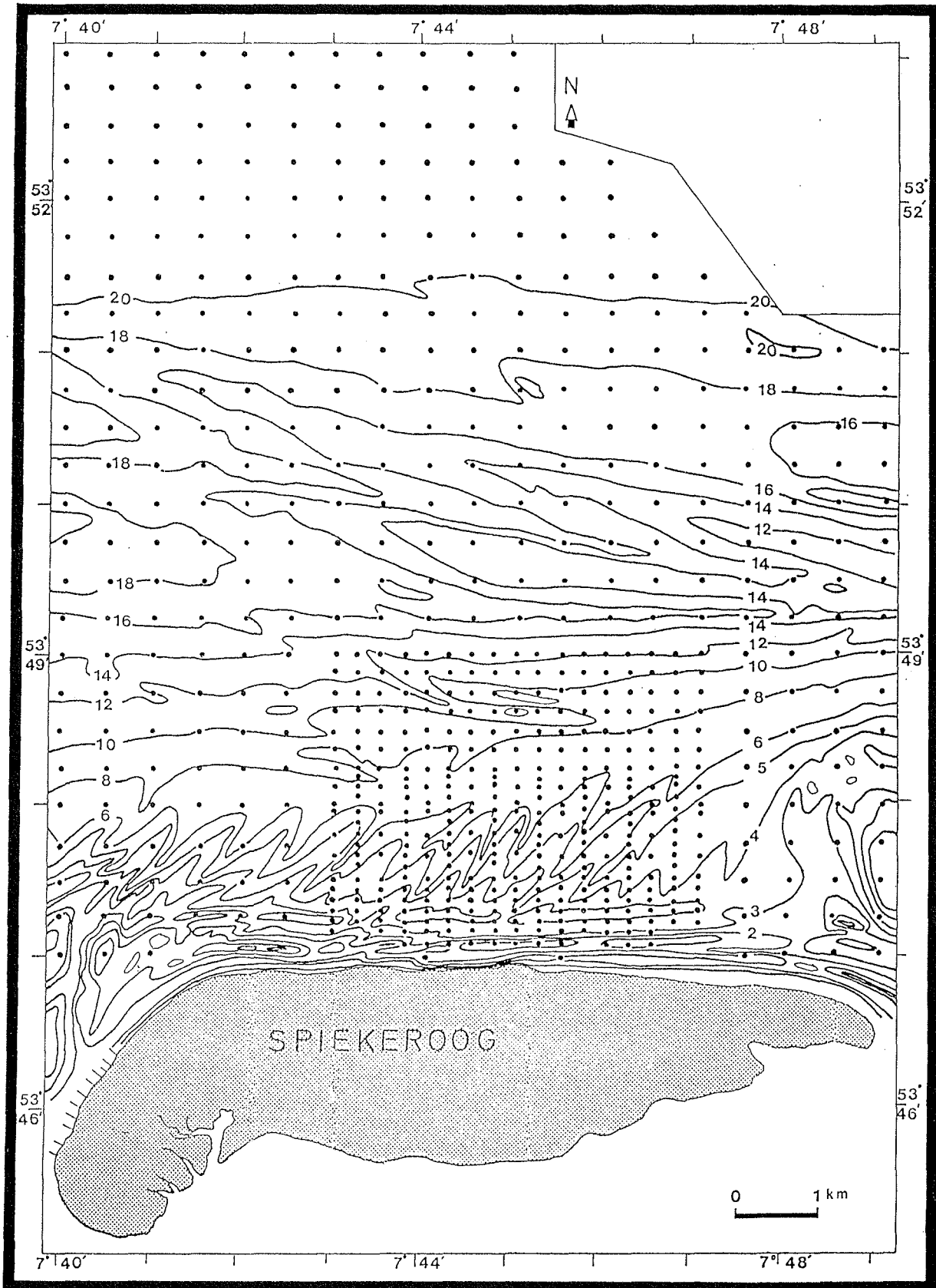


Fig. 13. Spiekeroog shoreface sediment sampling stations.

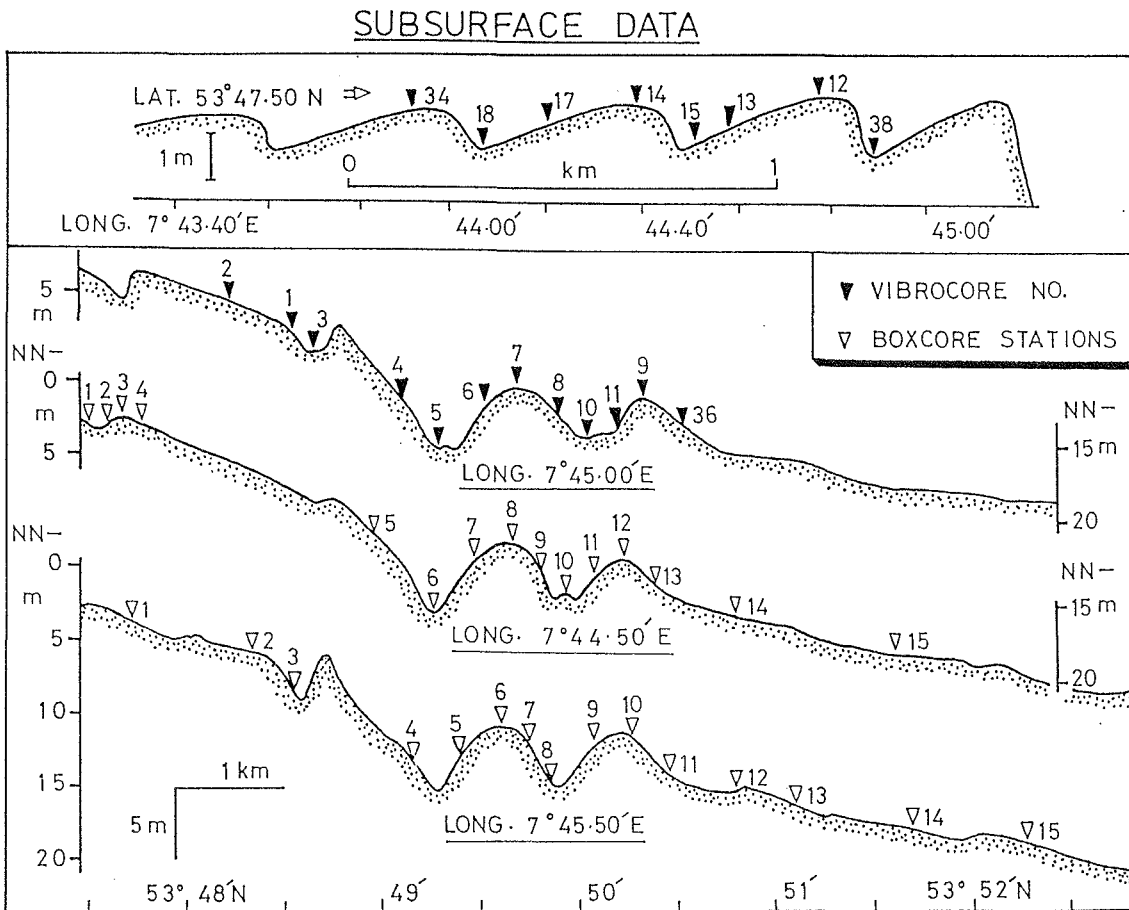


Fig. 14. Spiekeroog shoreface subsurface coring stations.

Seventy generally undisturbed core samples were obtained from the study area. The bulk of these, however, were retrieved along two coast-normal profiles (Longitude  $7^{\circ}44.50'$  and  $7^{\circ}45.50'E$ ), and were alternately sampled at intervals of 1-3 months in 1988/89. Standard sampling sites across the shoreface are shown in Fig. 14.

Due to problems relating to navigation and core penetration mentioned earlier, a complete series of samples as shown in Fig. 14 was rarely achieved. An additional problem

encountered during coring was the lack of a compass on the frame housing the box. Thus, in order to determine the orientation of the box on the seabed, the boxcore frame was allowed to freely drift while being lowered down the water column. The orientation of the box was read off the ship compass when, close to the bottom, the fins attached to it became aligned with the ship orientation which was generally parallel to the current direction.

The above problems did not apply to the core samples (16.5 x 12.5 x 30 cm) retrieved in the nearshore, since these were taken by divers who carefully measured core orientation at the time of penetration.

In general, these core samples enabled the evaluation of temporal and spatial variations of physical and biogenic structures on the sea bed. Sediment samples were also obtained at suitable intervals down the core depth. However, one of the obvious limitations of the present boxcoring technique is related to their small dimensions, which constrain proper recognition of larger-scale physical structures such as hummocky cross-stratification.

#### 4.2.3.3 Vibrocoring

Twenty, screwable square-box steel vibrocores (3 m long and 12 cm x 12 cm cross-sectional base area) were retrieved from the seabed in 1989 along two profiles shown in Fig. 14, using an electrically-powered hammering and vibrating system. Thirteen of these cores were located across the shoreface-connected ridge system along Longitude  $7^{\circ} 45.00'E$ , whereas 7 cores were taken from the saw-tooth bar morphology along Latitude  $53^{\circ} 47.60'N$ .

Most of the retrieved cores did not exceed 2 m in length, but were largely undisturbed. This coring device has the

advantage that the samples provide a stratigraphically longer record than those of the boxcores. On the other hand, the much smaller sample cross-sections of vibrocores are even more constraining to identification of larger-scale sedimentary structures than already observed for normal boxcores.

#### 4.2.3.4 Current metering

Half-hourly measurements of current velocities and directions were made along a vertical profile over a complete 12-hour tidal cycle at each of the 23 stations shown in Fig. 15. These observations were made exclusively during a relatively calm sea state and, at some stations, cover all of spring, mean and neap tidal conditions.

In all, the current record amounts to a time of over 400 hours. The data spatially spans all major bathymetric features seaward of the surf zone and thus provide, for the first time, a good opportunity (Section 6.3.2) for comparing the results of LAVELLE and SWIFT (1982) on flow characteristics on a North American Atlantic shoreface-connected ridge with a North Sea counterpart.

Data were acquired in two ways. Firstly, a General Oceanics direct read-out current meter (model 2035-MK11) with a standard rotatory propeller (model S2030R) was used. In measuring position, the meter is horizontally aligned with the current. With the aid of an attached weight and a graduated rope, the meter can be successively pulled through the water column. Typical elevations (in metres) above the sea bottom at which velocity observations were made are 0.5, 1, 2, and thereafter at 2 m increments up to about 1-2 m beneath the sea surface.

Depending on the depth of the water column and the steadiness of current flow, a complete set of current profile readings can be accomplished within 3-10 min. While the above

measuring procedure may replicate an expensive multiple-depth current metering package, the observation times are inadequate for assessing the effects of small-scale bursting phenomena on the flow record (HEATHERSHAW, 1974; GORDON, 1974; GROSS and NOWELL, 1983; DYER, 1986).

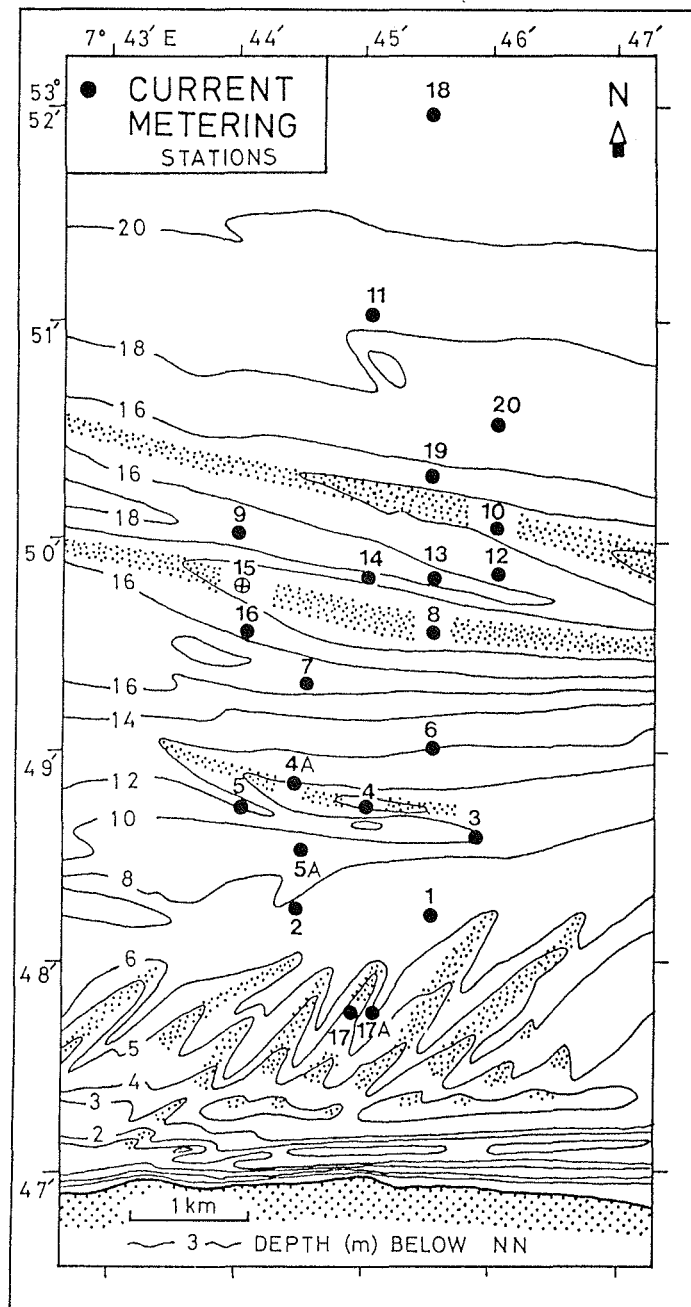


Fig. 15. Spiekeroog shoreface current metering stations.

Concurrently with the above equipment, a self-recording Interocean Systems impeller type current meter (model 135R) was also deployed. This meter registers every few seconds a current velocity and direction value. This instrument is suspended in the water column at a fixed and pre-determined depth with the aid of a winch on the vessel. However, its position relative to the sea bed constantly changes in response to the rising and falling tide.

Careful comparisons show that velocities indicated by this meter may be as much as 30% lower than the General Oceanics counterpart for a similar time and depth of measurement. A possible explanation for the observed discrepancy in velocity values between the two flow-meters may be signal dampening in the case of the Interocean current meter, the impellor of which rotates around an axis vertical to flow. Consequently, it is potentially more influenced by vertical turbulence in the water column produced, amongst others, by the heaving motion of the ship (FLEMMING, pers. comm.)

The current velocity data utilized in this report are those of the General Oceanics meter, and are considered in conjunction with the flow directions furnished by the Interocean meter. The recorded directions at each single but varying depth of the Interocean meter presupposes non-variation in the flow direction within the entire water column.

The essence of current velocity profile measurements described above was to enable the assessment of the bottom shear stress or frictional (shear) velocity, and their spatial and temporal variations. This fluid flow parameter is considered to be most descriptive of the degree of sediment movement at the sea bottom (NECE and SMITH, 1970).

GUST and SOUTHARD (1983) details at least 7 procedures for determining the bottom shear velocities. The law of the wall approach employed in this study presupposes uniformity in the

shear velocity and the coefficient of turbulence (von Karman's constant) within the boundary layer (Fig. 16). It is based on the commonly observed logarithmic nature of velocity profiles within this layer.

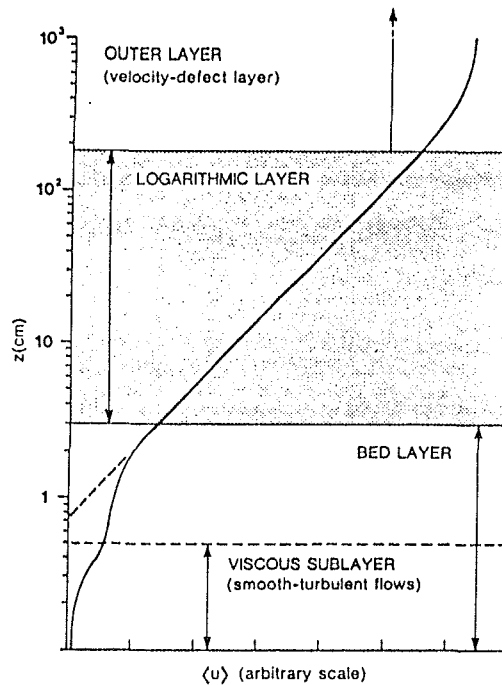


Fig. 16. Boundary-layer flow regime (after WRIGHT, 1989).

As exemplified in Fig. 17, in the study area, straight lines are obtained when data on current velocities and their corresponding depth (relative to sea bed) are plotted along the horizontal (arithmetic) and vertical (logarithmic) axis, respectively. The intersection on the depth ( $Z$ ) axis is referred to as the roughness length ( $Z_0$ ). Its value is dependent on the characteristics of the substrate underlying the flow.

The gradient of the straight lines is inversely related to the rate of change of velocity with depth ( $\delta u / \delta \log Z$ ) within the boundary layer, and its relation to the shear velocity ( $U_*$ ) is given by OPEN UNIVERSITY (1989) as:

$$U_* = 1/k \cdot \delta u / \delta \log Z$$

where  $k$  = von Karman's constant and has a value of 5.75 if a  $\log_{10}$  depth scale is used. It is noteworthy, however, that shear velocities calculated by the above procedure yield results which in many cases are suspect. One indication of the afore-stated is the very high values of the roughness length ( $Z_0$ ) obtained. Because plots of the current velocity profiles generally have logarithmic shapes, there is a tendency to believe that the  $Z_0$  values, being a graphically extracted variable, should reflect the situation in nature.

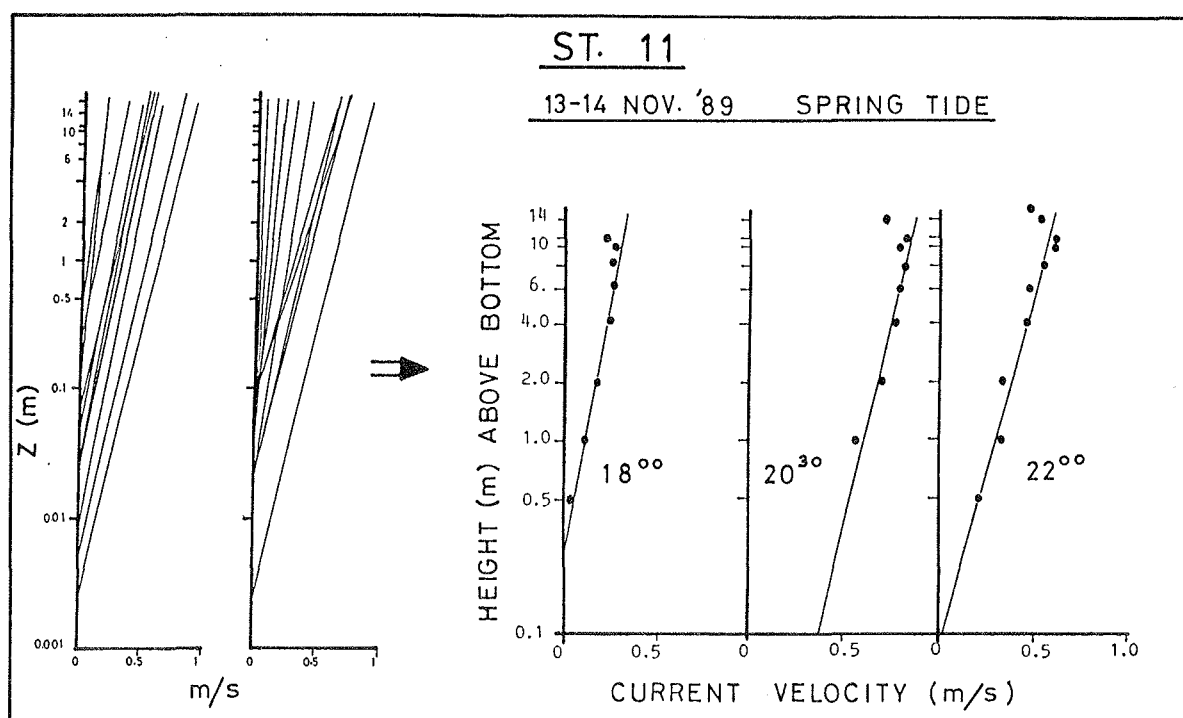


Fig. 17. Typical tidal variation in logarithmic current profiles on the Spiekeroog shoreface.

However, it has been shown by CHRISS and CALDWELL (1982) that within 15 cm of the sediment-water interface, in which conventional current meters are inoperable, current velocity profiles are usually also logarithmic but with a different gradient to the one above. The velocity gradient at this innermost boundary or bed layer is invariably steeper than their upper boundary layer counterpart, implying a correspondingly lower  $U_*$  value. It therefore seems obvious that

the observed roughness length and bottom shear values represent some summation of those due to form drag and skin friction (the latter being the actual shear stress exerted by the flow at the sea bed and defines sediment entrainment potentials).

Besides the logistic shortcomings addressed above, a realistic evaluation of  $U_*$  in the study area is further constrained by:

- (a) The flow is inherently non-steady and non-unidirectional and has acceleration - deceleration effects as well as oscillatory wave motions superimposed, whereas the logarithmic law is strictly applicable to a steady, unidirectional current.
- (b) As mentioned earlier, the calculated  $U_*$  values reflect both the skin friction and the form drag. The latter represents a retardation in flow and may be a consequence of:
  - (i) Unsteadiness of the flow in (a) above (e.g., GRANT and MADSEN, 1979).
  - (ii) Sea-bed undulations (e.g., SMITH and McLEAN, 1977).
  - (iii) Concentration of suspended sediments (e.g., ADAM and WEATHERLY, 1981; GLENN and GRANT, 1987; VILLARET and TROWBRIDGE, 1991).
  - (iv) Bedload transport (e.g., GUST and SOUTHARD, 1983).

The relative contributions of these to form drag are difficult to quantify. However, qualitative effects on some of the more common hydraulic parameters as synthesized by WRIGHT (1989) are listed in Table 3.

The fact that the estimated  $U_*$  values in this study incorporate various errors highlighted above, leading to an overestimation of the skin friction, is most evident when one compares the flow velocity for initiating sediment motion as a function of grain size and water depth given by RUBIN and McCULLOCH (1980) (see Appendix B-2) and the corresponding critical shear velocities (Appendix B-3). The tidal variations of the latter for some of the current stations are given in Appendix B-1.

TABLE 3. Factors affecting boundary-layer hydraulic parameters (after WRIGHT, 1989).

	$Z_o'$	$C_{100}$	$\tau$
Acc. Flow	Decrease	Decrease	Decrease
Dec. Flow	Increase	Increase	Increase
Wave-Current			
Interaction	Increase	Increase	Increase
Distributed Bed			Local Increase
Roughness	Increase	Increase	Space-averaged Decrease
Sediment			
Transport	Increase	Increase	Increase
Stratification	Increase	Decrease	Decrease

NOTE:  $Z_o'$  - apparent hydraulic roughness ;  $C_{100}$  - drag coefficient applicable to mean velocities at 1 m above the sea bed;  $\tau$  - skin friction shear stress

From the above comparison, it is concluded that the calculated  $U_*$  values may be at least 4 times higher than the actual skin friction velocities. Studies of CHRISS and CALDWELL (1982) suggest a similar order of magnitude. Difficult to ascertain, however, are the relative importance of the potential errors and their tidal variation.

#### 4.2.3.5 Temperature - Salinity Measurements

Knowledge of the vertical structure of temperature and salinity (T-S) of a water body is basic to understanding its dynamics and associated material transport. It is evident from the preceding section that stable density stratification

(sediment- or thermohaline-induced) of a water column would affect its boundary layer hydraulics.

Temperature and salinity were assessed in-situ at hourly intervals over a complete tidal cycle at 11 of the current observation stations using a cabled, dual-sensored Wheatston Bridge type (M.C. 5) salinity-temperature meter. This equipment has a readable accuracy of 0.05 ‰ and 0.2 °C respectively. Generally, data were obtained at 1 m and 5 m below the sea surface and near the seabed. The results of these measurements have been presented in Section 3.6.1.

### 4.3 Shore-Based Observations

#### 4.3.1 Beach profile surveys

Repetitive monitoring of beach profiles at a number of stations to assess temporal and spatial changes as initially envisaged was logistically constrained. Despite the latter constraint, the available data enable an assessment of the nature of beach morphology and its response to a storm-spring tide event.

Surveying was conducted using a standard theodolite along three coast-normal transects extending between an established bench mark and spring low water. The reference base level for elevation readings was the German topographic chart datum (NN).

By overlaying successive profiles of a given station, the net changes over the corresponding time-intervals were estimated from the differences in the areas underlying the profiles. On one occasion, surficial sediments were continuously sampled along a surveyed profile during the waning phase of a storm event.

#### 4.3.2 Beach sedimentary marks

The most common surface marks evident on the beach are rills, current ripples, water level and swash marks. These are not unique to the studied beach environment and thus merit no special emphasis. REINECK and SINGH (1975) provide a good documentation of the features. An additional remark on an attribute of swash marks, referred to as swash angle (ANTIA, 1989d), is given here.

Swash angle,  $\emptyset$ , (Fig. 18) is defined as the shoreward facing angle formed by the tangents drawn through the point of intersection of two adjacent swash marks. Essentially, as shown for a mesotidal, dissipative-prone Atlantic beach of Nigeria, Spiekerog Beach is also characterized by obtuse swash angle values, this being a manifestation of a similarity in surf zone processes.

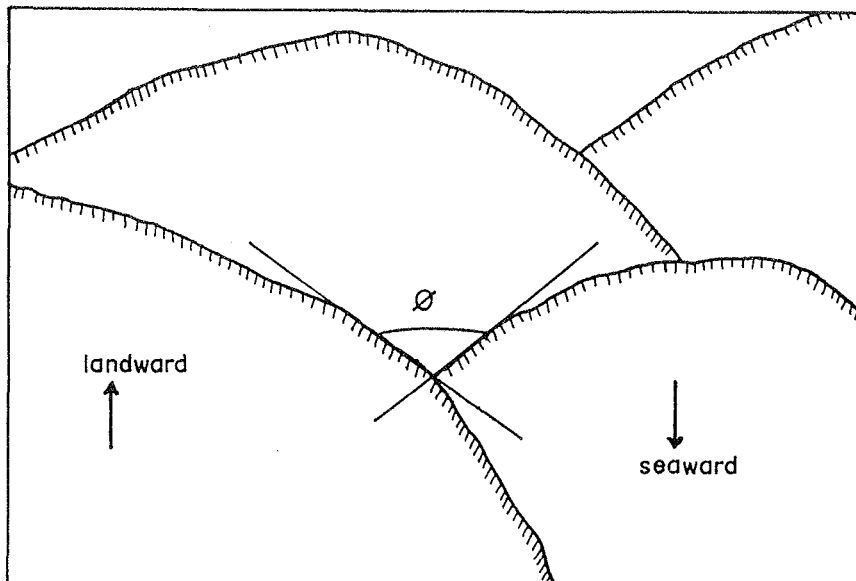


Fig. 18. Definition sketch of swash angle,  $\emptyset$ , (after ANTIA, 1989d).

#### 4.4 Laboratory Analyses

##### 4.4.1 Grain size measures and their interrelationships

In all, more than 1000 sediment samples were processed from the study area. These have been collected with grabs, boxcores, vibrocores and by hand from the beach. All samples were thoroughly washed to remove salts, and if organic matter was appreciable, further treated with hydrogen peroxide. The samples were then wet-sieved through a 62 micron mesh to separate the clay and silt fractions from other coarser (clastic and carbonaceous) materials. Only the sand fractions are of interest here. Thus, in the very few cases where carbonate materials constituted appreciable proportion of the representative samples, these were dissolved with 10% hydrochloric acid and then rewashed.

All the sand samples were oven-dried at 80°C and then continuously quartered using a mechanical splitter to a few grams of representative material. From the latter, about 1.5 gm was sub-sampled for grain-size analysis.

Size analysis was conducted using a version MC 86 macrogranometer (computerized settling tube) at the Senckenberg Institute, Wilhelmshaven. This equipment has a sedimentation length of 180 cm and cross-sectional diameter of 20 cm.

Following from the results of GIBBS (1972), the above settling tube dimensions, in conjunction with the sample weight, should yield less than 2% analytical inaccuracy. Moreover, his nomogram (p. 143) shows that for the above sample weight, the computed size statistics would have been based on between 5,000 and 10,000 grain particles.

The venetian blind at the top of the settling tube enables sediment grains to be released uniformly and instantaneously into the water column. These subsequently settle onto a pan of underwater balance at the bottom of the tube at rates which are

a function of the individual particle shape, size, density, as well as physical properties of the water medium such as temperature, viscosity and turbulence. The depositing particle weight is sensed as a positive voltage which is converted into binary numbers at a rate of 10,000 measurements per sec; these are subsequently integrated into a series of equal interval (0.02) logarithms of settling rate known as psi.

The psi-distribution displayed during sedimentation is the basis for computing moment and percentile measures of grain size distribution parameters of mean, median, sorting (standard deviation), skewness and kurtosis. No marked difference between the first and second moment measures and their percentile counterparts was evident for the sample set. However, large discrepancies exist between the third and fourth moment data and the percentile equivalent. For the sake of consistency, percentile measures would be adhered to.

However, it should be mentioned here that because the average value of the percentile measure, which is in reality the median, very highly correlates with the first moment counterpart, it is used throughout this study as a surrogate for the mean size. Furthermore, for the sake of conformity and easy comprehension, the percentile measures are in all illustrations and discussions referred to as graphic measures, because of their similarity. This is moreso, because verbal description of the percentile values follows that based on graphic statistics.

Generally, the value of a given phi grain-size statistic obtained by conversion from a psi-distribution depends on the input grain shape and density factors (1.18 and 2.65 g/cm<sup>3</sup> were used respectively) as well as the density and viscosity of the settling medium as reflected by its temperature. Again for ease of comparison, the psi-distribution resulting from different local settling temperature conditions was transformed to standard (20°C) settling rates after GIBBS et al. (1971). The equipment can be programmed to print out, besides the raw grain

size data, plots of three grain size distribution curves, namely, size frequency, cumulative frequency and log-probability.

The data employed from the above computation and plots include: mean settling velocity (cm/s), 1st and 50th (median) percentile (in phi units), sorting, skewness, kurtosis of both phi- and standard psi-distribution; weight % of sedimentation diameter and settling velocity class fractions (for the former at quarter, half and whole phi steps); number, percentage proportion, slope, phi-median and phi value of inflection points of the computer-truncated log probability grain size distribution segments. Some of the data are listed with their areal distribution charts in Appendices A, C, D and E.

The geological significance of grain size analysis are three-fold: assessment of sediment provenance, reconstruction of hydraulic conditions during transportation and deposition, and paleoenvironmental reconstructions. Opinions are divergent on both the efficiency of grain size parameters and the analytical procedure in fulfilling these tasks. In Chapter 5, the obtained grain size results are utilized to assess aspects of these. However, a brief comment and justification of the analytical procedure of grain sizes used is considered here.

In general, grain size distribution data of sands documented in the literature have been most commonly determined using either settling or sieving techniques. A number of studies (e.g., SENGUPTA and VEENSTRA, 1969; SANFORD and SWIFT, 1971; REED et al., 1975; FLEMMING, 1978; and KOMAR and CUI, 1984) have critically assessed both the significance and relationships of results from these sizing procedures. All these authors clearly favour settling techniques in view of the overall rapidity and reproducibility of results.

An additional and perhaps more important advantage of the settling technique commonly cited by its proponents is that grain-sorting in water is a response to their hydraulic

characteristics, and as such settling tube results more accurately replicates a real-world situation. Results of sieving can, however, match those of settling analysis for monomineralic and spherically shaped grains. However, SANFORD and SWIFT (1971) point that, in a strict sense of sedimentation, settling column should be subordinate as an analytical system to flume sorting. This is because natural sedimentation processes involve both bedload and suspension transport, the former not being adequately represented in settling column results. Accordingly, an ideal sedimentation parameter should be threshold stress of grain movement rather than settling velocity.

#### Interrelationships between grain size measures

In contrast to the commonly reported comparisons of settling - sieve results, very few reports (e.g., CLARKE, 1981) have considered the interrelationships between grain size statistics of psi and phi distributions. Thus, the results discussed below provide the modality for developing a functional scaling of summary statistics of psi-distribution that is comparable to that of the phi-distribution counterpart.

Firstly, mean standard settling velocity versus mean sedimentation diameter plot in Fig. 19 shows a typical Stoke's law relationship and, invariably, attests to the functionality of the settling tube and its computer software.

The sorting of psi-distribution versus the phi counterpart (Fig. 20) shows a distinct contrast. Although the areal pattern may be similar, the interpretation would be certainly different if phi-distribution-based scaling is utilized because of the correspondingly higher standard deviation values of the psi-distribution. As shown in Fig. 20, a "very well-sorted" psi-distribution of grain sizes should have a value of 6, if a similar interpretation as the phi-distribution counterpart is envisaged. As a rule-of-thumb, for standard deviation values

less than 1, the standard deviation value of psi-distribution will be 1.7 times larger than the phi-counterpart. In order for the verbal interpretation of sorting of both measures to be comparable, the sorting class boundaries of the psi-distribution must be accordingly scaled using the above factor.

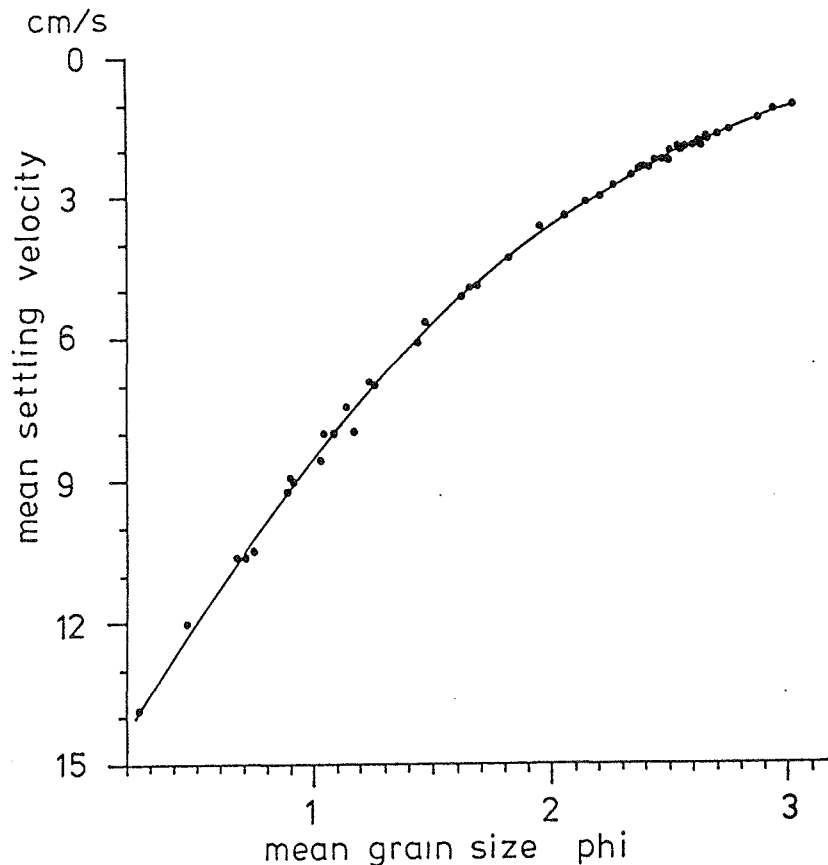


Fig. 19. Relationship between mean settling velocity (cm/s) and sedimentation diameter ( $\phi$ ) of shoreface sediments.

In contrast to the measure of sorting, skewness values of psi-distribution were only marginally higher (i.e., a more positive-prone skew) than their phi-distribution counterpart (Fig. 21). Kurtosis on the other hand (Fig. 22) revealed slightly elevated values for the phi-distribution than the psi counterpart. In general, using a common scale for the skewness and kurtosis of both psi- and phi-distributions will not result in a markedly different verbal interpretation.

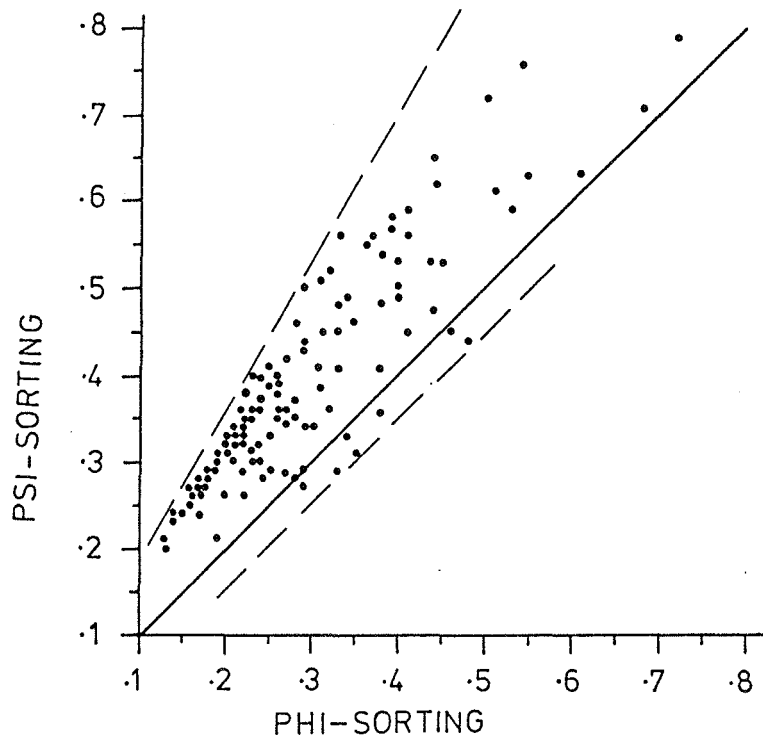


Fig. 20. Relationship between sorting of phi and psi distribution of shoreface sediments.

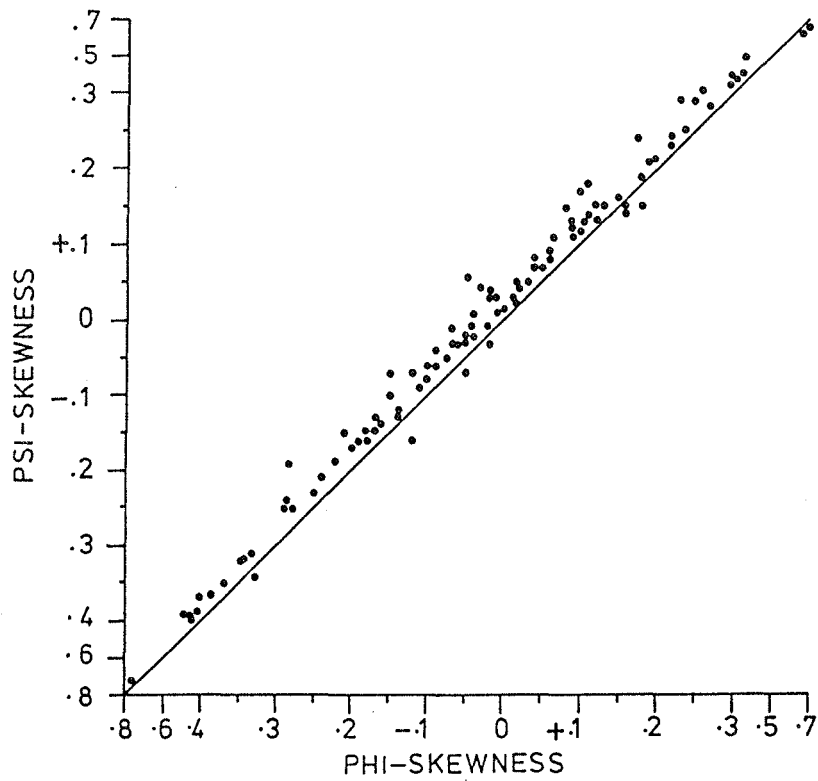


Fig. 21. Relationship between skewness of psi and phi distribution of shoreface sediments.

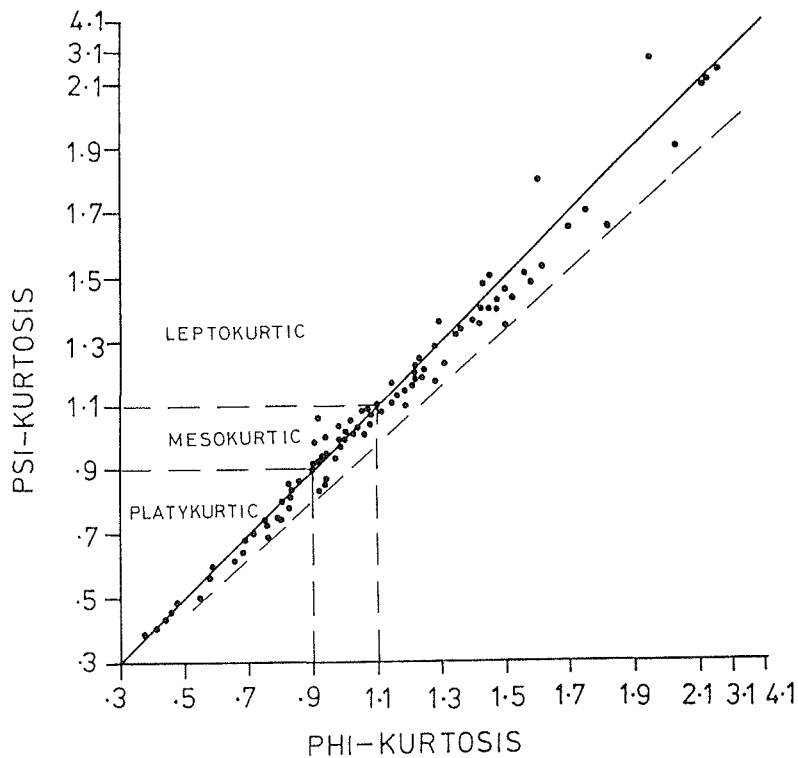


Fig. 22. Relationship between kurtosis of psi and phi distribution of shoreface sediments.

#### 4.4.2. Relief peels

Peeling is a commonly employed procedure to enhance the natural relief of sedimentary and biogenic structures within core samples. The cores (box and vibro) were laid horizontally on a firm surface, carefully opened, described, photographed and subsampled for grain size analysis. The sample surface was smoothed prior to applying the polyester resin. Two types of peeling techniques, dry and wet, were employed. All vibrocore samples were wet-peeled.

In the case of dry peeling, the boxcore samples were oven-dried at about 100°C for 12-24 hours. A 100:1 mixture ratio by weight of Araldite CY 221 resin and a HY 905 hardener, both products of CIBA-GEIGY GmbH, 7867 Wehr/Baden, Germany, was thinly and evenly poured onto the hot, smoothed sample surface. After a few hours of penetration, cooling and

hardening of the resin, the peel was extracted from the core. Information pertinent to core orientation and identification were inscribed on the resined surface, bearing in mind that the orientation of the peel is  $180^{\circ}$  out-of-phase with the latter. The peeled surface is subsequently carefully flushed with a water hose, left to dry, and then safely stored.

The wet peeling procedure was identical to the above, except that the resin mixture (100:2 part by weight of BÜFA P67 polyester and benzoyl-peroxide hardner, both products of BÜSING and FASCH GmbH, 2900 Oldenburg, Germany) was applied at room temperature. Where necessary, the resined surface of core samples was reinforced by one of two means. One approach involved glueing an overlapping plastic gauze at the surface, and this was typically the case for the vibrocore samples. A preferable and more effective alternative, typically employed for the boxcore samples, entailed laying the resined surface in an aluminium foil smeared with a few cm thick mixture of BÜFE P67 polyester and methylketonperoxide (MEKP) hardener to which a 1% cobalt catalysator is added. The latter two are products of VOSSCHEMIE GmbH, 2082 Uetersen, Germany.

## CHAPTER 5

### SHOREFACE SEDIMENT DISTRIBUTION, DYNAMICS AND BUDGET

#### 5.1 Introduction

The patterns of grain size statistics and distribution curves as well as bathymetric changes are presented in this chapter. These constitute the basis for the shoreface sediment dynamic modelling and zonation. As previously indicated in Section 4.4.1, sediment size characteristics are considered central to determining their provenance, palaeoflow and paleoenvironmental conditions.

A number of procedures for extracting the above information using grain size data exist in the literature. Although controversies exist on both the above procedures and the interpretations deduced (see e.g., McLAREN, 1981 and SAGOE and VISHER, 1982 for details of the trend of thoughts on the latter aspect), these procedures are nevertheless adopted in this study, in the hope that the results would clarify or add new dimensions to some of the current controversies. These procedures are briefly outlined below.

##### (a) Summary size statistics

The areal distribution pattern of summary size statistics such as mean, sorting, skewness and kurtosis (e.g., VALIA and CAMERON, 1977) is the most traditional sedimentological approach to environmental studies. It therefore merits no further discussion, except to state that sophisticated statistics are increasingly being applied to resolve spatial "trends" from "noise" in the data set (e.g., CHANNON and HAMILTON, 1976; CHAKRABARTI, 1977).

##### (b) Grain-size class fraction

Some authors (e.g., LIU and ZARILLO, 1987) utilize grain-size class fractions as textural tracers, much in the same

manner as modal sizes employed by CURRAY (1960) and DIAS and NEAL (1989). Not only are summary size statistics of polymodal sediments spurious, their unimodal counterparts are objectionable on the grounds that these represent an averaging process. As such, they may underscore and mask differences in response patterns of the individual size classes to a given hydrodynamic condition.

**(c) Bivariate and ternary diagram**

Representation of grain size statistics, sediment types or components (factors) of multivariate analyses in bivariate or ternary diagrams is a common routine among sedimentologists. To this category of bivariate plots belongs the C-M diagram of PASSEGA (1957, 1964). Perhaps with the exception of the latter, KLOVAN (1966) notes that the procedure used to delimit the different depositional environment domains in bivariate plots (arbitrary drawing of curves through data set) such as those presented by FRIEDMAN (1967) has no physical basis. In other words, environmental distinction is only feasible because of pre-knowledge of sample provenance.

The poor performance in applying a given empirical scatter plot to identify samples from other localities is amply documented in the literature. ROYSE (1968) considers the inaccuracies in environmental distinction from such empirical scatter plots to relate to the variable positions of their boundaries, these being a function of fluctuation in the flow transport competency, mixing of samples of diverse origin and data based on a poor quality analytical technique.

**(d) Grain-size distribution curve shape**

Shape characteristics of grain size distribution curves have been advocated as a strong tool in environmental reconstruction (e.g. , SINDOWSKI, 1957 ; TANNER, 1958, 1964; SPENCER, 1963; VISHER, 1969; MIDDLETON, 1976; BEIN and SASS,

1978; GREENWOOD, 1978). TANNER (1964) has also expressed reservations, but in a different sense from LUI and ZARILLO (1987), on the use of summary size statistics in environmental studies.

Indeed, like all the other authors, TANNER considers that an evaluation of the shape characteristics of grain size distribution curves may provide information regarding the nature, evolution and modification of sediment size distribution. These are basic to understanding dynamic and depositional processes in modern and ancient environments. He concluded that the non-consideration of curve shape characteristics may result in a situation where as much information is masked as are revealed by size statistics.

## 5.2 Sediment Distribution

### 5.2.1 Summary Sediment Size Statistics

Areal distribution patterns of summary sediment size statistics (mean, sorting, skewness and kurtosis) are generally considered to be a response to both their source characteristics and the energy conditions at deposition and / or during transportation (CADIGAN, 1961). While some authors stress the factor of source as exemplified by the proportional mixing model reported by FOLK and WARD (1957), MCKINNEY and FRIEDMAN (1970), CRONAN (1972), FLEMMING (1977), others are in favour of hydraulic energy, as evidenced by size-sorting models of SAHU (1964), DUANE (1964), FRIEDMAN (1967), SWIFT et al. (1972b), STAPOR and TANNER (1975), McLAREN (1981) and McLAREN and BOWLES (1985).

For the sake of clarity, comments on size statistical patterns in subsequent sections will be preceded by a brief evaluation of their mathematical relationship and flow regime expression. Verbal description of statistical data, except otherwise stated, follows that of FOLK and WARD (1957).

## 5.2.1.1 Mean

The mean of a particle size (or settling velocity) distribution expresses its mathematical average value. As earlier stated in Section 4.4.1, the first moment or mean is highly correlated with the percentile median. As a matter of fact, differences between both values are generally less than 5% or  $1/20 \phi$ , thus are too small to introduce errors in the interpretation of the results. The employment of percentile median, which for simplicity will be referred to as graphic mean, facilitates intercomparisons with the other percentile statistics in scatter plots. Furthermore, all other percentile measures are referred to and expressed as graphic measures in the following account.

The graphic mean is derived thus:

$$M_z = \frac{\phi_{16} + \phi_{50} + \phi_{84}}{3}$$

where e.g.,  $\phi_{16}$  = phi value of the 16th percentile

phi	mm	cm/s	Wentworth size class
-1	2.00	28	
-0.75	1.68	24	
-0.50	1.41	21	VERY COARSE SAND
-0.25	1.19	18	
0.00	1.00	15	
0.25	0.84	13	
0.50	0.70	10	COARSE SAND
0.75	0.60	9	
1.00	0.50	8	
1.25	0.42	6	
1.50	0.35	5	MEDIUM SAND
1.75	0.30	4	
2.00	0.25	3	
2.25	0.21	2.4	
2.50	0.18	2.0	FINE SAND
2.75	0.15	1.7	
3.00	0.13	1.1	
3.25	0.11	0.8	
3.50	0.09	0.6	VERY FINE SAND
3.75	0.07	0.4	
4.00	0.06	0.3	

The scaling and verbal description of mean sand-size particles are given above with their phi, mm, and settling velocities (cm/s) equivalents. The latter values are from GIBBS et al. (1971) and relate to diameter of glass spheres settling at 20°C in distilled water.

Given an equilibrium condition, the spatial variation in mean grain size should correlate well with the energy level of a depositional environment. This would imply a fining of sediments with a diminishing flow energy. A contrary trend can only relate to a factor of sediment source which may be, relative to the depocenter, local or remote in origin.

#### Mean sedimentation diameter

The phi mean-size distribution of surficial sediments on the shoreface (Fig. 23) is characterised by a centrally situated, 1.6-3.2 km wide, WNW-ESE aligned band of mostly medium to coarse grained sands (0.5-2.0 phi). This coarse-grained central band clearly correlates in alignment and extent with the shoreface-connected ridge bathymetry. It is flanked on either side by fine-grained sands showing a progressive seaward and shoreward fining pattern.

However, close to the shoreline and at the main tidal inlet-diametric upper shoreface margins, sediments again show a coarsening tendency. Coarsening in the former case is considered to represent a natural response to wave-breaking and winnowing of fines, whereas the latter reflects actual ebb current deposition of sediments scoured from the inlet floor.

Based on the above areal distribution pattern, a tripartite zonation of the shoreface is henceforth adopted, namely, an upper, a central and a lower shoreface subenvironment. The

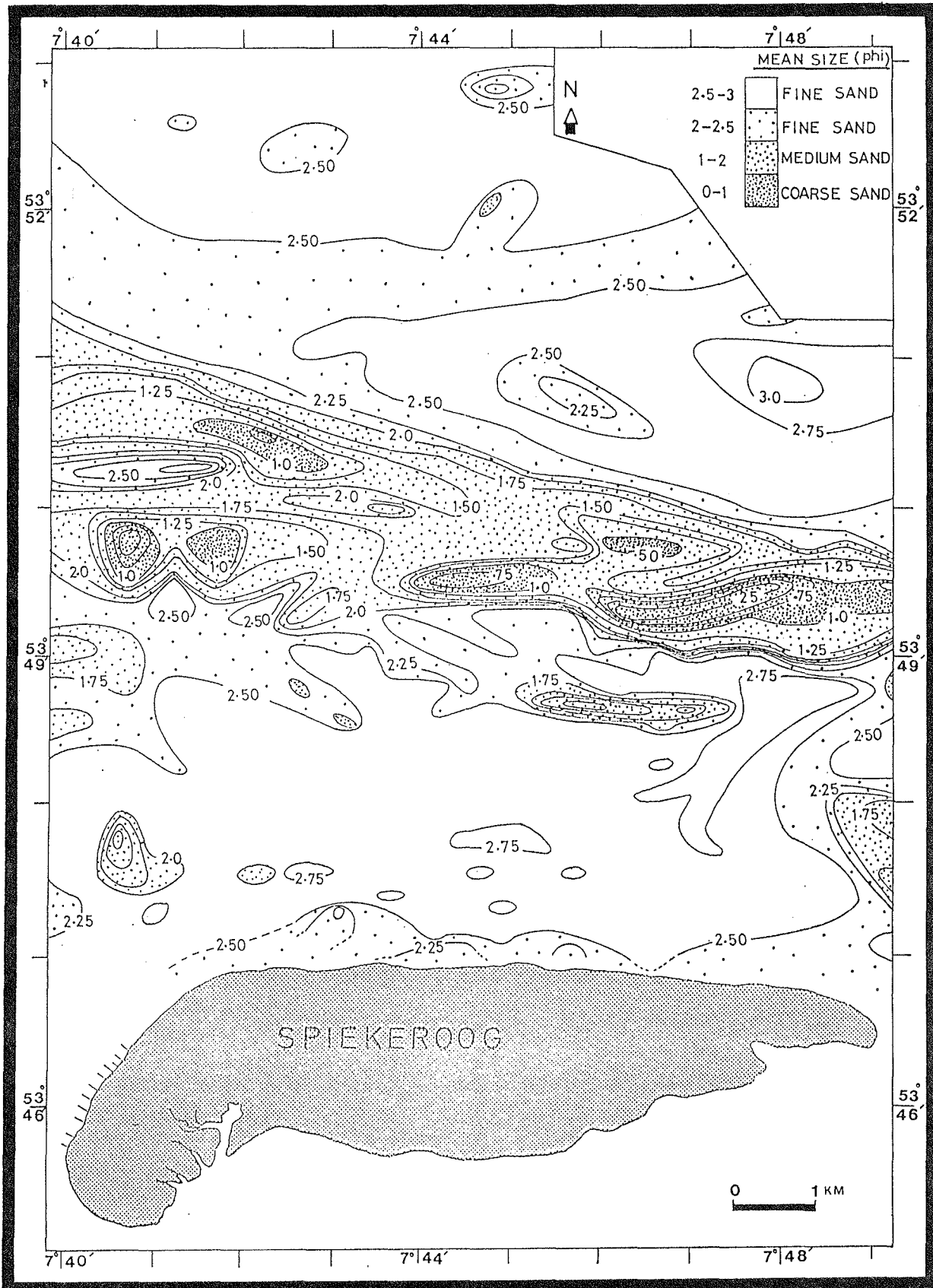


Fig. 23. Shoreface distribution of sediment mean sedimentation diameter (phi).

progressive seaward fining of sands from the coarse-grained central shoreface subenvironment is most typical of the western flank of the lower shoreface. The eastern flank, on the other hand, is characterized by a westward wedging tongue of 2.5-3 phi sediments embedded within a 2-2.5 phi sediment band. Because the finest patch of the fine sediment tongue occurs at a distal margin, which is diametric to the main inlet axis, its origin is accordingly associated with inlet ebb-flow fallouts. This implies that the coarser central shoreface band is "overpassed".

If the postulated origin of the tongue of fines is correct, as against an alternate view of being an artifact of dredging in this vicinity, then a similar pattern must be evident at comparable locations along the Frisian shoreface. Indeed, a presentation of sediment size charts of the Langeoog shoreface (west of Spiekeroog) by ZIELKE and FLEMMING (1991) supports the above contention.

Other important features worthy of note in Fig. 23 are :

(a) The coarse-grained (0-1 phi) sands composing the central shoreface are coastwise in trend but areally discontinuous; moreover, they are more abundant at the proximal (ESE or shallower water) end than at the distal (WNW or deeper water) counterpart, thus suggesting a proximal source of supply.

(b) Apart from the narrowness of the central shoreface band at the proximal end, grain size contours tend to be steeper than at the distal end, thus indicating better sortedness at the proximal end. This latter information is illuminating because it would suggest that the deposition of the central shoreface sediments must have been associated with very strong flow conditions culminating in proximally-derived "foreign" materials progressively diluting "native" sediments distally.

(c) The grain size contours at the central-lower shoreface transition are smooth while their central-upper shoreface counterpart are serrated with southeasterly protrusions. The 2.25 and 2.5 phi contours at the western flank best illustrate the latter.

The above protrusions conform to the predominantly southeasterly fair-weather flood-current direction in deeper water which, in shallower depth, veers coastwise (cf. Fig. 11f). By contrast, the ebb-current direction is conformable with the grain size contour trend of the central-lower shoreface transition.

On the basis of the above observations, it can therefore be concluded that the substrate sediments are responding to both periodic and episodic flow patterns.

#### Mean settling velocity

The mean settling velocity distribution presented in Fig. 24 depicts a pattern which is more conspicuous but reminiscent of that of the mean sedimentation diameter (phi) discussed earlier. Specifically, the central shoreface subenvironment is characterized by higher mean settling velocity (3-15 cm/s) sediments and is bounded on either side by lower mean settling velocity (< 3 cm/s) sediments of the upper and lower shoreface subenvironments.



Fig. 24. Shoreface distribution of sediment mean settling velocity (cm/s).

## 5.2.1.2 Sorting

Sorting describes the spread of a distribution from the mean. The graphical computation of this measure and its verbal description are given below:

$$= \frac{\phi_{84} - \phi_{16}}{4} + \frac{\phi_{95} - \phi_5}{6.6}$$

where e.g.,  $\phi_{16}$  = phi value  
of the 16th percentile

< 0.35	very well sorted
0.35-0.50	well sorted
0.50-0.70	moderately well sorted
0.70-1.00	moderately sorted
1.00-2.00	poorly sorted
2.00-4.00	very poorly sorted
> 4.00	extremely poorly sorted

From the view-point of fluid dynamics, SAHU (1964) considers sorting of a sediment distribution to relate to the fluctuations in the kinetic energy (velocity) conditions of a depositing agent about its average velocity. The textural imprint of the fluctuation is particularly obvious in the case of untruncated (well spread) distributions, in which case the sediment source is an important factor.

Distribution of sediment sorting is shown in Fig. 25. With the exception of discontinuous patches of poorly to well sorted sediments concentrated mostly along the axis of the central shoreface and the ebb-delta margins, the sediments are mostly very well sorted. The outline of the shoreface-connected ridge morphology is best defined by the 0.25 phi sorting contour. The very good sorting of the lower and upper shoreface sands suggests that the average flow energy suffices in segregating

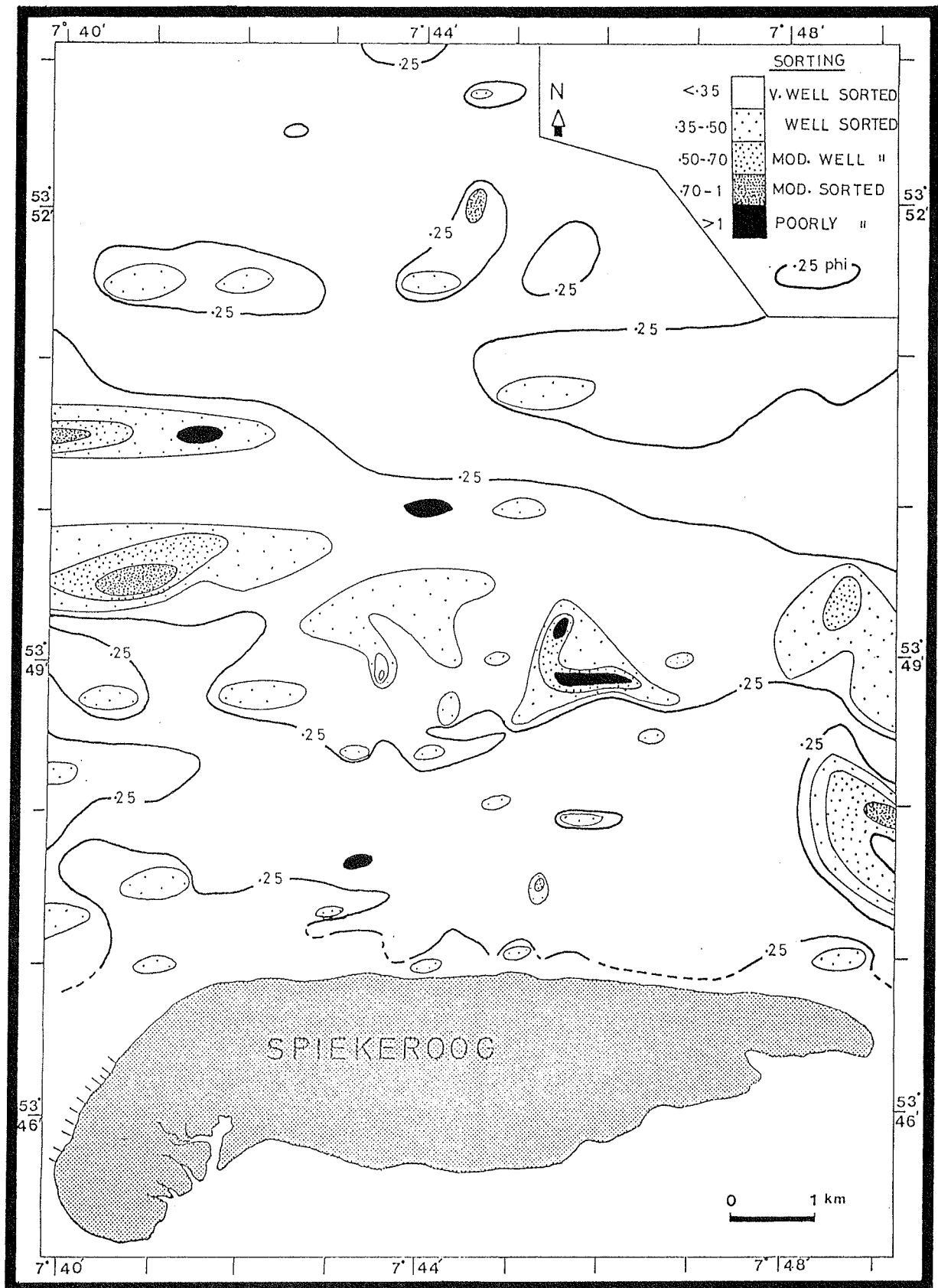


Fig. 25. Shoreface distribution of sediment sorting.

the sediments into a very narrow size range. By contrast, the relatively poorer sorting of the central shoreface sands must reflect textural disequilibrium with the average flow condition. The disequilibrium condition may be a consequence of influx of sediments (specifically coarser grains) from sources other than the shoreface region. The alternate view that the poorer sorting of the central shoreface sands is a consequence of diabathic sediment transport between the upper and lower shoreface zones is not supported by the mean grain size trends.

A feature of interest, however, is the lesser sorting of sediments in the proximal zone of each shoreface subenvironment as compared with the distal zone. This alternating cross-shore sorting pattern is examined in greater detail in Section 5.4.

#### 5.2.1.3. Skewness

Skewness is a measure of the asymmetry of a frequency distribution. The inclusive graphic skewness ( $SK_I$ ) is derived and described as shown below :

$$SK_I = \frac{\phi_{84} + \phi_{16} - 2(\phi_{50})}{2(\phi_{84} + \phi_{16})} + \frac{\phi_{95} + \phi_5 - 2(\phi_{50})}{2(\phi_{95} - \phi_5)}$$

where e.g.,  $\phi_{16}$  = phi value  
of the 16th percentile

-1.00 to -0.30	very negative skewed
-0.30 " -0.10	negative skewed
-0.10 " +0.10	nearly symmetric
+0.10 " +0.30	positive skewed
+0.30 " +1.00	very positive skewed

Positively- and negatively-skewed distributions have their mean values respectively on the finer and coarser sides of the median of a frequency curve, whereas a symmetrical distribution has an identical value of mean and median. Skewness can also be viewed as a function of sorting, in which case a distribution is skewed toward the poorer sorted half of a grain size frequency curve (CADIGAN, 1961). In relation to flow condition,

SAHU (1964) suggested that for an untruncated sediment distribution, skewness parameters should reflect the intensity, fluctuation and duration of flow relative to the normal condition. While the above interpretations of skewness seem quite simple, McLAREN (1981) and CLARK (1981) have shown that the evolution and sediment transport implications of this parameter can be controversial. Because of its significance in environmental reconstruction, and in order to rationally interpret the obtained results, a preview and clarification relating to the evolution of skewness signs are desirable.

### Models of skewness sign evolution

Essentially, skewness sign of a given size distribution would change through either selective "addition" or "extraction" of size classes in sufficient amounts. These modification types are respectively synonymous with the mixing and filtering / truncation processes of some authors.

As shown in Fig. 26, two types of mixing processes, "miscible" and "immiscible" can be distinguished. In the former (Case 1 a & b), the fine and coarse sediments added (stippled blocks) have size-classes which are represented within a native sediment population (unshaded blocks). For simplicity, the latter is considered to be initially symmetrically distributed. The resulting skewness signs in Case 1a and 1b are respectively negative and positive.

Cases 2-4 a and b are all identical in being immiscibly mixed, i.e., the added size-classes are not contained within the native population. Cases 2 and 3 indicate that skewness sign is also sensitive to the proportion of size classes (a function of sediment supply) added to the native sediments. Cases 3 a and 3 b should be respectively distinguishable from Case 1a and 1b based on their finer (coarser in Case 3 b) mean and mode as well as poorer sorting.

Modification of skewness due to material extraction from the size distribution of a native population is represented by

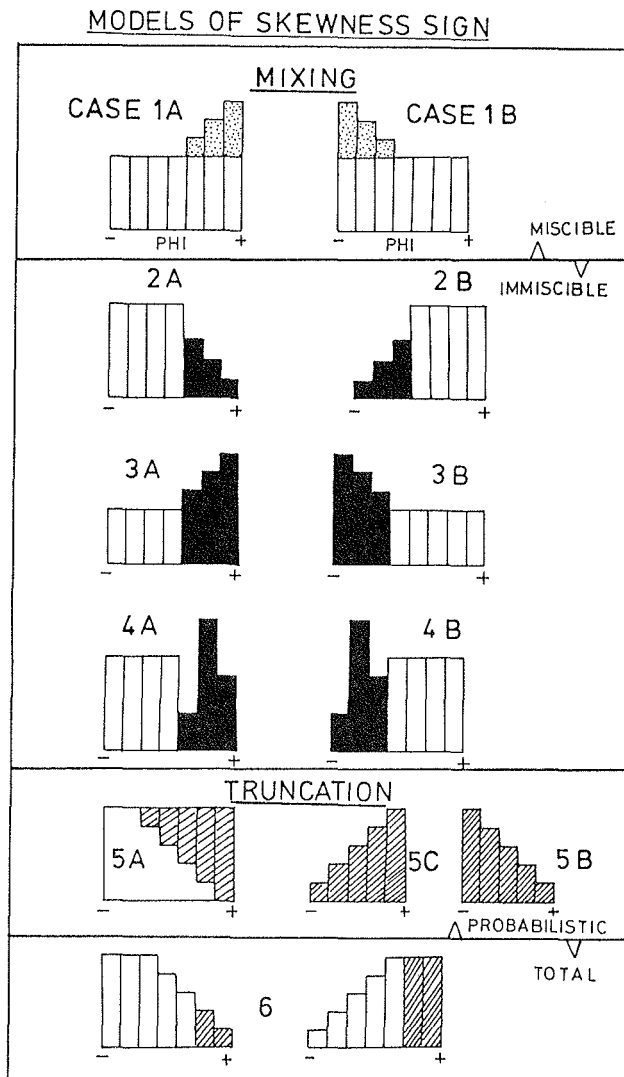


Fig. 26 Models of skewness sign evolution.

Case 5 (probability-based filtering) and Case 6 (total truncation) respectively. In the former, the lag (5a or the unhatched blocks) following extraction would generally be more positively skewed than the native sediments, whereas the extracted size classes (hatched blocks), assuming not subjected to mixing processes on deposition, would be negatively or positively skewed if respectively deposited totally (5c) or selectively (5b) (McLAREN, 1981).

By contrast, the lag (unhatched blocks) aftermath total truncation in Case 6 could be negatively, positively or even symmetrically skewed depending on the initial skewness of the native sediments and the extent (range of size classes) truncated. The latter factors, neglecting mixing processes, would determine the skewness sign of a totally deposited, truncated population. Selectively deposited counterpart will be prone to positive skewness as in Case 5b.

Finally, it should be stated that the spatial changes in skewness predicted are relative and may, in some instances, be strongly influenced by the initial grain size distribution.

#### Skewness distribution pattern

The skewness of the shoreface sediments for both phi and psi distribution based on FOLK and WARD's scaling showed an extremely erratic areal pattern (see Appendix C-1 for the former). However, on using a two-fold skewness scaling, i.e. positive and negative, a bathymetrically-related pattern emerged (Fig. 27).

Essentially, three coastwise alternating bands of positive and negative skewness are clearly recognizable. Furthermore, the proximal and distal zones of each of the three shoreface subenvironments are composed of a negative and a positive band, respectively.

Such a skewness zonation is reported for the first time from a shoreface environment. Its evolutionary process(es) may thus hold prospects for unravelling both steady and episodic sediment transport patterns and pathways in the study region. Since the latter is dealt with elaborately in Section 5.4, the ensuing account of skewness variation, which is based on the previously outlined model of skewness evolution (Fig. 26), is therefore still exploratory.

A cursory glance at Fig. 27 would suggest that the recurring skewness pattern within each of the shoreface

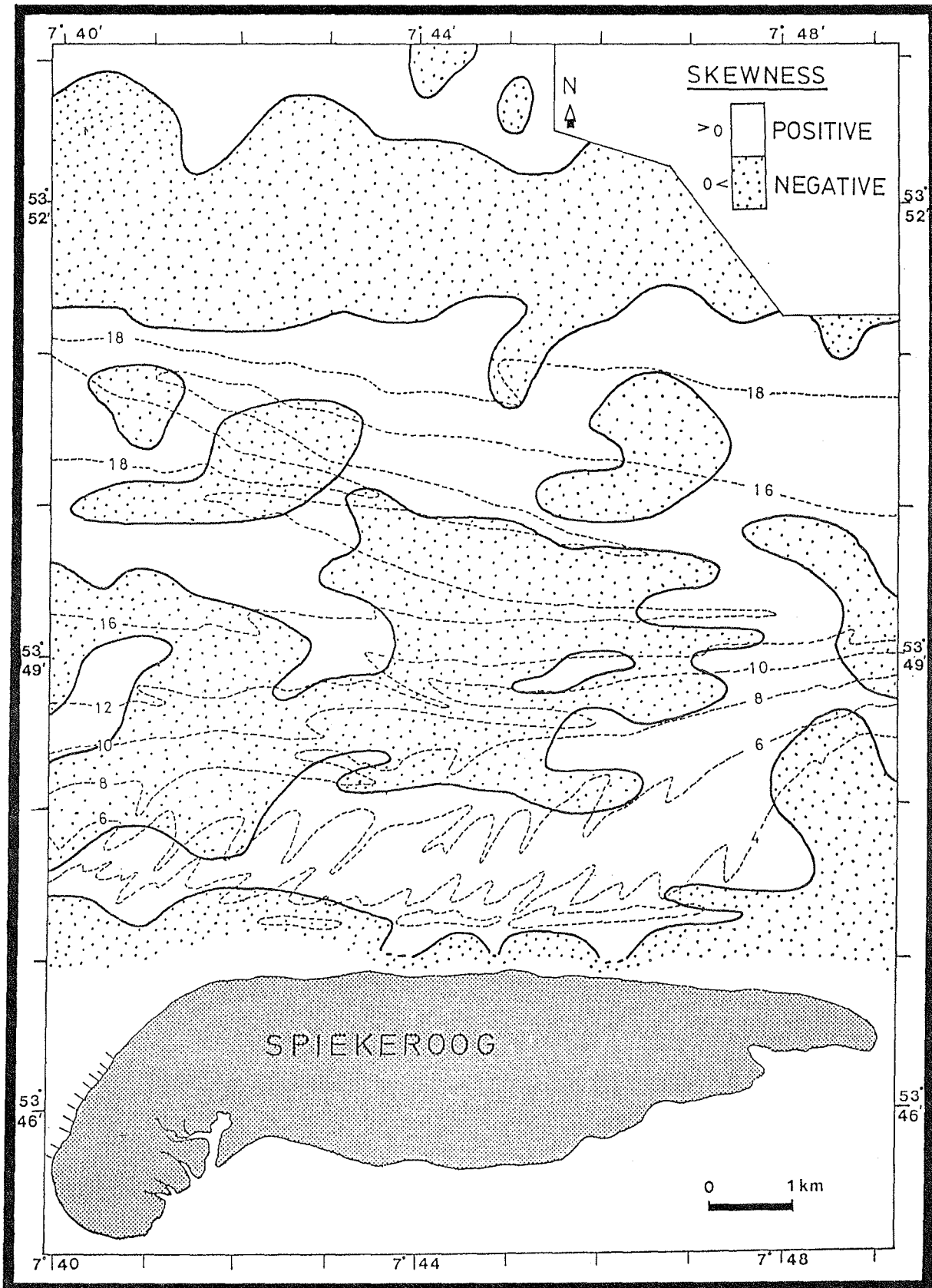


Fig. 27. Shoreface distribution of sediment skewness.

subenvironments cannot be a consequence of a similar process. The skewness pattern of the upper shoreface best fits a dual and continuous process of total truncation of the finer sizes of the beach-surf zone sediments by breaking waves leading to the observed lag of negative skewness (Case 6).

The truncated fines in suspension subsequently settle out and immiscibly mix (Case 2a) with the distal upper shoreface sands, endowing on these the observed positive skewness and slightly finer mean size. The slightly better sorting of the distal zone compared with the proximal counterpart probably implies either that the truncated sizes in suspension are very well sorted, and / or the fact that the proximal zone sediments have not fully attained textural equilibrium with the surf zone processes.

Following from SAHU's (1964) concept, the poorer sorting shown by the proximal sediments can be related to a greater fluctuation in the flow conditions, as would be typically expected in and landward of the surf zone of a dissipative beach system.

An alternate view of the upper shoreface skewness pattern involving a single sedimentary event is exemplified by Case 5 (see also McLAREN, 1981). It requires that the distal sands be derived through selective deposition (Case 5b) from a probabilistically-filtered source. The predicted positively skewed lag of the latter, however, contradicts the observation and hence is disregarded. Moreover, there is no logical reason in the study area for constraining changes in character of sediment distribution to a single sedimentary process.

The fact that the central shoreface sands are much coarser than their upper and lower shoreface counterparts suggests an origin other than the shoreface. Thus, skewness variation within this subenvironment can also not be viewed as a consequence of a single sedimentary event. The negatively-skewed, coarser and more poorly sorted proximal zone sediments are consistent with Case 2b and, to some extent, 4b immiscibly mixing processes. The skewness of the distal central shoreface

sands, on the other hand, may result from either Case 1b miscible mixing process (selectively deposited allochthonous coarse fraction source implied) or Case 2a (in which the finer fraction are selectively deposited from either a probabilistically winnowed allochthonous or proximal central shoreface source). From the point of view of a probably storm depositional mechanism of the central shoreface sands, Case 1b will result in a better sorted distal zone sediments than Case 2a, hence favoured.

Although the main source(s) of the central shoreface sands as a whole are at this stage not conclusively identified, the skewness and mean grain size considerations exclude the shoreface (in-situ) as a major contributor.

Finally, the evolution of the lower shoreface skewness zones, while appearing to incorporate elements of both the central and upper shoreface, is also unique. Specifically, the seabed effectiveness of waves in 18-22 m water depth is still appreciable. Under the above condition, preferential onshore transport of coarser fractions could cause a depletion of the latter in the distal lower shoreface - a variant of Case 6 and 5 - if conditions permit a complete or a probabilistic winnowing, respectively, of the coarse fraction. The winnowed sediment population in both cases will also be negatively skewed. Mixing (Case 2b or 1a) of the totally deposited, winnowed population with the proximal zone sediments will give rise to a negatively skewed pattern observed in the latter zone. The distal sands, representing a lag in this case, will be positively skewed and finer. Because the latter trend is indeed observed implies that the above process is quite feasible. It is however doubtful if grain sizes sufficiently coarse exist on the distal zone to form a distinct size range if incorporated in the proximal sediments as in Case 2b. On the otherhand, Case 1a will not result in a coarser proximal zone sediments.

Reverse (seaward) transport of coarse sands from the proximal zone (an invariant of Case 5 or 6) resulting from

amplitude modulation of the shoaling waves (SHI and LARSEN, 1984) could also cause the distal zone sediments to be positively skewed (Case 1 b) if the winnowed coarse fraction is selectively deposited. However, in this circumstance, the proximal sands, as a lag, should be positively skewed, better sorted and finer as the distal counterpart. This is the opposite of the observation and invariably cast doubts on the significance of the above amplitude-modulated or long wave size-sorting mechanism. A more plausible alternative is exemplified by Case 2b, in which the proximal lower shoreface is a beneficiary, as against its distal counterpart, of coarse fraction settling out during the depositional process of allochthonously derived central shoreface sands.

#### 5.2.1.4 Kurtosis

In a strict geometrical-statistical sense, BAKER (1967) considers kurtosis ( $K_G$ ) as a measure of peakedness of a frequency curve relative to a normal distribution of same mean and sorting. Any deviation from this would render any curve-shape connotation of this statistical parameter dubious. The parameter is however considered useful in partially expressing the deviation of a distribution curve from normality.

A simplistic view of graphic kurtosis is that it relates sorting within the central 90% to that of the central 50% of a frequency curve. This measure is derived and described thus:

$$K_G = \frac{(\phi_{95} - \phi_5)}{2.44 (\phi_{75} - \phi_{25})}$$

where e.g.,  $\phi_{95}$  = phi value of the 95th percentile

< 0.67	very platykurtic
0.67 - 0.90	platykurtic
0.90 - 1.11	mesokurtic
1.11 - 1.50	leptokurtic
1.50 - 3.00	very leptokurtic
> 3.00	extremely leptokurtic

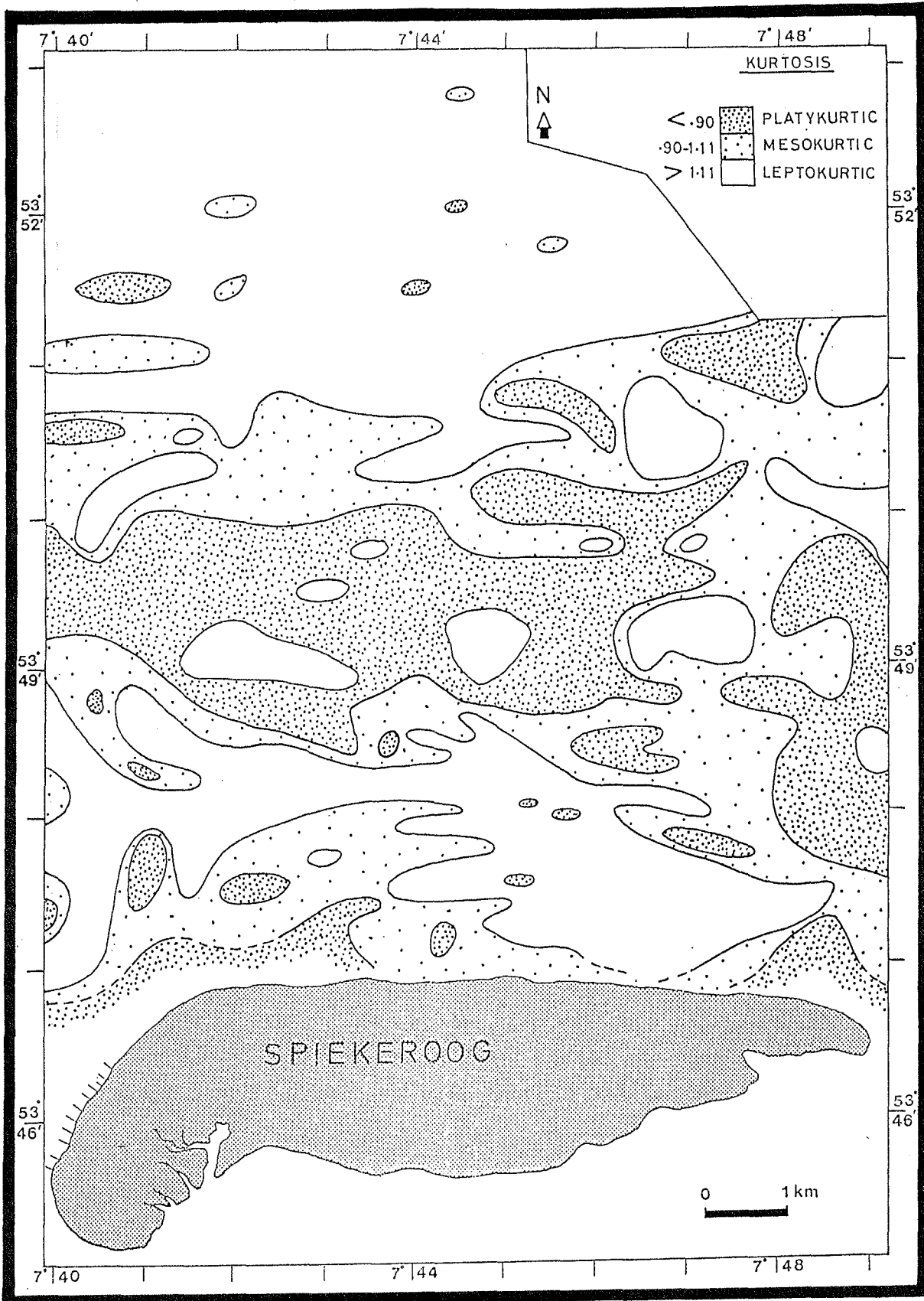


Fig. 28. Shoreface distribution of sediment kurtosis.

In relation to sorting, CADIGAN (1961) noted that a high value of kurtosis is likely to be associated with a well-sorted distribution, and vice versa. From a fluid dynamic point of view, SAHU (1964) notes that a leptokurtic distribution should result from a flow condition in which the fluctuation in velocity does not exceed 50% of its average velocity for a prolonged period of time.

In order to enhance clarity, a three-fold kurtosis scaling, based on FOLK and WARD (1957), has been employed for the phi-distribution of shoreface sediments presented in Fig. 28. Each of the three shoreface subenvironments reveal a particular kurtosis pattern. The lower shoreface is almost exclusively leptokurtic (high kurtosis values). The central shoreface is composed largely of a platykurtic (lower kurtosis value) band which correlates well in extent and orientation with the shoreface-connected ridge bathymetry. The platykurtic band is fringed longitudinally on either side by mesokurtic sands. The upper shoreface sands in the distal zone are leptokurtic (implying better sorting) as against mesokurtic to leptokurtic on the proximal counterpart.

The above distribution patterns corroborate the observations of CADIGAN (1961). The central shoreface sands, by virtue of their relatively poorer sorting, are typified by low kurtosis values (platykurtic proximally and mesokurtic distally). Although both upper and lower shoreface sands are very-well sorted, the latter is slightly superior and hence depicts higher kurtosis values. Finally, the almost exclusive occurrence of low kurtosis values within the central shoreface further supports the notion of an allochthonous origin of these sediments.

### 5.2.2 Sedimentation Diameter ( $\phi$ ) and Settling Velocity (cm/s) Class Fractions

The distribution patterns of sedimentation size class fractions at a whole, half and quarter  $\phi$  intervals as well as four settling velocity class fractions (1-1.5, 1.5-2, 2-2.5, > 2.5 cm/s) are described in subsequent sections. The velocity class fractions roughly correspond to quarter  $\phi$  intervals of fine sand, and may thus be designated as finer, medium, coarser and very coarse fine sand respectively.

Although the distribution patterns of all of the above size fractions correlate well with the earlier defined (based on summary statistics) tripartite zonation of the shoreface, some unique differences are, nevertheless, also evident.

Besides the distribution of whole  $\phi$  interval size fractions and a few other very instructive counterparts presented and discussed below, others are given in Appendix D and will only be briefly commented upon here.

#### 5.2.2.1 Whole- $\phi$ Size Classes

The distribution pattern of the 0-1  $\phi$  size fraction (coarse sand) given in Fig. 29 shows a marked depletion in the upper and lower shoreface and rarely compose 1% by weight of their sediments. This size fraction, by contrast, is well represented in the central shoreface sands where over 70% by weight is observed toward the proximal southeasterly end.

Besides the 1% contour defining the central shoreface margins, no other occurrence shows a longitudinal continuity over the entire central shoreface. This would suggest that the

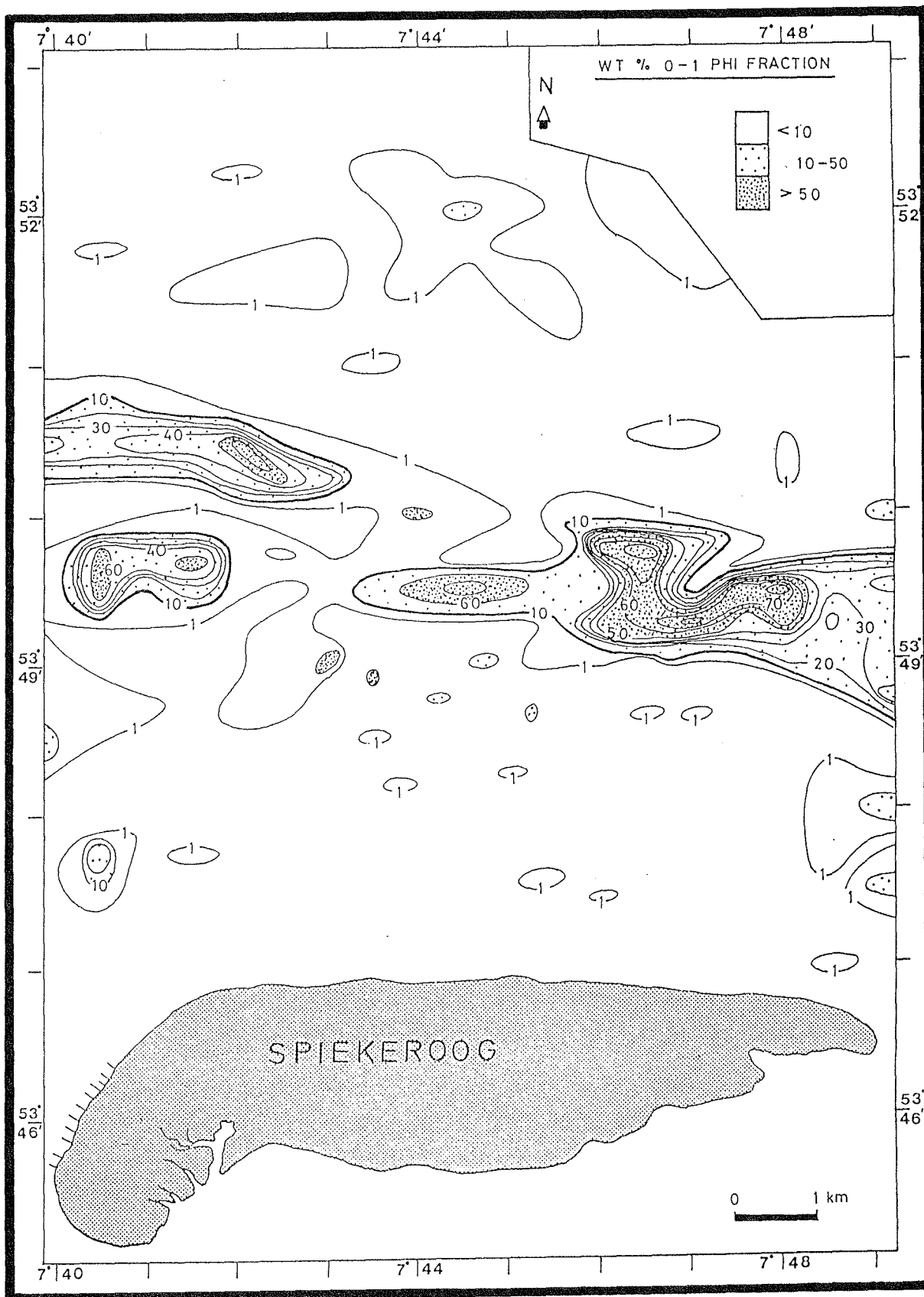


Fig. 29. Shoreface distribution of wt.-% of coarse sand (1-0 phi).

coarse sands were discretely deposited. Areally, the > 1% by weight 0-1 phi sands blanket about 25% of the shoreface area. Somewhat perplexing, however, is the preferential confinement of this size fraction to the intermediate water depth of the shoreface.

A conjecture that the coarse sands are concentrates of wave bottom activity on the shoreface is fraught with problems. For instance, while waves may preferentially cause onshore bottom transport of coarse materials from the lower shoreface or even greater depths to the central shoreface, a similarly selective wave transport of coarse sands from the upper shoreface offshore is most unlikely.

This being the case, the abrupt ceasure of onshore wave transport of coarse sands at intermediate depths becomes questionable, given the increasing wave transport efficiency with shoaling. A further shortcoming of the above conjecture relates to the out-of-phase relationship between the WNW-ESE orientation of the central shoreface sand deposit and the dominant NE-SW wave crestline trend.

The distribution pattern of 1-2 phi size fraction (medium sand) shown in Fig. 30 follows a similar pattern as the coarse sand. The upper and lower shoreface sands, with the exception of a few isolated patches offshore and close to the shoreline, contain only low proportions (< 10 % by weight) of medium sand. In contrast, the central shoreface is characterized by a longitudinally continuous belt of medium sand, reaching > 50% by weight

The modal size fraction of most of the central shoreface is thus composed of medium sand. Noteworthy, however, are most of the seemingly isolated patches of high proportions of medium sands at the ebb-delta margins of the upper shoreface. This observation would suggest a genetic affiliation of the central shoreface sands to an inlet source.

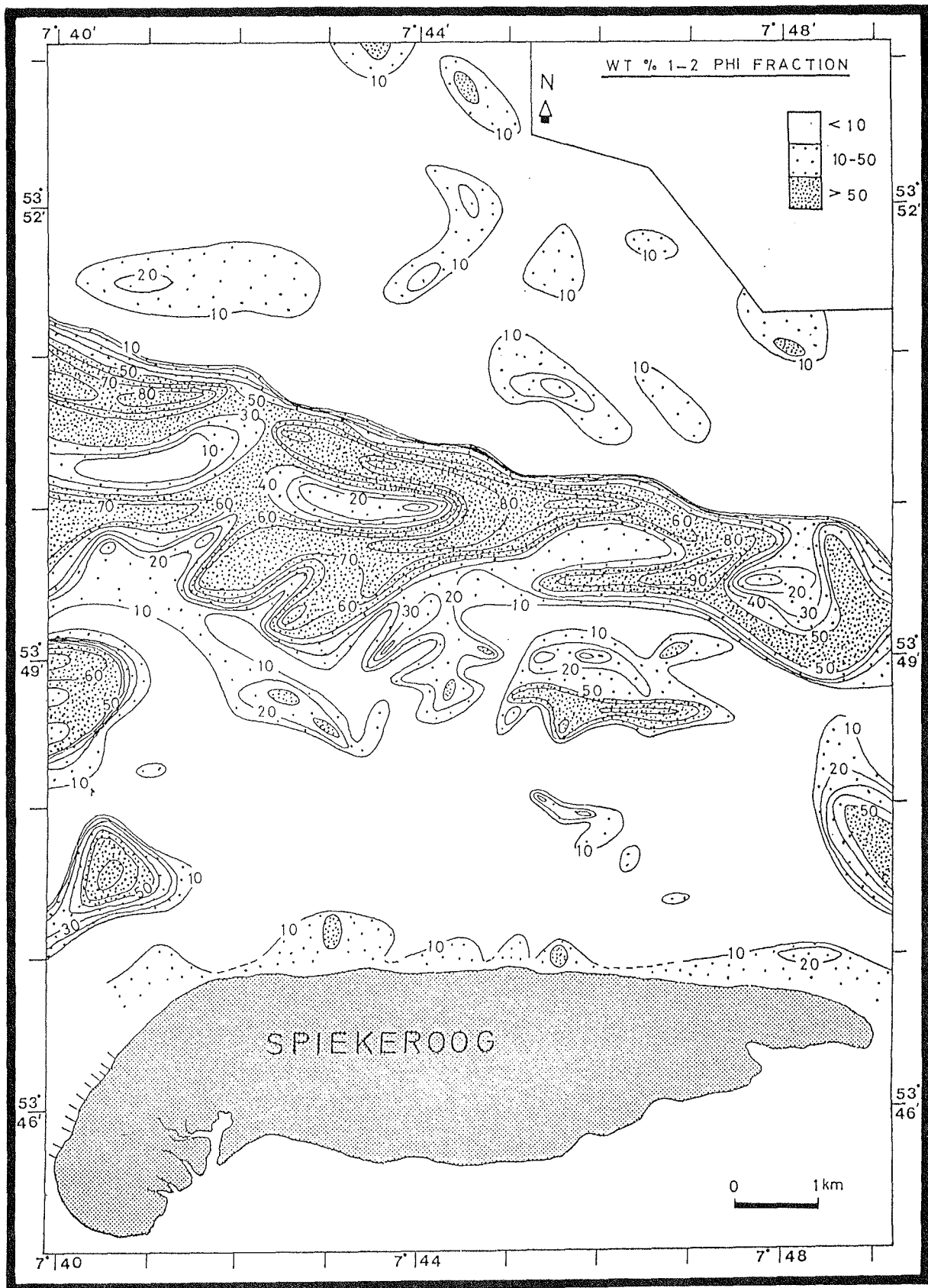


Fig. 30. Shoreface distribution of wt.-% of medium sand (1-2 phi).

The 2-3 phi fraction (fine sand) distribution pattern given in Fig. 31 is a corollary of the coarse and medium sand counterpart. The tripartite shoreface zonation is still well defined. However, in this case, the central shoreface subenvironment depicts a subordinate fine sand component; the latter component constitutes the modal sand fraction on both the upper and lower shoreface subenvironments, reaching concentrations of over 90% by weight.

The 3-4 phi (very fine sand) size fraction (Fig. 32) is most depleted on the central shoreface subenvironment (weight % < 1), with broad areas on the upper and lower shoreface depicting weight % ranging between 1 and 10.

A striking feature of the 3-4 phi size fraction is the tongue of very fine sand on the lower shoreface subenvironment. Its location with respect to the main tidal inlet clearly suggests that it represents accumulation of inlet ebb-flow fallouts.

#### 5.2.2.2 Half-Phi Size Classes

The half-phi shoreface sediment size classes charted are those of 1.5-2, 2-2.5, 2.5-3 and 3-3.5 phi. While their distribution patterns are obviously similar to those of the whole-phi size classes, a somewhat higher resolution in the local trends is evident.

The weight % of the 1.5-2 size fraction (Appendix D-1) shows that the half-phi modal size fractions of the central shoreface sands must be in the 1.5-2.5 phi range. This is most evident by the lower weight % of 1.5-2 phi fraction relative to the 1-2 phi counterpart, particularly at the southeasterly flank.

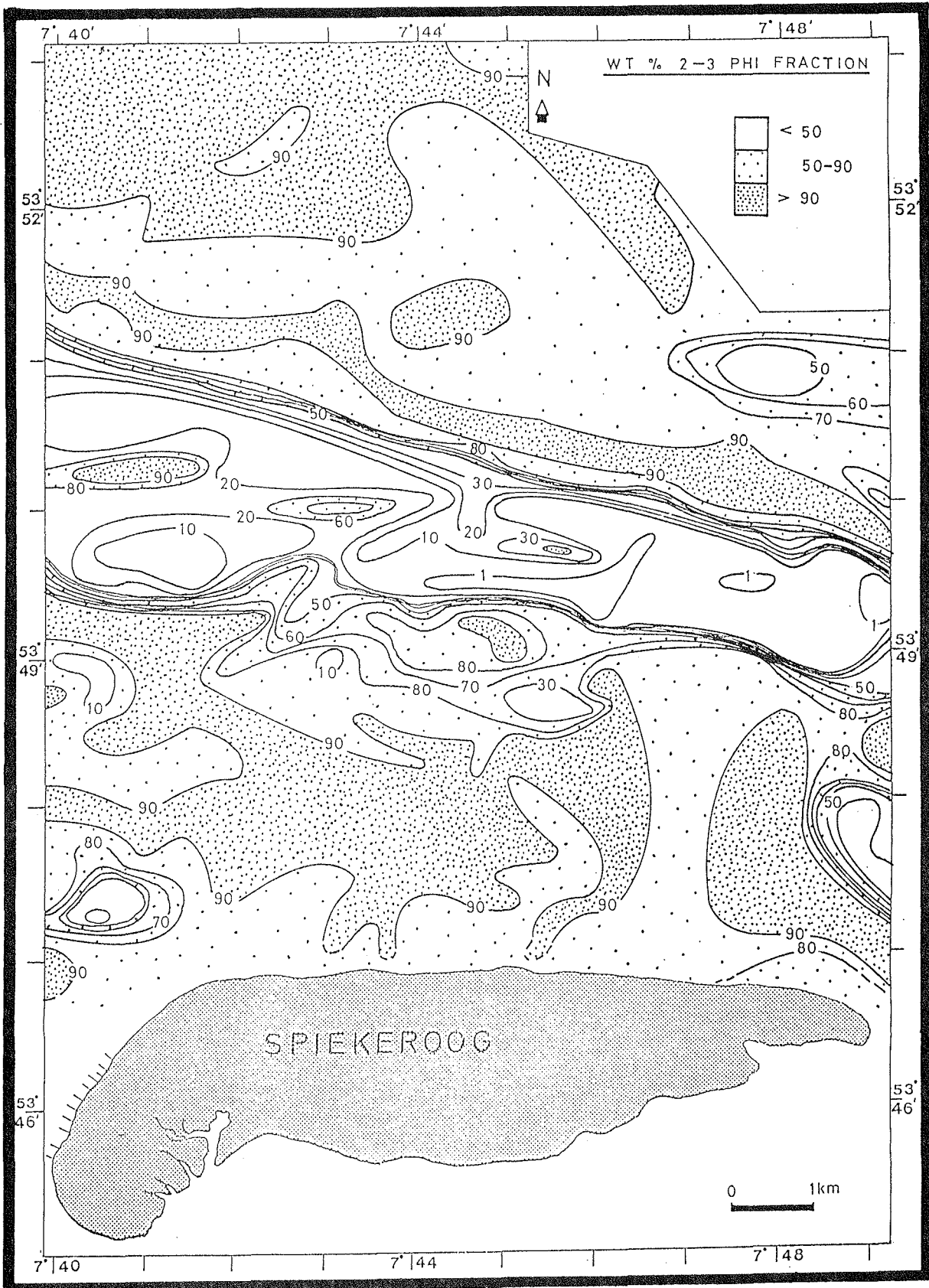


Fig. 31. Shoreface distribution of wt.-% of fine sand (2-3 phi).

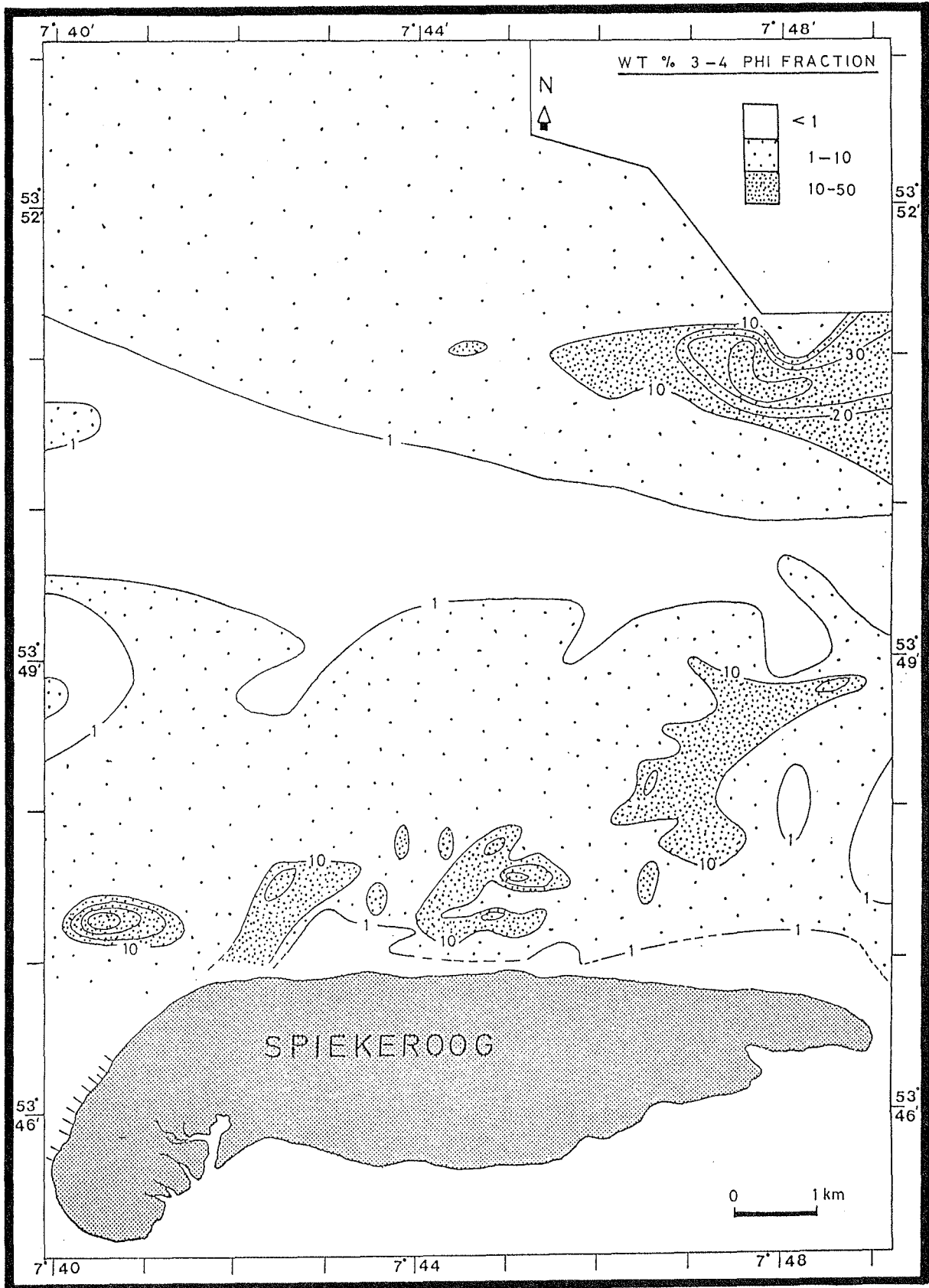


Fig. 32. Shoreface distribution of wt.-% very fine sand (3-4) phi.

Similarly, the whole-phi modal size class of the upper and lower shoreface sands of 2-3 phi is seen to shift to the finer end, i.e., 2.5-3 phi (Fig. 33). The latter trend also reveals the slightly coarser nature of the lower shoreface sands in comparison to their upper shoreface counterpart.

The 2-2.5 phi fraction (Appendix D-2) occurs in subordinate proportion relative to 2.5-3 phi on both the lower and upper shoreface. The 3-3.5 phi size class distribution pattern (Appendix D-3) is highly identical to the 3-4 phi counterpart as evidenced by their weight % contours and the areal extent of the lower shoreface tongue of fines. In essence, this indicates that the bulk of the very fine sand fraction is concentrated in the 3-3.5 phi size interval.

#### 5.2.2.3 Quarter-Phi Size Classes

As for the whole- and half-phi fractions, the quarter-phi counterparts all conform to the tripartite shoreface zonation. Grain size contrasts between the lower and upper shoreface sands are best illustrated by the 2.25-2.5 phi fraction distribution pattern (Fig. 34). Whereas this fraction is broadly distributed on the lower shoreface, it occurs sparsely on the upper shoreface.

The 2.5-2.75 phi fraction pattern (Appendix D-4), in contrast to the 2.25-2.5 phi counterpart, shows comparable weight frequencies on both the upper and lower shoreface. The 2.75-3 phi fraction distribution pattern (Fig. 35), on the other hand, is a corollary of the 2.25-2.5 phi counterpart, being broadly represented on the upper shoreface and sparsely represented on the lower shoreface.

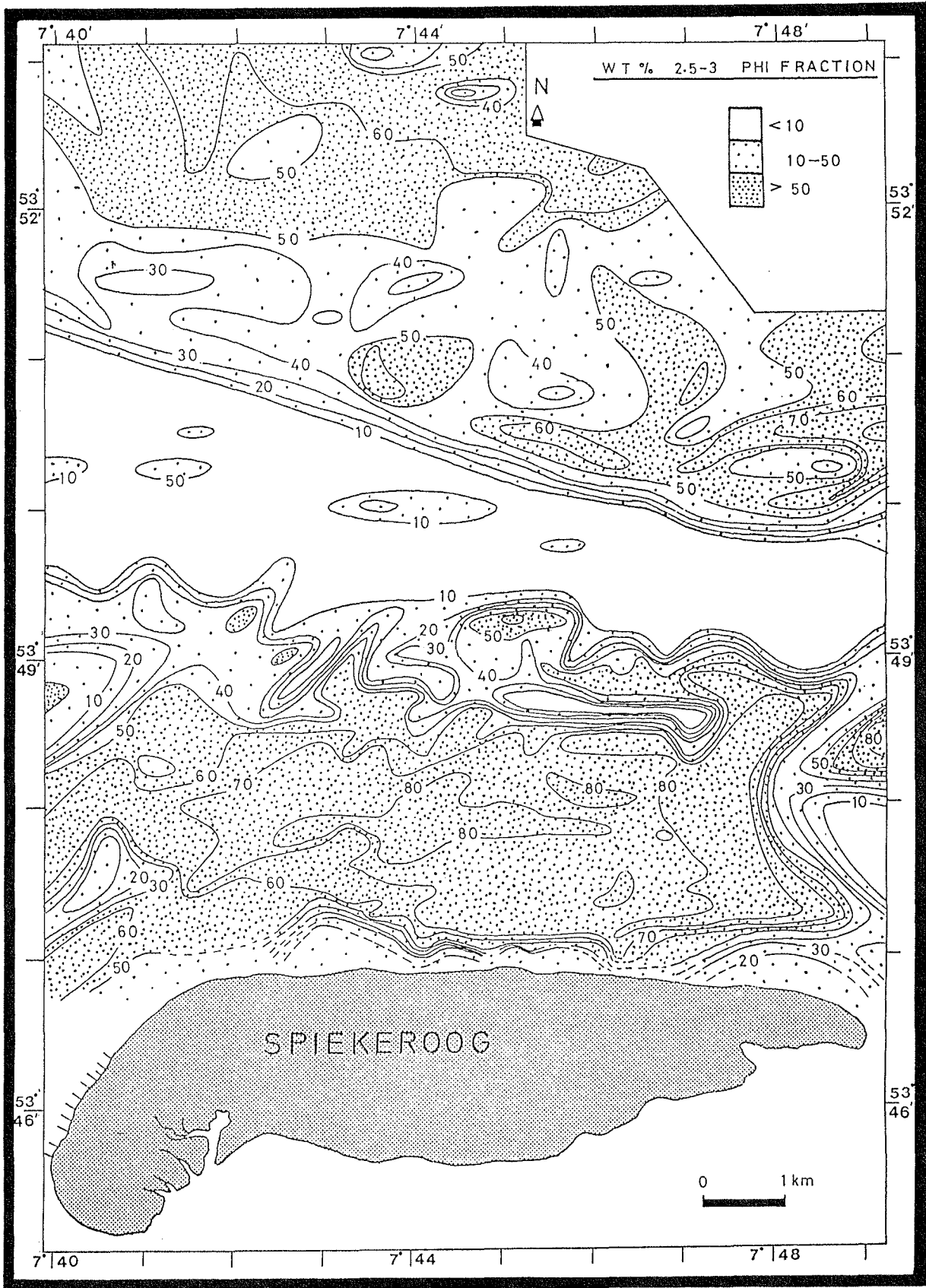


Fig. 33. Shoreface distribution of wt.-% of 2.5-3 phi sand fraction.

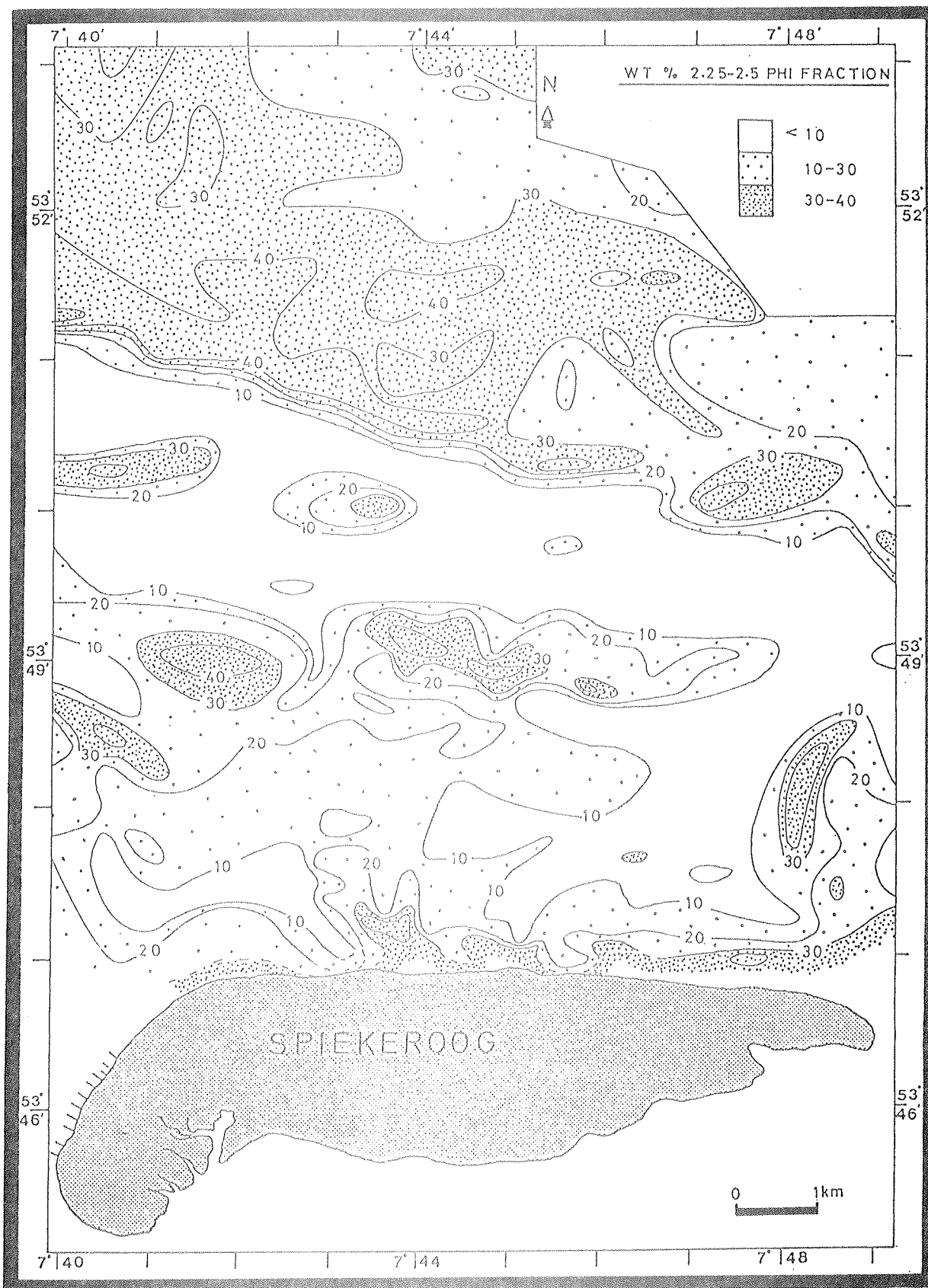


Fig. 34. Shoreface distribution of wt.-% of 2.25-2.5 phi sand fraction.

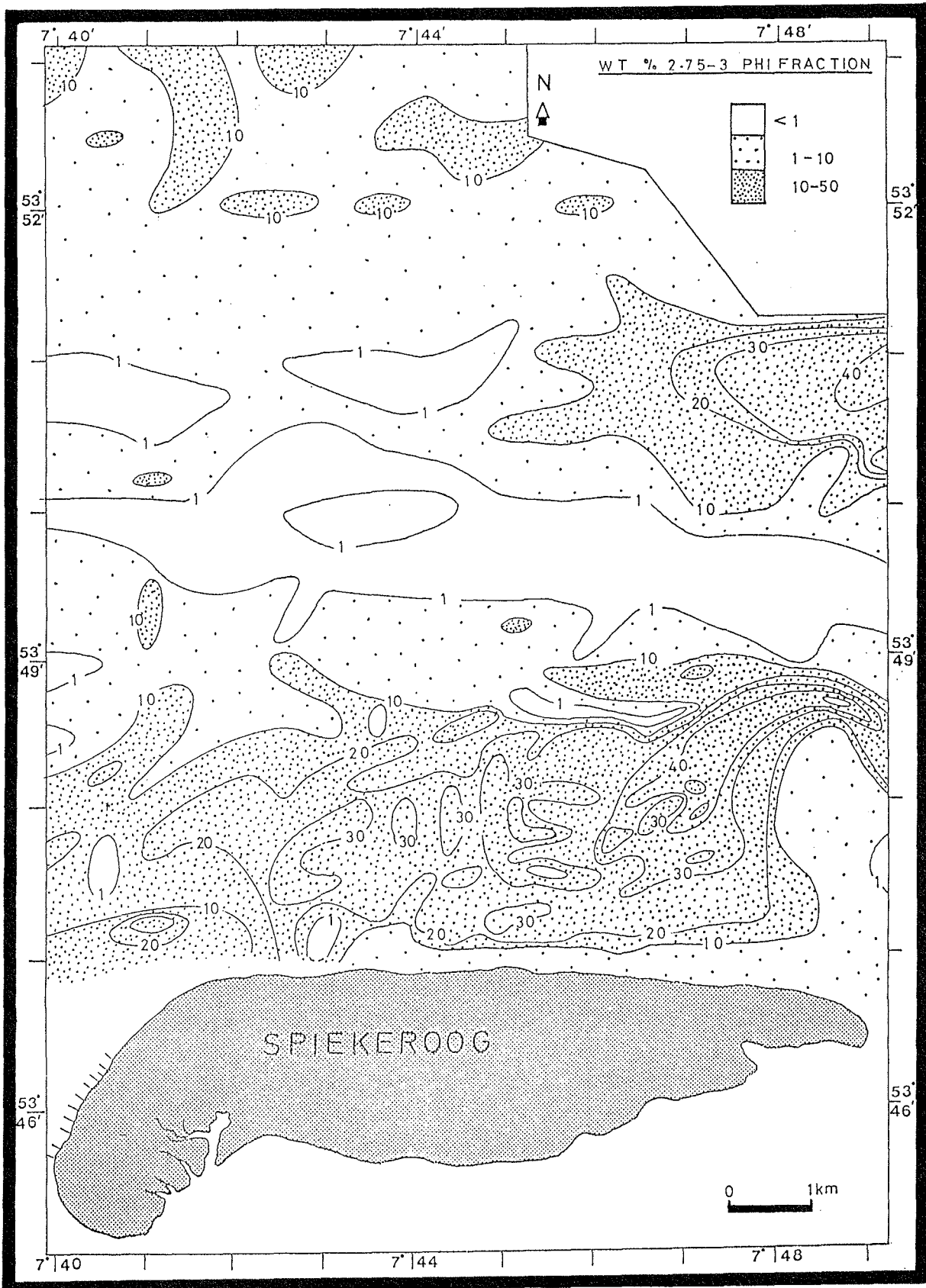


Fig. 35. Shoreface distribution of wt.-% of 2.75-3 phi sand fraction.

Quite instructive is the the relatively high concentration (10-50% by weight category) of the 2.75-3 phi fraction at the southeasterly margin of the lower shoreface subenvironment (north of Latitude  $53^{\circ} 50.00'N$ ). This category of fines also blankets the outer margin of the Harle ebb-delta, which in this part is mainly composed of medium-grained sands (cf. Fig. 30). The above fine sand fraction in the vicinity of the ebb-delta margin must have predominantly been deposited during fair-weather mean- and neap-tide ebb-currents, whereas a similar accumulation on the lower shoreface subenvironment suggests a more intensified (spring tide/storm) inlet out-flow.

All of the above size fractions are clearly subordinate (weight % < 10) constituents of the central shoreface sands. Sands on the lower shoreface subenvironment differ from their upper shoreface counterparts in being modally composed of 2.25-2.5 and 2.5-2.75 phi size fractions as against 2.5-2.75 and 2.75-3 phi on the latter.

In general, therefore, the upper shoreface sands are at least one quarter-phi interval finer than their lower shoreface counterparts. Ignoring the allogenic central shoreface sands for a moment, the general upper to lower shoreface coarsening size gradient observed in the distribution of fine sand indeed presents an anomaly where compared to the classical models of size decrease with offshore-diminishing energy. This anomalous trend differs from other shelf situations in that it is not a feature relating to offshore relict sediments, rather it is a product of recent shoreface processes.

#### 5.2.2.4 Settling Velocity (cm/s) Fractions

This section deals with the weight-% distribution of individual settling velocity fractions (> 2.5, 2.5-2, 2-1.5, 1.5-1 cm/s). With the exception of the > 2.5 cm/s distribution

chart (Fig. 36), all other charts are given in Appendix D-5, D-6 and D-7.

Although the distribution patterns of the fractions are very similar to their sedimentation diameter counterparts, they have the advantage in that spatial variations in frequency of sediment suspension for a given frictional velocity,  $u_*$ , can be readily visualized, assuming a settling-threshold velocity ratio of 1. In this case, the 1-1.5 velocity fraction (Appendix D-7) indicates that a mean  $u_* < 1.5$  cm/s would hardly set the central shoreface sands into suspension as against 10% by weight of the lower and upper shoreface sands.

The finer composition of the upper shoreface sands relative to the lower shoreface counterpart is illustrated by the 1.5-2 cm/s fraction (Appendix D-6). The converse is evident from the 2-2.5 cm/s fraction distribution pattern (Appendix D-5).

The sediment size contrast between the upper and lower shoreface is also highlighted by their respective settling velocities (Fig. 36). A very broad upper shoreface area reveals < 10% by weight of > 2.5 cm/s settling velocity sediments as against a range of 10-50% on the lower shoreface. On the other hand, the central shoreface is modally characterized by > 2.5 cm/s settling velocity sands, reaching > 90% in most cases.

Also noted is the high proportion of this velocity fraction in sediments at the inlet margins of the upper shoreface. Finally, in terms of sediment transport,  $u_*$  of the order of 2.5 cm/s would respectively suspend about 90%, 10%, and 70% by weight of the upper, central and lower shoreface sands.

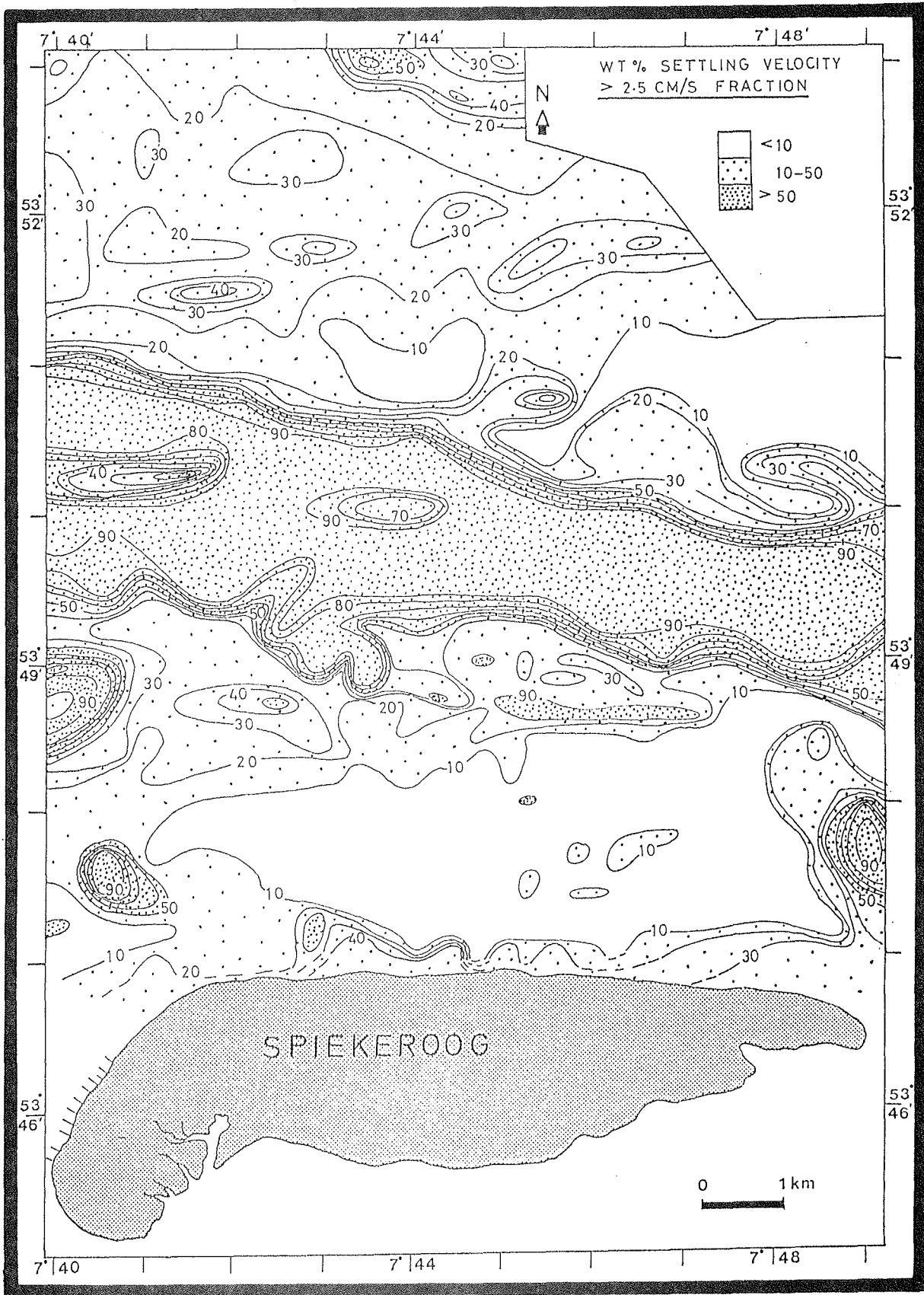


Fig. 36. Shoreface distribution of wt.-% of > 2.5 cm/s settling velocity sand fraction.

### 5.2.3 Bivariate Diagrams

Bivariate diagrams have the advantage in that pairs of summary size parameters can be directly compared and correlated with each other. Unlike the areal representation of size parameters, where trends are described on the basis of grouped data, trends in bivariate plots result from ungrouped data.

Results of statistical correlations of size parameter pairs, specifically identifying strengths in directional gradients within each of the shoreface subenvironments, are discussed in Chapter 7. The present results are based on randomly selected samples which, without swamping the diagrams with data points, nevertheless represent the spectrum for each of the shoreface subenvironments. The selective scatter plots thus reflect the general textural trends on the shoreface.

However, as earlier mentioned (Section 5.1), although delineation procedures of domains or environments in scatter plots in general are subjective, nevertheless, for certain site-specific applications, their usefulness cannot be underscored. This is particularly the case on the Spiekeroog shoreface, where the upper, central and lower shoreface subenvironments are constituted of texturally- and hydrodynamically-diverse facies zones (Chapter 7).

Finally, although patterns of grain-size parameters alone are not adequate for purposes of environmental or process interpretation, however, for a sufficiently large sample population, these parameters must be quite efficient in localized studies aimed at the above objectives. Consequently, in the following plots, the samples within each of the delimited domains (subenvironments) are representative of between 90-95% of those of their constituting facies zones. In this respect, the demarcations are "statistically" valid.

On the other hand, the outlying data points in all of the plots can be important geologically even if statistically insignificant.

#### 5.2.3.1 Mean vs. Sorting

This scatter plot (Fig. 37) reveals the bi-genetic nature of the shoreface sands, namely, an elliptically shaped finer population field of which the upper and lower shoreface sands are the main constituents, and a tilted, inverted V-shaped coarse population with the central and upper shoreface sands as major and minor constituents respectively.

The sediments comprising the fine and coarse population fields will henceforth be respectively referred to as native and foreign. The native population field can be subdivided into three domains, namely, an upper domain of exclusively upper shoreface sands, a medial domain of mixed but dominantly lower shoreface sands, and a lower domain of subequally mixed central and lower shoreface sands.

In general, the mean vs. sorting pattern is controlled more by mean size than sorting. The data, however, shows sorting to be best within the lower shoreface and worst within the central shoreface sands, a conclusion already reached from the areal distribution of kurtosis (Fig. 28). However, the orientation of the ellipse in Fig. 37 suggests that the native sediments improve in sorting with fining, and vice-versa.

The inverted V-shaped foreign sediment population shows two gradients of a similar trend above. Its left arm is steeper but the variation in sorting is narrower. The right arm shows the opposite, i.e., more variable sorting and a gentler gradient (comparable to that of the native population) of improved sorting with fining.

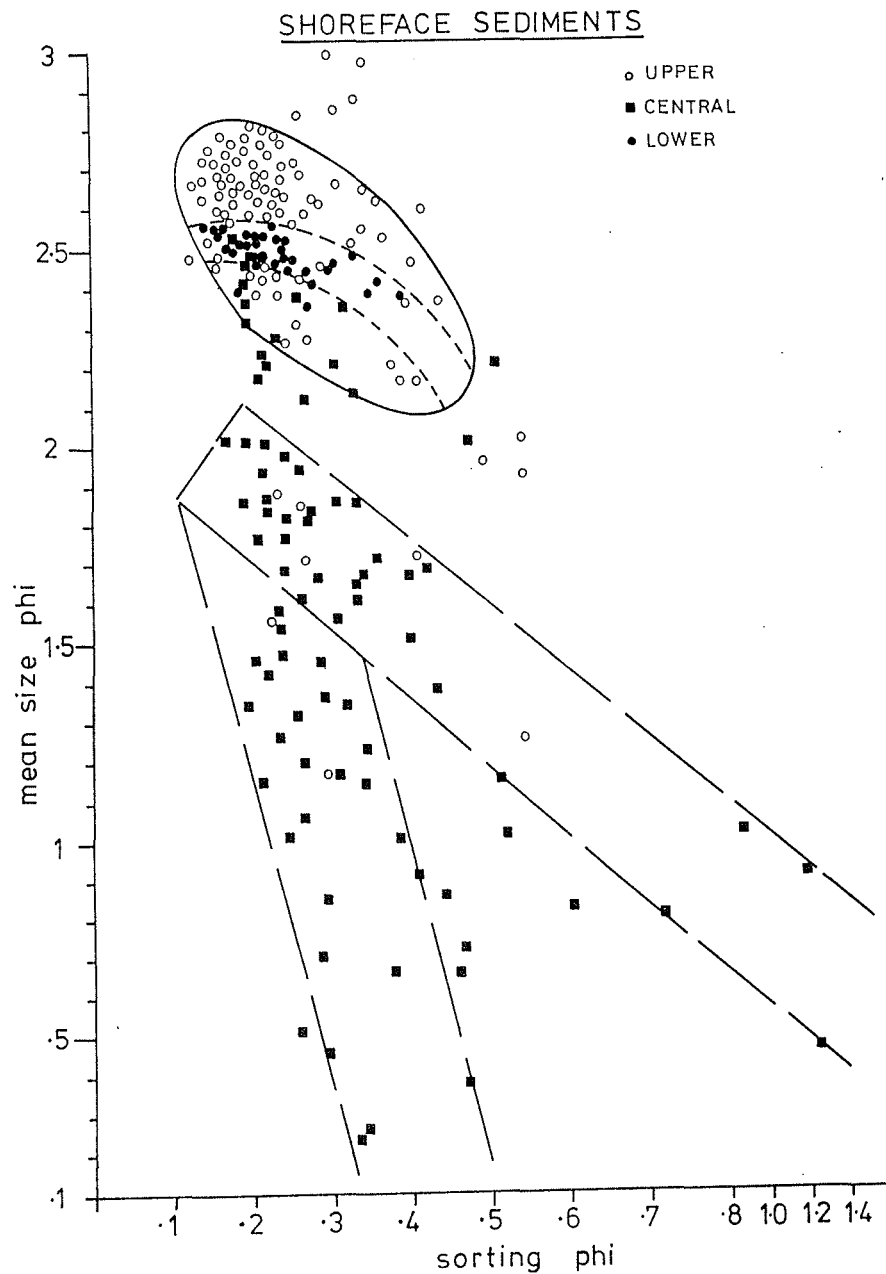


Fig. 37. Bivariate plot of mean grain size versus sorting.

#### 5.2.3.2 Mean vs. Skewness

As in the case of mean vs. sorting, the scatter plot of mean vs. skewness (Fig. 38) distinguishes a native population of fine-grained upper and lower shoreface sands from a cluster

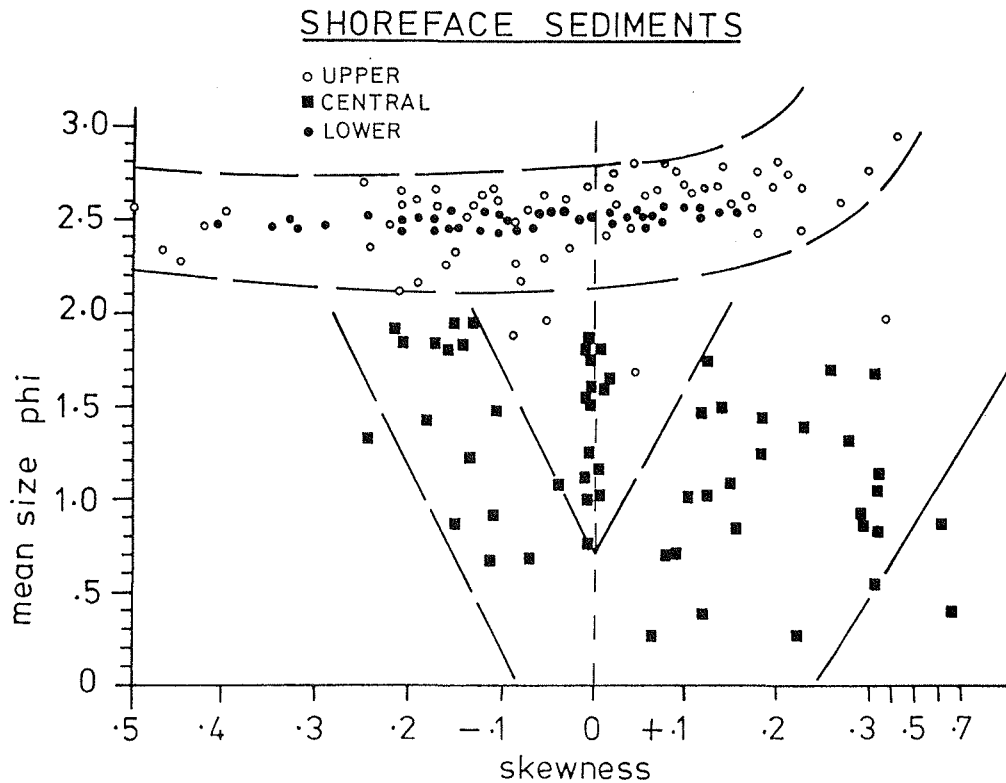


Fig. 38. Bivariate plot of mean grain size versus skewness.

of largely central shoreface sands. The former shows a slight increasing positive skewness with sediment fining. As discussed in Section 5.2.1.3, such a pattern is most likely a consequence of immiscible mixing of winnowed finer fractions with, in this case, near-symmetrically distributed sands. In general, the bulk of the native sediments are negatively skewed.

The coarse-grained foreign population, on the other hand, can be divided into three domains: a negatively skewed one, a positively skewed one, and a central domain of zero skewness. In comparison to the negatively skewed domain, the positively skewed one is more widely scattered.

To account for the contrasting size skewness trends, it is helpful to consider a horizontal reference (e.g.,  $1 \phi$  line) subdividing each of the sloping domains into two halves, upper and lower, the former being finer and more negatively skewed (left arm) or positively skewed (right arm).

By examining the skewness evolution models in Fig. 26, the mean-size vs. skewness relationship on the lower half of the left arm in Fig. 38 can be best accounted for by either of the following: Case 2b (immiscible mixing of an exponentially decreasing coarse population), Case 5c (total deposition of transported, probabilistically-winnowed, very coarse sediment source) or Case 6a (as a lag resulting from total truncation of a wide range of fines from a strong negatively-skewed native source).

The upper half can be a consequence of Case 3a (immiscible mixing of an exponentially increasing fine population). Cases 5 and 6 are also feasible, provided that the sediment source in the former is not very coarse, and in the latter, only a narrow range of fines are totally truncated. Case 1a (miscible mixing of an exponential decrease of coarse or increase of fine population) can be envisaged as an intermediate step in the above evolutionary process.

The positively sloping domain on the other hand would show the following sequence of skewness evolution: Case 3b (immiscible mixing of an exponentially increasing fine population), Case 5a (a lag of a probabilistically-winnowed very coarse source), Case 5b (selective deposition from a very coarse-grained suspension) and Case 6 (a lag following total truncation of fines from a strongly positively skewed source) are all applicable on the lower half.

Through an intermediate step of Case 1b (miscible mixing of an exponentially decreasing fine population), the upper half may result from Case 2a (immiscible mixing of an exponentially decreasing fine population). Other possibilities for the latter

are as in Case 5a (for a finer source population) and Case 5b (for a suspension population).

### 5.2.3.3 Mean vs. Kurtosis

The relationship between mean size and kurtosis (Fig. 39) reflects the same sediment size-dependent segregation of the native or upper and lower shoreface sands on the one hand, and the foreign or central shoreface counterpart on the other.

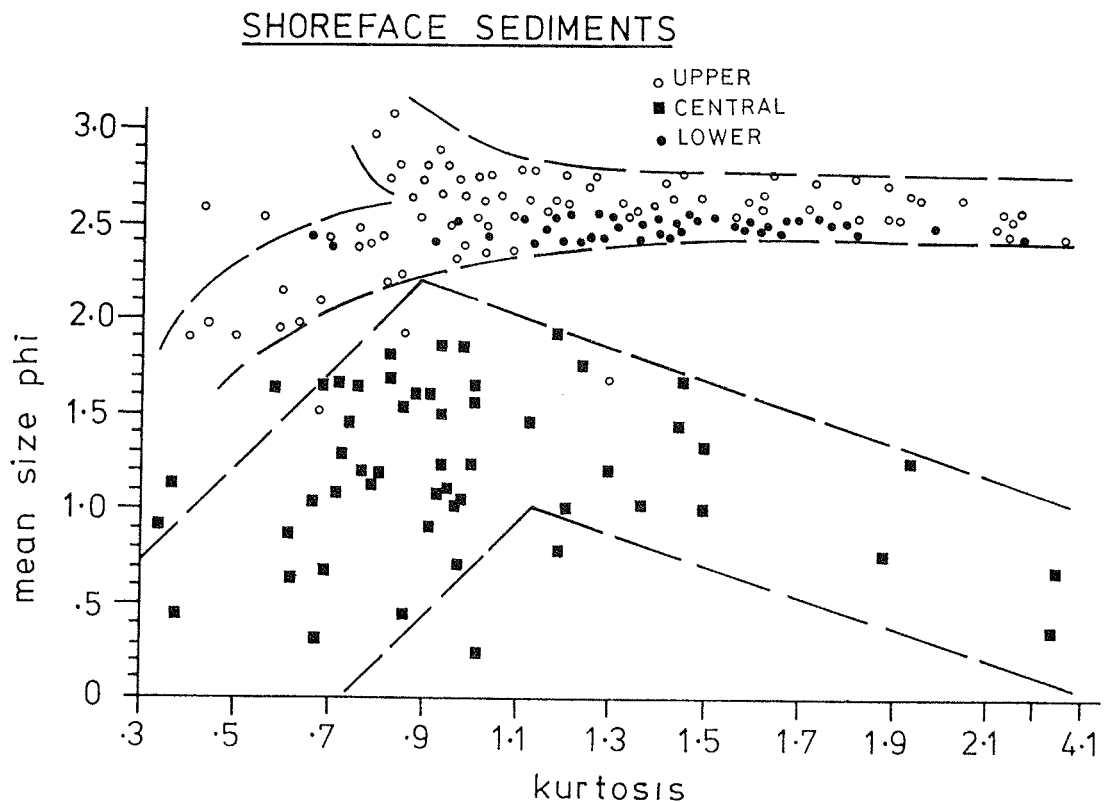


Fig. 39. Bivariate plot of mean grain size versus kurtosis.

Both the upper-shoreface native and the central shoreface foreign populations show a change in their pattern for kurtosis values in the range of 0.9-1.3, depending on the mean diameter.

With a decrease in kurtosis values below 0.9-1.3, both populations show a coarsening trend in their respective mean grain sizes. In addition, the upper shoreface native population shows a slightly fining trend along its upper margin, i.e., towards more platykurtic values, it shows a bi-directional evolution of mean size. However at higher kurtosis values, the native population remains invariant with respect to mean size. The foreign population, on the other hand, again increases in mean grain size, as is the case below the boundary kurtosis values of 0.9-1.3.

It is worth noting that, as in the mean size vs. sorting relationship, the mean-size vs. kurtosis pattern of the central shoreface sand population similarly takes the form of an inverted "V". This observation further corroborates the sorting vs. kurtosis relationship previously alluded to in Section 5.2.1.4.

#### 5.2.3.4 Sorting vs. Skewness

The relationship between sediment sorting and skewness given in Fig. 40 depicts two main domains. The lower saucer-shaped domain comprises sediments from all the shoreface subenvironments, whereas the upper bow-shaped domain is mainly constituted of central shoreface sands. Within the latter domain, sorting deteriorates with increasing positive skewness. In contrast, the saucer-shaped domain depicts both increasing positive and negative skewness tendencies with increasing unsortedness. Symmetric size distributions are associated with the best sorted sediments in the latter domain.

The above trends are very instructive in that, coupled with the mean grain size, a more reliable discrimination between the multiple skewness evolution cases becomes feasible. In general, the central shoreface sands differ from the upper and lower shoreface counterpart in being more prone toward positive

skewness. Referring again to the skewness evolution cases, it becomes quite evident from the extreme positive skewness, the poorer sortedness, and the coarseness of the central shoreface sands that they may be a source for the upper and lower shoreface sands, but not the converse.

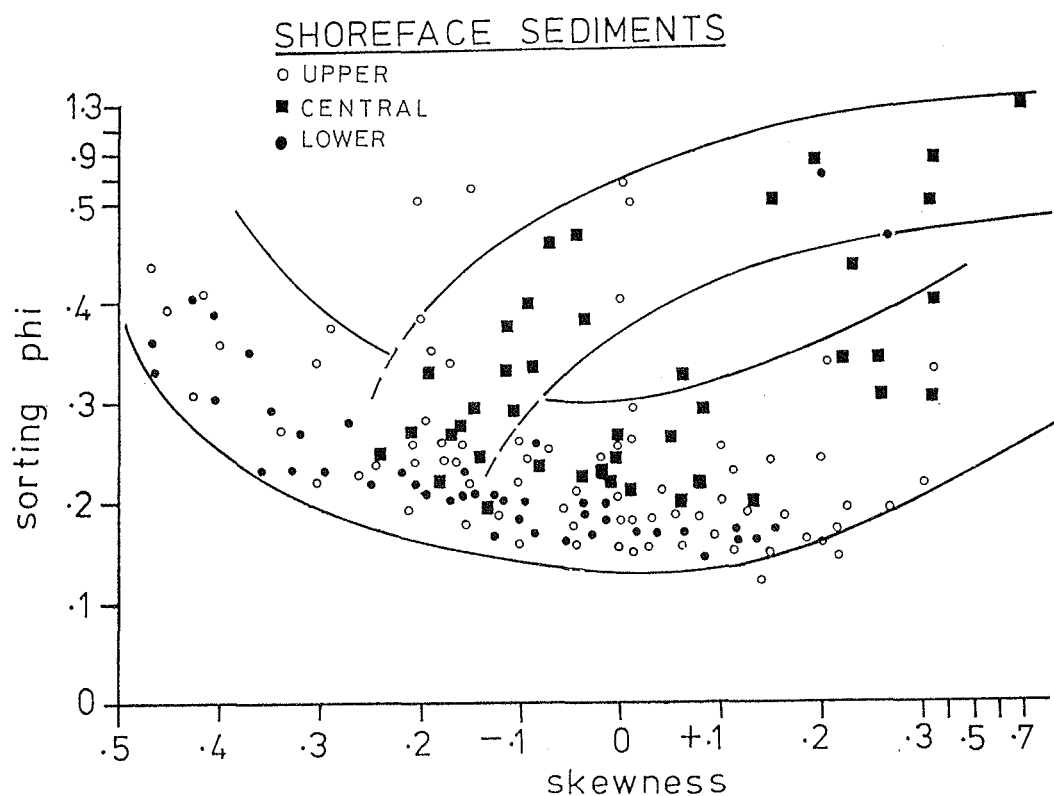


Fig. 40. Bivariate plot of sorting versus skewness.

#### 5.2.3.5 Sorting vs. Kurtosis

The relationship between sediment sorting and kurtosis (Fig. 41) is the most homogeneous of all of the size parameter pairs in that only a single domain exists in which sands from all the shoreface subenvironments are contained. The plot

reveals a steep gradient of improving sortedness with increasing kurtosis values up to the mesokurtic-platykurtic range of 0.9-1.3 where the best sorting is indicated. Beyond this range, sorting shows a subtle deteriorating tendency.

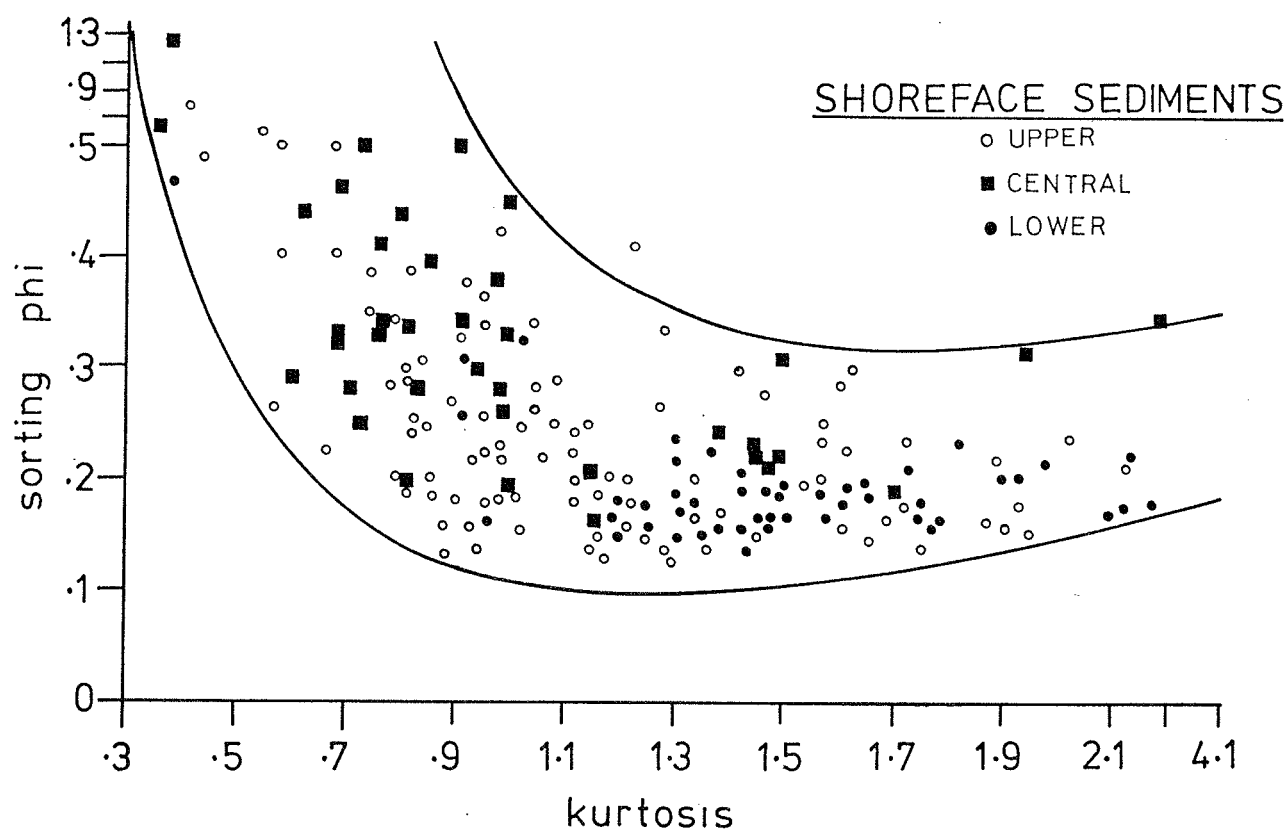


Fig. 41. Bivariate plot of sorting versus kurtosis.

#### 5.2.3.6 Skewness vs. Kurtosis

The skewness vs. kurtosis relationship shows two main rotated (90° anti-clockwise) V-shaped domains. For comparison purposes, two different plots are presented. In the first plot in which the upper shoreface data are excluded, the distinction between the central and lower shoreface sand fields is particularly pronounced, despite similarities in their trend (positive and negative skewness both tend to increase with decrease in kurtosis).

Importantly, the negligible overlap of data further strengthens the contention that these sands have different origins. Surprisingly, however, is the fact that in spite of the high sediment mobility on the shoreface, both central and lower shoreface sands still show a sharp segregation in their size statistics.

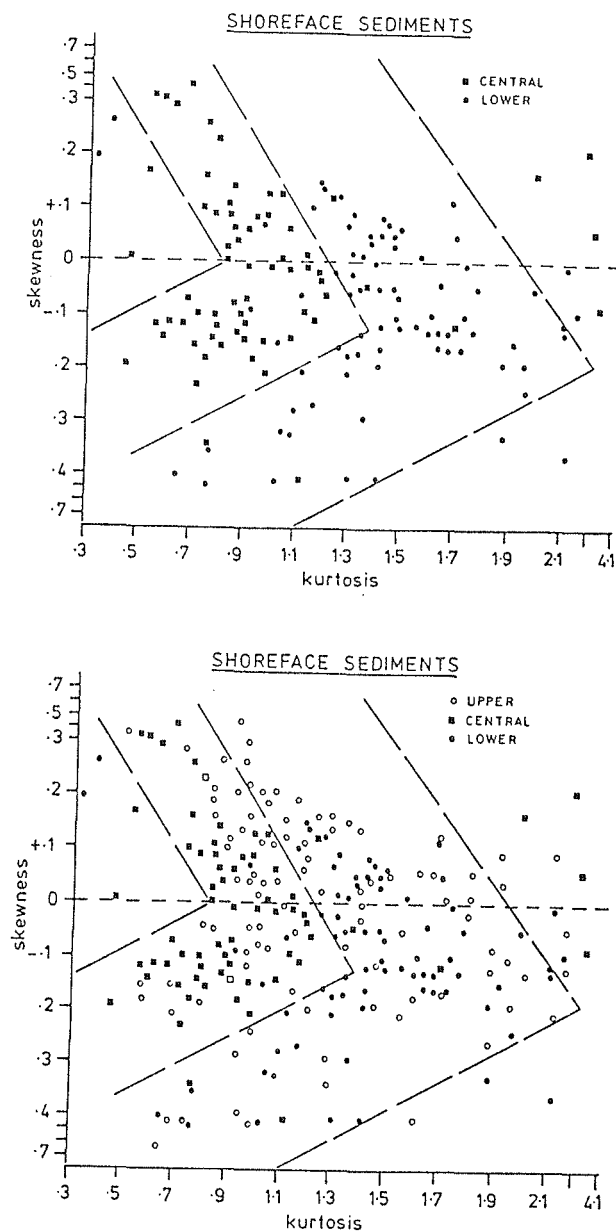


Fig. 42. Bivariate plot of skewness versus kurtosis.

In the second plot, data from the upper shoreface are inserted. Quite evident is the subequal and "well-mixed" distribution of the latter within the two domains, thus suggesting their dual origin. Of particular interest is the upper and central shoreface sand relationship. This relationship had been repetetively alluded to based on areal distribution of grain size statistics and fractions earlier presented.

In these and the foregone bivariate plots, the upper shoreface data most comparable to the central shoreface counterpart are those from the neighbourhood of the flanking inlet ebb deltas and, to some extent, close to the shoreline. In the absence of a cross-shore continuity of the central shoreface sands across the entire upper shoreface, the shoreline as a probable source of the former can be dismissed.

On the other hand, the seaward protruding patches and strings of central shoreface-comparable sands at the margins of the upper shoreface point to the inlets as potential sources of the central shoreface sands. This view-point will be elaborated upon in subsequent sections.

#### 5.2.3.7 C-M Plot of PASSEGA

The C-M diagram (PASSEGA, 1957, 1964) is essentially a bivariate plot of the diameter of the coarsest 1% or first percentile (C) and the median (M) of a cumulative frequency grain size distribution. PASSEGA (1964) notes that C-M patterns convey information on the transportational mechanisms of a sediment deposit. This assertion is examined in Section 5.4.3.

Pertinent at this point is the general distribution pattern of the shoreface sands on such a diagram (Fig. 43). The nomenclature and, to some extent, the demarcation of the various transport domains shown in the latter follows the

modifications of the original PASSEGA (1957) classification employed by FLEMMING (1978). For an easier comprehension, the comparisons are presented below :

Size Range	Terminology	
(C) phi	FLEMMING (1978)	PASSEGA (1964)
< 0	Traction	Rolling
0-0.65	Lower bottom suspension or (coarse) saltation 1	Bottom suspension and rolling
0.65-1.3	Upper bottom suspension or (fine) saltation 2	Bottom suspension and rolling
1.3-2.3	Graded suspension	Graded suspension
> 2.3	Uniform suspension	Uniform suspension
>>2.3		Pelagic suspension

Figure 43 shows clearly the close genetic relationship between the lower and upper shoreface sands on the one hand, and the dual character of the latter. Each of the shoreface subenvironment sands follows a specific pattern, reflecting differences in the transport modes. The corresponding areal distribution of the C-M groups is illustrated in Fig. 53.

In brief, from Fig. 43, the central shoreface sand population pattern is easily visualized as a long, baton-shaped (broader coarser end) band parallel to the C = M line, whereas the lower shoreface sand population pattern is a short strip parallel to the C axis. The upper shoreface sands show a tilted Y-shaped pattern in which the left arm is subparallel but closer to the C axis than the lower shoreface, and the right arm parallel to the C = M line.

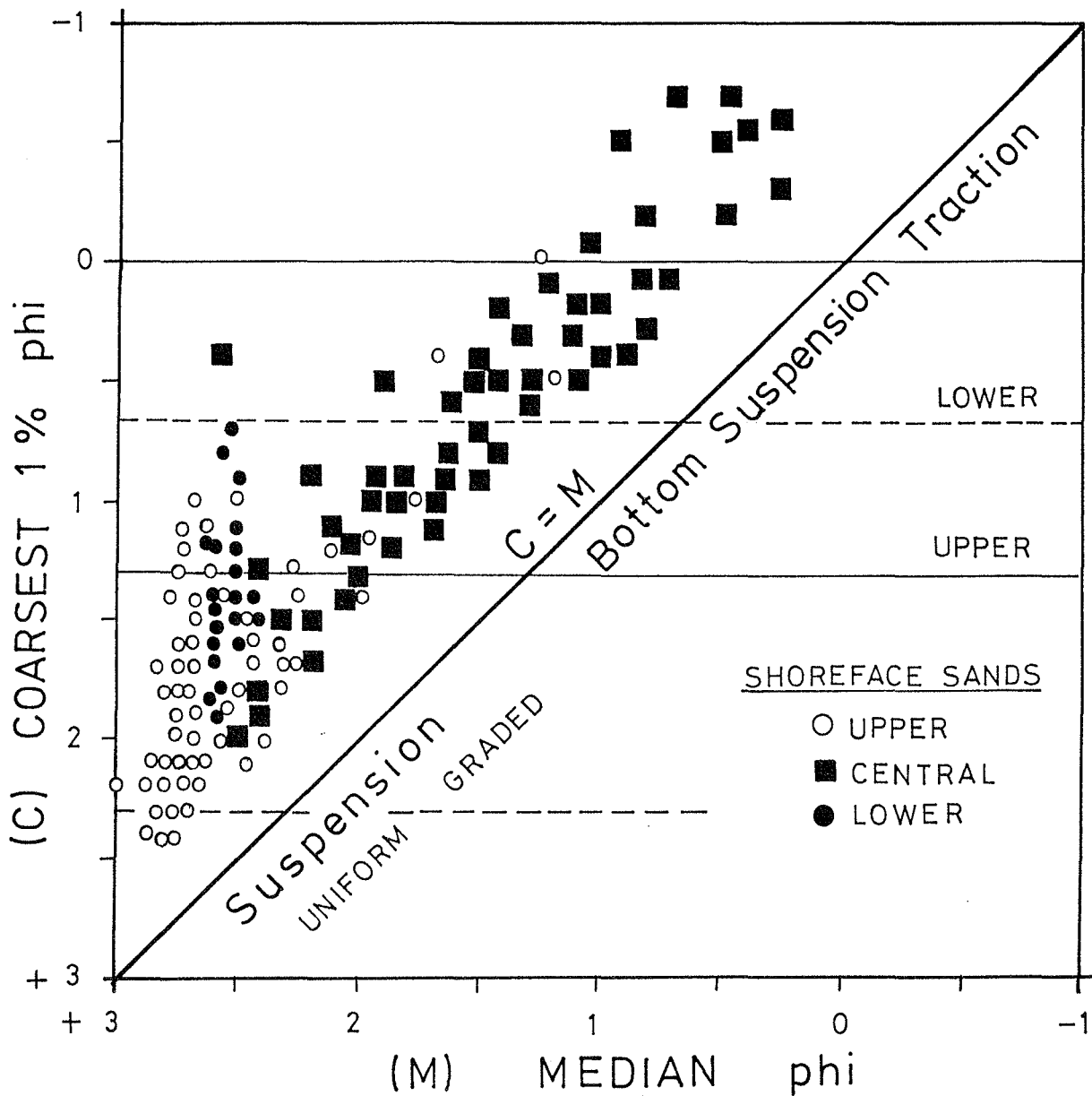


Fig. 43. C-M plot of shoreface sediments.

Finally, like most of the other discussed bivariate diagrams, the CM plot corroborates the allogenic nature of the central shoreface sands. In addition, the following size characteristics are suggested:

(a) By virtue of the closeness of the data points to the  $C = M$  line, the central shoreface sands on the whole show a highly uniform and much better sorting of the coarser half of their size distribution than those of the upper and lower shoreface; on the contrary, the coarser half size distribution of the lower and most of the upper shoreface sands clearly deteriorates in sorting despite their highly uniform median size, suggesting that these sediments are locally mixed with sands of the central shoreface and/or those similar in character to the latter.

(b) Contrary to the classical CM plot, the central-shoreface sands do not depict the typical kinking at the upper limit of the graded suspension, normally produced by an abrupt deterioration in sorting at this portion on the graph.

(c) The range in the ratio of C and M values (based on metric units), an index of sorting, is considered to reflect characteristics of the depositional media or mechanics (BULL, 1962). The upper, central and lower shoreface sands depict respectively the following ranges of C:M ratio: 1.2-3.3, 1.4-2, and 1.4-4. Note the narrower range for the central shoreface sands relative to the upper and lower shoreface counterpart. In particular, the larger values and range indicated by the lower shoreface sands relative to the upper shoreface counterpart support the contention of a correspondingly lower sediment mobility in deeper waters.

#### 5.2.4 Log-Probability Grain Size Curve Characteristics

All of the computer plots (at 0.02 phi interval) of the sedimentation diameter cumulative frequency distribution of the shoreface sands on an arithmetic-probability scale were composed of two to four (dominantly three) straight line segments. These are here designated as components A, B and C respectively for the upper, middle and lower segments.

Similar observations as above are replete in the literature of coastal and shelf grain size studies, e.g., FULLER (1961), TANNER (1964), VISHER (1969), REED et al. (1977), GREENWOOD (1978) and JAGO (1981). Although opinion is diversified in relation to the mechanics of evolution (e.g., mixture of normal, overlapping populations versus truncated normal populations) as well as the physical meaning of the segments, a school of thought considers and correlates these, i.e., components A, B and C with grain size fractions deposited from suspension, saltation and traction transport modes respectively.

The present intention is to describe the areal pattern of the relative proportion (weight %), phi-median, sorting (slope steepness) and inflection points ( $\phi$ ) of the components. Thus far, no systematic areal charting of such curve shape parameters has been undertaken. However, in order to facilitate the comparison of the current results with literature reports, both the A-B-C and the conventional suspension-saltation-traction designation for the above segments are interchangeably employed. In the very few instances where double saltation components are indicated, the median and sorting parameters described are that of the major saltation component.

#### 5.2.4.1 Weight-% of Curve Components A, B, and C

As shown in Fig. 44, the B- or saltation-component is the most significant or the mode across the entire shoreface. The C- or traction-component is largely confined to the coarse-grained central shoreface sand patches constituting > 50% by weight of the samples. By contrast, the A- or suspension-component hardly contributes more than 30% by weight of the curves. It occurs mostly in the proximal zones of both the upper and lower shoreface. The low representation of the suspension component at the southeasterly margin of the central

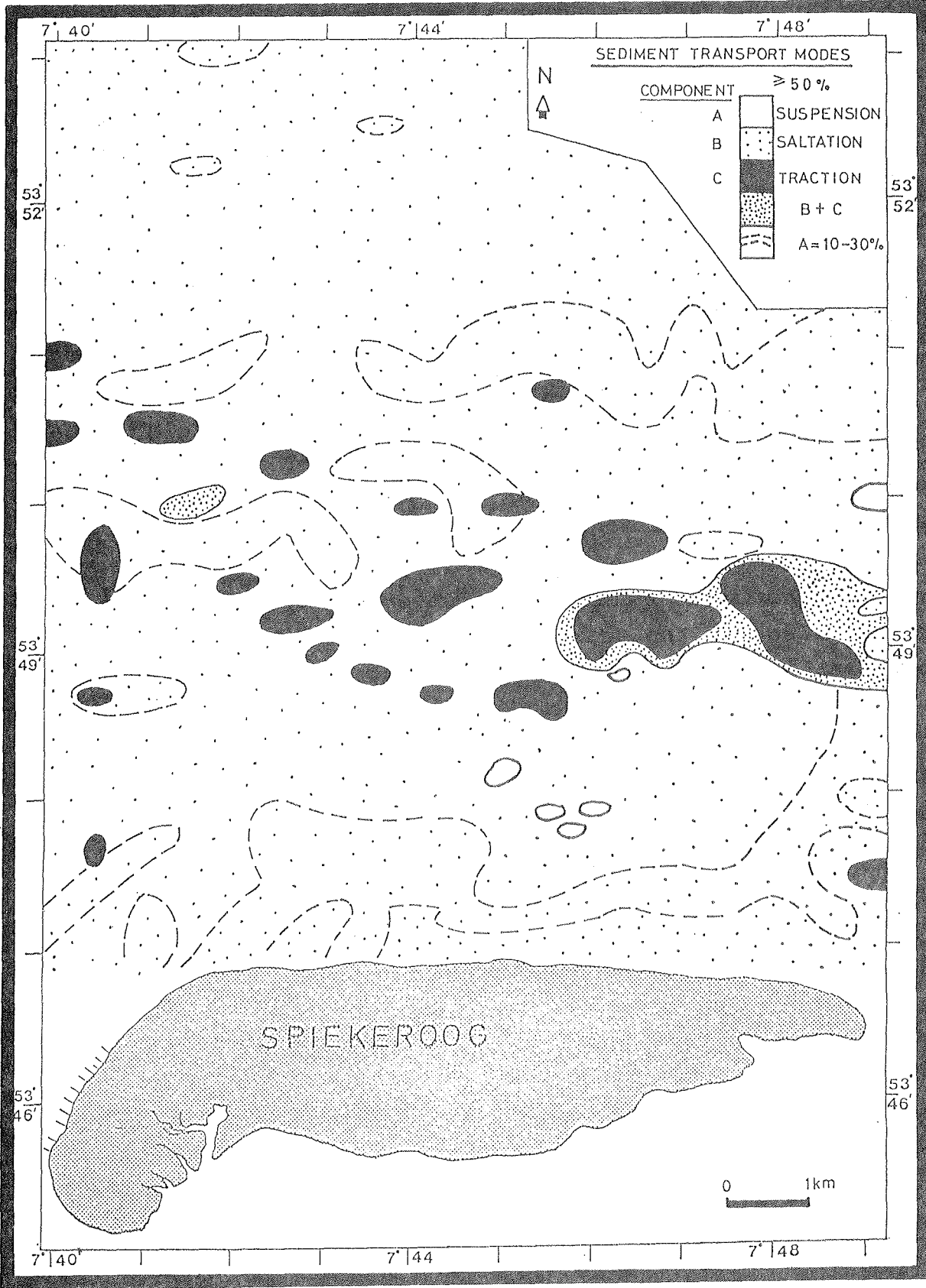


Fig. 44. Areal distribution of weight-% of log-probability curve components A-B-C of shoreface sediments.

shoreface, as compared to its northwesterly end, is worthnoting.

A closer examination of the curve-segment distribution patterns reveals that these too reflect the tripartite shoreface grain size patterns discussed earlier. In all cases, the upper- and lower-shoreface sands are contrasted from those of the central shoreface. This point is further emphasized by the distribution pattern of the saltation- or B-component (Fig. 45).

In brief, the B component depicts its lowest proportion (< 80% and often < 50% by weight) on the central shoreface. Similarly low values occur in the proximal or medial zones of the upper- and lower-shoreface subenvironments, with a higher proportion towards their distal zone. The genetic relationship between the inlet sediments and the central shoreface counterpart is further highlighted in the above distribution pattern.

#### 5.2.4.2 Phi-Median of Curve Components A, B and C

The areal distribution of the phi-median of components A, B and C are given in Figs. 46-48. All of these clearly corroborate the tripartite textural zonation of the shoreface and further demonstrate their genetic relationship.

The upper and lower shoreface sands are almost exclusively composed of suspension or A-component sediments having 3-3.5 phi median size as against < 3 phi for the central shoreface sands (Fig. 46). The latter values are also well represented close to the shoreline, while at the eastern inlet margin of the upper shoreface it forms a pattern that virtually links the central shoreface to the inlet-ebb delta morphology.

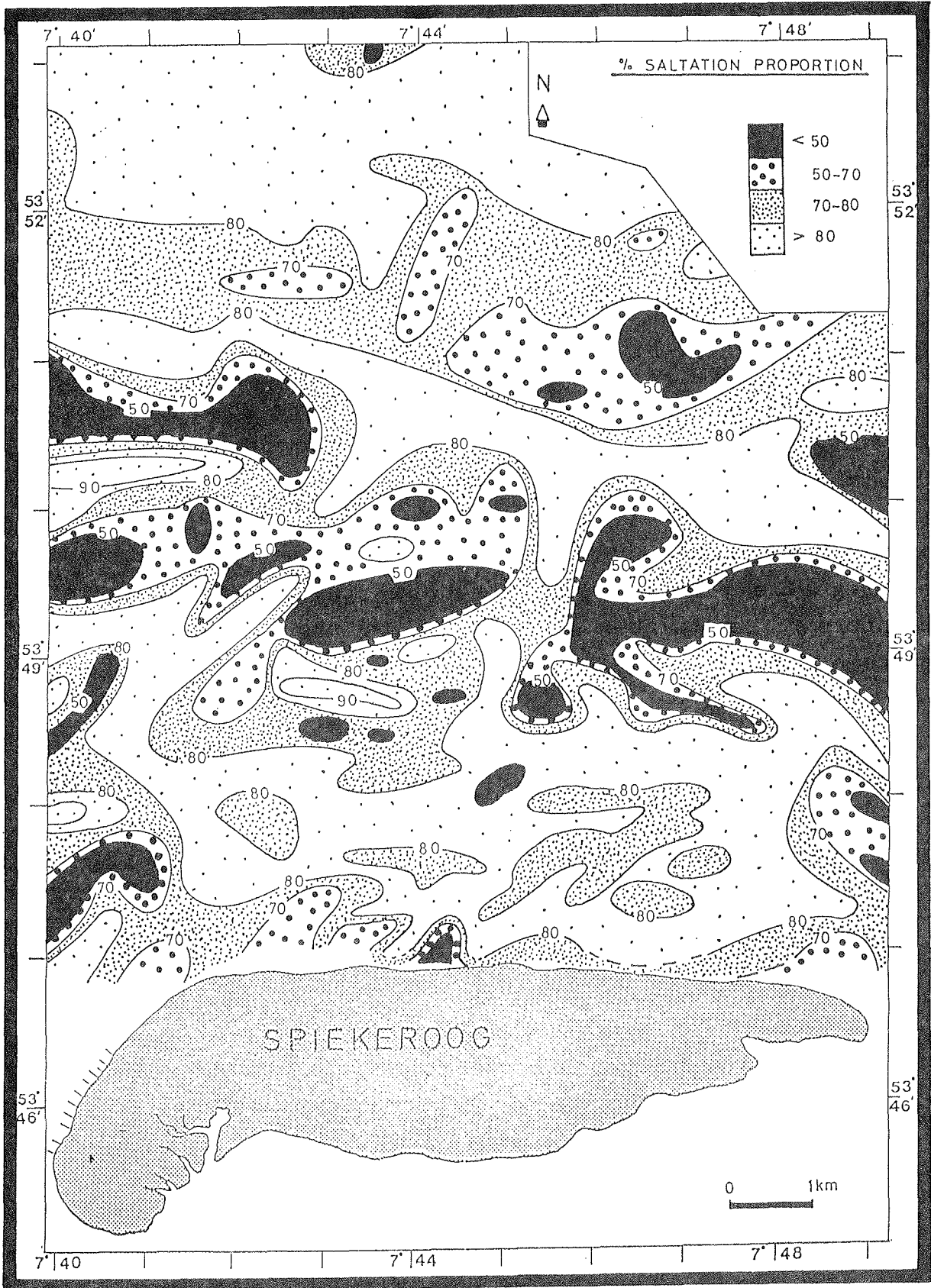


Fig. 45. Areal distribution of weight-% of log-probability curve component B (saltation population).

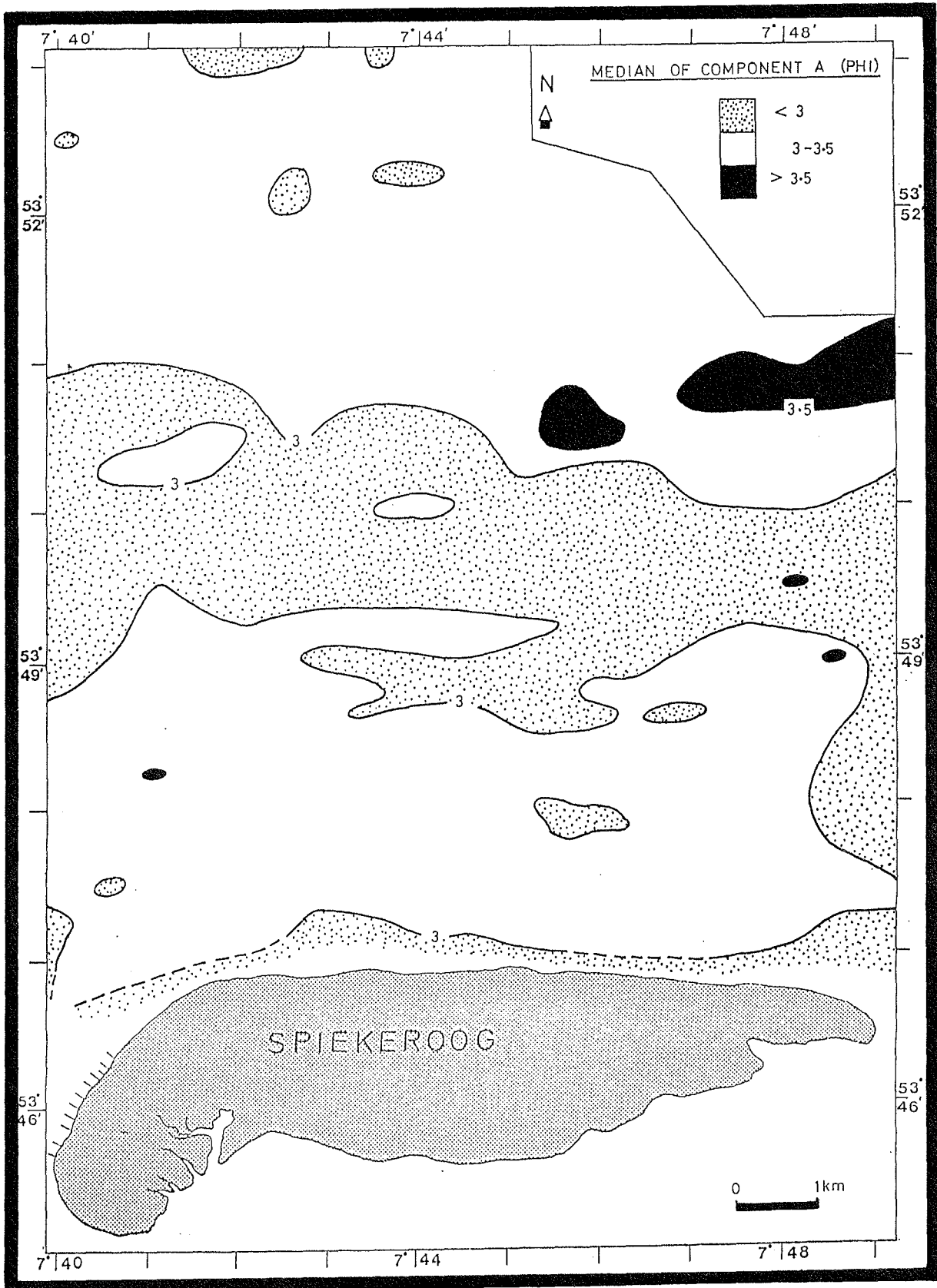


Fig. 46. Areal distribution of the phi-median of component A.

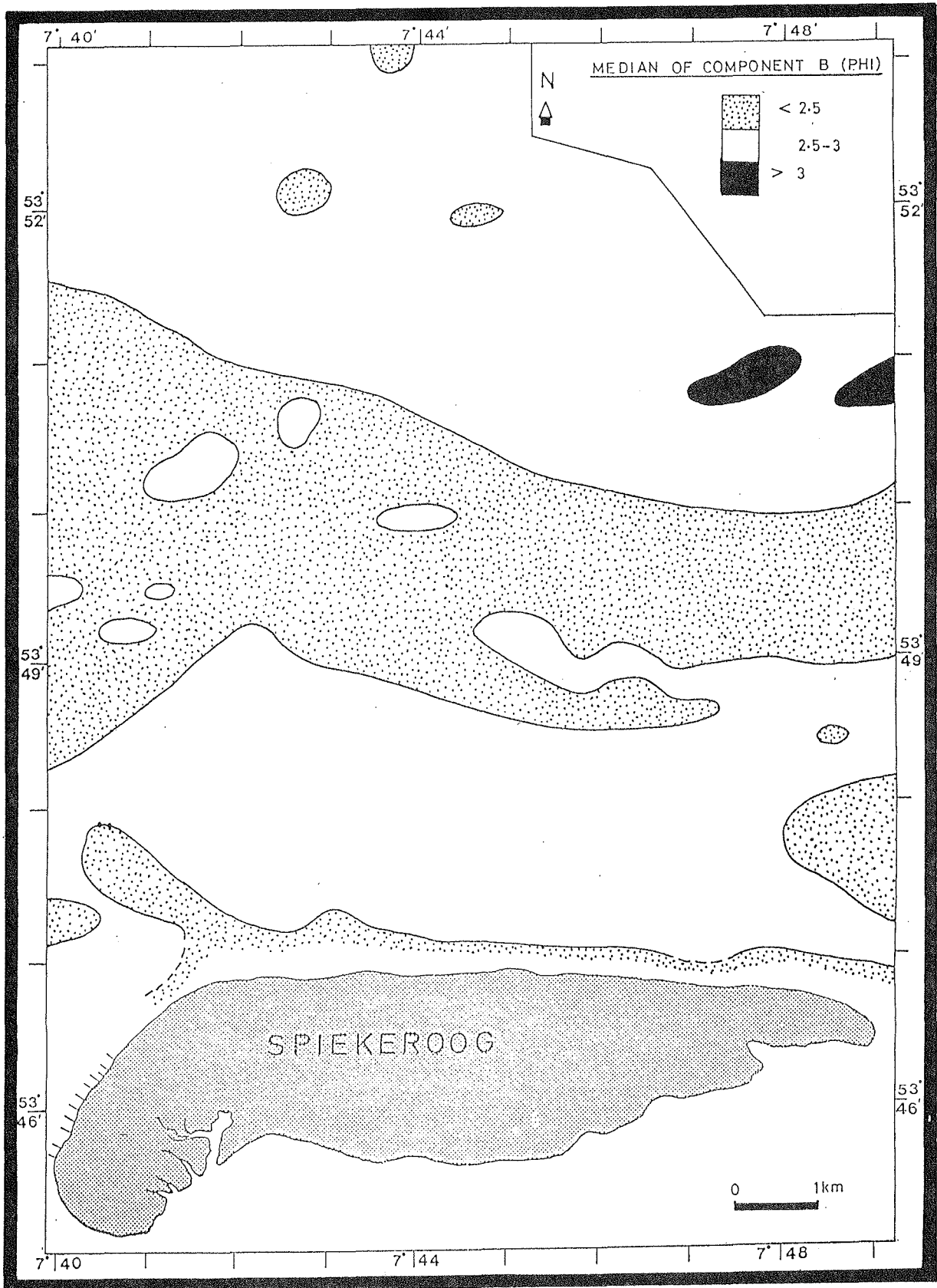


Fig. 47. Areal distribution of the phi-median of component B.

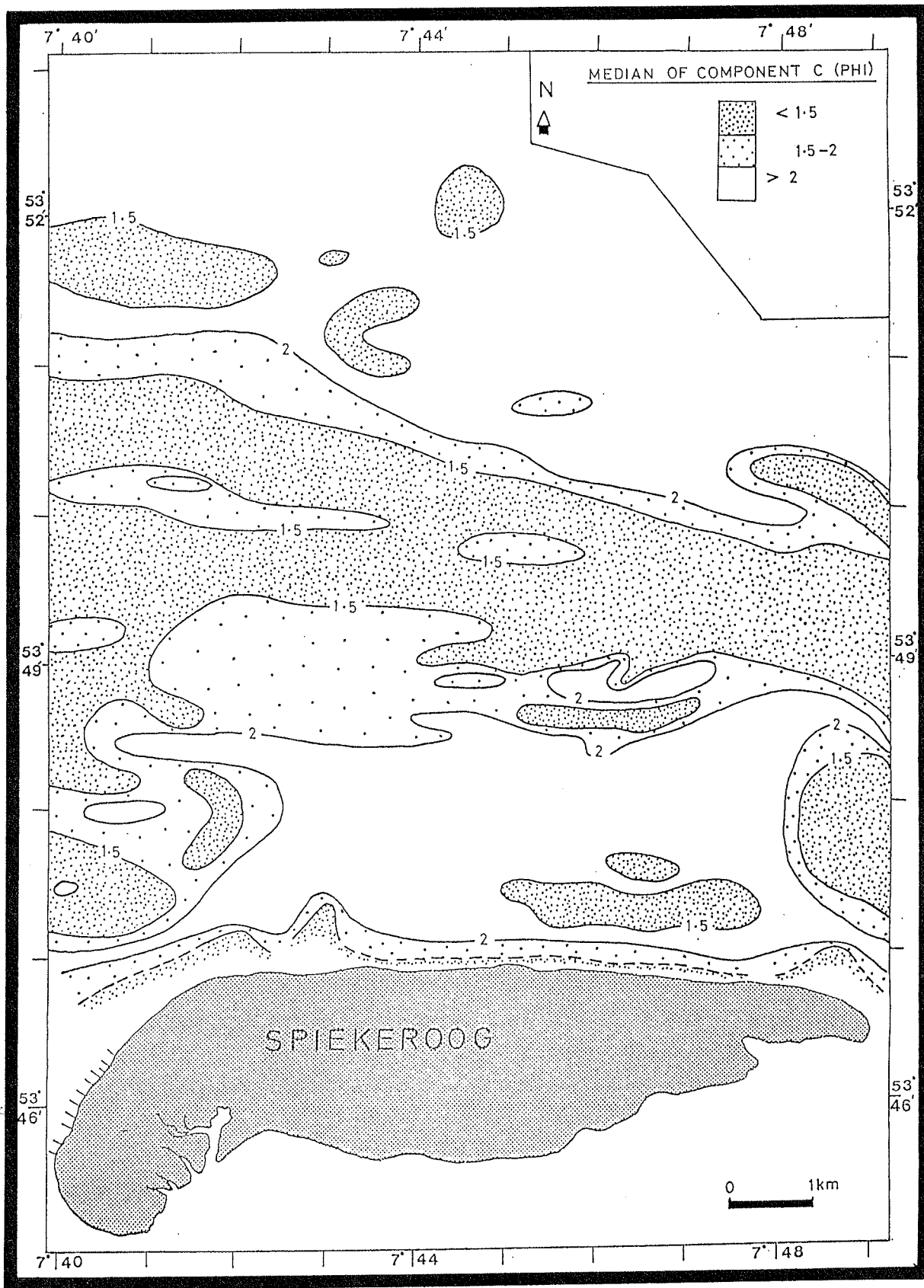


Fig. 48. Areal distribution of the phi-median of component C.

Similarly, the saltation or B-component (Fig. 47) depicts a coarser median size on the central shoreface ( $< 2.5 \phi$ ) than the adjacent upper and lower shoreface subenvironments ( $2.5-3.0 \phi$ ). The genetic relationship between the central shoreface and inlet sediments, however, is less conspicuous. The median size distribution of the traction- or C-component (Fig. 48), on the other hand, emphasizes the above relationship. As in previous cases, the median sizes are coarser ( $< 1.5 \phi$ ) on the central shoreface than on the upper and lower shoreface, where values are generally greater than  $2 \phi$ .

#### 5.2.4.3 Sorting Index of Components A, B and C

The steepness of the log-probability straight line segments designated previously as components is used as an index of their sorting. The higher the steepness values, the better the sorting.

The areal distribution of sorting of the components A and B is given in Appendix E-1 and E-2, whereas that of component C is presented Fig. 49. It is obvious that the saltation- or B-component shows the best sorting. The sorting of the A- or suspension-component depicts a less well-defined relationship with the shoreface bathymetry.

The upper shoreface sands, however, are best sorted. This is consistent with the high wave-winnowing intensity at this shallower water depth. In contrast to the suspension component, the sorting of the saltation component is better defined. A predictable improvement of sorting with distance from the central shoreface is evident. Also evident is the similarity in sorting of the upper shoreface flanks with that of the central shoreface.

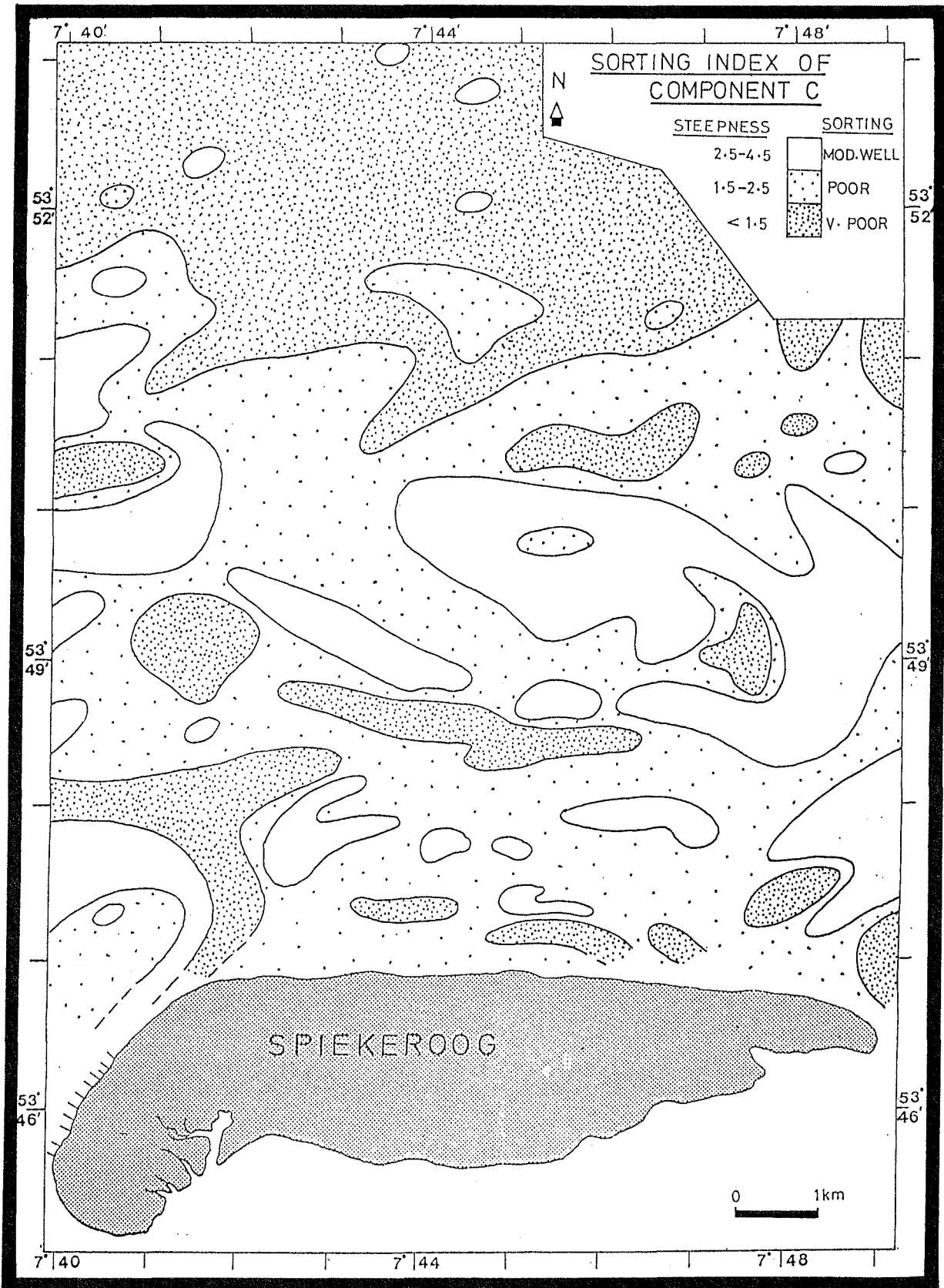


Fig. 49. Areal distribution of sortedness of component C.

Finally, the sorting pattern of the traction- or C-component (Fig. 49), though less well graded as that of the saltation-component, is illuminating in several respects. Firstly, this component is least well-sorted on the lower shoreface. This result can be viewed as a natural consequence of a diminishing flow energy with water depth. Incidentally, the best sorting does not occur on the shallow upper shoreface, but rather on the central shoreface.

The above observation leads to the conclusion that the central shoreface sands indeed have a foreign source. The broad patches of equally well-sorted traction components at the inlet-delta flanks of the upper shoreface further emphasizes their common origin. It also indicates that transport of sediment on the central shoreface must take place relatively close to the seabed, as required by traction transport.

#### 5.2.4.4 Inflection Points of Log-Probability Curve Components

The phi values of the fine and coarse inflection or truncation points, respectively defining the transition between the A-B (suspension-saltation) and B-C (saltation-traction) components are presented in Appendix E-3 and E-4. Again, the above distributions show a well-defined zonation. The A-B inflection values lie in the 2.75-3 phi range for the upper and lower shoreface subenvironments, but are coarser on the central shoreface (typically about 2 phi). Similarly, coarser inflection values are evident at the ebb-delta margins and close to the shoreline. On the other hand, the finest inflection points are associated with the tongue of fine sediments on the lower shoreface.

Several investigators presenting arguments for the hydraulic significance of the inflection points, are cited by SAGOE and VISHER (1977), who also present a theoretical model

of their relationship on the basis of a number of physical sedimentation parameters. The distribution pattern of the B-C break shows a central shoreface region of coarser ( $< 2 \phi$ ) values, flanked by finer (2-2.5  $\phi$ ) inflection values of the upper and central shoreface. Again, a close relationship between the inlet-delta margin patterns and those of the central shoreface is discernible.

### 5.3 Summary Remarks on Shoreface Sediment Texture

The above results indicate the existence of distinct patterns, both between and within the shoreface subenvironments. A summary of the latter is exemplified by the four cross-shore profiles presented in Fig. 50.

Quite evident is the fact that sands at the distal zone of each of the subenvironments depict a consistently finer mean grain-size, better sorting and (a more) positively skewed than their proximal counterpart. Except for the lower shoreface, the distal sands also clearly have elevated kurtosis values. Significant is also the relative displacement of the modal size class of the distal sand toward the fine end in most of the histograms.

The central-shoreface sands, on the other hand, show clear contrasts to the upper and lower shoreface counterparts in relation to their areal distribution of summary size statistics, grain size fractions and the proportion and properties of their subpopulations, as well as in the pattern of distribution in bivariate plots.

These results demonstrate the complex interplay of sediment supply and hydrodynamic processes (steady and episodic) in shaping and sustaining the shoreface. The mechanics through which the aforementioned are achieved are examined in the next section.

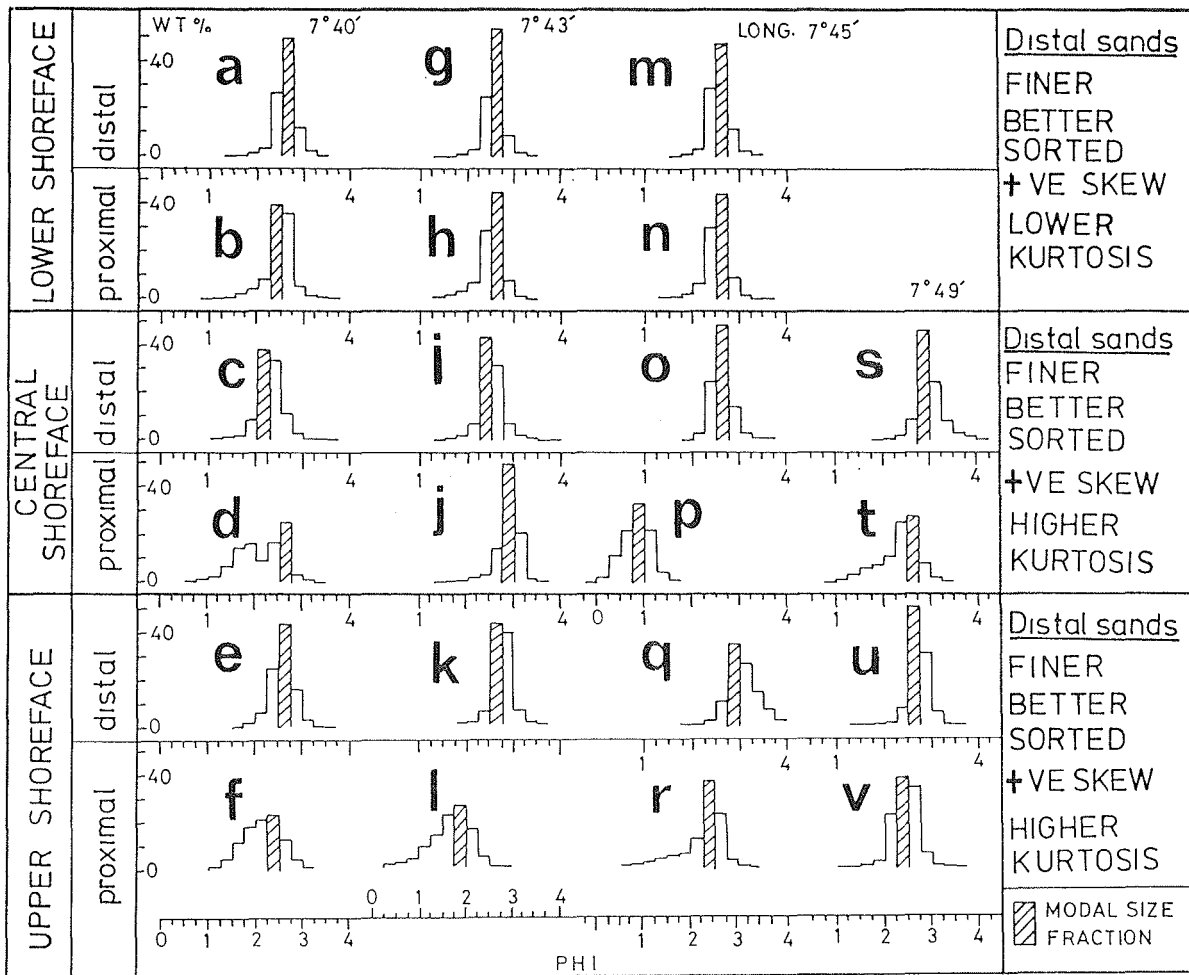


Fig. 50. Patterns of grain size statistical variation between and within the shoreface subenvironments.

#### 5.4 Shoreface Sediment Dynamics: Comparison of Some Texture-Based Sediment Transport Models

A wide variety of models are currently in use for qualitatively predicting sediment transport patterns and pathways based on the grain size characteristics outlined in the previous section. The success ratio of the majority of these models, however, is rarely uniformly satisfactory when applied to a spectrum of different coastal settings.

One of the main reasons for the reported inconsistencies in the predictive power of these models is inherent in their underlying assumptions, these being rarely verified by independent means. In this section, an attempt is made to evaluate the interrelationships and the relative merits of a few of the more commonly employed models by applying them to Spiekeroog shoreface.

#### 5.4.1 Size-Sorting Model

The underlying principles of a variety of size-sorting models are well elucidated by SWIFT et al. (1972b). Essentially, it entails that the flow or transporting medium exerts a discernible imprint in their deposits via some transition probabilities. In a broad sense, the gradient along the transport path may be progressive or punctuated, and may relate to granulometric, petrographic, geochemical or even palaeontologic-biotic parameters. The physical mechanism of size-sorting itself is often related to some probability functions, which thus define the variants of the model (Fig. 51).

Restricting attention to the granulometric parameters, the approach of SWIFT et al. (1972b), albeit conceptual, is remarkable in that it is based on a probabilistic analysis of population dynamics rather than a mere description of the summary statistics of grain size distribution.

As shown in Fig. 51, all the variants of a sorting model predict a decreasing mean grain-size with distance, depth or diminishing flow energy. Moreover, sorting is predicted to improve, while kurtosis increases towards more leptokurtic values. On the other hand, all the variants of the size-sorting model predict a generally more negatively skewed sediment distribution with distance.

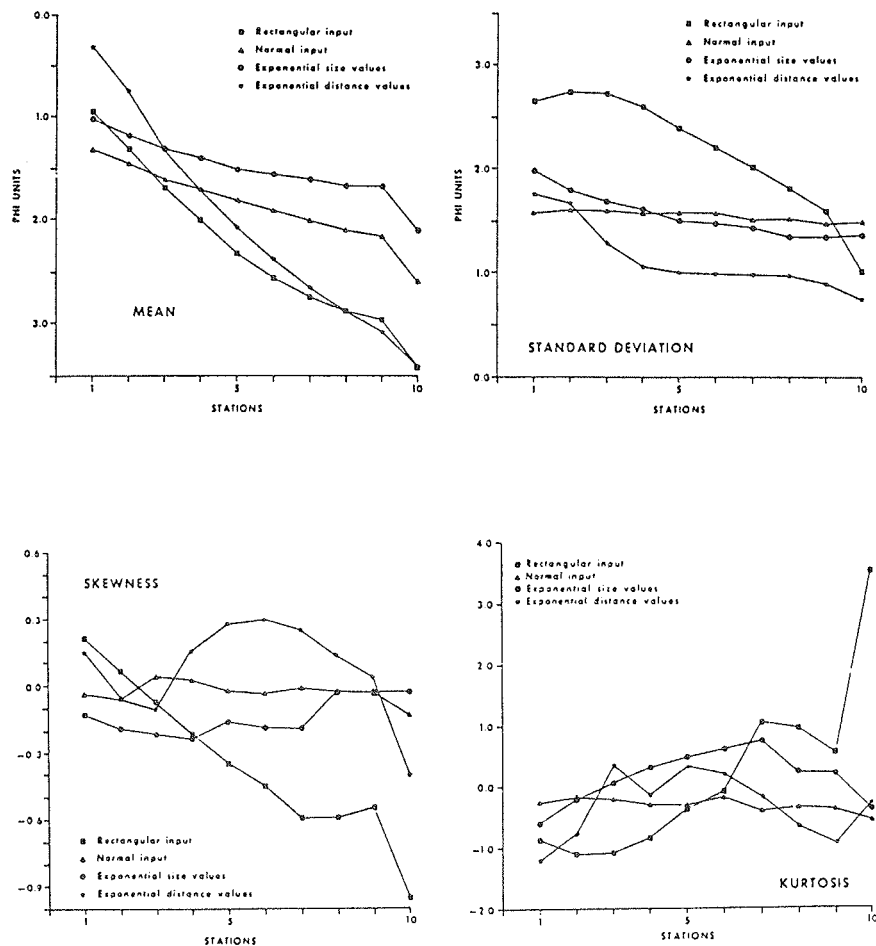


Fig. 51. Variants of a sediment size-sorting model (after SWIFT et al., 1972b).

Textural trends as a reflection of transport path, as amply documented in the literature and exemplified above, are most obvious in (a) environments approaching a closed system, and (b) where the flow is essentially unidirectional or, if reversing, strongly asymmetric.

HAMILTON et al. (1980) have observed that transport path predictions (at least in relation to mean size) are not necessarily true under a reversing tidal current system where opposing flows are competent to entrain a similar spectrum of

grain sizes. While the repetitive selective transport of such a flow system ultimately leads to very-well sorted end-products, the mean grain-size would relate more to the most easily entrained grains rather than the coarser bedload substrate.

In order to assess whether the size-sorting approach is representative, a chart of primary mode-distribution at 0.1 phi intervals (Fig. 52) is first examined. The modal class is a preferable size descriptor to mean size in mixed-mode sediments.

The grain size modal distribution pattern is very similar to that of mean size illustrated in Fig. 23. A central shoreface of coarser-mode sands is flanked on either side by finer-mode sands of the upper and lower shoreface. A coarsening of modal values can be noted at the inlet flanks of the upper shoreface. Also, the upper-shoreface sands have slightly finer modes ( $> 2.6$  phi over much of the area) than the lower shoreface counterpart. The inlet-fallout fines at the eastern margin of the proximal lower shoreface seem to form an upward-fining sedimentary sequence.

Considering all three shoreface subenvironments, it is quite obvious that the depicted gradient in sediment mode is not in conformity with any of the variants of a size-sorting model. In addition, sorting, skewness and kurtosis all show discrepancies across the shoreface. This would firstly imply that the shoreface of Spiekeroog is not a closed system in that extraneous materials have been, or are still being introduced onto the central shoreface. Secondly, it demonstrates the inappropriateness of the size-sorting model of SWIFT et al. (1972b) on the Spiekeroog shoreface.

Interestingly, even with the exclusion of the central shoreface deposit, the gradient of the sediment mode (and invariably mean size) between the upper and lower shoreface subenvironment is also not consistent with a classical

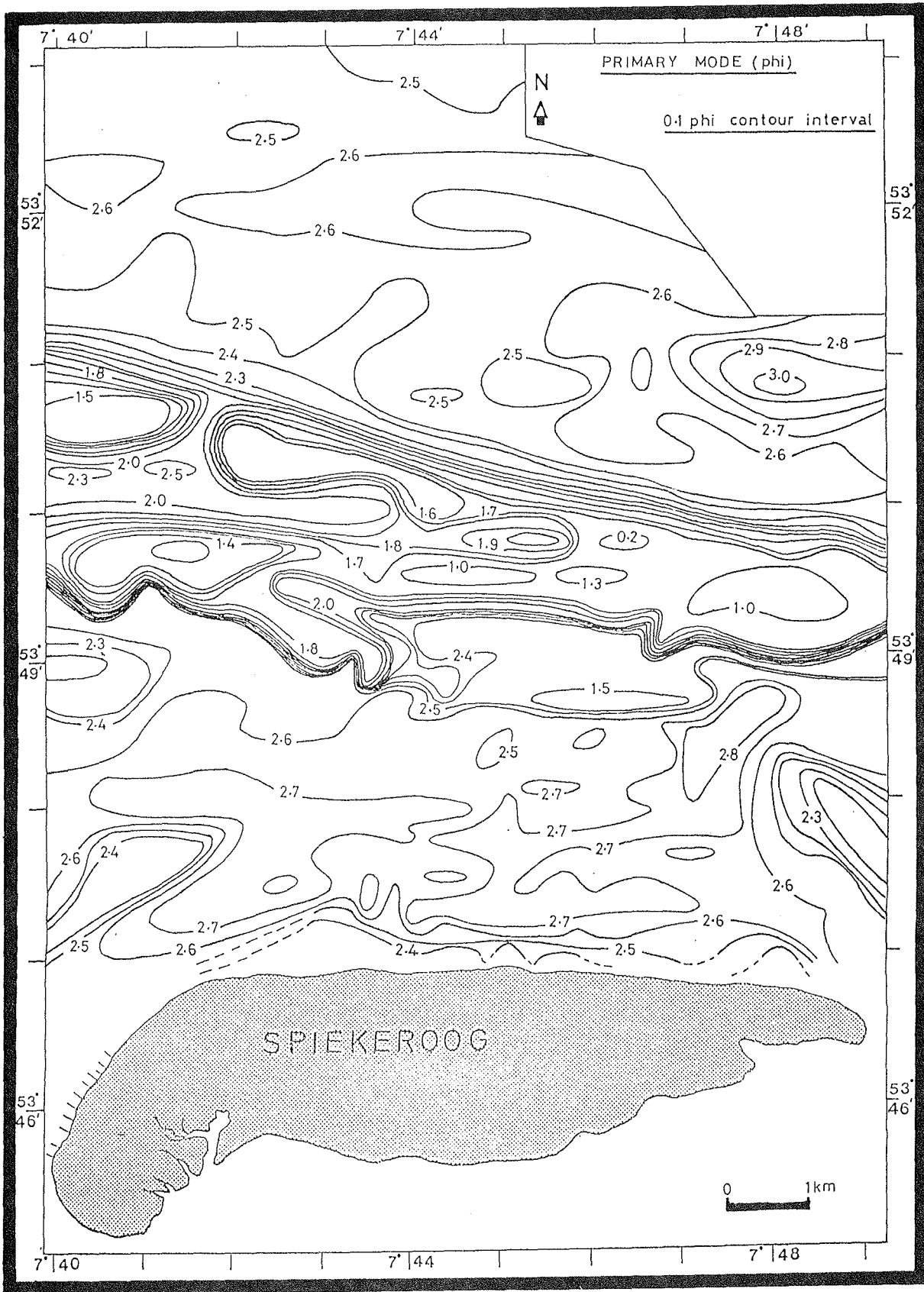


Fig. 52. Areal distribution of shoreface grain size modes.

size-sorting model, in that the lower shoreface sands are on the whole coarser.

Finally, both the areal skewness pattern in Fig. 27 and the observed alternation in proximal and distal sand characteristics (Fig. 50) suggest that size sorting on the Spiekeroog shoreface is punctuated, i.e., locally confined within the shoreface subenvironments rather than progressively developed across these. In this respect, the observations of HAMILTON et al. (1980) are corroborated, especially when taking each of the shoreface subenvironments as a closed system.

Specific textural patterns outlined above may be accounted for by the fact that tidal current velocities, at least on the central shoreface (see Chapter 7), increase distally both during ebb and flood stages. This being the case, the current-mobilized sands in the distal zones should form a better sorted, if not also finer blanket over the depositional surface during slack water than their proximal counterparts. With wave effects superimposed, the distal sands should indeed be finer than their proximal zone counterparts.

#### 5.4.2 VISHER'S Model

The above model is actually a refinement of ideas of DOEGLASS (1946), SINDOWSKI (1958) and MOSS (1963) who, although identifying the relationship between grain size curves and specific sedimentary environments, did not relate these to the depositional processes (VISHER, 1969). VISHER postulated that straight line segments in log-probability plots reflect the three sediment transport modes of suspension, saltation and traction already recognized by fluid dynamists some decades earlier.

From his empirical studies, he noted that there was a discernible difference in the mixing or relative composition,

sorting, size range and truncation pattern of the subpopulations in the different sedimentary environments, and that these disparities have bearing on the prevailing pattern and intensity of fluid motion.

In particular, the traction - saltation (or coarse) truncation and the saltation-suspension (or fine) counterpart have been found to have a bearing on flow hydraulics (e.g., MIDDLETON, 1976). JAGO (1980) examined MIDDLETON's assertion that the settling velocity corresponding to the phi-value of the coarse truncation was of the same order of magnitude as the shear velocity of the flow. He obtained much higher shear velocities than predicted by the inflection point, but noted that the discrepancy could perhaps relate to a wrong estimate of the drag coefficient used in computing the shear velocity.

Even without recourse to rigorous hydrodynamics, several characteristics of the subpopulations have been shown in Section 5.2.4 to display well-defined, bathymetry-related areal patterns which justify a genetic differentiation of the shoreface sands on the one hand and, through comparisons, a contemplation of plausible processes on the other.

Whatever the nature of the processes operating within each of the shoreface subenvironments, the spatial homogeneity of the curve shape parameters of their composing sands suggests a certain degree of distinctiveness of these processes. Observations of VISHER's empirical studies having a bearing on the present study are:

(a) An identical coarse truncation point of 1.5 phi for the inlet sediments as that observed for the inlet margin and central shoreface sands of the study area (Appendix E-4). The upper and lower shoreface sands depict corresponding values in the 2-2.5 phi range. As illustrated by GIBBS et al. (1971; p.11, Fig. 1), the junction between Stokes' and Impact's settling velocity law occurs at 2.25 phi which is comparable to

the coarse truncation value observed. FULLER (1961) also found a highly consistent coarse inflection point of 2 phi in shallow marine sands and considered this break to delimit size populations whose settling behaviour is defined by the above laws. It should be noted, however, that Stoke's law relates to settling in still water, i.e. a laminar condition. FLEMMING (pers comm.) suggests that under turbulent conditions, the above inflection point values may signify the transition between saltation and suspension of grain particles.

(b) Turbidity current deposits are characterized by a poorly sorted suspension (A-component) and saltation (B-component) population and, when a traction (C-component) population is present, is expectedly better sorted. Furthermore, a large variability in the curve shape can be expected due to inherent fluctuations in current velocity and density. These observations are in conformity with the data on the central shoreface sands earlier presented. Compared to the adjacent subenvironments, the traction component is best sorted on the central shoreface, the contrary being the case for the other two components. In addition, the fine truncation point is most variable on the central shoreface (1.5-2.75 phi) as against 2.75-3 phi on the adjacent subenvironments.

Applying the concept of VISHER (1969) to the above results, one could argue that the central shoreface sands were deposited from a turbidity-like or density current. This view-point is elaborated upon in Chapter 7. However, it can be recalled from Fig. 44 that, along the central shoreface axis, the suspension population or component A increases in amount distally (northwesterly), perhaps in response to the declining transport competency of the density current.

In any case, in view of the lack of direct on-the-spot observations, the above interpretation is inevitably tentative. This is more so because inflection points in grain-size curves can also evolve from a mixture of two or more distinct populations (TANNER, 1964; FLEMMING, 1978).

#### 5.4.3 PASSEGA'S Model

The areal distribution of sediment transport modes based on a modified scheme of PASSEGA (1957, 1964) is given in Fig. 53. It is obvious that the transport modes of the central shoreface subenvironment differ from their upper and lower shoreface counterpart. Whereas the latter two shoreface sands are almost exclusively deposited from graded-suspension transport mode, the former reveals areally, subequal representation of the two bottom suspension modes. The latter modes are interspersed with a traction mode. The pattern at the eastern margin of the central shoreface is remarkable in its extent and "sortedness" from traction to lower bottom suspension and upper bottom suspension distally.

The above sequence is a strong indicator of a declining sediment transport competency from the proximal, southeasterly end. Being a regime of reversing flow, one might have of course expected a mirror image of the above transport sequence at the distal end of the central shoreface. The present results, therefore, suggest that the sands on the central shoreface are derived from the eastern inlet source and are subsequently dispersed distally, and not the converse.

It is recalled from the C-M plot of Fig. 43 that the central shoreface sands formed a continuous pattern parallel to the  $C = M$  line. One of the implications of this was that the coarser sediments were very much better sorted than those of the adjoining shoreface. The above result correlates well with the better sorting of the component C or traction population indicated by the central shoreface sands. In terms of an index of maximum sorting (PASSEGA, 1964), the central shoreface sand pattern has a value of 0.75. Thus, these sands are much better sorted than those recorded by the former from wave and turbidity deposits. Unfortunately, both deposits can not be differentiated on the basis of the above sorting index.

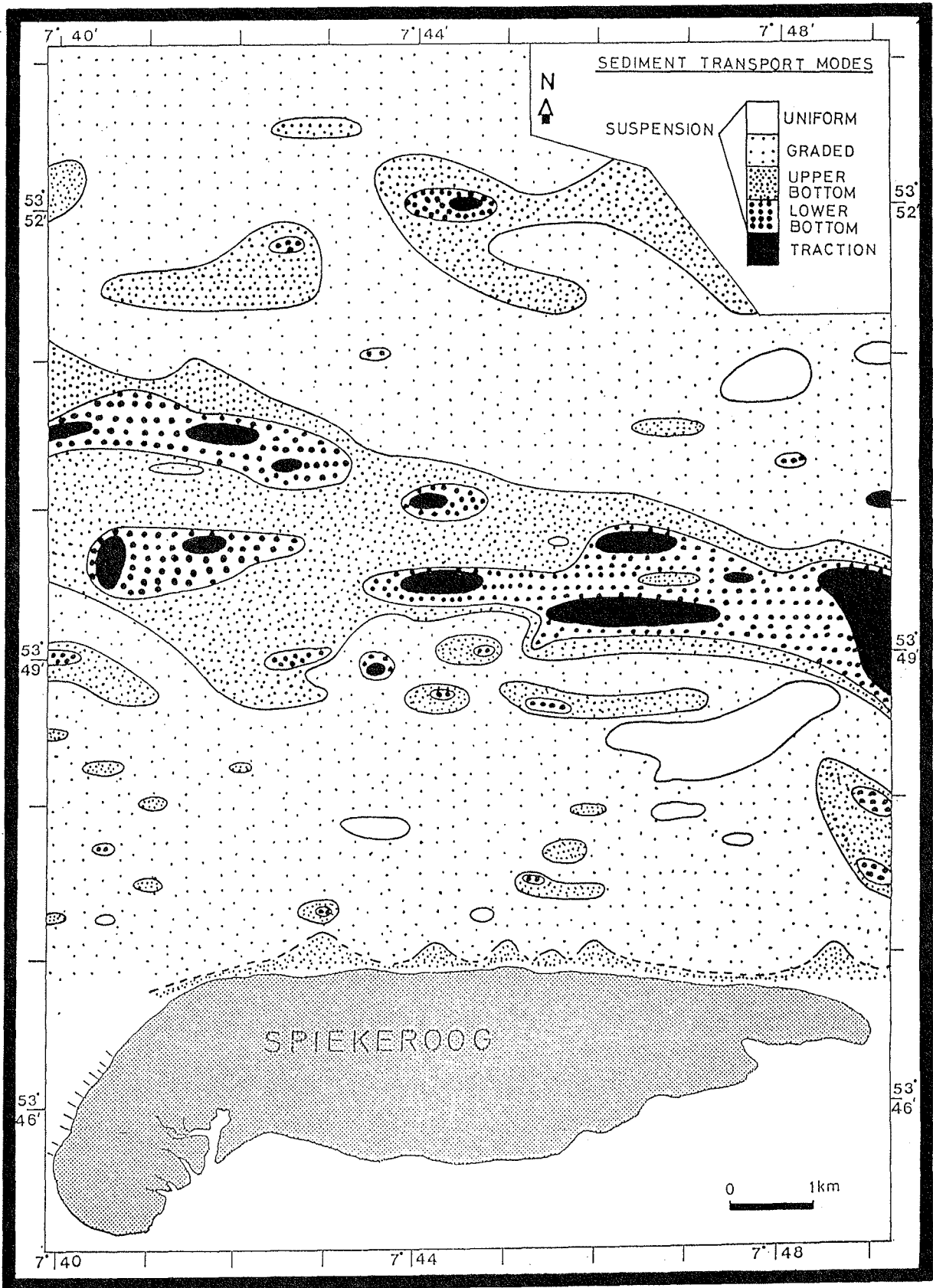


Fig. 53. Areal distribution of C-M based shoreface sediment transport modes.

The absence of a kink in the CM pattern of the central shoreface sands would suggest that the density current from which the central shoreface sands have been, and are being, derived was laterally and longitudinally graded. The good sorting of the central shoreface coarser fractions may additionally imply that, while the depositional events may have been episodic, the depositional process must have been steady in each case.

#### 5.4.4 McLAREN'S Model

The model of McLAREN, (1981) and its modified version (McLAREN and BOWLES, 1985) are in reality a variant of the size-sorting model, in as much as the textural gradient between a potential source and a deposit is related by some form of transport probabilities. The authors refer to the latter as sediment transfer functions.

A low energy transfer function is negatively skewed, and as such successive deposits in a direction of declining flow energy should become finer and more negatively skewed. By contrast, a high energy function is less negatively skewed, and deposits in a declining flow direction should as a result be coarser and more positively skewed than the source. As shown in Fig. 54, the variance or sorting may initially deteriorate, but would ultimately decrease (improved sortedness) with distance.

The areal distribution patterns of mean size, sorting and skewness for the studied shoreface, as summarized in Fig. 50, clearly contradict the modified model of McLAREN and BOWLES. The shoreline - outer surf zone situation is less ambiguous and is drawn upon to illustrate the inconsistency of the above.

Shoreline sands are coarser and negatively skewed, whereas the outer surf zone sands show the converse. Irrespective of the transfer function employed, none recognizes a cross-shore

transport trend to exist between these two shoreface zones, although shore-normal pattern of bar migration documented, for example by FLEMMING (1991), must be in response to such a pattern of sediment transport. It would thus seem that the 1981 version of the McLAREN model referred to in Section 5.2.1.3 is more creditable.

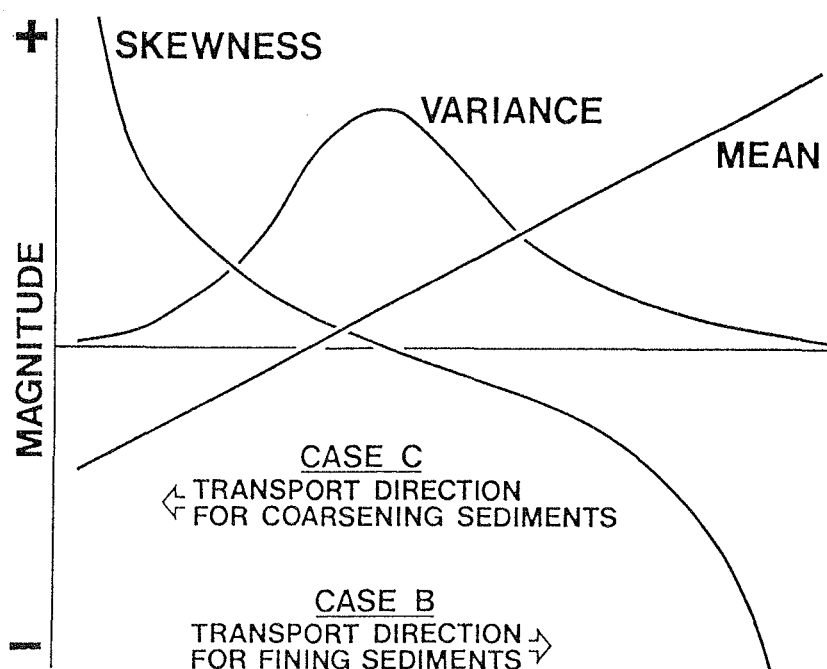


Fig. 54. Sediment source-deposit predictive model (after McLAREN and BOWLES, 1985).

#### 5.4.5 Storm-Sedimentation Model

It is apparent by now that the Spiekeroog shoreface is not a closed system and that the central shoreface sands are allogegenic. All of the areal distribution charts of grain size statistics and curve shape parameters attest to a tripartite zonation of the shoreface.

It is a well established fact that the coarse fractions of sediment size distributions are a reliable indicator of sediment dynamics and provenance. This is primarily because of their relatively low mobility under "normal" flow conditions. The areal distribution pattern of the coarsest percentile illustrated in Fig. 55 corroborates this conclusion.

Generally, two types of high energy processes leading to a concentration of coarse fractions can be envisaged, namely a "negative" and a "positive" one. The former is exemplified in the study area along the shoreline, where winnowing of fines results in a coarse lag. The positive counterpart entails an extraneous supply of coarse material, as is invoked for the central shoreface.

Even a cursory examination of Fig. 55 makes it clear that the central shoreface sands cannot be autochthonous, neither in the sense of representing in-situ winnowed lag deposits nor as reflecting a local source. The flanking finer sand sheets of the upper and lower shoreface defy any such in-situ origin, a conclusion that is corroborated by the fact that vibrocore data (Section 6.3.4.1) indicate the coarse sediments on the central shoreface to be merely surface concentrates.

By contrast, the upper shoreface inlet margin first-percentile values show marked similarities and continuity with the central shoreface counterpart to invoke a tidal inlet origin of the latter. The sizes of sands involved dictate that the bulk of the sediment supply from within the inlets should occur during episodic storms when the ebb flow intensity is strongly amplified.

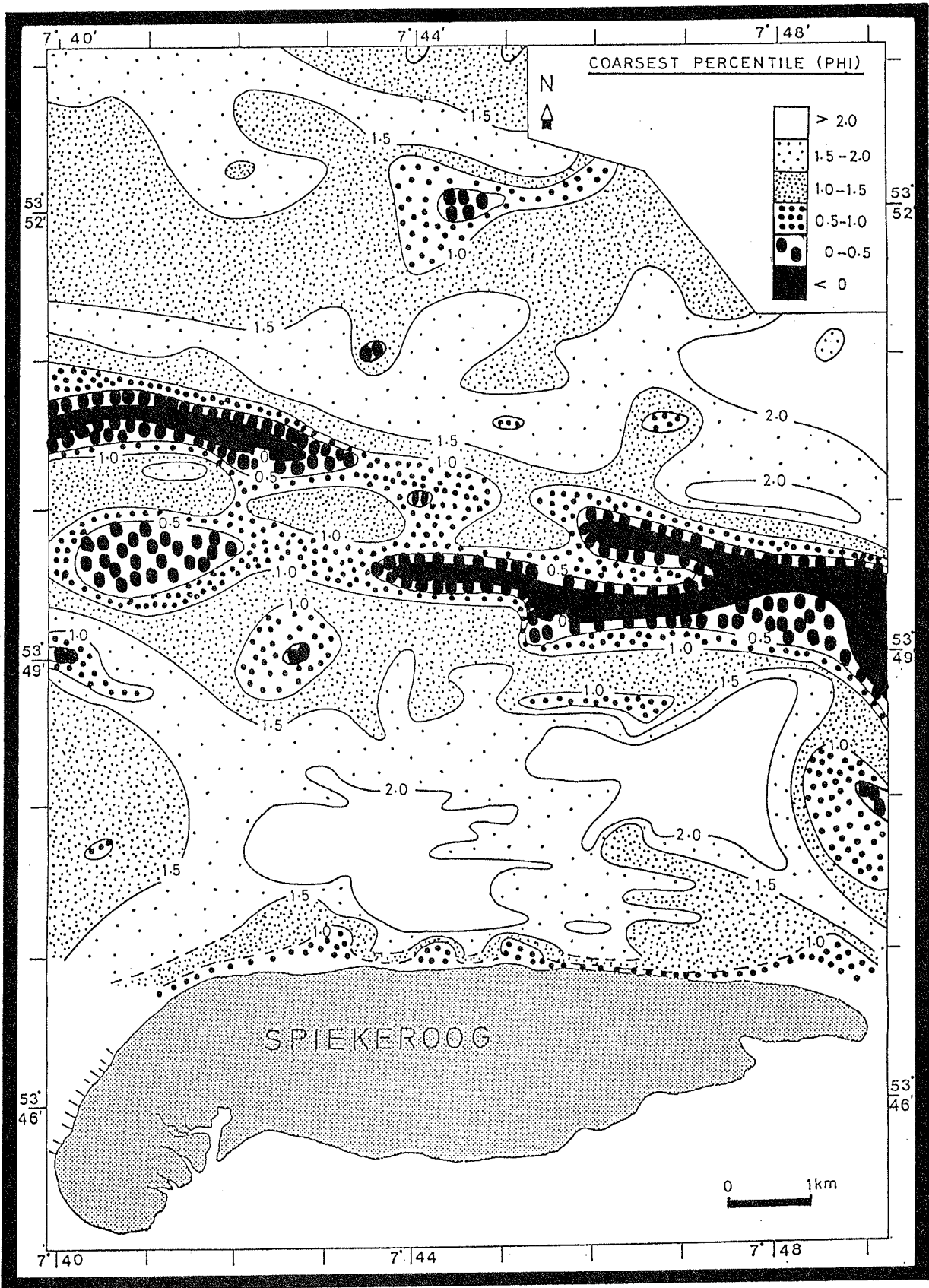


Fig. 55. Areal distribution of the phi coarsest percentile.

#### 5.4.6 Summary Remarks on Sediment Transport Models

A comparative evaluation of the existing qualitative sediment transport models does show that:

(1) The central shoreface sands are allogenetic and have been steadily deposited over time from density currents emanating from the inlets during episodic storm events.

(2) The upper and lower shoreface sands both have a similar principal mode of transport, representing saltation (VISHER) or graded suspension (PASSEGA).

(3) Size-sorting is more significant within, as against between, the shoreface subenvironments.

(4) The sediment transport trends predicted by the model of McLAREN and BOWLES (1985) are not realistic in the present study area.

#### 5.5 Shoreface Sediment Budget

Sediment budgeting is a very important tool in modelling flow / substrate interaction. The time-scale and water depth covered by the budget calculations may, however, be decisive in determining the representivity (event or cumulative response) and the utility of the results.

In general, budget results from shallow depths are most reliable for shorter time intervals because of the inherently high sediment mobility in this region. The results presented here are based on a 15-year time interval and are hence deemed to represent more of the cumulative or average response in the distal shoreface region. While sediment budget patterns between the survey dates are expectedly real, the accuracy of the calculations is dependent on the accuracy of the sounding charts.

The general pattern of volumetric erosion and accretion of the sea floor over the 15-year time interval is shown in Fig. 56. The contour interval is  $2.5 \times 10^3 \text{ m}^3$ , this corresponding to a net depth difference of 25 cm over a  $100 \text{ m}^2$  surface area. The budget area is limited by the extent of sounding to between the shoreline and water depth of 12-14 m relative to NN. Hence, calculations do not incorporate data from the lower shoreface zones and the distal central counterpart. The accretional regions are stippled, and are flanked on either side by negative budget regions. The zero line is delimited by the bold contour.

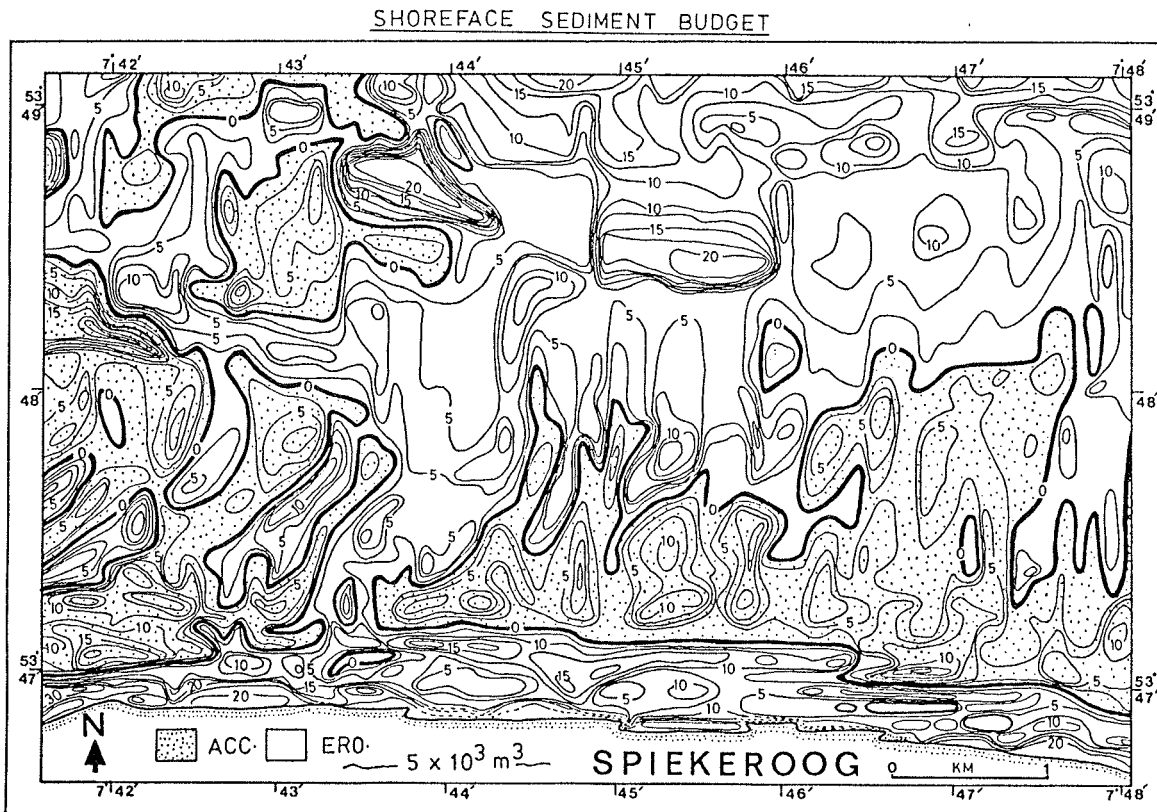


Fig. 56. Areal pattern of volumetric shoreface erosion and accretion.

### 5.5.1 Erosional Pattern

Relative to the 1960 chart, a total of 14.4 million  $m^3$  of sand was removed from the budget area over the 15-year time interval. The region of sand deficit (volumetric) or negative budget (Fig. 57) constitutes about two-third of the shoreface budget area.

Two major seabed erosional provinces are distinguishable: a relatively narrow shoreline - inner surf zone province and a much broader outer shoreface province. Within both regions, strong gradients in the magnitude of volumetric change are apparent. The higher ( $> 10 \times 10^3 m^3$ ) sand deficit regions are stippled more densely in the figure.

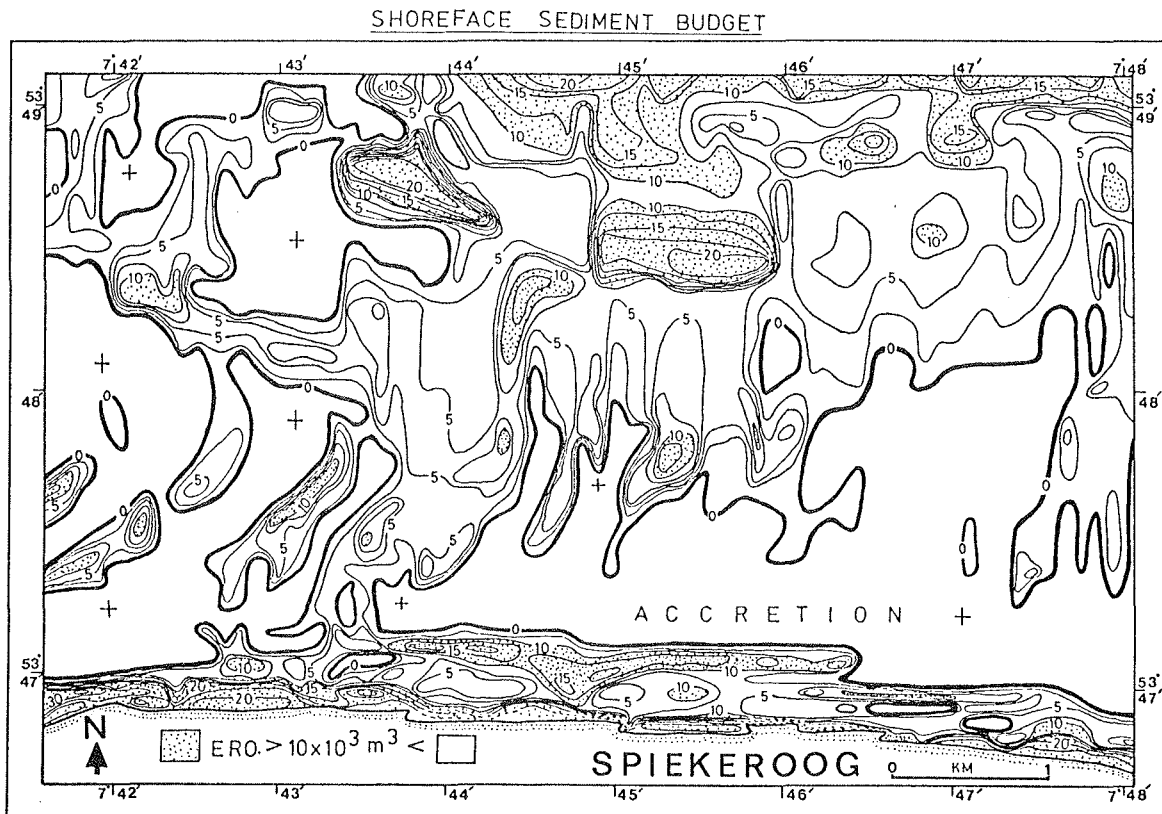


Fig. 57. Negative volumetric shoreface sediment budget pattern.

While the occurrence of a high negative budget close to the shoreline and just seaward of it can be conceived to reflect wave breaking processes and trough scouring, a similar degree of deficit in deeper waters cannot be due (solely) to wave action. Since the latter high-deficit region corresponds in location and orientation to the shoreface-connected ridge morphology, tidal (probably storm-amplified) currents are invoked to have been responsible for the observed deepening. Unfortunately, the offshore limitation of the budget area precludes an assessment of sediment budget changes in the main ridge area of the central shoreface. Consequently, it is a matter of speculation if the observed sand volume deficit would have been balanced by a corresponding surplus further offshore.

Finally, it is noted that unlike the smooth landward margin of the positive budget region, the seaward counterpart is indented or incised. These indentations in fact correspond to the swales of the sawtooth bar morphology. Although few of these incisions, especially in the central part, show spacings comparable to that of the above morphology, the poorly defined pattern is due to the high mobility of the latter. Each of the swales reveals a deepening of the order of 0.5-1 m over the 15-year period.

#### 5.5.2 Accretional Pattern

The accretional region is largely confined to latitudes  $53^{\circ} 47'$  and  $53^{\circ} 48'N$  (Fig. 58). This defines the medial upper shoreface or the saw-tooth bar zone. However, a further accretional province occurs at the northwestern part of the budget area.

The latter is particularly instructive in that it corresponds to the deeper distal end of the shoreface-connected ridges. This occurrence would support the grain size statistical inference that the major transport trend along the

central shoreface is from southeast to northwest. In all, only 1.4 million  $m^3$  of accretion was apparent during the budget interval, relative to the 1960 chart.

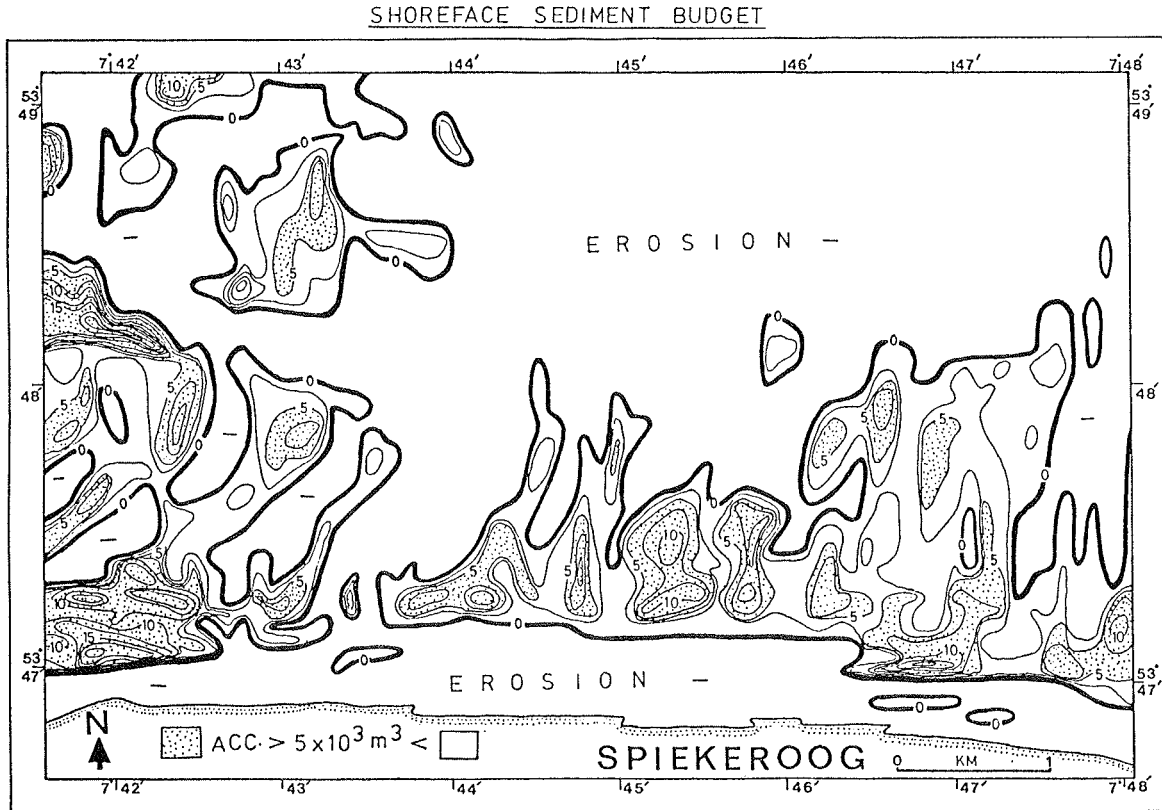


Fig. 58. Positive volumetric shoreface sediment budget pattern.

### 5.5.3 Summary Remarks on Sediment Budget Patterns

In order to better assess the spatial variability of the sediment budget analyses above, data were latitudinally partitioned into five cross-shore shoreface zones (Fig. 59). The latter reveals a net loss of sand from the budget area over the 15-year interval estimated at 13 million  $m^3$ . The maximum net cross-shore loss of sand (1.8 million  $m^3$ ) was from Zone 1 (shoreline-inner surf or beach). It can be speculated that much

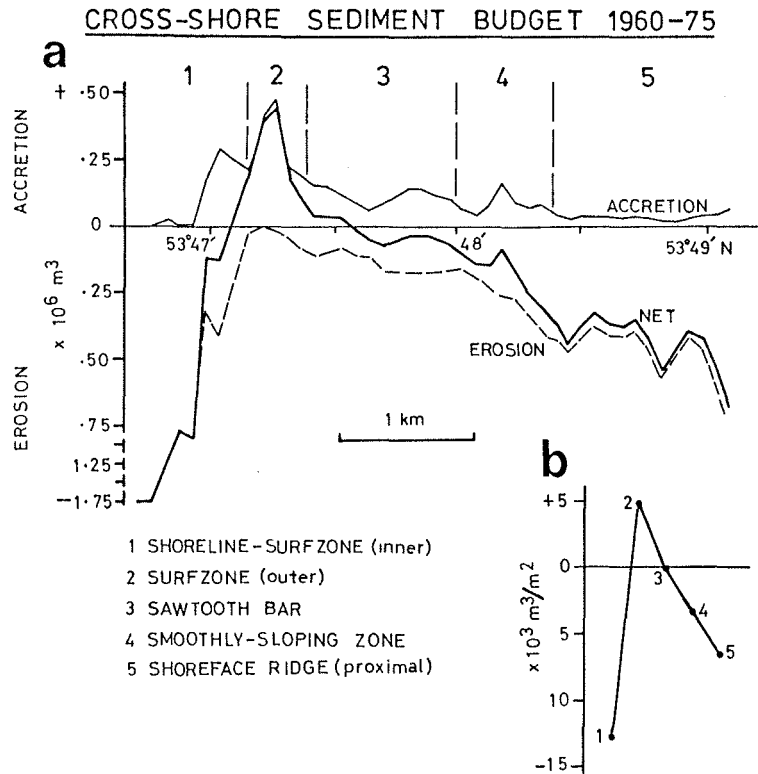


Fig. 59. Cross-shoreface sediment budget variation. (A) Accretional, erosional and net cross-shore volumetric budget curves. (B) Net volumetric change per total surface area of the morphozones.

of the above negative budget may have resulted from the severe storm of 1962 in which the eroded beach sands were deposited in the outer surf zone.

Beyond the outer surf zone of net positive budget values, corresponding to the isolated shore-parallel outer bar or Zone 2 in Fig. 59a, a steadily increasing net sediment loss is observed. The net volumetric change per total surface area of the different morphozones of the shoreface (Fig. 59b) reveals a similar pattern as that of the net total cross-shore

earlier discussed. Because the positive budget in Zone 2 is inadequate to offset the total loss from the budget area, it is evident that this budget segment of the shoreface is a net sediment export region.

Although it is not clear at this stage where the eroded sediment was exported to, it is anticipated that a positive budget would be evident seaward of the examined budget boundary. This is borne out of the fact that the central shoreface sands and part of the proximal lower shoreface counterpart, especially the tongue of fines, are extraneous.

Besides the cross-shore pattern, the alongshore counterpart (Fig. 60) was found to be similarly illuminating. The latter is limited to the wave-dominated upper shoreface subenvironment. The pattern of net volumetric change pattern over the 15-year interval shows a positive budget close to the flanking ebb-deltas and a negative budget close to the centre line of the island.

As schematized above, the pattern is in conformity with a wave refraction / longshore drift-reversal process which appears to have been first documented for mesotidal inlets (HAYES, 1970 cf., BOOTHROYD, 1985). The report of DEAN and WALTON (1975) also corroborates the significance of wave refraction in sand-trapping processes around inlets.

Essentially, the above process leads to a development of a nodal zone on either side of which longshore currents flow in opposite directions. The nodal zone is expected to be depleted of sand and hence erosional in character. The nodal zone concept has been shown to occur on various scales (e.g., ASHLEY et al., 1986) and also along microtidal coasts which are tide-dominated (REYNOLDS, 1988). The latter observed that the nodal zone of sand depletion migrates downcoast with increasing size of the ebb-delta.

ALONGSHORE UPPER SHOREFACE VOLUMETRIC  
CHANGE (1960-75)

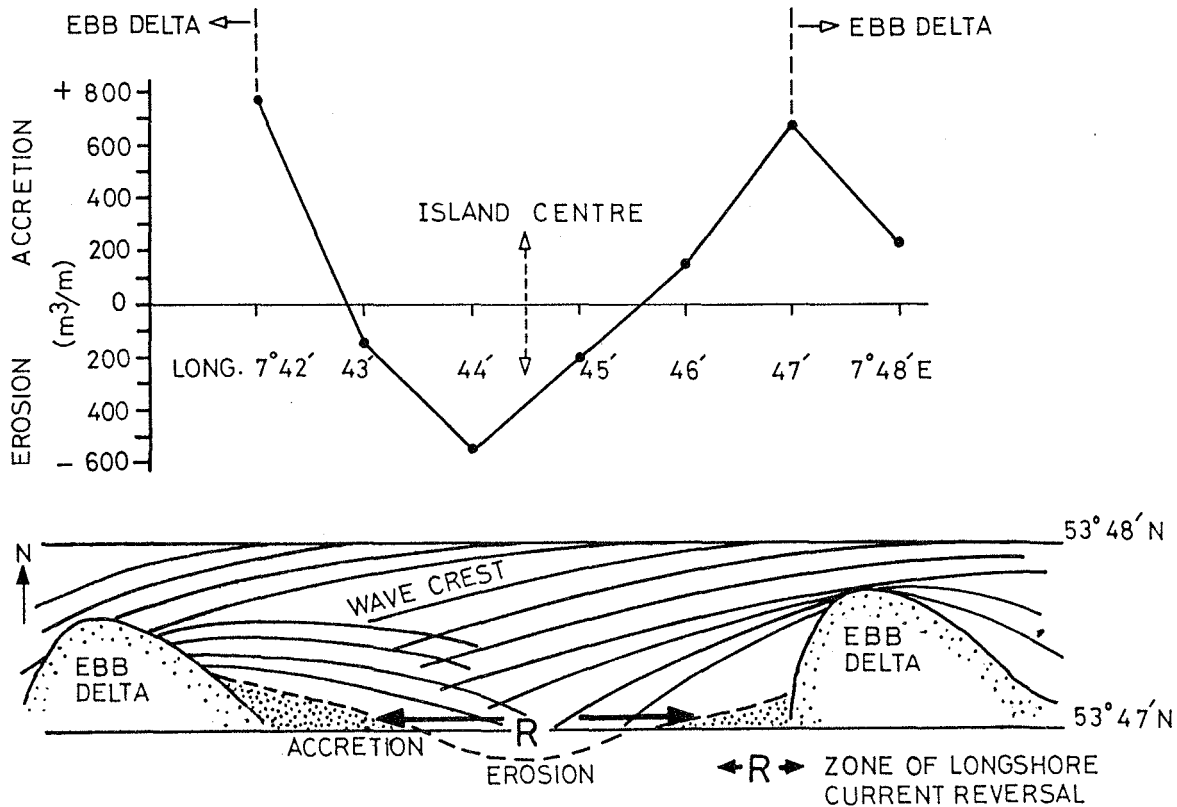


Fig. 60. Alongshore shoreface sediment budget variation.

MIKESH et al. (1969) (cf. OERTEL and HOWARD, 1972) have also documented sand depletion at mid-island shorelines of the Georgia (USA) coast. OERTEL and HOWARD (1972) relate the latter observation to sediment gyres - a variant of sand trapping mechanism developed by wave-induced currents during the ebbing tide.

This alongshore pattern off Spiekeroog represents the first reported evidence of such a nodal zone along a Frisian barrier island. It mitigates against the often implied opinion of a continuous eastward-directed longshore sand transport within the littoral zone of the Frisian islands (FRELS, pers. com). While a strong and consistent eastward longshore transport within the beach and surf zone region is easily conceived based on their eastward-opening, shoreline-acute breaker angles, and

from results of tracer experiments (FRELS, pers. comm), the summarizing data of Fig. 60 shows that this is not necessarily the case in each of the wave-dominated upper shoreface zones. Further implications of these and other sediment budget patterns in deducing flow patterns are considered in Chapter 6.

## CHAPTER 6

### HYDRODYNAMICS, MORPHODYNAMICS AND SEDIMENTARY FACIES ASSOCIATIONS OF THE SHOREFACE SUBENVIRONMENTS

#### 6.1. Introduction

In this chapter, the process-response characteristics between the upper, central and lower shoreface subenvironments on the one hand, and their constituting zones on the other, are contrasted. In order to enhance comparisons between the results of the present study and those of previous studies (Section 2.2), the discussion will endeavour to focus on each of the following three aspects: hydrodynamics, morphodynamics and sediment facies.

Hydrodynamics constitutes the process variable, whereas morphodynamics and facies development represent the response variables. Discussion on hydrodynamics will be based on measured or inferred fluid motions; morphodynamics involves time-varying changes in bottom morphology/bathymetry, whereas facies embody variations in sediment size statistics and on sedimentary structures (physical and biogenic) examined, as well as bedform predictions based on empirical studies (e.g., RUBIN and McCULLOCH, 1980).

The subdivision of the shoreface subenvironments may either relate to actual bottom morphology and/or based on terminologies reflecting seaward increasing seaward distances (e.g., proximal, medial and distal).

#### 6.2 Upper Shoreface Subenvironment

The upper shoreface subenvironment is divided into four facies zones : shoreline-beach (SB), surf (S), sawtooth bar (STB), and smoothly sloping transitional (SST) zones.

For convenience, the surf zone is subdivided into an inner and an outer zone, of which the former will be discussed along with the more genetically and dynamically related shoreline-beach zone counterpart.

## 6.2.1 Hydrodynamics, Morphodynamics and Facies

### 6.2.1.1 Shoreline-Beach Zone

#### Hydrodynamics:

The shoreline-beach and inner surf zones constitute the proximal region of the upper shoreface. Some details on shoreline and surf-zone hydrodynamics considered to be applicable to the study area have already been presented in Section 2.2.1

For instance, the dominantly spilling wave-breaking pattern observed is consistent with the wave-breaker height, period and beach slope relationship documented by GALVIN (1968). Based on a fair-weather mean wave height of 1.5 m, the most seaward breaking depth will generally be above the NN-2 m isobath relative to the mean sea-level. This depth serves as a boundary between the inner and outer surf zones.

The generally shoreline-oblique (north-westerly emanating) incidence of breaking waves is suggestive that eastward flowing longshore current must be a potential sediment transport medium in the proximal upper shoreface region. Evidence from changes in bottom topography and sediment size parameters (to be discussed subsequently) is consistent with the above.

Nevertheless, there is still a dearth of information on volumetric rates and temporal variability of sediment transport by longshore currents in the study area. Also uncertain is the relative importance of a continuous as opposed to a cellular nature of the transport pattern, although sediment budget

calculations for the upper shoreface as a whole (Fig. 60) suggest a reversal in the net easterly longshore pattern.

Besides wind-generated surface gravity waves and their associated currents (longshore and cross-shore), the cursorily observed longshore sinuosity of wave swash excursions on the beach provides a compelling reason to believe that low frequency oscillations (edge waves) of uncertain character and origin must be an intermittently important process variable in this zone. Similar inferences have been made elsewhere (e.g., HUNTLEY et al., 1977; KATOH, 1981). These sinuous swash patterns are most obvious in the study area on occasions where rising tides coincide with high waves.

The general lack of time-series measurements of the process variables in this zone implies that the strength and pattern of waves and currents and, in the case of edge waves, also the mode have to be inferred from the morphology, grain size statistical parameters and facies characteristics of the sea floor.

#### **Morphodynamics :**

With respect to morphodynamics, limited short-term ground observations have been made in this zone. Most of the information on physical changes are based on intermediate- and long-term records, as are respectively exemplified by the evaluation of aerial photos (FLEMMING, 1990b) and historical charts (Fig. 61; FITZGERALD et al., 1984).

Taken together, the above data reveal some very significant changes to have taken place on historical time scales and that the present-day morphodynamics of the shoreline-beach and inner surf zones are substantial. The salient variations are:

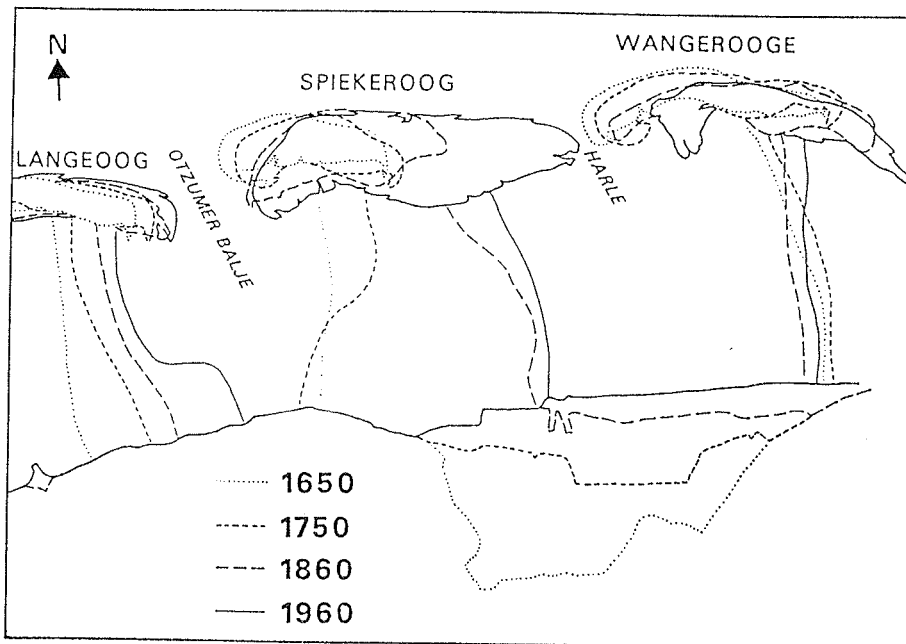


Fig. 61. Historical change in East Frisian barrier island shoreline position and size. Note the changes in backbarrier water sheds. (after FITZGERALD et al., 1984).

(a) A 4.6 km (89%) eastward island and hence shoreline growth over the past 310 years (1650-1960). This increase has been largely accommodated by a 3.8 km decrease in width of the eastward flanking Harle Inlet. The westward fringing Otzumer Balje Inlet showed only a marginal width decrease of 30 m over the same interval. A corresponding deepening of these inlets (on the average 6-10 cm/yr) would be shown to have played a major role in the evolution of the central shoreface morphology and facies.

(b) Along the shoreline an eastward-opening oblique bar-trough topography is evident. The bars seem to be attached to the shoreline at quasi-periodic spacings of about 900m (cf. FLEMMING, 1990b). Knowledge of the dynamics and flow pattern associated with the bars in the study area is still rudimentary. However, some general remarks are useful.

The above shoreline-attached oblique bar system seems to have a greater temporal stability in form and position (being recognizable on both 1960 and 1975 topographic charts) than similar features reported by CHAPPELL and ELIOT (1979) from a microtidal, high energy coast of Australia.

On both coastline settings, as well as on some sections of the mesotidal Atlantic coast of Aquitaine, France, the acute angle formed by the bar relative to the shoreline opens in the direction of the subordinate longshore transport. This would suggest an intimate association between bar development, if not origin, and the obliquely shoaling surface gravity waves and/or their generated longshore currents. The ephemeral nature of the bar form on the Australian coast most probably reflects the high variability of the wave regime.

Finally, some comments on the origin of the bars seem appropriate. As a first step, the mechanisms of formation of physically, if not genetically, related surf zone longshore bars are considered. Controversies still exist on this topic, particularly with respect to the multiple linear types. The various postulates discussed so far in the literature can be accommodated within two broad classes of wave-period dependent forcing models, i.e. a gravity and an infragravity wave model.

To the first class includes waves which may be standing (e.g., CARTER et al., 1973; LAU and TRAVIS, 1973), breaking (MILLER, 1976; GREENWOOD and DAVIDSON-ARNOTT, 1979; DALLY, 1987) or progressive (BOCZAR-KARAKIEWICZ and DAVIDSON-ARNOTT, 1987). The second class incorporates infragravity waves or surf-beat and is favoured, amongst others, by SHORT (1975), SALLENGER et al. (1985) and AAGARD (1991).

Both classes of models show varying degrees of deficiencies when strictly applied to natural observations. For instance, although some variants of the breaking wave hypothesis (GREENWOOD and DAVIDSON-ARNOTT, 1979; DALLY, 1987) show

spilling rather than plunging breakers to be associated with bar formation, the cross-shore spacing and location of the bars are not predictable. In any case, SALLENGER et al. (1985; p.250) have shown that the breaker type pattern (spilling or plunging) is not a significant factor in bar generation, at least during storm events. However, an all year-round observation on a moderate- to high-energy coast by ANTIA (1989c) reveals that the longshore bar-trough topography tended to be more stable or persistent along beach segments characterized by a low spilling/plunging breaker ratio value.

Two basic shortcomings of the surf-beat mechanism have been highlighted by DALLY (1987). The first concerns the non-stationarity of the nodes and antinodes of the oscillation, given their broad-band nature (GUZA and THORNTON, 1985), and the associated ambiguity of respectively relating the location of a bar crest to either the node or antinode as a function of the dominance of sediment transport mode (bedload or suspension). The second shortcoming is the irony of explaining the seaward increasing amplitude of bars in nature (e.g., GREENWOOD and DAVIDSON-ARNOTT, 1975) by a correspondingly offshore decaying surf-beat oscillation.

The above queries are being addressed in recent studies. For example, the possibilities of a preferential selection (bottom morphology effected) or a temporal segregation (a function of the external forcing) of a dominant surf-beat characteristic have been discussed (BAUER and GREENWOOD, 1990 p.194-196; AAGAARD, 1991 p.802, 809-811). Secondly, much of the recent field evidence suggest bar crests to form at the antinodes. It should be noted, however, that DALLY's queries arose from the results of a rather simplistic (compared to real-world circumstances) but not necessarily explicit laboratory studies.

Furthermore, while some variants of the gravity wave model may indeed be significant under certain surf zone

conditions, e.g. where bars are exclusively linear and shore-parallel, this can certainly not be the case where (i) linear bars are succeeded seaward or shoreward by rhythmic bars (e.g., BOCZAR-KARAKIEWICZ and DAVIDSON-ARNOTT, 1987; AAGARD, 1991), and (ii) linear bars are transformed to crescentic ones (SALLENGER et al., 1985; SONNENFIELD and NUMMEDAL, 1987; BAUER and GREENWOOD, 1991).

In the case of the Spiekeroog surf zone, the situation is somewhat peculiar because elements of both models are exhibited. While the evolution of the shore-parallel outer surf zone bar (Section 6.2.1.2) may have bearing with a variant of the wave-breaking cross-shore flow hypothesis (although their crescentic seaward outer margin suggests subsequent edge wave modification), the along-coast positioning and quasi-periodic spacing of the shoreline-attached oblique bars are neither in consonance with a solely shore-normal progressive wave model proposed by BOCZAR-KARAKIEWICZ and DAVIDSON-ARNOTT (1987), nor the turbulent dynamics and cross-shore standing wave models of other authors.

HOLMAN and BOWEN (1982) have demonstrated theoretically how the interaction of different edge wave modes can generate similar rhythmic features. The significance of the latter study is the ability to simultaneously generate both linear and rhythmic bar forms.

(c) Beach morphology (Figs. 62a, b) is generally of low gradient (commonly 1:80 - 1:125) and at some sections may be characterized by a ridge and runnel (or trough) topography. The dynamics of the Spiekeroog beach system seem to respond mainly to a seasonal summer/winter variation in wave energy (cf. FLEMMING, 1990b). However, in addition to a seasonal berm oscillation of 80-100 m, a retreat of the order of 200-300 m was found to be associated with severe episodic storm surges such as those of 1962 and 1976, with a beach recovery period of the order of 10-15 years.

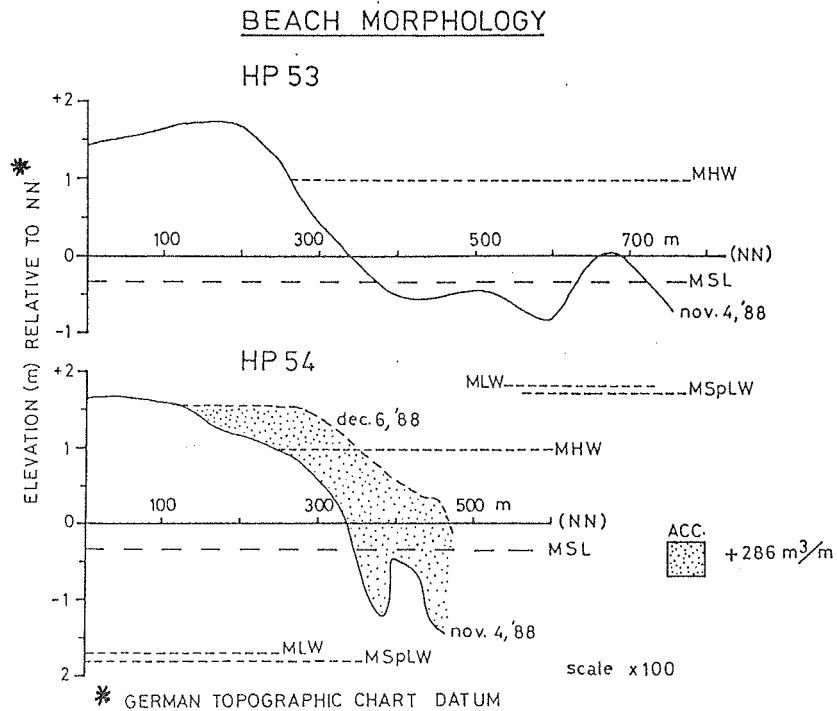


Fig. 62a. Spiekeroog beach profiles indicating short-term fluctuations.

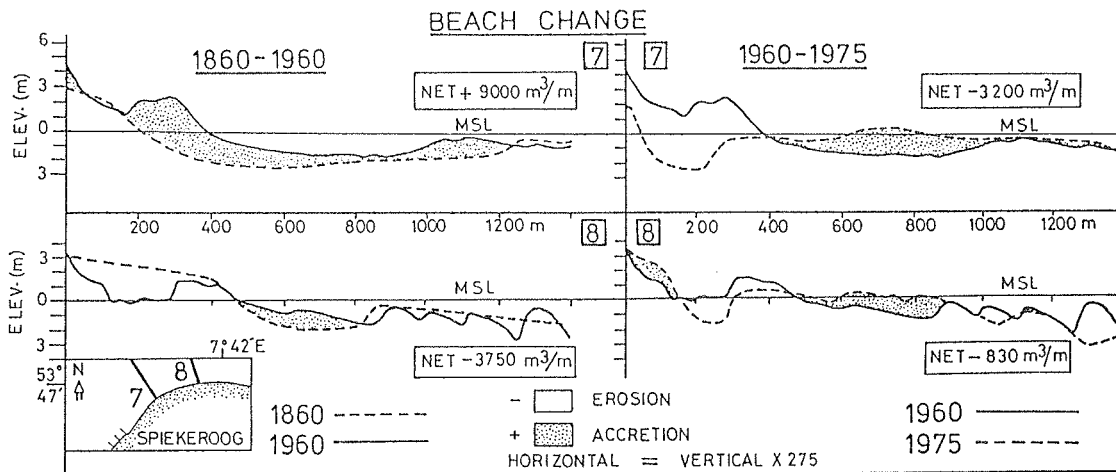


Fig. 62b. Spiekeroog beach profiles indicating the intermediate- to long-term active zone (modified from HOMEIER and LUCK, 2978)

In Fig. 62b, centennial and decadal beach changes are compared for two profiles located at the western flank of the island. The contrasts evident in Profile 7 over the two time-intervals clearly emphasize the inherent dangers of over-dependence on "long-term" data in engineering designs on beaches, i.e., beaches are highly dynamic geomorphic systems whose attributes should be assessed on brief time-scales.

The beach profile comparisons in Fig. 62b demonstrate that in this particular case, the active beach zone has remained unchanged over the period 1860-1975. Finally, the result of the 15-year (1960-1975) period in which a decrease in net sediment deficit is evident between Profile 7 and 8 would seem to suggest an eastward longshore sediment transport along the beaches (see also Section 5.5).

(d) Figure 62a is further instructive in that a net accretion ( $286 \text{ m}^3/\text{m}$  of beach length), instead of erosion, was observed along the illustrated survey profile following a December 4-5 1988 storm event, the latter coinciding with a spring tide. This observation emphasizes the fact that, irrespective of the incident wave energy levels, the response pattern of a beach is strongly determined by the antecedent beach-state (WRIGHT and SHORT, 1983).

WRIGHT and SHORT (1983) indicate a strongly dissipative beach-state to be the most stable, being the result of extreme erosional activity (Fig. 4). Thus, as long as flow conditions (also storms) are less intense as that responsible for maintaining the above beach-state, the beach can even accrete as observed. The result further corroborates an earlier assertion (e.g., SHORT and HESP, 1982; ANTIA, 1991) that, under certain beach-states (most commonly dissipative), a retreat of the berm is not necessarily synonymous with a net loss in beach volume over a given time-interval.

(e) Consideration of beach slope and typical range of wave conditions along the East Frisian coast in general (Section 3.6.4) suggests that Spiekeroog is modally characterized by an extremely dissipative beach-state. As a matter of fact, the computed values of the surf-scaling parameter ( $\mathcal{E}$ ), computed based on the equation of GUZA and INMAN (1975) :

$$\mathcal{E} = H (2\pi/T)^2 / g (\tan\beta)^2$$

(where  $H$ ,  $T$ ,  $\beta$  and  $g$  respectively designate wave-breaking height, wave period, bottom slope and gravitational acceleration,  $m/s^2$ ), is mostly in the 1000-2000 range. This range of values, which is double to four times the value reported in the literature (e.g., WRIGHT et al., 1982a), evidently places Spiekeroog into an extremely dissipative beach category.

(f) The absence of rhythmic features in the surf zone of Spiekeroog is considered to relate to its mesotidal character. This follows from the suggestion of WRIGHT et al. (1982a) that a large transient variability of the surf-scaling parameter, as would typically be the case along meso- to macro-tidal shorelines could lead to a suppression of the growth of resonant phenomena such as edge waves - at least those resulting from wave-wave interaction.

(h) Sediment budget calculations over the 15-year interval from 1960-1975 (cf. Fig. 59a) indicate a net loss of about 1.8 million  $m^3$  of sand from the beach. This is equal to 14% of the total volume removed from the budget area. Changes in the inner surf zone were also considerable, depicting a loss of  $900 \times 10^3 m^3$ , but sharply changing to a net gain at its outermost boundary. The cumulative net volumetric change per unit area (Fig. 59b) was highest in the shoreline-beach and inner surf zones, accounting for 55 % of the loss within the budget area.

(i) In order to examine the possible significance of longshore sediment transport processes on the upper shoreface over the above budget period, the result of the alongshore sediment budget presented in Fig. 60 was re-evaluated for 6 adjacent uniform area (1.1 km long and 0.3 km wide) compartments of the proximal (beach-inner surf) and distal (smoothly sloping transitional) zones of the above subenvironment (Table 4).

Table 4. Alongshore sediment budget data for two upper shoreface zones.

	7° 42'	43'	44'	45'	46'	47'	48'
Distal ( $\times 10^6 \text{ m}^3$ )	+2.3	-5.3	-4.5	-5.3	-0.8	+0.1	
Proximal ( $\times 10^6 \text{ m}^3$ )	-15.8	-15.2	-11.1	-6.3	-2.2	-5.1	

A number of points are quite instructive from Table 4, albeit, inconclusive. Firstly, there is a general eastward decrease in volumetric erosion. Sand budget calculations for each of the two westernmost, central and eastern longitudinal compartments of the proximal zone yielded losses of 31, 17 and 7 million  $\text{m}^3$  respectively. Maximum erosion occurred at the westernmost compartment, which is consistent with the expected role of the contiguous Otzumer Balje inlet as a barrier to longshore sediment supply to the western (updrift) beach segment of Spiekeroog.

On the other hand, the Harle inlet acts as a trap to sediments drifting towards the easternmost segment of the island. In general the above data suggest a marked and continuous alongshore sediment transport in the beach and inner surf zones. In contrast to the entire shoreface data (Fig. 60), evidence for a longshore sand transport reversal at a km scale is lacking. Such a reversal in pattern seems to obtain on the

distal zone between  $7^{\circ} 45'$  to  $7^{\circ} 46'E$  longitude where erosion magnitude is higher than at the bounding compartments.

Secondly, there is a considerable disparity in volumetric changes between the proximal and distal longshore patterns as a whole. This is easily anticipated, and most likely reflects a diminishing efficiency of longshore sediment transport with increasing water depth.

g) It was previously mentioned that the recurring longshore sinusoidal swash excursion pattern observed along the shoreline may be an expression of longshore standing edge-waves in the nearshore. This being the case, edge-wave activity, other than storm-associated alongshore rhythmic foredune scouring/breaching should be reconstructable along the lines of ANTIA (1990a) using sediment budget patterns.

ANTIA (1990a) hypothetically related alongshore rhythmic patterns in volumetric beach change magnitudes along Ibeno Beach, southeastern coast of Nigeria, to a longshore standing edge wave. Both the Spiekeroog and Ibeno beaches have many features in common to speculate such a relationship on the former. With the exception of being respectively storm- and swell-dominated, both beaches share the following attributes: oblique incidence of high-energy waves, mesotidal regime, fine grained sands and a gentle nearshore gradient, and are bounded on either side by shoreface protruding sandy shoals (ebb deltas / estuarine mouth bars).

The main difference between the two case studies is their respective data base. Ibeno data consist of monthly 2-D beach surveys across a unit width of beach length, whereas those of Spiekeroog are based on a 15-year sediment budget. Each data point for the latter case shown in Fig. 63 represents a net sum of the beach-inner surf zone depth change, for different shoreline or budget lengths, but of a constant width of 100 m. In order to maintain a uniform budget area ( $100 \text{ m}^2$ ), this not

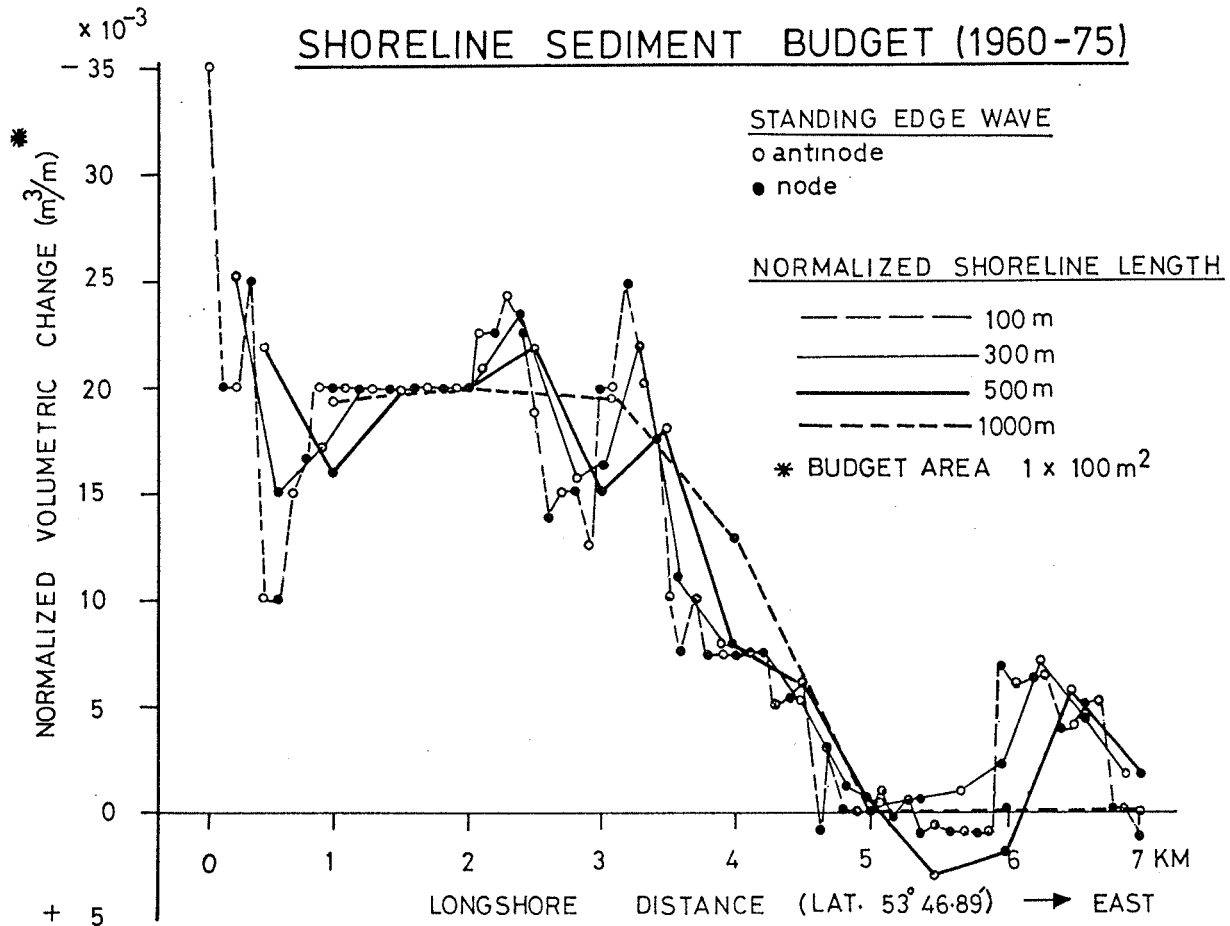


Fig. 63. Rhythmicity in shoreline sediment budget.

being critical to pattern identification, the volumetric changes associated with the different shoreline lengths were normalized by simply dividing the volumetric change values with the respective budget lengths.

To test the probable effect of edge waves on the sea floor, these budget or shoreline lengths were in each case assumed to represent a half ( $L/2$ ) of the most frequently occurring, hypothetical edge-wave length ( $L$ ). The antinodal position is in all cases presumed to be located adjacent to the updrift ebb delta, downdrift of which nodal positions alternate with the former at distances corresponding to the budget lengths.

Of all the postulated  $L/2$  edge-wave lengths, only the 500 m value shows a longshore pattern of nodal-antinodal

volumetric change that is consistent with a standing edge-wave oscillation. This is exemplified by the alternating occurrence of higher and lower volumetric erosion values at the antinodal and nodal points respectively. The strong alongshore (W-E) volumetric change gradient observed would suggest that the edge-wave oscillations are (a) generally weak relative to the wave-induced (easterly-directed) longshore currents, or (b) are spatially weaker on the downdrift (eastern) shoreline segment, and/or (c) the edge-wave oscillation is an ephemeral phenomenon. All of these would explain the noted longshore gradient in sediment transport in the proximal upper shoreface region.

The implication of these results to the sawtooth bar morphology showing comparable longshore spacing will be elucidated later. It should be noted that the antinodal and nodal points in Fig. 63 respectively designate high and low erosion areas. This is justified by the fact that erosion rates at or close to the shoreline should be more intense around the antinodes of a standing edge wave oscillation where the interaction between the elevated mean sea level and incident waves often leads to an intensification of swash-backwash (e.g., ANTIA, 1990a) or, under favourable storm events, overwash processes (e.g., DOLAN et al, 1979).

These essentially one-dimensional horizontal flow patterns are analogous to those considered to initiate swash cusps on reflective beaches (INMAN and GUZA, 1982). While a 2-D horizontal (cellular) flow pattern may develop following cusp formation on reflective beaches, this is rarely the case on the subaerial portion of strongly dissipative beaches. The contrary is however the case on the adjacent surf zones, where drift velocities associated with a standing oscillation generate a variety of rhythmic 3-D longshore features collectively called surf zone cusps by INMAN and GUZA (1982).

Based on the above considerations, the relative importance

of a Mode 0 or mode 1 (1 km long) standing edge wave oscillation on cross-shore volumetric changes are assessed (Fig. 64). In conformity with theoretical predictions of the offshore decay in edge wave oscillation, the frequencies of higher erosion at the edge-wave antinodes relative to the nodes decrease from 86% close to the shoreline to 66% in 7-8 m and 57% in 12-13 m of water depth. Alternatively, the degree of discrepancy between the relative bed-level change due to edge-wave activity increases from 14% to 43% in < 2 m to 13 m of water depth.

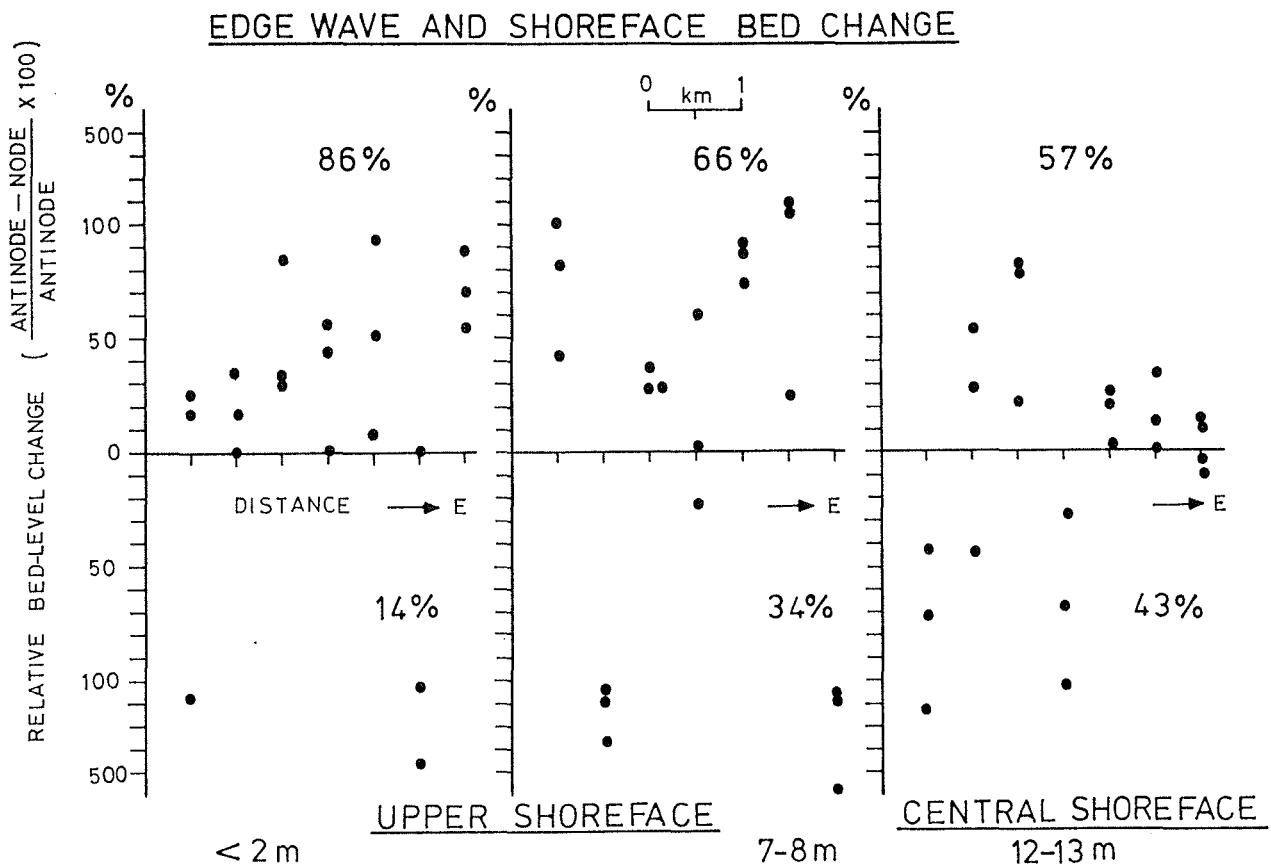


Fig. 64. Mode (0,1) edge wave effect on shoreface bed change.

**Sediment Facies :**

The sedimentary facies associations of the beach and inner surf zone of Spiekeroog are expectedly similar to those of the other East Frisian Islands described by REINECK (1976) as well as CHOWDHURI and REINECK (1978), given the similarity of their process variables. These and other authors (e.g., CLIFTON et al., 1971; DAVIDSON-ARNOTT and GREENWOOD, 1976; SHORT, 1984) have all documented systematic shore-normal variations in the suite of sedimentary structures and textures in the nearshore region, these being in response to the changing intensity and pattern of the wave-driven flow field (e.g., wave shoaling, wave-generated currents and swash-backwash).

Facies zones 1 and 2 of REINECK (1976) extend from the low water line to about 3 m depth and correspond, in part, to the proximal upper shoreface region of this study. Sedimentary structures are nearly exclusively physical, with a preponderance of horizontal lamination and air-escape cavities in the fine sands above mean sea-level. Below mean sea-level, REINECK (1976) documents an increased proportion of large-scale cross-stratification to characterize the coarser-grained inner troughs of the shore-attached oblique bars, as against oscillatory ripple lamination in the outer, finer-grained counterpart.

Cross-shore profiles of grain size statistical parameters for the upper shoreface (Fig. 65) show a consistent pattern, sediments of the proximal zone (represented by Lat.  $53^{\circ} 47.08'$ ) being the coarsest. Sorting, skewness and kurtosis values are almost identical in both the proximal and the distal zone (Lat.  $53^{\circ} 48.25'$ ). In both zones, sediments are less well sorted, skewness signs are negative and kurtosis values lowest.

The cross-shore patterns are consistent with a shore-normal sediment transport processes, in which breaking waves and intense longshore currents cause fines winnowed from the

proximal zone to be deposited seawards. However, the abrupt changes in grain size statistical trends at the distal zone is suggestive of some shoreward transport of coarser fractions from the adjacent central shoreface subenvironment.

UPPER SHOREFACE CROSS-SHORE GRAIN SIZE  
STATISTICS VARIATION

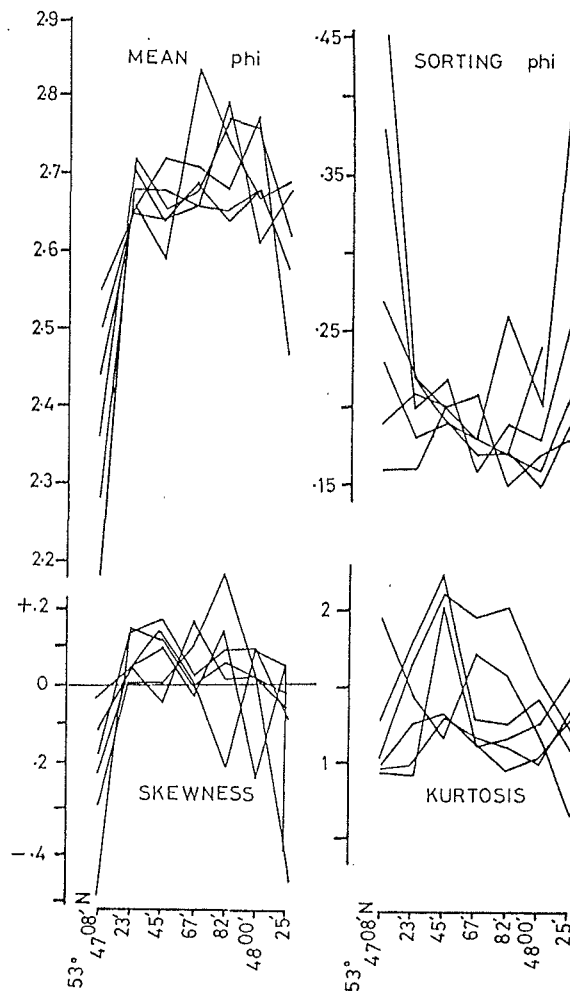


Fig. 65. Cross-shore profiles of upper shoreface grain size statistical parameters.

The shoreward-asymmetrical orbital velocities of even day-to-day waves can effectively account for the latter. The negative skewness depicted in both zones are respectively explained by Case 6 (total truncation of fine size classes) or 2b (immiscible admixture of coarse fractions) of the skewness sign evolution model (Fig. 26).

The alongshore variation in grain size statistics for three representative zones of the upper shoreface subenvironment are illustrated in Fig. 66. The number of samples on which the latter profiles are based varies from 5 to 11 and are spaced 560 m apart. Quite obvious is the fact that the proximal zone

UPPER SHOREFACE ALONGSHORE GRAIN SIZE  
STATISTICS VARIATION

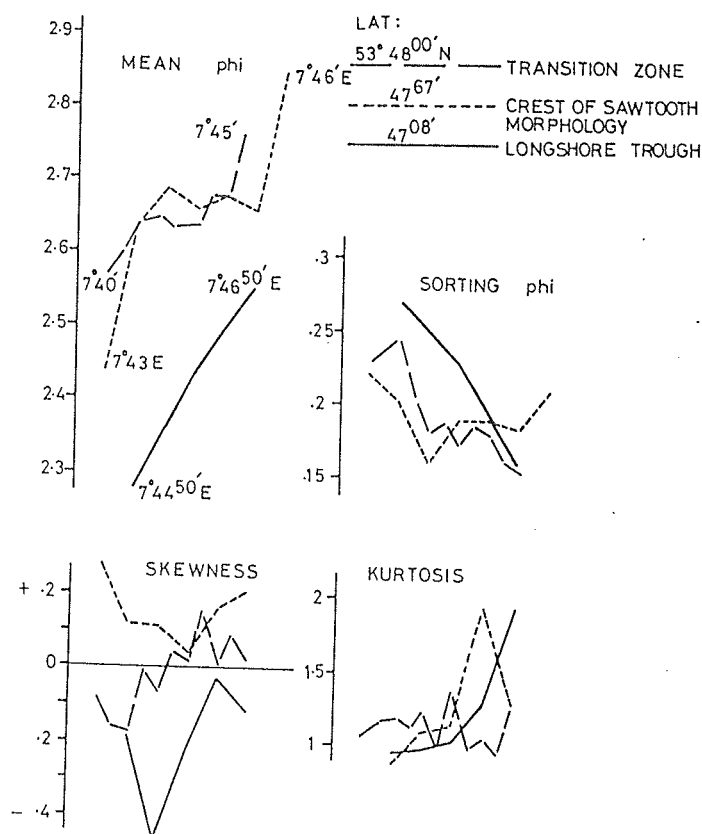


Fig. 66. Alongshore profiles of upper shoreface grain size statistical parameters.

sediments, as exemplified by the longshore trough data, are coarsest, least sorted, and most negatively skewed. The latter also reveals classical textural indices of a size-sorting transport model, i.e., a well-defined eastward grain size fining, coupled with improving sorting, a reduction in negative skewness and an increasing kurtosis. The lower negative skewness can be viewed in terms of immiscible mixing of finer fractions downdrift or selective deposition of sediments in transport, thus corroborating the transport trend inferred from the alongshore variation in sediment budget.

Similar textural trends as above were evident at the distal or smoothly sloping transitional zone, and to some extent on the crests of the saw-tooth bar morphology. However, the more pronounced trends evident from the trough data may be explained by the fact that wind-wave generated shore-parallel currents are easily confined and/or tend to attain maximum velocities within such morphologies (e.g., GREENWOOD and SHERMAN, 1984).

The beach profile above the mean water line also exhibits a very subtle cross-shore grain size pattern (Fig. 67), which may be instructive in understanding the processes in operation during a storm, when the samples were collected.

Beach face sediments are coarser, poorer sorted and depict lower kurtosis values than either of the berm and backshore counterparts; a more negative skewness relative to the adjacent berm is also indicated. The coarser and more negatively skewed beach face sediments, relative to the upper profile, appear to have been an intensification of a pre-storm attribute, with more fines being winnowed (total truncation) during the storm process. Grain size statistics of berm and backshore sediments tend to suggest enhanced overwash processes, whereby coarser sand fractions from the berm or beach face are immiscibly mixed with the backshore counterpart, culminating in their relatively poorer sorting and more negative skewness.

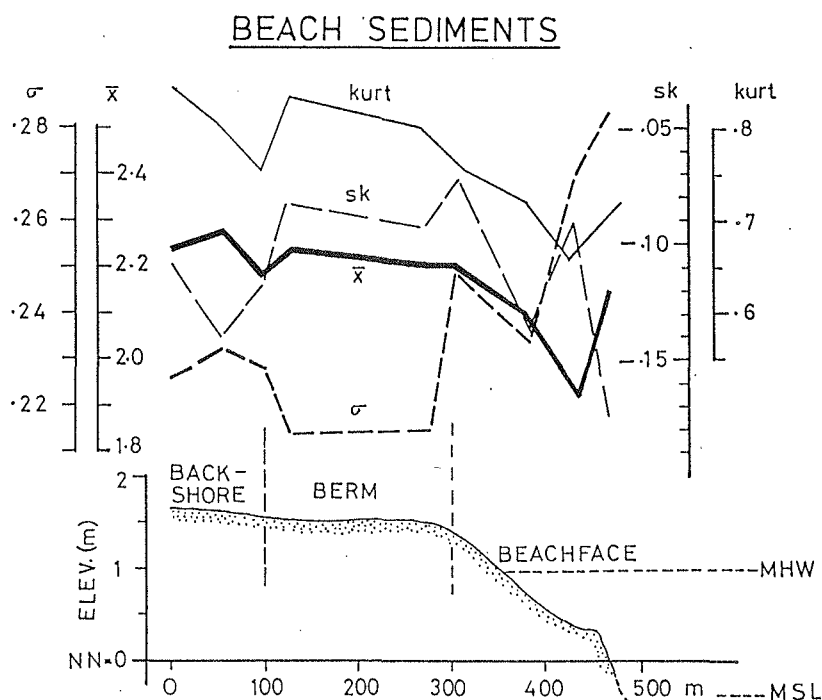


Fig. 67 Shore-normal variation in beach grain size statistical parameters during a storm event.

Finally, the poorest sorting evident on the beach face is a consequence of immiscible admixture of fallout of fines, winnowed from the upper reaches of the beach profile, following beach inundation and the associated landward translation of the breaker position.

Grain size statistical parameters on the berm show little variation. Aeolian processes with a dominantly onshore impact, as in the case of the study area, should normally result in a much finer, better sorted, more positively skewed and more leptokurtic backshore sediments than the berm counterpart. Some of the converse trends (e.g., better sortedness and more positive skewed berm sediments) must, therefore, reflect modifications associated with the storm event.

In order to accommodate both textural and accretional changes of the beach profile during this particular storm event, the following explanation is offered. The observed beach inundation must have been accompanied by landward bottom transport of sediments from the adjacent surf zone. The precise mechanisms for the latter are speculative at this stage, because flow data are lacking. Even where data exist, there is no general consensus in opinion, at least on dissipative beaches, on the relative significance of vertical versus horizontal segregation of surf zone currents (WRIGHT et al, 1982a). Thus, GREENWOOD and SHERMAN (1984) state : ".....a plethora of theories exist for predicting shore-normal transport ". In the studied case, shoreward-asymmetric wave orbital motion and/or intense overwash during the waxing storm phase, and subsequent seaward-directed transport of fines, largely by ebb storm-surge flow during the waning phase, are invoked.

#### 6.2.1.2 Surf zone (Outer)

The outer surf zone is about 500 m wide and is confined to between NN-2 m and NN-3 m depth contours.

#### Hydrodynamics:

As in the case of the shoreline-inner surf zone, measurements on fluid motion in the outer surf zone are lacking. However, based on water depth consideration, the major sedimentological and morphological changes in this zone are likely to be storm-associated. However, combined flows involving non-storm wave orbital and tidal currents should also cause marked physical changes on a day-to-day basis. Limited evidence however exist for the latter.

### Morphodynamics:

The outer bar, prominently displayed on the 1975 bathymetric chart, is the only significant morphological feature in this zone. This is a shore-parallel bar which is breached in several places. It is characterized by straight and rhythmic shoreward and seaward outlines respectively (Fig. 7). The non-linearity of the seaward margin could relate to the subordinate role of longshore bottom sediment transport in the region contiguous to it, compared with the shoreline-inner surf zone shoreward of the outer bar.

A comparison of 1960 and 1975 nearshore topographic charts has led to the speculation (FLEMMING and ANTIA, 1989) that the outer bar may have evolved sometime between both dates. Sediment budget over the above 15-year period (e.g., Figs. 57-59) clearly identifies the shoreline-beach/inner surf zone as the source of the outer bar sands. In fact, the outer surf zone is the only shoreface zone yielding a net volumetric accretion and a positive areal budget (approx.  $5000 \text{ m}^3 / \text{m}^2$ ) over the budget period.

The location of the outer bar some 600-700 m from the 1975 shoreline attests to the swiftness of the seaward-directed flow (rip currents, undertow, ebb storm-surge flow etc.) and rapid seaward bar migration during the responsible storm event. Furthermore, the antecedent morphodynamic state of the beach (in contrast to that of the surf zone) must have been reflective at the waxing phase of the storm event. If the opposite was the case, then as exemplified by beach response to the 1988 storm event, the outer bar might not have developed since beach accretion (or marginal erosion) would have taken precedence over intense erosion.

The persistence (beyond 1975) and storm wave-dampening role of the outer bar may have partly contributed to the relatively smaller scale of beach berm retreat of 200 m during the

1976 storm-surge event as against 300 m during the 1962 counterpart (FLEMMING, pers. comm).

#### Facies:

The facies characteristics of the outer surf zone have not been examined in any detail due to logistical difficulties. Sediments are, however, fine grained, well sorted and are devoid of muds and shelly components. The very high wave orbital velocities in this depth range (Section 3.6.4), even under non-storm conditions, would suggest a dominance of upper flow regime sedimentary structures (mainly horizontal lamination).

#### 6.2.1.3 Saw-tooth Bar Zone : Genesis and Dynamics

The medial (NN-4 to NN-6 m) upper shoreface zone of Spiekeroog (Fig. 7) is characterized by a quasi-rhythmic NE-SW striking morphology, referred to as "Sägezahnriffe" (saw-tooth bars) by REINECK (1963). In plan view, these features could be mistaken for transverse sand bars, which are usually oriented either perpendicular or at high angles to the shoreline (e.g., NIEDORODA, 1973). Such transverse bars have been reported from several coastlines. Indeed some of the literature reports document transverse bars of similar morphometrics as the saw-tooth bars. On the other hand, the facies and morphodynamic characteristics of the transverse bars are rarely reported.

The main geomorphic characteristics of transverse bars have been synthesized by NIEDORODA (1973). However, these are not necessarily conformable with the observations of WRIGHT and SHORT (1983). Opinion certainly differs on the origin of the transverse bars. For purposes of comparison with the saw-tooth

bars, both the geographically-spread observations of NIEDORODA and the "site-specific" counterpart of the latter authors are considered.

Transverse bars are extensions of the beach form, and are typical of low wave-energy and small tidal-range coastlines (NIEDORODA, 1973). Additionally, their long axis is directed to the mean annual wave approach direction; moreover they modify the nearshore flow field through wave refraction and energy concentration on their crests. WRIGHT and SHORT (1983) on the other hand observe transverse bars to be typical of modally intermediate-state beaches (Fig. 4).

By contrast to the transverse bars, the saw-tooth bars are completely detached from the shoreline and are situated seaward of the fair-weather surf zone of an energetic coast. The tidal range along the study area is also higher than in typical transverse bar settings reported by NIEDORODA (1973). As such, the saw-tooth bars are features yet to be described from other coastal settings.

Consequently, the Frisian barrier island coast qualifies as a type locality for the saw-tooth bar morphology. Although not specifically focused on saw-tooth bar genesis and dynamics, the studies of REINECK (1976), DÖRJES (1976), WUNDERLICH (1983) and AIGNER and REINECK (1983) have shed light on some aspects of their sedimentology and biology, which are useful in a genetic interpretation of the feature. With the exception of the study of WUNDERLICH (1983) offshore of Spiekeroog island, all the other investigations were concentrated off the island of Norderney.

The saw-tooth bars are sculptured into a gently sloping (1:550) fine sand (2.5 -2.75 phi) substrate. They are 1.5-2 km

in length, have a relief of about a metre that planes off in a seaward direction, and a time-history mean spacing of  $460 \pm 200$  m. In cross section (e.g., Fig. 14), they are asymmetrical with the steeper side facing eastwards. The latter form has invoked the notion in the local literature (e.g., REINECK, 1963; see also EHLERS, 1988, for some of the earlier studies) that these bars must be subaqueous flow-transverse bedforms (giant ripples, sand waves or dunes).

The flow-transverse bedform postulate of saw-tooth bar genesis has been examined by FLEMMING and ANTIA (1990) from a variety of view-points and found to be inconsistent. A notable objection of a flow-transverse bedform nature includes the fact that their spacing (460 m) versus mean grain-size (2.5-2.75 phi) relationship does not conform to any existing empirical data set as exemplified by Fig. 66a, which would limit the spacing in this case to about 70 m. Their height, by contrast, could be accommodated by the bedform theory.

Although empirical data on which Figs. 68a and b are based are sufficiently large ( $n = 1491$ ) and span an array of environments, one may for the sake of argument consider the data coverage to be "incomplete" and hence not decisive to discard the bedform theory. A non-debatable fact for rejecting the flow-transverse bedform nature of the feature, however, is based on their internal structure. Box cores and detailed vibrocore data (to be discussed later) corroborate the opinion of WUNDERLICH (1983) that the saw-tooth bars are devoid of cross-strata and as such can not be interpreted as representing flow-transverse bedforms.

A core from within a trough, recovered by divers, revealed seaward dipping strata, as against horizontal laminae on the crest (Fig. 69). Furthermore, the shoreward extension of the channels through breaches on the outer parallel bar on one hand, and their embayed seaward side on the other (FLEMMING and ANTIA, 1989) is suggestive of a rip current origin of the troughs. Thus, in the light of the preceding

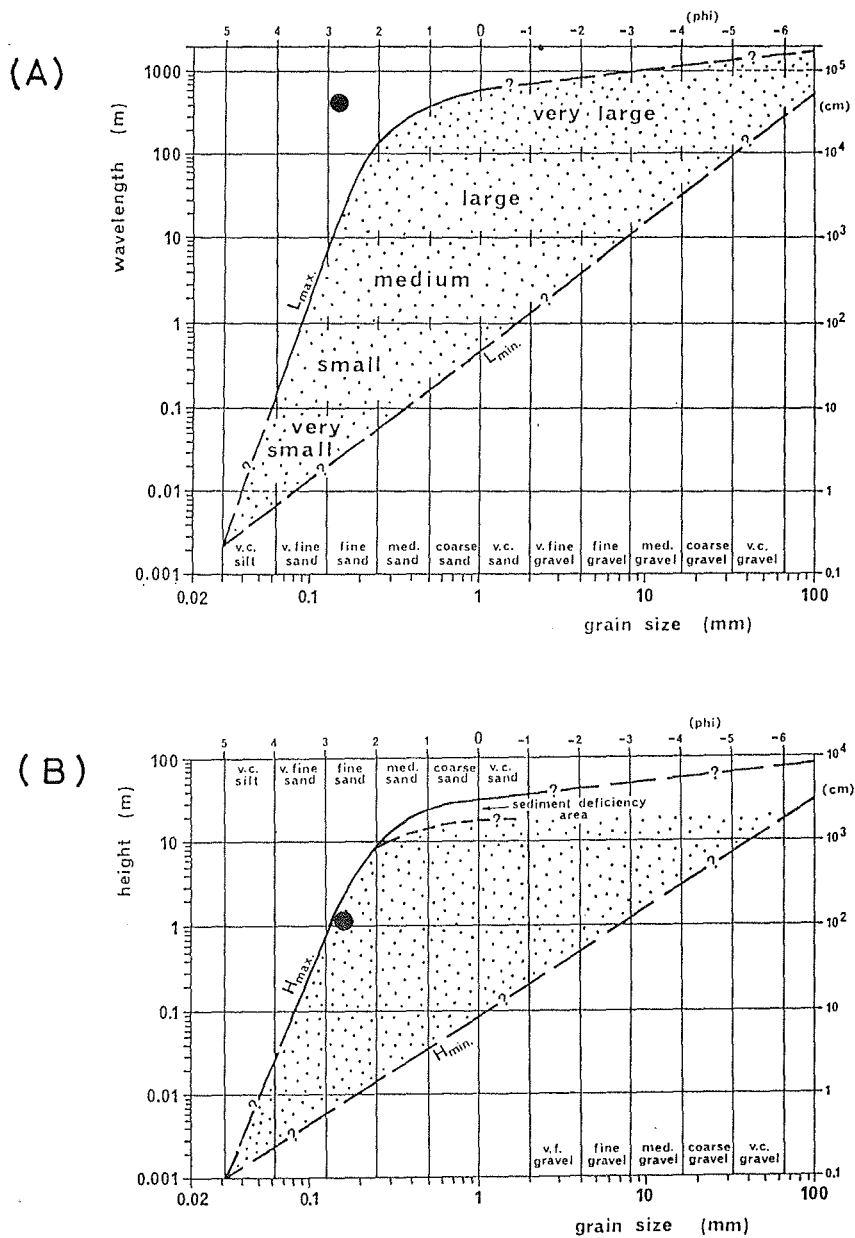


Fig. 68. (a) Empirical relationship of bedform wavelength versus mean grain size (after FLEMMING, 1988, 1990a). (b) Empirical relationship of bedform height versus mean grain size (after FLEMMING, 1988, 1990a). (● SAWTOOTH BAR)

arguments, supplemented by other subsequent evidence, the saw-tooth bar morphology will henceforth be considered as a rip channel-ridge crest morphology, with more emphasis on the channels, than the bars.

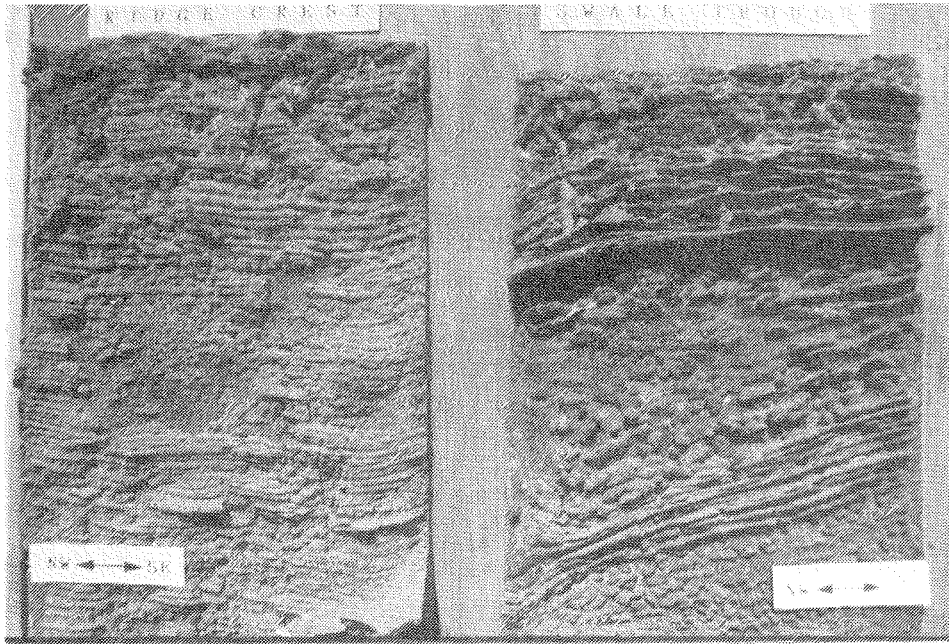


Fig. 69. Relief peels from the saw tooth bar (rip and ridge) morphology (courtesy of B. W. FLEMMING).

Additional evidence against a transverse flow origin of the saw-tooth bar morphology is provided by the trends of rip channel axes over time shown in (Fig. 70). These have been compiled from semi-sequential sounding charts spanning a 37-year time interval (1950-1987). In the first instance, the axes are curvilinear and somewhat too chaotic in orientation to represent trough-crestlines of a dune morphology formed by shore-parallel flows. Secondly, by filtering out the "noise" from the above trends, resulting mostly from incomplete or sectionalized soundings, one can clearly define 12 almost equidistant axis clusters. It is also doubtful whether steadily migrating dunes over a comparable time-period would result in a pattern of segregated crest-line clusters, instead of one which is spatially continuous.

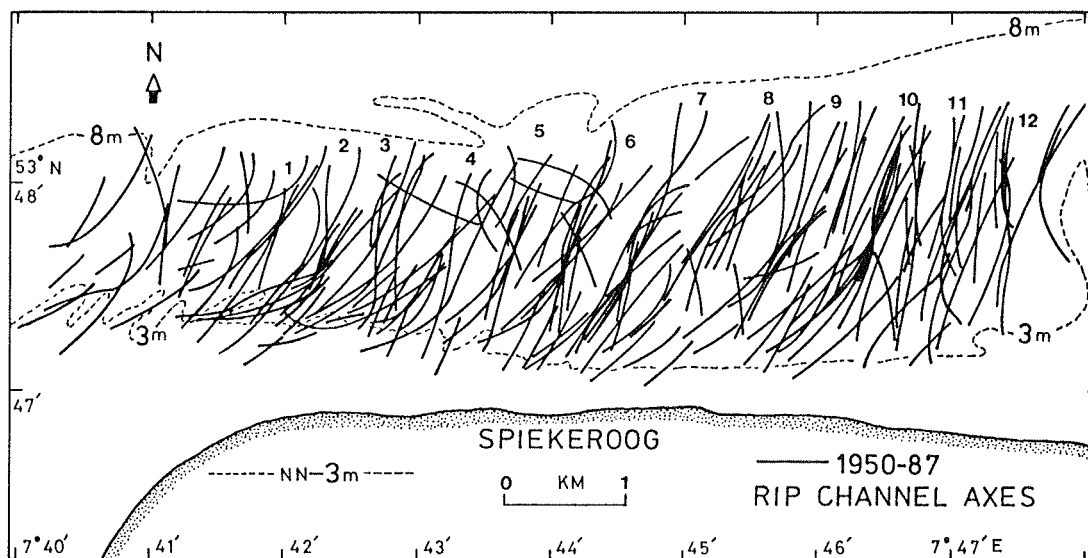


Fig. 70. Spatial trend of rip channel axes.

As shown in Fig. 71, each of the axis clusters is characterized by a hinge point around and about which the axes seem to "oscillate" and translate. The latter motion is however subordinate. The above noted axis oscillation is incompatible with subaqueous dune dynamics driven by an easterly directed mean flow in the region. The latter may, however, contribute to their cross-sectional asymmetry during, as against after formation. Based on the data presented in Fig. 71, further details regarding the time-history dynamics of the channels were investigated.

The procedure entails determining the angular displacement ( $\theta$ ) of each of the rip channel axes relative to a shore-normal plane through a hinge point. To ensure computational accuracy, only channels extending at least 500 m seaward and shoreward in length from the hinge point were evaluated. Furthermore, a distinction was made between dynamic trends of the upper (relative to the hinge point) and lower channel axis segments. The former and the latter respectively represent the distal and proximal channel segments and, as shown in the definition sketch in Fig. 72a, their displacements relative to the shore-normal plane and the shoreline trend are denoted with the subscripts 1 and 2.



SPATIAL DYNAMICS OF RIP CHANNELS

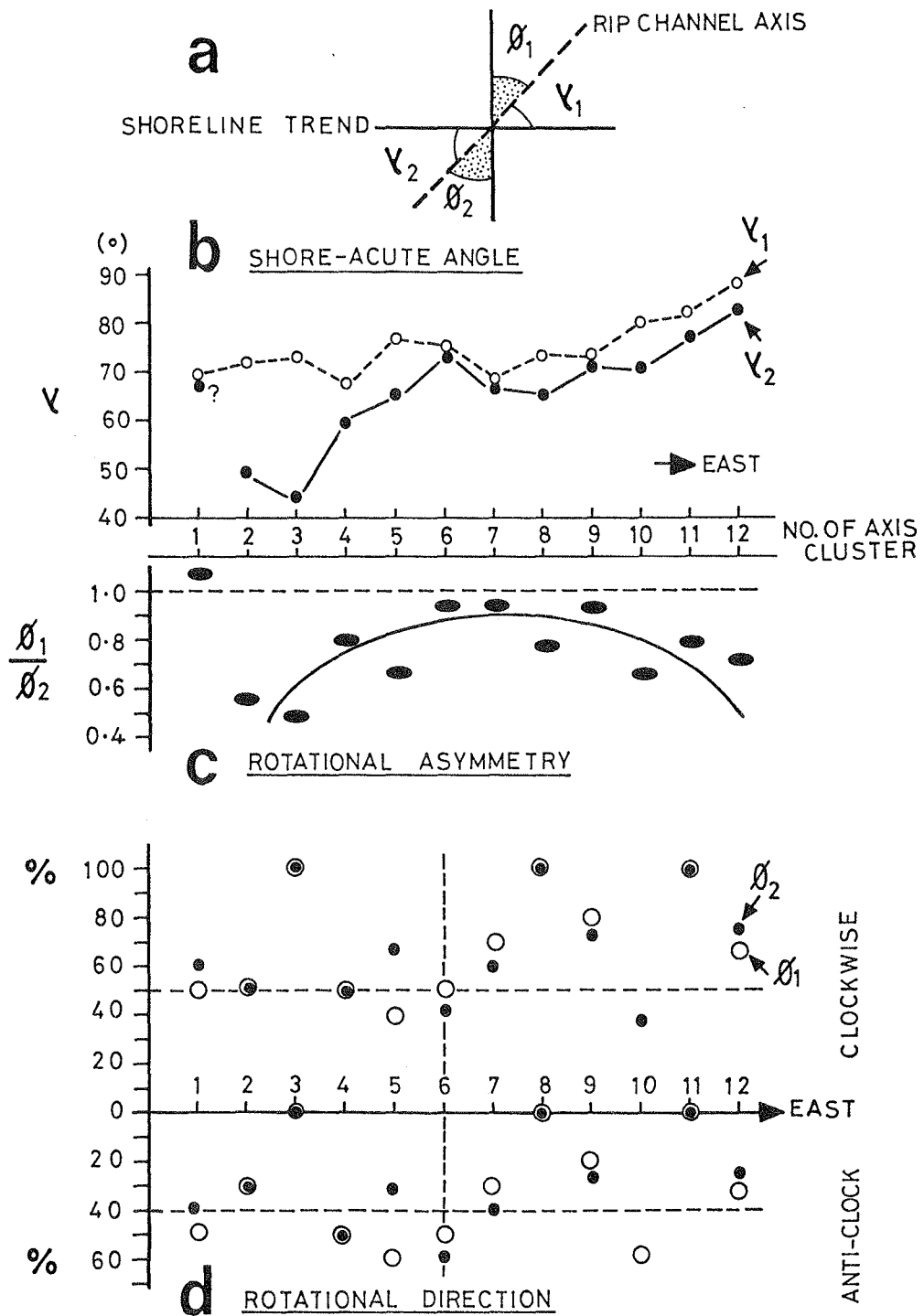


Fig. 72. (a) Definition sketch of rip channel axis dynamic parameters. (b) Spatial variation in mean cluster rip channel axis shore-acute angle. (c) Mean cluster rotational asymmetry of rip channel axis. (d) mean cluster frequencies of rotational direction of rip channel axis.

Quite instructive from the mean cluster shore-acute angle data in Fig. 72b is the fact that both channel axis segments tend to increase in inclination relative to the shoreline trend, i.e., become more perpendicular eastwards. Furthermore, the W-E gradient of angular inclination is much steeper for the lower, shoreward channel segment than for the upper, seaward counterpart.

If the axes were indeed crest- or trough-lines of flow-transverse bedforms, then the implication of the above results would be that their generating eastward directed flow should show a continual and spatially consistent anti-clockwise veering of the order of  $20^{\circ}$  to  $40^{\circ}$  over a distance of just 10 km, this corresponding to the island length.

Although spatially-confined, shoreface current measurements conducted as well as basic reasoning negate the notion that easterly-directed littoral currents in the northern hemisphere and shallow water-depth study setting should veer in such a sense and at the scale indicated. Also, the speculation that the eastwards increasing, shore-normal orientation of the axes eastwards may relate to a post-formational weakening of the littoral flow cannot be substantiated at the present time. An eastward positive or increasingly less negative volumetric sand budget change on the distal and proximal upper shoreface (Table 4) may seem to suggest this fact.

However a closer examination of Fig 72b suggests the converse to be the case. If an eastward weakening of longshore currents were to be accepted as the cause of the spatial variation in axis inclination, then the shore-acute angle of the lower channel segment should have been larger and the rotational asymmetry shown in Fig. 72c should have resulted in values greater than unity, i.e.  $\theta_2 < \theta_1$ , because of the generally stronger alongshore littoral currents at shallower water depths.

Figure 72d further supports the above contention. Stronger eastward-directed longshore currents acting on a shore-normal lower channel segment should cause it to swing in an anti-clockwise direction. Thus a high %-frequency of anti-clockwise rotation within the lower axis clusters (dark circles), particularly those at the western sector (clusters 1 to 6), should be evident. The results demonstrate the opposite.

The %-frequency of anti-clockwise rotation of the lower axis clusters do not only lack a pronounced alongshore gradient, their frequencies are subordinate (< 40 % on the average) to their clockwise counterpart. However, to invoke a westerly-directed and diminishing driving force on the lower channel segments as a cause of their observed spatial pattern of rotation depicted in Fig. 72d would contradict the asymmetry of the morphology. In essence, the time- and spatially-varying shoreline inclination of the channel axes is an attribute coupled more to their mechanism of generation than to a post-formational modification of the antecedent counterpart.

The above observations are compelling enough to discard the flow-transverse bedform nature of the saw-tooth bars. The generating mechanism of these features will become evident in the following evaluation of their spatial and temporal dynamic patterns. A total of 111 pairs of channel axes were evaluated in relation to their temporal rotational sense and magnitude ( $^{\circ}$ ) for both the upper ( $\delta\theta_1$ ) and lower ( $\delta\theta_2$ ) segments (Fig. 73).

Three salient facts emerge from the representation in Fig. 73. Firstly, none of the channel segments indicates a statistically significant angular-displacement versus time relationship. This can be interpreted to reflect a high dynamic equilibrium in channel mobility over time. Secondly, for both channel segments, the degree of clockwise re-orientation or rotation is more pronounced than the anti-clockwise counterpart. Rotational values exceeding  $20^{\circ}$  are more common in the former than in the latter. Thirdly, the clockwise rotation of the lower, shoreward channel segments is more intense than that of the upper, seaward counterparts.

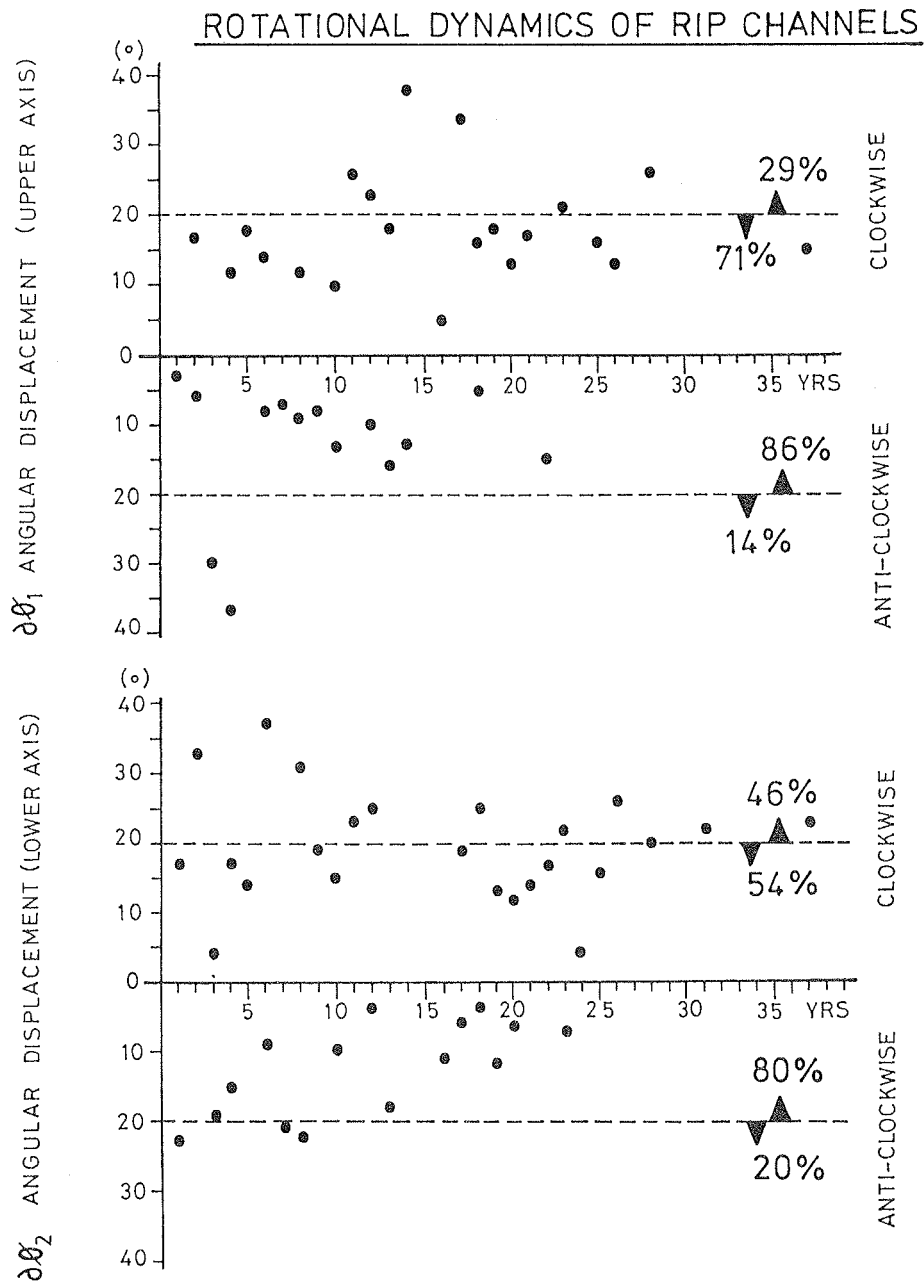


Fig. 73. Temporal variation in magnitude and sense of rip channel axis rotation.

The observed temporal pattern of both channel segment oscillations can be grouped into four rotational modes: two cyclic and two counter-cyclic motions (Fig. 74). The cyclic dynamic modes are characterized by both upper and lower axis

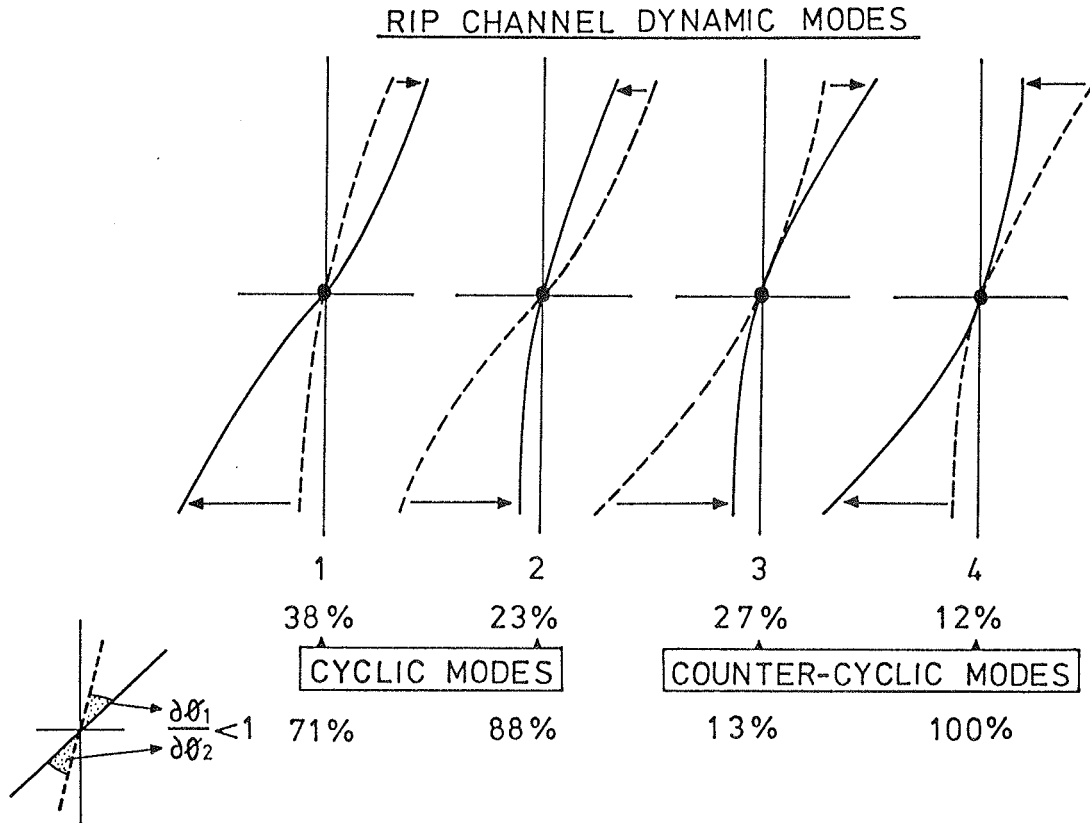


Fig. 74. Rip channel dynamic modes.

segments depicting clockwise (Mode 1) and anti-clockwise (Mode 2) angular displacement relative to a pre-existing channel orientation. The counter-cyclic rotational modes, on the other hand, are typified respectively by a clockwise (Mode 3) and an anti-clockwise (Mode 4) angular displacement of the upper channel segment, with a converse pattern in their lower channels.

Mode 1 rotational pattern was found to be the most frequently occurring (38%). It was the principal type (>50%) in 7 of the 11 assessed cluster axis sets (cluster 1 was excluded because verification was limited by an inadequate data set). Mode 2 (23%) was the major pattern of two of the axis clusters. The relatively high occurrence of the counter-cyclic Modes 3 (27%) and 4 (12%) and their cyclic counterparts does demonstrate the complexity of the flow field

on the medial zone of upper shoreface subenvironment. The complex nature of the flow within the above zone is further attested to by the frequencies of rotational asymmetry associated with the different rotational modes. For example, with the exception of Mode 3, the angular displacement of the lower channel is frequently larger than their upper counterpart, irrespective of the sense of change of the former.

Mean-tide current measurements made over a tidal cycle on the crest and in the channel of the ridge and rip morphology during a fair-weather condition (Fig. 75 a, b) did

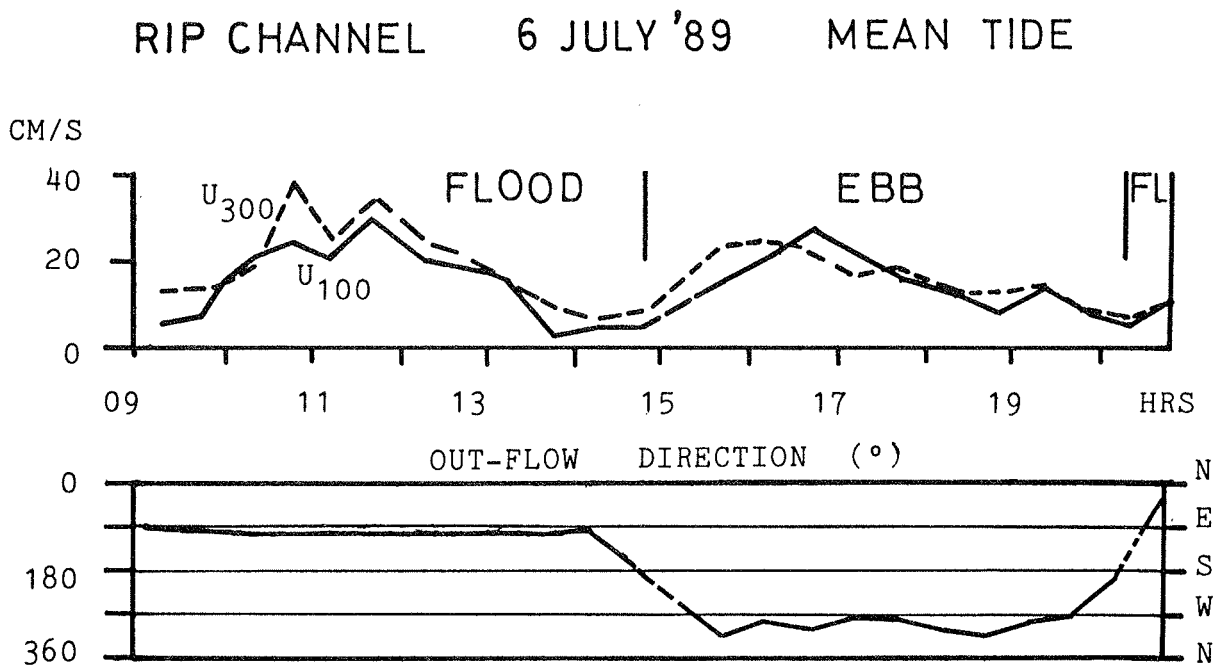


Fig. 75 (a). Fair-weather tidal current measurements in a swale of the saw-tooth bar (rip and ridge morphology).

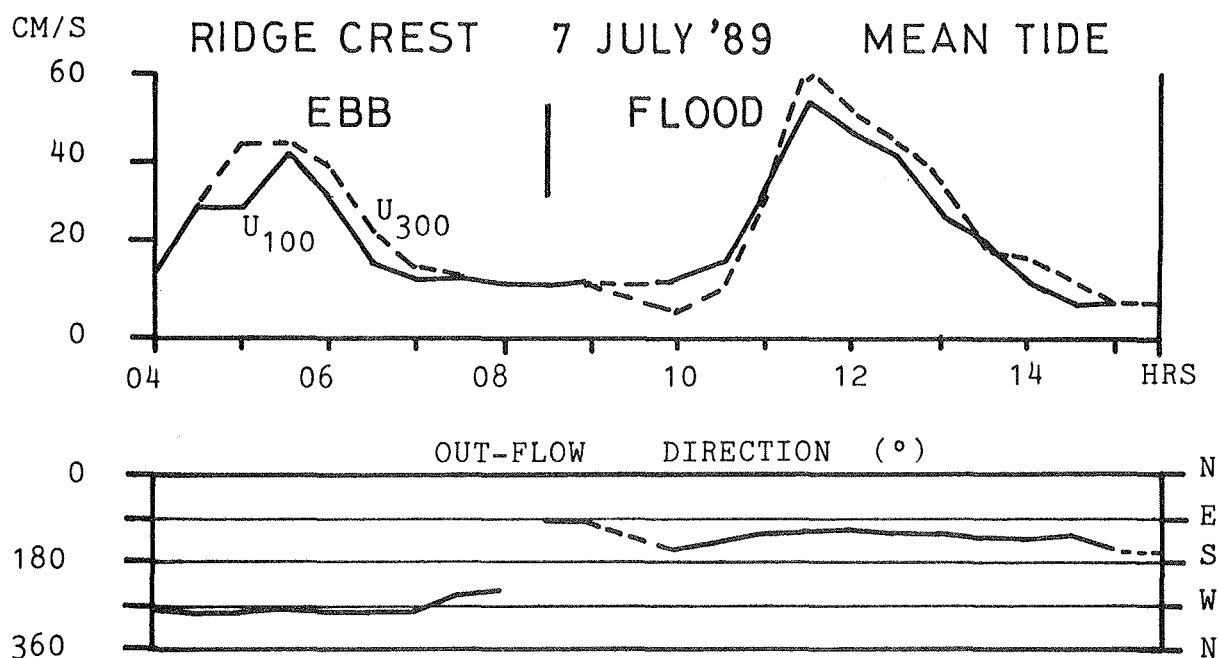


Fig. 75 (b). Fair-weather tidal current measurements on a crest of the saw-tooth bar (rip and ridge morphology).

not show any complexity in pattern. Maximum flood and ebb velocities (and flow direction) on the crest at 100 cm above bottom were respectively 54 cm/s (Az.  $125^{\circ}$ ) and 42 cm/s (Az.  $275^{\circ}$ ). Their channel counterparts were 28 cm/s (Az.  $100^{\circ}$ ) and 28 cm/s (Az.  $295^{\circ}$ ).

The implications of the above data are that for the 2.5-2.75 phi substrate sands, which have a threshold of motion

of about 30 cm/s, the sediments in the rip channels would only be mobilized during storm conditions or when waves act in concert with the fair-weather currents. On the other hand, bedform/grain size stability diagrams as a function of water depth and flow velocity given in Appendix B-2 indicate that on the crest both tidal flows can independently generate ripples but not dunes.

The above flow records clearly suggest that the genesis and dynamics of the ridge and rip morphology must be related to storm action. The dynamic behaviour of the rip channels in response to specific storm events has therefore been evaluated and the results presented in Fig. 76 (see also Appendix F). The storm data have been synthesized from the annual reports of the Forschungstelle Küste, Norderney.

In virtually all of the documented cases, the Mode 1 rotational pattern was typically associated with, but not limited to, storm surge heights > 3 m. Furthermore, post-storm rip channel axis orientation depicts as much as 20° smaller shore-acute angle than the pre-storm counterpart.

In the absence of actual storm flow measurements on the upper shoreface, ideas about the origin of the rip channel and crest morphology must inevitably be deductive, being mainly based on the available data of morphometrics and morphodynamics. However, additional supporting evidence, based on a detailed facies analysis will also be presented.

One of the most striking attributes of the saw-tooth morphology is undoubtedly their quasi-periodic alongshore spacing. As indicated in Section 2.2.1, the interest in variously scaled rhythmic coastal features has grown in recent times. However, in contrast to the present study, all of the rhythmic features discussed to-date are either shore-attached or confined to the surf zone. Nevertheless, a general consensus exists on the role of edge waves in their generation.

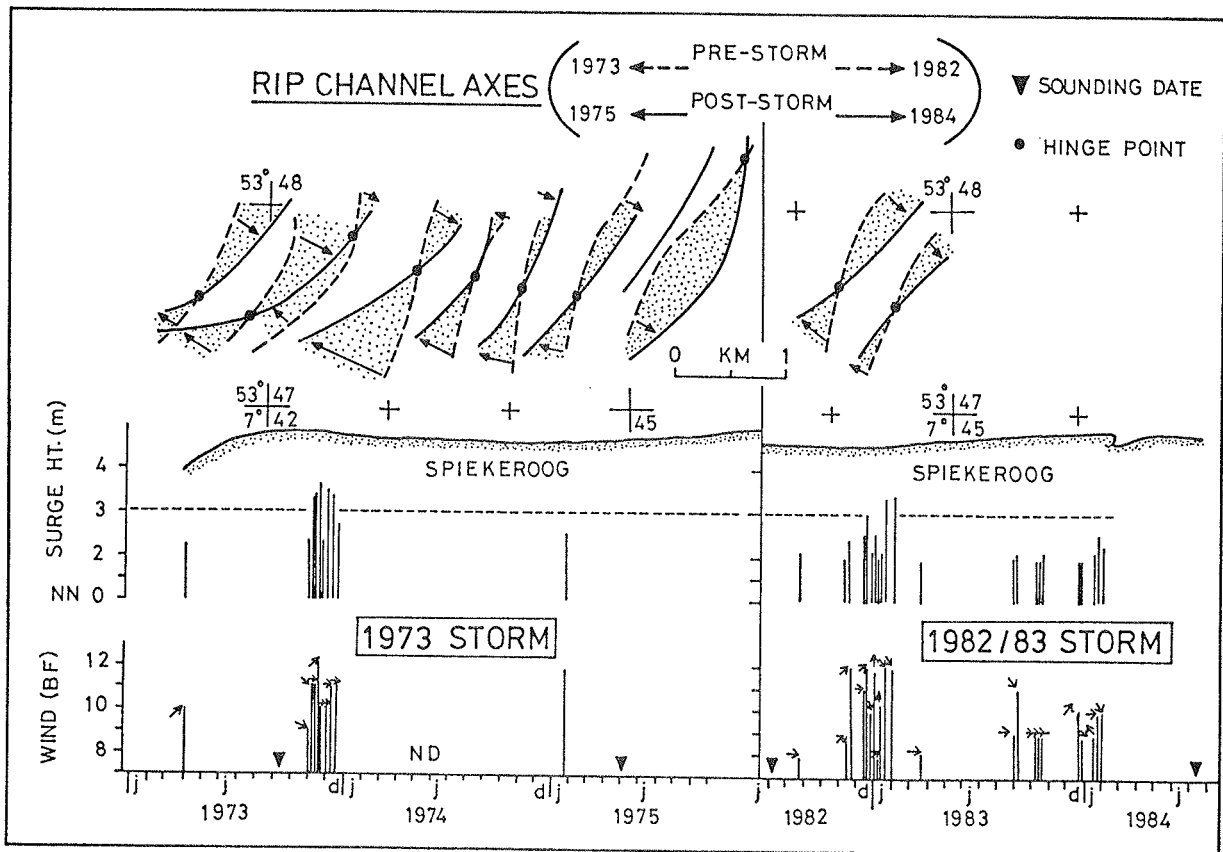


Fig. 76. Rip channel response to 1973 and 1982/83 storm events.

In the absence of any other suitable alternative, a possible edge wave-related origin of the sawtooth bar (rip-ridge) morphology is explored.

Edge waves, of which a variety of types exist, essentially represent a class of surface oscillatory motion which is trapped near the shore and propagates alongshore. In contrast to swells and seas with shoreline-parallel or oblique crests, the crests of edge waves are essentially shore-normal.

Unlike normal gravity waves, edge waves are not only characterized by a wavelength ( $L_e$ ) and period ( $T_e$ ), but also a mode number ( $n$ ), which denotes the number of zero-crossings of the mean sea surface in the offshore direction (HOLMAN and KOMAR, 1986). The edge-wave dispersion relation for a plane beach is expressed (e.g., URSELL, 1952) as :

$$L_e = g / 2\pi (T_e)^2 \sin [ (2n + 1) \beta ]$$

where  $g$  is gravitational acceleration ( $10 \text{ m s}^{-2}$ ),  $\beta$  is the sea floor slope and  $n$  is an interger which defines the offshore profile of the edge wave.

It is apparent from the given relationship that the edge wave length is a direct function of its period, mode number and sea floor slope. The maximum amplitude occurs at the shoreline and decreases with increasing mode number. Where the edge wave is standing alongshore, as against progressing, alongshore alternation in amplitude highs (antinode) and lows (node) is well defined along the shore, this being instrumental in the development of rhythmic morphologies. This means that the spacing of a rhythmic morphology so generated would equal a halve of the edge wave length.

Thus, a basic pre-requisite for the stability of the edge-wave generated morphology, therefore, is that the edge waves must be of the standing type and that it depicts consistent physical dimensions in time. In the study area, standing edge waves could be generated by reflection of a progressive edge wave at the downdrift ebb-delta.

The beauty of the edge wave model is its flexibility and the liberty granted to match almost any scale of a rhythmic feature to one or more of the almost infinite family of edge wave patterns. On the other hand, the lack of direct field

verification may deter from, but not disprove the credibility of employing an edge wave model to explain the origin of rhythmic features.

Taking a mean rip channel spacing of 460 m ( $L_e = 920$  m) and an average slope of  $0.0974^\circ$  for the medial zone of the upper shoreface, a variety of long-period standing edge wave patterns can be considered to have contributed to the development of the observed rhythmic morphology, e.g., Mode 1,  $T_e = 340$  s; Mode 2,  $T_e = 330$  s; Mode 3,  $T_e = 280$  s etc.

It should be noted that the above edge wave patterns are merely approximations of a time-history average channel dimension. Moreover, the predicted edge wave is extremely sensitive to the value of the nearshore slope. Thus, the previously suggested Mode 3 ( $T_e = 150$  s) edge wave (FLEMMING and ANTIA, 1990) was based on just a 2.4% steeper slope as that employed above.

In this writer's opinion, hypothetical matching of the spacing of a rhythmic morphology to a given length (and period) of edge waves, as done above, is less critical than the choice of the mode or even the type (synchronous or subharmonic) of the edge wave itself. This is not only from the point of energetics but also the configuration of the morphology. For example, the offshore structure of edge wave modes greater as one should definitely cause the channels, by virtue of their length, to depict a cross-shore meandering or rhythmicity, instead of a straight or curvilinear pattern as evidenced.

The latter consideration speaks in favour of a Mode 0 or 1 edge wave pattern as playing a key role in the genesis of the observed morphology. Furthermore, based on energetics, because of the rapid offshore decay in amplitude of higher-mode edge waves, their efficiency in confining seaward returning flows in channels extending some 2.5 km

away from the shoreline is questionable. However, as will be shown shortly, the latter consideration is less critical than the evidence of the cross-shore channel shape.

As previously noted by many authors, the generating mechanism(s) of infragravity oscillations is (are) still unclarified. In the main, four hypotheses exist: (a) interaction of shoaling waves of different frequencies (forced wave release mechanism), e.g., MUNK (1949) cf. GUZA and THORNTON (1989), (b) time-varying breakpoint of grouped incident waves (surf zone localized), e.g., SYMONDS et al. (1982), (c) a longshore-moving pressure distribution over a sloping bed, e.g., GREENSPAN, 1956; EVANS, 1988, and (d) a longshore uniform current over a small protrusion on the sloping bed, e.g., YIH, 1984 ; EVANS, 1988.

Whereas the former two are indirect and may not necessarily generate long period edge waves, i.e. alongshore infragravity oscillations, the latter two seem to be direct generating mechanisms. The perturbed longshore current mechanism is particularly attractive because, in this case, the maximum amplitude of the oscillation need not necessarily be at the shoreline. Furthermore, there would be no restriction as to the dominance of higher modes over the lower ones.

In the study area, the updrift (Otzumer) delta can serve as a topographic protrusion for the perturbation of the recurring easterly-directed storm currents, thereby generating progressive edge waves, which are then reflected at the downdrift (Harle) delta to produce a longshore standing oscillation. Based on the formulation of EVANS (1988), the near-bottom longshore current velocity required to generate, for example, a longshore standing, 920 m long, Mode 0, 1, 2, 3 edge wave is respectively 1.6, 2.7, 3.5 and 4.2 m/s. The sparse storm flow data from the study region speak in favour of Mode 0 and 1 edge waves as the most frequently excited, therefore corroborating the earlier assertion of their key role in the the origin of the rhythmic morphology.

The nodal positions of the oscillation define the location of channel incisions by the seaward returning flow during the storm relaxation phase. However, a similar interaction between the downdrift ebb delta and the shoreface ebb storm surge flow in generating edge waves would be limited by the inlet outflow.

As with other edge-wave generating mechanisms, a strong decay of the oscillation seawards is predicted by the topography-perturbed model (EVANS, 1988). However, it has been demonstrated (HOLMAN and BOWEN, 1982) that a standing edge wave need not necessarily only result from progressive edge waves of similar mode, amplitude and opposing travel direction in order to initiate a longshore rhythmic morphology. No study known to the writer from the study region has considered the effect of a shore-parallel flow on a longshore standing oscillation. This writer's postulate, as presented in Fig. 77, is consistent with a recent formulation on such interaction by HOWD et al. (1992).

In essence, a strong alongshore flow would distort the sinusoidal pattern of the oscillation, causing it to skew. In the case of the study area, an eastward skew is expected. The above interaction is completely independent of, and has no bearing on, the longshore wave-length and offshore extent of the oscillation. The degree of skewness of the oscillation would, however, depend on the duration and vigour of the interaction.

Generally, an eastward decreasing skewing of the oscillation with diminishing intensity of the alongshore flow can be expected. Moreover, at any given longshore position, cross-shore asymmetry in the flow-induced skewing of the oscillation can be further expected. Because of the smaller amplitude of the oscillation distally, skewing of the latter would be more pronounced. However, the writer is further of the opinion that due to imperfect reflection at the downdrift ebb delta and other nonlinearities, the envelop of an excited alongshore standing oscillation should strongly

FLOW INTERACTION AND RIP DYNAMICS

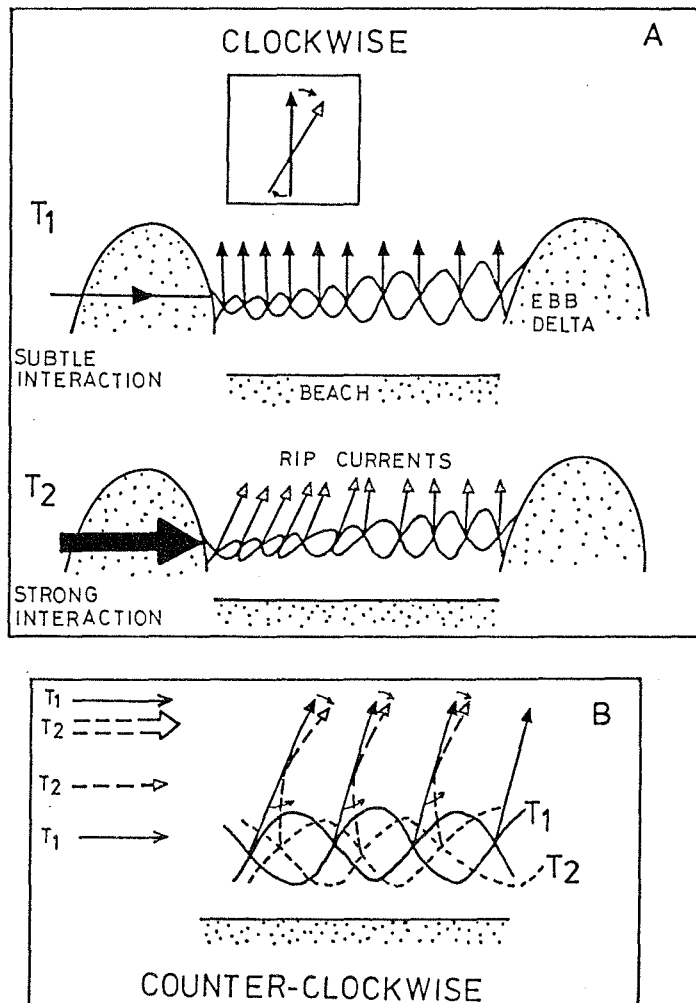


Fig. 77. (a) Interaction between longshore flows and a standing edge wave oscillation and the resulting rip channel orientation (b) Interaction between a longshore flow and out-of-phase edge wave oscillations.

diminish in the updrift direction, as is also the case in the offshore direction. This postulate is borne out of the fact that nonlinear effects, such as fluctuations in the longshore current intensity in the course of a storm surge event and the consequent damping of the antecedent resonance, would be most pronounced in the coastal sector proximal to the updrift ebb delta.

Against the above background, the spatial and temporal dynamic behaviour of the channel axes outline earlier can be rationally explained. Three of the more salient features are addressed here : (a) the time-consistent, spatially-varying orientation of the channel axis (Fig. 72 b); (b) the predominance of clockwise rotation over space and during storm events (Fig. 76 and Appendix F); and (c) the pattern of rotational asymmetry (Fig. 72c). However, it is re-emphasized that the channel axis orientation is an intrinsic attribute of their genesis and, this being the case, is suggestive of the distortion of the standing oscillation by transient storm currents persisting even after triggering the oscillation.

Interaction between the easterly directed shore-parallel storm flow and the longshore standing oscillation triggered by it can be viewed from the following perspectives. Firstly, the shore-normal symmetry of the standing oscillation (Mode 1 edge wave is advocated) is distorted (eastward skewed) to an extent dictated by the superimposed longshore flow intensity and duration. Because flow interaction is consistently more intense close to the updrift ebb delta, a corresponding eastward diminishing skew of the standing oscillation or increasing shore-acute angle of the channels should be expected.

Secondly, the distorted orientation of the oscillation defines the channelized course of the seaward returning ebb surge. As illustrated in Fig. 77a, where a subsequent storm event at time  $T_2$  leads to an intense skewing of the oscillation, the incised rip channels can be visualized to have been displaced clockwise relative to the pre-existing  $T_1$  counterpart. The above displacement defines the Mode 1 channel rotation pattern. The converse of the above, i.e., channel incision associated with a strong distortion of the oscillation succeeded by that of a subtle distortion would result in a Mode 2 pattern.

Thus, the earlier noted spatial dominance of Mode 1 channel rotation pattern would indicate an increasing intensity of

subsequent storm surge events. The fact that Mode 1 also tends to be dominant during episodes of storm surge > 3 m in height further emphasizes the significance of longshore flow-induced distortion of standing edge-wave oscillation as a cause of channel dynamics. On the other hand, the preponderance of counter-cyclic rotational Modes 3 and 4 at the western sector could be a response to a strong cross-shore (proximal versus distal) segregation in the intensity of flow interactions and kinetics.

In reality, however, as shown in Fig. 77b, the counter-cyclic rotational Modes 3 and 4 are a consequence of (a) a slight out-of-phase relationship between the antecedent and instantaneous oscillation ( $T_1$  and  $T_2$  respectively) and (b) variable cross-shore gradient in longshore flow interaction. A combination of condition (a) with a uniform longshore flow at  $T_1$  and a non-uniform counterpart at  $T_2$  would give rise to a counter-cyclic Mode 3 dynamic pattern, whereas the converse results in a Mode 4 dynamic pattern.

In general, the temporal changes in rotation patterns can be intricately related to the varying degree of interaction between the above edge-wave oscillation and shoreface flow. For instance, a given storm event, while inducing a similar edge-wave character as that of its predecessor, may interact less intensively with it.

One of the major implications of Fig. 77, as elucidated above, is that the channel axes as depicted in in Figs. 70 and 71 are not simply re-aligned antecedent channels but indeed are newly created ones. Thus, the oscillatory dynamic pattern previously referred to should be viewed in the latter perspective.

The pattern of rotational asymmetry given in Fig. 72c is not very easily explained by the above model. This difficulty is inevitable because the data have not been decomposed into the different rotational patterns. It is surmised, however,

that the noted pattern may have a bearing on Fig. 77b, in which a cross-shore varying longshore flow intensity interacts with a longshore standing infragravity oscillation that is slightly out of phase, e.g. with a 10 % longer wavelength, relative to the antecedent situation. Thus, the rotational asymmetry pattern underlies the earlier mentioned distinctiveness in flow kinetics and direction at the proximal and distal ends of the rip channels.

Figure 72d has revealed that the axis clusters (7-12) in the eastern sector of the study area contrast from their western counterparts (1-6) in consistently depicting > 50% clockwise rotation or a Mode 1 rotation pattern, compared with a large variability in the western sector.

Finally, it is important to note that the occasionally observed, lateral rip channel translation, as against re-alignment about the defined hinge points, suggests that the edge-wave oscillation, whatever the generating mechanism, can deviate from its "normal" pattern. While the exact circumstances (e.g., storm-surge height, duration, direction etc.) under which the deviations ensue are unknown, explanations presented with respect to Fig. 77b are feasible. Instructive, however, is the fact that the longevity of the latter is always brief (annual scale), since successive surveys usually reveal spatial coherence in channel location about the defined hinge points.

A further evaluation of the morphodynamics of the sawtooth bar or rip-ridge zone showed the smallest change in sediment budget of all the zones examined (Fig. 59a), with almost zero volumetric change per  $m^2$  of the sea floor (Fig. 59b). This result is a strong indication of differences in the hydrodynamic regime of this zone compared with the adjacent counterparts. The above differences must be most dramatic during storm events, in which case the sediment budget incorporates more of the latter signal than that of the fair-weather condition. This inference follows from the

fair-weather flow records from the budget zones, which indicate almost a similar frequency of sediment entrainment.

**Sediment facies:**

The ridge and rip channel morphology or saw-tooth bar zone shows a high uniformity in the textural characteristics of its surficial sediments (Fig. 78). Grain sizes are in the fine sand range and are very well sorted. Skewness is either positive or symmetrical, whereas kurtosis varies between mesokurtic and platykurtic. The textural data show neither a predictable grain

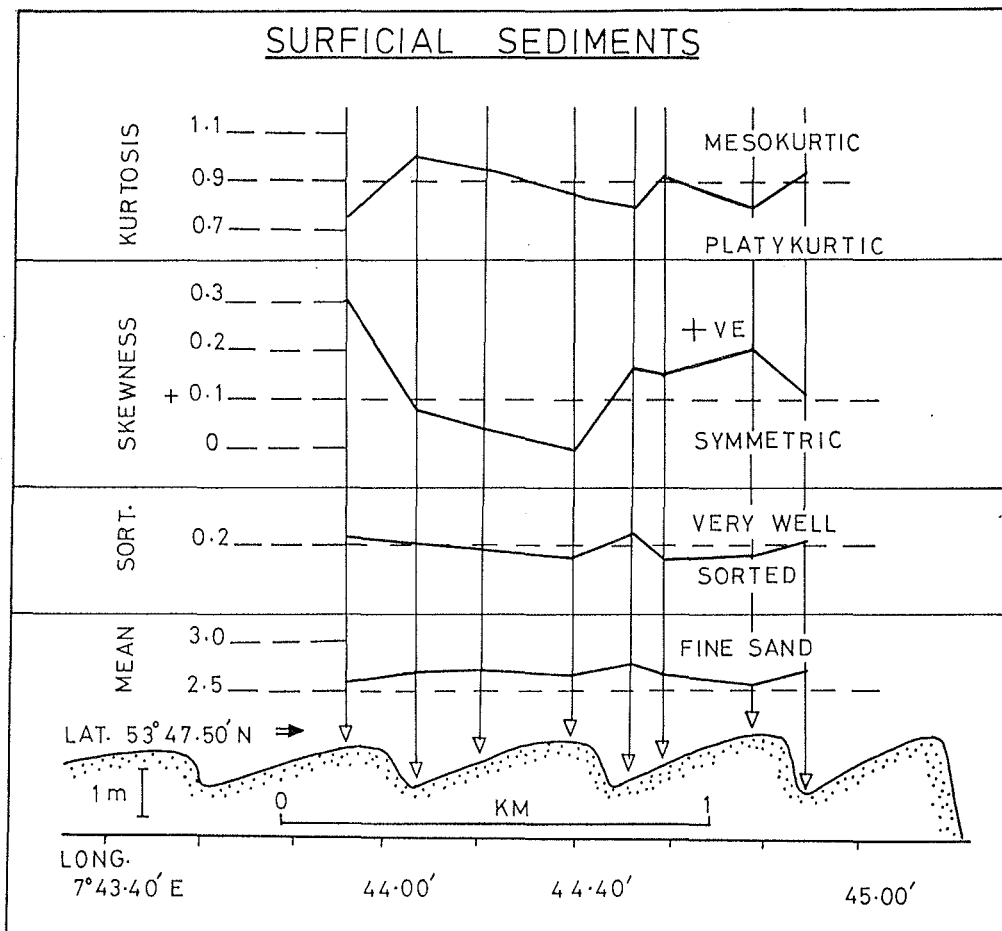


Fig. 78. Surficial grain size statistics of the rip channel and and ridge morphology.

size trend between adjacent channels, stoss sides and crests of the morphology nor alongshore in general. However, over a longer cross-section (Fig. 66) the mean grain-size of the crests do show a discernible eastward fining trend.

Vertically, statistical grain-size parameters are identical to their surficial counterparts, being similarly homogeneous (Figs. 79-82). Moreover, all core sections are composed of 70-90% fine sand (Fig. 83). The %-composition of very fine sand (Fig. 84), however, shows some variation between individual morphological components. This variation could have bearing on the flow conditions on the morphology. The very fine sand fraction is most depleted on the crest and most abundant in the channel.

The above sediment distribution pattern corroborates the observation of DÖRJES (1976) who also associated the impoverishment of macrofauna in the swales or channels relative to the crests of the rhythmic morphology to the higher concentration of fines in the former.

Finally, the upward depletion of the very fine sand fraction in the channel and adjacent flank could reflect a transition from a waning storm phase to a normal condition.

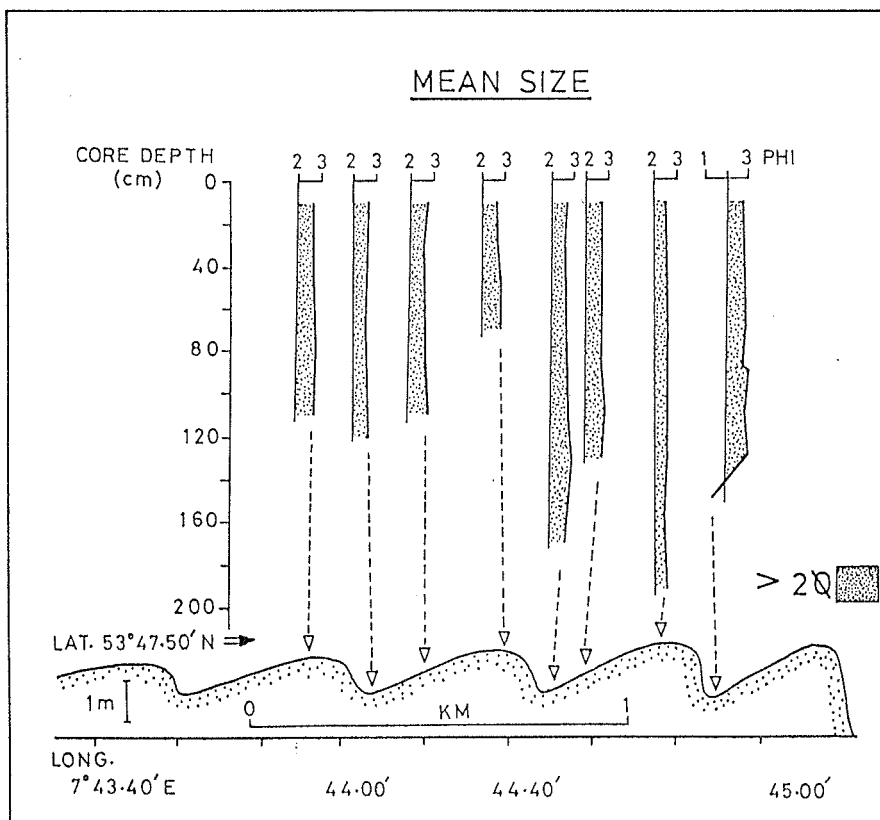


Fig. 79. Vertical variation in mean grain-size across the rip channel and ridge morphology.

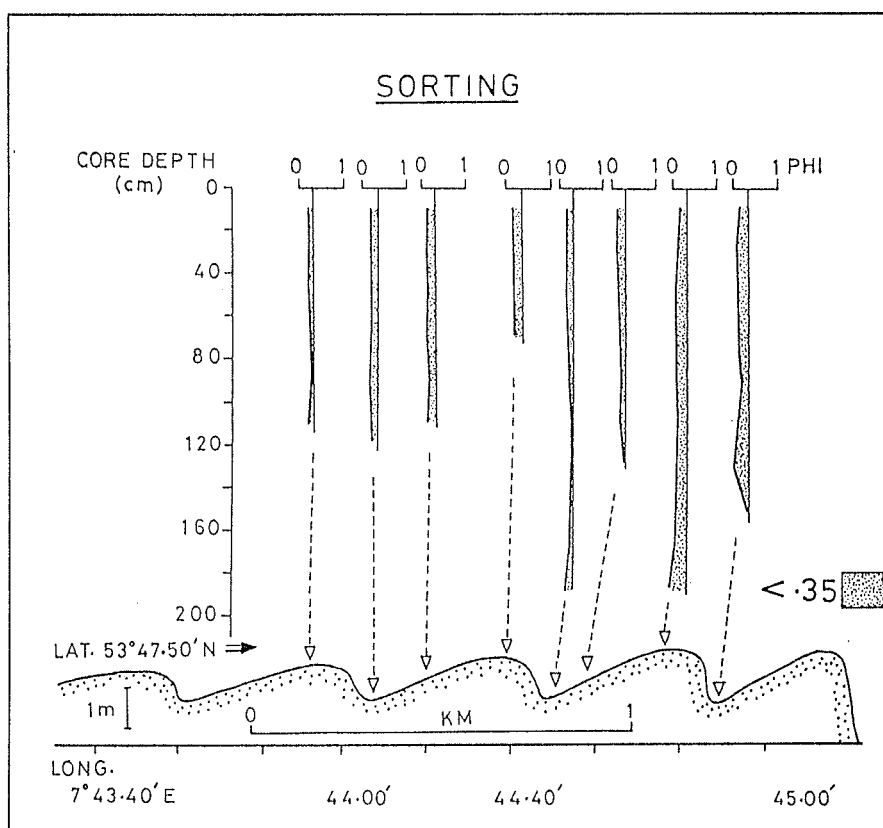


Fig. 80. Vertical variation in sediment sorting across the rip channel and ridge morphology.

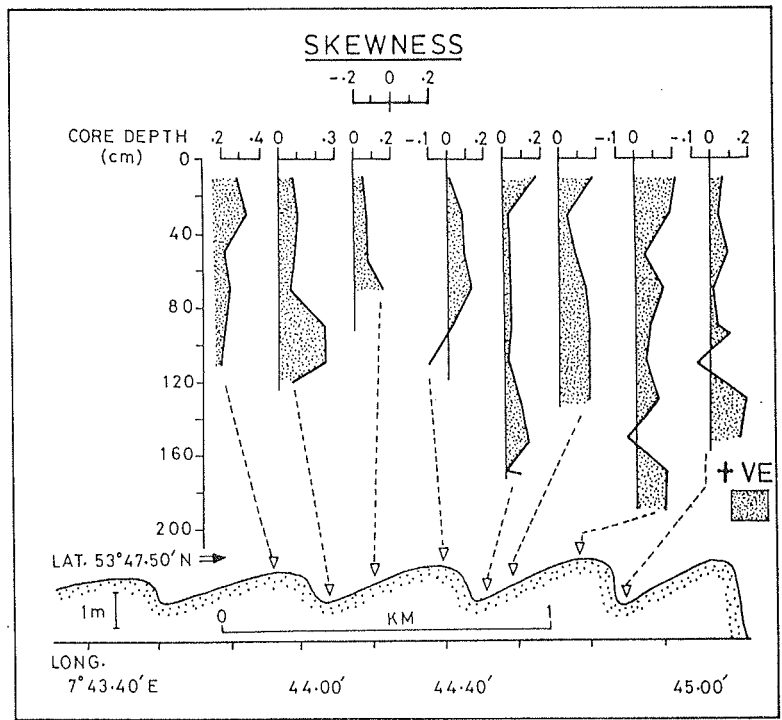


Fig. 81. Vertical variation in skewness of sediments across the rip channel and ridge morphology.

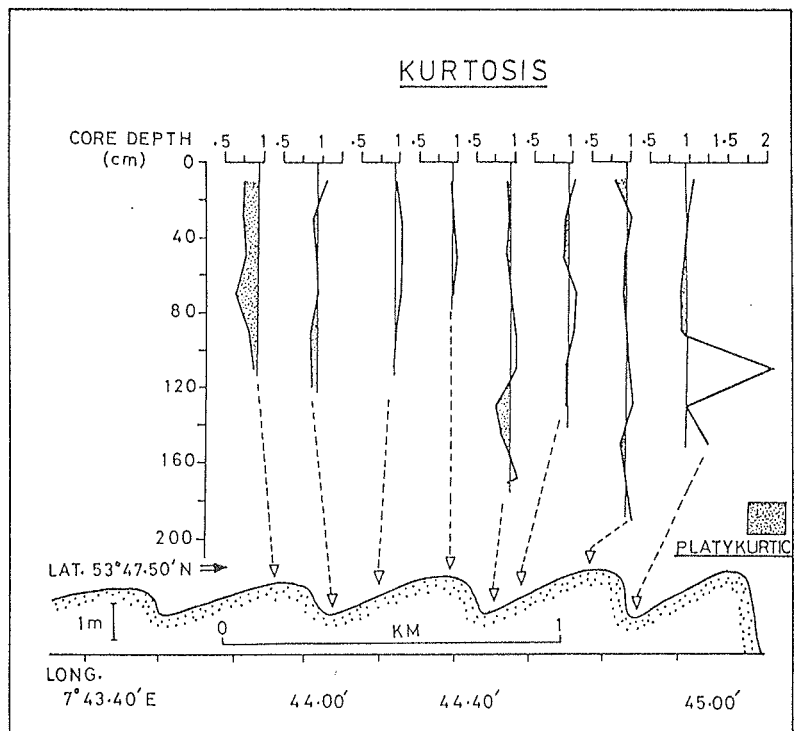


Fig. 82. Vertical variation in kurtosis of sediments across the rip channel and ridge morphology.

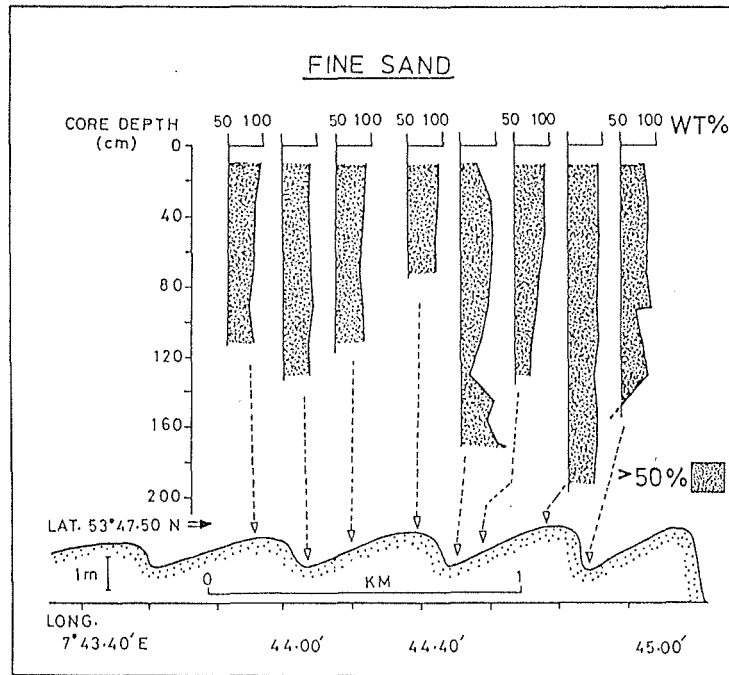


Fig. 83. Vertical variation in wt.- % distribution of fine sand fraction across the rip channel and ridge morphology.

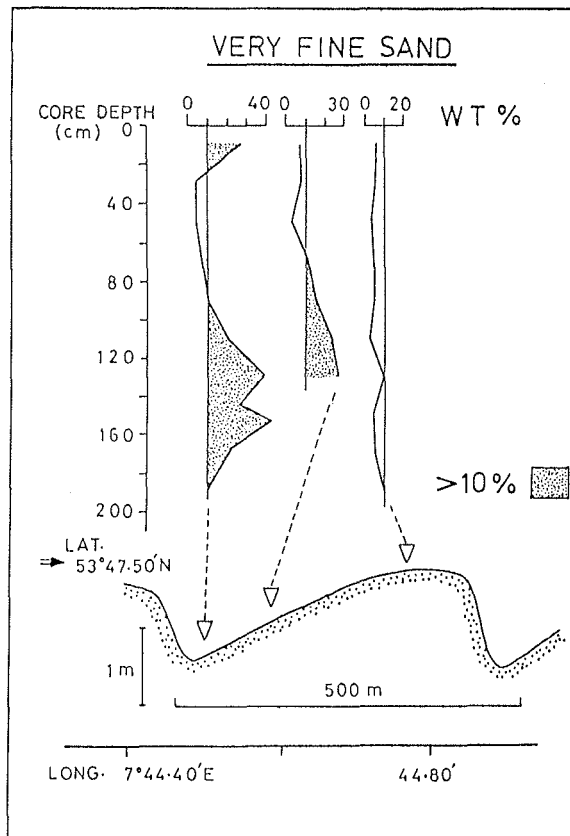


Fig. 84. Vertical variation in wt.-% distribution of the very fine sand fraction across the rip channel and ridge morphology.

The vertical sequence of sedimentary structures of the rip and ridge morphology given in Fig. 85 is to a considerable extent uniform. Horizontally-laminated fine sands constitute 50-90 % of the core sections. This is in accord with empirical observations, predicting greater than 70% exceedence of the upper flat bed orbital threshold velocities (about 70 cm/s) in fine sand (see Appendix B-2) at water depths shallower than 10 m (cf. Fig. 12c).

There are, however, marked variations in the relative distribution of alternating mud-sand laminae and shell fragments. The channel sequences revealed a greater abundance of these. Bioturbation structures are sparse due to the high energy conditions prevailing on the upper shoreface subenvironment in general.

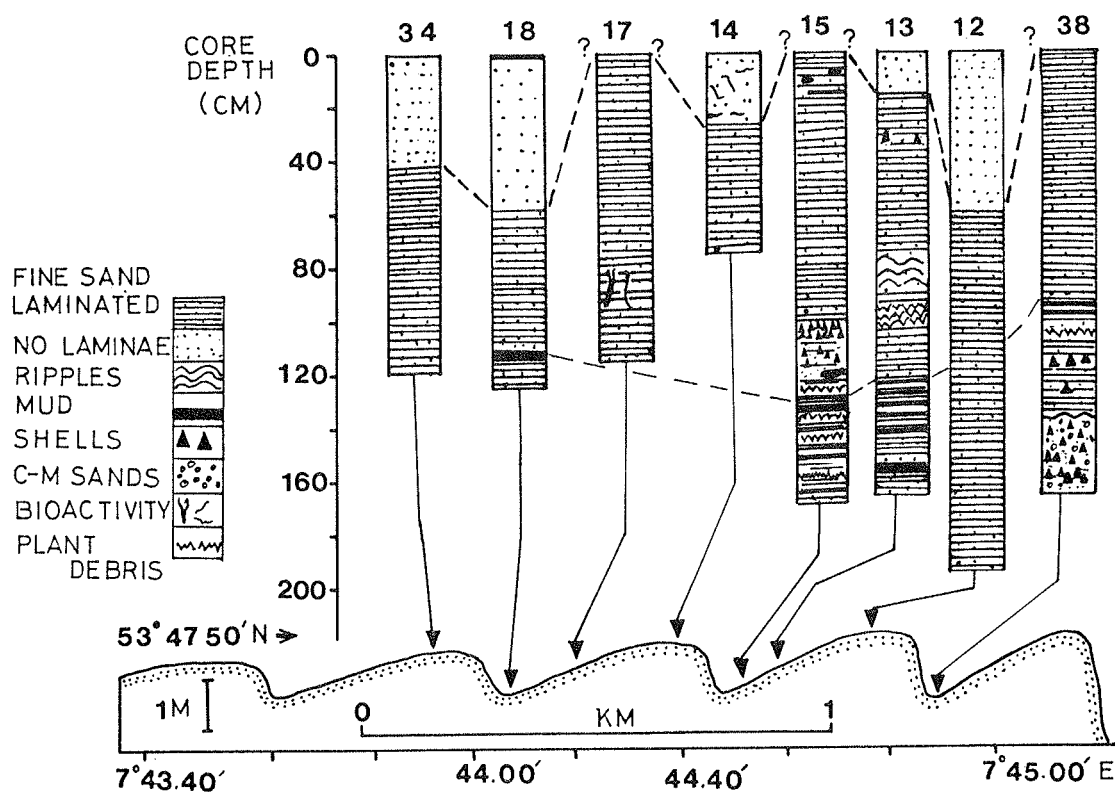


Fig. 85. Vertical sequence of sedimentary structures across the rip channel and ridge morphology.

#### 6.2.1.4 Smoothly Sloping Transitional Zone

The smoothly sloping transitional zone (SSTZ) defines the distal end of the upper shoreface subenvironment and links the latter to the central shoreface. In this 6-8 m water depth (relative to NN) zone, wave influence at the seabed is still pronounced. Even the coarsest sediment constituting the substrate can be entrained in > 80% of the time.

Tidal currents, as exemplified in Fig. 86, are flood dominated (see also Section 3.6.3) and at peak flow can initiate sediment transport. Nonetheless, transport efficiency is expectedly higher under the combined influence of tidal and wave orbital currents during both the flood and the ebb phase. The morphosedimentary characteristics of this zone, as discussed earlier, is consistent with this conclusion.

Principally, the alongshore sediment budget data presented in Table 4 show a net accretion in regions proximal to the ebb deltas, whereas erosion is higher off the centre of the island. This suggests that wave-induced reversals in longshore sediment transport is more pronounced in this zone and that data from this zone contribute more to the overall upper shoreface pattern illustrated in Fig. 60.

By comparison, changes in the proximal upper-shoreface sediment budget are as much as 60 % higher, while the longshore gradient in the budget magnitudes is less steep on average, i.e. shows a more continuous change than observed in the transitional zone. The steadier gradient in the proximal zone has two implications :

(a) standing edge waves in the study area are more commonly generated by longshore current/topography interactions (in which case the maximum amplitude is situated further away from the shoreline);

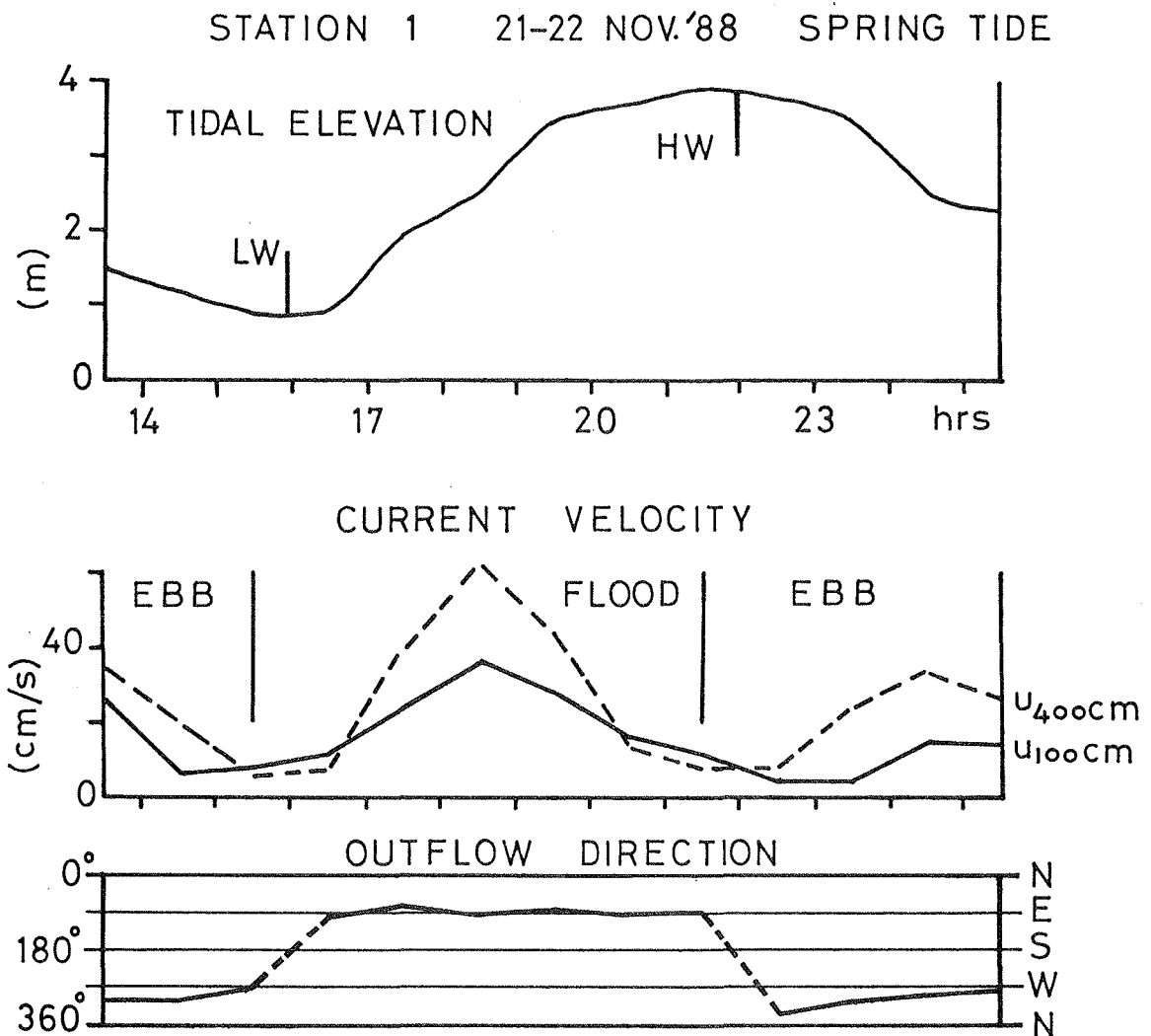


Fig. 86. Typical fair-weather tidal current pattern on the smoothly sloping upper shoreface transitional zone.

(b) where the maximum amplitude of the standing oscillation occurs at the shoreline, it shows that the oscillation itself is incapable of curtailing a continuous coastwise sediment transport induced by breaking waves.

Surficially, transitional zone sediments show a similar alongshore gradient in statistical grain size parameters as observed in the medial and proximal upper-shoreface

counterparts (Fig. 66). The sediments become finer, better sorted and more positively skewed in an easterly transport direction. Vertically, as shown in Figs. 87a and 87b, the mean size and sorting values remain quite uniform, except at the base of most cores where medium sands and less well sorted sands are found. Because of the discrete occurrence of the latter, a relationship with a specific storm event is plausible.

On the other hand, skewness (Fig. 87c) and kurtosis (Fig. 87d), especially in the two distal cores, showed a markedly more variable, but nevertheless correlative pattern. In particular, negative skewness on the upper 60 cm core section can be related to immiscible admixture of coarser size classes in the course of, or aftermath deposition of the central shoreface sands. This view is corroborated by the upper shoreface cross-shore grain size statistical trends of Fig. 67. This pattern shows transitional zone sands (positioned at lat.  $53^{\circ} 48.00'$  and  $53^{\circ} 48.25'$  in the figure) are coarser than those of the medial saw-tooth bar zone. As such, the fine sediment components transported by the rip currents must be "overpassing" the distal part of the transitional zone during storms; if not, then the coarser sands on the central shoreface are being mixed with those of the transitional zone, possibly by shoaling waves.

At it will be shown in Section 6.3.3.1, the central shoreface sands depict a marked textural change at about the same core depth as indicated above.

The %-composition of the sand fractions (Fig. 88 a-c) shows fine sand to be the dominant grain size. Vibrocore and repetitive boxcore data (see Section 6.3.3.2) consistently depict a finely horizontally-laminated sand sequence in this zone. As on the saw-tooth bar crests, shell fragments and mud laminae are rare. By contrast, bioturbation is persistent and significant, especially in its distal reaches.

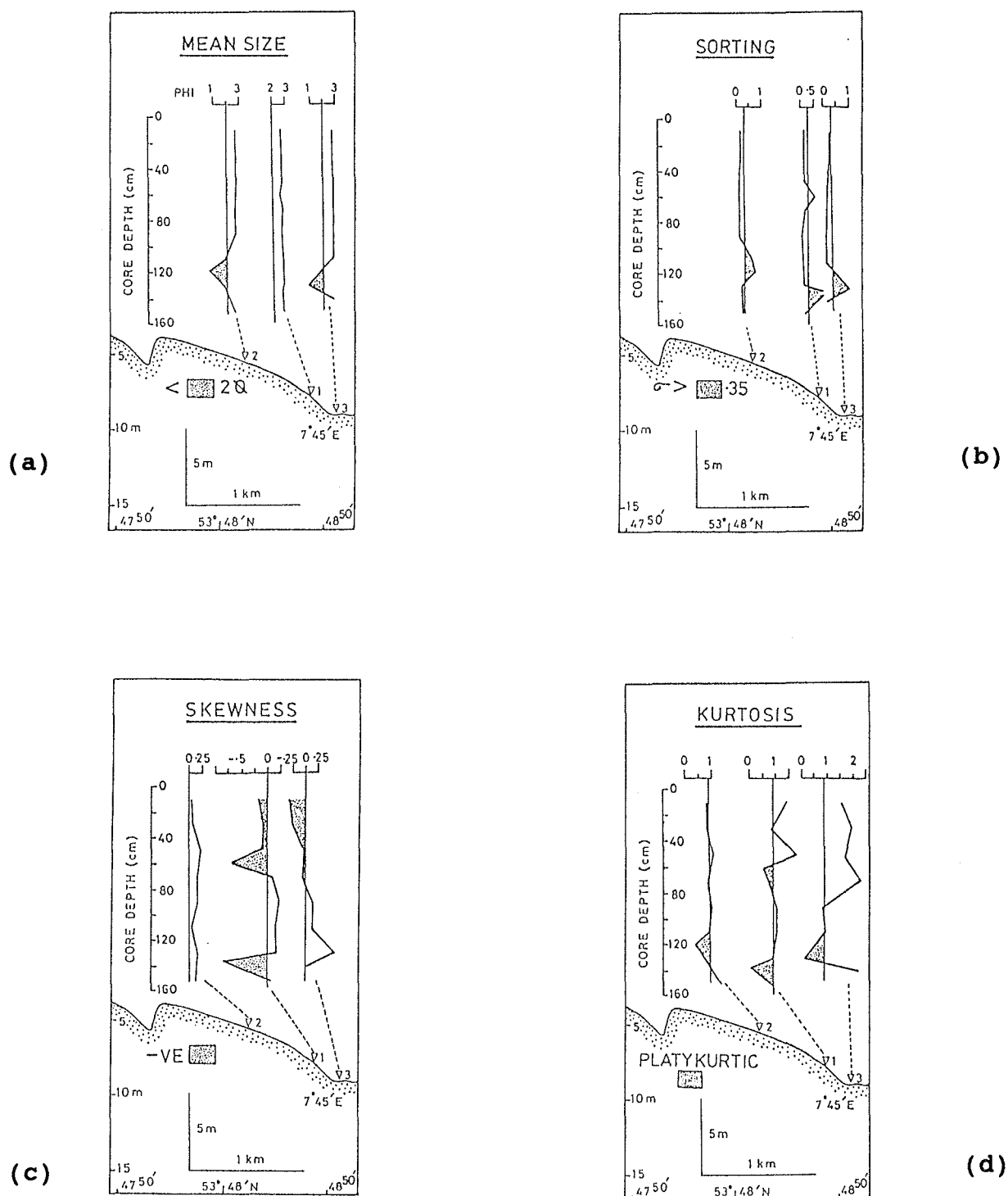
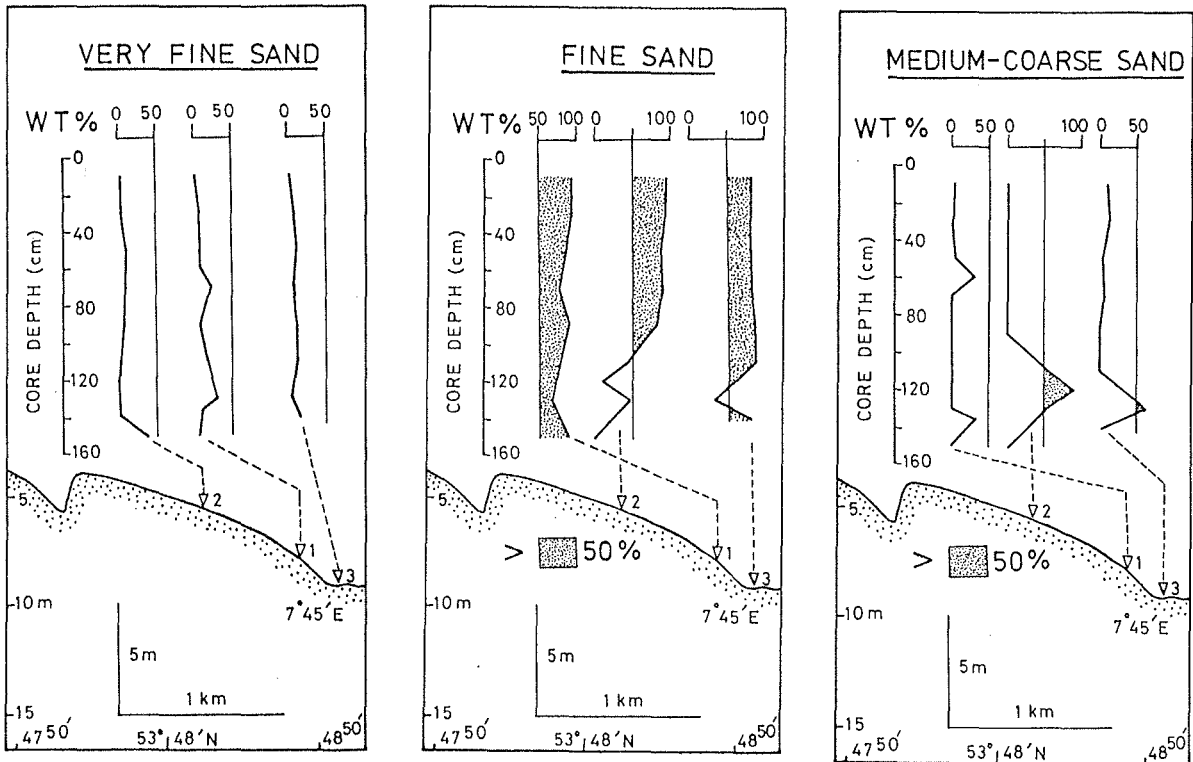


Fig. 87. Vertical variation in (a) mean grain-size, (b) sediment sorting, (c) sediment distribution skewness and (d) sediment distribution kurtosis on the smoothly sloping upper shoreface transitional zone.



(a)

(b)

(c)

Fig. 88. Vertical variation in wt.-% of (a) very fine sand, (b) fine sand and (c) medium-coarse sand on the smoothly sloping upper shoreface transitional zone

### 6.2.2 Summary Remarks on the Upper Shoreface Subenvironment

The 2.5-3.5 km wide upper shoreface subenvironment has been subdivided into 4 zones of generally high mean flow intensity which can in > 80% of the time mobilize bottom sediments. The flows differ both in scale and structure over time and space. Sediment budget analysis and textural data suggest both cross-shore and alongshore flow patterns to be significant. The alongshore sediment budget pattern supports the contention that the mean shore-parallel currents are higher in magnitude and steadier in direction on the proximal relative to to the distal upper shoreface.

Besides tidal and storm-induced currents, as well as wind-waves and their associated currents, edge waves evidently play a significant role in this subenvironment. It is hypothesized that due to their peculiar generating mechanism, involving ebb-delta-induced perturbations of westerly to northwesterly emanating storm currents, their major morphological expression is less apparent at the shoreline and in the surf zone than beyond the latter. In addition, high-energy choppy waves coupled with the large tidal range in the study area, might suppress the coherence of any standing edge wave oscillation within and shoreward of the surf zone.

By comparison, the recurrence of rhythmic shoreline features on the fine-grained, high-energy, mesotidal Ibeno Beach along the southeastern coast of Nigeria, may relate to the prevailing ocean swell climate. A saw-tooth bar morphology, however, is not observed along this coast, despite the fact that the beach is bounded on both sides by a seaward protruding bathymetry as is the case in Spiekeroog. Reasons for the absence of this rhythmic morphology are probably because (a) of its plano-concave nearshore profile whereas Spiekeroog has a convex profile, this enhancing channelization by rip currents, and (b) because steady and intense shore-parallel storm currents are rare whereas they are recurrent on Spiekeroog.

Texturally, it has been shown that the different upper shoreface zones depict varying degrees of discernible grain-size statistical parameters both alongshore and cross-shore. The regression trends presented in Fig. 98 show the following characteristics :

- (a) The best correlated pairs of grain-size statistical parameters are skewness vs. mean, sorting vs. mean, and skewness vs. sorting;
- (b) The cross-shore pattern is generally better defined than the alongshore counterpart for any given pair of grain-size parameters;

## UPPER SHOREFACE GRAIN SIZE REGRESSION TREND

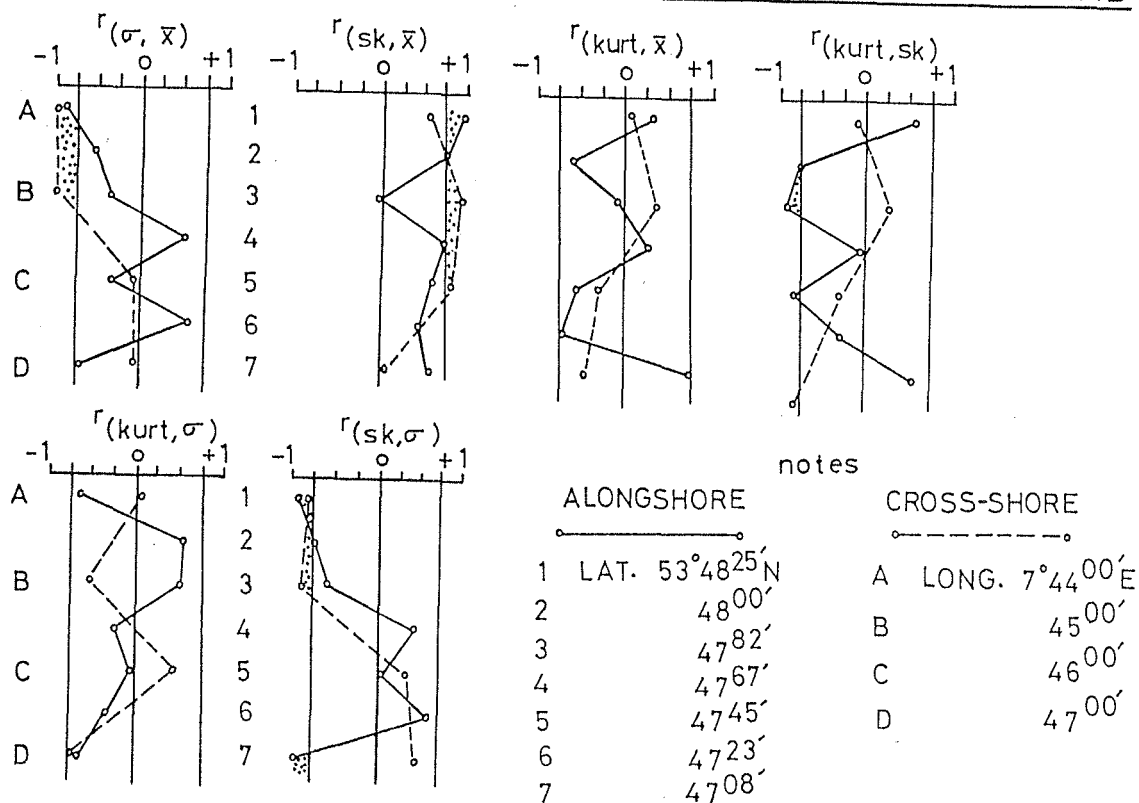


Fig. 89. Regression trends of cross-shore and alongshore upper shoreface grain-size statistical parameters.

(c) The cross-shore correlation coefficients tend to decrease eastwards towards the ebb-delta, probably due to the increasing influx of allogenic sediments from the inlet; and

(d) The alongshore correlation coefficients were high and consistent in the proximal and distal zones but variable and weak in the medial (sawtooth bar) zone. The implication of the above is that alongshore sediment transport is least intensive on the medial zone. Two plausible reasons may be adduced to explain this: (i) the occurrence of standing edge-wave oscillations may constrain a continuous longshore transport, or (ii) this zone is not sufficiently exposed to either the wave-generated longshore current or the transient storm counterpart.

Finally, in conformity with the flow regime and the narrow range of sediment characteristics, the upper shoreface facies principally comprises horizontally-laminated fine sands. The sands are clean and very well sorted. Sand-mud laminae are most commonly encountered within the rip channels. Shells and bioturbation structures are generally rare, except in the distal reaches of the transitional zone, where burrowing becomes appreciable and persistent.

### 6.3 Central Shoreface Subenvironment

The central shoreface subenvironment is the domain of the WNW-ESE striking shoreface-connected ridge system (Fig. 7). Four such ridge crests are recognized in the study area and are, coastward, designated as outermost, outer, inner and innermost. A similarly trending set of two ridge crests occur just northward of Fig. 7. These could be considered as inner shelf ridges. Much of the emphasis is placed on the outer and inner ridges over which detailed investigations were conducted. The northwestward continuation of these beyond the study area necessitates an overview of the regional characteristics of the ridges.

A sediment distribution chart of the German Bight published by the Deutsches Hydrographisches Institut (DHI) in 1981 (No. 2900; 1:250 000), as modified in Fig. 90, provides a good basis for such an overview. It should be mentioned, however, that the sediment map is based on an average density of 1 sample per 2 km<sup>2</sup> and as such is 16-64 times coarser gridded than that of the present study. A further shortcoming is that the tidal inlets, which are on average 2 km wide, are inadequately represented on the map.

Nonetheless, the following regional characteristics of the ridges are evident from the latter:

- (1) The sand bodies are elongate in shape, typically being 10-25 km in length and discontinuous coastwise;
- (2) They are surficially composed of mainly medium-coarse sands;
- (3) They have a shoreline-oblique orientation with a westward-opening shore-acute angle ( $\theta$ ) which is somewhat larger to the west;
- (4) They are situated in water depth  $> 10$  m;
- (5) Their long axis strike is similar to sediment bands occurring in deeper waters (especially 10-20% muddy sand);
- (6) The sediments similar in texture to those of the ridges are limited in occurrence to the inlets, around Helgoland (40 km NE of Spiekeroog) and to the shoreface of Borkum Island. In fact, the latter is also a shoreface-ridge but apparently differs from the others in its massiveness. Line A-A' defines its longitudinal trend.

#### 6.3.1 Genesis of Shoreface-Connected Ridges : Criteria and Constraints of Existing Models

From the literature study presented in Section 2.2.2, it is readily apparent that the most intensively investigated shoreface ridge environment is situated on the eastern seaboard of the United States. The results accrued in the studies of SWIFT and co-workers from the latter region have subsequently been extended to other localities, e.g. the North Sea (SWIFT et al., 1978), the Canadian shelf (HOOGENDOORN and DALRYMPLE, 1986) and the Argentine shelf (PARKER et al., 1982).

It is worth mentioning from the outset that the intensity of the flow regime and, by implication, its potential sediment transport capacity along the Atlantic shoreface-shelf province of the American continent is several orders of magnitude lower

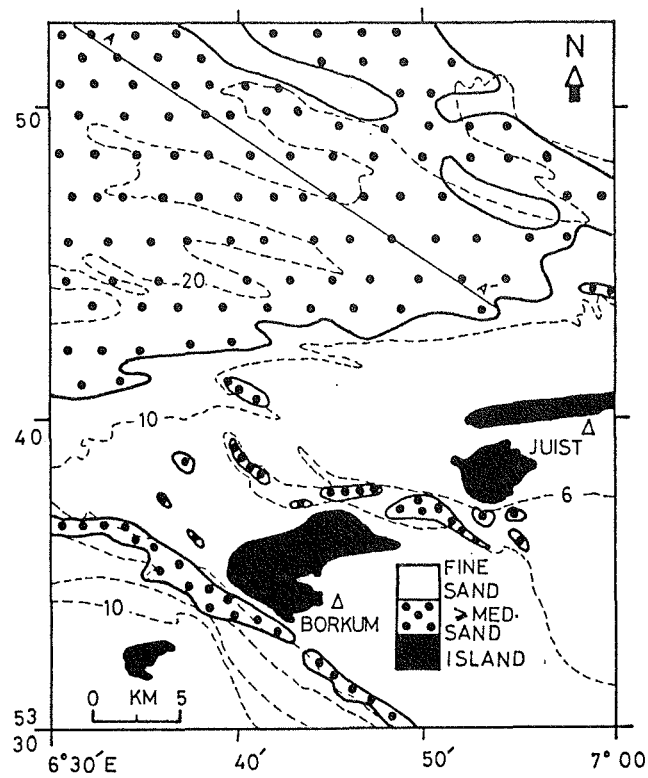
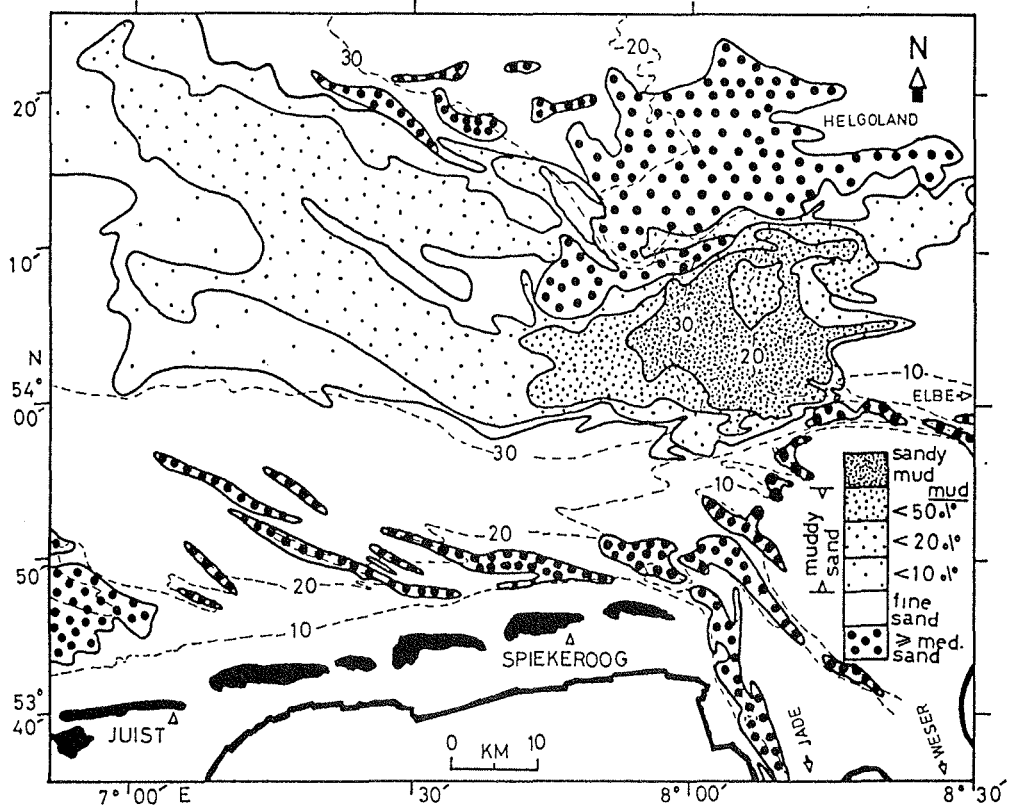


Fig. 90. Sediment size distribution in the German Bight (modified from DHI, 1981).

than that of the southern North Sea. Moreover, sediment transport on the former is storm-dependent and hence limited in time, whereas in the North Sea even fair-weather combined flows would effect continuous sediment transport in > 80% of the time, with intensified rates during recurring storm events.

The above disparities, in the writer's opinion, limit any direct extrapolation of the generating and maintaining mechanisms of the ridges on the Atlantic shelves to those of the North Sea study area, inspite of the fact that these ridges display certain similar characteristics. Principal among these similarities are (a) the oblique ridge orientation relative to the regional major flow direction, (b) the textural-topography asymmetry and (c) an underlying flat reflector which is not part of the ridge structure (e.g., SWIFT et al., 1978).

Historically, shoreface and shelf ridges have been viewed as features of relict (pre-Holocene), recent (post-Holocene) or combined relict-recent origin. The current literature reveals some consensus with regard to a recent evolution of the ridges. By contrast, the mechanism of formation is still a subject of debate. The principal postulates are based on : (a) stability analyses of flows which are transverse (SMITH, 1970) and oblique (HUTHNANCE, 1981) to the morphology; (b) helical flow (HOUBOLT, 1968; SWIFT et al., 1978); (c) progressive infragravity waves (BOCZAR-KARAKIEWICZ et al., 1990); (d) internal waves (BOCZAR-KARAKIEWICZ et al., 1991); and ebb-delta retreat path (McBRIDE and MOSLOW, 1991). The possibility of the ridges having evolved as breaking storm wave-formed bars has also been considered (DUANE et al., 1972).

Following a scrutiny of the underlying principles of the above models, none is deemed suitable to account for the evolution of the ridges in the studied area. McBRIDE and MOSLOW (1991) rightly noted that all of the above hypotheses were speculative and that not a single one can simultaneously account for their origin, orientation and distribution.

As a matter of fact, the existing models merely address specific attributes of the ridges, some of which may have no bearing on the primary process of their generation. The principal flaws of the individual models will be addressed in the course of following discussions.

Based on data from the shoreface ridges studied, a set of criteria and constraints, which any rational explanation of ridge genesis should consider and unequivocally account for, are outlined below.

- (1) Water depth of occurrence: is it dictated by sediment supply and/or flow energy?
- (2) Ridge longevity: is it determined by waves?, tides? or mean currents (storm or normal)?
- (3) Ridge orientation: is it dependent on tidal inlet/shoreline retreat rates or defines actual flow direction?
- (4) Vertical grain-size pattern: does it depict erosional or depositional processes?
- (5) Longitudinal and cross-shore grain-size patterns: has it developed contemporaneously or is it a post-formational modification?
- (6) Longitudinal and cross-shore ridge morphology and relief patterns: are these developed contemporaneously or do they reflect post-formational changes?
- (7) Longitudinal and cross-shore sediment budget pattern; and
- (8) Ridge morphology hydraulics.

The basic principles of a model that most reasonably explain ridge genesis along the Frisian barrier island coast are outlined below. However, the main discussion on the development and dynamic sequence of the ridges will be deferred until their hydrodynamics, morphodynamics and facies attributes have been examined.

### 6.3.1.1 Diverged Inlet Storm Ebb Current (DISEC) Model : A Novel Approach to Ridge Genesis

Hydraulics and sediment dynamics of tidal inlets (and estuaries) are elaborately documented in the following treatise: CRONIN (1975), BRUNN (1978) and AUBREY and WEISHAR (1986). Comparatively less is known about the interaction between inlet flows and the adjacent nearshore circulation (DAVIS and FOX, 1981), particularly during storms.

Flow patterns reconstructed from field measurements and morphodynamic processes are generally restricted to the proximity of the shoreline (TODD, 1968; DAVIS and FOX, 1981; OERTEL and HOWARD, 1972, OERTEL, 1986). The tempestite model (e.g., AIGNER and REINECK, 1982; MYROW, 1992) represents storm-related offshore example of such an interaction.

In general there is consensus that during the ebbing phase, shore-parallel flows at the updrift side of an inlet would be diverged seaward by the inlet ebb flow (TODD, 1968; OERTEL and HOWARD, 1972). In reality, the shoreface current is never entirely diverted and need not always be deflected. Nor can it be presupposed that the inlet ebb flow can be diverged in its entirety. The tempestite stratigraphy and the concentration of fines on the lower shoreface of the study area, at positions diametric to the inlet mouth, corroborate the latter.

The flow that is deflected (inlet versus shore-parallel) would depend on their relative strengths, which can vary vertically and distally. Thus, temporal and spatial variability in flow being diverged is feasible. These facts are evident in the morphologic model of ebb-delta configuration presented by OERTEL (1986).

For reasons to be discussed later, the flow diversion model presented in Fig. 91 relates principally to storm events during which the inlet ebb flows are jet-like. ÖZSOY (1986) presents a

## DISEC - INLET FLOW DIVERSION MODEL

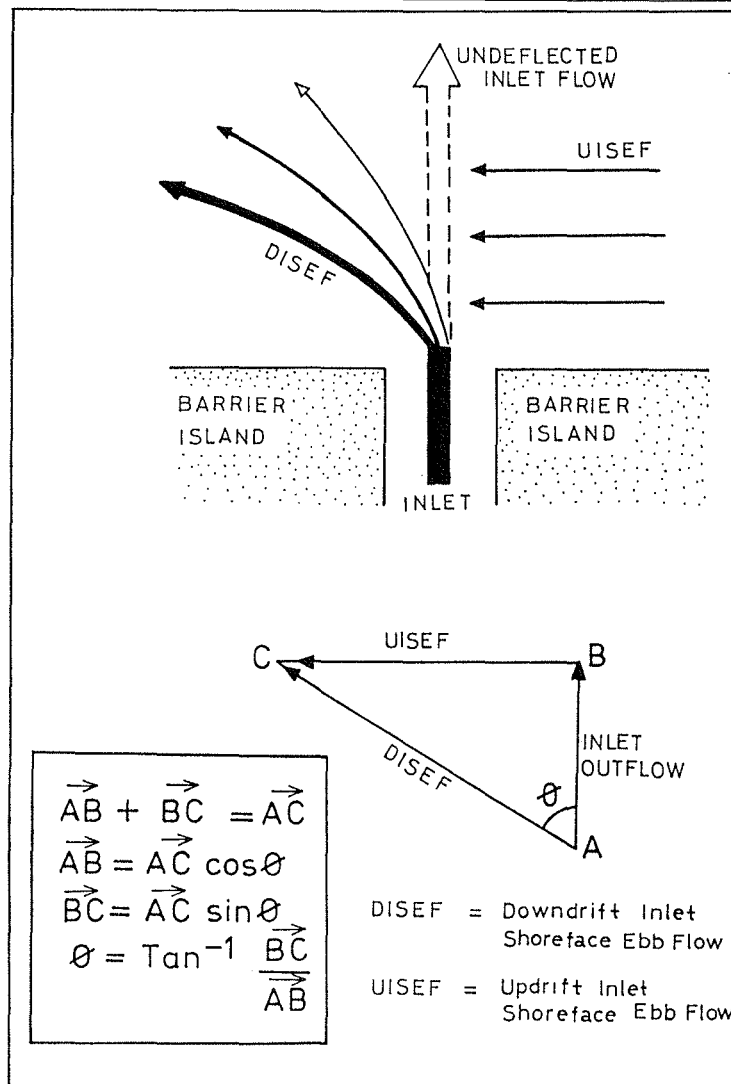


Fig. 94. Principles of flow diversion (DISEC) model.

rigorous treatment of tidal inlet ebb-jet dynamics. In contrast to the existing flow divergence models, the present one considers the inlet ebb-jet to be stratified, as a consequence of which the velocity of the denser near-bed flow, produced by the additional factor of bottom frictional resistance of a generally gentle sea floor slope, is much lower than that in the upper water column.

Thus, a two-fold pattern of inlet ebb-jet (IEJ) interaction with the shoreface ebb-flow at the updrift side of an inlet (UISEF) is postulated. The lower column of the IEJ would generally be deflected to form the shoreface ebb-flow at the downdrift side of the inlet (DISEF), whereas its swifter upper column may continue virtually undeflected over a much longer offshore distance. In the latter case it is the UISEF that veers, except at the waning stage of IEJ. Based on elementary vector analyses and trigonometry, the following are evident :

- (a) The bottom diverged flow (DISEF), being a resultant of UISEF and IEJ, will always be swifter than either of its components; and
- (b) The shoreline-obliquity of DISEF increases with higher UISEF-IEJ velocity ratios.

Although ÖZSOY's (1986) inlet jet model was based on a somewhat different premise (e.g., unstratified and undeflected IEJ), some of his results are quite logical and can, with appropriate modification for divergence, be incorporated into the model presented here. In particular it was shown that:

- (a) The cone-shaped inlet jets may be characterized by a core or centerline of maximum velocity;
- (b) Maximum deposition would occur at both margins of the centerline, whereas the core may be either erosional or depositional, depending on flow intensity;
- (c) Depositional patterns depend on bottom friction and topography, settling velocities of sediments and the initial velocity at the inlet. In particular, sediments with higher settling velocities are confined to the vicinity of the inlet mouth; and
- (d) The jet shows, longitudinally, a seaward diminishing gradient of deposition.

A supporting evidence of flow diversion in nature is inferred by this writer from the results of trace metals (Cr, Cu, Ni and Zn) studies of bottom sediments on the New Jersey

inner-shelf ridges presented by HALL et al. (1987). As exemplified in Fig. 92, the concentration pattern of the above metals, the sources of which are located upstream of Delaware Bay, parallels the ridge trend. Such a pattern can only be due to a northeasterly deflection of the ebbing estuarine flow.

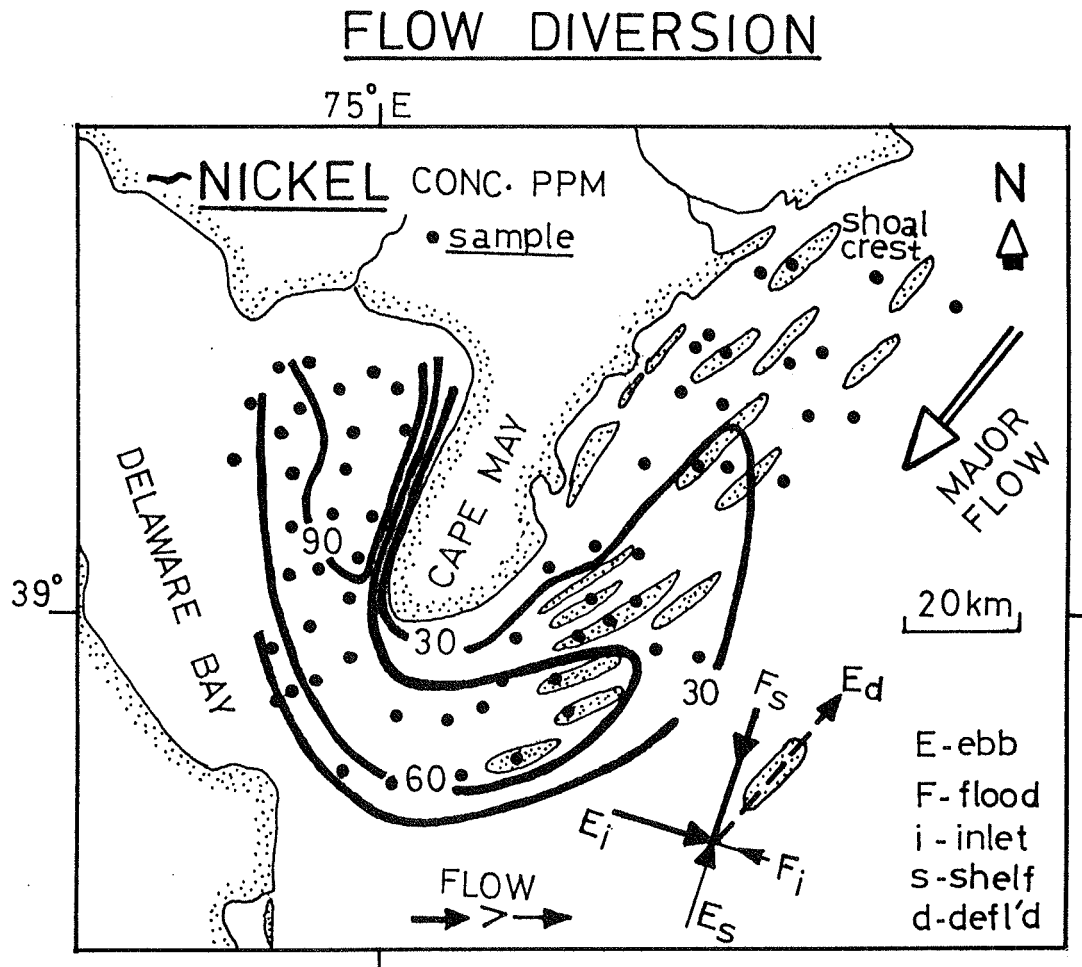


Fig. 92. Heavy metal distribution pattern as a response to flow diversion (modified from HALL et al., 1987).

In the absence of such a deflection, the pattern of concentration should have had a southeasterly orientation. Furthermore, the ridge-parallel pattern would also not have been apparent, at least not close to the coastline, if the coast-parallel flow was diverged instead of the estuarine flow.

With the above background information, some of the criteria for ridge genesis outline earlier can now be commented upon. The DISEC model predicts that, like the trace metals, the sediments forming the ridges emanate from the inlets and because their transport is related to DISEF, they are impoverished at, or bypass, water depths shallower than 10 m.

Relatively high inlet outflow velocities, such as recorded during storms (Section 3.6.3), would be required to effect such a bypass. Under this circumstance, shoreface ridges along the Frisian barrier island coast can only form seaward of the terminal lobe of the ebb deltas, which is generally in water depth of  $> 6$  m. The flow direction of DISEF defines the obliquity of a ridge relative to the shoreline, whereas ridge longevity is related to recurring deposition associated with DISEF. Finally, sediments should decrease in size (lower settling velocities) longitudinally in a northwesterly direction.

Of all of the ridge genesis models, only that of McBRIDE and MOSLOW (1991) on the North American Atlantic shelf (Fig. 93) is conceptually related to the DISEC model in that it identifies a genetic relationship between a propensity for ridge development with inlet dynamics and deposits. Noteworthy is the fact that these authors explain the "vexing" problem of ridge orientation to inlet dynamics without recourse to a major regional sand transport direction often invoked by other workers.

However, the credibility of the above model is severely limited in that the mechanics of "joining" the stranded ebb tidal deposits on the one hand, and their moulding to a ridge-trough system on the other, are unclarified. Consequently, many attributes of the ridge morphology outlined earlier are not accounted for.

Furthermore, the discrepancies between the established and the model-predicted inlet/shoreline dynamics, both in scale and

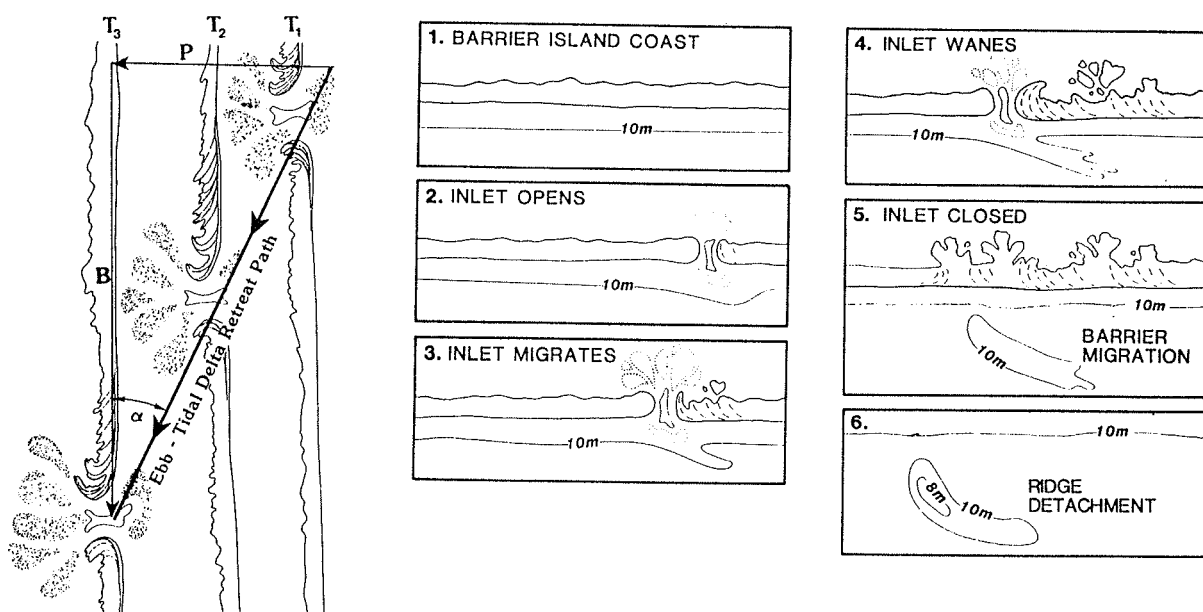


Fig. 93. Ebb-delta retreat path model of shoreface ridge genesis (from McBRIDE and MOSLOW, 1991).

rate, additionally invalidate the prospect of the above evolution model of shoreface ridges along the Frisian barrier island coast. For example, with an average shore-acute ridge angle of  $14^{\circ}$  and a lateral inlet migration rate of 13 m/yr, the predicted shoreline recession rate of 4 m/yr turns out to be four times the rate reported by STREIF (1986) (cf. SCHUBERT, 1990) for the neighbouring barrier islands.

Similarly, using well known data such as the ridge length (10 km) as a surrogate for the retreat path length and the above mean ridge angle, the model predicts a 9.7 km lateral migration of the Harle Inlet. The above value is clearly incompatible with a maximum Frisian inlet migration of 4 km. Thus, as a mechanism of origin for the Frisian ridges, the ebb delta retreat model must be discarded.

### 6.3.2 Hydrodynamics

It was shown in Section 3.6 that the fluid motion on the shoreface as a whole is capable of frequently mobilizing the surficial sediments. This logically implies that the longevity of the ridges would be endangered if their orientation was not conformable with that of the principal (net) flow, responsible for sediment transport on a day-to-day basis.

This being the case, one can visualize the ridge orientation as an equilibrium response to the principal flow regime on the central shoreface. Consequently, currents and water mass transport associated with shoaling waves are clearly subordinate in role since the major trend of wave crests in the region (NE-SW) is non-conformable with the ridge orientation. In a similar sense, breaking waves as a generating mechanism can be discarded even though commensurate wave heights ( $> 10$  m) may occur in  $< 0.1\%$  of the time. By contrast, as shown in Fig. 11f, the tidal flow directions show a much more ridge-trend conformable pattern. Because the tidal flow pattern referred to above persists for more than 6000 hours annually, in the course of which sediments are also mobilized, it is considered responsible for maintaining the ridges once initiated.

Figure 11f, however, also shows that both flood and ebb currents on the shoreface are mutually evasive. Whereas the flood currents in deeper waters flow at a high angle to the shoreline, its obliquity increasing towards shallower water, the ebb currents show the converse of the above. The latter is denoted DISEF in Fig. 91. It was further noted that the ebb currents displayed considerably less variability in flow direction than the flood current.

In general, the above fair-weather ebb current patterns support the the diversion model initially invoked for storm conditions. Thus, as anticipated for storm conditions, the apparently less stratified fair-weather inlet outflow would be

expected to decelerate in deeper water and hence be more vulnerable to deflection from a shore-normal orientation than at the proximal inlet mouth.

As such, DISEF in about 8-10 m of water depth is less shoreline-oblique than in deeper water. The cross-shore component of DISEF in the above water depth may contribute to the typically observed shore-normal textural-topographic asymmetry (Section 6.3.3.1) predicted by SMITH (1970).

An additional observation concerning the flow record over the shoreface ridges is that, irrespective of the tidal cycle, the  $U_{100}$  velocities of DISEF tend to increase with distance offshore, both within the troughs and on the crests of the ridges (Fig. 94). Velocities are higher and correlation better in the troughs than over the crests.

This offshore increase in velocity of DISEF further attests to the diminishing outflow velocities and damping of UISEF away from the inlet mouth. Because the angle of deflection,  $\theta$ , of the inlet outflow from a shore-normal plane is likely to be larger distally, trigonometric relations show that DISEF velocities must be correspondingly higher.

In contrast to the cross-shore flow data, corresponding longitudinal data is not available at present and must thus be inferred from indirect sources such as sediment characteristics and sea floor morphodynamics.

Finally, none of the flow data acquired so far suggests a helical flow pattern with which ridge genesis is commonly associated. Such a pattern must persist in the study area, even in non-storm conditions, if the ridge morphology is to be maintained. Furthermore, since the principal flow pattern was not shore-normal, the ridges could not have evolved as a flow-transverse bedform, notwithstanding their conformable textural-topographic attributes as suggested by SMITH 's (1970) model.

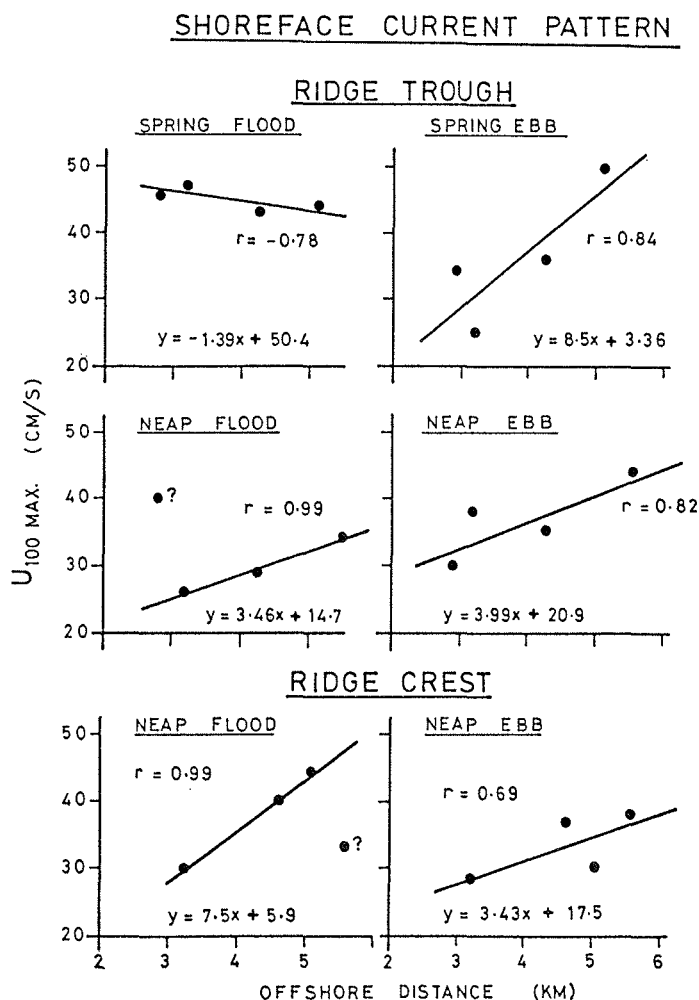


Fig. 97. Variation in peak flow velocities (at 100 cm above bottom,  $U_{100}$ ) with distance within the ridge morphology.

### 6.3.3 Morphodynamics

The dynamics of the shoreface ridges and aspects of their evolution are better visualized in the light of their geometry and morphometrics. They are noticeably non-parallel, converging towards the coast and diverging seaward. They have a westward opening, mean crest-trough shore-acute angle of  $17^\circ$  for the outer and  $10^\circ$  for the inner ridge respectively. Henceforth, their shallower near-coast end will be referred to as proximal and the northwesterly seaward counterpart as distal.

From a longitudinal perspective, the ridge orientation is inlet jet- or cone-shaped. It would therefore seem that all that is needed to initiate this morphology is a divergence of a storm inlet-jet. The troughs of the morphology can then be viewed as the high velocity centerline or core, which ÖZSOY (1968) showed to be erosional under intense flow conditions.

Furthermore, the ridge morphology (relief) wedges out distally. As would be expected for a waning jet entering deeper waters, its sediment entrainment capacity would be increasingly devoid of a lateral gradient and, accordingly, produce a less well-defined relief. None of the flow models on ridge genesis outlined earlier can unambiguously explain the above cone and wedging-out characteristics of the ridges.

A typical cross-ridge profile at Long.  $7^{\circ} 45.00'E$  (see Fig. 14) can be described as follows:

(1) The inner ridge has a relief of 5.3 m, a width of 2.1 km and a spacing of 1.6 km, whereas the outer ridge has corresponding measures of 3.5 m, 1 km and 1.2 km respectively, with steepnesses in the 0.003-0.004 range. The cross-sectional area of the inner ridge is 2.25 times larger than that of the outer ridge.

(2) Both ridges have seaward and landward flank slopes in the range of  $0.5^{\circ}$ - $1^{\circ}$ , those of the landward flanks being steeper. Ridge asymmetry is higher for the outer ridge (slope variation of 48%) than for the inner ridge with a slope variation of 24%.

In contrast to this local picture, a set of cross-sectional profiles (Fig. 95) indicates:

(1) Ridge asymmetry varies alongshore and not necessarily in a similar sense on both ridges. The inner ridge sections show lesser variability and tend to be landward asymmetric or symmetrical. In contrast, the outer ridge more commonly indicates an alternation of landward and seaward asymmetry. The predominantly landward asymmetry (i.e., gentler landward slope)

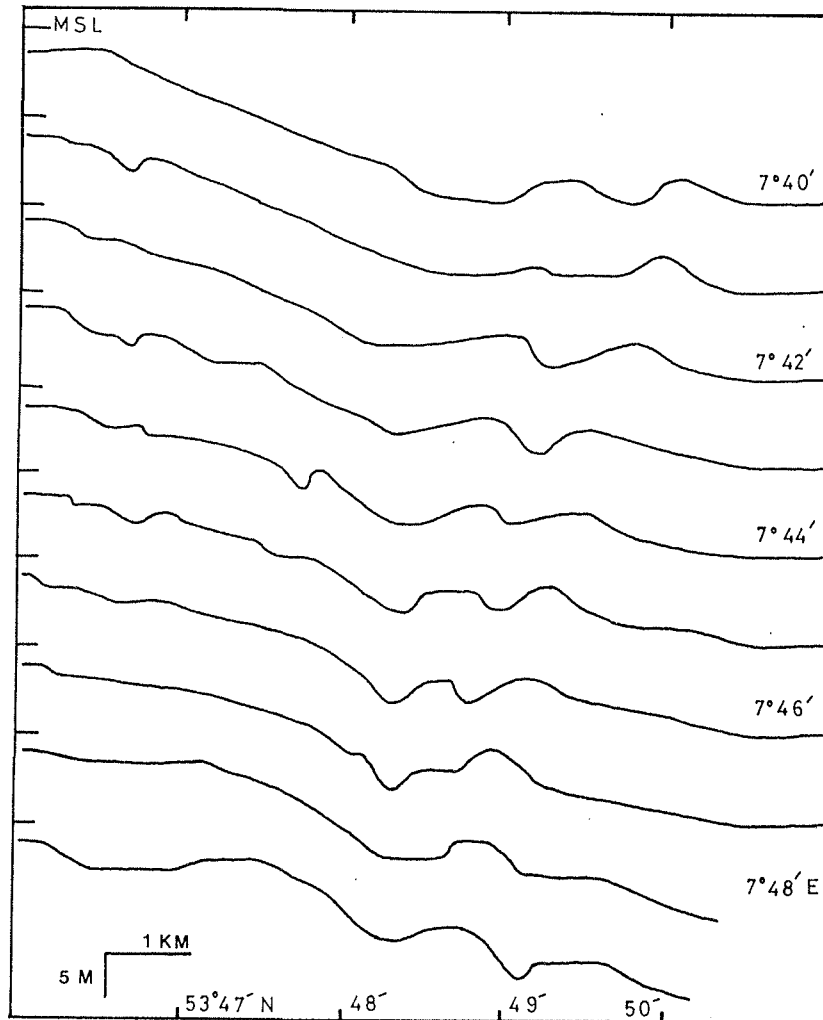


Fig. 95. Cross-sectional profiles of the shoreface bathymetry.

of the inner ridge may be a direct response to various types of seaward return flows associated with storm events, including rip currents. In this respect, the inner ridge cross-shore profile is comparable to that of a transverse bedform.

(2) Crest shape is also variable and may be either rounded or plateau-like. Similarly, troughs, 200-600 m in width, may be either V- or U-shaped.

The morphodynamic behaviour of the ridges has been assessed by (a) comparing temporal variations in trough axes over the period 1950-1987, and (b) longitudinal and cross-shore sediment budget patterns between 1960-1975.

The spatial pattern of trough axes is illustrated in Fig. 96. Quite evident is the fact that the axes form a set of well-defined clusters. This suggests a well-structured nature of the generating and maintaining flow regime. The latter conclusion corroborates the DISEC model, since the DISEF path is better controlled than the highly variable direction of the storm-amplified flood currents.

As on the Atlantic shelf of the United States, coastwise elongation of the shoreface-connected ridge morphology through headward trough erosion is discernible along the Frisian coast (Fig. 97). However, the data on the migration rate presented from Assateague island, U.S. coast, by SWIFT and FIELD (1981), is several order of magnitude lower than the Frisian counterpart. For instance, while the latter reported no change in ridge pattern over a time-period of about 10 years, Spiekeroog ridges showed an average annual landward migration of 80 m/yr over an eight-year time-interval (1965-1973).

Of particular interest in Fig. 97 is the intense erosion of the Wangerooge ridge troughs, which over the time interval of 1990-1992 attains a maximum of 1 km, or an annual average of 500 m/yr. Over the latter interval, a seaward migration tendency was evident. The headward erosion of the Spiekeroog counterpart is relatively smaller, showing a maximum annual average of 80 m/yr.

Finally, on both Frisian Islands the tips of the ridges are also retreating downcoast, but at rates which may be comparable (in the case of Spiekeroog) or much smaller (in case of Wangerooge) to that of trough erosion.

In order to ascertain spatial disparities in shoreface ridge dynamics, a total of ten trough-axis panels indicated in Fig. 96 were evaluated. Longitudinal variations were also examined along the longer troughs based on comparisons of data from the two panels on their distal (western) and proximal (eastern) sectors.

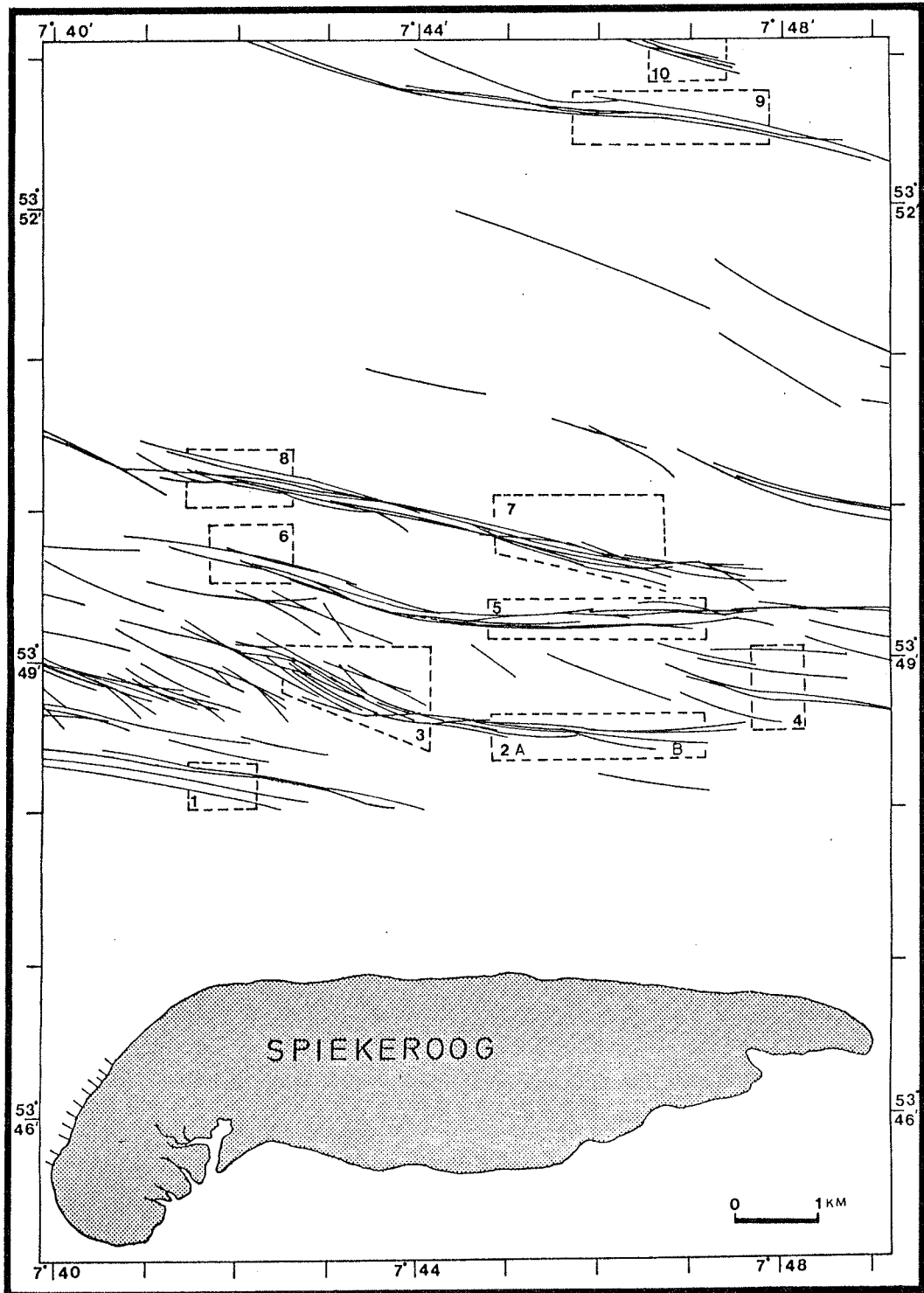


Fig. 96. Spatial pattern of shoreface-connected ridge trough axes.

SHOREFACE RIDGE DYNAMICS

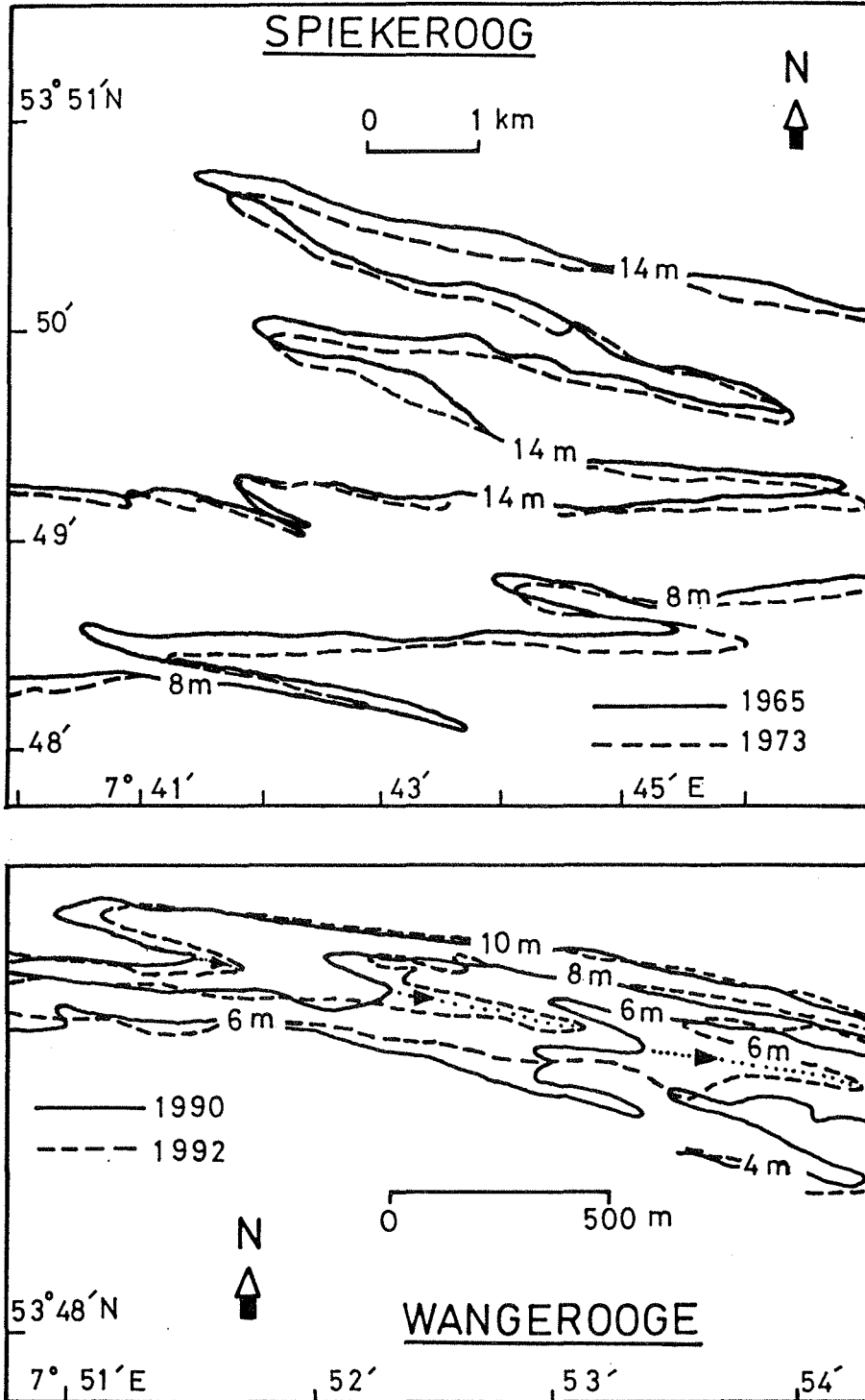


Fig. 97. Headward erosion of Frisian barrier island shoreface-connected ridge troughs.

In the individual panels shown in Fig. 98, each axis was compared with a successive one and both the absolute and the mean rate, as well as the mode of migration were documented. With respect to the latter, the translation of any given axis pair can either be exclusively landward or seaward, or diabathic in character. The above cross-shore dynamic patterns can only be a response to a net flow momentum during storm events associated with coastal storm surges and its ebb counterparts.

The absolute translational values of the trough axes (m) illustrated in Fig. 99 did not show any definite time progressive variation in both cross-shore directions. This is in conformity with the rapidity of reversals in the direction of translation. Quite instructive is the fact that over an interval of just one year, the extent of seaward and shoreward translation may amount to about 100 m and 200 m respectively. On average, shoreward translation seems to be slightly larger in magnitude.

The implications of Figs. 98 and 99 are that some storm flows are more energetic during their waxing (flood) phase, whereas others attain higher energy during the waning or ebb phase. It is not at all clear whether surge elevations can furnish further information on the relative importance of the above. This writer is of the opinion that the storm direction may be more valuable in predicting the aforementioned.

As shown in Fig. 100, the shoreward translation of the morphology, at least in the eastern sector, seemed to be particularly pronounced (maximum 200 m/yr) during the 1967 storm, although storm surge height was less than 3 m. The latter rate compares well with that of the 1982/83 event, which had a higher surge height, but was more variable in direction.

SHOREFACE RIDGE DYNAMICS (1950-87)

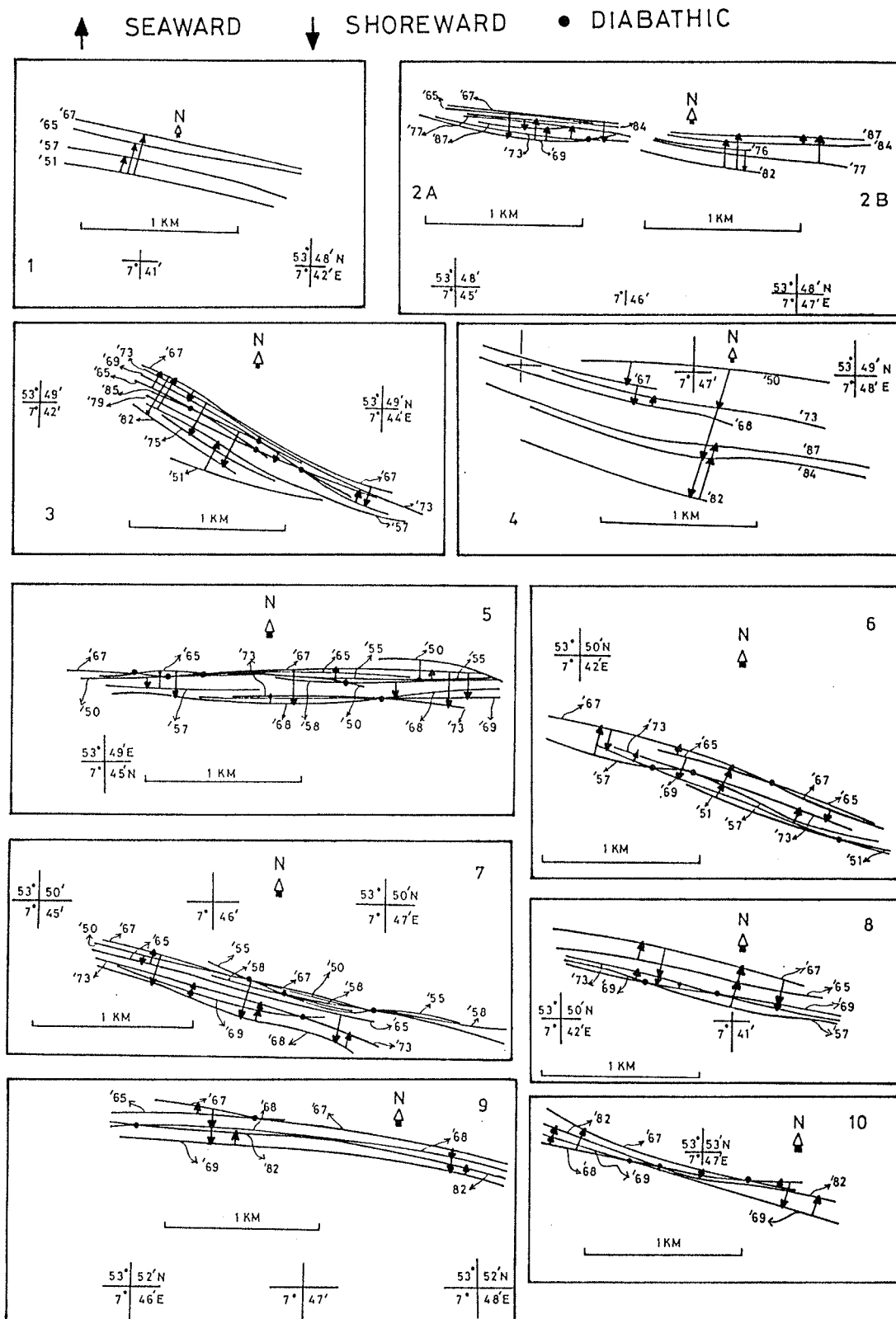


Fig. 98. Temporal variations in shoreface-connected ridge trough axis trends.

### SHOREFACE RIDGE DYNAMICS

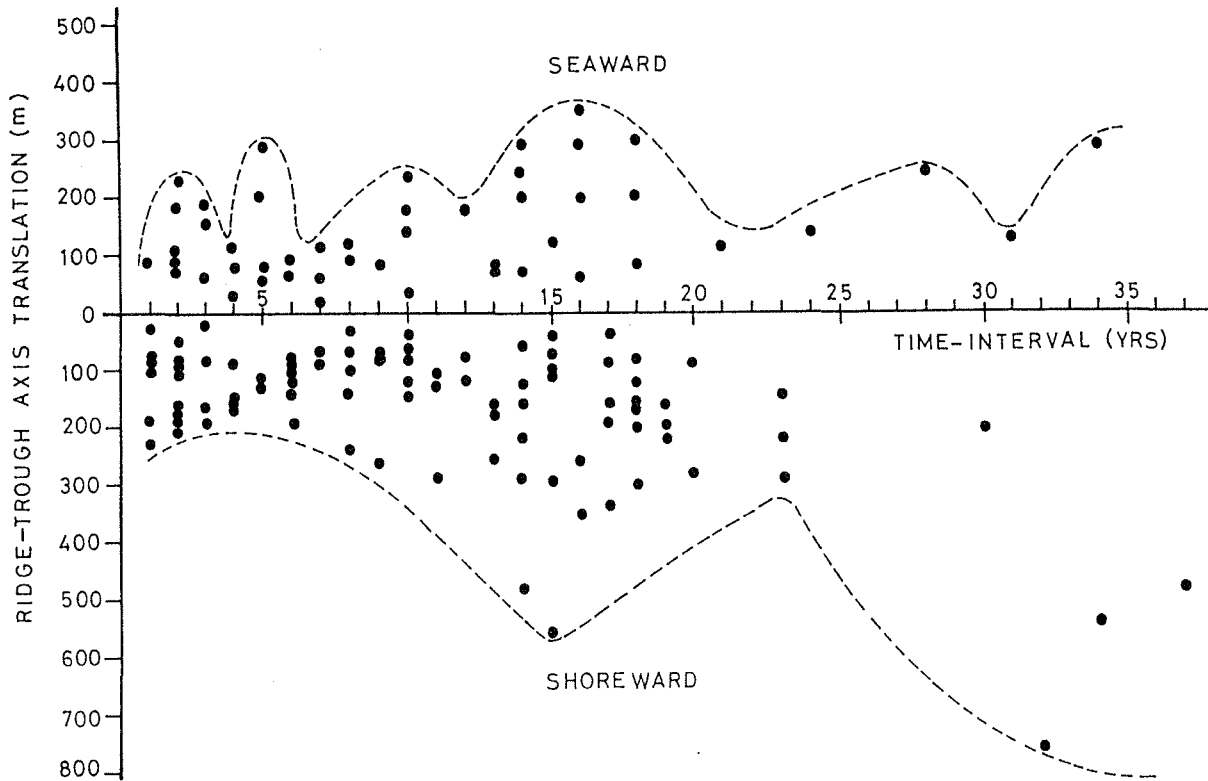


Fig. 99. Temporal variations in absolute magnitudes of shoreface-connected ridge trough axis translation.

Figure 101a shows that there are indeed spatial variations in the trough translation patterns. With the exception of trough axis cluster 1 and 2/3, all others showed a higher frequency of shoreward translation. This result is very illuminating in that the former panels, by virtue of their proximity to the coastline, would be most subjected to the impact of the ebb storm-surge. By contrast, the distal axis clusters are much more influenced by the onshore-directed storm surge, hence their more frequent shoreward translation.

The mean translation rate (m/y) and %-variation from the mean for the various trough axis clusters are given in Fig. 101b. Both patterns are well correlated for the seaward translation, but lack a defined spatial trend. The shoreward translation rate, on the other hand, increases with offshore distance in accordance with the frequency pattern.

SHOREFACE RIDGE DYNAMICS : STORM EFFECT

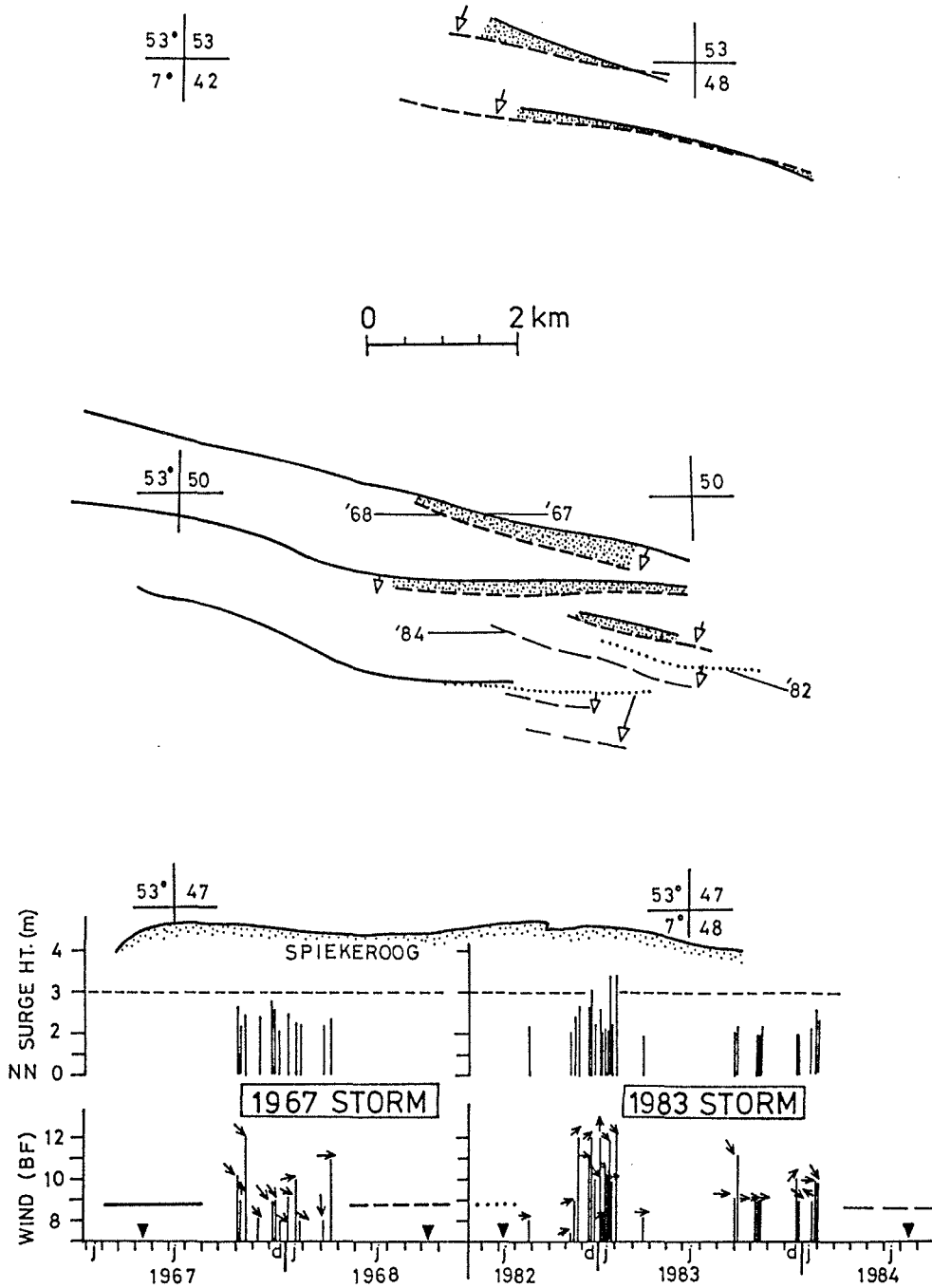


Fig. 100. Shoreface-connected ridge trough axis translation at the eastern sector in response to 1967 and 1982/83 storm events

## SHOREFACE RIDGE DYNAMICS

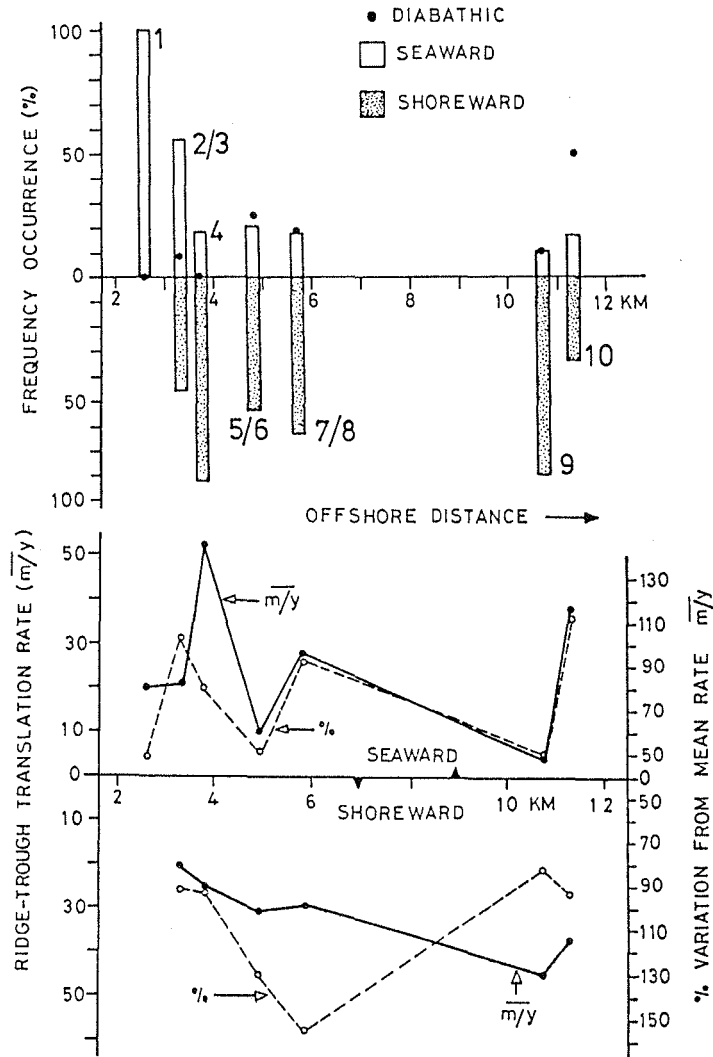


Fig. 101. (a) Frequency % of dynamic pattern of shoreface-connected ridge. (b) Shoreface-connected ridge trough axis mean translation rate and % variation from the mean.

Finally, the hypothesis that the ridge morphology may have evolved from a re-orientation of shore-parallel bars formed by a variety of flow mechanisms such as a non-breaking progressive infragravity waves (BOCZAR-KARAKIEWICZ et al., 1990) or their breaking storm counterpart was tested.

In either of the above cases, axis clusters of the eastern sector should exhibit larger shoreward translation rates, while the western sectors should depict larger seaward translation rates.

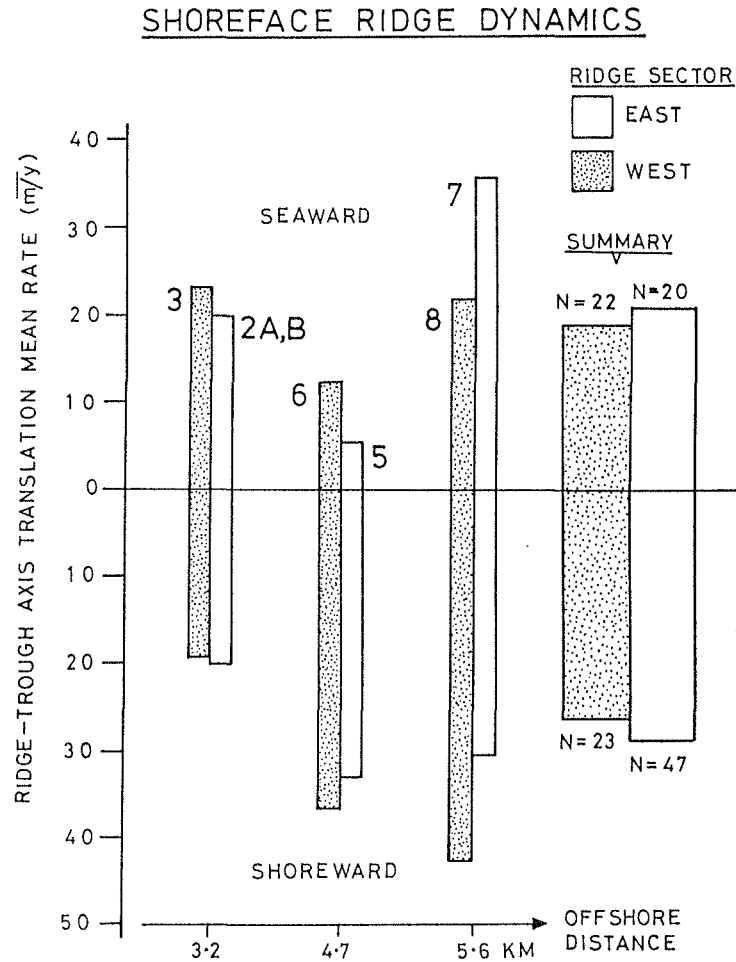


Fig. 102. Relative rates of shoreface-connected ridge trough axis translation at their eastern and western sectors.

Figure 102 demonstrates that the above hypothesis is very unlikely. Only the dynamics of trough axis cluster 3/2A,B (see Fig. 96) conform to the above postulate. However, the relative mean translation rates between the eastern and western sectors

in the latter case are too marginal. At least a 1.5 km translation (seaward or shoreward) would be required to realign a shore-parallel bar to the ridge trend. Data given in Fig. 99 indicate that such a scale of translation is unrealistic. Thus, neither of the wave hypotheses has merit as ridge generating mechanisms.

Sediment budget calculations for a cross-shore section of the innermost ridge morphology (Fig. 103a) indicate erosion to be most intensified within the trough (1.8 m<sup>3</sup>/m<sup>2</sup>), with a diminishing volume across the crest to the seaward flank. By comparison, trough erosion is twice that of the seaward flank.

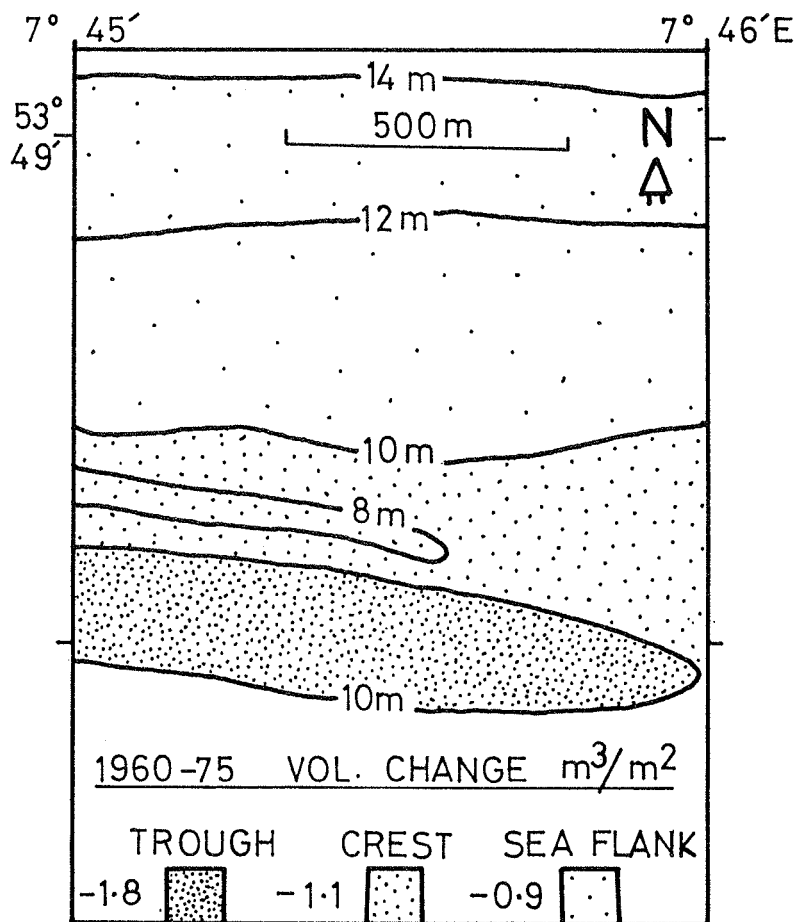


Fig. 103a. Cross-shore variation in sediment budget of the inner shoreface ridge morphology.

It is not clear at this stage whether the budget changes in the ridge morphology zones are mutually exclusive or inter-dependent. The latter would imply a steady transfer of sediments from the trough across the crest to the seaward flank.

Longitudinal sediment budget changes within the trough (Fig. 103 b) shows distally diminishing volumetric erosion. The erosion intensity at the head of the trough is more than 350% of the value at the mouth of the trough.

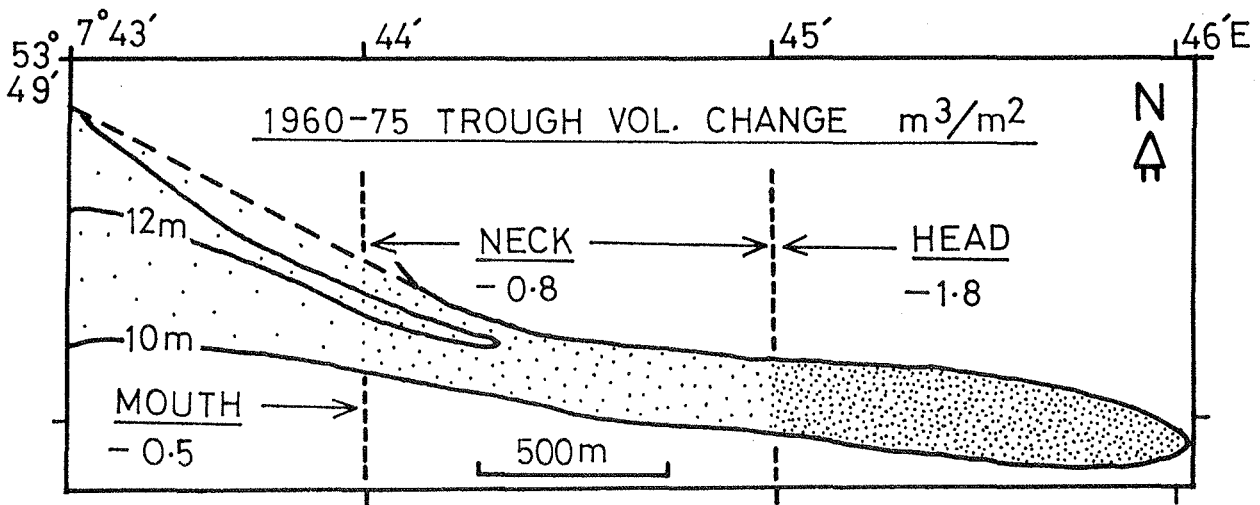


Fig. 103b. Longitudinal variation in sediment budget of the inner trough of the shoreface ridge morphology.

Farther from the mouth, as noted in Section 5.5.2, a positive budget is revealed. This budget trend indicates the principal flow on the central shoreface to be northwesterly-directed, which is in consonance with the prediction of the DISEC model. It is pertinent to state here that, although storm flood currents may intensify headward (downcoast) erosion of the trough as documented in Fig. 97, sediment transport itself is effected by northwesterly-directed flows.

It is noteworthy that an often cited attribute of the ridges, that their shore-acute angles open into the principal sediment transport direction (DUANE et al., 1972; SWIFT et al., 1978; SWIFT and FIELD, 1981), is not only contradicted by the diversion model but it is found to be non-critical to ridge genesis. The latter observation has also been made by other authors.

#### 6.3.4 Facies

It is obvious from the size statistics, class fractions and curve shapes of the surficial sediments discussed in Chapter 5 that the central shoreface sands are distinct from those of the contiguous shoreface subenvironments. In the following sections the distinctiveness of these sands and their sedimentary structures is further explored. This is based on a systematic surface and subsurface sampling of their morphozones: ridge crest, trough, seaward and landward flanks. The subsurface data in particular should enable an estimate of the ridge volume and, consequently, an evaluation of the inlet source of sand for their formation as predicted by the DISEC model.

##### 6.3.4.1 Sediment Size Statistics : Cross-shore, Longitudinal and Vertical Patterns

###### (A) Cross-shore Textural Pattern

Results of size statistics obtained from repetitive cross-ridge sediment sampling carried out along two transects are summarized in Figs. 104-107 (Long.  $7^{\circ} 44.50'$ ) and Appendix C-2 to C-5 (Long.  $7^{\circ} 45.50'$ ). On both transects the ridge morphozone size statistics clearly differ from those of the bounding subenvironments as pointed out earlier.

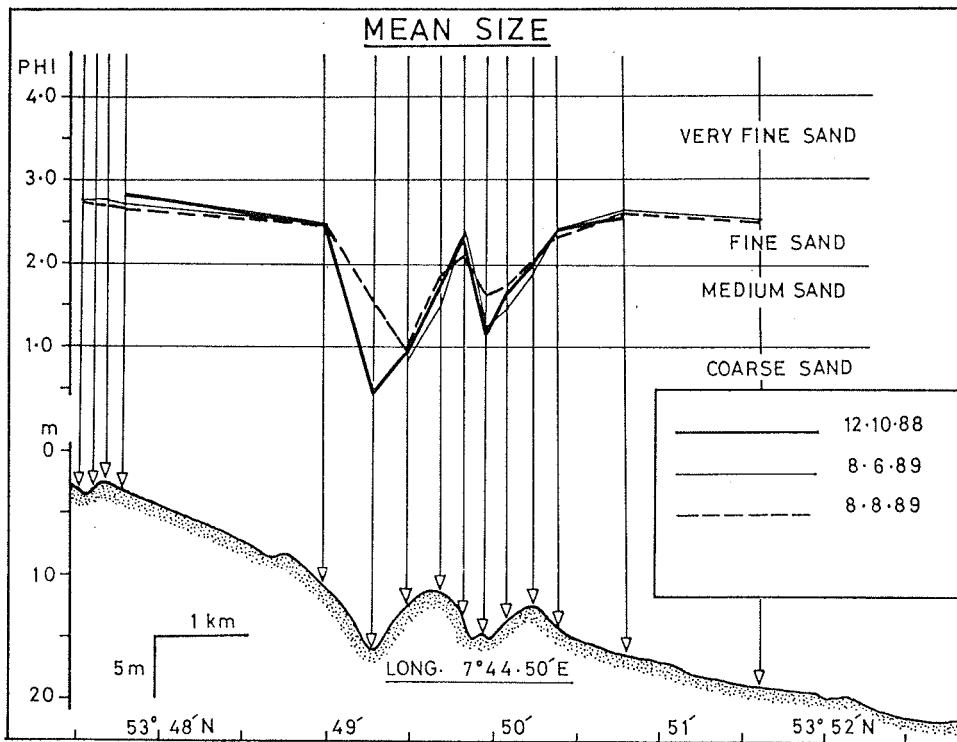


Fig. 104. Temporal cross-shore variation in mean surficial grain size of the shoreface ridge morphology.

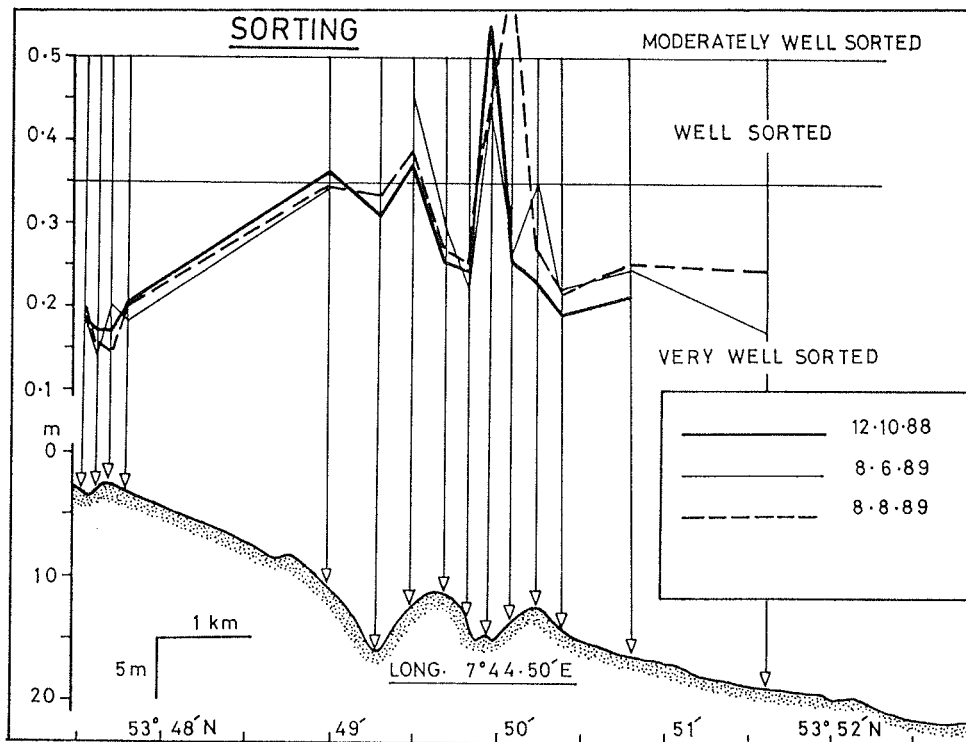


Fig. 105. Temporal cross-shore variation in sorting of shoreface ridge surficial sediments.

Mean grain size (Fig. 104) and sorting (Fig. 105) showed the most consistent temporal pattern. Consistency in the mean grain size pattern as shown above has also been reported by SWIFT et al. (1978) further to the west of the study area. This writer shares their opinion that the pattern is a manifestation of equilibrium response to the flow regime.

Particularly striking is the fact that both the inner and outer ridge morphology reveals finer mean sizes on the seaward flanks than on the landward counterparts. However, with respect to the ridge morphozones, the sands of the seaward flank are the finest while the coarsest sands occur in the troughs (see also Fig. 115).

Occasionally, landward flank sands may be slightly coarser or are of comparable mean size as those in the troughs. Finally, the mean grain size for any ridge morphozone, as well as the gradient between any adjacent morphozone, was consistently larger for the inner than the outer ridge.

Without recourse to post-formational modification, the cross-ridge textural segregation can be viewed as an inherent attribute of the diverged storm flow deposition. In this case, such a flow can be conceived as being comprised of streamlines whose laterally (seaward) diminishing velocities are directly proportional to their sediment transport competence. Gravitational (dynamic) settling of sands from such a flow should thus yield deposits which are laterally graded and fining seaward. The implication of the latter would be that the outer and inner ridges are not contemporaneous, i.e., resulted from different flow events. ÖZSOY's ideal ebb-jet model would suggest the contrary. That this is not the case is also evident from the difference in the average shore-acute angle of both ridges ( $17^{\circ}$  and  $10^{\circ}$  respectively), among other textural and geometric attributes.

Sorting of sediments on both ridges was best on the seaward flanks and worst in the outer trough (Fig. 105). The marked

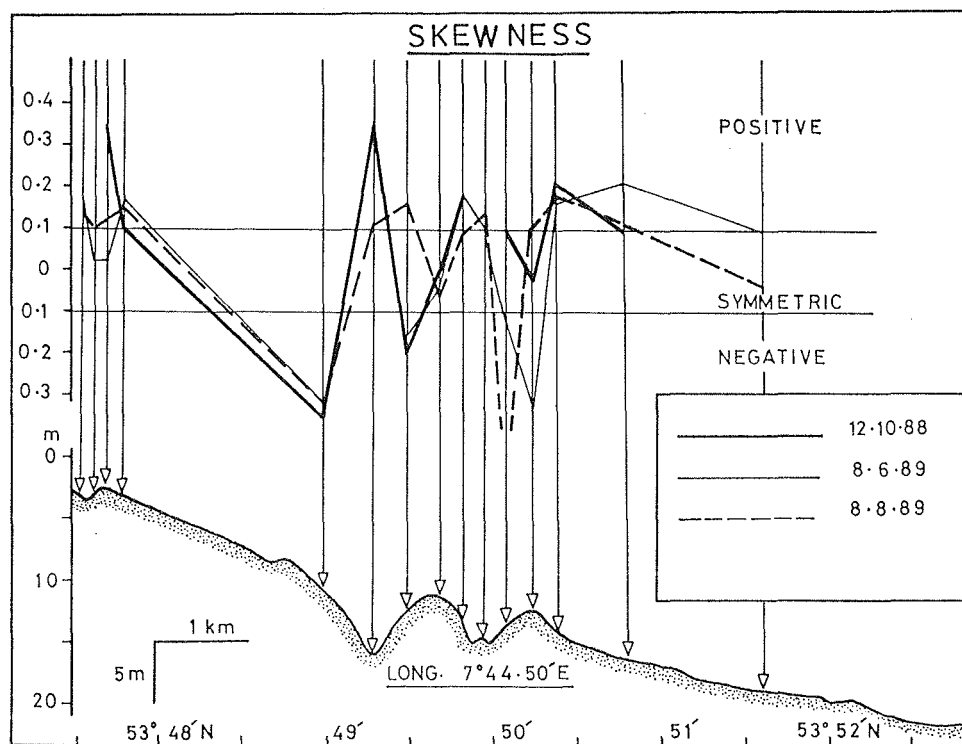


Fig. 106. Temporal cross-shore variation in skewness of grain size distribution of shoreface ridge surficial sediments.

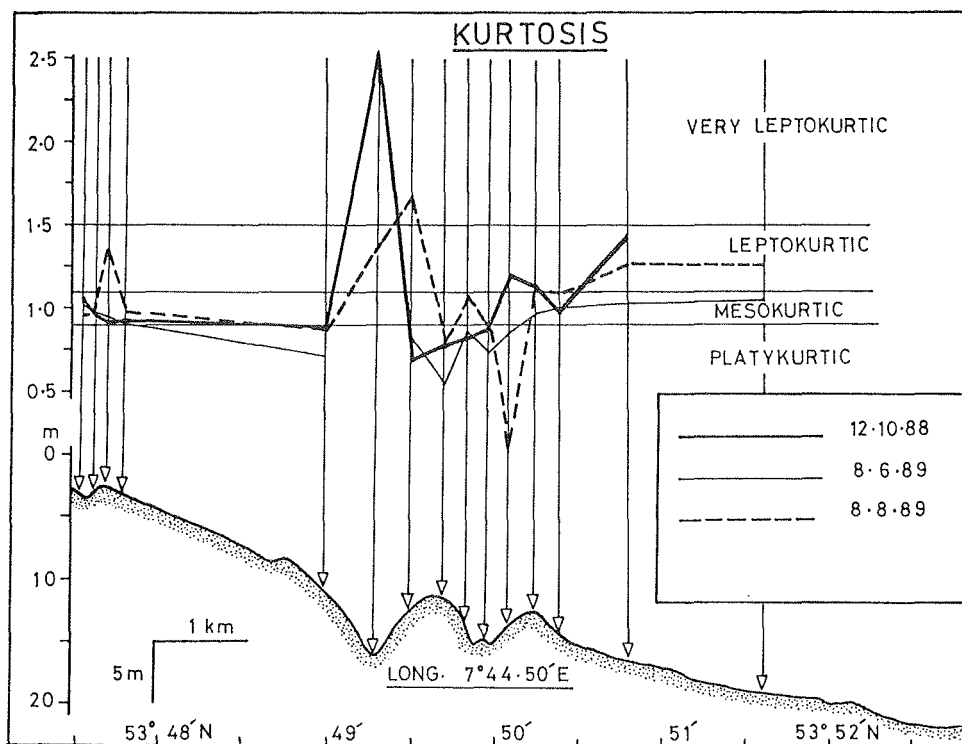


Fig. 107. Temporal cross-shore variation in kurtosis of shoreface ridge surficial sediments.

difference in sorting of the outer and the inner trough is particularly surprising given the fact that peak bottom flow velocities in the troughs tend to increase distally (Fig. 94). It is surmised that because the outer trough sediments are coarser than those of the adjacent inner-ridge seaward flank and crest, their poor sorting must relate to storm deposition.

Skewness (Fig. 106) and kurtosis (Fig. 107), as previously mentioned, showed high temporal variability. The variation of the latter is largely inverse to the former. On the other hand, on both ridges, the landward flank sands are more negatively skewed than those of the adjacent troughs. This would imply that the troughs are sinks for fines (immiscible mixing of these), whereas winnowing (truncation) of fines from the landward flanks may account for their negative skewness. Moreover, compared with the landward flank, these seaward flank sands are more prone to positive skewness. This is in accord with SMITH's (1970) analysis of shear stress distribution on bedforms subjected to a transverse flow. As further asserted by SWIFT et al. (1978), and exemplified by the indicated ridge profile, the seaward flanks would be steeper because of its accretionary tendency, this being due to a lower shear stress relative to the landward counterpart.

The extent to which these variations depend on the changing flow conditions will be evaluated later from their accompanying sedimentary structures. It is surmised that the high positive skewness of inner trough sands on 12.10.88 may have been due to an intense offshore flow on the upper shoreface, resulting in a large influx of seaward transported fines.

An alternative and more likely origin of the positive skewness of the inner trough sands, in the light of Fig. 115 and their coarse mean size, is a proportional increase in the existing coarser size classes brought about by a differential or selective deposition during a high-energy transport event. Their relatively good sorting makes this interpretation all the more likely.

Bivariate plots of grain size statistical pairs of the surficial sands of the ridge morphozones given in Figs. 108-113 further provide insights as to their distinctiveness and genesis. For this purpose, only unimodal samples were evaluated. All of the plots, except kurtosis vs. skewness (Fig. 113), exhibit three distinct textural domains: seaward flank, crest and a mixed trough-landward flank.

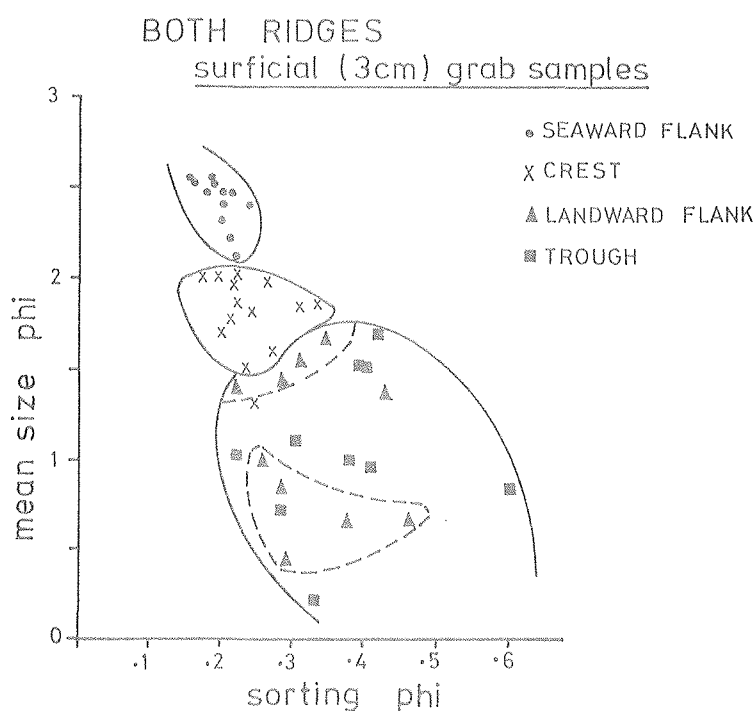


Fig. 108. Bivariate plot of mean grain size versus sorting of shoreface ridge surficial sediments.

In general, seaward flank sediments are the finest (fine sand), best sorted, predominantly positively skewed and meso-leptokurtic. The mean grain size is their most distinguishing attribute. The contiguous crest sands differ from the above in being slightly coarser, less well sorted, more negative skewed and meso-platykurtic. Figure 110 shows that platykurtic and leptokurtic distributions were both lacking in sands finer than 1.75 phi and coarser than 1 phi. Kurtosis was more variable for sands with 1-1.75 phi mean size.

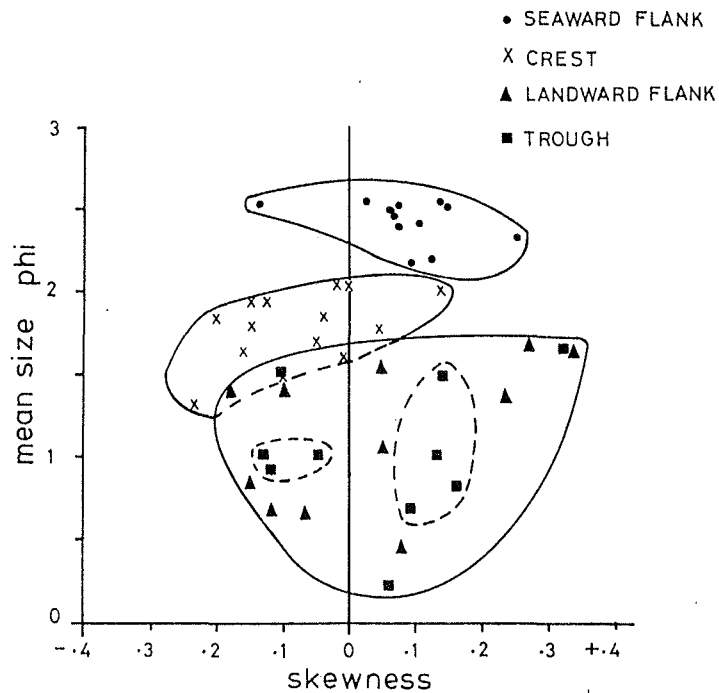


Fig. 109. Bivariate plot of mean grain size versus skewness of shoreface ridge surficial sediments.

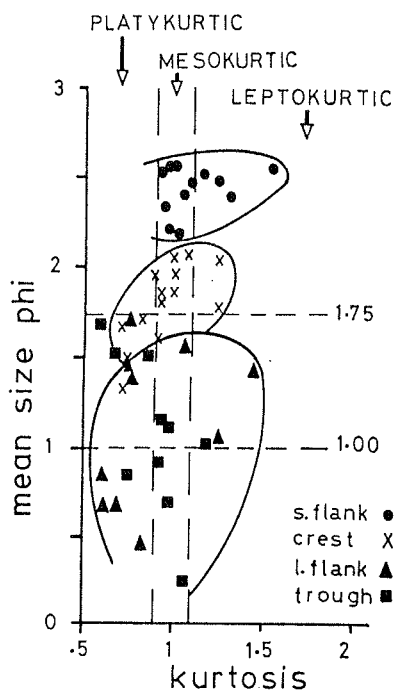


Fig. 110. Bivariate plot of mean grain size versus kurtosis of shoreface ridge surficial sediments.

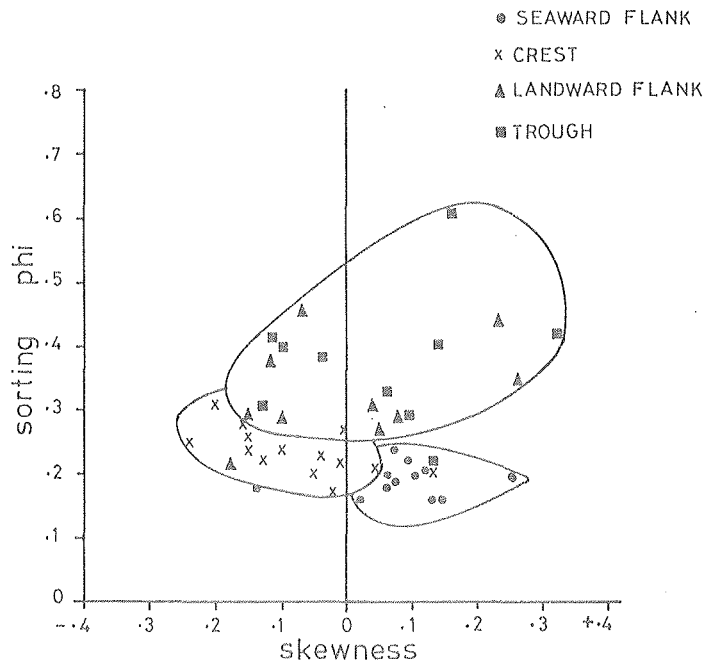


Fig. 111. Bivariate plot of sorting versus skewness of shoreface ridge surficial sediments.

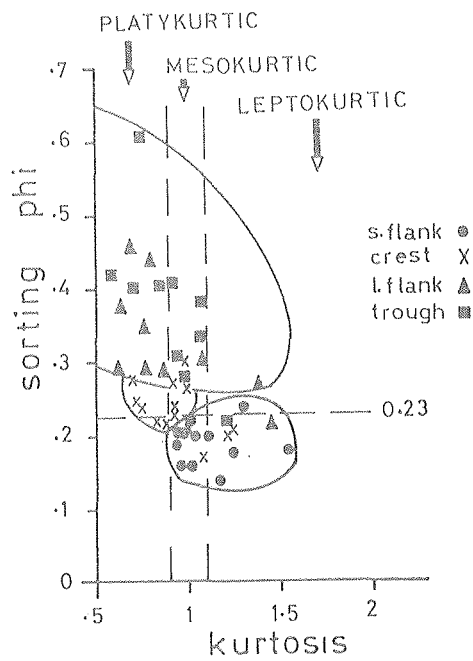


Fig. 112. Bivariate plot of sorting versus kurtosis of shoreface ridge surficial sediments.

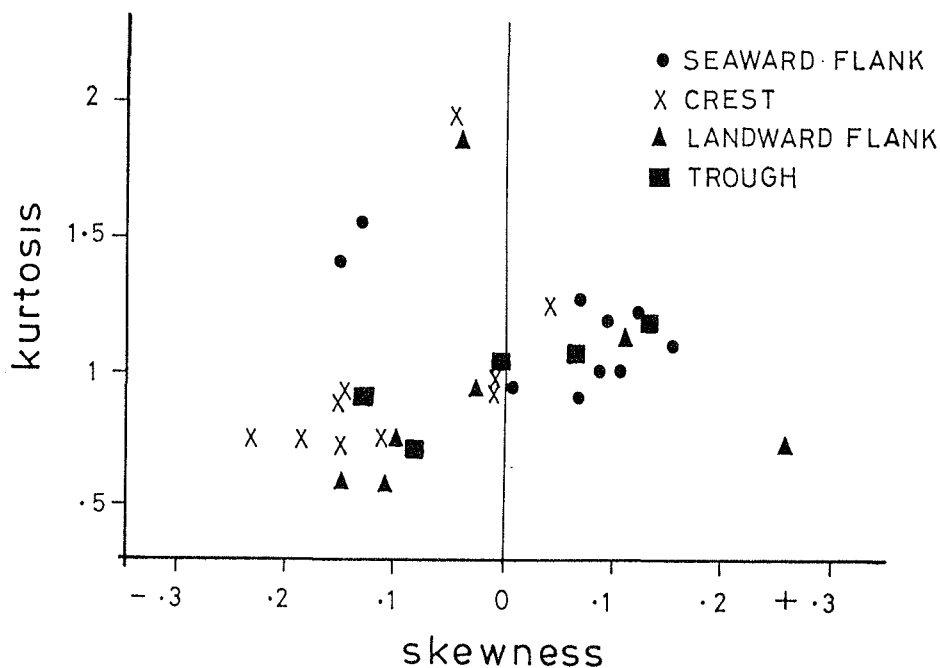


Fig. 113. Bivariate plot of kurtosis versus skewness of shoreface ridge surficial sediments.

Finally, as a single population, the landward flank and trough sands differ from the crest and seaward flanks in being coarser ( $< 1.5 \phi$ ) and more poorly sorted. Skewness showed subequal positive and negative tendencies. As in the case of the crest sands a meso-platykurtic distribution is typical. As shown in Fig. 112, the latter range of kurtosis is typically associated with sorting values  $> 0.23$ , whereas better sorted sands tend to be meso-leptokurtic.

The textural similarity between trough and landward flank sands noted above seems to relate more to their depositional processes than an aftermath of deposition. It is very doubtful whether sand bodies and bedforms developed in-situ from an initially smooth and texturally homogeneous substrate would exhibit such a large trough-crest or crest-flank mean size difference observed on these ridges. Neither mean grain sizes of troughs and crests of nearshore wave-formed bars (e.g., MOTHERSILL, 1969) nor of transverse bedforms in shallow sea environments are known to exhibit such a variation.

This being the case, the concept of helical flow forming a morphology with a ridge crest spacing of the order of a kilometer can be questioned on the following grounds: (1) effectiveness of entraining medium sands from the bottom in water depths  $>10$  m, and (2) efficiency of laterally transporting these over considerable distances, both shoreward and seaward, onto a crest unhindered by intense onshore-offshore directed momentum flux associated with storm-generated cross-shore flows. In any case, the non-parallel orientation of the ridges is inconsistent with such a development.

A final attribute of the surficial sands of the ridge morphozones considered is their CM pattern. As shown in Fig. 114a, the data mostly plot along a narrow band close and parallel to the  $C = M$  line, suggesting high sortedness. Again, as in the case of the bivariate plots just discussed, the crest and seaward flank sediments are, in contrast to the landward flank and trough counterparts, defined by distinct transport modes.

The pattern in general suggests a progressive cross-shore size-sorting in the manner depicted in Fig. 115 above. The histogram given in Fig. 114b is a summary of the frequency of specific transport modes depicted in sands of a given morphozone. Thus the seaward flank, crest, and trough sands are modally deposited as graded suspension, upper bottom suspension and lower bottom suspension respectively. The landward flank sands exhibit both lower bottom suspension and traction depositional modes. On the other hand, Fig. 114c shows the relative frequencies of the different ridge morphozone sands comprising a given depositional mode. The pattern is identical to the former, excepting the fact that sands of the landward flank are the principal constituents of the traction depositional mode. In general, the consistently high sortedness of the morphozone sands need not only reflect post-depositional processes, but, as earlier mentioned, may be the result of differential settling rates dictated by a cross-shore variation

in the velocity of the transporting storm flow (DISEC). Even fair-weather peak ebb-flow ( $U_{100}$ ) measurements over the ridge morphology earlier presented support the latter.

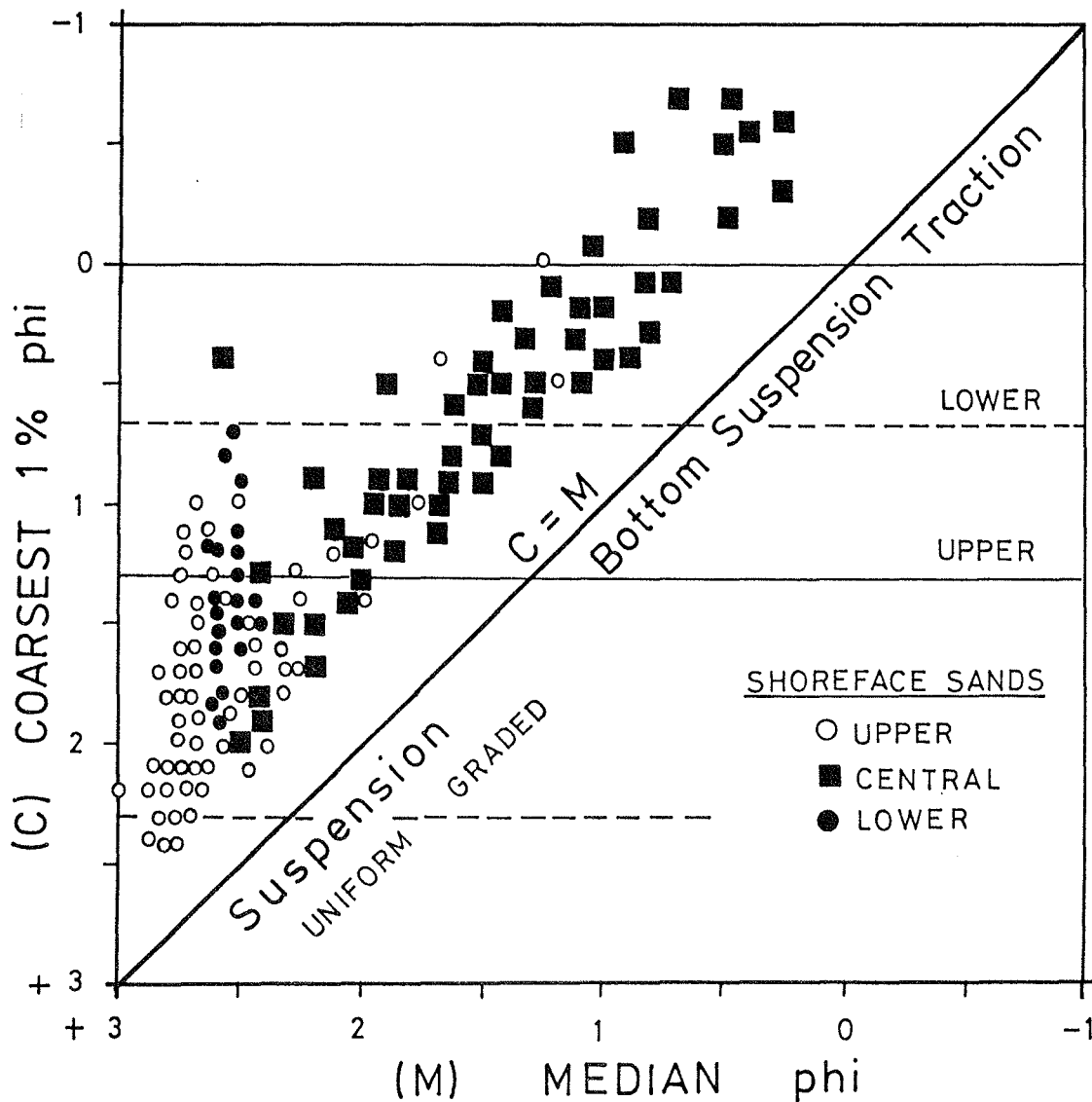


Fig. 114. (a) C-M pattern of shoreface ridge surficial sediments, (b) Frequency-% of transportational modes reflected in sediments of the respective shoreface ridge morphozones, (c) Frequency-% of the different ridge morphozone sediments associated with a given transportational mode.

## SHOREFACE-CONNECTED RIDGE SEDIMENTS

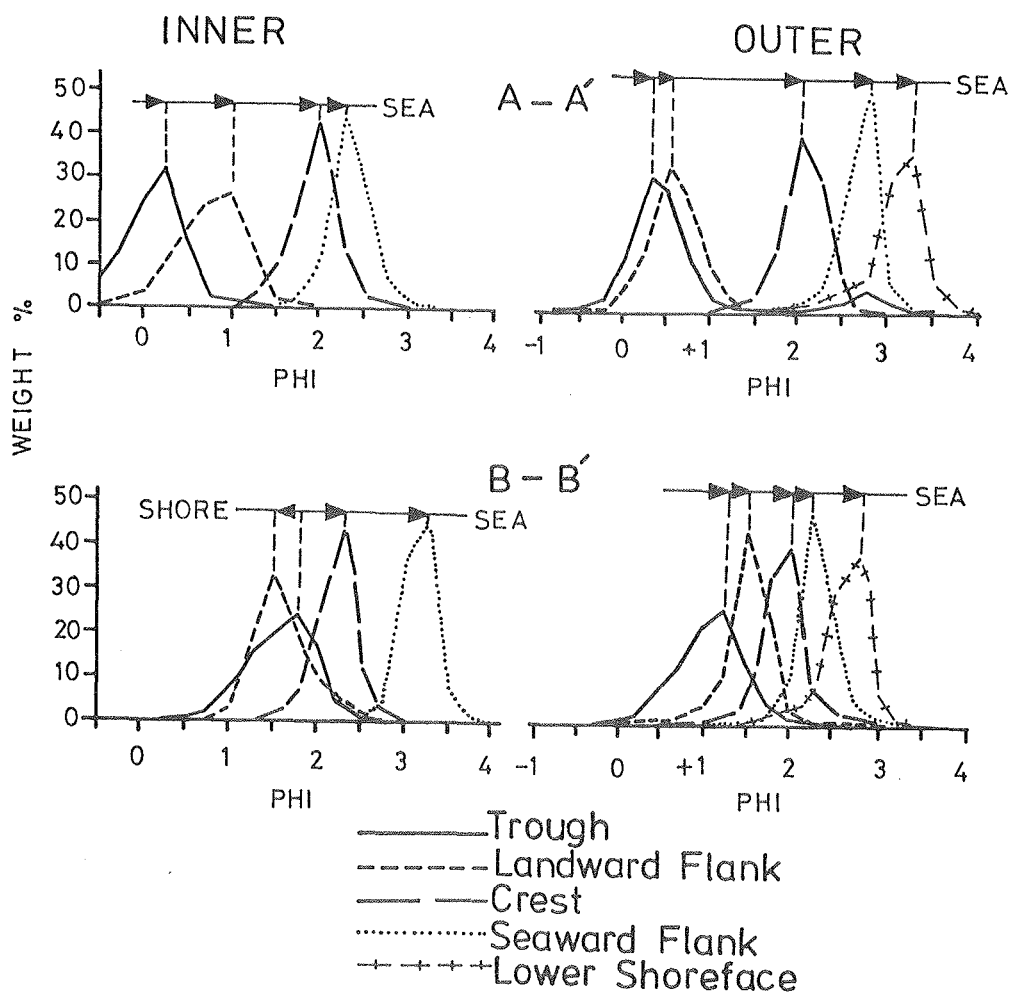


Fig. 115. Progressive cross-shore size-sorting of shoreface ridge surficial sediments.

### (B) Longitudinal Textural Pattern

One of the basic implications of the DISEC model of shoreface-connected ridge evolution earlier discussed is a well-defined, longitudinal pattern in grain size statistical parameters. Interestingly, because of the peculiar nature of the flow regime over the ridge morphology, the downcurrent rate and pattern of textural change are higher and opposite to those of the lower and upper shoreface subenvironments.

Specifically, since sediment deposition is effected by DISEF, which is northwesterly directed, mean grain sizes of the ridge morphozones should fine or decrease in settling velocities toward the distal (northwesterly) end, as against eastwards on the contiguous upper and lower subenvironments, in response to the principal eastward directed flow pattern in the study region.

Indeed, results already presented for the upper shoreface zones is in accord with this view. Because of the opposing and strong fair-weather tidal flow influence on the sediment dynamics in deeper waters, the ridge morphozones were sectorized longitudinally into a distal (northwesterly), a middle and a proximal (southeasterly) sector, for each of which average settling velocities were computed.

TABLE 5. Longitudinal variation in average settling velocities (cm/s) of shoreface sands.

		Distal	Middle	Proximal
<b>LOWER</b>				
<b>SHOREFACE</b>		2.2	2.1	2.1
	OUTER CREST	3.9	3.8	4.3
<b>CENTRAL</b>	OUTER TROUGH	8.3	6.8	12.8
<b>SHOREFACE</b>	INNER CREST	3.7	4.6	6.6
	INNER TROUGH	6.8	3.3	12.7
<b>UPPER</b>				
<b>SHOREFACE</b>		2.8	1.8	2.3

As shown in Table 5 above, settling velocity values are consistently larger at the proximal end of the morphology relative to the distal sector as predicted by the model. This gradient is particularly remarkable within the troughs as compared to the crests, which is also a reflection of their

variable CM pattern. Also noteworthy is the apparent lack of a gradient on the lower shoreface, whereas the upper shoreface shows a discernible easterly fining pattern.

Figure 116 shows a similar relationship (see also Appendix C-6), but in particular demonstrates that in the middle section of the inner trough, much finer modes occur than in the distal sector. Interestingly, this middle sector spatially corresponds to the well-developed rip-channel position on the medial upper shoreface zone and hence may be a sink of sediments transported by these currents. Furthermore, sorting, while remaining almost uniform along the crest, perceptibly deteriorates distally in the trough (see also Appendix C-6).

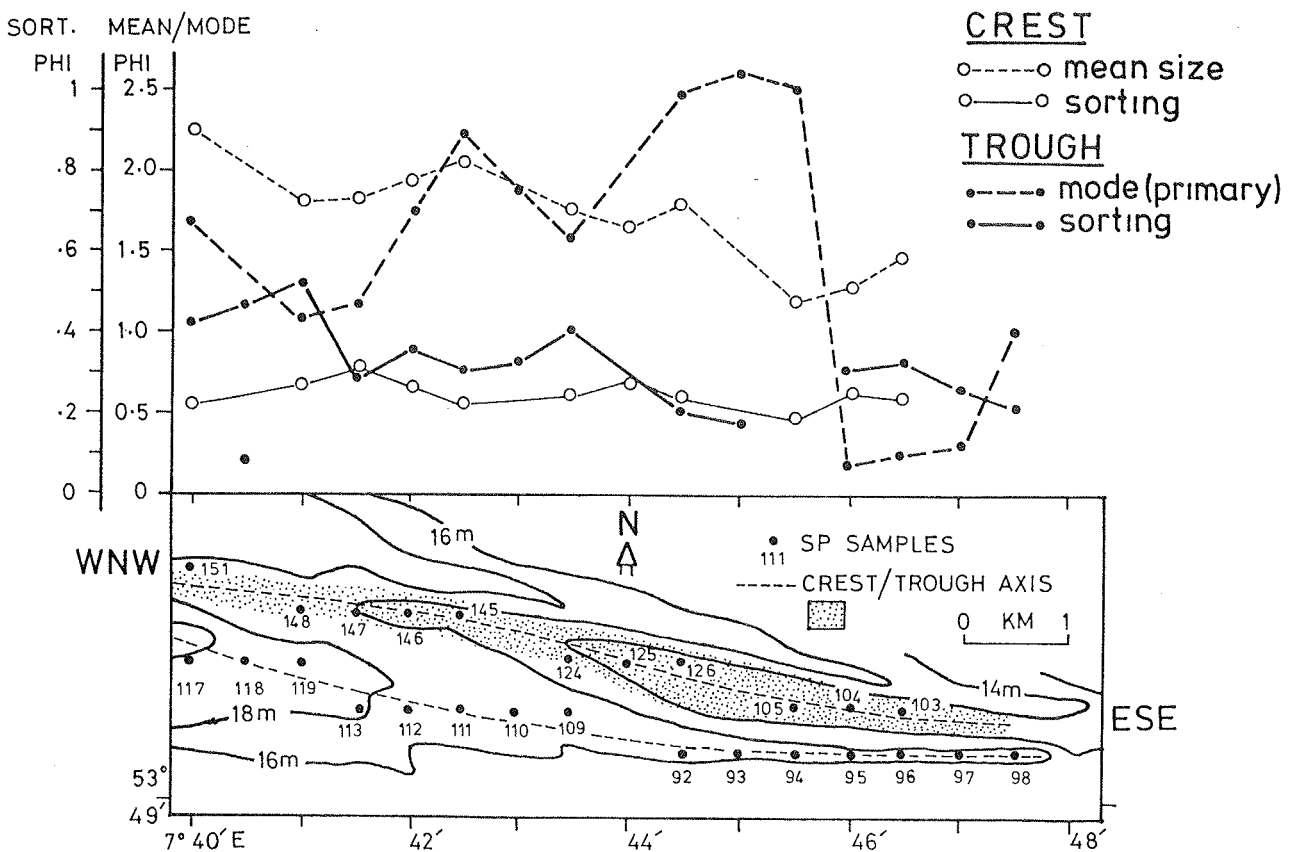


Fig. 116. Longitudinal grain size statistics variation of surficial shoreface ridge crest and trough sediments.

Downcurrent deteriorating sorting, as depicted above, is a logical consequence of a highly energetic flow. Unlike equilibrium flows, under intense flow conditions a much larger range of sediment sizes than usual are entrainable, the successive downdrift deposition of which introduces a correspondingly increasing textural disequilibrium with their native counterpart. By similar logic, sorting should be better at the proximal sector because of a combined effect of differential deposition of coarser grains and winnowing of finer ones brought about by turbulence during the inlet-jet diversion process.

The kurtosis pattern of the trough sediments (Appendix C-6), with elevated values proximally and a steep longitudinal gradient, is consistent with the model prediction. The skewness trend shown by the latter is very illuminating with respect to the above sediment dynamic pattern. Positive-prone skewness sign is evident both at the proximal and distal sectors of the ridge morphology, with a minimum value (slightly negative skewness sign) at the middle sector.

The positive skewness at the proximal sector cannot be due to a "tail" of fines because of their susceptibility to being winnowed by the high flow turbulence. Neither would winnowing of finer size classes, especially if probabilistic, lead to a negative skewness. Because of the high sortedness and coarse mean grain size at this sector, the positive skewness must invariably be related to an increasing proportion of the coarser size classes comprising the native sediment size distribution.

With transport distance from the inlet, the storm-flow-entrained grain sizes being deposited may still be coarser than the native counterpart, but because of their low proportion (e.g., due to hindered settling), skewness sign becomes negative. Finally, at the distal sector of the ridge the deposits settling from the flow must be much finer than the native counterpart, hence their positive skewness, fine mean grain size and poor sorting.

## (C) Vertical Textural Pattern

The vertical variations in grain size statistical parameters and fractions from the different shoreface ridge morphozones is illustrated in Figs. 117-120 and 122-124. The mean grain size (Fig. 117) in the study area shows a well-defined correlation across the ridges. In general, core lithology (mean size  $< 2$  phi) can, with depth, change abruptly (Core no. 6 and 9) or gradually (7 and 8), fluctuate (10 and 11) or be highly uniform (36 and 5).

In contrast to the inner ridge morphozones, the outer zones show a vertically fluctuating textural pattern consistent with storm-induced sedimentation, these being at the distal end

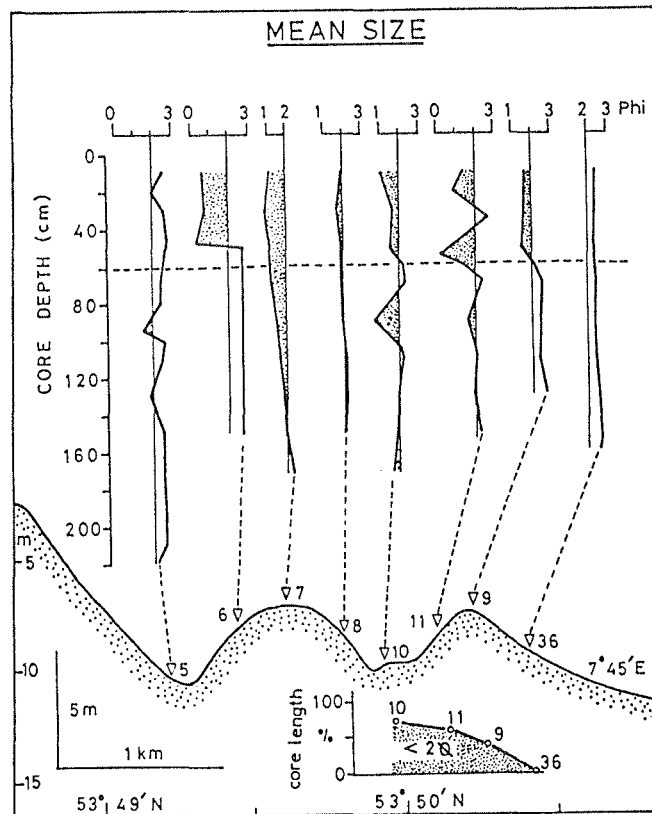


Fig. 117. Vertical variation in mean grain-size of the shoreface ridge sediments.

of the diverged inlet flow. The inset illustrates that the %-proportion of medium and coarser sands in the cores from the outer ridge predictably decreases distally.

With the exception of the inner ridge crest, sand of  $< 2$  phi mean size is impoverished or entirely lacking in core depths below 60 cm. This result, particularly as exemplified by Core no. 6 and 9, suggests that the ridge morphology is merely blanketed by coarser grains. The surficial coarser grain cover may be viewed as an indication of vertical growth of the ridges. It is to be noted that coarse grains do occur within the uppermost 10 cm of the inner trough, as exemplified in their cross-shore profiles, but are not apparent in Core no. 5 due to non-sampling.

The vertical variation in sorting shown in Fig. 118 shows that a cross-shore seaward improving pattern within each ridge morphology is discernible in both their coarse superficial and finer subsurface sediments. This result would imply that the processes moulding and maintaining the ridge morphology have been consistent over time.

Vertical discontinuity in sortedness is subtle and is most apparent on the landward flanks and in troughs. This break also occurs at about 60 cm of core depth and, with the exception of the inner trough, is indicated by an improvement in sorting. As noted earlier, the inner trough is more susceptible to influx of fines from the upper shoreface and this would explain its highly variable sorting. Three major influx events are recorded in this core at the following depths:  $< 30$ , 50-150 and  $>210$  cm.

The vertical skewness pattern shown in Fig. 119 is less predictable; although discontinuity also occurs at depth, the skewness sign of the adjacent morphozones is usually inconsistent. It is surmised that the disparity in the skewness sign of the surficial (upper 60 cm) sands between the inner and outer ridge crest/seaward flank is related to the variable size

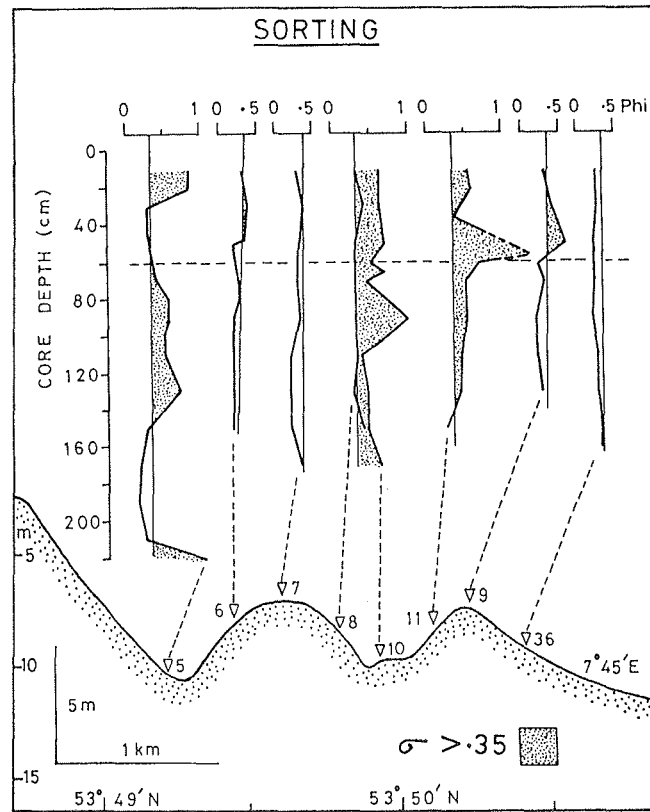


Fig. 118. Vertical variation in sorting of the shoreface ridge sediments.

range of sediments in suspension during the storm events. The negative skewness sign of the inner ridge crest and seaward flanks reflect deposits in which the finer half of the size distribution in transport depict a comparable increase relative to their coarser half. The converse is certainly the case on the landward flank, more so given the fact that deposition seems to take place by traction or lower bottom suspension (cf. Fig. 114).

At the distal outer ridge, surficial skewness reflects a variation of the landward flank with a much higher proportion of the coarser half (hence positive skewness prone) through

either an increased proportion of the finer half or immiscible admixture of minor quantities of coarser sizes on the crest (hence negative skewness) to a seaward flank characterized by immiscible admixture of fines (hence positive skewness).

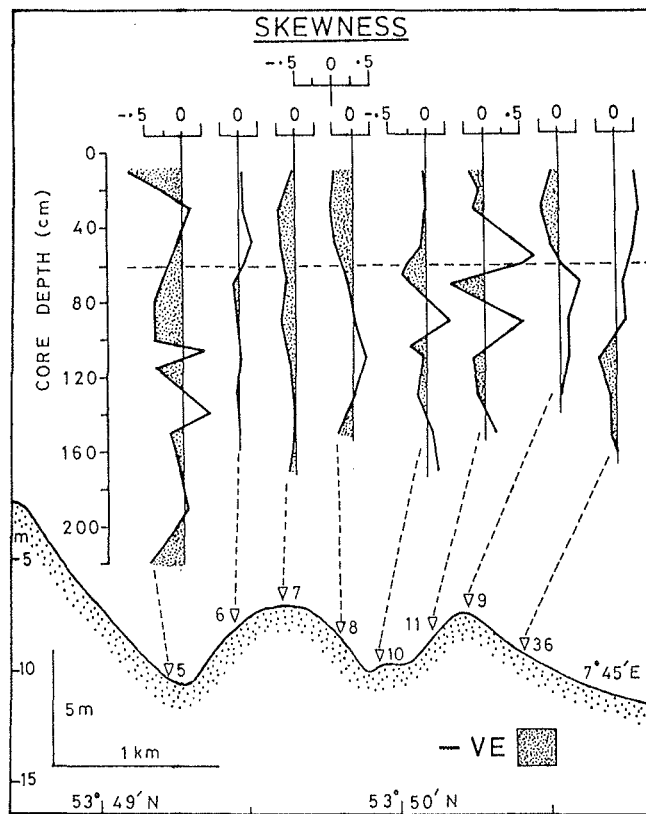


Fig. 119. Vertical variation in skewness of the shoreface ridge sediments.

The kurtosis pattern (Fig. 120) also depicts a vertical discontinuity of variable character on the ridge morphozones at a core depth of about 60 cm. With the exception of the troughs, sands which are platykurtic are rare or rapidly diminish beneath 60 cm core depth, suggesting downcore improving sortedness.

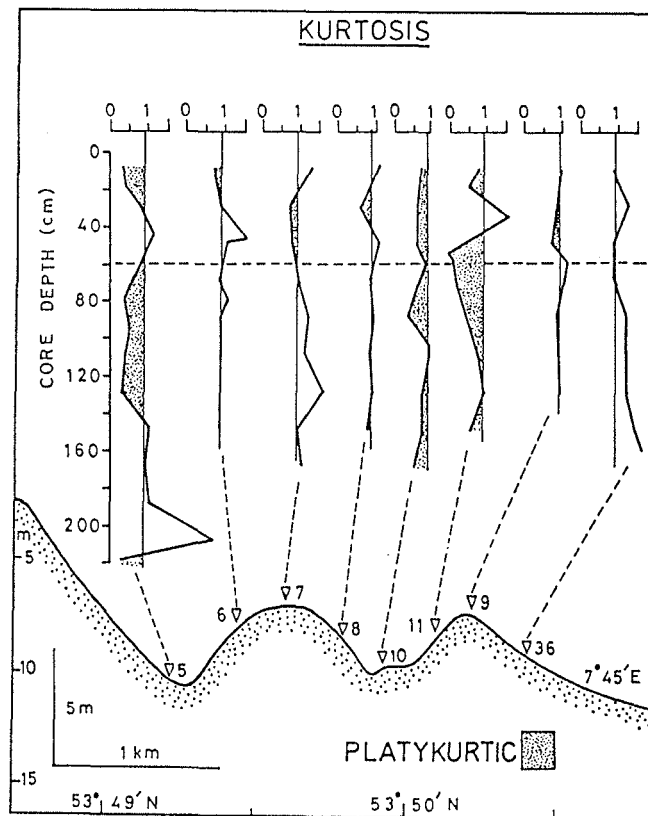


Fig. 120. Vertical variation in kurtosis of the shoreface ridge sediments

Finally, Fig. 121 shows that textural segregation between the ridge morphozones has always been an inherent attribute of their development. The surficial coarser grained fraction of both (outer and inner) ridges, however, was better segregated than the finer subsurface counterpart. It is noteworthy that in these bivariate plots, the landward flank and trough sediments tend to depict a genetic relationship. Interestingly, the surficial and subsurface inner trough sediments are generally finer, but less sorted, than those of other morphozones.

The per cent variation of the sediment fractions in the cores indicates that very fine sand (Fig. 122) constitutes typically < 10% by weight, a notable exception being the landward flank of the inner ridge with almost 90% in its lower section. The adjacent crest shows an increasing proportion of very fine sand with core depth.

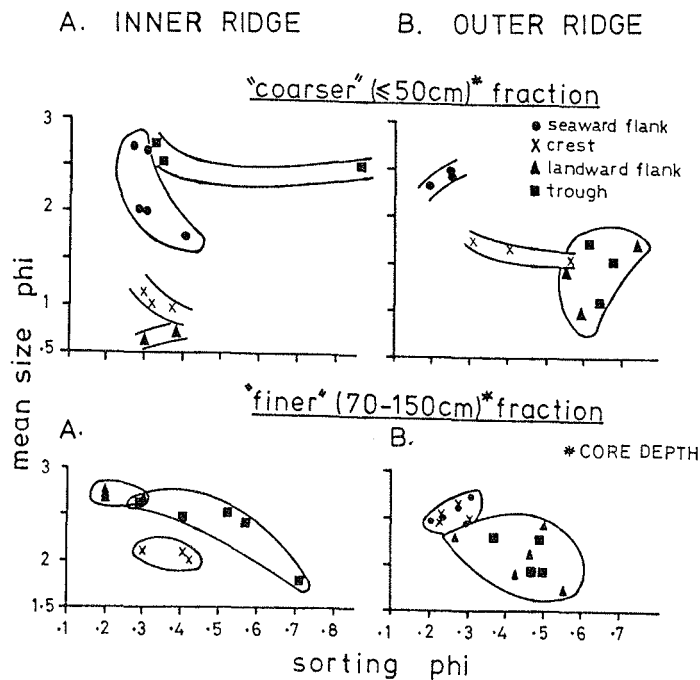


Fig. 121. Bivariate plots of mean grain size versus sorting for the coarser and finer lithologic units of the inner and outer shoreface ridges.

The impoverishment of the very fine sand fraction in the inner trough relative to the aforementioned counterparts would imply either that this morphozone as a depocenter was "overpassed" by the seaward transporting flows or that the very fine sand deposits have been completely reworked. The thin or discontinuous capping of medium-coarse sands must have enhanced their reworking compared to the crest or landward flank. It appears logical that the very fine sand fraction of the latter two morphozones would be underlain by fine sands similar to those constituting the subsurface of the outer ridge.

The fine sand fraction (Fig. 123) is most abundant in the inner trough and at the seaward flank of the outer ridge. A sharp vertical discontinuity at 60 cm core depth is indicated on the outer ridge crest. However, because Core 5 has the greatest subsurface penetration, one can conclude that the shoreface is composed primarily of fine sands.

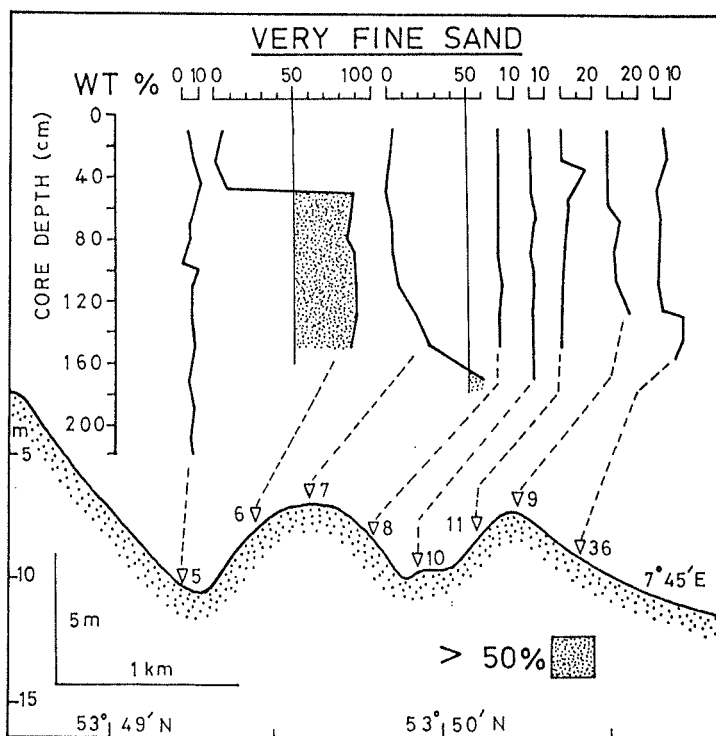


Fig. 122. Vertical variation in wt.-% of very fine sand of the shoreface ridge sediments.

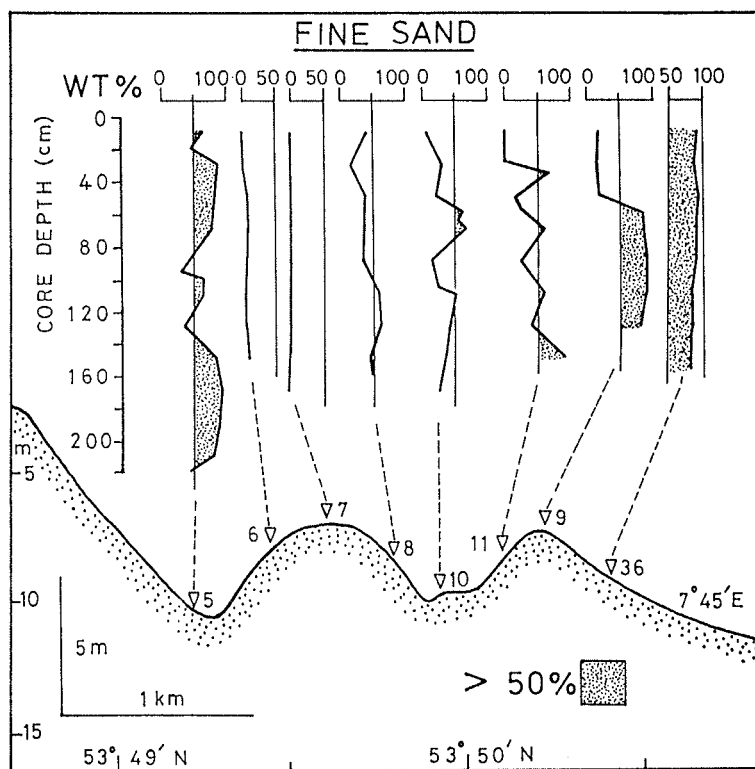


Fig. 123. Vertical variation in wt.-% of fine sand of the shoreface ridge sediments.

Medium to coarse sands in appreciable amounts occur intermittently within this morphozone (Fig. 124), perhaps in response to storm events. The latter representation is comparable in pattern to that of the mean size.

Due to the general discontinuous or fluctuating pattern of the > 50% by weight of medium to coarse sands beneath 60 cm core depth, but more so because these sands occur in amounts typically < 10% by weight on the upper and lower shoreface, it is difficult to conceive how their origin can be a consequence of in-situ winnowing. It is furthermore doubtful how an in-situ winnowing process can concurrently give rise to a coarsening upward, updrift (proximal) and coastward pattern.

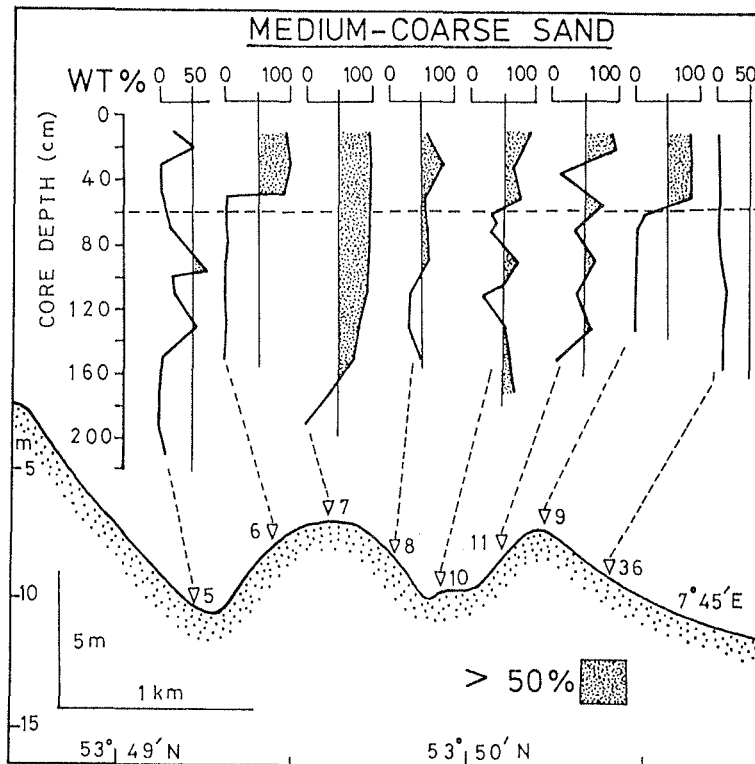


Fig. 124. Vertical variation in wt.-% of medium-coarse sand of the shoreface ridge sediments.

### Medium-coarse sand budget of the ridge morphology

Because all indications point to an allogenetic nature of the surficial sediments of the central shoreface ridge morphology, the suitability of the inlets as a potential source of supply in accord with the DISEC model is worth verifying.

Taking the ridge base level as a reference, and taking an average ridge length of 10 km for the study area, both ridges reveal a sand volume of 49 million m<sup>3</sup>. Based on vibrocore data, the medium to coarse grained surficial blanket is estimated at 1.4 million m<sup>3</sup> or 2.9% of the above ridge volume.

It is well known that the main channels of the Frisian barrier island inlets are deeper than 10-15 m and as such have scoured into the Pleistocene substrate. The writer's unpublished sediment studies on the Ameland Inlet of the Netherlands as well as others, e.g. SHA (1990) and SCHUBERT (1990) show that the inlet gorge and main ebb channel are characterized by sands of similar grain size as those blanketing the ridge morphology.

The inlet sediments are composed of up to 30% by weight of medium to coarse sand. Because these channels deepen at a rate of 6-10 cm/yr, sediments for ridge building is constantly replenished.

Although the emphasis of the sediment budget calculation is on the medium-coarse sand fraction, it is logical that prior to inlet incision into the Pleistocene substrate only fine sands were available for transportation by the diverged inlet jets; this, therefore, explains why the subsurface of the ridge morphozones is composed of fine sand succeeded abruptly in some cases by coarser fractions.

The size distribution patterns of sediments within the inlets flanking the study area have been documented by SCHUBERT (1990). Based on a very conservative estimate of 5 cm thickness

for the areal pattern, the volume of medium to coarse sands within the Otzumer and Harle inlets amount to at least 854, 000 and 357, 000 m<sup>3</sup> respectively. These comprise 60% and 25% respectively of the estimated coarse fraction of the ridge morphology. The larger volume within the Otzumer Inlet is probably related to its more intense scouring/winnowing flow, as might be expected from its smaller main inlet cross-sectional area.

Indeed, an assessment of the current data from the above author at comparable tide conditions and locations within both inlet systems indicate that the peak ebb/flood velocity ratio in the Otzumer Inlet is about 20-40% higher than in the Harle. A similar order of magnitude within the main channels can be expected.

The postulated model for the shoreface-connected ridge genesis along the East and West Frisian coast requires the bulk of the ridge sand to emanate from the inlets at the eastern end of each barrier island, in this case the Harle. Thus, with a supply of the modestly estimated coarse fraction volume of the Harle Inlet annually, the present surficial cover of the ridge could have been emplaced within a 4-year time-period.

#### 6.3.4.2 Sedimentary and Biogenic Structures

Data on the above are based primarily on a set of vibrocores and repetitive boxcoreing. It should be noted that the documented facies need not necessarily reflect an equilibrium response to the instantaneous flow regime. However, the recurrence of certain attributes within the cores may indeed indicate the likelihood of their preservation in the rock record.

It appears beneficial to first discuss the results from the vibrocores (Fig. 125) before evaluating temporal variabilities

in the facies of the different ridge morphozones evident in the boxcores (Fig. 126; Appendix G1-G3). The salient points evident from Fig. 12 are as follows :

(1) Horizontally laminated sands are the most common sedimentary structure. The upper core section on the ridge morphozones tends to be coarser, homogeneous to poorly bedded and enriched in shelly materials.

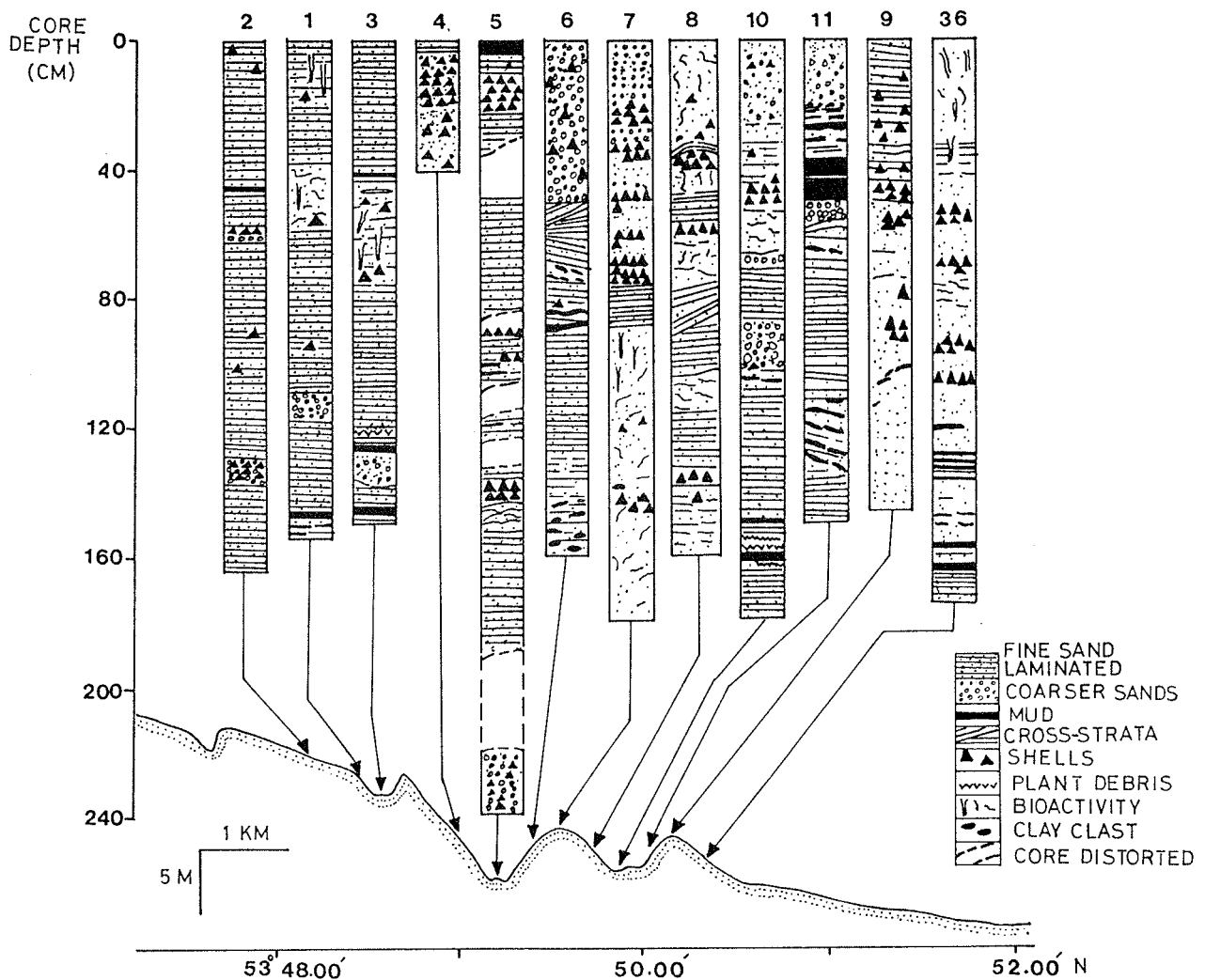


Fig. 125. Vertical sequence of shoreface sedimentary structures.

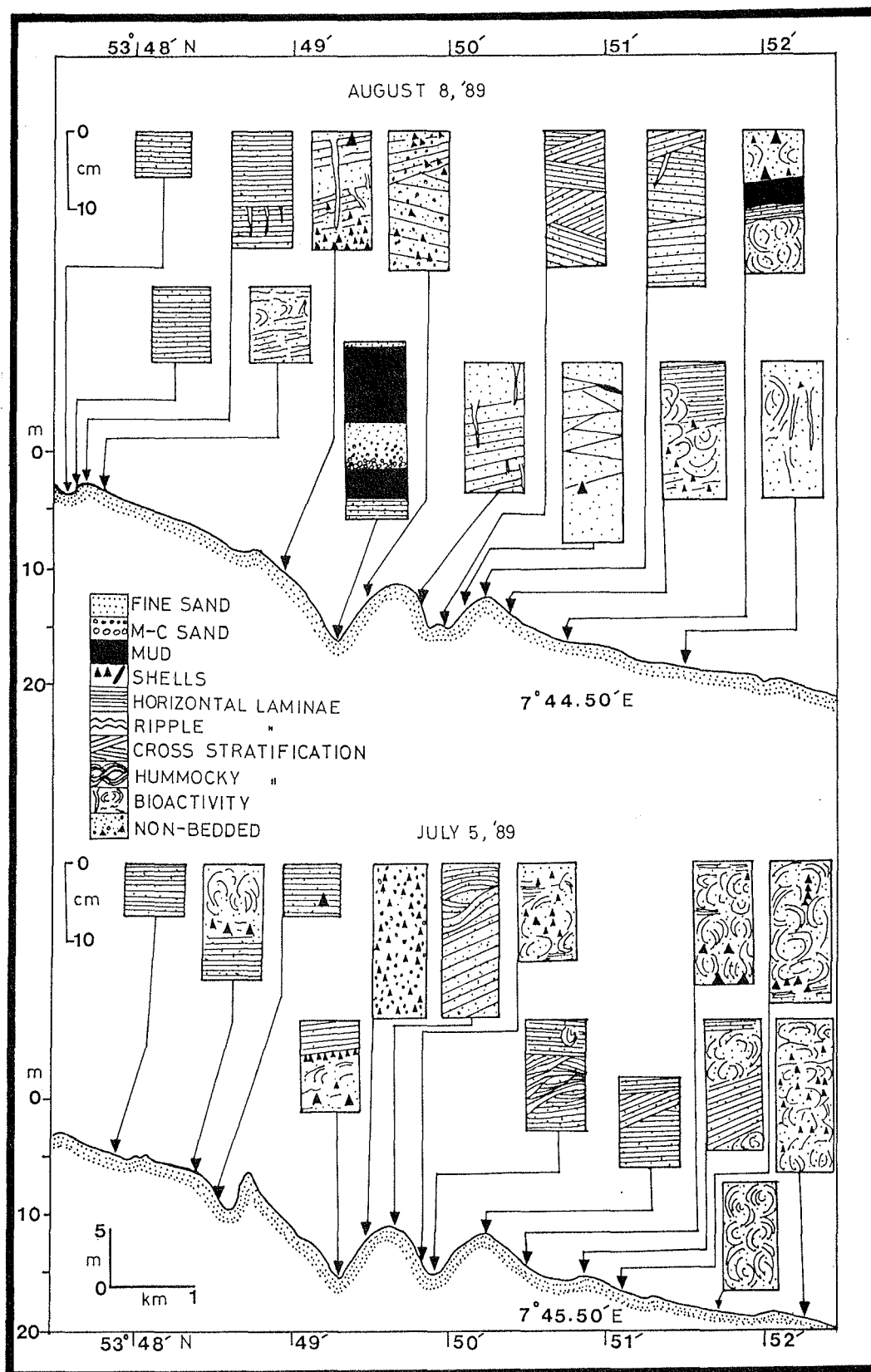


Fig. 126. Temporal variability in surficial sequence of shoreface sedimentary structures.

(2) Physical sedimentary structures in general decrease in significance within the cores from the upper shoreface down to the lower shoreface. Bioturbation shows the opposite trend.

(3) A single or more upward-fining storm sequences are evident in all the shoreface subenvironments. The basal unit of the sequence may consist either of a coarser, clean sand fraction, a shell bed or both.

(4) The storm sequence is typically 10-18 cm thick. The thickest sequence, which is about 30-40 cm, occurs within the central shoreface ridge trough, whereas it is lacking on the corresponding ridge crests.

#### 6.3.3.2.1 Ridge Trough

The inner and outer troughs exhibit marked differences in their sedimentary sequences. Further illuminating is the fact that there is a higher lateral variability in the inner trough as compared to the outer one. Much of the disparity between the two trough facies is related to the greater depth of the inner trough, but also its native sediments.

The inner trough facies is composed of either stratified or massive to poorly bedded medium to pebble (up to 3 cm diameter) sized sediments (Plate 1a). The stratified sequence is in the main (70 % of the time) a consequence of storm sedimentation and is typically characterized by a single or by repetitive upward fining sequences with a surficial veneer (3-10 cm thick) mud layer, all of which are horizontally bedded.

Shelly material is generally subordinate but tends to be concentrated in the the basal unit of the storm sequence. Biogenic activity is rare and cross-stratification is occasionally encountered in the uppermost core section only.

This may indicate a reponse to the fair-weather flow regime, whereby the upper mud unit of the storm sequence has been reworked.

In contrast to the inner trough, the outer one less commonly exhibits marked storm sequences. Nonetheless, sedimentary structures are very variable. These range from apparent lack of bedding to stratified sets : cross bedding, horizontal bedding and swaley (hummocky ?) bedding (Plate 1b). Pebbly and very coarse sands, as well as shells, are comparatively rare. Bioturbation, when evident, appears to be more intensive than within the inner trough.

#### 6.3.3.2.2 Ridge Flanks

The landward and seaward flanks of both the inner and outer ridges show a discernible distinction in their facies character. Further distinction exists between similar flanks of both ridges.

The landward flank of the inner ridge exhibits a very high content of shells which is associated with the constituting medium-coarse grained sands (Plate 1c). Bioturbation is rare. This facies is often massive to poorly bedded. In the latter case this can include bundlewise tidal cross-stratified or low-angle landward-dipping beds. Its seaward counterpart exhibits principally a gentle landward dipping stratification with moderate to intense bioturbation; this facies is generally devoid of shells and mud beds (Plate 1d).

The higher propensity toward bioturbation on the seaward flanks in comparison to the landward counterpart would initially suggest a less intense flow condition on the former. However, the current records do not strongly support the above assertion. One is thus inclined to relate the above propensity to the finer and better sorted sediment of the seaward flank, a

view further corroborated by a similar pattern on the outer ridge.

The outer landward flank facies differs from the inner counterpart in its finer grained texture, very low content of shelly material and in being more commonly bedded: horizontal, cross-stratified or swaley bedding. On the other hand, as on the inner ridge, the outer seaward flank tends to be bioturbated, but less so than the inner ridge counterpart. Horizontal stratification is quite common, thus further contrasting it from the inner ridge counterpart, which is typified by low angle plane stratification.

Finally, unlike the troughs, the flanks show a higher lateral consistency in their facies. The inherent grain size texture appears to play a strong role in the facies variability of the morphozones, given the fact that their flow conditions vary little in intensity. In particular, there is a noticeable decrease in the content of shelly materials distally across the morphology. This is the contrary to what would normally be expected because diminishing energy downshelf should provide a more conducive habitat for the benthic organisms.

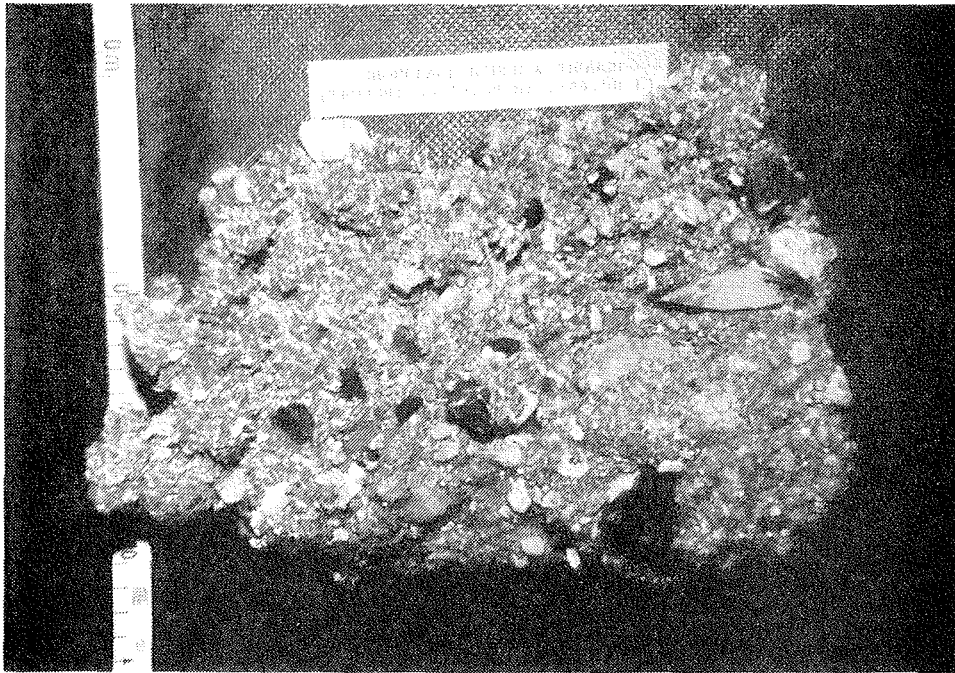
The pattern indicated above corroborates the fact that extraneous sediments played a dominant role in ridge genesis as predicted by the DISEC model. The association of the shelly materials with the coarser grained fractions of the proximal central shoreface is indicative of hydraulic equivalence.

Interestingly, there are clear indications from relief peels, as illustrated in Fig.126, that shell content tends to be higher within the inner troughs and on landward flanks of the eastern transect (bottom cross-section) than in its western counterpart. This further supports the contention of a longitudinal segregation of materials in the downdrift or northwesterly flow direction of the diverged inlet ebb-jet or DISEC.

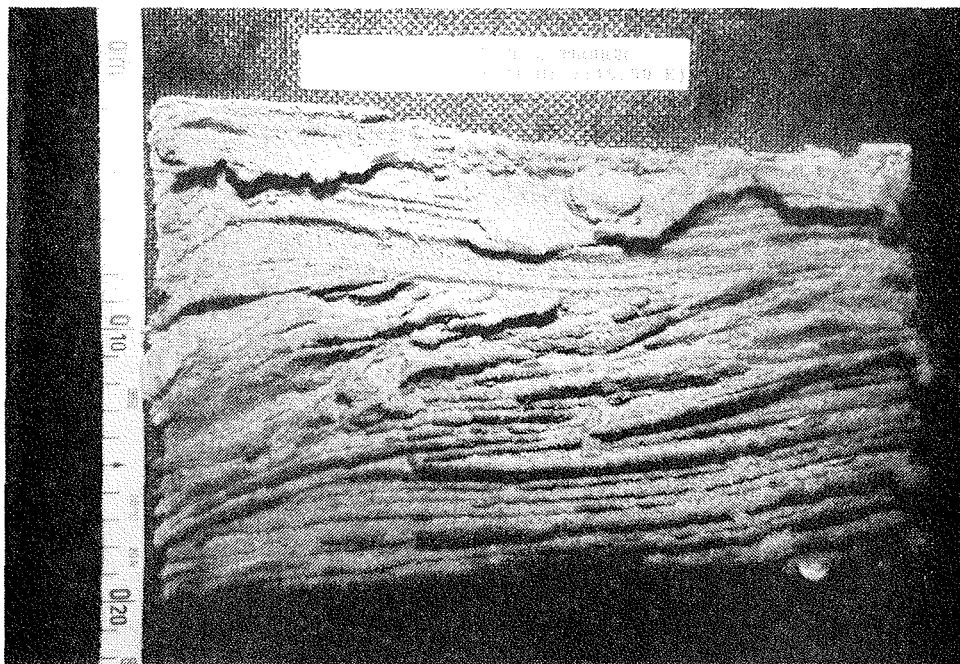
#### 6.3.3.2.1 Ridge crest

On both the outer and inner ridge crests low angle cross-stratification was the most common sedimentary structure. The dominantly medium sands of the crest facies general lack shells and mud; burrowing, though very rare, is apt to occur on the outer crest.

PLATE 1

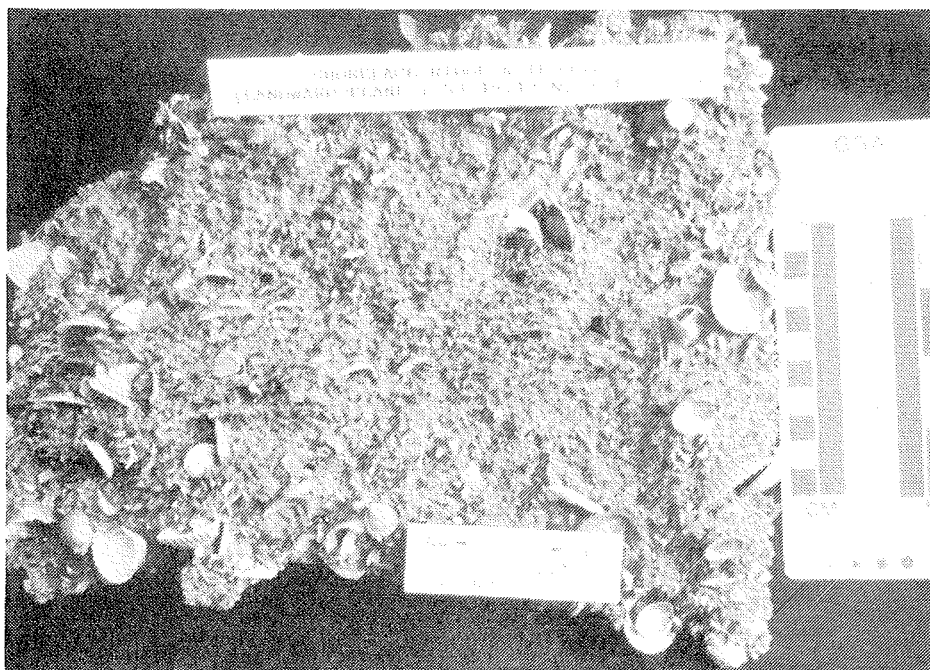


(a) Massive medium to pebbly sand inner trough facies.



(b) Swaley (hummocky?) bedded fine-medium sand outer trough facies.

## PLATE 1 contd.

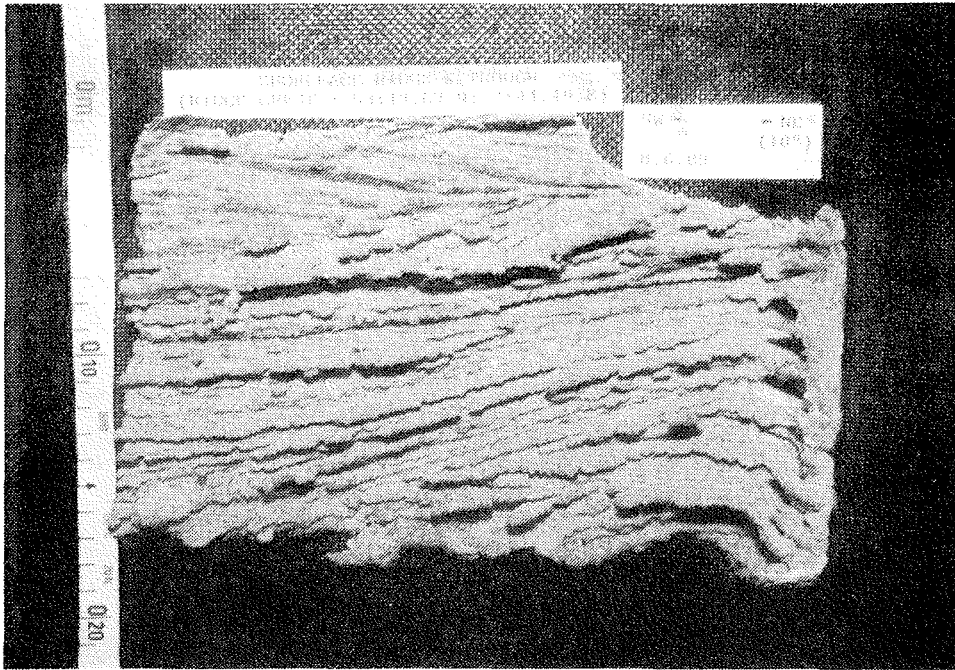


(c) Shelly-rich medium- to coarse-grained inner landward flank facies.

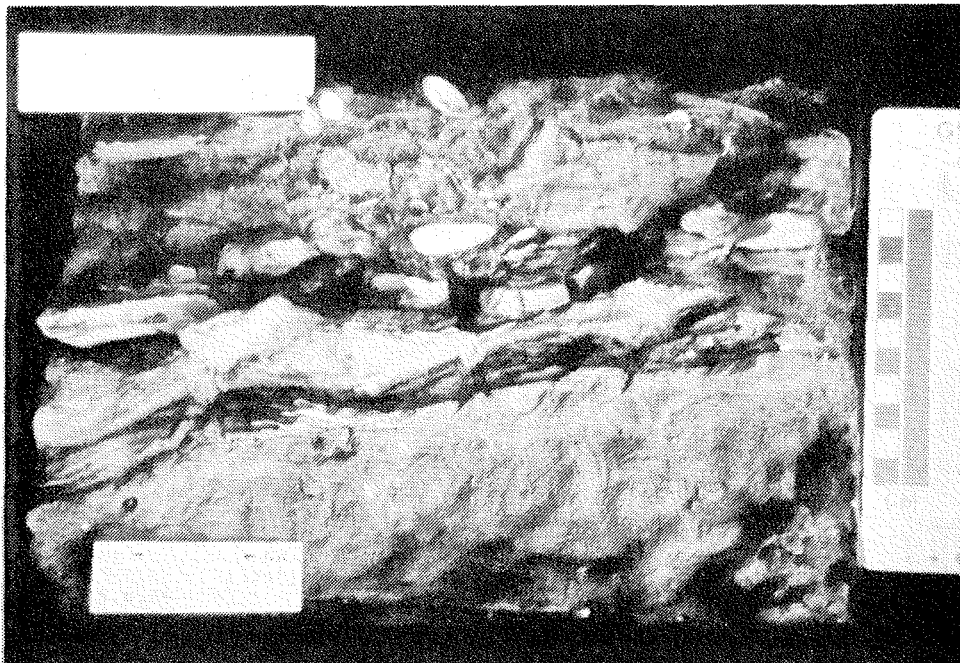


(d) Gently dipping fine sand seaward flank facies. Note the completely bioturbated lower section of the peel.

## PLATE 1 contd.



(e) Low angle cross-stratified fine- to medium-grained crest facies.



(f) Completely bioturbated fine sand lower shoreface facies. Note the mud bed horizon in the middle of peel.

### 6.3.5 Development and Dynamic Sequence of Frisian Barrier Island Shoreface-Connected Ridges

Considerations of the attributes of the shoreface-connected ridges earlier outlined and fully discussed in the preceding sections leave no doubt that these are intricately related to their genesis as predicted by the DISEC model, and hence contemporaneous. The DISEC model is the only existing model that unambiguously explains principal attributes of ridge morphology without recourse to other divergent generating mechanisms. This fact alone demonstrates its credibility.

By virtue of their energetic environment, the ridges are extremely dynamic. Moreover, vibrocore grain size data suggest an upward growth of the ridge. Although these modifications do not mar their moulding mechanism, it is meaningful to examine how the ridges may be maintained, especially in the light of the former.

A six-fold cyclic sequence of ridge development and dynamics along the Frisian barrier island coast is given in Fig. 127. This provides, in a generalized way, an insight as to the response character of the ridge morphology under a variety of storm and tidal flow regimes.

The first sequence commences with the divergence of the inlet jet during the waxing storm ebb phase. At first, the finer grained Holocene deposits, as presently found on the barrier islands, would be deposited in a longitudinally WNW-wedging configuration along the path of the diverged flow (DISEF). With further scouring of the inlet, coarser grain sizes would similarly be transported and emplaced over the pre-existing finer grained sand body.

In this model the offshore distance of a sand body is related to the intensity of divergence and also the material in

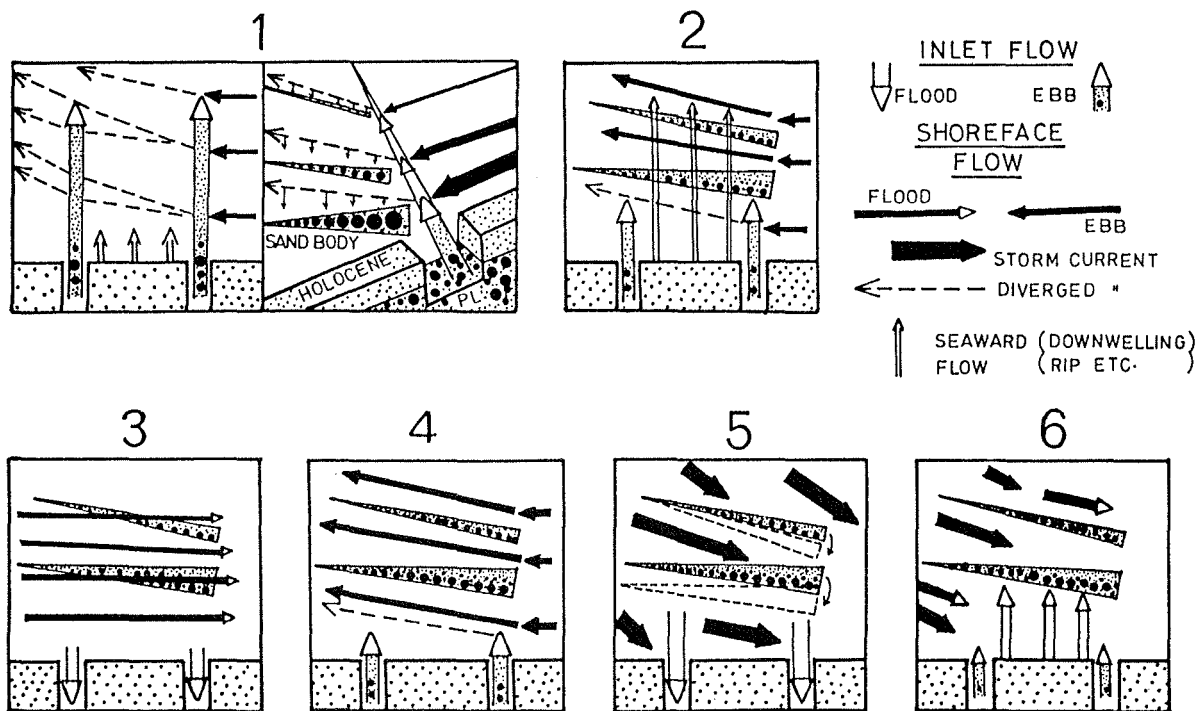


Fig. 127. Development and dynamic sequence of the Frisian barrier island shoreface-connected ridges.

STAGE	EFFECT
(1) EBB STORM WAXING -----	Sand body emplacement (or dynamics if pre-existing)
(2) EBB STORM WANING -----	Trough scouring and textural segregation
(3) NORMAL FLOOD FLOW -----	Textural segregation and trough scouring
(4) NORMAL EBB FLOW -----	Crestal aggradation and trough erosion
(5) STORM FLOOD WAXING ----	Ridge dynamics
(6) STORM FLOOD WANING ----	Texture-morphology asymmetry intensified

transport. As such these bodies need not have developed simultaneously. In any case, it is quite evident that the sand body closest to shore would be the coarsest and, as also noted, most enriched in shells. This also applies to the landward margin of the sand bodies in general. Moreover, because of the downdrift decreasing flow competence, the sand bodies would fine distally.

As the inlet jet diminishes in intensity during the waning ebb storm phase (stage 2), the previously deposited sand bodies would tend to channelize the shoreface ebb-flow, thus initiating the scouring of ridge troughs. At some point in stage 2, seaward return flows like rip currents and gradient currents may attain intensities effective to intensify cross-ridge textural segregation in the manner proposed by SMITH (1970). The longitudinally varying inner-ridge asymmetry may owe its origin to the above rip currents.

At the return to normal tidal flow conditions, the flood currents (stage 3) would primarily enhance the cross-ridge textural segregation since the flow direction is generally oblique to the morphology. Some trough scouring should also be apparent.

The succeeding shoreface ebb currents or DISEF (stage 4), the direction of which is essentially parallel to ridge trend, could enhance crestal upward aggradation if materials are entrained in sufficient quantities, particularly during spring tides. Trough erosion may also persist. The magnitude of erosion, as already documented in Fig. 103b, is highest at the trough neck. This is because of its comparatively smaller width and hence swifter currents.

Stage 5 represents the waxing phase of storm-amplified flood currents. Except for storms travelling in the direction of ridge orientation, most others should, through direct momentum impact, cause a cross-shore (commonly coastward) translation of the ridge morphology. Ridge-aligned storm flows

on the other hand may greatly intensify trough scouring.

The waning storm flood phase (stage 6) is typified by early seaward returning flows which further accentuate the textural-topography asymmetry. Some seaward shifting of the ridge morphology may also be apparent. However much of the latter translation is likely to occur at stage 2.

#### 6.3.6 Summary Remarks on the Central Shoreface Subenvironment

The central shoreface differs markedly from its contiguous counterparts in its bottom topography and texture. The shoreface-connected ridge morphology constituting this subenvironment has been well documented elsewhere, principally off the Atlantic coast of the United States.

While these various ridge systems reveal a number of common features, their dynamic environments are very different. The studied North Sea ridges show much higher dynamic rates than those reported elsewhere. The Atlantic shoreface ridges are dynamic during short-period storm events, whereas even fair-weather flow along the North Sea coast can induce sediment transport over the ridges, daily, in > 80% of the time.

Thus, unless the transport pathways are comparable to those of ridge trends, the longevity of the Frisian ridges would be endangered. The implication of the above is that the flow field moulding and maintaining the ridges must be oriented more or less like the latter.

In the above respect, the tidal currents are the most likely candidate in the study area. A comprehensive flow measurement program instituted by LAVELLE and SWIFT (1982) over a ridge topography has led to a similar view-point. There are,

however, some notable disparities between the Frisian ridge flow pattern and those documented by the above authors, the most important being the higher velocities over the southern North Sea ridge field.

The non-occurrence of ridges in water depths shallower than the distal margin of the ebb deltas ( $< 6$  m) in the studied area is elucidated in a novel approach on their moulding and maintenance called DISEC (diverged inlet storm ebb current). By contrast, the occurrence of the Atlantic ridges in depths as shallow as 3 m would, in the context of the DISEC model, be related to the low tidal range ( $< 1.5$  m) and the correspondingly very weak inlet or estuarine ebb-jets relative to the coast-parallel ebb currents; under such circumstances, divergence of the inlet out-flow is virtually confined near the coastline.

A multiplicity of factors and ridge features favour and confirm the DISEC model as the most creditable mechanism of moulding and maintaining the southern North Sea shoreface-connected ridges.

Texturally, the central shoreface ridge sands depict a very wide range, which is also manifested in the variable transport modes. Cross-ridge mean grain size and sorting trends were temporally consistent, suggesting a well defined flow pattern. In contrast to the expected regional trend, mean grain sizes along the ridge morphozones fine in a northwesterly direction.

Finally, core data indicate facies of the central shoreface ridge morphozones to be variable, both surficially and in the subsurface. Storm sequences are commonly encountered. Particularly worthy of note is the fact that the coarse-grained sediments evident on the surface rarely continue at depth beyond 60 cm. This coarse sediment blanket is thus a signature of the continuing aggradation of the morphology through sediment deposition. The ridges have been built, and are being maintained, by sediments whose source are the inlets fringing the barrier islands.

#### 6.4 Lower Shoreface Subenvironment

The lower shoreface subenvironment is for convenience divided into two zones : proximal and distal. The latter zone extends northward of Lat.  $53^{\circ} 52.75'$ .

##### 6.4.1 Hydrodynamics, Morphodynamics and Facies

Wave orbital velocities in water depth range of the lower shoreface subenvironment during fairweather condition are estimated to exceed the threshold of the fine sands up to about 50% of the time (cf. Fig. 12b, c) but considerably more when storm-swells and seas prevail. Similarly, these sediments would also be entrained by the peak tidal flows during spring and neap.

Tidal flow directions differ markedly on the upper and lower shoreface. The increased ebb-current obliquity on the lower shoreface is certainly a consequence of increasing divergence of the inlet outflow with depth. By contrast, the increasing shoreward obliquity of the flood currents seems to relate to the increasing longshore component of momentum flux of the shoaling waves.

The occurrence of a broad patch of fines at the proximal zone as well as the ridge trough lines, delineated on the distal counterpart, clearly suggest that this subenvironment must be strongly influenced during high energy conditions.

Besides the above hydrodynamic factors, gradients in grain size statistical parameters and primary sedimentary structures attest to sediment mobility in this subenvironment. On the whole, like the upper shoreface sands, graded suspension (Figs. 43, 53) or saltation (Fig. 44) modes of transport are most typical.

It was noted in Fig. 104b that ridge trough axis clusters 9 and 10 showed the highest shoreward mean translation rate of 44 m/yr, a fact which can logically be related to the impact of net onshore flow-momentum. Interestingly, a high offshore translation rate (38 m/yr) is also indicated by cluster 10. The latter appears anomalous in view of the fact that axis cluster 9, which lies adjacent to it, exhibits a rate of about 5 m/yr.

The distal and proximal zones of the lower shoreface subenvironment can be distinguished texturally by the finer, better sorted and positively skewed sediment characteristics in the distal zone (Fig. 128; see also Fig. 50). Kurtosis values are partly somewhat lower or remain constant. The evolution of these grain size patterns has already been discussed in various sections of Chapter 5 and need not be repeated here.

Requiring emphasis, however, is the fact that because the coarser grains of the lower shoreface occur on the proximal zone contiguous to the central shoreface ridges, their origin is inevitably the consequence of the inlet-jet divergence (DISEF) responsible for the moulding and maintenance of the ridges. The mere fact that the ridges are not moulded on the proximal lower shoreface zone is attributable to the ephemeral nature of DISEF.

In addition to the textural distinction within the lower shoreface subenvironment, it was previously noted that sediments of this environment, when compared with the upper shoreface counterparts, exhibited coarser mean grain sizes. The coarsest percentile distribution (Fig. 55) appropriately illustrates this disparity.

The lack of a discernible mean grain size pattern from the three longshore transects on the lower shoreface shown in Fig. 128 was anticipated because of the texturally strong imprint of DISEF which, although ephemeral, defines a transport direction which opposes the easterly long-term net flow

in the region. However, the farther seaward from the regular influence of DIESEF such as at the distal transect, the stronger some grain size trends become. The aforementioned is also applicable to sediment sorting, skewness and kurtosis.

### LOWER SHOREFACE CROSS-SHORE GRAIN SIZE STATISTICS VARIATION

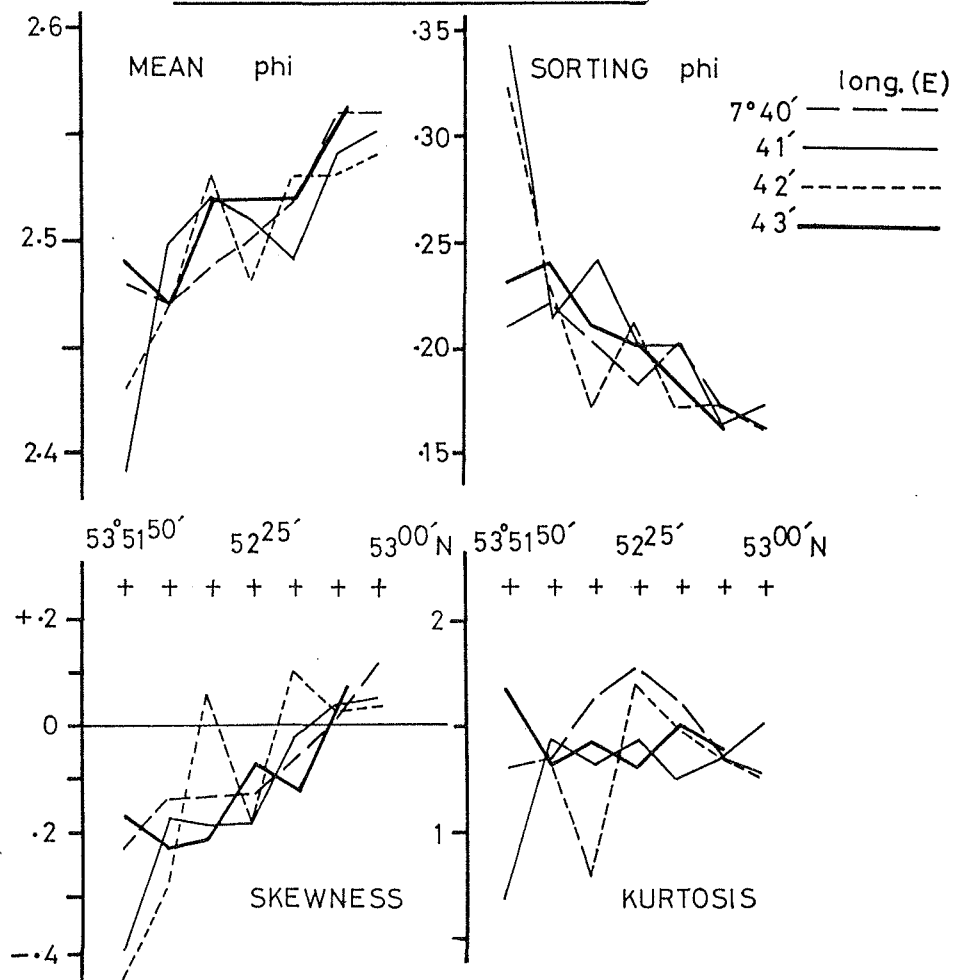


Fig. 128 Cross-shore variation in grain size statistical parameters of lower shoreface sediments

The facies of the lower shoreface subenvironment (Fig. 128, Plate 1f and Appendix G1-G3) is constituted in the main of biogenic structures - burrows of Echinocardium cordatum and other forms of bioactivity leading to considerable destruction

LOWER SHOREFACE ALONGSHORE GRAIN SIZE  
STATISTICS VARIATION

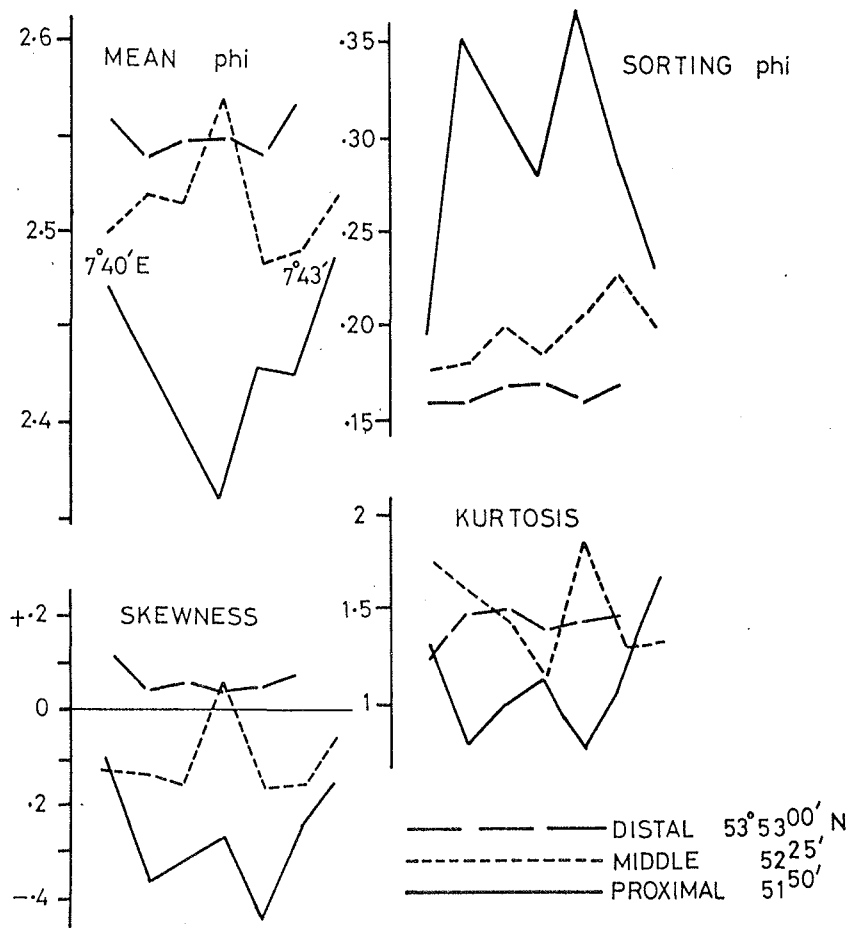


Fig. 129. Alongshore variation in grain size statistical parameters of lower shoreface sediments

of pre-existing physical structures. Shelly materials are much higher in content than on the upper shoreface. Relatively thick layers of mud occasionally occur as intercalation with fine sand, these being attributed to high-energy events.

#### 6.4.2 Summary Remarks on the Lower Shoreface Subenvironment

Texturally, the lower shoreface shows a more defined cross-shore than longshore gradient (Fig. 129). The best correlated grain size statistical pairs are sorting/mean, skewness/sorting and skewness/mean. In conformity with a

LOWER SHOREFACE GRAIN SIZE REGRESSION TREND

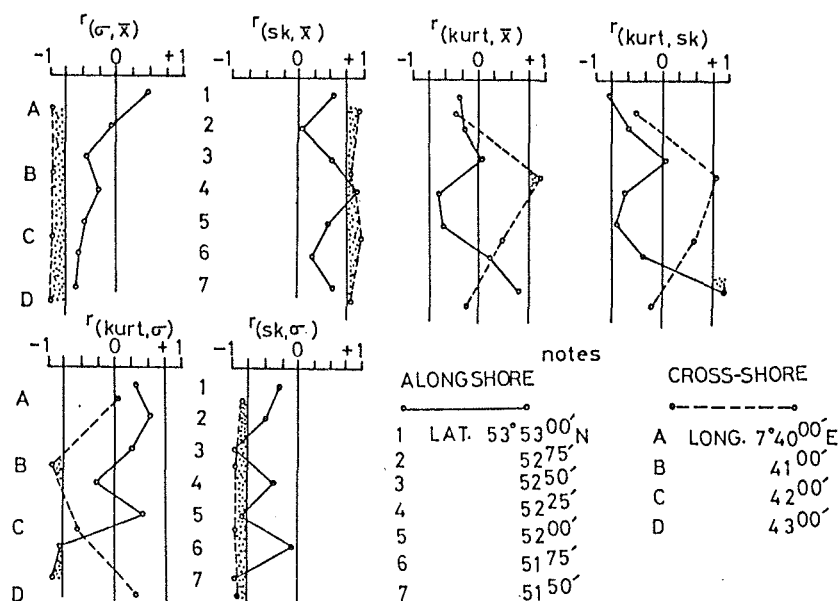


Fig. 130. Regression trend of cross-shore and alongshore lower shoreface grain size statistical parameters.

downshelf energy gradient, the sediment facies is dominated by bioturbation. Moreover, the accumulation of fines in locations diametrically opposed to the main inlet axis clearly suggest that the morphosedimentary character of the lower shoreface is to a considerable extent dependent on high-energy events.

### 6.5 Shoreface Stratigraphic Model

The factors on which the evolution of the different stratigraphic sequences of shallow marine deposits depend are fairly well known (e.g., THOM, 1983; DAVIES and CLIFTON, 1987). On the other hand, information on the relative composition and characteristics of shoreface deposits in the rock-record is still scanty. DAVIES and CLIFTON (1987) have, however, suggested that shoreface deposits would constitute the major component of a nearshore progradational sequence, the opposite being the case for a transgressive counterpart.

The character of the shoreface deposit is somewhat controversial. Whereas HOBDAV and READING (1972) concluded, based on a study of a Precambrian shallow marine sequence in northern Norway, that shoreface deposits would bear more the imprints of fair-weather processes, KUMAR and SANDERS (1976) assert storm deposits to be dominant. The natural consequence of the aforementioned is that there is hardly any standard shoreface stratigraphic model. The following section considers aspects of the above highlighted controversies.

#### 6.5.1 Transgressive Sequence

The transgressive shoreface stratigraphic sequence of Spiekeroog (Fig. 131) should consist of three principal units corresponding to the tripartite shoreface subenvironments (upper, central and lower) earlier identified. Legends to Figs. 131 and 132 are as presented in Fig. 126.

The lowermost unit of the transgressive sequence is the present-day upper shoreface facies. The preservation potential of this unit appears to be the poorest as the shoreface continually retreats landwards. Where preserved, the facies would be dominantly composed of fine to medium sand with horizontal and gently dipping lamination.

The above basal unit would be overlain by the highly variable facies of the central shoreface subenvironment. The most diagnostic features of this latter unit are the swaley/hummocky and tidal cross-strata of the distal zone overlain by one or all of the following proximal zone facies: storm-graded bedding with a non-stratified basal component of shelly fragments, coarse grained and gravelly (pebbly) sands or both, succeeded upwards by horizontally laminated fine sand, capped by variedly thick mud beds; gentle to moderately steep stratification; non-bedded (massive) shelly-rich coarse-grained sand.

TRANSGRESSIVE SHOREFACE STRATIGRAPHY

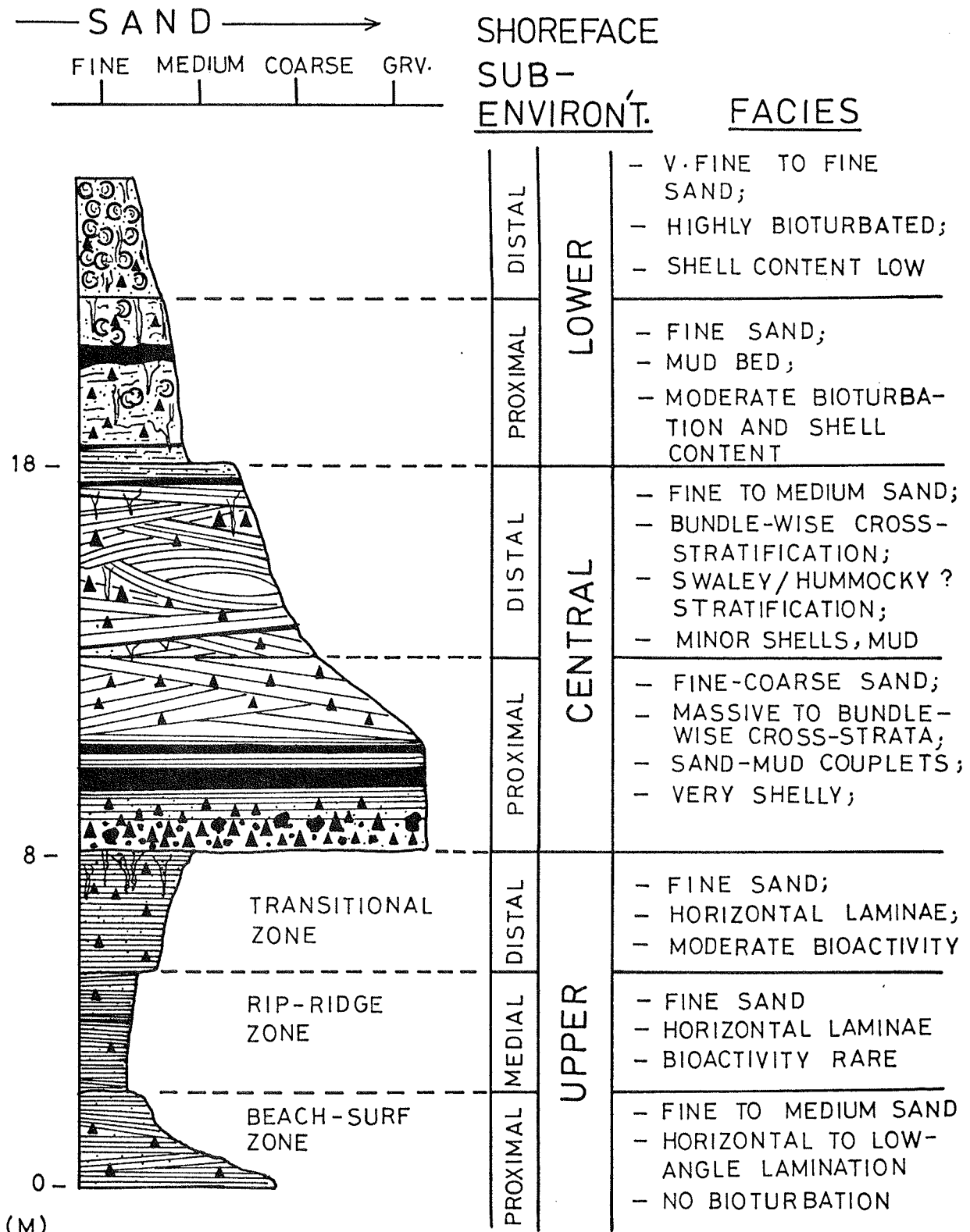


Fig. 131. Transgressive shoreface stratigraphic sequence.

In any case, the central shoreface facies should show an upward coarsening and shelly-rich sequence. The preservation potential of this facies is considered particularly good and both storm- and fair-weather deposits may occur subequally in the rock-record. The same applies to the upper shoreface facies except that due to the generally high day-to-day flow energy conditions, distinction between both deposit types may be impracticable.

The topmost unit of the transgressive sequence is characterized by a predominantly fine sand which, as shown earlier, may be slightly coarser than that of the upper shoreface. It is however much more bioturbated, mostly by Echinocardiun cordatum. This unit would be similarly well represented in the rock-record. In this case, the facies evident would be predominantly fair-weather deposit.

#### 6.5.2 Regressive Sequence

The regressive stratigraphy of the shoreface of Spiekeroog (Fig. 132) reveals a similar suite of sedimentary and biogenic structures in the vertical as that of the transgressive counterpart. The principal difference is that the upper shoreface facies would in the regressive record constitute the topmost part of the sequence, whereas the lower shoreface facies will occur at the bottom.

In general, the regressive sequence would be more completely preserved in the rock record than the transgressive counterpart. However, as documented by the studies of BOSE et al. (1988), many of the facies of the upper shoreface morphozones described from the study area can indeed be preserved in a transgressive rock-record.

REGRESSIVE SHOREFACE STRATIGRAPHY

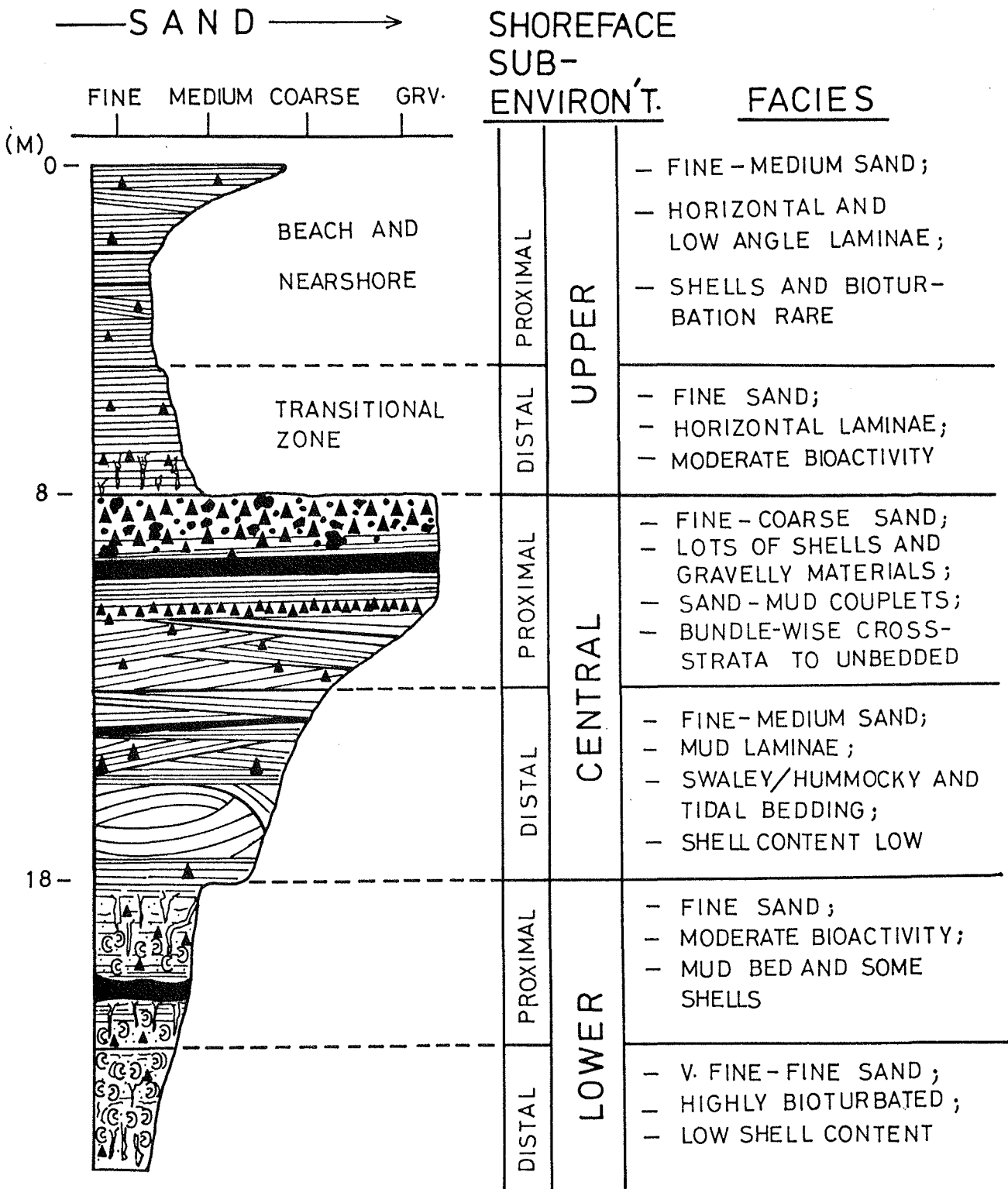


Fig. 132. Regressive shoreface stratigraphic sequence.

## CHAPTER 7

### GENERAL CONCLUSIONS : RESULTS, IMPLICATIONS, AND APPLICATIONS

This study was geared towards improved insights on process-response characteristics of a barrier island shoreface situated in a mesotidal, high energy (wave-tidal current) North Sea setting. The shoreface, as defined in this study, extends from the beach to water depths of about 25 m.

The process variables in a broader sense embody fluid motions and bioactivities causing continuous or episodic changes in bottom morphology and sedimentary characteristics. The latter two represent the response variables.

On the basis of hydrodynamics, bottom morphology and sedimentary facies, the shoreface can be divided into 3 subenvironments: an upper, a central and a lower shoreface. Each of these subenvironments is comprised of distinct morphosedimentary zones.

For purpose of clarity and coherence, salient results and related implications and/or applications will follow the specific objectives of the study as defined in Section 2.3.1.

#### (1) Scale and structure of shoreface flow

(a) Direct measurements and indirect evidence from bottom morphology and sediment size parameters support the contention that coast-parallel and cross-shore fluid motions are significant on the shoreface. Knowledge of such flow patterns, especially the temporal variability, can be beneficially employed in virtually all coastal marine investigations, in which tracking or tracing of particulate matter (including pollutants) is of prime importance.

(b) The upper shoreface fluid motions are primarily wave-driven. Three wave regimes are distinguished, namely, normal ( $H_{sig}$  1-2 m,  $T=$  4-8 s), sea ( $H_{sig}$  2.5-3.5 m,  $T=$  6-8 s) and storm-swell ( $H_{sig} > 3.5$  m,  $T=$  8-10 s). These respectively occur in 67%, 16% and 8% of the time.

(c) Wave breaking occurs in 80% of the time in  $< 4$  m depth. Nevertheless, the mean orbital velocities associated with these waves can effectively mobilize sediments on the upper and central shoreface in  $> 80\%$  of the time, but less frequently on the lower shoreface. It was indicated that due to wave refraction at the inlet ebb-delta located at the western part of the study area, wave-induced easterly longshore currents reveal a reversal in flow direction beyond the fair-weather surf zone.

Given the size and the easterly asymmetry of the ebb deltas along the East Frisian coastline, wave-generated alongshore flow reversals are likely to occur close to the middle of the barrier island length. Within the surf zone itself, a very strong easterly longshore current can be inferred from the sediment size gradient and sediment budget pattern. The opposite is the case on the medial upper shoreface zone, which is characterized by saw-tooth bars. The above results imply that the middle section of these barrier islands are potentially prone to erosion and, hence, breaching. This is due to a continual deficit of sand budget over time. As such, engineering structures may be advisable at these locations especially where threats to lives and property are high.

(d) Besides wind-generated waves, long-period standing edge waves are speculated to develop during storm conditions. The actual edge wave generating mechanism is not well understood, but may be variable. However, distinctly variable is also the physical character or mode of the edge waves. From the point of view of energetics, among others, the domination of the seaward region beyond the fair-weather surf zone by a Mode 1 infragravity oscillation is favoured.

(e) An attractive edge-wave generating mechanism seaward of the surf zone requires a topographic perturbation of an easterly directed transient storm flow. The updrift (Otzumer) ebb-delta bathymetry is suitable in this respect. The downdrift (Harle) counterpart, on the other hand, would act as a bounding surface for reflecting the updrift delta-induced, downcoast propagating edge wave, giving rise to a longshore standing oscillation. Such an interaction is conceived to be confined close to the distal margin of the deltas. Consequently, the morphological expression of the edge wave is not apparent within the fair-weather surf zone.

(f) The rhythmic morphology on the medial upper shoreface is conceived to be a product of rip-like channelized flows. The latter is a consequence of interaction between a sheet-like, seaward returning storm surge and the above longshore standing oscillation.

(g) In contrast to the domination of the upper shoreface by wave-induced flows, tidal currents are the major agent of sediment transport on the central and lower shoreface subenvironment. Records of neap, mean and spring tidal current velocities show a tendency towards a flood-tide dominance, with a weak time asymmetry. The combined  $U_{100}$  max velocity averages of spring flood, spring ebb, neap flood and neap ebb currents were respectively 48, 37, 35 and 33 cm/s. Under all these tidal conditions, threshold velocities required to initiate local sediment transport are attained during a significant fraction of the tidal cycle.

(h) Finally, it was shown that the inlet ebb-flow, particularly the resultant of its interaction with the shoreface counterpart called DISEF, plays a major role in the morphosedimentary characteristics of the central and lower shoreface subenvironments.

(2) Grain size distribution

(a) Patterns of surficial grain size statistical parameters, weight-% of size fractions and probability curve shape characteristics suggest that, whereas the lower and upper shoreface sands are genetically related, those of the central shoreface are allogenetic.

(b) The lower and upper shoreface sands are fine grained (< 3 cm/s settling velocity), very well sorted and dominantly meso-leptokurtic. The central shoreface sands are typically medium-coarse grained (3-18 cm/s settling velocity), less well sorted and meso-platykurtic. Each of the shoreface subenvironments reveal a coast-parallel band of positive and negative skewness. The latter occurs in their proximal part where sands are also coarser, less well sorted and reveal elevated kurtosis values.

(c) The alternating bands of skewness sign noted above is not exclusively hydrodynamically effected. On the other hand, it supports the assertion of an influx of extraneous sediment.

(d) The weight-% size fraction patterns reveal that the lower shoreface sands are somewhat coarser than those of the upper shoreface. This cross-shore anomaly is intricately related to the deposition of the central shoreface sands and strongly supports an inlet source rather than an offshore source for the extraneous sediments found on the central shoreface.

(e) Finally, the characteristics of the probability size distribution curves exhibit areal patterns which are consistent with the 3-fold textural division of the shoreface. It is significant that the coarsest component (C or traction subpopulation) showed the best sortedness on the central shoreface. This implies that the depositional conditions are very energetic, most likely resembling density currents. The B component (or saltation subpopulation) constitutes the mode of all the shoreface subenvironment sands.

### (3) Sediment transport trends and pathways

(a) Sediment textural patterns in a highly dynamic shoreface, such as that of Spiekeroog Island, must represent a time-averaged response to both the cross-shore and alongshore flow regime. The coarse-grained central shoreface band bounded on either side by contrasting finer-grained sands is indicative of a larger scale coastline-oblique flow regime.

A smaller scale counterpart, relating to wave-generated longshore currents, is evident on the proximal region of the upper shoreface. This is manifested by a very marked eastward fining sediment gradient. By contrast, the central shoreface sands depict a northwesterly fining gradient, even though easterly-directed currents (storm and tidal) are dominant.

(b) Given the efficiency of sediment mobilization on the central shoreface, the contrast in the direction relative to that of the upper shoreface is suggestive of disequilibrium conditions dictated by episodically opposing flow patterns on the former. The conflict between the processes forming and maintaining the central shoreface sands and the easterly-directed net flow on the lower shoreface endows an unpredictable alongshore textural trend on the latter.

(c) Statistically, the cross-shore textural gradient is generally better correlated than the alongshore one. However, such a cross-shore gradient need not necessarily be a consequence of a coast-normal flow. The alternating skewness signs demonstrate this point. With the exception of the upper shoreface, where cross-shore textural changes are unequivocally related to wave breaking and seaward transport of fines and/or rip current activity, a similar pattern on the central and lower shoreface cannot be attributed to the latter processes or on wave amplitude-modulated sediment transport reversal described by SHI and LARSEN (1984). A more likely mechanism

relates to a laterally (deeper-depth) diminishing transport competence of coastline-oblique storm flows associated with the central shoreface sands.

(d) A number of sediment transport models have been evaluated and all point to an allogenetic nature of the central shoreface sands. A storm sedimentation model best accounts for the larger scale features of the latter deposit. Progressive size-sorting patterns, which are temporally consistent, observed within the central shoreface morphozones may, however, be enhanced by the day-to-day processes.

#### (4) Moulding and morphodynamics of the shoreface

(a) Two shoreface morphologies have been studied in detail. These are the saw-tooth bars on the upper shoreface and the shoreface-connected ridges occurring principally on the central shoreface.

(b) The rhythmic saw-tooth bars, as earlier mentioned, are speculated to represent a rip and ridge morphology scoured on the convex upper shoreface profile by seaward-directed channelized flows.

(c) A number of independent lines of evidence negate a previously held opinion that the above morphology represents flow-transverse bedforms migrating alongshore. Particularly instructive are : (i) the spatially-varying channel inclination relative to the shoreline, (ii) the exclusively horizontally laminated internal structure of the morphology as a whole, and (iii) the non-conformable grain size-wave length relationship with empirical results.

(d) The spatially- and temporally-varying orientation of the rip channels has been shown to depend on the degree of distortion of the standing oscillation. Specifically, due to imperfect reflection, frictional dissipation of energy as well as a continuous forcing at the updrift ebb delta sector, the

standing oscillation must be skewed eastwards, with an easterly diminishing asymmetry of the oscillation relative to a shore-normal transect.

(e) The location and spatial variability in the orientation of the inferred rip channels are both functions of the edge wave oscillation and the degree of interaction with transient storm flows at the time of generation. Depending on the character of the latter, incised channels may deviate in the above respect from the time-averaged or equilibrium condition. The fact that the channel location tends to coincide temporally is suggestive of the coherent nature of the edge wave generating mechanism. In general and in contrast to a rip channel location, the orientation is commonly highly variable, as would be expected, given the variable nature of storm intensity, duration and direction.

(f) On the basis of the above variable orientation of the alongshore rhythmic channel system, a four-fold rotational dynamic mode has been established, two of which are cyclic and two anti-cyclic. It was found that during very intense storm events, the channels tend to adopt smaller shoreline-acute angles as defined by the cyclic rotational mode 1. The latter rotational mode also was the most frequently occurring over time. Finally, it should be mentioned that successive channel orientations do not simply symbolize a re-alignment of pre-existing channels, but rather represent newly incised ones.

(g) The generating mechanisms of shoreface-connected ridges have been meticulously examined based on existing models. None of the latter unequivocally explains the morphometric and textural attributes of the studied ridges, although some similarities in characteristics are apparent. The latter includes their orientation relative to the regional flow direction, textural and topographic asymmetry and their seismically flat base.

More difficult to account for by the commonly-cited models are : (i) the non-occurrence of the morphology at the present time in water depths shallower than the distal margin of the ebb deltas, (ii) the longitudinal grain size gradient which is the converse of that anticipated for an easterly storm flow, (iii) the longitudinally WNW-wedging out ridge relief and positive-prone sediment budget, (iv) upward-coarsening ridge lithology and (V) the higher tendency of ebb current dominance in the ridge troughs.

(i) A novel model of ridge genesis and maintenance appropriate to the Frisian coast called DISEC (Diverged Inlet Storm Ebb Current) has been outlined and discussed. All of the characteristics of the ridge system can be logically explained with the above model. However, the latter does not preclude the modifying effects of other flow regimes and patterns. This is particularly evident from the six-fold development and dynamic sequence presented.

(j) In contrast to other ridges, those investigated are highly mobile with maximum cross-shore translations of the order of 100-200 m in one year and also displaying changes in bottom elevation of up to 2 m. The above rates, in addition to the a coastwise trough elongation in the 80-500 m/y, attest to the high instability of the sea floor and should profoundly influence engineering developments and constructions on or through the shoreface.

#### (5) Shoreface facies association

(a) The upper shoreface is characterized by horizontally laminated clean fine sands. Shells are generally rare and bioturbation becomes apparent at the distal smoothly sloping transitional zone of the upper shoreface.

(b) The central shoreface facies is the most variable. Distinctions are obvious between the ridge morphozones as a

whole and between their outer and inner counterparts. The inner ridge morphozones are texturally coarser than their outer ridge counterparts. Shell content markedly decreases distally. Physical structures range from non-bedded sets in troughs and landward flanks to low-angle dipping and swaley/hummocky stratification on the crest and seaward flanks. Bioturbation is generally more common on the seaward flank than on the landward counterpart.

(c) The lower shoreface facies is mainly fine-grained with an abundance of bioturbation structures. Shells are more common than on the upper shoreface.

(d) In general, a single or several upward-fining storm sequences are evident in all the shoreface subenvironments. The basal unit of the sequence may comprise either a coarser, clean sand fraction, a shell bed, or both. The thickest sequence (30-40 cm) occurs within the central shoreface ridge trough. Such sequences are lacking on the ridge crests.

(e) The central shoreface facies also differs from its adjacent counterparts in the vertical grain size pattern. In most of the morphozones, a sharp distinction between a surficial coarse-grained sand sequence (generally 60 cm thick) and an underlying fine-grained counterpart is possible.

#### (6) Shoreface stratigraphic sequences

The distinction between a regressive and a transgressive shoreface stratigraphic sequence is relatively simple. In the former case, beach and nearshore sediment facies characterized mostly by horizontally laminated fine sands compose the upper sequence, whereas the highly bioturbated and commonly fine sand-mud facies of the lower shoreface occur at the bottom of the sequence. Moreover, the central shoreface facies will show an upward coarsening and shelly-rich pattern. The transgressive stratigraphic record, on the other hand, would show vertical patterns opposite to those of the regressive sequence outlined above.

## REFERENCES

- AAGARD, T. 1991. Infragravity waves and nearshore bars in protected, storm-dominated coastal environments. *Marine Geology*, 94, 181-203.
- ADAMS, C. E. and WEATHERLY, G. L. 1981. Some effects of suspended sediment stratification on the oceanic boundary layer. *Journal of Geophysical Research*, 86, 4161-4172.
- AIGNER, T. and REINECK, H. -E. 1982. Proximity trends in modern storm sands from the Helgoland Bight (North Sea) and their implications for basin analysis. *Senckenbergiana maritima*, 14, 183-215.
- AIGNER, T. and REINECK, H. -E. 1983. Seasonal variation of wave-base on the shoreface of the barrier island Norderney, North Sea. *Senckenbergiana maritima*, 15, 87-92.
- ANTIA, E. E. 1987a. A geomorphic model of beach changes in Nigeria. In : KRAUS, N. C. (Ed.), *Coastal Sediments '87*. American Society of Civil Engineers, New York, p. 1793-1808.
- ANTIA, E. E. 1987b. Preliminary field observations on beach cusp formation and characteristics on tidally- and morphodynamically-distinct beaches on the Nigerian coast. *Marine Geology*, 78, 23-33.
- ANTIA, E. E. 1989c. Surf zone breaker types, subaqueous bar topographies and sandy beach transformation on the Nigerian coast. *Coastal Zone Specialty Symposium*, South Carolina. American Society of Civil Engineers, New York, p. 1674-1687.
- ANTIA, E. E. 1989d. Swash mark and swash angle on texturally, tidally, and morphodynamically-distinct beaches. *Geologie en Mijnbouw*, 68, 297-300.

ANTIA, E. E. 1990a. Beach response to edge wave resonances: field evidence from the west African coast. In : BRUUN, P. and JACOBSEN, N. K. (Eds.), Skagen Symposium. Journal of Coastal Research, Special Issue 9, 591-604.

ANTIA, E. E. 1991. Beach change magnitudes in relation to dynamic phases on dissipative coasts. Proceedings, Coastal Zone '91, California. American Society of Civil Engineers, New York, p. 3193-3203.

ASHLEY, G. M., HASLEY, S. D. and BUTEX, C. B. 1986. New Jersey's longshore current pattern. Journal of Coastal Research, 2, 453-463.

AUBREY, D. G. and WEISHAR, L. 1988. (Eds.), Hydrodynamics and Sediment Dynamics of Tidal Inlets. Springer Verlag, New York, 456 pp.

BAINES, W. P. and KNAPP, D. J., 1965. Wind-driven water currents. Journal of Hydraulic Division, American Society of Civil Engineers, 91 (HY2), 205-221.

BAKER, R. A. 1967. Kurtosis and peakedness. Journal of Sedimentary Petrology, 38, 679-681.

BALSILLIE, J. H. 1983. The transformation of wave height during shore-breaking: the alpha wave peaking process. Beach and Shores, Florida Department of Natural Resources, Technical Memorandum, no. 83-4, 33 pp.

BÄTJE, M. 1986. Salzgehalt und Wassertemperatur an der ostfriesischen Küste. Jahresbericht, Forschungsstelle Küste, Norderney, 125-145.

BAUER, B. O. and GREENWOOD, B. 1990. Modification of a linear bar-trough system by a standing edge wave. Marine Geology, 92, 177-204.

BEHRE, K. -E., MENKE, B. and STREIF, H. 1979. The Quaternary development of the German part of the North Sea. In : OELELE, E., SHÜTTENHELM, R. T. E., WIGGERS, A. J. (Eds.), The Quaternary History of the North Sea. Acta Universitatis Upsaliensis Symposium, Annum Quingentesimum Celebrantis, 2, 85-113.

BEIN, A. and SASS, E. 1978. Analysis of log-probability plots of recent Atlantic sediments and its analogy with simulated mixtures. *Sedimentology*, 25, 575-581.

BELDERSON, R. H. 1986. Offshore tidal and non-tidal sand ridges and sheets - differences in morphology and hydrodynamic setting. In : KNIGHT, R. J. and McLEAN, J. R. (Eds.), Shelf Sands and Sandstones. Canadian Society of Petroleum Geologists, Memoir 11, 293-302.

BELDERSON, R. H., JOHNSON, M. A. and KENYON, N. H. 1982. Bedforms. In : STRIDE, A. H. (Ed.), Offshore Tidal Sands, Processes and Deposits. Chapman and Hall, London, 27-57.

BELKNAP, D. F. and KRAFT, J. C. 1985. Influence of antecedent geology on stratigraphic preservation potential and evolution of Delaware's barrier systems. In : Oertel, G. F. and LEATHERMAN, S. P. (Eds.), Barrier Islands, *Marine Geology*, 63, 235-262.

BEREK, E. P. and DEAN, R. G. 1982. Field investigation of longshore transport distribution. Proceedings, 18th International Conference on Coastal Engineering, American Society of Coastal Engineers, p. 1620-1639.

BOCZAR-KARAKIEWICZ, B. and DAVIDSON-ARNOTT, R. G. D. 1987. Nearshore bar formation by non-linear wave processes - a comparison of model results and field data. *Marine Geology*, 77, 287-304.

BOCZAR-KARAKIEWICZ, B. AMOS, C. L. and DRAPEAU, G. 1990. The origin and stability of sand ridges on Sable Island Bank, Scotian Shelf. *Continental Shelf Research*, 10, 683-704.

BOCZAR-KARAKIEWICZ, B. and BONA, J. L. 1986. Wave-dominated shelves: a model of sand-ridge formation by progressive, infragravity waves. In : KNIGHT, R. J. and McLEAN, J. R. (Eds.), Shelf Sands and Sandstones. Canadian Society of Petroleum Geologists, Memoir 11, 163-179.

BOCZAR-KARAKIEWICZ, B., BONA, J. L. and PELCHAT, B. 1991. Sand ridges and internal waves on continental shelves. Proceedings of Coastal Sediments, Washington. American Society of Civil Engineers, New York, p. 527-541.

BODGE, K. R. and DEAN, R. G. 1987. Short-term impoundment of longshore transport. In : KRAUS, N. C. (Ed.), Coastal Sediments '87, American Society of Civil Engineers, New York, p. 468-483.

BOOTHROYD, J. C. 1985. Tidal inlets and tidal deltas. In : DAVIS, R. A. (Ed.), Coastal Sedimentary Environments. Springer-Verlag, New York, 445-532.

BOSE, P. K., CHAUDHURI, A. K. and SETH, A. 1988. Facies, flow and bedform patterns across a storm-dominated inner continental shelf: Proterozoic Kaimur Formation, Rajasthan, India. Sedimentary Geology, 59, 275-293.

BOWEN, A. J. 1969. Rip currents 1. Theoretical investigations. Journal of Geophysical Research, 23, 5467-5478.

BOWEN, A. J. and Inman, D. L. 1969. Rip currents 2. Laboratory and field observations. Journal of Geophysical Research, 74, 5479-5490.

BOWEN, A. J. and INMAN, D. L. 1971. Edge waves and crescentic bars. Journal of Geophysical Research, 76, 8662-8671.

BOWEN, A. J. and INMAN, D. L. 1972. Reply to comments on paper: A. J. Bowen and D. L. Inman, "Edge waves and crescentic bars". Journal of Geophysical Research, 77, 6632-6633.

BOWMAN, D. and GOLDSMITH, V. 1983. Bar morphology of dissipative beaches: an empirical model. *Marine Geology*, 51, 15-33.

BOWMAN, D., ROSEN, D. S., KIT, E., ARAD, D. and SLAVICZ, A. 1988a. Flow characteristics at the rip current neck under low energy conditions. *Marine Geology*, 79, 41-54.

BOWMAN D., ARAD, D., ROSEN, D. S., KIT, E., GOLDBERY, R., and SLAVICZ, A. 1988b. Flow characteristics along the rip current system under low-energy conditions. *Marine Geology*, 82, 149-167.

BRUUN, P. 1978. *Stability of Tidal Inlets : Theory and Engineering*. Elsevier, Amsterdam, 506 pp.

BULL, W. B. 1962. Relation of textural (CM) patterns to depositional environment of alluvial-fan deposits. *Journal of Sedimentary Petrology*, 32, 211-216.

CACCHIONE, D. H., GRANT, W. D., DRAKE, D. E., and GLENN, S. M. 1987. Storm-dominated boundary layer dynamics on the northern Californian continental shelf: measurements and predictions. *Journal of Geophysical Research*, 92, 8244-8264.

CADIGAN, R. A. 1961. Geologic interpretation of grain-size distribution measurements of Colorado Plateau sedimentary rocks. *Journal of Geology*, 69, 121-142.

CARTER, T. G., LIU, P. L. F. and MEI, C. C. 1973. Mass transport by waves and offshore sand bedforms. *Journal of Waterways, Harbors and Coastal Engineering Division, American Society of Civil Engineers*, 99, 165-184.

CASTON, V. N. D. 1972. Linear sand banks in the Southern North Sea. *Sedimentology*, 18, 63-78.

CASTON, V. N. D. 1979. The Quaternary sediments of the North Sea. In : BANNER, F. T., COLLINS, M. B. and MASSIE, K. S. (Eds.), *The North-West European Shelf Seas : The Sea Bed and the Sea in Motion*. Elsevier, Amsterdam, 195-270.

CHAKRABARTI, A. 1977. Mass-spring-damper system as the mathematical model for the pattern of sand movement for an eroding beach around Digha, West Bengal, India. *Journal of Sedimentary Petrology*, 47, 311-330.

CHANG-SHU, Y. and SONG-JIA, S. 1988. Tidal sand ridges on the East China Sea Shelf. In : DE BOOER, P. L., VAN GELDER, A. and NIO, S. -D. (Eds.), *Tide-Influenced Sedimentary Environments and Facies*. D. Reidel Publishing Company, Dordrecht, 23-38.

CHANNON, R. D. and HAMILTON, D. 1976. Wave and tidal current sorting of shelf sediments southwest of England. *Sedimentology*, 23, 17-42.

CHAPELL, J. and ELLIOT, I. G. 1979. Surf-beach dynamics in time and space - an Australian case study , and elements of a predictive model. *Marine Geology*, 32, 231-250.

CHOWDHURI, K. R. and REINECK, H. -E. 1978. Primary sedimentary structures and their sequence in the shoreface of barrier island Wangerooge (North Sea). *Senckenbergiana maritima*, 10, 15-29.

CHRISS, T. M. and CALDWELL, D. R. 1982. Evidence for the influence of form drag on bottom layer flow. *Journal of Geophysical Research*, 87, 4184-4154.

CLARK, M. W. 1981. More skewed against skewing. In : NIO, S.-D SHÜTTENHELM, R. T. E. and VAN WEERING, Tj. C. E. (Eds.), *Holocene Marine Sedimentation in the North Sea Basin*. IAS Special Publication 5, Blackwell Scientific Publications, Oxford, 111-121.

CLIFTON, H. E. 1976. Wave-formed sedimentary structures - a conceptual model. In : DAVIS, R. A. and ETHINGTON, R. L. (Eds.), Beach and Nearshore Sedimentation. SEPM Special Publication 24, 126-148.

CLIFTON, H. E., HUNTER, R. E. and PHILLIPS, R. L. 1971. Depositional structures and processes in the non-barred high energy nearshore. Journal of Sedimentary Petrology, 41, 651-670.

CLOS-ARCEDEC, A. 1962. Etude sur les vues aeriennes, des alluvions littorales d'allure periodique, cordons littoraux et fostons. Bull. Soc. Fr. Photogramm, 4, 13-21.

COOK, D. O. 1970. The occurrence and geological work of rip currents off southern California. Marine Geology, 9, 173-186.

COOK, D. O. and GORSLINE, D. S. 1972. Field observations of sand transport by shoaling waves. Marine Geology, 13, 31-55.

CROMWELL, J. E. 1971. Barrier coast distribution : a world wide survey. 2nd National Coastal and Shallow Water Research Conference, Abstract, p. 50.

CRONAN, D. S. 1972. Skewness and kurtosis in polymodal sediments from the Irish Sea. Journal of Sedimentary Petrology, 42, 102-106.

CRONIN, L. E. 1975. (Ed.), Estuarine Research. Vol. 2. Geology and Engineering. Academic Press, Inc., New York, 587 pp.

CURRAY, J. R. 1960. Tracing sediment masses by grain-size modes. 21st Session International Geological Congress, Norden, p. 119-130.

DALLY, W. R. 1987. Longshore bar formation - surf beat or undertow ? In : KRAUS, N. C. (Ed.), Coastal Sediments '87. American Society of Civil Engineers, New York, p. 71-86.

DALRYMPLE, R. A. 1975. A mechanism for rip current generation on an open coast. Journal of Geophysical Research, 80, 3485-3487.

DALRYMPLE, R. A. and LOZANO, C.L. 1978. Wave-current interaction models for rip currents. Journal of Geophysical Research, 83, 6063-6071.

DAVIDSON-ARNOTT, R. G. D. and GREENWOOD, B. 1976. Facies relationships on a barred coast, Kouchibouguac Bay, New Brunswick, Canada. In : Davis; R. A. and Ethington, R. L. (Eds.), Beach and Nearshore Sedimentation. SEPM Special Publication 24, 149-168.

DAVIES, J. L. 1964. A morphogenetic approach to world shorelines. Zeitschrift für Morphologie, 8, 27-42.

DAVIS, R. A. and BALSAN, P. S. 1990. Comparison of tidal shelf sand ridges, southern Florida and the North Sea. 13th International Sedimentological Congress, Nottingham, U.K., Abstract Volume, p. 121-122.

DAVIS, R. A. and CLIFTON, H. E. 1987. Sea level change and the preservation potential of wave-dominated and tide-dominated coastal sequences. In: NUMMEDAL, D., PILKEY, O. H. and HOWARD, J. D. (Eds.), Sea-Level Fluctuation and Coastal Evolution. Society of Economic Paleontologists and Mineralogists Special Publication No 41, 167-178.

DAVIS, R. A. and FOX, W. T. 1981. Interaction between wave- and tide-generated processes at the mouth of a microtidal estuary, Matanzas River, Florida. Marine Geology, 40, 49-68.

DAVIS, R.A. and HAYES, M.O. 1984. What is a wave-dominated coast ? *Marine Geology*, 60, 313-329.

DEAN, R. G. 1973. Heuristic models of sand transport in the surf zone. *Proceedings, Conference on Engineering Dynamics in the Surf Zone, Sydney*, p. 208-214.

DEAN, R. G. and WALTON, T. L. 1975. Sediment transport in the vicinity of inlets with special reference to sand trapping. In: CRONIN, L. E. (Ed.), *Estuarine Research*. Academic Press, New York, 129-150.

DEMAREST, J. M. and LEATHERMAN, S. P. 1985. Mainland influence on coastal transgression: Delmarva Peninsula. In : OERTEL, G.F. and LEATHERMAN, S.P. (Eds.), *Barrier Islands*. *Marine Geology*, 63, 19-33.

DETTE, H. H. 1977. Ein Vorschlag zur Analyse eines Wellenklimas. *Die Küste*, 31, 166-180

DHYR-NIELSEN and SORENSEN, T. 1970. Sand transport phenomena on coasts with bars. *Proceedings, 12th International Conference on Coastal Engineering, American Society of Civil Engineers, New York*, p. 855-866.

DIAS, J. M. A. and NEAL, W. J. 1990. Modal size classification of sands : an example from the Northern Portugal Continental Shelf. *Journal of Sedimentary Petrology*, 60, 426-437.

DICKINSON, K.A., BERRYHILL, H. C. and HOLMES, C.W. 1972. Criteria for recognizing ancient barrier island coastlines. In : RIGBY, J.K. and HAMBIN, W.K. (Eds.), *Recognition of Ancient Sedimentary Environments*. Society of Economic Paleontologists and Mineralogists Special Publication No 16, 192-214.

DOEGLASS. D. J. 1946. Interpretation of the results of mechanical analysis. *Journal of Sedimentary Petrology* 16, 19-40

DOLAN, R. and HAYDEN, B. 1983. Patterns and prediction of shoreline change. In : KOMAR, P. D. (Ed.), Handbook of Coastal Processes and Erosion. CRC Press, Inc., Boca Raton, Florida. 123-149.

DOLAN, R., HAYDEN, B. and FELDER, W. 1979. Shoreline periodicities and edge waves. Journal of Geology, 87, 175-185.

DÖRJES, J. 1976. Primärgefüge, Bioturbation und Makrofauna als Indikatoren des Sandversatzes im Seegebiet vor Norderney (Nordsee). II. Zonierung und Verteilung der Makrofauna. Senckenbergiana maritima, 8, 171-188.

DUANE, D. B. 1964. Significance of skewness in recent sediments, Western Pamlico Sound, North Carolina. Journal of Sedimentary Petrology, 34, 867-874.

DUANE, D. B., FIELD, M. E., MEISBURGER, E. P., SWIFT, D. J. P. and WILLIAMS, S. J. 1972. Linear shoals on the Atlantic inner continental shelf, Florida to Long Island. In : SWIFT, D. J. P., DUANE, D. B. and PILKEY, O. H. (Eds.), Shelf Sediment Transport, Processes and Pattern. Dowden, Hutchinson and Ross, Inc., Stroudsburg, 447-498.

DYER, K. R. 1986. Coastal and Estuarine Sediment Dynamics. John Wiley and Sons, Chichester, 342 pp.

EHLERS, J. 1988. Morphodynamics of the Wadden Sea. A. A. Balkema, Rotterdam, 397 pp.

ELLIOT, T. 1978. Clastic shorelines. In : READING, H. G. (Ed.), Sedimentary Environments and Facies. Elsevier, New York, 143-177.

EVANS, D. V. 1988. Mechanisms for the generation of edge waves over a sloping beach. Journal of Fluid Mechanics, 186, 379-391.

FISHER, J. J. 1982. Barrier Islands. In : SCHWARTZ, M. L. (Ed.), The Encyclopedia of Beaches and Coastal Environments. Hutchinson Ross Publishing Company, Stroudsburg, 124-133.

FITZGERALD, D. M., PENLAND, S and NUMMEDAL, G. 1984. Control of barrier island shape by inlet sediment passing : East Frisian Islands, West Germany. Marine Geology, 60, 355-376.

FLEMMING, B. W. 1977. Depositional Processes in Saldanha Bay and Langebaan Lagoon. Professional Research Series No. 2, National Research Institute of Oceanology, CSIR, South Africa, 215 pp.

FLEMMING, B. W. 1988. Zur Klassifikation subaquatischer, strömungstransversaler Transportkörper. Bochumer geologische und geotechnische Arbeiten, 29, 44-47.

FLEMMING, B. W. 1990a. On the relationships between height, spacing and grain size in subaqueous, flow-transverse bedforms. 13th International Sedimentological Congress, Nottingham, U.K. Abstract Volume, p.170.

FLEMMING, B. W. 1990b. Zur holozäne Entwicklung, Morphodynamik und faziellen Gliederung der mesotidalen Düneninsel Spiekeroog (Südliche Nordsee). In : WILLEMS et al (Eds.), Beiträge zur Geologie und Paläontologie Norddeutschlands. Berichte Nr. 10, Fachbereich Geowissenschaften der Universität Bremen, 13-73.

FLEMMING, B. W. and ANTIA, E. E. 1989. Origin of the nearshore ridge and swale topography along the mesotidal barrier island coast of the southern North Sea. 2nd International Research Symposium on Clastic Tidal Deposits. Calgary, Canada. Abstract, 34-35.

FLEMMING, B. W. and ANTIA, E. E. 1990. Interaction between storm-induced resonance and nearshore morphodynamics along the Frisian barrier island coast, southern North Sea. 13th International Sedimentological Congress, Nottingham, U.K. Abstract Volume, p. 171.

FOLK, R. L. and WARD, W. C. 1957. Brazos River bar: a study in the significance of grain size parameters. *Journal of Sedimentary Petrology*, 27, 3-26.

FORTNUM, B. C. H. 1978. Waves recorded by M.V. Fatima in the Northern North Sea. Report No 59, Institute of Oceanographic Sciences, U.K. 10 pp.

FRIEDMAN, G. M. 1967. Dynamic processes and statistical parameters compared for size frequency distribution of beach and river sands. *Journal of Sedimentary Petrology*, 37, 327-354.

FÜHRBÖTER, A. 1974. Einige Ergebnisse aus Naturuntersuchungen in Bradungszonen. *Mitteilungen Leichtweiß-Institut*, Heft 40.

FULLER, A. O. 1961. Size distribution characteristics of shallow marine sands from the Cape of Good Hope, South Africa. *Journal of Sedimentary Petrology*, 31, 256-261.

GADOW, S. and REINECK, H. -E. 1969. Abländiger Sandtransport bei Sturmfluten. *Senckenbergiana maritima*, 1, 63-78.

GALVIN, C. J. 1967. Longshore current velocity: a review of theory and data. *Review of Geophysics*, 5, 287-304.

GALVIN, C. J. 1968. Breaker type classification on three laboratory beaches. *Journal of Geophysical Research*, 73, 3651-3659.

GIBBS, R. J. 1972. The accuracy of particle size analyses utilizing settling tubes. *Journal of Sedimentary Petrology*, 42, 141-145.

GIBBS, R. J., MATTHEWS, M. D. and LINK, D. A. 1971. The relationship between sphere size and settling velocity. *Journal of Sedimentary Petrology*, 41, 7-18.

GIENAPP, H. 1973. Stromungen während der Sturmflut vom 2. November 1965 in der Deutschen Bucht und ihre Bedeutung für den Sedimenttransport. *Senckenbergiana maritima*, 5, 135-151.

GIERLOFF-EMDEN, H. G. 1961. Nehrungen und Lagunen : Pettermans Geographische Mitteilungen, 105 (2), 81-92; 105 (3), 161-176.

GLAESER, J. D. 1978. Global distribution of barrier islands in terms of tectonic setting. *Journal of Geology*, 86, 283-297.

GLENN, S. M. and GRANT, W. D. 1987. A suspended sediment stratification correction for a combined wave and current flows. *Journal of Geophysical Research*, 92, 8244-8264.

GOLDSMITH, V., BOWMAN, D. and KILEY, K. 1982. Sequential stage development of crescentic bars: Hahoterim Beach, southeastern Mediterranean. *Journal of Sedimentary Petrology*, 52, 233-249.

GORDON, C. M. 1974. Intermittent momentum transport in a geophysical boundary layer. *Nature*, 248, 392-394.

GRANT, W. D. and MADSEN, O. S. 1979. Combined wave and current interaction with a rough bottom. *Journal of Geophysical Research*, 84, 1979-1808.

GREENSPAN, H. P. 1956. The generation of edge waves by moving pressure distribution. *Journal of Fluid Mechanics*, 1, 574-592.

GREENWOOD, B. 1978. Spatial variability of texture over a beach-dune complex, North Devon, England. *Sedimentary Geology*, 21, 27-44.

GREENWOOD, B. and DAVIDSON-ARNOTT, R. G. D. 1975. Marine bars and nearshore sedimentary processes, Kouchibouguac Bay, New Brunswick. In : HAILS, J. and CARR, A. (Eds.), *Nearshore Sediment Dynamics and Sedimentation*. John Wiley and Sons, London, 123-150.

GREENWOOD, B. and DAVIDSON-ARNOTT, R. G. D. 1979. Sedimentation and equilibrium in wave-formed bars: a review and case study. *Canadian Journal of Earth Sciences*, 16, 312-332.

GREENWOOD, B. and MITTLER, P. R. 1985. Vertical sequence and lateral transitions in facies of a barred nearshore environment. *Journal of Sedimentary Petrology*, 55, 366-375.

GREENWOOD, B. and SHERMAN, D. J. 1984. Waves, currents, sediment flux and morphological response in a barred nearshore system. *Marine Geology*, 60, 31-61.

GROSS, T. F. and NOWELL, A. R. M. 1983. Mean flow and turbulence scaling in a tidal boundary layer. *Continental Shelf Research*, 2, 109-126.

GUST, G. and SOUTHARD, J. B. 1983. Effects of weak bed load on the universal law of the wall. *Journal of Geophysical Research*, 88, 5939-5952.

GUZA, R. T. and DAVIS, R. E. 1974. Excitation of edge waves by waves incident on a beach. *Journal of Geophysical Research*, 79, 1285-1291.

GUZA, R. T. and INMAN, D. L. 1975. Edge waves and beach cusps. *Journal of Geophysical Research*, 80, 2997-3012.

GUZA, R. T. and THORNTON, E. B. 1978. Variability of longshore currents. *Proceedings, 16th Conference on Coastal Engineering. American Society of Civil Engineers, New York*, p. 756-775.

GUZA, R. T. and THORNTON, E. B. 1985. Observations of surf beat. *Journal of Geophysical Research*, 90, 3161-3172.

GUZA, R. T. and THORNTON, E. B. 1989. Run-up and surf beat. In: SEYMOUR, R. J. (Ed.), *Nearshore Sediment Transport*. Plenum Press, New York, 173-181.

HALL, M. J., NADEAU, J. E. and NICOLICH, M. J. 1987. Sediment transport from Delaware Bay to the New Jersey inner shelf. *Journal of Coastal Research*, 3, 469-474.

HAMBLIN, A. P., DUKE, W. L. and WALKER, R. G. 1979. Hummocky cross stratification - indicator of storm-dominated shallow-marine environments. *American Association of Petroleum Geologists*, 63, 460-461.

HAMILTON, D., SOMMERVILLE, J. H. and STANFORD, P. N. 1980. Bottom currents and shelf sediments, southwest of Britain. *Sedimentary Geology*, 26, 115-138.

HAYDEN, B., DOLAN, R. and FELDER, W. 1979. Spatial and temporal analysis of shoreline variations. *Coastal Engineering*, 2, 351-361.

HAYES, M. O. 1967. Hurricanes as geologic agents, South Texas coast. *American Association of Petroleum Geologists Bulletin*, 51, 937-956.

HAYES, M. O. 1975. Morphology of sand accumulations in estuaries: an introduction to the symposium. In : CRONIN, L. E. (Ed.), *Estuarine Research*, Vol. 2. Academic Press, New York, 3-22.

HAYES, M. O. 1979. Barrier island morphology as a function of tidal and wave regime. In : LEATHERMAN, S. P. (Ed.), *Barrier Islands*. Academic Press, New York, 1-27.

HEATHERSHAW, A. D. 1974. 'Bursting' phenomena in the sea. *Nature*, 248, 394-395.

HINE, A. C. and SNYDER, S.W. 1985. Coastal lithosome preservation : Evidence from the shoreface and continental shelf off Bogue Banks, North Carolina. In : OERTEL, G. F. and LEATHERMAN, S. P (Eds.), Barrier Islands. Marine Geology, 63, 307-330.

HOBDAV, D. K. and READING, H. G. 1972. Fair weather versus storm processes in shallow marine sand bar sequences in Late Precambrian of Finnmark, north Norway. Journal of Sedimentary Petrology, 42, 318-324.

HOLLIGAN, P. M., AARUP, T. and GROOM, S. B. 1989. The North Sea satellite colour atlas. Continental Shelf Research, 9, 665-765.

HOLMAN, R. A. 1981. Infragravity energy in the surf zone. Journal of Geophysical Research, 86, 6442-6450.

HOLMAN, R. A. and BOWEN, A. J. 1984. Longshore structure of infragravity wave motions. Journal of Geophysical Research, 89, 6446-6452.

HOLMAN, R. A. and BOWEN, D. J. 1982. Bars, bumps and holes: Models for the generation of complex beach topography. Journal of Geophysical Research, 87, 457-468.

HOMEIER, H. and LUCK. G. 1978. Strandveränderungen und Dünenabbrüche im Nordwestern der Insel Spiekeroog. Jahresbericht, Forschungsstelle für Insel- und Küstenschutz, Norderney, 29, 127-147.

HOOGENDOORN, E. L. and DALYRMPLE, R. W. 1986. Morphology, lateral migration, and internal structures of shoreface-connected ridges. Sable Island Bank, Nova Scotia, Canada. Geology, 14, 400-403.

HOUBOLT, J. J. H. C. 1968. Recent sediments in the Southern Bight of the North Sea. Geologie en Mjnbouw, 47, 245-273.

HOWARD, J. D. and REINECK, H. -E. 1972. Georgia coastal region, Sapelo Island, U.S.A. - sedimentology and biology, IV: physical and biogenic sedimentary structures of the nearshore shelf. *Senckenbergiana maritima* 4, 81-123.

HOWARD, J. D. and REINECK, H. -E. 1981. Depositional facies of high energy beach to offshore sequence: comparison with low energy sequence. *American Association of Petroleum Geologists Bulletin*, 65, 807-830.

HOWD, P. A., BOWEN, A. J. and HOLMAN, R. A. 1992. Edge waves in the presence of strong longshore currents. *Journal of Geophysical Research*, 97, 11357-11371

HUNTLEY, D. A. 1976. Long period wave motion on a natural beach. *Journal of Geophysical Research*, 81, 6441-6449.

HUNTLEY, D. A. 1980. Edge waves in a crescentic bar system. In : McCANN, S. B. (Ed.), *The coastline of Canada*. Geological Survey of Canada, Paper 80-10, 111-121.

HUNTLEY, D. A. and BOWEN, A. J. 1973. Field observations of edge waves. *Nature*, 243, 160-162.

HUNTLEY, D. A. and BOWEN, A. J. 1975. Field comparisons of edge waves and their effect on beach material. *Journal of Geological Society of London*, 131, 69-81.

HUNTLEY, D. A., GUZA, R. T. and BOWEN, A. J. 1977. A universal form for shoreline run-up spectra? *Journal of Geophysical Research*, 82, 2577-2581.

HUNTLEY, D. A., GUZA, R. T. and THORNTON, E. B. 1981. Field observations of surf beat, 1, progressive edge waves. *Journal of Geophysical Research*, 83, 1913-1920.

HUTHNANCE, J. M. 1981. On one mechanism forming linear sand banks. *Estuarine, Coastal Shelf Science*, 14, 79-99.

INMAN, D. L. and NORDSTROM, C. E. 1971. On the tectonic and morphologic classifications of coasts. *Journal of Geology*, 79, 1-21.

INMAN, D. L. and GUZA, R. T. 1982. The origin of swash cusps on beaches. *Marine Geology*, 49, 133-148.

JAGO, C. F. 1980. Contemporary accumulation of marine sand in a macrotidal estuary, southwest Wales. *Sedimentary Geology*, 26, 21-49.

JAGO, C. F. 1981. Sediment response to waves and currents, North Yorkshire Shelf, North Sea. In : NIO, S.-D, SHÜTTENHELM, R.T.E. and VAN WEERING, Tj. C. E. (Eds.), *Holocene Marine Sedimentation in the North Sea Basin*. IAS Special Publication 5, 283-301.

JAGO, C. F. and HARDISTY, J. 1984. Sedimentology and morphodynamics of a macrotidal beach, Pendine Sands, SW Wales. *Marine Geology*, 60, 123-154.

JOHNSON, H. D. 1978. Shallow siliciclastic seas. In : READING, H. G. (Ed.), *Sedimentary Environments and Facies*. Blackwell Scientific Publications, Oxford, 557 pp.

JONES, T. A. 1969. Skewness and kurtosis as criteria of normality in observed frequency distributions. *Journal of Sedimentary Petrology*, 39, 1622-1627.

KATOH, K. 1981. Analysis of edge waves by means of empirical eigenfunctions. *Report Port Harbour Institute, Japan*, 20, 3-51.

KING, C. A. M. 1959. *Beaches and Coasts*. Edward Arnold Publishers Ltd., London, 403 pp.

KLEIN, G. De V. 1970. Depositional and dispersal dynamics of intertidal sand bars. *Journal of Sedimentary Petrology*, 40, 1095-1125.

KLOVAN, J. E. 1966. The use of factor analysis in determining the depositional environments from grain size distributions. *Journal of Sedimentary Petrology*, 36, 115-125.

KOCH, M and NIEMEYER, H. D. 1978. Sturmtiden-Strommessungen im Bereich des Norderneyer Seegats. *Jahresbericht, Forschungsstelle für Insel- und Küstenschutz, Norderney*, 29, 91-108.

KOMAR, P. D. 1971. Nearshore cell circulation and the formation of giant cusps. *Geological Society of America Bulletin*, 82, 2643-2650.

KOMAR, P. D., NEUDECK, R. H. and KULM, L. D. 1972. Observations and significance of deep-water oscillatory ripple marks on the Oregon Continental Shelf. In : SWIFT, D. J. P., DUANE, D. B. and PILKEY, O. H. (Eds.), *Shelf Sediment Transport, Process and Pattern*. Dowden, Hutchinson and Ross, Inc., Stroudsburg, 601-619.

KOMAR, P. D. 1974. Oscillatory ripple marks and the evaluation of ancient wave conditions and environments. *Journal of Sedimentary Petrology*, 44, 169-180.

KOMAR. P. D. 1976. *Beach Processes and Sedimentation*. Prentice-Hall, New Jersey, 429 pp.

KOMAR. P. D. and CUI, B. 1984. The analyses of grain-size measurements by sieving and settling-tube techniques. *Journal of Sedimentary Petrology*, 54, 603-614.

KOMAR, P. D. and HOLMAN, R. A. 1986. Coastal processes and the development of shoreline erosion. *Annual Review Earth and Planetary Science*, 14, 237-265.

KREISA, R. D. 1981. Storm-generated sedimentary structures in subtidal marine facies with examples from the middle and upper Ordovician of southwestern Virginia. *Journal of Sedimentary Petrology*, 51, 823-848.

KUMAR, N and SANDERS, J. E. 1976. Characteristics of shoreface storm deposits: modern and ancient examples. *Journal of Sedimentary Petrology*, 46, 145-162.

LAU, J. and TRAVIS, B. 1973. Slowly varying Stokes waves and submarine longshore bars. *Journal of Geophysical Research*, 78, 4489-4497.

LAVELLE, J. W. and SWIFT, D. J. P. 1982. Near-shore currents measured in ridge-and-swale topography off Long island, New York. *Journal of Geophysical Research*, 87, 4190-4194.

LAVELLE, J. W., SWIFT, D. J. P., GADD, P. E., STUBBLEFIELD, W. L., CASE, F. N., BRASHEAR, H. R. and HAFF, K. W. 1978a. Fair weather and storm transport on the Long Island, New York, inner shelf. *Sedimentology*, 25, 823-842.

LAVELLE, J. W., YOUNG, R. A., SWIFT, D. J. P. and CLARK, T. L. 1978b. Near-bottom sediment concentration and fluid velocity measurements on the inner continental shelf, New York. *Journal of Geophysical Research*, 83, 6052-6062.

LEATHERMAN, S. P. 1976. Barrier island dynamics : overwash processes and eolian transport. *Proceedings, 15th Coastal Engineering Conference, Honolulu, American Society of Civil Engineers, New York, p. 1958-1974.*

LEE, A. J. 1980. North Sea : Physical oceanography. In : BANNER, F. T. , COLLINS, M. B. and MASSIE, K. S. (Eds.), The North-west European Shelf Seas : The Sea bed and The Sea in Motion. Elsevier, Amsterdam, 467-493.

LEONT`YEV, O. K. and NIKIFOROV, L. G. 1965. Reasons for the world-wide occurrence of barrier beaches. *Oceanology*, 5, 61-67.

LIU, J. T. and ZARILLO, G. A. 1987. Partitioning of shoreface sediment grain-sizes. In : KRAUS, N. C. (Ed.) Coastal Sediments '87. American Society of Civil Engineers, New York, p. 1533-1548.

LIU, J. T. and ZARILLO, G. A. 1990. Shoreface dynamics : Evidence from bathymetry and surficial sediments. *Marine Geology*, 94, 37-53.

LONGUET-HIGGINS, M. S. 1972. Recent progress in the study of longshore currents. In : MEYER, R. E. (Ed.), Waves on Beaches and Resulting Sediment Transport. Academic Press, New York, 203-248.

LUCK, G. 1976. Protection of the littoral and seabed against erosion - Fallstudie Norderney. *Forschungstelle Norderney, Jahresbericht 1975, Band 27*, 9-78.

LUCK, G. and NIEMEYER, H. D. 1976. Seegangsmessungen im Bereich der ostfriesischen Inseln und Watten. *Meerestechnik*, Nr. 4, Band 7.

LÜDERS, K. 1968. Sediments of the North Sea. In : TRASK, P. D. (Ed.) , Recent Marine Sediments. Dover Publications, Inc., New York, 232-342.

LUDWICK, J. C. 1978. Coastal currents and bottom sediment transport off Virginia Beach, Virginia. *Journal of Geophysical Research*, 83, 2365-2372.

LUDWIG, G., MÜLLER, H. and STREIF, H. 1981. New dates on Holocene sea-level changes in German Bight. In : NIO, S. -D, SHÜTTENHELM and VAN WEERING, Tj. C. E. (Eds.), Holocene Marine Sedimentation in the North Sea Basin. IAS Special Publication 5, 211-219.

LYNE, V. D., BUTMAN, B. and GRANT, W. D. 1990. Sediment movement along the U.S. east coast continental shelf - I. Estimates of bottom stress using the Grant-Madsen model and near-bottom wave and current measurements. Continental Shelf Research, 10, 397-428.

LYNE, V. D., BUTMAN, B. and GRANT, W. D. 1990. Sediment movement along the U.S. east coast continental shelf - II. Modelling suspended sediment concentration and transport rate during storms. Continental Shelf Research, 10, 429-460.

MADSEN, O. S. 1976. Wave climate of the continental margin : elements of its mathematical description. In : STANLEY, D. J. and SWIFT, D. J. P. (Eds.), Marine Sediment Transport and Environmental Management. John Wiley and Sons, New York, 65-87.

MARTINS, L. R. 1965. Significance of skewness and kurtosis in environmental interpretation. Journal of Sedimentary Petrology, 35, 768-770.

McKINNEY, T. F. and FRIEDMAN, G. F. 1970. Continental shelf sediments of Long Island, New York. Journal of Sedimentary Petrology, 40, 213-248.

McLAREN, P. 1981. An interpretation of trends in grain size measures. Journal of Sedimentary Petrology, 51, 611-624.

McLAREN, P. and BOWLES, D. 1985. The effects of sediment transport on grain-size distributions. Journal of Sedimentary Petrology, 55, 457-470.

McLEAN, S. R and SMITH, D. J. 1979. Turbulence measurements in the boundary layer over a sand wave field. *Journal of Geophysical Research*, 84, 7791-7808.

MIDDLETON, G. V. 1976. Hydraulic interpretation of sand size distributions. *Journal of Geology*, 84, 405-426.

MIDDLETON, J. H., CAHIL, M. L. and HSIEH, W. W. 1987. Edge waves on the Sydney (Australia) coast. *Journal of Geophysical Research*, 92, 9487-9493.

MILLER, R. L. 1976. Role of vortices in surf zone prediction : sedimentation and wave forces. In : DAVIS, R. A. and ETHINGTON, R. L. (Eds.), *Beach and Nearshore Sedimentation*. SEPM Special Publication 24, 92-114.

MORTON, R. A. 1979. Subaerial storm deposits formed on barrier flats by wind-driven currents. *Sedimentary Geology*, 24, 105-122.

MORTON, R. A. 1981. Formation of storm deposits by wind-forced currents in the Gulf of Mexico and the North Sea. In : NIO, S.-D, SHÜTTENHELM, R.T.E. and VAN WEERING, Tj. C. E. (Eds.), *Holocene Marine Sedimentation in the North Sea Basin*. IAS Special Publication 5, 385-397.

MOSS. A. J. 1963. The physical nature of common sandy and pebbly deposits, 2. *American Journal of Science*, 261, 297-343.

MOTHERSILL, J. S. 1969. A grain size analysis of longshore-bars and troughs, Lake Superior, Ontario. *Journal of Sedimentary Petrology*, 39, 1317-1324.

MURRAY, S. P. 1970. Bottom currents near the coast during hurricane Camille. *Journal of Geophysical Research*, 75, 4579-4582.

MYROW, P. M. 1992. Bypass-zone tempestite facies model and proximity trends for an ancient muddy shoreline and shelf. *Journal of Sedimentology*, 62, 99-115.

NECE, R. E. and SMITH, J. D. 1970. Boundary shear stress in rivers and estuaries. *Journal of Waterways and Harbour Division, American Society of Civil Engineers*, 96, 335-358.

NEUMANN, H. 1966. Die Beziehung zwischen Wind und Oberflächenströmung auf Grund von Triftkartenuntersuchungen. *Deutsche Hydrographische Zeitschrift*, Jahrgang 19, Heft 6, 253-266.

NEUMANN, H. and MEIER, C. 1964. Die Oberflächenströme in der Deutschen Bucht. *Deutsche Hydrographische Zeitschrift*, Jahrgang 17, Heft 1, 1-40.

NIEDORODA, A. W. 1973. Sand bars along low energy beaches. Part 2: Transverse bars. In: COATES, D. R. (Ed.), *Coastal Geomorphology*. Allen and Unwin Ltd., London, 103-113.

NIEDORODA, A. W. and SWIFT, D. J. P. 1981. Maintenance of the shoreface by wave orbital currents and mean flow: observations from the Long Island coast. *Geophysical Research Letters*, 8, 337-348.

NIEDORODA, A. W., SWIFT, D. J. P., FIGUEIRODO, A. G. and FREELAND, G. L. 1985. Barrier island evolution, middle Atlantic shelf, U.S.A. Part II : Evidence from the shelf floor. In : OERTEL, G. F. and LEATHERMAN, S. P. (Eds.), *Barrier Islands*. *Marine Geology*, 63, 363-396.

NIEDORODA, A. W., SWIFT, D. J. P. and HOPKINS, T. S. 1985. The shoreface. In : Davis, R. A. (Ed.), Coastal Sedimentary Environments (2nd Edition). Springer-Verlag, New York, 716 pp.

NIEDORODA, A. W., SWIFT, D.J. P., HOPKINS, T. S. and MA, C. M. 1984. Shoreface morphodynamics on wave-dominated coasts. Marine Geology, 60, 331-354.

NIEMEYER, H. D. 1976. Der Verlauf der Sturmtiden vom Januar 1976 im Bereich der Ostfriesischen Inseln. Forschungsstelle Norderney, Jahresbericht 1975, Band 27, 79-106.

NIEMEYER, H. D. 1979 Untersuchungen zum Seegangsklima im Bereich der ostfriesischen Inseln und Küste. Die Küste, 34, 53-70

NUMMEDAL, D. and SNEDDEN, J. W. 1987. Sediment exchange between the shoreface and the continental shelf - evidence from the modern Texas coast and the rock record. In : KRAUS, N. C. (Ed.), Coastal Sediments '87. American Society of Civil Engineers, New York, p. 2110-2125.

OERTEL, G. F. 1977. Geomorphic cycles in ebb deltas and related patterns of shore erosion and accretion. Journal of Sedimentary Petrology, 47, 1121-1131.

OERTEL, G. F. 1985. The barrier island system. In : OERTEL, G. F. and LEATHERMAN, S. P. (Eds.), Barrier Islands. Marine Geology, 63, 1-18.

OERTEL, G.F. 1988. Processes of sediment exchange between tidal inlets, ebb deltas and barrier islands. In : AUBREY, D. G. and WEISHAR, L. (Eds.), Hydrodynamics and Sediment Dynamics of Tidal Inlets. Springer Verlag, New York, 297-318.

OERTEL, G. F. and HOWARD, J. D. 1972. Water circulation and sedimentation at estuary entrances on the Georgia coast. In : SWIFT, D. J. P., DUANE, D. B. and PILKEY, O. H. (Eds.), Shelf Sediment Transport, Process and Pattern. Dowden, Hutchinson and Ross, Stroudsburg, 411-427.

OFF, T. 1963. Rhythmic linear sand bodies caused by tidal currents. American Association of Petroleum Geologists Bulletin, 85, 1319-1328.

OPEN UNIVERSITY, 1989. Waves, Tides, and Shallow-Water Processes. Pergamon Press, Oxford, 187 pp.

ORFORD, J. D and CARTER, R. W. G. 1984. Mechanisms to account for the longshore spacing of overwash throats on a coarse clastic barrier in southeast Ireland. Marine Geology, 56, 207-226.

OTHMAN-SHAY, J and GUZA, R. T. 1987. Infragravity edge wave observations on two California Beaches. Journal of Physical Oceanography, 17, 644-663.

ÖZSOY, E. 1986. Ebb-tidal jets : A model of suspended sediment and mass transport at tidal inlets. Estuarine, Coastal and Shelf Science, 22, 45-62.

PARKER, G., LANFREDI, N. W. and SWIFT, D. J. P. 1982. Seafloor response to flow in a southern hemisphere sand-ridge field: Argentine Inner Shelf. Sedimentary Geology, 33, 195-216.

PASSEGA, R. 1957. Texture as characteristic of clastic deposition. American Association of Geologists Bulletin, 41, 1952-1984.

PASSEGA, R. 1964. Grain size representation by CM patterns as a geological tool. Journal of Sedimentary Petrology, 34, 830-874.

POSTMA, H. 1982. (Ed.), Hydrography of the Wadden Sea: Movements and properties of water and particulate matter. Report 2 of the Wadden Sea Working Group. A. A. Balkema, Rotterdam, 75 pp.

REED, W. E., LE FEVER, R. and MOIR, G. J. 1975. Depositional environment interpretation from settling velocity ( $\Psi$ ) distributions. Bulletin Geological Society of America, 86, 1321-1328.

REINECK, H. -E. 1958. Kastengreifer und Lotröhre " Schnepfe", Geräte zur Entnahme ungestörter, orientierter Meeresgrundproben. Senckenbergiana lethae, 39, 42-48, 54-56.

REINECK, H. -E. 1963. Sedimentgefüge im Bereich der südlichen Nordsee. Abhandlungen Senckenbergischen Naturforschende Gessellschaft, Frankfurt am M, 505, 138 pp.

REINECK, H. -E. 1976. Primäregefüge, Bioturbation und Makrofauna als Indikatoren des Sandversatzes im Seegebiet vor Norderney (Nordsee). I. Zonierung von Primärgefügen und Bioturbation. Senckenbergiana maritima, 8, 155-169.

REINECK, H. -E. and SINGH, I. B. 1972. Genesis of laminated sand and graded rhythmites in storm sand layers of shelf mud. Sedimentology, 18, 123-128.

REYNOLDS, W. J. 1988. Ebb-tidal delta dynamics for a tide-dominated barrier island. In : AUBREY, D. G. and WEISHAR, L. (Eds.), Hydrodynamics and Sediment Dynamics of Tidal Inlets. Springer-Verlag, New York, 348-363.

ROELVINK, J. A. and STIVE, M. J. F. 1989. Bar-generating cross-shore flow mechanisms on a beach. Journal of Geophysical Research, 94, 4785-4800.

ROYSE, C. F. Recognition of fluvial environments by particle-size characteristics. *Journal of Sedimentary Petrology*, 38, 1171-1178.

RUBIN, D. M. and McCULLOCH, D. S. 1980. Single and superimposed bedforms: a synthesis of San Francisco Bay and flume observations. *Sedimentary Geology*, 26, 207-231.

SAGOE, K. O. and VISHER, G. S. 1977. Population breaks in grain-size distributions of sand - a theoretical model. *Journal of Sedimentary Petrology*, 47, 285-310.

SAHU, B. K. 1964. Depositional mechanisms from the size analysis of clastic sediments. *Journal of Sedimentary Petrology*, 34, 73-83.

SALLENGER, A. H., HOLMAN, R. A. and BIRKEMEIER, W. A. 1985. Storm-induced response of a nearshore-bar system. *Marine Geology*. 64, 237-257.

SANFORD, R. B. and SWIFT, D. J. P. 1971. Comparison of sieving and settling techniques for size analysis, using a Benthos rapid sediment analyzer. *Sedimentology*, 17, 257-264.

SCHUBERT, H. 1990. Entstehung, Vorkommen und Nutzung sublitoraler Schillanreicherungen im Gebiet um Spiekeroog. Beiträge zur Meerestechnik Nr. 12, Technische Universität Clausthal-Zellerfeld, 190 pp.

SCHWING, F. B., KJERFVE, B. J. and SNEED, J. E. 1983. Nearshore currents on the South Carolina continental shelf. *Journal of Geophysical Research*, 88, 4719-4729.

SCOTT, J. T. and CSANADY, G. T. 1976. Nearshore currents off Long Island. *Journal of Geophysical Research*, 81, 5401-5409.

SENGUPTA, S, and VEENSTRA, H. J. 1968. On sieving and settling techniques for sand analysis. *Sedimentology*, 11, 83-98.

SHA, L.P. 1990. Sedimentological studies of the ebb-tidal deltas along the West Frisian Islands, The Netherlands. *Geologica Ultraiectina*, 64, Rijksuniversiteit te Utrecht, 159 pp.

SHEPARD, F. P. 1950. Longshore bars and longshore troughs. Beach Erosion Board. Technical Memo 15, 32 pp.

SHI, N. C. and LARSEN, L. H. 1984. Reverse sediment transport induced by amplitude-modulated waves. *Marine Geology*, 54, 181-200.

SHIPP, R. C. 1984. Bedforms and depositional sedimentary structures of a barred nearshore system, eastern Long Island, New York. *Marine Geology*, 60, 235-259.

SHORT, A. D. 1975. Multiple offshore bars and standing waves. *Journal of Geophysical Research*, 80, 3838-3840.

SHORT, A. D. 1978. Wave power and beach stages: a global model. *Proceedings, 16th Conference on Coastal Engineering, Hamburg. American Society of Civil Engineers, New York*, p. 1145-1162.

SHORT, A. D. 1979. Three dimensional beach stage model. *Journal of Geology*, 87, 553-571.

SHORT, A. D. 1980. Beach response to variations in breaker height. *Proceedings, 17th International Conference on Coastal Engineering, Sydney*, p. 1016-1035.

SHORT, A. D. 1984. Beach and nearshore sand facies: southeast Australia. *Marine Geology*, 60, 261-282.

SHORT, A. D. 1985. Rip-current type, spacing and persistence, Narrabeen Beach. *Marine Geology*, 65, 47-71.

SHORT, A. D. and HESP, P. A. 1982. Wave, beach and dune interactions in southeastern Australia. *Marine Geology*, 48, 259-284.

SINDOWSKI, K. -H. 1970. Das Quartär im Untergrund der Deutschen Bucht (Nordsee). *Eiszeitalter und Gegenwart* 21, 33-46.

SINDOWSKI, K. -H. 1973. Das ostfriesische Küstengebiet - Inseln, Watten und Marshen. *Sammlung geologischer Führer* 57. Gebrüder Borntraeger, Berlin, 162 pp.

SINDOWSKI, K. H. 1957. Die synoptische Methode des des Kornkuven-Vergleiches zur Ausdeutung fossilee Sedimentationsräume. *Geologisches Jahrbuch*, 73, 237-275.

SMITH, J. D. 1970. Stability of a sand bed subjected to a shear flow of low froude number. *Journal of Geophysical Research* 30, 5928-5940.

SMITH, J. D. and McLEAN, S. R. 1977. Spatially averaged flow over a wavy surface. *Journal of Geophysical Research*, 82, 1735-1746.

SONNENFIELD, D. L. and NUMMEDAL, D. 1987. Morphodynamics and sediment dispersal of a tideless surf zone. In : KRAUS, N. C. (Ed.), *Coastal Sediments '87*. American Society of Civil Engineers, New York, p. 1938-1949.

SONU, C. J. 1972. Comments on paper by A. J. Bowen and D. L. Inman, "Edge wave and crescentic bars". *Journal of Geophysical Research*, 77, 6629-6631.

SONU, C. J. 1973. Three-dimensional beach changes. *Journal of Geology*, 81, 42-64.

SONU, C. J. and VAN BEEK, J. L. 1971. Systematic beach changes on the Outer Banks, North Carolina. *Journal of Geology*, 79, 416-425.

SPENCER, D. W. 1963. The interpretation of grain size distribution curve of clastic sediments. *Journal of Sedimentary Petrology*, 33, 180-190.

STAHL, L., KOCZAN, J. and SWIFT, D. J. P. 1974. Anatomy of a shoreface connected ridge system on the New Jersey Shelf: implications for the genesis of the shelf surficial sand sheet. *Geology*, 2, 117-120.

STAPOR, F. W. and TANNER, W. F. 1975. Hydrodynamic implications of beach, beach ridge and dune grain size studies. *Journal of Sedimentary Petrology*, 45, 926-931.

STIVE, M. J. F. and WIND, H. G. 1986. Cross-shore mean flow in the surf zone. *Coastal Engineering*, 10, 325-340.

STREIF, H. 1989. Barrier islands, tidal flats, and coastal marshes resulting from a relative rise of sea level in East Frisia on the German North Sea coast. *Proceedings, KNGMG Symposium on Coastal Lowlands, Geology and Geotechnology, The Hague*, p. 213-223.

STREIF, H. 1990. *Das ostfriesische Küstengebiet. Sammlung Geologischer Führer 57. Gebrüder Borntraeger, Berlin, 376 pp.*

STREIF, H. and KÖSTER, R. 1978. Zur Geologie der deutschen Nordseeküste. *Die Küste*, 32, 30-49.

STUBBLEFIELD, W. L. and SWIFT, D. J. P. 1976. Ridge development as revealed by sub-bottom profiles on the central New Jersey Shelf. *Marine Geology*, 20, 315-334.

STUBBLEFIELD, W. L. and SWIFT, D.J.P. 1981. Grain size variation across sand ridges, New Jersey continental shelf. *Geo-Marine Letters*, 1, 45-48.

STUBBLEFIELD, W. L., LAVALLE, W. J., SWIFT, D. J. P. and MCKINNEY, T. F. 1975. Sediment response to the present hydraulic regime on the central New Jersey Shelf. *Journal of Sedimentary Petrology*, 45, 337-358.

SUHAYDA, J. N. 1974. Standing waves on beaches. *Journal of Geophysical Research*, 79, 3065-3071.

SUNAMURA, T. and HORIKAWA, K. 1974. Two dimensional transformation due to waves. *Proceedings, 14th International Coastal Engineering Conference, Copenhagen, American Society of Civil Engineers, New York*, p. 920-938.

SUTER, J. R. and PENLAND, S. 1987. Evolution of Cat Island Pass, Louisiana. In : Kraus, N.C. (Ed.), *Coastal Sediments '87*, American Society of Coastal Engineers, New York, p. 2078-2093.

SVENDSEN, I. A. 1984. Mass flux and undertow in a surf zone. *Coastal Engineering*, 8, 347-365.

SVENDSEN, I. A., SCHÄFFER, H. A. and HANSEN, J. B. 1987. The interaction between the undertow and the boundary layer flow on a beach. *Journal of Geophysical Research*, 92, 11845-11856.

SWIFT, D. J. P. 1975a. Barrier island genesis : evidence from the central Atlantic shelf, eastern U.S.A. *Sedimentary Geology*, 14, 1-43.

SWIFT, D. J. P. 1975b Tidal sand ridges and shoal-retreat massifs. *Marine Geology*, 18, 105-134.

SWIFT, D.J. P. 1976. Coastal sedimentation. In: STANLEY, D. J., SWIFT, D. J. P. (Eds.), Marine Sediment Transport and Environmental Management. John Wiley and Sons, New York, 225-310.

SWIFT, D. J. P. and FIELD, M. E. 1981. Evolution of a classic ridge field, Maryland Sector, North American Inner Shelf. *sedimentology*, 28, 461-482.

SWIFT, D. J. P., DUANE, D. B. and MCKINNEY, T. F. 1973. Ridge and swale topography of the Middle Atlantic Bight, North America : secular response to the Holocene hydraulic regime. *Marine Geology*, 15, 227-247.

SWIFT, D. J. P., KOFOED, J. W., SAULSBURY, F. P. and SEARS, P. 1972a. Holocene evolution of the shelf surface, central and southern shelf of North America. In : SWIFT, D. J. P., DUANE, D. B., and Pilkey, O. H. (Eds.), Shelf Sediment Transport Process and Pattern. Dowden Hutchinson and Ross, Inc., Strousburg, 499-574.

SWIFT, D. J. P., LUDWICK, J. C. and BOEHMER, W. R. 1972b. Shelf sediment transport: A probability model. In : SWIFT, D. J. P., DUANE, D. B. and PILKEY, O. H. (Eds), Shelf Sediment Transport : Processes and Patterns. Dowden, Hutchinson and Ross, Inc., Stroudsburg, 195-223.

SWIFT, D. J. P., NIEDORODA, A. W., VINCENT, C. E. and HOPKINS, T. S. 1985. Barrier island evolution, middle Atlantic Shelf, U.S.A. Part I : Shoreface dynamics. In : OERTEL, G. F. and LEATHERMAN, S. P. (Eds.), Barrier Islands. *Marine Geology*, 63, 331-361.

SWIFT, D. J. P., PARKER, G., LANFREDI, N. W., PERILLO, G. and FIGGE, K. 1978. Shoreface-connected sand ridges on American and European shelves: a comparison. *Estuarine, Coastal Marine Research*, 7, 257-273.

SWIFT, D. J. P., THORNE, J. A. and OERTEL, G. F. 1986. Fluid processes and sea-floor response on a modern storm-dominated shelf : Middle Atlantic shelf of North America. Part II: Response of the shelf floor. In: KNIGHT, R. J. and MCLEAN, J. R. (Eds.), Shelf Sands and Sandstones. Canadian Society of Petroleum Geologists, Memoir 11, 191-211.

SWIFT, D.J. P., HOLLIDAY, B., AVIGNONE, N. and SHIDELER, G. 1972b. Anatomy of a shoreface ridge system, False Cape, Virginia. *Marine Geology* 12, 59-84.

SYMONDS, G., HUNTLEY, D. A. and BOWEN, A. J. 1982. Two dimensional surf beat : long wave generation by a time-varying breakpoint. *Journal of Geophysical Research*, 87, 492-498.

TALBOT, M. M. B. and BATE, G. C. 1987. Distribution patterns of rip frequency and intensity in Algoa Bay, South Africa. *Marine Geology*, 76, 319-324.

TANNER, W. F. 1958. The zig-zag nature of Type I and Type IV curves. *Journal of Sedimentary Petrology*, 28, 372-357.

TANNER, W. F. 1964. Modification of sediment size distributions. *Journal of Sedimentary Petrology*, 34, 156-164.

THOM, B. G. 1983. Transgressive and regressive stratigraphies of coastal sand barriers in southeast Australia. *Marine Geology*, 56, 137-158

THORNTON, E. B. and GUZA, R. T. 1982. Energy saturation and phase speeds measured on a natural beach. *Journal of Geophysical Research*, 87, 9499-9508.

THORNTON, E.B. and GUZA, R. T. 1983. Transformation of wave height distribution. *Journal of Geophysical Research*, 88, 5925-5938.

TODD, T. W. 1968. Dynamic diversion : influence of longshore current-tidal flow interaction on chernier and barrier island plains. *Journal of Sedimentary Petrology*, 38, 734-746.

URSELL, F. 1952. Edge waves on a sloping beach. *Proceedings, Royal Society of London, Series A*, 214, p. 79-97.

VALIA, H. S and CAMERON, B. 1977. Skewness as a paleoenvironmental indicator. *Journal of Sedimentary Petrology*, 47, 784-793.

VILLARET, C. and TROWBRIDGE, J. H. 1991. Effects of stratification by suspended sediments on turbulent shear flows. *Journal of Geophysical Research*, 96, 10659-10680.

VISHER, G. S. 1969. Grain size distributions and depositional processes. *Journal of Sedimentary Petrology*, 39, 1074-1106.

WRIGHT, L. D. 1987. Shelf-surfzone coupling: cross-shore transport mechanisms on the shoreface. In: Kraus, N. C. (Ed.), *Coastal Sediment '87*, American Society of Civil Engineers, New York, p. 25-40.

WRIGHT, L. D. 1989. Benthic boundary layers of estuarine and coastal environments. *Reviews in Aquatic Sciences*, 1, 75-95.

WRIGHT, L. D., CHAPPELL, B. G., THOM, B. G., BRADSHAW, M. P. and COWELL, P. 1979. Morphodynamics of reflective and dissipative beach and inshore systems : southeastern Australia. *Marine Geology*, 32, 105-140.

WRIGHT, L. D., GUZA, R.T. and SHORT, A. D. 1982a. Dynamics of a high energy dissipative surf zone. *Marine Geology*, 45, 41-62.

WRIGHT, L. D., NIELSEN, P., SHORT, A. D. and GREEN, M. O. 1982b. Morphodynamics of a macrotidal beach. *Marine Geology*, 50, 97-128.

WRIGHT, L. D. and SHORT, A. D. 1983. Morphodynamics of beaches and surf zones in Australia. In : KOMAR, P. D. (Ed.), *Handbook of Coastal Processes and Erosion*. CRC Press, 35-64.

WRIGHT, L. D. , BOON, J. D., KIM, S. C. and LIST, J. H. 1991. Modes of cross-shore sediment transport on the shoreface of Middle Atlantic Bight. *Marine Geology*, 96, 19-51.

WUNDERLICH, F. 1972. Georgia coastal region. Sapelo Island, U.S.A. - sedimentology and biology, III: beach dynamics and beach development. *Senckenbergiana maritima*, 4, 15-45.

WUNDERLICH, F. 1983. Sturmbedingter Sandversatz vor den ostfriesischen Inseln und im Gebiet des Großen Knechtsandes, Deutsche Bucht, Nordsee. *Senckenberg maritima*, 15, 199-217.

YIH, C. -S. 1984. Edge waves created by a longshore current over a ridge in the sea bed. *Proceedings, 15th Symposium on Naval Hydrodynamics, Hamburg*, p. 367-371.

ZIEGLER, P. A. and LOUWERENS, C. J. 1979. Tectonics of the North Sea. In : OELE, E. , SCHÜTTENHELM, R. T. E. and WIGGERS, A. J. (Eds.), *The Quaternary History of the North Sea. Acta Universitatis Upsaliensis Symposium, Annum Quingentesimum Celebrantis*, 7-22.

ZIELKE, U. and FLEMMING, B. W. 1991. Morphologie und Sedimentologie des Langooger Inselsockels (Südliche Nordsee). *Poster Presentation, Sediment '91, Wilhelmshaven*.

**Appendix A. Sediment sample position and principal grain size statistical parameters.**

Sample Number	Lat.	Long.	Mean (cm/s)	PHI-P e r c e n t i l e				
				Mean	Sort	Skew	Kurt	
SP								
1	53°	7°	46.98	1.625	2.781	0.181	0.070	1.138
2			46.49	1.625	2.752	0.197	0.086	1.198
3			46.00	1.866	2.671	0.168	0.024	1.414
4			45.51	2.000	2.612	0.241	-0.215	1.554
5			45.01	1.625	2.756	0.154	0.021	1.257
6			44.50	1.741	2.683	0.162	0.092	0.960
7			44.00	1.866	2.682	0.180	0.012	1.031
8			43.51	1.866	2.642	0.186	0.159	0.988
9			43.01	1.866	2.640	0.173	0.022	1.384
10			42.48	1.866	2.636	0.189	0.054	0.984
11			42.51	1.866	2.647	0.182	-0.064	1.217
12			41.51	1.866	2.643	0.205	-0.013	1.125
13			41.00	2.000	2.608	0.264	-0.172	1.708
14			40.30	2.000	2.597	0.176	-0.165	1.149
15			40.01	2.000	2.567	0.229	-0.084	1.060
16			40.05	2.144	2.531	0.370	-0.400	0.959
17			40.54	1.866	2.619	0.288	-0.194	1.460
18			41.02	2.297	2.450	0.286	-0.198	0.788
19			41.50	2.000	2.587	0.251	-0.078	1.097
20			42.00	2.000	2.611	0.231	-0.176	1.612
21			42.52	2.000	2.592	0.160	-0.030	1.400
22			43.00	1.866	2.627	0.180	0.049	0.976
23			43.54	2.000	2.583	0.165	-0.088	1.889
24			44.02	2.000	2.580	0.271	-0.343	1.284
25			44.51	2.000	2.584	0.207	-0.086	1.342
26			45.01	1.866	2.620	0.202	-0.058	1.567
27			45.50	1.866	2.655	0.193	0.065	1.176
28			46.01	1.741	2.685	0.183	-0.006	1.062
29			46.50	2.297	2.471	0.471	-0.429	0.690
30			47.01	1.625	2.781	0.155	0.191	1.151
31			47.51	1.866	2.684	0.163	0.134	0.934
32			48.00	1.866	2.651	0.143	0.217	1.073
33			47.50	1.625	2.782	0.166	0.188	1.302
34			47.00	1.625	2.769	0.150	0.198	0.980
35			46.50	4.000	1.935	0.415	-0.247	0.637
36			46.01	1.866	2.661	0.121	0.188	1.316
37			45.50	1.866	2.679	0.152	0.090	1.052
38			45.00	1.866	2.632	0.180	-0.029	1.016
39			44.48	2.000	2.567	0.177	-0.036	1.079
40			44.01	2.000	2.586	0.188	-0.113	1.158
41			43.50	2.144	2.508	0.306	-0.364	1.064
42			43.00	4.000	1.883	0.432	0.389	0.416

## PHI-P e r c e n t i l e

Sample Number	Lat.	Long.	Mean (cm/s)	Mean	Sort	Skew	Kurt	
SP								
43	53°	48.50	7° 42.52	2.000	2.558	0.235	-0.269	1.136
44		48.50	42.00	2.000	2.559	0.234	-0.338	1.036
45		48.50	41.50	2.144	2.542	0.226	-0.275	1.387
46		48.50	41.00	2.000	2.537	0.219	-0.101	1.211
47		48.51	40.50	2.297	2.482	0.184	0.126	0.923
48		48.50	40.01	6.964	1.262	0.243	0.051	2.024
49		48.75	40.02	2.144	2.519	0.197	-0.177	1.396
50		48.76	40.52	4.000	1.902	0.476	0.095	0.491
51		48.76	41.01	2.000	2.571	0.204	-0.101	1.577
52		48.76	41.52	2.144	2.517	0.240	-0.165	0.908
53		48.75	42.01	2.297	2.447	0.458	-0.548	0.622
54		48.75	42.52	4.000	1.916	0.449	0.047	0.510
55		48.75	43.00	2.297	2.569	0.251	-0.169	0.960
56		48.76	43.51	1.866	2.631	0.180	-0.075	1.084
57		48.75	44.02	2.000	2.566	0.276	-0.393	1.497
58		48.74	44.51	2.828	2.276	0.409	0.006	0.479
59		48.75	45.01	4.595	1.763	0.293	0.025	0.848
60		48.75	45.56	4.595	1.761	0.431	0.354	0.549
61		48.75	46.00	2.144	2.549	0.209	-0.119	1.292
62		48.76	46.50	2.297	2.473	0.420	-0.423	0.609
63		48.75	47.02	2.144	2.574	0.271	-0.276	1.394
64		48.76	47.50	1.741	2.779	0.200	0.078	0.979
65		48.75	48.02	1.625	2.769	0.144	0.224	0.884
66		49.01	48.00	6.964	1.249	0.454	0.176	0.996
67		49.02	47.51	2.000	2.578	0.301	-0.275	1.160
68		49.01	47.00	2.144	2.486	0.298	-0.214	1.196
69		49.02	46.50	1.866	2.619	0.247	-0.060	1.125
70		49.01	46.01	2.828	2.285	0.498	-0.291	0.677
71		49.00	45.50	2.144	2.506	0.450	-0.590	0.613
72		49.00	45.50	2.144	2.505	0.174	-0.068	1.422
73		49.01	44.50	2.144	2.496	0.255	-0.193	1.324
74		49.01	44.00	2.297	2.454	0.216	-0.020	0.923
75		49.00	43.50	5.278	1.631	0.509	0.037	0.593
76		49.01	43.00	9.849	0.797	0.300	0.047	1.198
77		49.00	42.50	2.297	2.532	0.248	-0.227	2.068
78		49.00	42.00	2.297	2.454	0.241	-0.283	1.476
79		49.00	41.50	2.297	2.433	0.217	-0.046	1.132
80		49.00	41.00	2.639	2.340	0.240	0.086	0.804
81		49.00	40.48	4.000	1.884	0.286	0.252	0.907
82		49.10	40.00	5.657	1.511	0.302	-0.090	0.942
83		49.25	40.00	2.462	2.392	0.206	0.008	0.833
84		49.24	40.51	2.297	2.452	0.203	-0.090	0.904
85		49.25	41.01	2.144	2.545	0.238	-0.149	1.082
86		49.25	41.50	2.144	2.493	0.292	-0.410	1.124
87		49.26	42.00	2.000	2.558	0.142	-0.062	1.200
88		49.25	42.51	5.278	1.628	0.344	0.080	1.015
89		49.25	43.00	3.482	2.034	0.397	0.170	0.524
90		49.25	43.50	2.639	2.328	0.246	0.098	0.843
91		49.24	44.02	3.249	2.148	0.437	-0.122	0.577
92		49.25	44.50	2.144	2.500	0.216	-0.099	1.146
93		49.25	45.01	1.866	2.656	0.187	-0.121	1.708
94		49.25	45.50	2.144	2.530	1.104	-0.848	0.372
95		49.25	46.02	16.000	0.028	0.321	-0.117	0.677

Sample Number	Lat.	Long.	Mean (cm/s)	PHI-P e r c e n t i l e				
				Mean	Sort	Skew	Kurt	
SP								
96	53°	49.25	7° 46.52	13.929	0.245	0.335	0.067	3.430
97		49.26	47.00	12.126	0.515	0.256	0.323	3.546
98		49.25	47.52	8.574	1.030	0.222	0.128	1.206
99		49.25	48.02	9.190	0.877	0.442	0.298	0.610
100		49.50	48.00	10.556	0.704	0.284	0.085	0.981
101		49.50	47.52	13.929	0.244	0.332	0.060	1.073
102		49.50	47.00	5.657	1.541	0.239	-0.010	0.869
103		49.50	46.48	5.657	1.498	0.235	-0.102	0.736
104		49.50	46.00	6.498	1.319	0.250	-0.239	0.729
105		49.51	45.50	7.464	1.200	0.190	-0.129	0.806
106		49.50	45.01	9.849	0.855	0.292	-0.149	0.602
107		49.50	44.48	10.556	0.676	0.376	-0.117	0.619
108		49.50	44.00	10.556	0.678	0.463	-0.072	0.692
109		49.50	43.50	5.657	1.508	0.404	-0.096	0.701
110		49.50	43.00	4.000	1.878	0.334	-0.014	1.017
111		49.50	42.50	3.031	2.216	0.307	0.010	0.747
112		49.50	42.00	4.595	1.736	0.365	0.115	0.848
113		49.50	41.50	7.464	1.186	0.299	0.047	0.878
114		49.50	41.00	2.000	2.559	0.752	-0.757	0.421
115		49.50	40.50	9.849	0.823	0.724	0.357	0.907
116		49.50	40.00	3.031	2.201	0.504	-0.206	0.451
117		49.75	40.05	4.925	1.693	0.422	0.315	0.575
118		49.75	40.52	12.996	0.399	0.477	0.121	2.093
119		49.76	41.00	8.000	1.092	0.529	0.105	0.730
120		49.75	41.50	9.849	0.844	0.605	0.156	0.737
121		49.76	42.02	5.657	1.501	0.399	0.143	0.859
122		49.75	42.50	6.498	1.386	0.437	0.232	0.786
123		49.76	43.01	6.498	1.695	0.349	0.259	0.752
124		49.70	43.51	4.595	1.767	0.248	-0.007	1.144
125		49.75	44.03	4.925	1.663	0.279	-0.159	0.709
126		49.75	44.50	4.287	1.812	0.242	-0.148	0.917
127		49.74	45.00	4.000	1.914	0.266	-0.211	0.982
128		49.73	45.52	3.031	2.204	0.223	0.078	0.959
129		49.76	46.01	13.929	0.269	0.348	0.215	2.980
130		49.75	46.52	12.126	0.459	0.294	0.080	0.860
131		49.75	47.03	8.000	1.071	0.267	0.053	1.373
132		49.70	47.50	5.278	1.608	0.270	-0.002	0.913
133		49.75	48.02	3.482	2.061	0.171	-0.017	1.083
134		50.00	48.01	2.000	2.547	0.163	0.134	0.996
135		50.00	47.50	2.144	2.524	0.185	0.070	0.912
136		50.00	47.02	2.297	2.475	0.212	0.147	0.791
137		50.00	46.50	4.000	1.941	0.216	-0.130	0.887
138		50.00	46.01	4.925	1.651	0.330	-0.189	0.760
139		50.01	45.50	6.063	1.454	0.286	-0.103	0.749
140		50.00	45.01	4.925	1.670	0.400	0.331	0.689
141		50.00	44.50	5.278	1.566	0.312	0.004	1.077
142		50.00	44.01	12.126	0.460	1.254	0.650	0.212
143		50.00	43.51	2.462	2.358	0.326	-0.354	0.764
144		50.00	43.00	3.031	2.184	0.218	0.094	1.004
145		50.00	42.50	3.482	2.064	0.223	-0.014	0.999
146		50.00	42.02	3.732	1.948	0.261	-0.150	0.983
147		50.00	41.50	4.287	1.858	0.307	-0.201	0.982
148		50.00	41.00	4.287	1.819	0.273	-0.169	0.825

Sample Number	Lat.	Long.	Mean (cm/s)	PHI-P e r c e n t i l e				
				Mean	Sort	Skew	Kurt	
SP								
149	53°	50.00	7° 40.50	4.000	1.830	0.275	-0.033	1.252
150		50.00	40.05	4.287	1.849	0.228	0.017	1.042
151		50.25	40.01	2.828	2.247	0.221	0.079	0.918
152		50.25	40.53	2.639	2.328	0.198	0.136	1.044
153		50.26	41.02	2.000	2.546	0.208	0.007	1.147
154		50.25	41.52	2.144	2.522	0.156	0.114	1.161
155		50.25	42.02	8.000	1.119	0.308	0.132	0.946
156		50.25	42.52	9.190	0.905	0.410	-0.119	0.915
157		50.24	43.02	6.964	1.242	0.344	-0.022	0.931
158		50.25	44.01	5.657	1.482	0.242	0.124	1.139
159		50.25	44.01	4.925	1.686	0.234	0.020	1.446
160		50.25	44.52	4.000	1.938	0.243	-0.020	1.195
161		50.25	45.02	2.639	2.308	0.239	0.143	0.866
162		50.25	45.50	2.297	2.475	0.182	0.099	0.899
163		50.25	46.00	2.144	2.546	0.157	0.016	0.978
164		50.25	46.52	2.000	2.541	0.180	-0.135	1.554
165		50.25	47.03	2.000	2.566	0.229	-0.151	1.142
166		50.24	47.50	2.297	2.472	0.241	0.052	0.803
167		50.20	48.06	2.144	2.499	0.209	-0.171	2.742
168		50.50	48.00	1.625	2.765	0.203	0.221	0.939
169		50.50	47.50	2.000	2.607	0.215	0.105	1.051
170		50.50	47.01	2.297	2.424	0.306	-0.157	1.516
171		50.50	46.60	2.140	2.542	0.273	-0.196	1.656
172		50.50	46.60	2.297	2.459	0.407	-0.314	0.777
173		50.50	45.50	2.000	2.571	0.192	0.124	1.233
174		50.50	45.00	2.000	2.583	0.188	0.155	1.124
175		50.51	44.50	2.297	2.480	0.179	0.055	1.239
176		50.50	44.01	2.297	2.472	0.196	0.056	1.061
177		50.51	43.50	3.030	2.218	0.214	0.121	0.955
178		50.50	43.00	4.000	1.870	0.228	-0.040	0.933
179		50.50	42.51	5.278	1.612	0.332	-0.091	0.896
180		50.50	42.00	10.556	0.745	0.473	-0.046	1.884
181		50.50	41.48	9.190	0.912	1.208	0.299	0.342
182		50.50	41.01	8.574	1.029	0.382	-0.041	0.975
183		50.50	40.50	7.464	1.150	0.524	0.342	0.797
184		50.50	40.00	8.000	1.055	0.849	0.347	0.677
185		50.70	40.00	6.498	1.362	0.306	0.267	1.500
186		50.75	40.50	6.964	1.227	0.238	-0.079	1.308
187		50.75	41.04	6.063	1.434	0.220	-0.180	1.449
188		50.75	41.50	4.595	1.783	0.214	0.037	1.252
189		50.75	42.02	3.482	2.029	0.196	0.133	1.243
190		50.76	42.52	2.639	2.337	0.199	0.248	0.931
191		50.75	43.02	2.462	2.404	0.237	0.070	1.297
192		50.74	43.53	2.144	2.508	0.204	-0.089	1.060
193		50.76	44.03	2.000	2.570	0.215	0.108	1.425
194		50.74	44.51	2.144	2.522	0.207	0.087	1.534
195		50.75	45.01	2.462	2.391	0.370	-0.306	0.790
196		50.75	45.53	3.732	2.008	0.443	0.305	0.652
197		50.75	46.00	2.000	2.574	0.297	0.284	0.996
198		50.74	56.50	2.144	2.507	0.320	-0.011	1.272
199		50.75	47.02	1.741	2.685	0.249	0.192	0.996
200		50.73	47.51	1.231	3.019	0.277	0.175	0.908
201		50.74	48.02	1.231	3.031	0.234	0.233	0.826

## PHI-P e r c e n t i l e

Sample Nunmer	Lat.	Long.	Mean (cm/s)	Mean	Sort	Skew	Kurt	
SP								
202	53°	51.00	7°48.00	1.320	2.948	0.294	0.217	0.794
203		51.00	47.50	1.231	3.008	0.301	0.191	0.716
204		51.01	47.00	1.414	2.895	0.352	0.170	0.668
205		51.00	46.50	2.000	2.607	0.297	0.323	0.989
206		51.00	46.02	2.000	2.591	0.337	0.264	1.007
207		51.00	45.51	2.000	2.572	0.332	0.041	1.078
208		51.01	45.02	2.297	2.465	0.294	-0.085	1.491
209		51.00	44.50	2.000	2.571	0.250	0.194	1.285
210		51.00	44.00	2.144	2.527	0.202	0.089	1.410
211		51.00	43.51	2.000	2.564	0.192	0.070	1.758
212		51.00	43.00	2.297	2.473	0.197	0.145	1.315
213		51.01	42.50	2.144	2.519	0.194	0.090	1.136
214		51.00	42.00	2.297	2.422	0.191	0.017	1.170
215		51.01	41.48	2.462	2.411	0.200	0.103	1.040
216		51.00	41.03	2.462	2.378	0.209	0.192	0.904
217		51.00	40.50	3.482	2.041	0.193	0.400	0.989
218		51.00	40.00	4.000	1.879	0.268	0.008	1.028
219		51.27	40.00	2.462	2.394	0.183	0.055	1.231
220		51.25	40.51	2.297	2.472	0.192	0.021	1.184
221		51.25	41.03	2.297	2.454	0.221	-0.070	1.244
222		51.25	41.54	2.297	2.465	0.250	-0.123	1.235
223		51.25	42.04	2.297	2.471	0.210	-0.053	1.556
224		51.27	42.51	2.297	2.451	0.245	-0.174	1.307
225		51.26	43.00	2.000	2.516	0.168	0.006	1.440
226		51.26	43.51	2.297	2.437	0.208	-0.120	1.430
227		51.24	44.00	2.144	2.501	0.181	-0.037	1.396
228		51.25	44.50	2.144	2.510	0.196	0.121	1.373
229		51.25	45.02	2.144	2.510	0.235	0.041	1.165
230		51.24	45.54	2.297	2.497	0.236	-0.098	1.788
231		51.27	46.00	2.144	2.502	0.236	0.072	1.782
232		51.25	46.50	2.144	2.547	0.205	0.096	1.355
233		51.25	47.00	2.144	2.536	0.236	0.061	1.487
234		51.26	47.50	2.297	2.473	0.254	-0.330	1.250
235		51.50	47.00	2.144	2.500	0.211	-0.009	2.305
236		51.50	46.50	2.297	2.450	0.213	-0.066	1.218
237		51.52	46.00	2.144	2.543	0.204	-0.117	1.712
238		51.51	45.46	2.297	2.451	0.304	-0.403	1.313
239		51.51	45.01	2.297	2.474	0.246	-0.135	1.674
240		51.50	44.52	2.297	2.468	0.189	-0.050	1.421
241		51.50	44.01	2.462	2.355	0.408	-0.437	0.692
242		51.50	43.52	2.297	2.460	0.210	-0.198	1.915
243		51.51	43.00	2.144	2.488	0.227	-0.163	1.688
244		51.50	42.50	2.297	2.424	0.281	-0.278	1.106
245		51.50	42.00	2.297	2.426	0.366	-0.473	0.767
246		51.50	41.50	2.462	2.359	0.278	-0.274	1.168
247		51.50	41.01	2.462	2.388	0.393	-0.405	0.657
248		51.50	40.50	2.462	2.392	0.353	-0.376	0.778
249		51.50	40.00	2.297	2.475	0.208	-0.132	1.354
250		51.74	40.02	2.297	2.469	0.222	-0.216	1.303
251		51.75	40.53	2.297	2.464	0.247	-0.117	1.349
252		51.74	41.00	2.144	2.497	0.210	-0.163	1.421
253		51.75	41.50	2.144	2.502	0.245	-0.206	1.132
254		51.75	42.02	2.297	2.469	0.232	-0.297	1.365

## PHI-Percentile

Sample Number	Lat.	Long.	Mean (cm/s)	Mean	Sort	Skew	Kurt	
SP								
255	53°	51.79	7°42.50	2.144	2.506	0.200	-0.168	1.643
256		51.74	43.02	2.297	2.467	0.237	-0.215	1.300
257		51.74	43.50	2.144	2.504	0.188	-0.106	1.492
258		51.75	44.00	2.144	2.510	0.237	-0.330	1.818
259		51.74	44.51	2.297	2.475	0.308	-0.407	1.424
260		51.75	45.02	2.144	2.527	0.198	-0.068	1.484
261		51.74	46.00	2.297	2.448	0.277	-0.320	1.050
262		51.74	46.00	2.144	2.504	0.182	-0.002	1.412
263		51.75	46.52	2.297	2.472	0.296	-0.351	1.099
264		52.00	46.01	2.000	2.554	0.178	-0.051	2.096
265		52.00	45.45	2.144	2.547	0.173	-0.003	1.747
266		52.01	45.00	2.144	2.497	0.179	-0.091	2.744
267		52.00	44.48	8.000	1.127	0.859	0.198	0.323
268		52.00	44.00	2.144	2.531	0.187	-0.110	2.366
269		52.00	43.50	2.000	2.539	0.203	-0.046	1.473
270		52.00	43.00	2.144	2.522	0.211	-0.195	1.416
271		52.02	42.50	2.000	2.557	0.181	-0.050	1.347
272		52.01	42.00	2.144	2.531	0.165	0.069	0.976
273		52.00	41.50	2.144	2.527	0.196	-0.124	1.434
274		52.00	41.00	2.144	2.515	0.236	-0.176	1.307
275		52.01	40.05	2.000	2.517	0.197	-0.117	1.562
276		52.02	40.02	2.297	2.486	0.201	-0.129	1.647
277		52.24	40.02	2.144	2.501	0.178	-0.134	1.769
278		52.23	40.50	2.144	2.518	0.180	-0.138	1.609
279		52.25	41.02	2.144	2.512	0.204	-0.179	1.426
280		52.24	41.56	2.000	2.559	0.186	0.060	1.154
281		52.23	42.05	2.297	2.483	0.205	-0.182	1.895
282		52.25	42.51	2.144	2.488	0.229	-0.163	1.273
283		52.24	43.03	2.144	2.523	0.197	-0.065	1.305
284		52.25	43.52	2.144	2.518	0.173	-0.132	2.442
285		52.25	44.02	2.144	2.520	0.231	-0.365	2.268
286		52.24	44.54	2.000	2.568	0.184	-0.100	1.749
287		52.25	45.01	2.000	2.564	0.157	0.014	1.351
288		52.23	45.55	2.000	2.564	0.148	0.076	1.434
289		52.21	46.11	2.000	2.544	0.224	-0.248	1.977
290		48.00	47.51	1.741	2.680	0.152	0.066	0.968
291		47.75	47.50	1.741	2.724	0.167	0.185	0.882
292		47.51	47.49	1.866	2.670	0.164	0.057	1.169
293		47.24	47.52	1.866	2.649	0.155	-0.004	1.620
294		47.03	47.52	2.462	2.383	0.238	-0.244	0.987
295		48.25	47.99	2.297	2.446	0.205	-0.044	0.800
296		48.01	48.00	2.297	2.429	0.210	-0.075	1.020
297		47.76	47.90	2.144	2.499	0.166	0.033	1.036
298		47.50	48.01	2.000	2.605	0.144	0.144	0.944
299		47.25	48.00	1.866	2.654	0.141	-0.067	1.752
300		47.01	48.00	2.828	2.279	0.294	-0.194	0.819
301		51.00	48.50	1.516	2.823	0.309	-0.039	1.521
302		50.76	48.51	1.414	2.903	0.279	0.101	1.220
303		50.51	48.51	1.741	2.721	0.221	0.060	0.923
304		50.24	48.49	3.031	2.220	0.256	0.044	0.826
305		50.01	48.50	2.000	2.601	0.163	0.117	1.149
306		49.76	48.51	4.925	1.713	0.200	-0.046	0.816
307		49.50	48.51	7.464	1.149	0.679	-0.277	0.365

Sample Number	Lat.	Long.	Mean (cm/s)	PHI-P e r c e n t i l e			
				Mean	Sort	Skew	Kurt
SP							
308	53° 49.25	7° 48.52	8.000	1.099	0.510	0.098	0.920
309	49.99	48.49	6.964	1.256	0.320	-0.003	1.949
310	48.76	48.49	1.414	2.882	0.157	0.177	0.976
311	48.49	48.50	2.639	2.326	0.259	-0.059	0.838
312	48.26	47.49	2.144	2.544	0.627	-0.665	0.551
313	48.00	48.50	5.278	1.935	0.541	-0.159	0.585
314	47.75	48.51	3.249	2.147	0.543	-0.213	0.681
315	47.49	48.50	2.144	2.515	0.189	-0.136	1.137
316	47.25	48.50	2.000	2.577	0.131	0.022	0.889
317	47.02	48.50	2.639	2.349	0.393	-0.450	0.756
318	51.01	49.04	1.414	2.909	0.245	0.373	1.022
319	50.75	49.01	1.320	2.937	0.218	0.238	1.275
320	50.50	49.03	1.741	2.693	0.188	0.297	0.996
321	50.25	49.02	1.516	2.790	0.197	0.196	1.076
322	49.99	49.00	2.297	2.436	1.269	-0.822	1.118
323	49.74	49.01	2.639	2.308	0.134	0.146	1.244
324	49.51	48.98	11.314	0.641	0.339	0.087	0.818
325	49.25	49.01	6.964	1.229	0.413	-0.291	0.762
326	49.00	49.01	2.462	2.428	0.440	-0.433	0.803
327	48.74	49.00	3.031	2.186	1.193	-0.504	0.249
328	48.50	49.00	1.741	2.694	0.168	0.128	1.217
329	48.26	49.00	1.741	2.692	0.179	0.010	1.201
330	47.98	49.00	4.925	1.652	0.798	-0.046	0.280
331	47.74	48.99	3.732	1.984	0.256	-0.066	0.859
332	47.50	49.01	6.964	1.266	0.548	0.077	0.913
333	47.25	49.01	2.297	2.465	0.222	-0.156	0.993
334	47.99	48.99	2.144	2.496	0.174	-0.097	1.347
335	47.77	40.00	2.000	2.638	0.242	-0.182	1.575
336	47.51	40.02	2.000	2.575	0.225	0.019	0.968
337	47.27	40.03	3.031	2.168	0.405	-0.086	0.593
338	47.00	39.94	2.000	2.592	0.214	-0.002	1.186
339	47.74	40.51	7.464	1.174	0.299	0.038	1.601
340	47.51	40.51	4.925	1.713	0.265	0.036	1.293
341	47.25	40.48	2.000	2.610	0.206	-0.023	1.219
342	47.02	40.50	2.000	2.591	0.242	-0.136	1.120
343	47.74	41.00	2.000	2.626	0.210	0.050	0.864
344	47.47	41.01	3.732	1.962	0.498	0.351	0.448
345	47.27	41.00	1.414	2.882	0.332	0.317	0.928
346	47.01	41.01	2.297	2.505	0.359	-0.183	0.750
347	47.74	41.52	1.866	2.624	0.229	-0.110	1.474
348	47.50	41.50	1.625	2.766	0.209	0.020	1.206
349	47.27	41.50	2.000	2.571	0.269	-0.112	1.050
350	NO DATA						
351	47.75	41.99	1.866	2.672	0.199	-0.068	0.993
352	47.49	42.00	5.657	1.553	0.225	-0.004	0.675
353	47.25	42.01	2.000	2.558	0.251	-0.074	1.048
354	NO DATA						
355	47.76	42.51	1.741	2.702	0.181	0.028	0.914
356	47.49	42.51	1.516	2.840	0.260	0.096	0.839
357	47.25	42.51	1.866	2.658	0.346	-0.176	0.969
401	53.00	40.01	2.000	2.563	0.164	0.131	1.261
402	53.01	40.51	2.144	2.536	0.163	0.051	1.474

## PHI-Percentile

Sample Number	Lat.	Long.	Mean (cm/s)	Mean	Sort	Skew	Kurt	
SP								
403	53°	52.98	7° 41.03	2.144	2.548	0.170	0.059	1.495
404		53.02	41.53	2.000	2.554	0.167	0.047	1.384
405		53.00	42.02	2.000	2.542	0.157	0.049	1.422
406		52.99	42.53	2.000	2.566	0.167	0.067	1.455
407		53.01	43.02	2.000	2.588	0.214	-0.145	1.922
408		53.01	43.47	4.595	1.715	0.307	0.345	0.924
409		53.00	44.02	2.462	2.418	0.264	-0.089	0.917
410		52.99	44.52	2.114	2.506	0.202	-0.019	1.306
411		52.98	45.03	2.000	2.553	0.171	0.154	1.187
412		52.76	45.01	2.297	2.440	0.249	-0.147	1.032
413		52.71	44.45	3.732	1.965	0.471	0.257	0.392
414		52.74	43.95	2.000	2.571	0.160	-0.047	1.465
415		52.73	43.43	2.000	2.555	0.145	0.073	1.296
416		52.74	42.96	2.000	2.556	0.155	0.044	1.384
417		52.74	45.49	2.000	2.556	0.165	0.006	1.565
418		52.75	41.97	2.144	2.533	0.174	0.031	1.472
419		52.74	41.97	2.000	2.548	0.172	0.045	1.697
420		52.76	40.98	2.144	2.538	0.164	0.049	1.362
421		52.72	40.47	2.144	2.538	0.174	-0.045	1.777
422		52.75	39.97	2.000	2.557	0.168	0.007	1.322
423		52.47	40.00	2.144	2.509	0.198	-0.099	1.609
424		52.48	40.53	2.000	2.551	0.188	-0.040	1.650
425		52.48	41.04	2.297	2.486	0.176	-0.023	1.250
426		52.51	41.53	2.000	2.584	0.170	0.091	1.324
427		52.48	42.03	2.144	2.530	0.165	0.108	1.686
428		52.49	42.53	2.297	2.486	0.330	-0.473	1.030
429		52.47	43.02	2.144	2.521	0.201	-0.120	1.497
430		52.50	43.53	2.000	2.561	0.164	0.103	1.164
431		52.49	44.02	2.000	2.567	0.161	0.110	1.155
432		52.48	44.51	2.000	2.570	0.149	0.146	1.202
433		52.49	45.02	2.000	2.557	0.228	-0.163	1.724
HD 1	53°	48.20	7° 43.25	2.000	2.572	0.218	-0.207	1.198
2		48.20	43.75	1.866	2.639	0.254	-0.362	1.485
3		48.21	44.24	1.866	2.672	0.160	-0.045	1.180
4		48.12	44.76	1.866	2.625	0.181	-0.037	1.656
5		48.20	45.25	2.000	2.607	0.187	-0.135	1.171
6		48.20	45.75	1.866	2.661	0.179	-0.146	1.233
7		48.20	46.26	1.741	2.694	0.154	-0.025	1.038
8		48.21	46.75	1.741	2.716	0.161	0.059	0.973
9		48.12	43.01	1.741	2.654	0.164	0.075	0.996
10		48.11	43.25	1.866	2.667	0.175	-0.143	1.222
11		48.12	43.51	1.866	2.631	0.189	-0.181	1.282
12		48.11	43.75	1.866	2.663	0.196	-0.188	1.454
13		48.12	43.99	1.866	2.663	0.173	-0.144	1.609
14		48.12	44.24	1.741	2.698	0.169	0.009	1.396
15		48.11	44.52	1.866	2.676	0.172	-0.125	1.486
16		48.21	44.74	1.866	2.665	0.218	-0.107	1.137
17		48.12	45.00	1.741	2.680	0.163	-0.051	1.005
18		48.11	45.25	1.625	2.742	0.190	-0.182	1.452
19		48.13	45.50	1.741	2.708	0.167	-0.046	0.964
20		48.12	45.73	1.741	2.703	0.182	-0.034	1.127
21		48.12	46.01	1.866	2.645	0.211	-0.138	0.876

Sample Number	Lat.	Long.	PHI-P e r c e n t i l e					
			Mean (cm/s)	Mean	Sort	Skew	Kurt	
HD								
22	53° 48.12	7° 46.24	1.741	2.702	0.189	-0.073	1.210	
23	48.12	46.49	1.516	2.814	0.202	0.160	1.151	
24	48.12	46.74	1.741	2.774	0.193	0.043	0.970	
25	48.12	47.01	1.516	2.844	0.163	0.123	1.104	
26	48.05	43.25	1.625	2.792	0.195	0.084	1.047	
27	48.04	43.75	1.741	2.724	0.174	-0.017	1.021	
28	48.07	44.25	1.741	2.686	0.159	0.072	1.057	
29	48.06	44.74	2.462	2.414	0.488	-0.303	0.485	
30	48.06	45.25	3.732	1.947	0.321	0.199	0.863	
31	48.05	45.74	1.741	2.699	0.169	-0.062	1.341	
32	48.06	46.25	1.625	2.754	0.162	0.091	1.269	
33	48.05	46.75	1.741	2.687	0.159	0.096	1.283	
34	47.96	43.00	1.625	2.743	0.150	0.067	1.224	
35	47.96	43.22	1.866	2.648	0.192	-0.012	0.990	
36	47.98	43.49	1.866	2.622	0.189	-0.058	1.072	
37	47.95	43.75	1.741	2.685	0.172	0.078	0.923	
38	47.97	43.99	1.741	2.685	0.164	-0.020	1.145	
39	47.98	44.25	1.741	2.703	0.176	-0.105	1.423	
40	47.96	44.59	1.741	2.690	0.180	-0.109	1.490	
41	47.96	44.75	1.741	2.698	0.161	0.095	1.280	
42	47.97	44.98	1.625	2.774	0.142	0.070	1.085	
43	47.96	45.24	1.741	2.692	0.181	-0.099	2.265	
44	47.98	45.51	2.462	2.435	0.441	-0.357	0.522	
45	47.98	45.75	3.031	2.203	0.504	-0.057	0.568	
46	47.97	46.01	2.000	2.609	0.342	-0.449	1.244	
47	47.97	46.24	1.741	2.730	0.210	0.166	0.797	
48	47.97	46.91	1.741	2.679	0.223	0.122	1.032	
49	47.96	46.76	1.625	2.755	0.173	0.297	1.000	
50	47.97	47.99	1.516	2.800	0.159	0.114	1.170	
51	47.90	43.25	1.625	2.742	0.161	0.114	1.042	
52	47.90	43.75	1.741	2.732	0.142	0.174	1.287	
53	47.80	43.75	1.741	2.679	0.148	0.152	1.359	
54	47.90	44.74	2.144	2.488	0.129	0.137	1.298	
55	47.91	45.25	1.866	2.665	0.134	0.078	1.170	
56	47.91	45.75	1.866	2.667	0.153	0.058	1.665	
57	47.90	46.25	1.741	2.734	0.163	0.055	1.160	
58	47.90	46.74	1.625	2.768	0.147	0.105	1.059	
59	47.82	42.98	1.741	2.714	0.178	0.045	0.962	
60	47.82	43.25	2.297	2.643	0.237	0.105	1.133	
61	47.82	43.50	1.866	2.670	0.163	0.090	0.966	
62	47.80	43.75	1.741	2.731	0.181	0.071	1.000	
63	47.81	44.01	1.866	2.639	0.192	0.267	0.943	
64	47.82	44.24	1.741	2.746	0.173	0.204	1.023	
65	47.82	44.50	1.866	2.647	0.169	0.085	1.104	
66	47.82	44.76	1.625	2.774	0.159	0.043	1.446	
67	47.82	45.00	1.625	2.768	0.168	0.070	1.135	
68	47.82	45.23	1.866	2.672	0.158	-0.008	1.414	
69	47.82	45.50	1.625	2.790	0.165	0.138	0.946	
70	47.83	45.74	1.741	2.677	0.216	-0.125	1.884	
71	47.83	46.00	1.741	2.735	0.152	0.021	1.252	
72	47.82	46.26	1.625	2.746	0.225	-0.266	1.818	
73	47.82	46.50	2.144	2.683	0.261	-0.210	1.571	
74	47.82	46.74	1.866	2.801	0.221	0.302	0.904	

## PHI-Percentile

Sample Number	Lat.	Long.	Mean (cm/s)	Mean	Sort	Skew	Kurt	
HD								
75	53°	47.82	7° 47.00	2.000	2.719	0.193	0.218	0.831
76		47.75	43.24	2.297	2.656	0.223	0.162	0.962
77		47.76	43.75	2.144	2.697	0.227	0.284	0.712
78		47.75	44.25	2.000	2.775	0.244	0.196	0.834
79		47.74	44.73	1.516	2.986	0.347	0.205	0.784
80		47.74	45.24	2.297	2.473	0.184	0.263	0.862
81		47.75	45.74	2.297	2.656	0.342	-0.308	1.298
82		47.76	46.25	2.144	2.712	0.240	0.146	1.406
83		47.76	46.76	2.000	2.783	0.197	0.227	0.845
84		47.68	43.01	2.297	2.436	0.215	0.281	4.540
85		47.66	43.25	2.144	2.504	1.094	0.826	0.090
86		47.67	43.50	1.741	2.639	0.196	0.120	0.891
87		47.67	43.75	1.741	2.692	0.169	0.111	1.033
88		47.67	44.01	1.741	2.687	0.161	0.111	1.107
89		47.67	44.25	1.866	2.681	0.218	0.035	1.003
90		47.52	44.51	1.866	2.657	0.177	0.039	1.147
91		47.67	44.75	1.741	2.718	0.241	-0.025	2.017
92		47.66	44.98	1.741	2.677	0.178	-0.002	1.113
93		47.68	45.24	1.625	2.755	0.185	0.201	1.174
94		47.68	45.50	1.866	2.661	0.172	-0.01	1.947
95		47.66	45.76	1.866	2.661	0.224	-0.205	2.222
96		47.66	46.01	1.516	2.828	0.209	0.174	1.278
97		47.67	46.25	1.866	2.619	0.360	-0.400	1.169
98		47.67	46.51	1.741	2.711	0.182	0.014	1.715
99		47.67	46.75	1.741	2.703	0.177	0.008	1.877
100		47.66	47.01	1.625	2.771	0.155	0.056	1.620
101		47.60	43.25	1.866	2.673	0.229	0.046	0.939
102		47.59	43.75	1.866	2.660	0.210	0.110	1.010
103		47.60	44.24	1.866	2.674	0.170	0.166	1.236
104		47.58	44.75	1.866	2.689	0.201	0.123	1.101
105		47.61	45.25	1.516	2.811	0.207	0.135	1.057
106		47.61	45.75	1.741	2.712	0.204	0.012	1.542
107		47.61	46.25	1.866	2.660	0.314	-0.437	1.622
108		47.60	46.76	1.741	2.688	0.219	-0.138	2.020
109		47.53	43.00	1.741	2.736	0.221	0.077	0.967
110		47.52	43.25	2.000	2.571	0.175	0.054	1.815
111		47.54	43.50	1.741	2.697	0.179	-0.052	1.106
112		47.52	43.74	1.866	2.675	0.152	0.114	1.185
113		47.53	43.99	1.866	2.634	0.174	-0.008	1.696
114		47.53	44.25	1.741	2.712	0.186	0.022	1.027
115		47.66	44.51	1.625	2.796	0.236	0.220	0.959
116		47.52	44.75	1.741	2.682	0.178	-0.059	1.115
117		47.51	45.00	1.231	3.005	0.302	0.197	0.820
118		47.53	45.23	1.866	2.639	0.869	-0.620	0.430
119		47.52	45.51	1.625	2.783	0.177	0.208	0.929
120		47.52	45.76	1.741	2.708	0.186	0.064	1.241
121		47.52	45.99	1.741	2.687	0.198	0.092	1.142
122		47.53	46.25	1.741	2.681	0.162	0.039	1.514
123		47.53	46.51	1.625	2.791	0.198	0.100	1.141
124		47.52	46.76	1.741	2.691	0.184	0.047	1.939
125		47.51	47.01	2.144	2.550	0.201	0.124	1.683
126		47.44	43.00	1.741	2.678	0.259	0.096	0.981
127		47.46	43.25	2.000	2.565	0.183	0.113	1.061

## PHI-Percentile

Sample Number	Lat.	Long.	Mean (cm/s)	Mean	Sort	Skew	Kurt	
HD								
128	53°	47.45	7° 43.51	1.741	2.706	0.258	0.174	0.905
129		47.45	43.76	2.144	2.547	0.166	0.005	1.210
130		47.44	44.00	1.866	2.643	0.215	0.024	2.033
131		47.45	44.25	1.866	2.645	0.155	0.063	1.193
132		47.46	44.51	1.741	2.680	0.199	0.165	1.303
133		47.44	44.75	1.866	2.656	0.150	0.095	1.125
134		47.44	44.99	1.866	2.651	0.186	0.121	1.324
135		47.46	45.24	2.144	2.540	0.422	-0.507	1.233
136		47.44	45.49	1.866	2.642	0.192	0.091	2.206
137		47.44	45.74	1.866	2.645	0.221	-0.124	2.316
138		47.44	46.01	2.000	2.592	0.198	-0.052	2.331
139		47.45	46.25	1.741	2.704	0.165	0.067	1.538
140		47.45	46.49	1.741	2.716	0.195	0.127	1.137
141		47.45	46.76	1.741	2.683	0.173	0.116	1.458
142		47.45	47.00	1.741	2.696	0.159	0.013	2.187
143		47.37	43.00	2.144	2.505	0.342	0.026	1.040
144		47.37	43.24	1.866	2.636	0.246	0.070	0.870
145		47.38	43.49	1.414	2.863	0.316	0.110	0.849
146		47.38	43.75	2.000	2.595	0.206	0.069	1.027
147		47.38	44.02	1.625	2.773	0.244	0.172	0.926
148		47.37	44.25	1.741	2.714	0.194	0.159	0.836
149		47.37	44.51	1.866	2.662	0.204	0.122	1.127
150		47.44	44.75	1.741	2.683	0.188	0.041	1.045
151		47.36	45.01	1.866	2.626	0.166	0.064	1.553
152		47.38	45.26	1.741	2.699	0.179	0.043	1.459
153		47.38	45.51	1.866	2.650	0.168	0.088	1.582
154		47.36	45.76	1.866	2.648	0.208	-0.026	1.795
155		47.37	45.99	1.741	2.679	0.155	0.031	1.245
156		47.37	46.24	1.866	2.660	0.158	0.092	1.977
157		47.38	46.49	1.866	2.656	0.189	-0.001	2.431
158		47.35	46.46	2.000	2.589	0.263	-0.052	1.655
159		47.38	47.00	1.741	2.700	0.185	-0.025	2.236
160		47.30	43.00	4.595	1.739	0.406	-0.158	0.685
161		47.31	43.25	2.297	2.430	0.264	0.086	0.775
162		47.29	43.50	1.866	2.670	0.235	0.071	0.952
163		47.31	43.76	2.000	2.592	0.217	0.040	0.974
164		47.30	43.99	1.866	2.669	0.222	0.124	0.903
165		47.31	44.26	2.000	2.611	0.170	0.124	1.023
166		47.30	44.50	1.866	2.643	0.200	-0.013	1.058
167		47.29	44.75	1.516	2.842	0.266	0.208	0.884
168		47.31	45.00	1.866	2.625	0.189	0.000	1.318
169		47.29	45.25	1.741	2.715	0.230	0.201	0.960
170		47.29	45.51	2.000	2.600	0.186	-0.121	2.263
171		47.29	45.73	1.866	2.628	0.187	0.051	1.504
172		47.29	45.99	1.866	2.618	0.172	0.132	1.559
173		47.31	46.25	1.866	2.658	0.186	0.098	1.577
174		47.30	46.51	2.000	2.579	0.187	0.130	2.186
175		47.30	46.75	1.866	2.633	0.181	-0.015	2.388
176		47.31	47.01	1.866	2.669	0.194	-0.105	2.103
177		47.22	43.00	4.000	1.888	0.226	-0.090	0.891
178		47.22	43.24	2.639	2.331	0.219	-0.158	0.993
179		47.23	43.51	2.462	2.391	0.209	-0.039	1.044
180		47.22	43.74	2.462	2.499	0.172	0.174	0.882

## PHI-Percentile

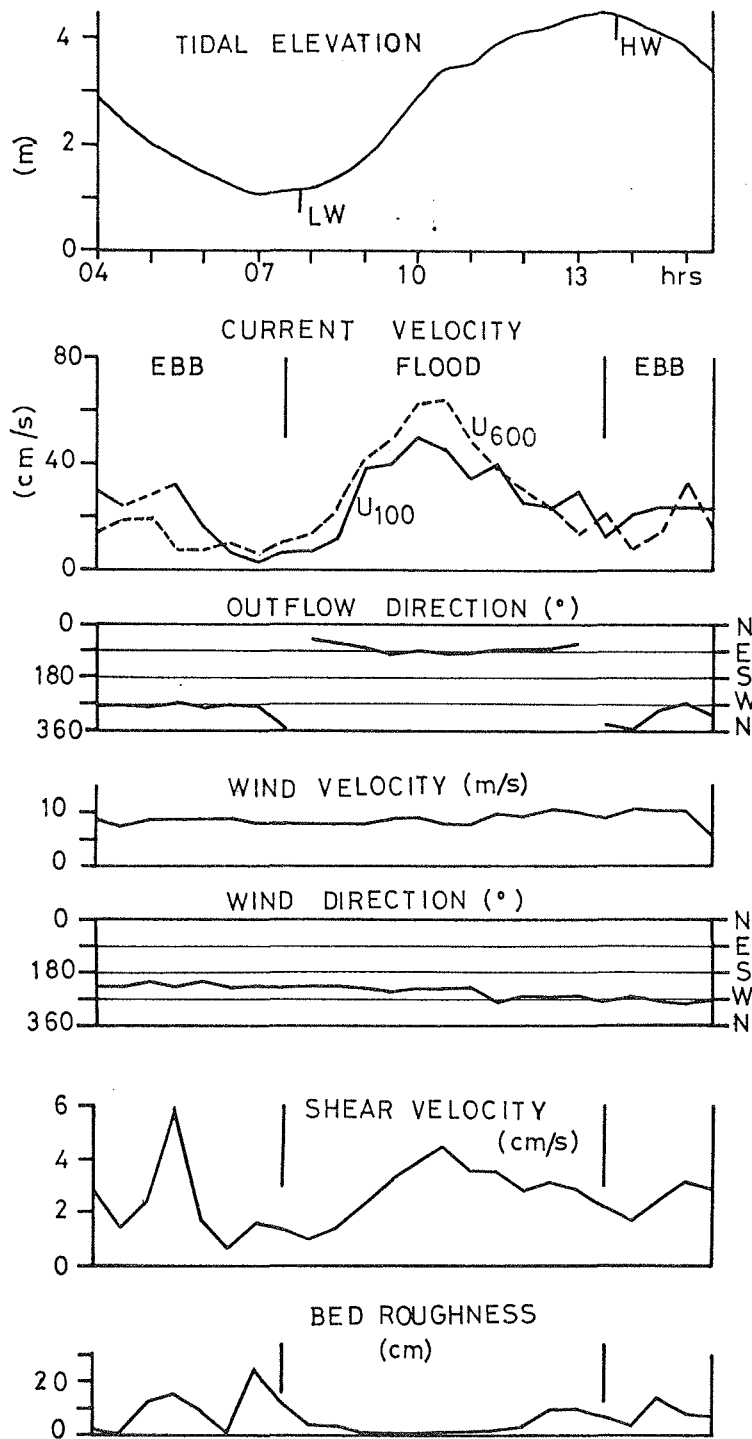
Sample Number	Lat.	Long.	Mean (cm/s)	Mean	Sort	Skew	Kurt	
HD								
181	53°	47.22	7° 44.00	1.741	2.709	0.202	0.017	0.905
182		47.22	44.26	1.741	2.691	0.233	0.197	0.846
183		47.23	44.50	1.741	2.683	0.217	0.131	0.980
184		47.23	44.76	1.741	2.717	0.217	0.138	1.162
185		47.23	45.00	1.741	2.716	0.222	0.139	1.264
186		47.25	45.25	1.741	2.685	0.223	0.107	1.181
187		47.21	45.51	1.866	2.652	0.175	0.045	1.638
188		47.22	45.76	1.741	2.684	0.206	0.083	1.255
189		47.23	46.00	1.866	2.660	0.212	0.045	1.812
190		47.21	46.24	1.741	2.687	0.195	0.106	1.475
191		47.22	46.49	1.866	2.664	0.161	0.043	1.430
192		47.22	46.75	1.866	2.654	0.140	0.094	1.709
193		47.22	47.01	1.866	2.636	0.143	0.080	1.414
194		47.15	43.00	4.595	1.763	0.302	0.017	0.761
195		NO DATA						
196		47.15	43.49	2.828	2.272	0.249	-0.090	1.086
197		47.15	43.74	2.297	2.461	0.160	0.013	0.960
198		47.14	44.00	1.866	2.615	0.203	0.107	1.125
199		47.15	44.25	1.866	2.625	0.277	0.090	0.900
200		47.15	44.49	2.000	2.599	0.163	0.092	0.961
201		47.15	44.74	1.741	2.692	0.201	0.099	0.904
202		47.16	45.01	1.866	2.671	0.190	0.094	0.900
203		47.16	45.24	1.866	2.647	0.178	0.164	1.002
204		47.14	45.50	1.866	2.665	0.195	0.079	1.302
205		47.15	45.76	1.866	2.564	0.150	0.025	1.182
206		47.15	46.00	2.000	2.629	0.161	0.041	1.019
207		47.14	46.24	1.866	2.658	0.146	0.087	0.988
208		47.15	46.50	1.866	2.577	0.221	-0.017	2.078
214		47.07	43.74	2.639	2.312	0.203	0.033	1.019
215		47.09	44.00	2.144	2.525	0.152	0.064	1.077
216		47.07	44.26	3.031	2.172	0.392	-0.204	0.827
217		47.07	44.49	2.828	2.276	0.269	-0.169	0.963
218		47.06	44.75	2.144	2.518	0.159	0.058	1.138
219		47.08	44.99	2.639	2.362	0.438	-0.474	0.981
220		47.08	45.25	2.297	2.486	0.208	-0.200	1.219
221		47.09	45.50	2.297	2.439	0.232	-0.223	1.028
223		47.07	46.01	2.144	2.503	0.186	-0.029	1.276
224		47.07	46.25	2.000	2.589	0.157	0.005	1.086
225		47.08	46.49	2.000	2.549	0.164	-0.109	1.946
232		47.01	44.01	3.031	2.209	0.376	-0.293	0.935
238		47.01	45.50	4.287	1.845	0.267	-0.181	0.576
245		49.00	43.25	2.144	2.518	0.204	-0.100	0.983
246		49.00	43.74	2.462	2.415	0.256	-0.097	0.879
247		49.00	44.26	2.639	2.352	0.457	-0.522	0.646
248		48.99	44.74	4.925	1.665	0.555	-0.041	0.594
249		48.99	45.24	2.462	2.369	0.555	-0.519	0.562
250		49.00	45.74	3.249	2.103	0.424	-0.093	0.504
251		49.00	46.24	2.144	2.489	0.326	-0.304	0.845

Sample Number	Lat.	Long.	Mean (cm/s)	PHI-Percentile				
				Mean	Sort	Skew	Kurt	
HD								
252	53°	49.00 7°	46.76	5.657	1.520	0.562	0.193	0.659
253			43.00	2.00	2.564	0.165	0.023	1.223
254			43.26	2.000	2.614	0.208	0.072	1.733
255			43.51	12.126	0.438	1.262	0.782	0.168
256			43.75	2.828	2.261	0.324	-0.106	0.700
257			44.01	3.031	2.214	0.337	-0.099	3.665
258			44.25	3.249	2.133	0.271	0.086	0.780
259			43.50	2.297	2.425	0.191	0.069	0.866
260			43.75	2.297	2.461	0.223	-0.104	1.118
261			45.99	2.297	2.472	0.209	-0.086	1.044
262			45.24	2.462	2.414	0.368	-0.448	0.762
263			45.50	2.000	2.556	0.229	-0.165	1.181
264			45.75	2.000	2.563	1.209	0.759	0.190
265			46.01	2.144	2.524	0.382	-0.444	0.752
266			46.25	2.297	2.482	1.474	0.497	0.185
267			46.50	2.000	2.575	0.286	-0.401	4.291
268			46.24	2.144	2.508	0.267	-0.134	1.092
269			47.01	1.866	2.666	0.220	0.267	1.091
270			43.26	2.144	2.524	0.198	-0.032	0.860
271			43.76	2.000	2.625	0.144	0.084	1.090
272			44.24	7.464	1.151	0.348	0.074	1.697
273			44.75	2.462	2.399	0.260	-0.020	0.898
274			45.24	4.925	1.677	0.347	0.152	0.691
275			45.74	2.462	2.389	0.247	0.069	0.850
276			46.24	2.144	2.522	0.311	-0.339	0.912
277			46.76	2.144	2.539	0.351	-0.343	0.820
278			42.99	2.462	2.408	0.310	-0.172	0.614
279			43.25	2.144	2.545	0.251	-0.134	0.997
280			43.51	2.462	2.416	0.286	-0.166	1.117
281			43.74	2.000	2.573	0.189	-0.066	0.972
282			44.00	2.297	2.476	0.343	-0.352	0.936
283			44.25	2.297	2.467	0.371	-0.450	0.917
284			44.50	1.741	2.663	0.194	-0.057	1.393
285			44.75	1.866	2.658	0.201	-0.018	1.343
286			45.01	3.249	2.099	0.475	0.188	0.385
287			45.25	6.498	1.380	0.298	-0.013	1.616
288			45.50	7.464	1.219	0.272	-0.022	0.992
289			45.75	7.464	1.145	0.210	-0.009	0.811
290			46.00	6.498	1.318	0.179	-0.031	0.790
291			46.25	6.498	1.342	0.197	0.001	1.016
292			46.50	5.278	1.587	0.232	0.026	1.603
293			46.76	6.063	1.456	0.208	-0.055	0.927
294			47.00	4.287	1.868	0.198	-0.068	1.793
295			43.26	2.000	2.585	0.281	-0.313	0.760
296			43.76	2.000	2.583	0.371	-0.265	0.815
297			44.26	1.866	2.675	0.192	-0.114	1.764
298			44.76	2.144	2.528	0.278	-0.241	1.332
299			45.24	1.866	2.640	0.176	-0.075	1.163
300			45.75	1.741	2.700	0.141	0.125	1.045
301			46.24	1.741	2.691	0.139	0.206	0.850
302			46.75	1.516	2.819	0.162	0.221	0.990
303			43.00	1.866	2.630	0.207	-0.116	1.533
304			43.25	2.000	2.576	0.415	-0.487	0.544

## PHI-P e r c e n t i l e

Sample Nummer	Lat.	Long.	Mean (cm/s)	Mean	Sort	Skew	Kurt	
HD								
305	53°	48.37	7° 43.51	1.866	2.645	0.223	-0.206	1.107
306		48.38	43.74	1.866	2.626	0.256	-0.250	0.892
307		48.39	44.00	2.000	2.569	0.368	-0.424	0.918
308		48.37	44.24	2.000	2.601	0.249	-0.150	0.888
309		48.39	44.49	2.000	2.578	0.267	-0.243	1.874
310		48.38	44.75	1.866	2.647	0.194	-0.111	1.301
311		48.37	45.00	1.866	2.639	0.202	-0.078	1.286
312		48.37	45.24	2.000	2.584	0.249	-0.213	1.121
313		48.37	45.50	1.866	2.640	0.178	0.000	1.039
314		48.37	45.75	1.741	2.692	0.174	0.040	0.873
315		48.38	46.99	1.866	2.671	0.164	0.037	0.898
316		48.38	46.26	1.866	2.675	0.164	0.124	0.844
317		48.38	46.50	1.741	2.692	0.164	0.165	0.952
318		48.38	46.75	1.741	2.705	0.164	0.165	0.928
319		48.37	46.99	1.414	2.919	0.245	0.286	1.165
320		48.25	43.25	1.866	2.627	0.200	-0.091	1.254
321		48.26	43.75	2.000	2.566	0.244	-0.209	1.093
322		48.26	44.25	1.866	2.628	0.200	-0.046	1.440
323		48.26	44.76	1.516	2.843	0.131	0.306	0.892
324		48.24	45.24	1.866	2.636	0.198	0.044	0.950
325		48.24	45.76	1.866	2.614	0.218	0.120	0.953
326		48.25	46.24	1.866	2.649	0.191	0.187	0.835
327		48.26	46.76	1.741	2.722	0.203	0.217	0.774

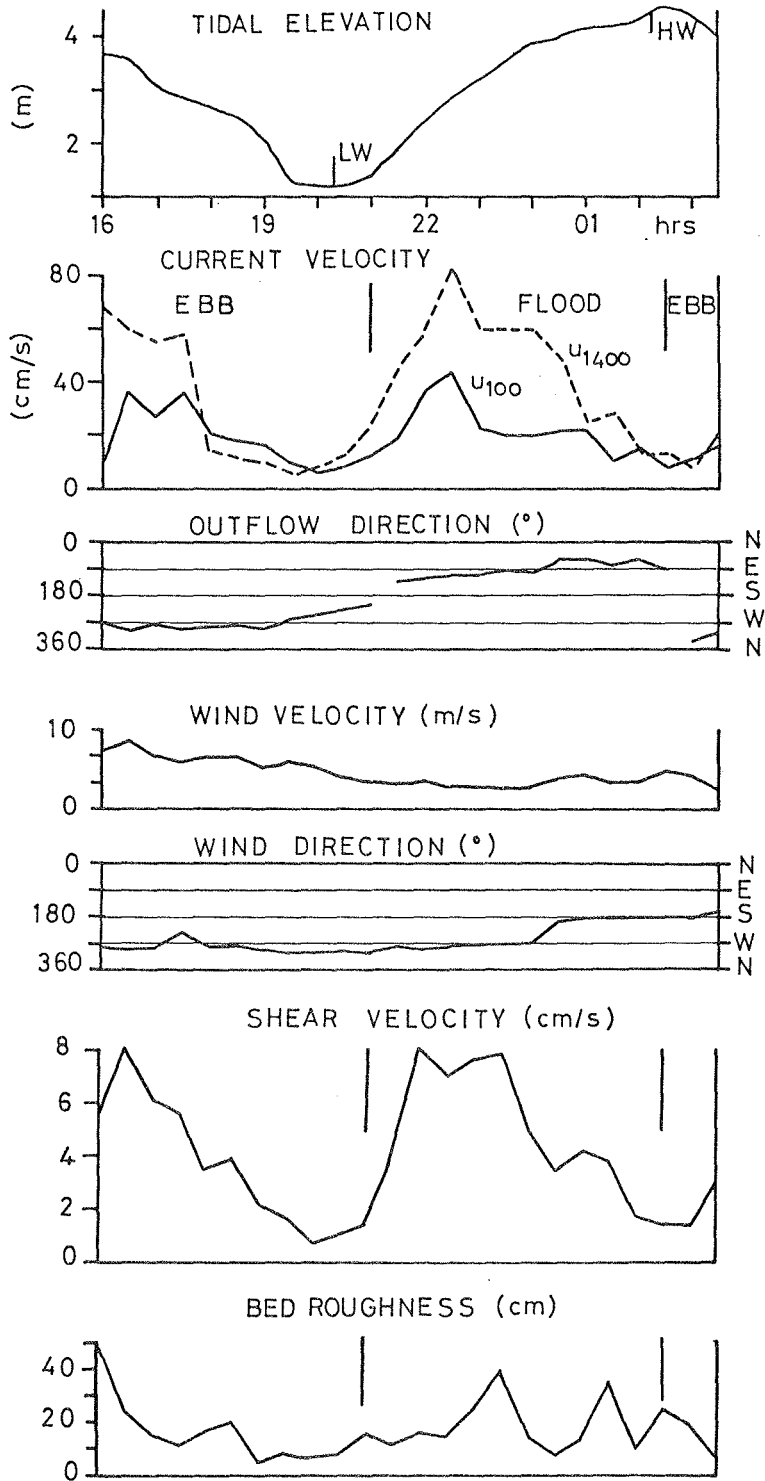
STATION 6 18 AUG. '89 SPRING TIDE



MEAN GRAIN SIZE = 0.18 mm

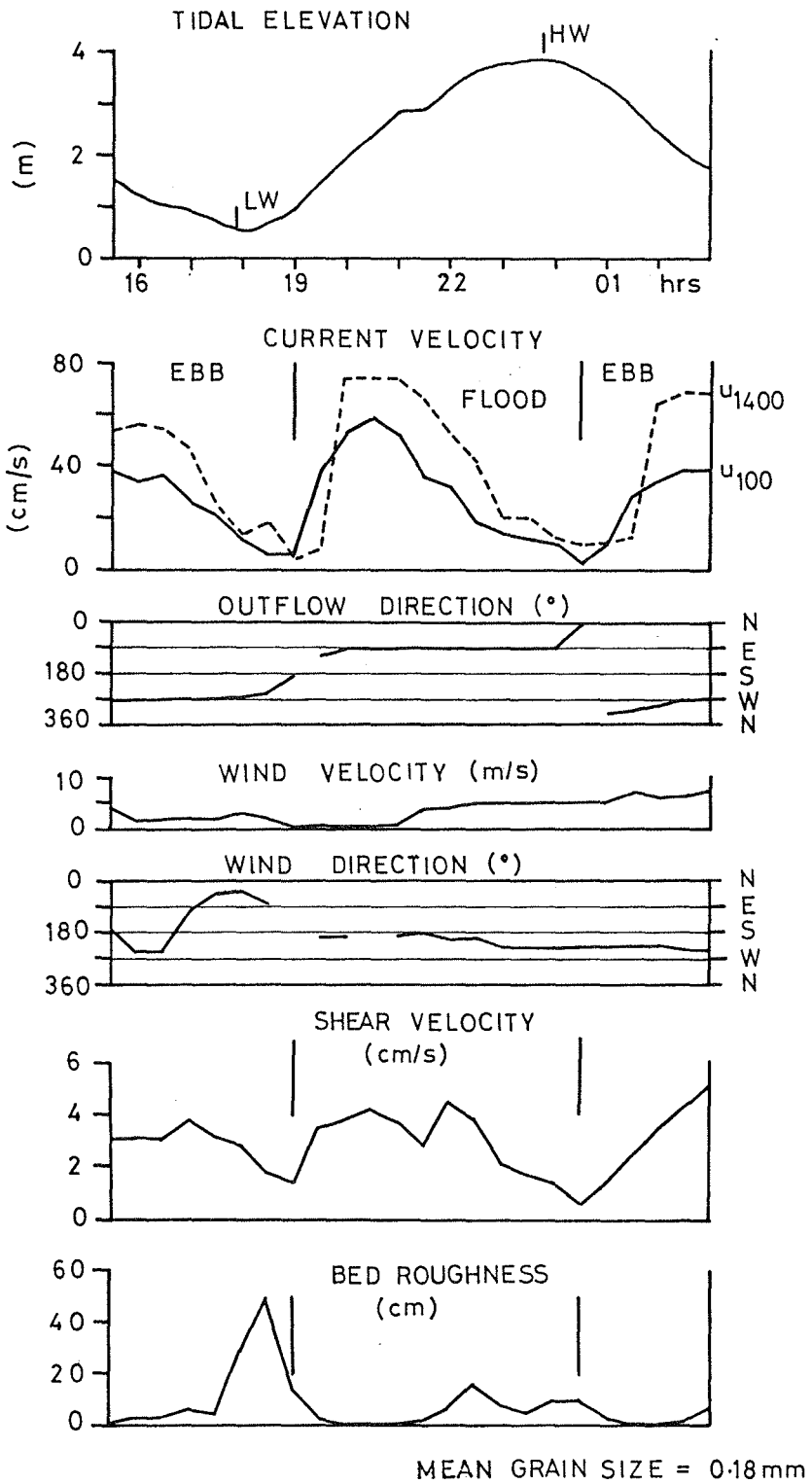
Appendix B-1. Data on tidal variation in current velocities and direction as well as boundary-layer hydraulic parameters at some stations.

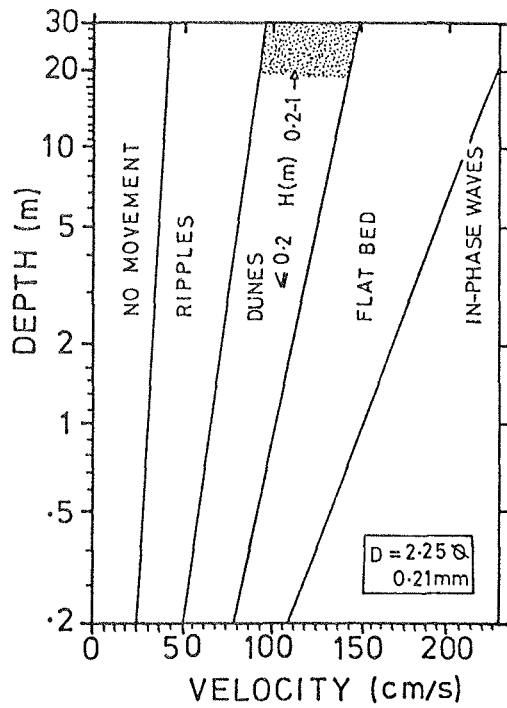
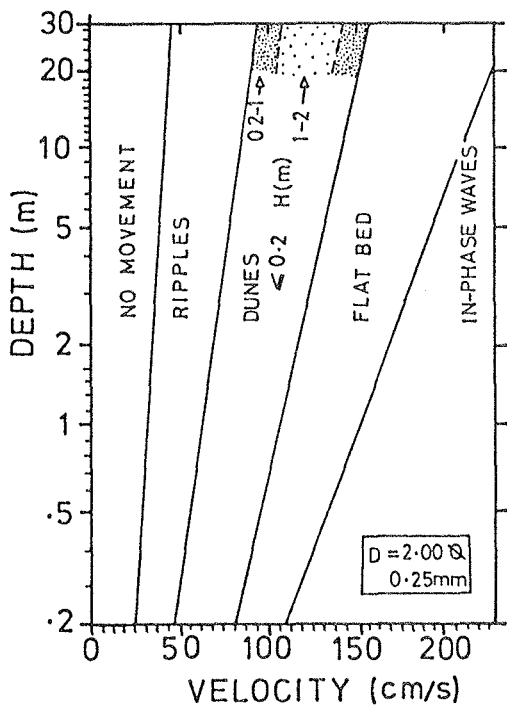
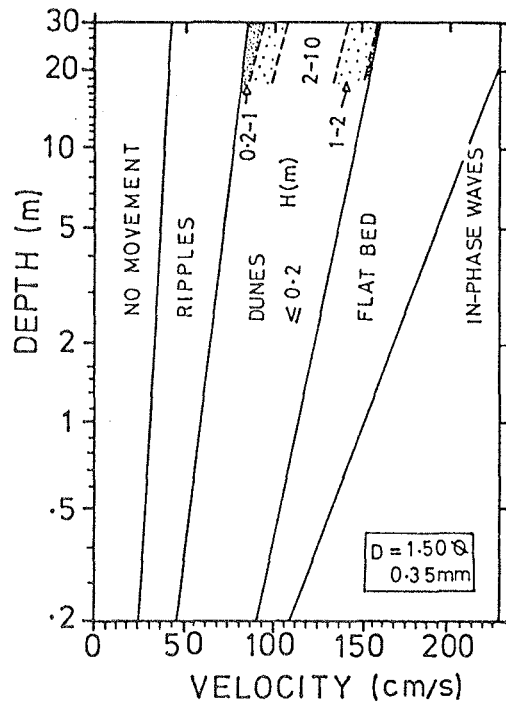
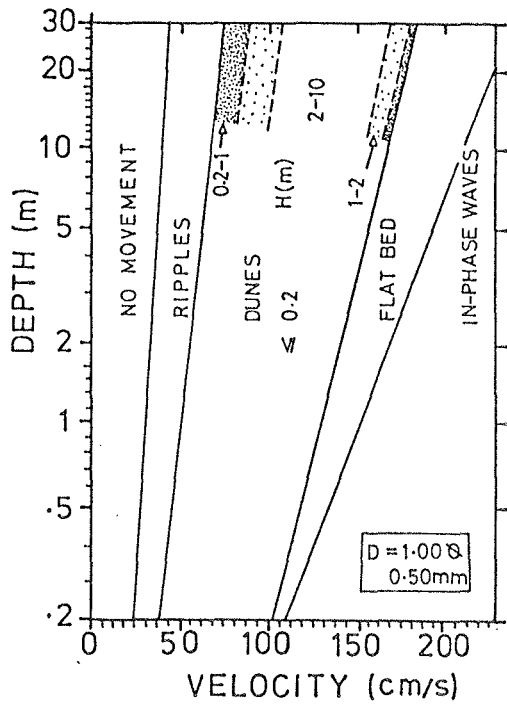
STATION 7 18-19 AUG.'89 SPRING TIDE



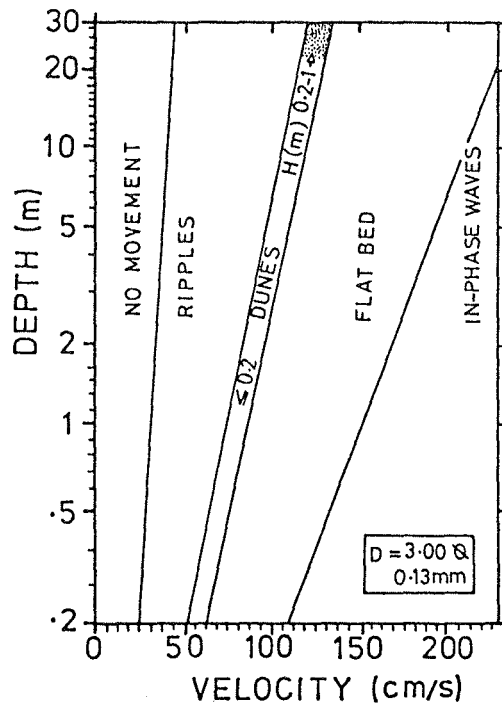
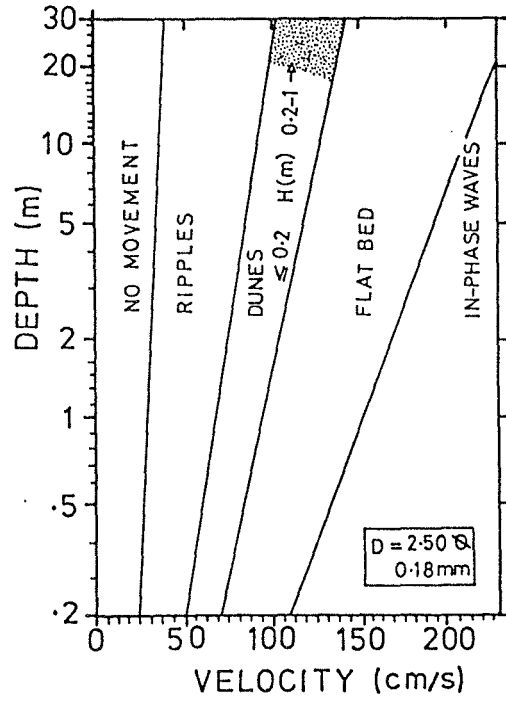
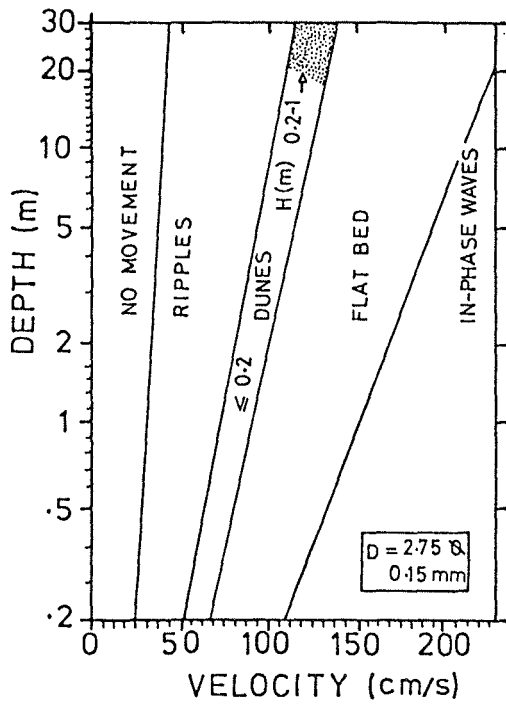
MEAN GRAIN SIZE = 0.18mm

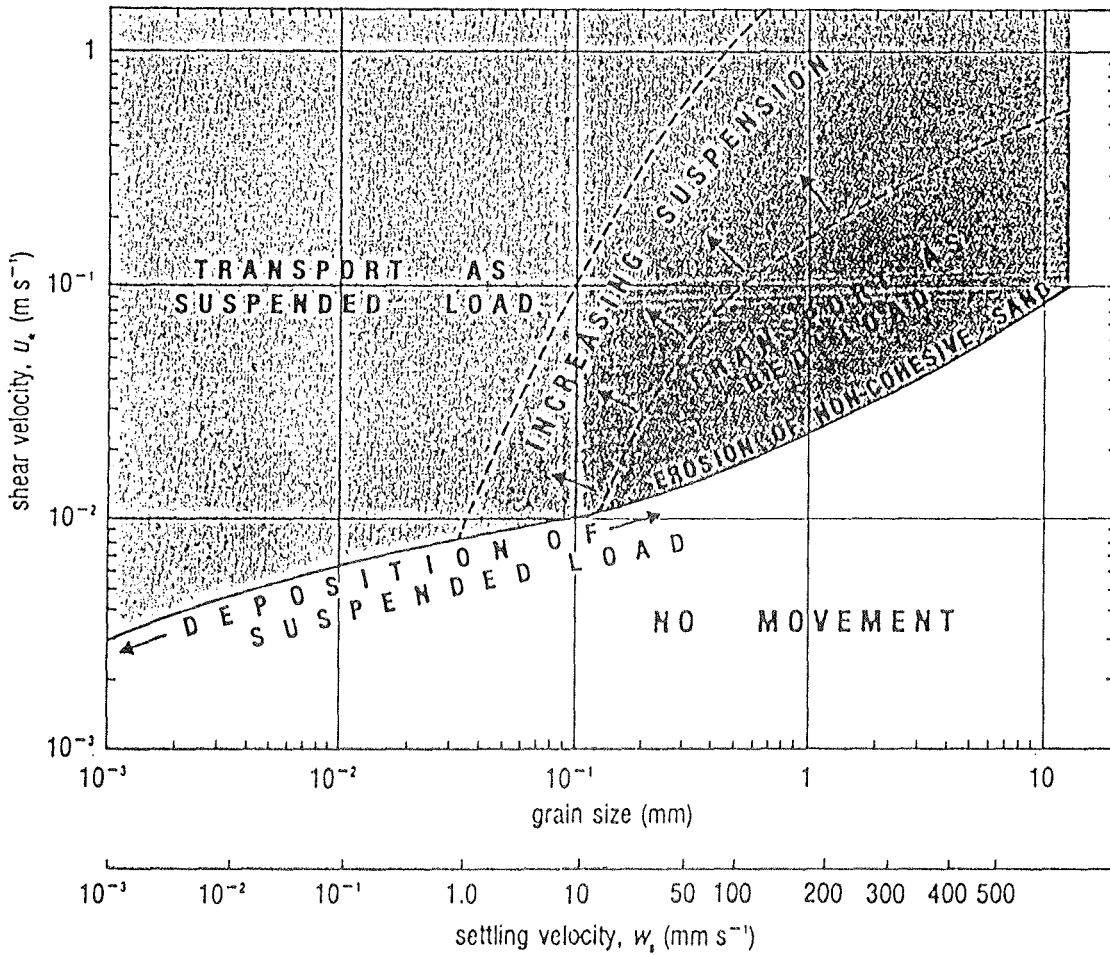
STATION 11 13-14 NOV. '89 SPRING TIDE



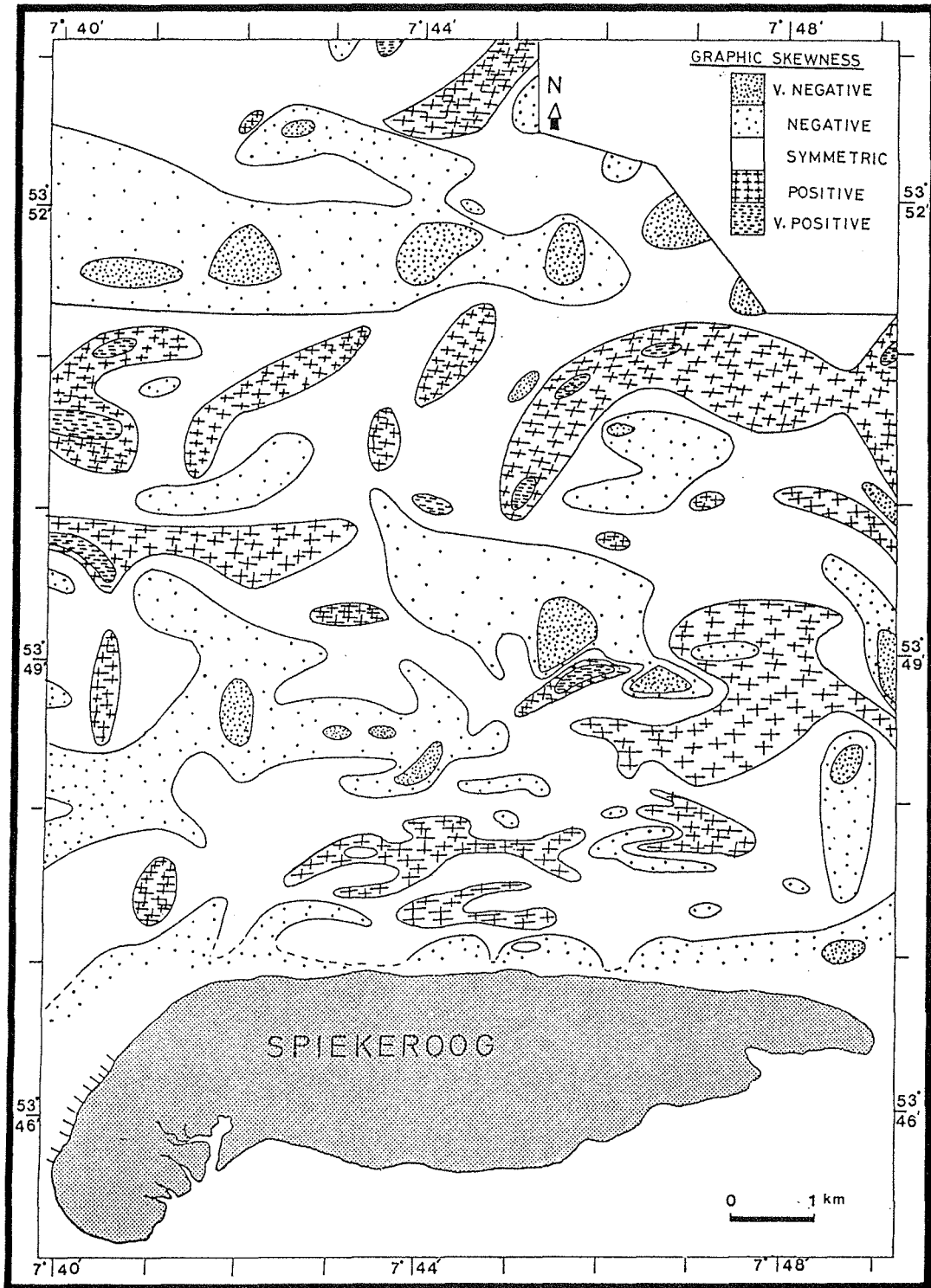


Appendix B-2. Panels of RUBIN and McCULLOCH's (1980) bedform stability diagram.

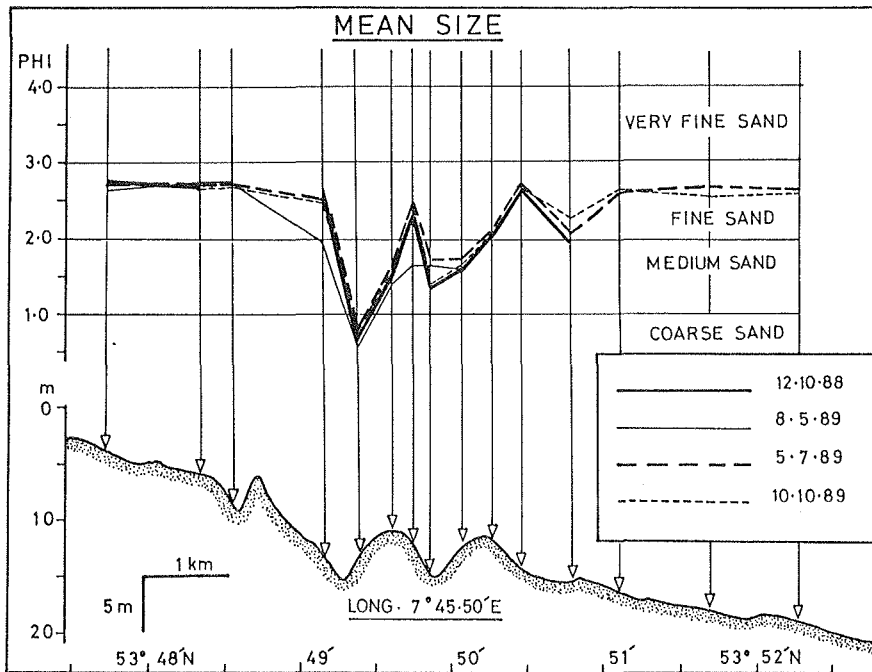




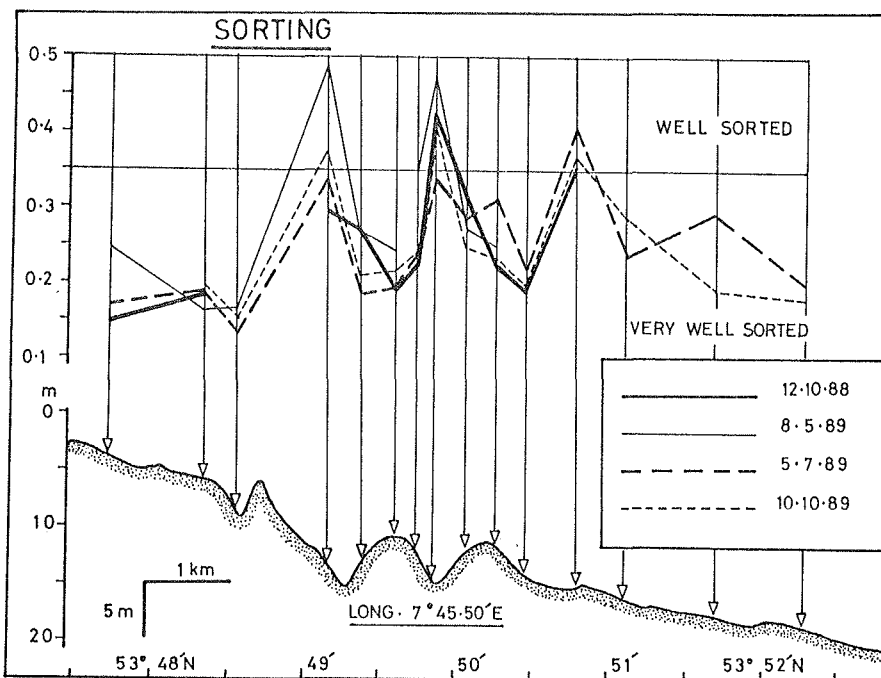
Appendix B-3. Sediment transport threshold as a function of shear velocity (after OPEN UNIVERSITY, 1989).



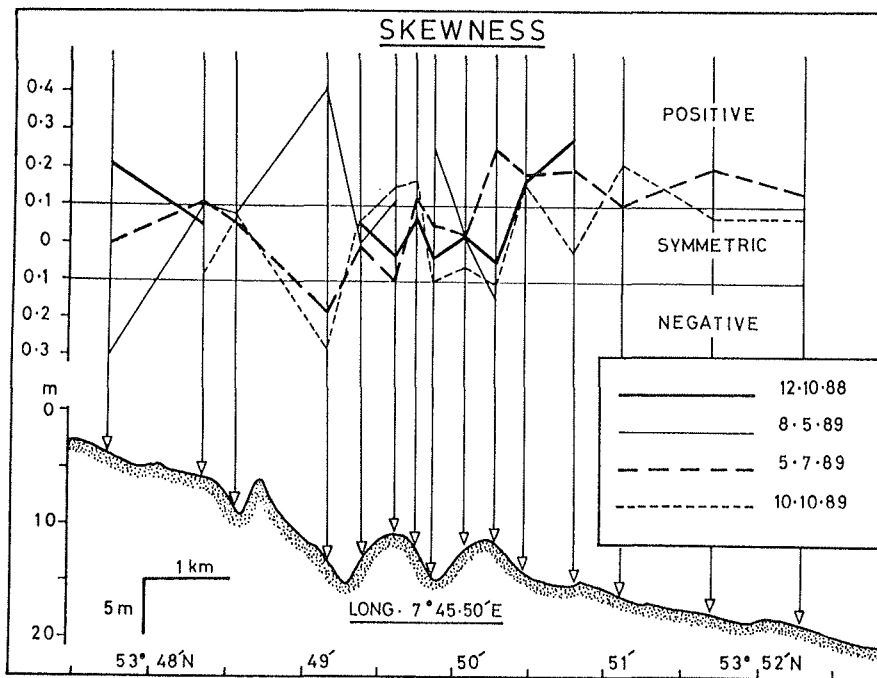
Appendix C-1. Areal distribution in skewness of shoreface sediments.



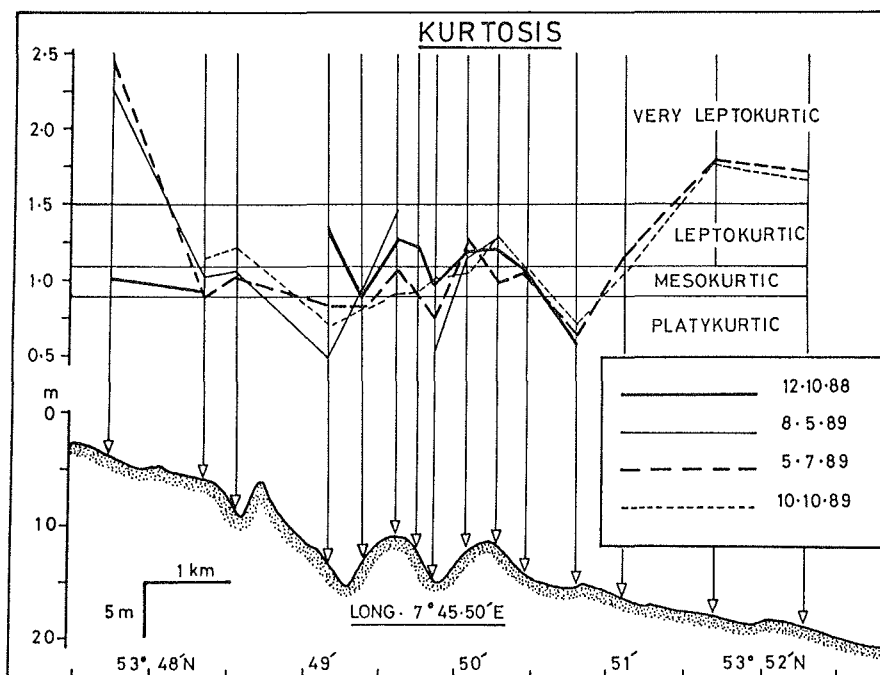
Appendix C-2. Cross-shore temporal variation in mean grain size of shoreface ridge surficial sediments.



Appendix C-3. Cross-shore temporal variation in sorting of shoreface ridge surficial sediments.

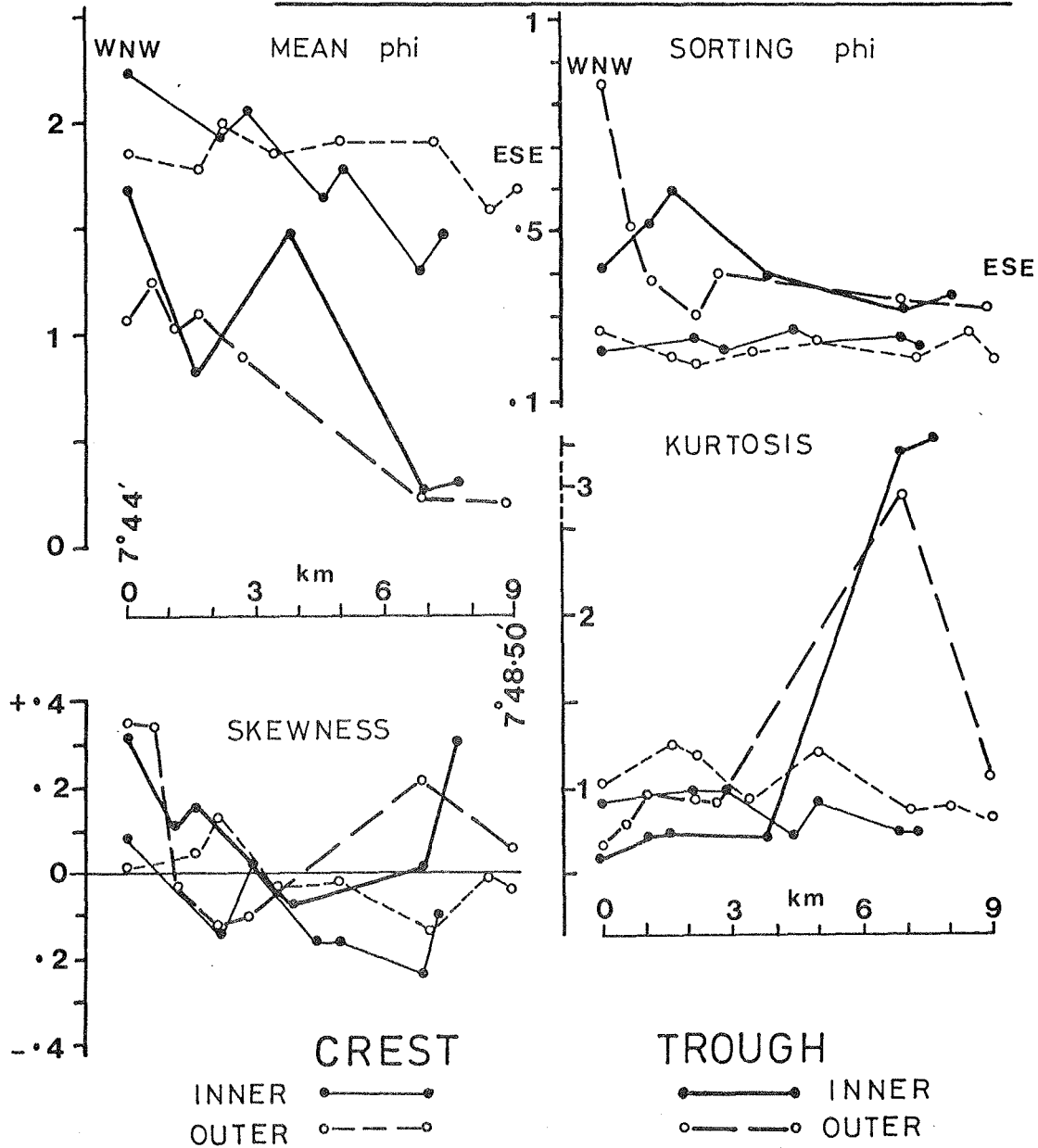


Appendix C-4. Cross-shore temporal variation in skewness of shoreface ridge surficial sediments.

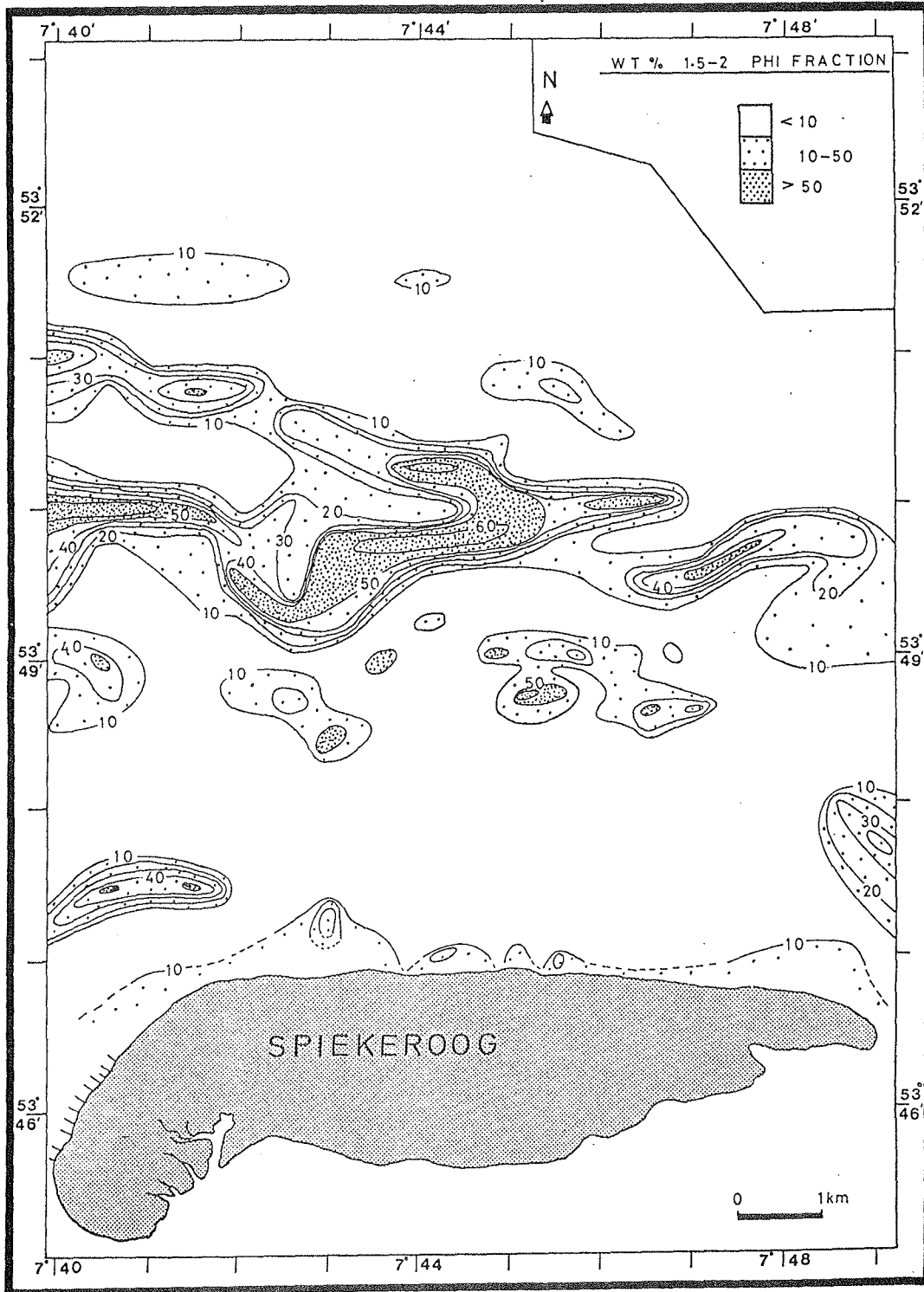


Appendix C-5. Cross-shore temporal variation in kurtosis of shoreface ridge surficial sediments.

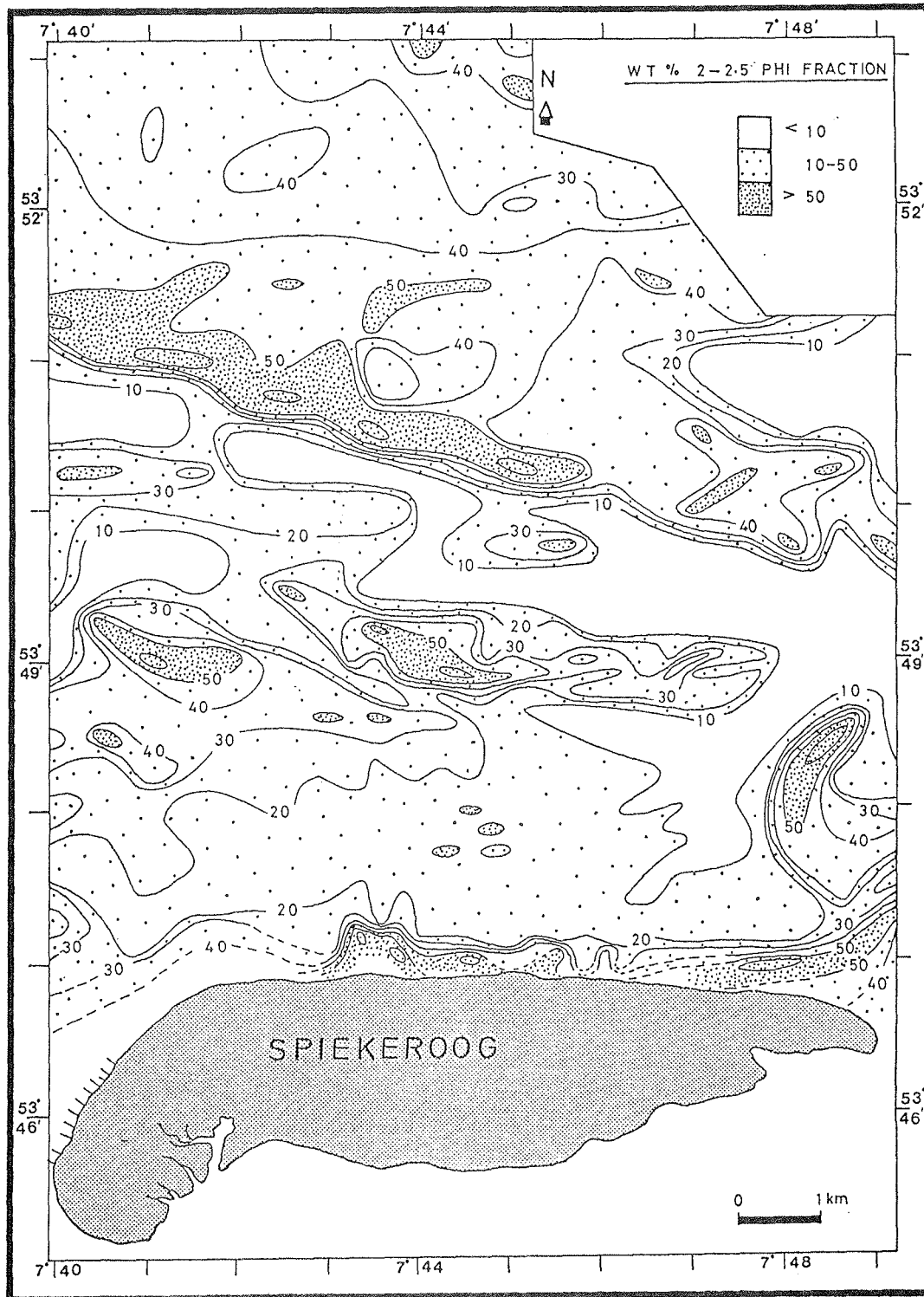
GRAIN SIZE STATISTICS ALONG AXES OF SHOREFACE—  
CONNECTED RIDGE MORPHOLOGY



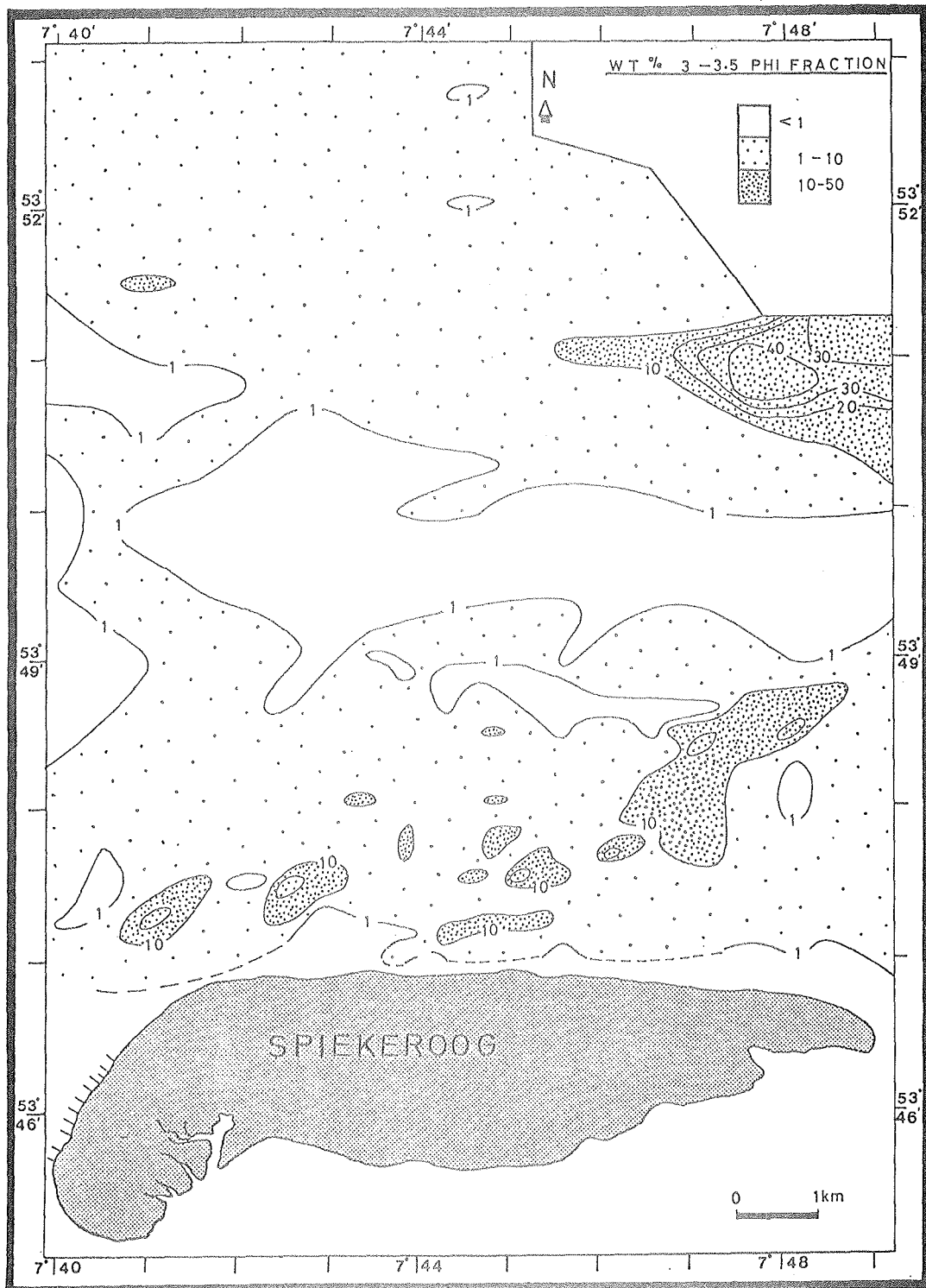
Appendix C-6. Alongshore variation in central shoreface surficial grain size statistical parameters.



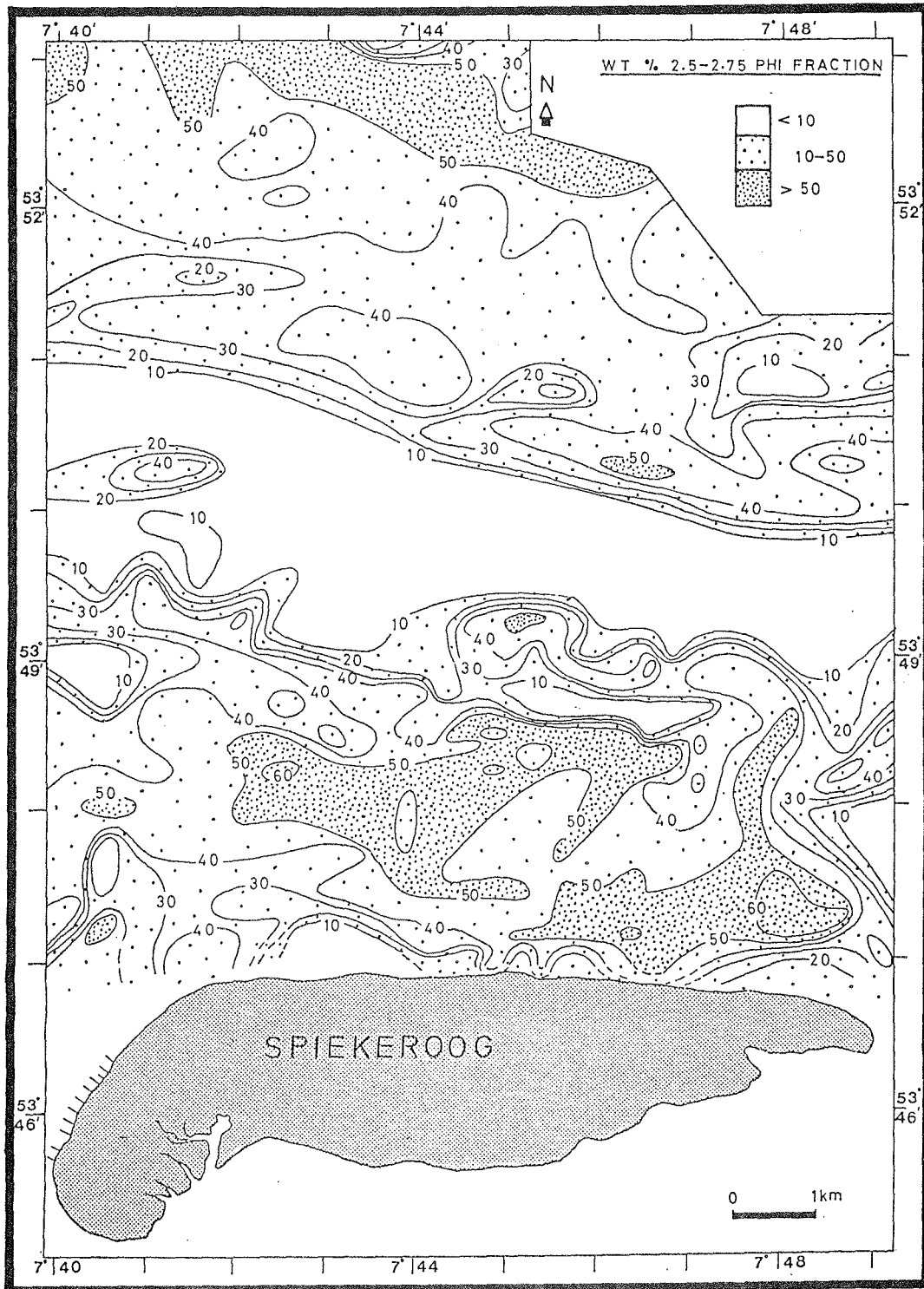
Appendix D-1. Shoreface distribution of wt.-% of 1.5-2 phi sand fraction.



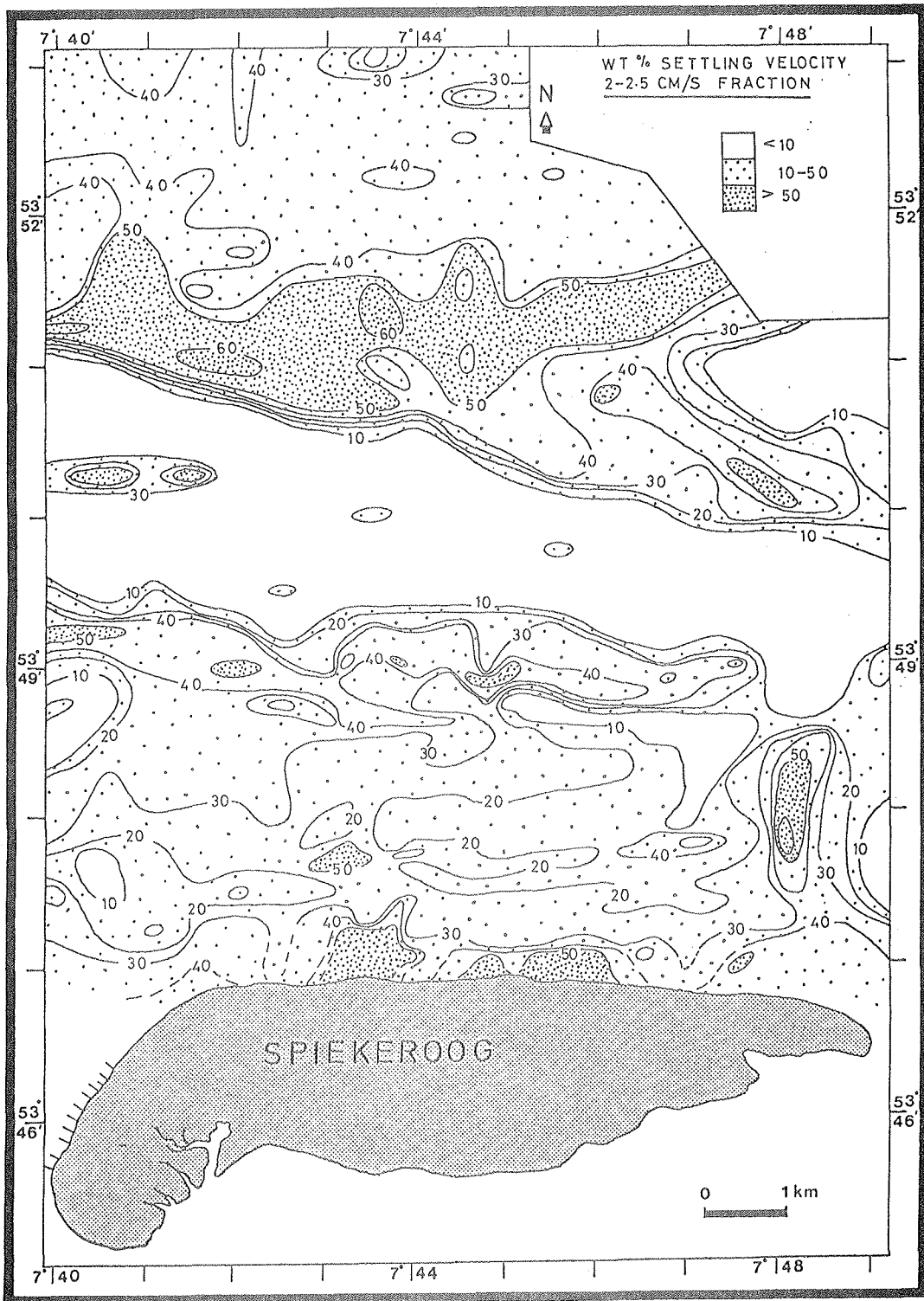
Appendix D-2. Shoreface distribution of wt.-% of 2-2.5 phi sand fraction.



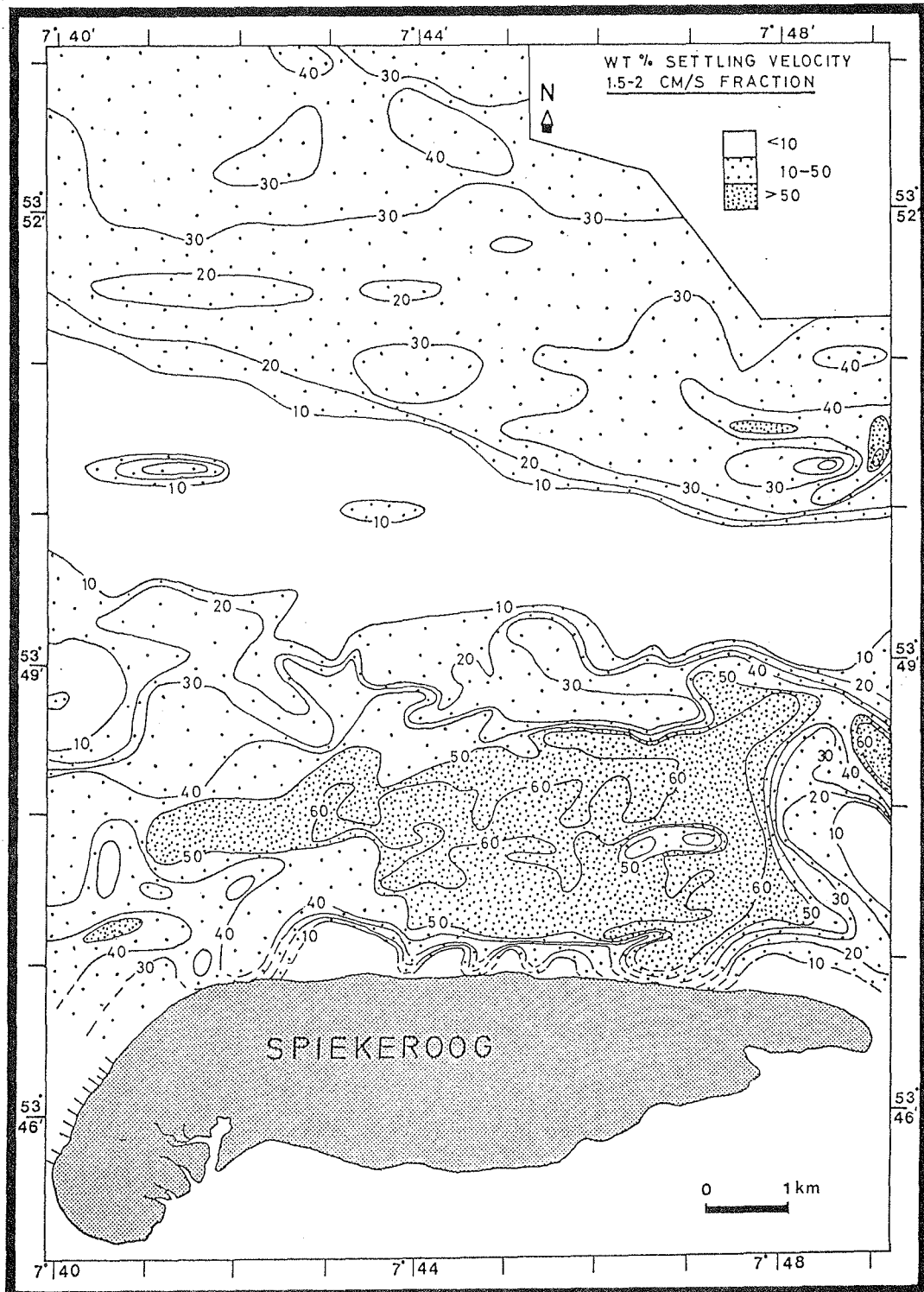
Appendix D-3. Shoreface distribution of wt.-% of 3-3.5 phi sand fraction.



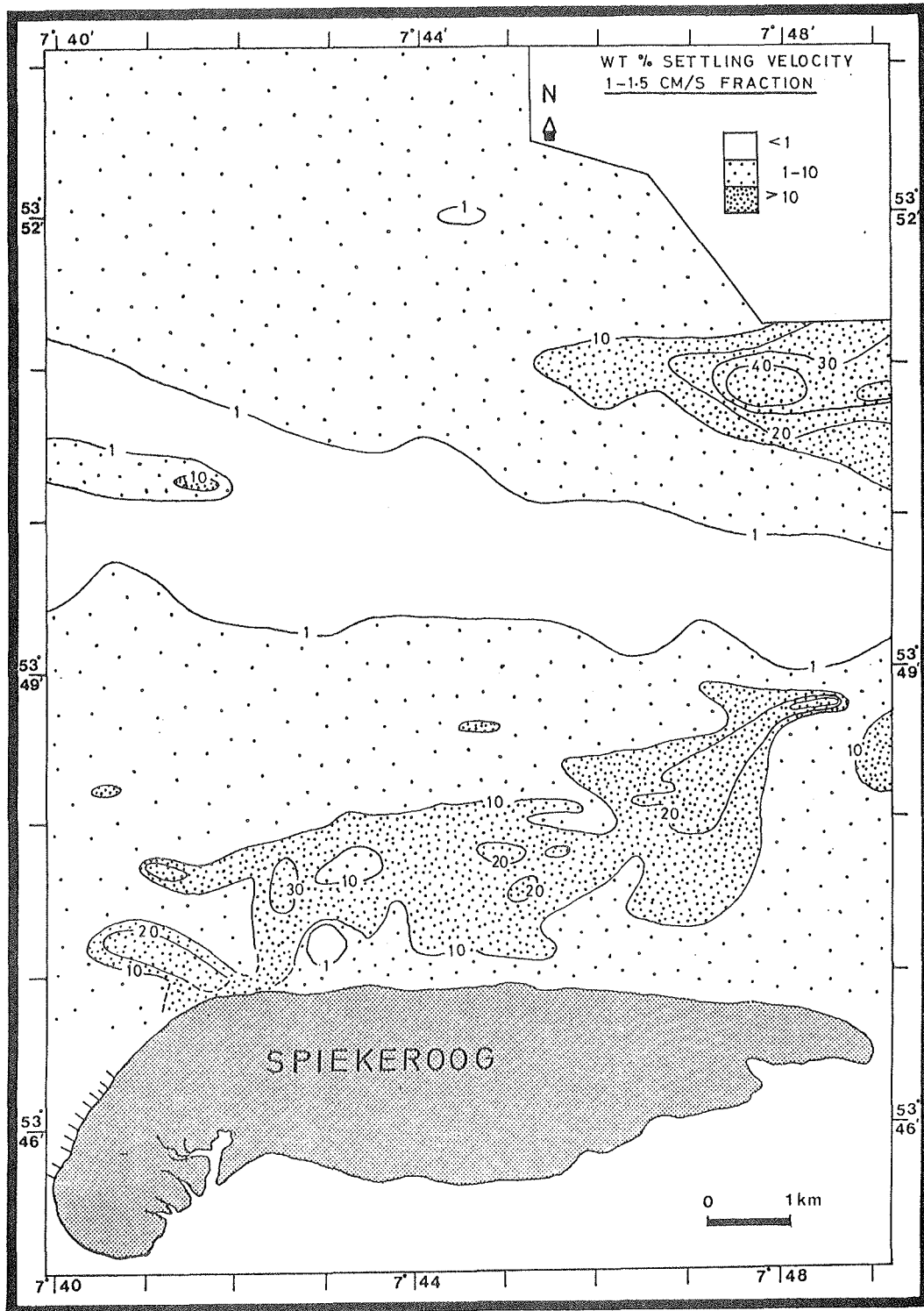
Appendix D-4. Shoreface distribution of wt.-% of 2.5-2.75 phi sand fraction.



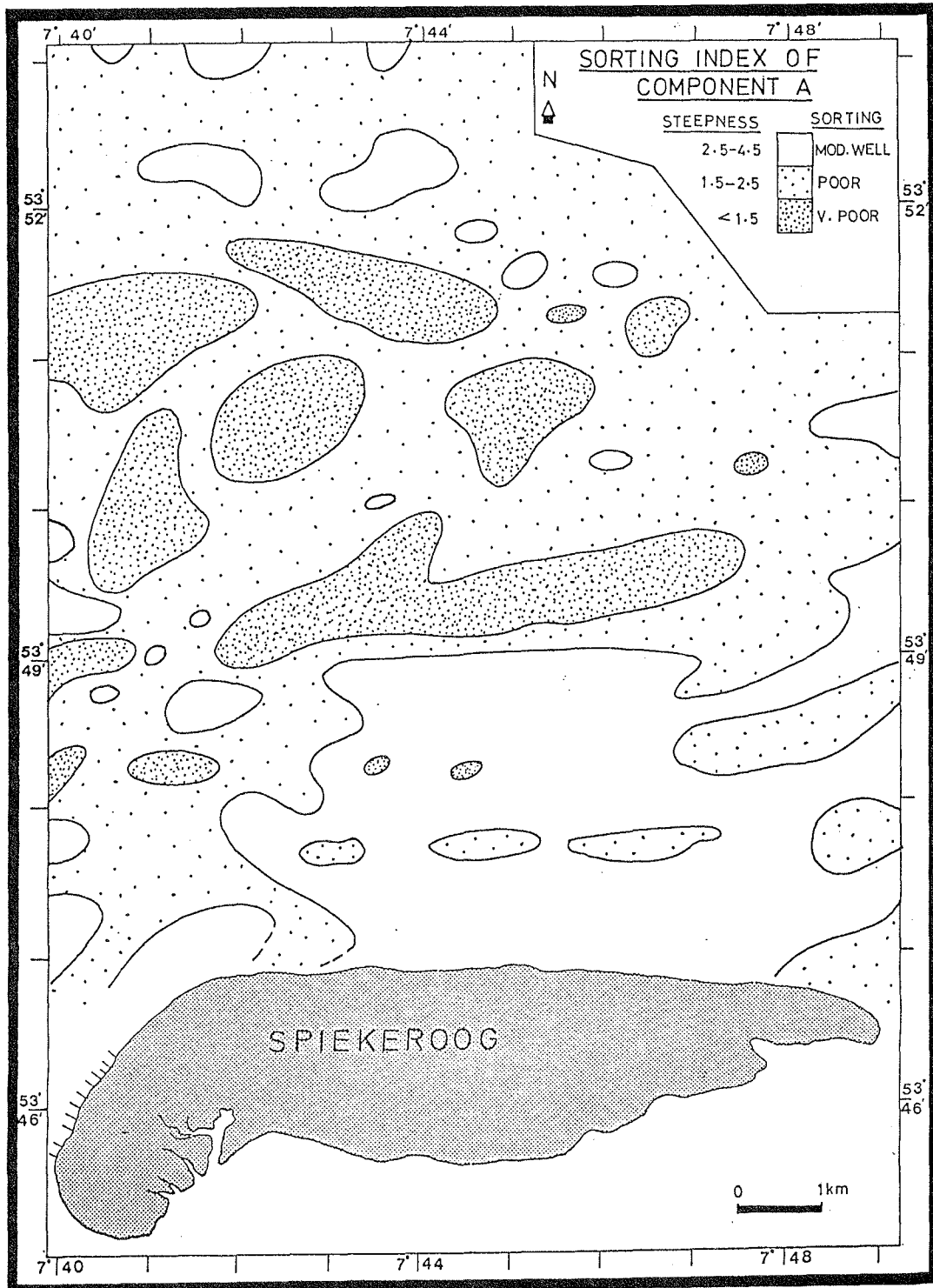
Appendix D-5. Shoreface distribution of wt.-% of 2-2.5 cm/s sand fraction.



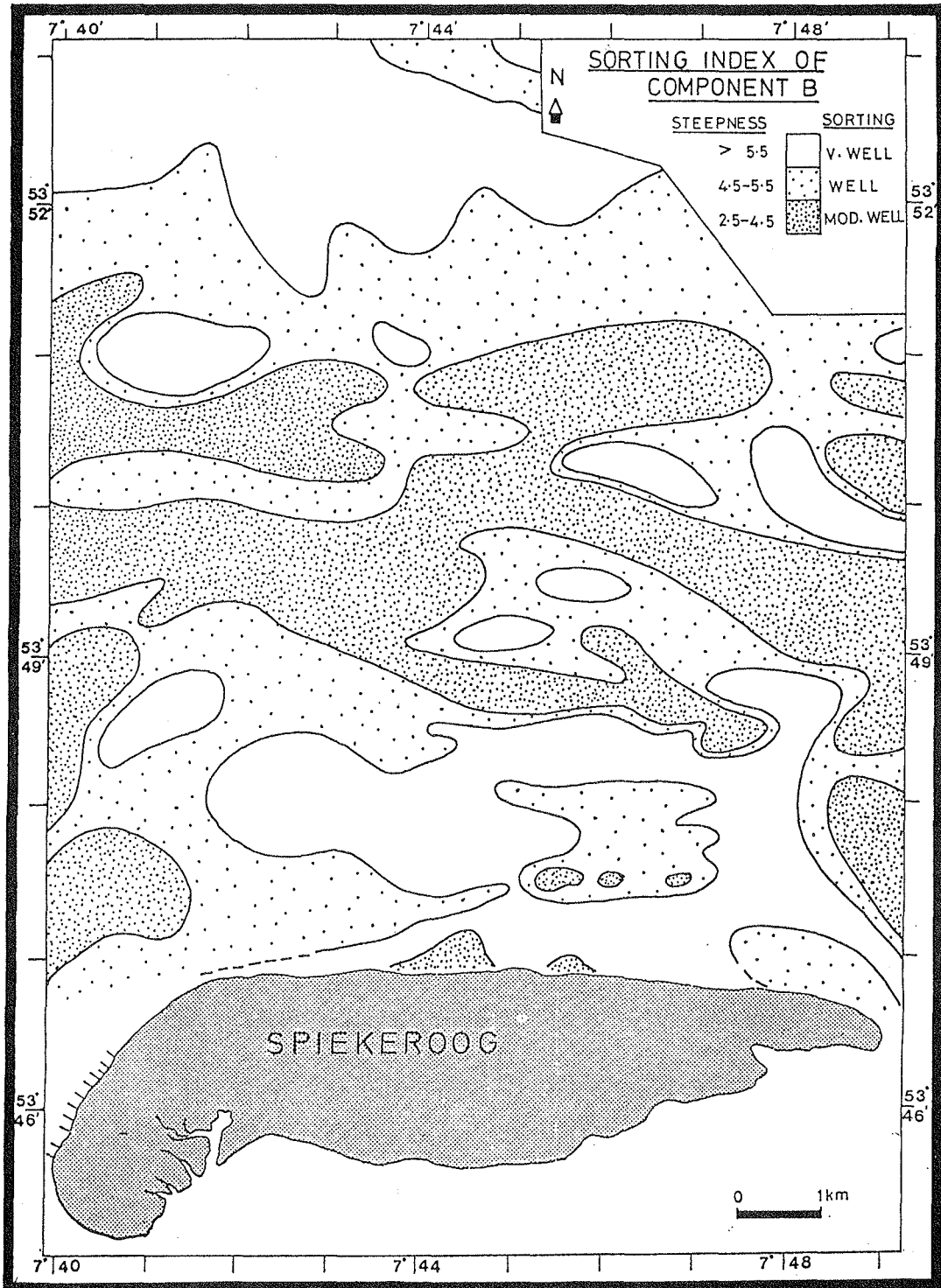
Appendix D-6. Shoreface distribution of wt.-% of 1.5-2 cm/s sand fraction.



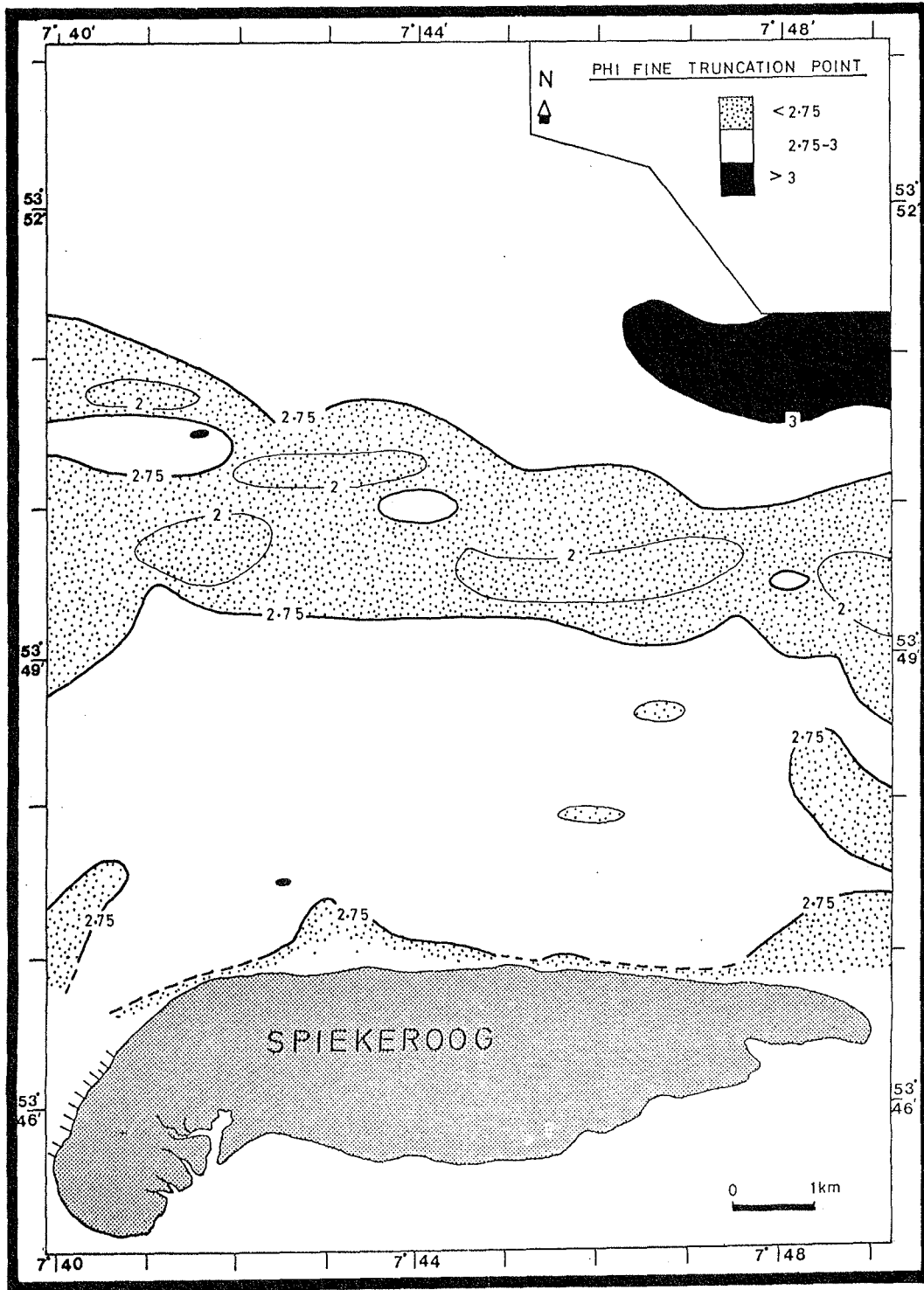
Appendix D-7. Shoreface distribution of wt.-% of 1-1.5 cm/s sand fraction.



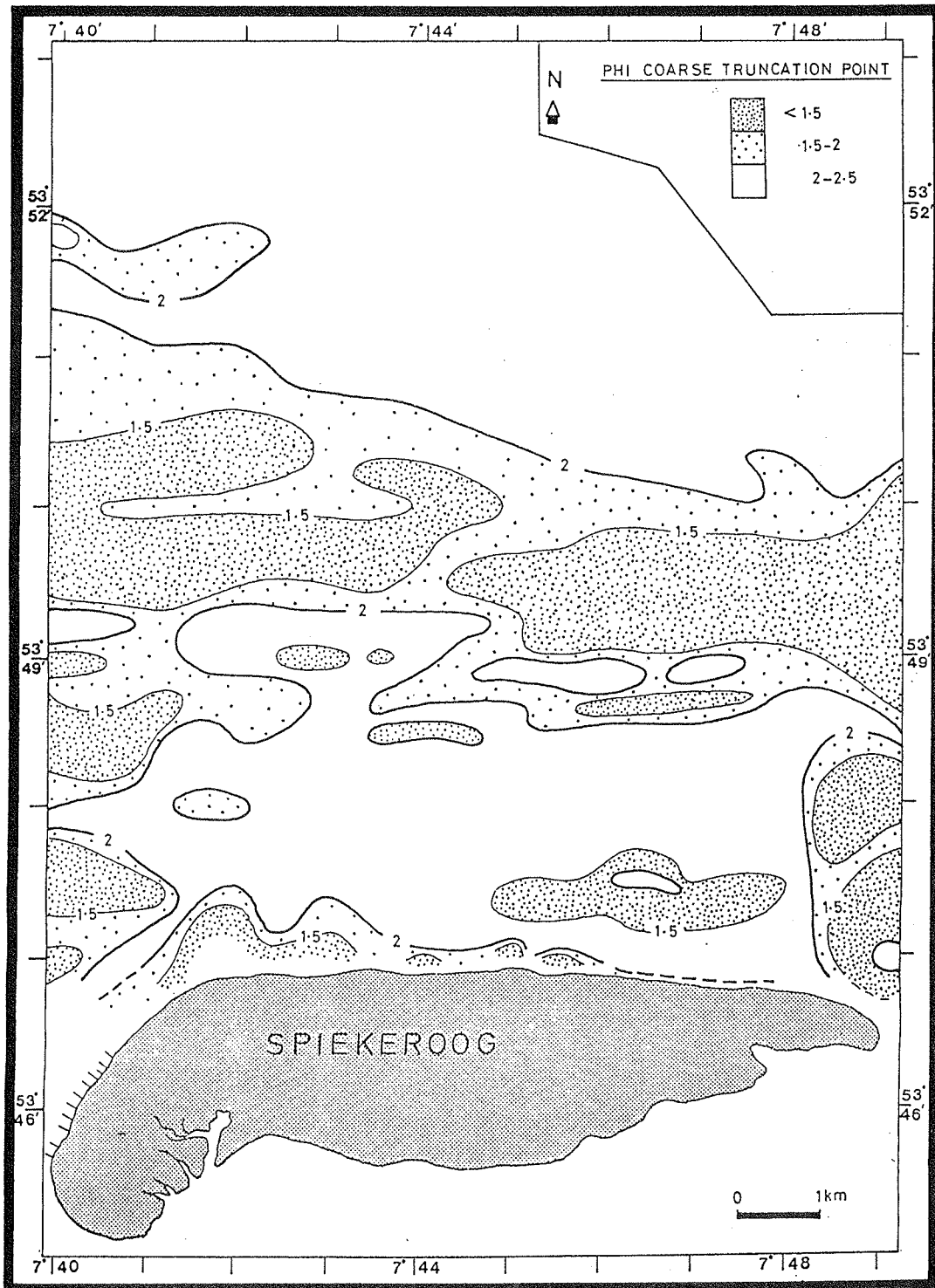
Appendix E-1. Shoreface distribution of the sorting of Component A (Suspension population).



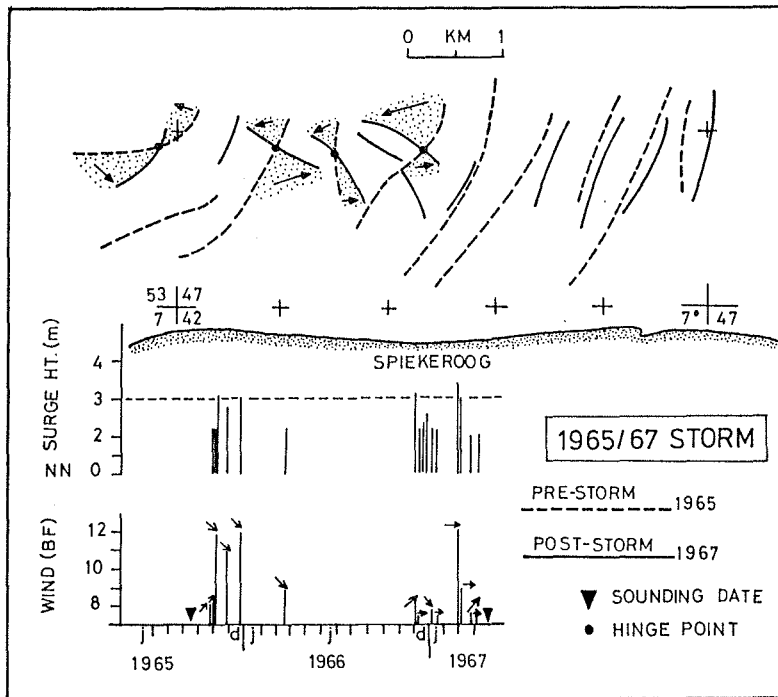
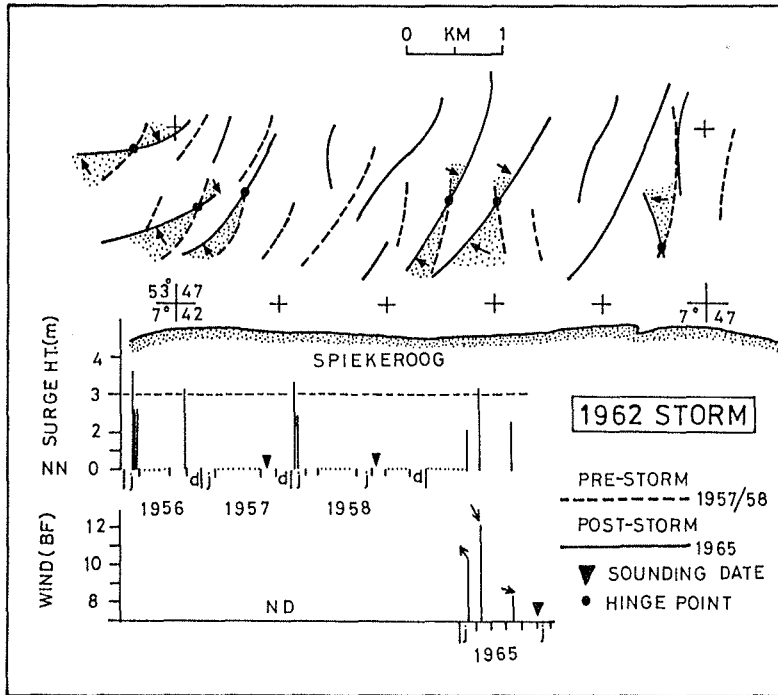
Appendix E-2. Shoreface distribution of the sorting of Component B (Saltation population).



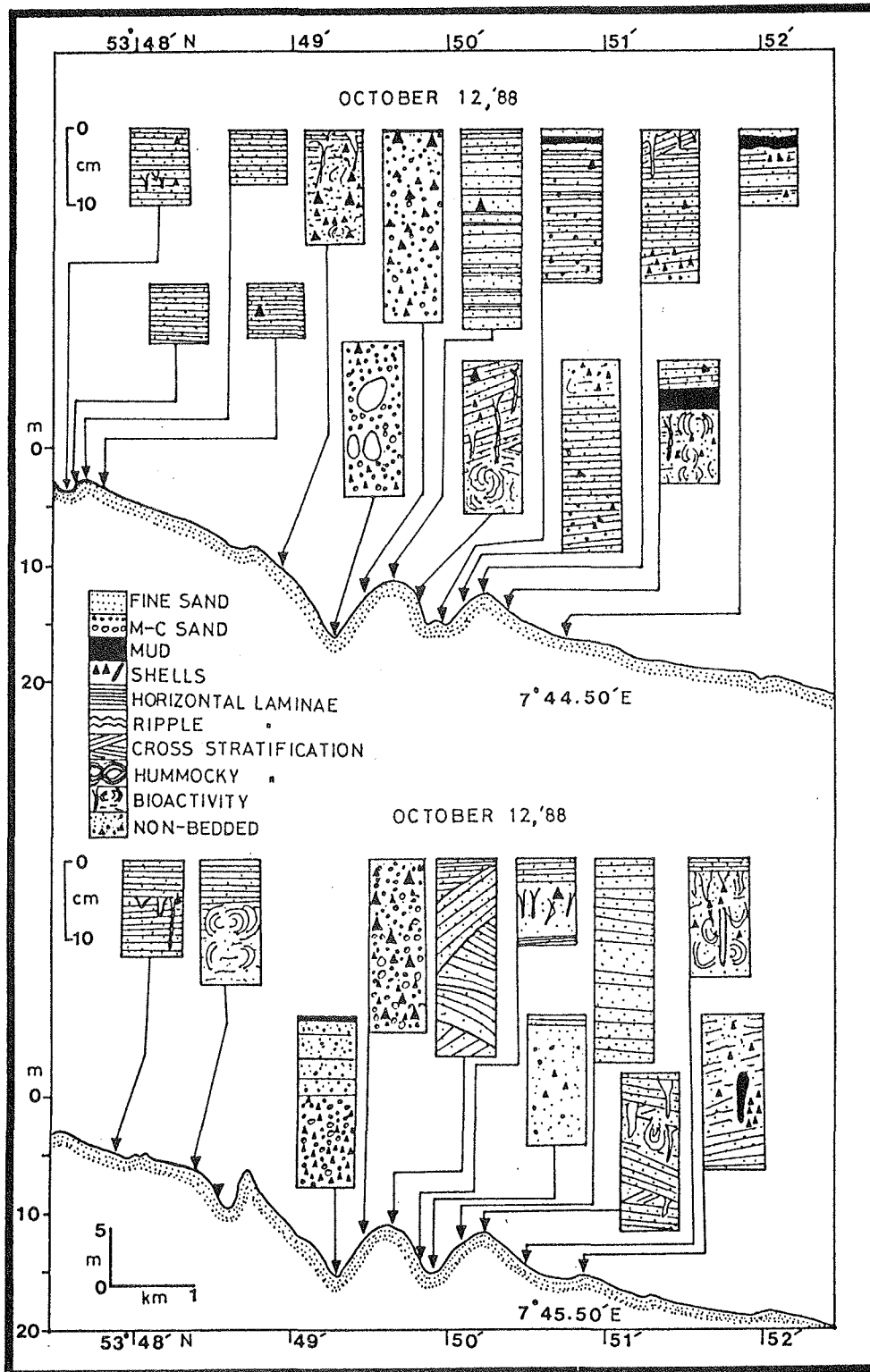
Appendix E-3. Shoreface distribution of the phi fine-truncation point (suspension-saltation transition).



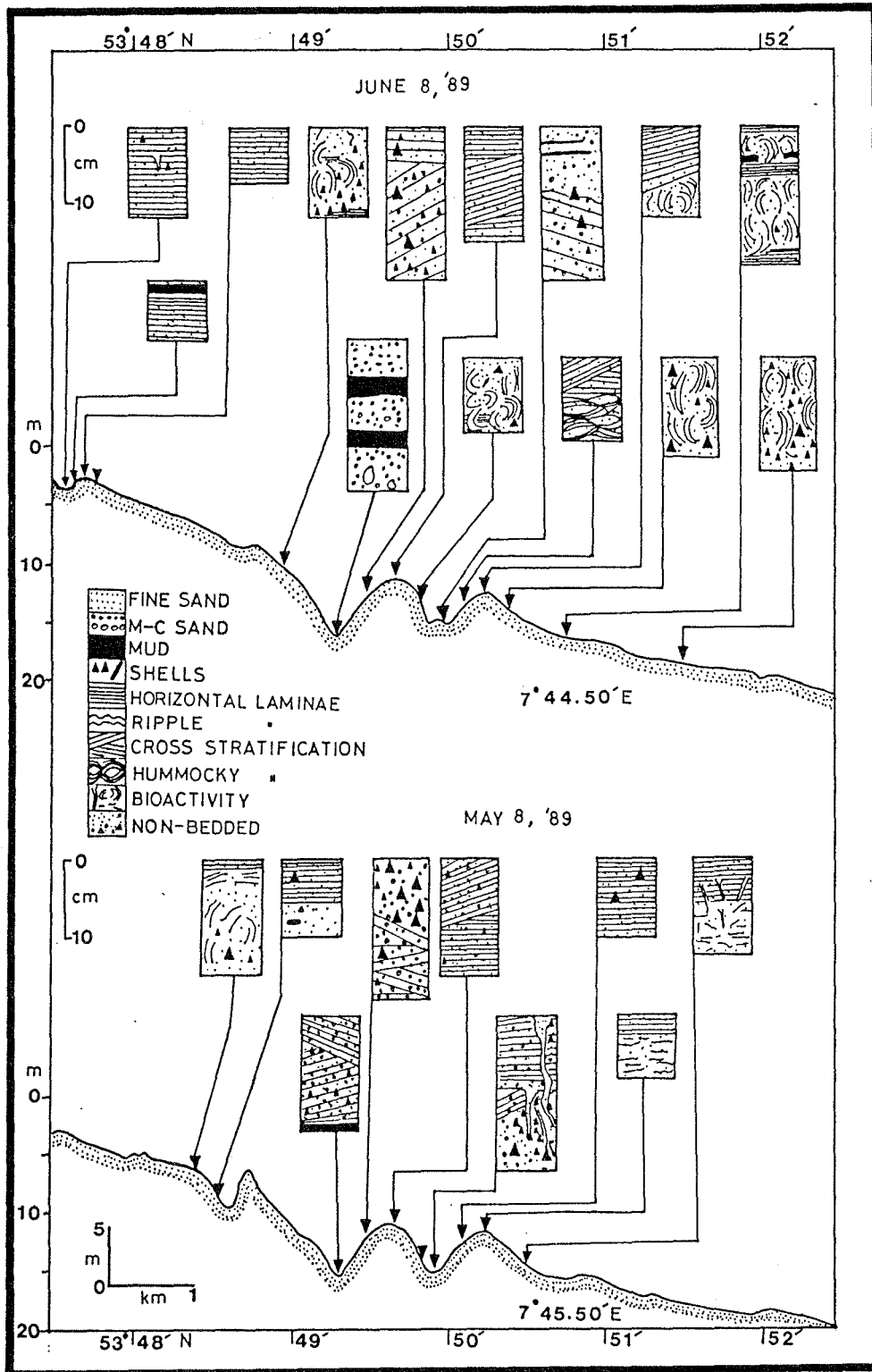
Appendix E-4. Shoreface distribution of the phi coarse-truncation point (saltation-traction transition).



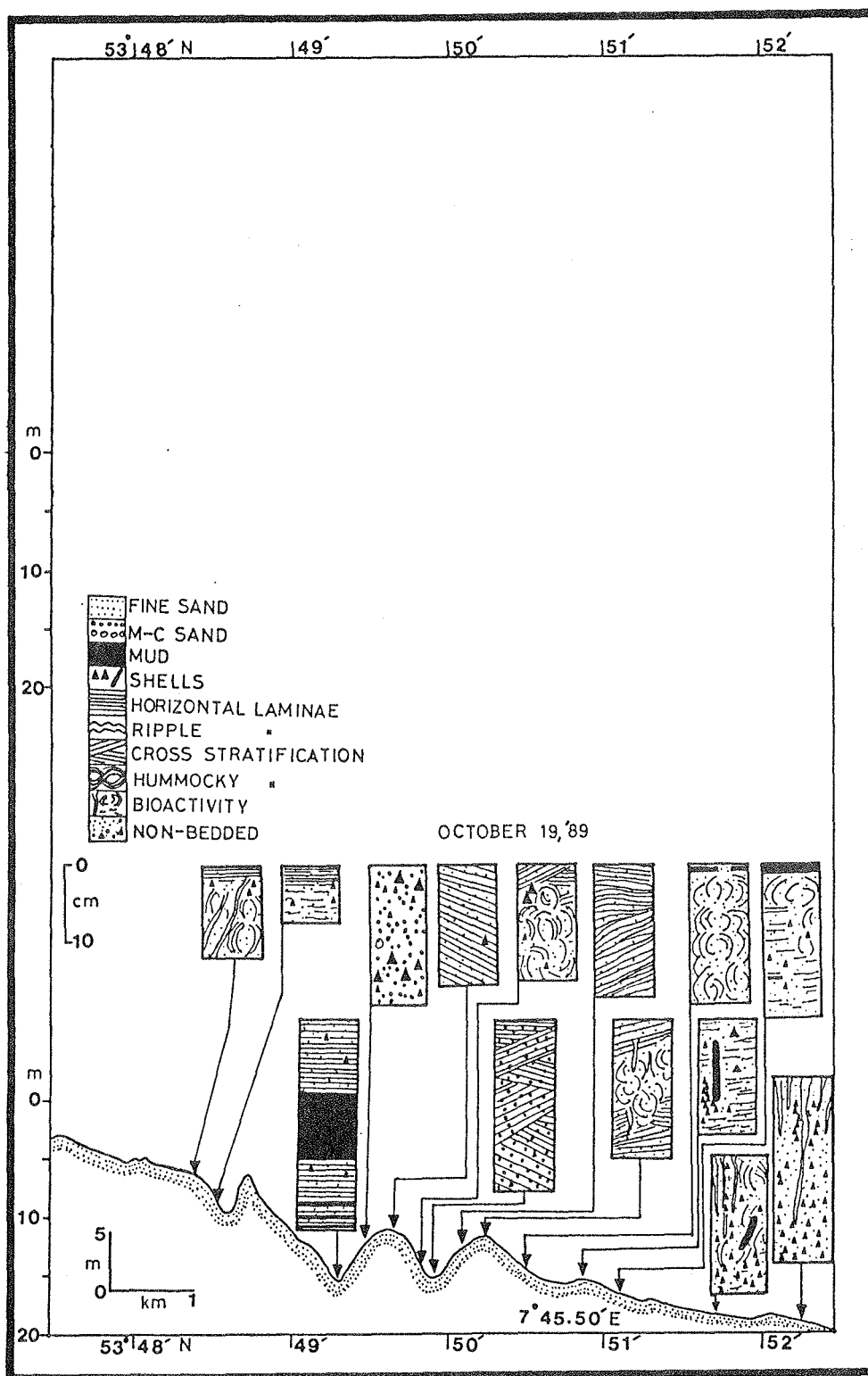
Appendix F. Dynamic patterns of rip channels in relation to 1962 and 1965/67 storm events.



Appendix G-1. Sequence of shoreface surficial sedimentary structures: October, 1988.



Appendix G-2. Sequence of shoreface surficial sedimentary structures: May/June 1988.



Appendix G-3. Sequence of shoreface surficial sedimentary structures: October, 1989.